



HAL
open science

Design, synthesis and optimization of new CXCR1/2 receptors antagonists for the treatment of exudative AMD

Marie Fabre

► **To cite this version:**

Marie Fabre. Design, synthesis and optimization of new CXCR1/2 receptors antagonists for the treatment of exudative AMD. Organic chemistry. Université Côte d'Azur, 2021. English. NNT : 2021COAZ4044 . tel-04213493

HAL Id: tel-04213493

<https://theses.hal.science/tel-04213493>

Submitted on 21 Sep 2023

HAL is a multi-disciplinary open access archive for the deposit and dissemination of scientific research documents, whether they are published or not. The documents may come from teaching and research institutions in France or abroad, or from public or private research centers.

L'archive ouverte pluridisciplinaire **HAL**, est destinée au dépôt et à la diffusion de documents scientifiques de niveau recherche, publiés ou non, émanant des établissements d'enseignement et de recherche français ou étrangers, des laboratoires publics ou privés.



$$\rho \left(\frac{\partial v}{\partial t} + v \cdot \nabla v \right) = -\nabla p + \nabla \cdot T + f$$

$$e^{i\pi} + 1 = 0$$

THÈSE DE DOCTORAT

Conception, synthèse et optimisation de
nouveaux antagonistes des récepteurs
CXCR1/2 pour le traitement de la DMLA
exsudative

Marie FABRE

Institut de Chimie de Nice

Présentée en vue de l'obtention
du grade de docteur en chimie
d'Université Côte d'Azur

Dirigée par Rachid BENHIDA,
Co-dirigée par Cyril RONCO,
Co-encadrée par Luc DEMANGE

Soutenue le : 25 juin 2021

Devant le jury, composé de :

Pr. Gilles PAGÈS, Directeur de recherche
INSERM, Université Côte d'Azur

Dr. Ling PENG, Directeur de Recherche CNRS,
Aix-Marseille Université

Dr. Sandrine FIGUEL, Maître de Conférences
HDR, Institut Curie, Université Paris-Saclay

Dr. Baptiste RONAN, Chef d'équipe Small
Molecule Medicinal Chemistry, Sanofi

Pr. Stéphanie BAILLIF, Professeur des
Universités-Praticien hospitalier, CHU Pasteur 2

Dr. Rachid BENHIDA, Directeur de Recherche
CNRS, Université Côte d'Azur

Dr. Cyril RONCO, Maître de Conférences HDR,
Université Côte d'Azur

Pr. Luc DEMANGE, Professeur, Université de
Paris

Université Côte d'Azur

École doctorale « Sciences Fondamentales et Appliquées »

Conception, synthèse et optimisation de nouveaux antagonistes des récepteurs CXCR1/2 pour le traitement de la DMLA exsudative

Jury :

Pr. Gilles PAGÈS	Directeur de recherche INSERM, Université Côte d'Azur	Président du jury
Dr. Ling PENG	Directeur de Recherche CNRS, Université Aix-Marseille	Rapporteur
Dr. Sandrine FIGUEL	Maître de Conférences HDR, Institut Curie, Université Paris-Saclay	Rapporteur
Dr. Baptiste RONAN	Chef d'équipe Small Molecule Medicinal Chemistry, Sanofi	Examineur
Pr. Stéphanie BAILLIF	Professeur des Universités- Praticien hospitalier, CHU Pasteur 2	Examineur
Dr. Rachid BENHIDA	Directeur de Recherche CNRS, Université Côte d'Azur	Directeur de thèse
Dr. Cyril RONCO	Maître de Conférences HDR, Université Côte d'Azur	Co-directeur de thèse
Pr. Luc DEMANGE	Professeur, Université de Paris	Co-encadrant de thèse

Abstract

In western countries, exudative age-related macular degeneration (AMD) is one of the leading causes of blindness in the elderly. This disease is characterized by an abnormal vascularization of the choroid and a strong intraocular inflammation. Currently, only anti-VEGF symptomatic treatments exist, which rely on humanized monoclonal antibodies (mAbs) and recombinant fusion glycoprotein targeting pro-angiogenic factors. Moreover, only 30% of the patients present a durable response to this treatment.

The blockage of the ERL⁺ CXCL cytokines signaling pathway has been proposed as a promising alternative to target simultaneously choroid vascularization and inflammation. Indeed, this sub-family of cytokines is specifically involved both in inflammation and in the early stage of the pro-angiogenic signal.

Two compounds of diarylurea family, MCK133 and MCK140, have established a proof of concept *in vitro* and *in vivo*. Therefore, a new series of compounds has been designed that features the same pharmacophore but with new chemical functions,azole core, to enhance the activity and the physicochemical properties.

Four series based on the pharmacophore were considered: two with an imidazole core and two with a triazole core. Synthetic pathways to each of these families have been studied. One of them, 1-benzyl-*N*³-1*H*-1,2,4-triazole-3,5-diamine series allowed to synthesize various compounds thanks to a new straightforward synthetic pathway, aimed at modifying two key parts of the structure. The structure-activity relationships of these series were studied thanks to their biological evaluations on exudative AMD models. Therefore, the preparation of 63 final analogues possessing the desired pharmacophore and 14 1*H*-1,2,4-triazole intermediates, permitted the identification of a Lead compound. The perspectives of this thesis are the evaluation of this compound on several *in vivo* models of exudative AMD.

Finally, the last part of this manuscript presents two annexe projects: (i) the study of the biamidines transfer to biguanides and (ii) the stability study of NRPa-308.

Keywords: organic synthesis, 1,2,4-triazole, RSA, CXCR 1/2 receptors, exudative AMD

Résumé

Dans les pays occidentaux, la dégénérescence maculaire liée à l'âge (DMLA) exsudative est l'une des principales causes de cécité chez les personnes âgées. Cette maladie est caractérisée par une vascularisation anormale de la choroïde et une forte inflammation intraoculaire. Actuellement, seuls les traitements symptomatiques anti-VEGF existent, à base d'anticorps monoclonaux humanisés et des glycoprotéines de fusion recombinantes ciblant les facteurs pro-angiogéniques. À l'heure actuelle, uniquement 30 % des patients présentent une réponse durable aux traitements.

Le blocage de la voie de signalisation des cytokines ERL⁺ CXCL a été proposé comme une alternative prometteuse pour cibler simultanément la vascularisation de la choroïde et l'inflammation. En effet, cette sous-famille de cytokines est impliquée à la fois dans le processus inflammatoire et dans le stade précoce du signal pro-angiogénique.

Deux composés de la famille des diarylurée, MCK133 et MCK140, ont permis d'établir une preuve de concept *in vitro* et *in vivo*. À partir de ces composés, nous allons concevoir et développer des familles de composés basés sur le même pharmacophore mais avec de nouvelles fonctions chimiques, le noyau azole, pour améliorer l'activité et les propriétés physico-chimiques.

Quatre séries de composés basées sur le pharmacophore ont été envisagées : deux avec un noyau imidazole et deux avec un noyau triazole. Les voies d'accès synthétiques à chacune de ces familles ont été étudiées. L'une d'elles les 1-benzyl-*N*³-1*H*-1,2,4-triazole-3,5-diamine a permis la synthèse d'un certain nombre d'analogues, visant à modifier deux parties clés de la structure. Les relations structures-activité de cette série ont été étudiées à l'aide de leurs évaluations biologiques sur plusieurs modèles de DMLA exsudative. Grâce à la préparation de 63 analogues finaux possédant le pharmacophore désiré et de 14 intermédiaires 1*H*-1,2,4-triazole, un Lead prometteur a été identifié. Les perspectives de cette thèse sont l'évaluation de ce composé sur plusieurs modèles *in vivo* de DMLA exsudative.

Finalement, la dernière partie de ce manuscrit présente deux projets annexes : (i) une étude du transfert des biamidines vers les biguanides et (ii) l'étude de la stabilité du NRPa-308.

Mots-clés : synthèse organique, 1,2,4-triazole, RSA, récepteurs CXCR 1/2, DMLA exsudative

À mon grand-père, Emile Fabre (1934-2020)

ACKNOWLEDGMENTS

Cette thèse de doctorat est l'aboutissement de trois années de travail à l'Institut de Chimie de Nice (ICN) de l'université Côte-d'Azur dans le groupe molécules bioactives. Je vois une réelle différence entre la chimiste que je suis aujourd'hui et celle d'il y a trois ans. Cela a été un travail long, parfois difficile, parfois plaisant et toujours passionnant. Mais un doctorat ne se fait pas seul et je tiens à remercier les personnes qui y ont participé.

Je remercie en premier lieu l'ANR et le consortium TARMAC qui a permis le financement de ma thèse. Ce consortium regroupe l'Institut de Chimie de Nice (ICN) de l'université Côte-d'Azur composée du Dr. Rachid Benhida, du Dr. Cyril Ronco et du Pr. Luc Demange ; de l'équipe de l'Institut de recherche sur le cancer et vieillissement de Nice (IRCAN) avec le Pr. Gilles Pagès et le Dr. Maeva Dufies ; et du centre hospitalier Universitaire de Nice avec le Pr. Stéphanie Baillif. Je remercie également la collaboration d'Iris Pharma avec le Dr. Sophie Antonelli.

Je tiens à remercier mon directeur de thèse, le Dr. Rachid Benhida, pour m'avoir accueilli dans son équipe et au sein de l'ICN. Vous m'avez permis d'évoluer scientifiquement en me confiant ce projet et en me faisant confiance pour le mener à bien. Grâce à vous j'ai pu toucher à toutes les parties de ma thèse, la conception, la synthèse, la partie biologique et clinique avec notamment l'écriture de la revue, contribuant à faire de moi la chimiste médicinale que je suis aujourd'hui.

Un grand merci à mon co-directeur de thèse, le Dr. Cyril Ronco, qui a obtenu son HDR durant ma thèse (un 25 juin), ce qui m'a permis de devenir sa première doctorante officielle... et quelle fierté ! Grâce à nos échanges quotidiens, à toutes les propositions de projets, de papiers, d'idées de nouvelles réactions et récemment pour avoir corrigé ma thèse avec bienveillance et rapidité, j'ai pu réaliser ce doctorat au mieux. Tes actuels et prochains doctorants ont de la chance de t'avoir comme directeur de thèse.

Merci au Pr. Luc Demange qui a été en co-supervision depuis Paris. Depuis que tu m'as recruté, j'ai beaucoup appris à tes côtés. Tu m'as permis de faire de belles présentations et tu étais toujours là pour y assister. Ton soutien, tes nombreux messages, commentaires lors des corrections, tes appels, tes propositions de projets et surtout ta bonne humeur m'ont beaucoup aidé tout au long de ma thèse.

Je souhaite ensuite remercier l'ensemble des membres de mon jury de thèse. Tout d'abord le Dr. Ling Peng et le Dr. Sandrine Piguel pour avoir accepté d'évaluer mon travail de doctorat en tant que rapporteurs. Puis, le Pr. Gilles Pagès d'avoir accepté de présider ce jury. Pour finir, je remercie le Dr.

Baptiste Ronan et le Pr. Stéphanie Baillif d'avoir accepté d'examiner ma thèse. Merci également au Pr. Baillif de m'avoir accueilli et expliqué la partie clinique de la DMLA, ce qui fut très enrichissant pour mon sujet de thèse.

J'exprime mes sincères remerciements à l'équipe du Pr. Gilles Pagès pour sa collaboration sur les évaluations biologiques effectuées dans son unité. Merci Gilles de m'avoir accueilli dans ton équipe pour que je pratique moi-même les tests sur mes molécules, d'avoir été membre de mon jury de comité de thèse et maintenant de me faire l'honneur d'être le président de mon jury de thèse. Merci au Dr. Maeva Dufies pour la réalisation des nombreuses expériences biologiques et pour avoir pris le temps de me les expliquer. Merci à Olivia Rastoin d'avoir fait les évaluations sur mes composés et de m'avoir enseigné la pratique expérimentale.

Merci au Dr. Elisabeth Taffin-de-Givenchy d'avoir été membre de mon jury de comité de thèse et pour sa présence et son aide en tant que directrice de l'ED-SFA. Merci aux Dr. Marc Gaysinski et au Dr. Lionel Massi pour leurs aides sur les multiples analyses de RMN et de LCMS. Merci au Dr. Patrick Deschamps pour la cristallographie de mes molécules et pour m'avoir reçu à Paris. Et finalement, merci au Dr. Nathalie Lagarde pour la réalisation du docking sur les composés.

Je voudrais remercier les permanents du groupe molécule bioactives avec qui j'ai pu avoir d'intéressantes conversations, le Pr. Nadia Patino, le Dr. Audrey Di Giorgio, le Dr. Maria Duca, le Dr. Benoit Michel, le Dr. Alain Burger et le Dr. Mohamed Mehiri.

For my colleagues and the RB team, I switch to English because I had the chance to work in the 508 lab, mainly with foreign chemists. Leticia, obrigada for everything: your support, your kindness, your help, and your chocolates. Спасибо Rostyslav for sharing a wonderful project, allowing us to submit our paper, and for all our discussions from the first day of this thesis. Sorry I could not learn your complex language even though you tried. Thank you in all languages to the whole RB team for our discussions in chemistry or other, meals of *non-permanent* workers and for sharing the lab with me: Lou (in particular for our collaboration on the introduction's review), Mauro, Anthony, Aicha, Zakaria, Mathilde, Sarah, Kévin, Julien, Sacha, Pascal, and all the trainees. Thank you also to all the ICN members for these shared moments: Ngoan, Najiba, Guillaume, Céline, Chloé, Steve, Romain, Alexandra, Paula, and probably other names to cite...

Merci à Laurie Chiara et à la compagnie BAL pour le travail effectué sur « ma thèse en 180 secondes » (MT180), exercice enrichissant où malheureusement la finale s'est tenue à huis clos à la veille du début de la pandémie du covid-19.

D'un point de vue plus personnel, je tiens à remercier mes amis de toujours, des amis qui m'accompagnent pour certains depuis mon enfance. Malgré la distance vous êtes toujours là pour moi et je me rends compte de la chance de vous avoir. Je commencerais par mon grand ami le Dr. Jason que je connais depuis 24 ans maintenant. Merci pour tes nombreux conseils sur la vie de thésard que nous avons partagé. J'espère que notre longue amitié, si précieuse, continuera toute notre vie (avec de nombreux partages de tourtons et saucissons). Maxime, depuis l'époque du lycée où nous sommes devenues amis, nous étions dans des villes éloignées qui n'empêchais pas nos nombreux appels mais passé 1 an près de toi au moment de ce début de thèse a été une vraie chance. Aurélie et Étienne à distance également mais toujours partant pour se retrouver, on retourne à Rome ou à Madrid ? Chloé et Elodie, ces études ont commencé avec vous et je vous rattrape enfin pour le diplôme, plus qu'à boire un verre toutes ensemble (chez nous ou à Grenoble). Et finalement la chimiste, une pensée particulière pour ma Laetitia qui m'a accompagné à mon premier stage à l'étranger à York, nos discussions autour d'une bonne bouteille de vin sont toujours un plaisir. Et à tous les autres... Hâte de vous revoir.

Merci à mes amis d'ici, du quotidien avec lesquels je partage depuis 3 années des cinémas qui étaient une joie de chaque semaine mais aussi des FIJ, des voyages (d'ailleurs merci à Jérémie du Vietnam pour l'invitation à ton mariage), des réveillons et tant d'autres choses trop longues à citer... Merci Thibaut, Morgane, Nicolas, Noélie et à distance Étienne.

Et tout ça aussi pour aboutir à un ami qui est devenu mon amour, un des plus grands soutiens de cette dernière année de thèse qui m'a écouté inlassablement parler de ma thèse avec un calme parfait, pour tes encouragements et tes conseils, François, merci !

Et en dernier, ceux sans qui je n'aurais pas pu faire une thèse : ma famille. Merci à chaque membre, mes grands-mères (Jacqueline et Yvonne), ma marraine, mon parrain, mes tantes, mes oncles, cousines, cousins, mon filleul. Un remerciement spécial à mes deux grands frères, Jérémie et Antonin. Notre relation fraternelle est si importante pour moi, merci pour votre soutien sans faille durant cette thèse et depuis toujours. Merci à mes parents, Catherine et Jean-Dominique, vous faire une liste de pourquoi vous remercier prendrais bien plus d'une thèse. Vous avez cru en moi tout au long de ma vie, sans votre soutien et votre amour qui m'ont toujours motivé à aller plus loin, à me dépasser, je n'aurais pas pu atteindre le bout de ces 10 années d'études.

CONTENT

Abstract.....	5
Résumé.....	7
Acknowledgments	11
Abbreviations	19
General Introduction	23
Chapter 1. Exudative age-related macular degeneration (AMD): Evolution of the different treatments	27
1.1 Introduction	29
1.1.1 The complexity of the eye’s anatomy.....	29
1.1.2 The different eye diseases.....	31
1.2 Pathogenesis, development and characteristics of AMD	32
1.2.1 Pathogenesis	32
1.2.2 Epidemiology and Risks factors of AMD	34
1.2.3 AMD characteristics	35
1.3 Atrophic (dry) AMD treatments	39
1.3.1 Visual cycle	39
1.3.2 Amyloid β ($A\beta$).....	43
1.3.3 Choriocapillaris (CC) atrophy.....	45
1.3.4 RPE and photoreceptors loss: Stem cells (SC)	47
1.3.5 Oxidative stress.....	50
1.3.6 Neuroprotection	53
1.3.7 Inflammatory pathways	55
1.4 Exudative (wet) AMD treatments.....	62
1.4.1 Phototherapies	63
1.4.2 Anti-VEGF drugs.....	66
1.4.3 Anti-PDGFs.....	80

1.4.4	Angiopoietin 2 inhibitors.....	81
1.4.5	Miscellaneous targets	82
1.4.6	Stem cell transplant	85
Chapter 2.	Development of dual antiangiogenic /anti-inflammatory compounds targeting the CXCR1/2 receptors.....	89
2.1	CXCL Chemokine family and their receptors.....	92
2.2	CXCR1/2 known antagonists	93
2.3	Proofs of concept of CXCR1/2 antagonists effects in angiogenic pathologies.....	96
2.3.1	In cancers	98
2.3.2	In AMD	99
2.4	Design of new series of CXCR1/2 antagonists.....	100
2.4.1	Rationale	100
2.4.2	Envisaged series.....	101
2.4.3	Structural properties and similarities of the predicted pharmacophores and diarylureas	102
Chapter 3.	Synthesis of the imidazole series.....	103
3.1	<i>N</i> , phenyl-1 <i>H</i> -imidazol-2-amine synthesis (Series A).....	105
3.1.1	A1: Aza-Hantzsch pathway: Unexpected product	105
3.1.2	A2: <i>S_NAr</i> pathway	116
3.1.3	A3: Pyrimidinium pattern pathway.....	121
3.2	1-benzyl-1 <i>H</i> -imidazol-2-amine synthesis (Series B)	125
3.2.1	B1: Aza-Hantzsch pathway	126
3.2.2	B2: Riley oxidation pathway	129
3.2.3	B3: Pyrimidinium pathway	131
Chapter 4.	Synthesis of the triazole series	135
4.1	<i>S_NAr</i> approach (Series C & D)	137
4.2	1-benzyl- <i>N</i> ³ -1 <i>H</i> -1,2,4-triazole-3,5-diamine (Series D)	139
4.2.1	1 <i>H</i> 1,2,4-triazole intermediates.....	140

4.2.2	Benzyl-1,2,4-triazole: First results	143
4.2.3	Series D ₁ : functionalization with different benzyl groups.....	152
4.2.4	Series D ₂ : functionalization of R ¹ group	172
	General conclusion and perspectives	175
Chapter 5.	Annexe projects	181
5.1	Biamidine transfer in biguanides compounds.....	183
5.1.1	Introduction.....	183
5.1.2	Results and discussion	184
5.1.3	Conclusions.....	191
5.2	Stability analyses of NRPa-308	192
	Experimental part	197
	References.....	291

ABBREVIATIONS

μM: Micromolar	CRT: thickness of central retina
A2E: <i>N</i> -retinylidene- <i>N</i> -retinylethanolamine	CT: control
Aβ: Amyloid β	CXCL: Chemokine (C-X-C motif) ligand
ABCA4: ATP-Binding Cassette Subfamily A Member 4	CXCR: Chemokines receptor
Akt: Protein kinase B	DCM: Dichloromethane
AMD: Age-related Macular Degeneration	DHA: Docosahexaenoic acid
ANG: angiopoietin	DIPEA: <i>N,N</i> -Diisopropylethylamine
AREDS: Age-Related Eye Disease Study	DMAP: 4- <i>N,N</i> -diméthylaminopyridine
BCVA: best corrected visual acuity	DME: diabetic macular edema
bFGF: basic fibroblast growth factor	DMF: Dimethylformamide
BMI: body mass index	DMSO: Dimethyl sulfoxide
Boc: <i>t</i> -butyloxycarbonyl group	DTC: differentiated thyroid cancer
BrM: Bruch's membrane	ELR: glutamate-leucine-arginine motif
<i>n</i>-BuLi: <i>n</i> -Butyllithium	EC₅₀: Efficient dose 50
CC: choriocapillaris	EPA: eicosapentaenoic acid
CFH: complement factor H	ERK: Extracellular signal–regulated kinases
CFI: complement factor I	ESI: Electrospray ionization
CNRS : Centre National de la Recherche Scientifique (National Center of Scientific Research)	EtOH: Ethanol
CNV: choroidal neovascularization	Et₃N: Triethylamine
COPD: chronic obstructive pulmonary diseases	FAF: fundus autofluorescence
	FDA: U.S. Food and Drug Administration
	FGF-R: fibroblast growth factor receptor

GA: geographic atrophy

GFP: green fluorescent protein

h: hour(s)

HAS : “Haute Autorité de Santé”

HCMEC: human choroidal microvascular endothelial cells

HDL-C: High-Density Lipoprotein Cholesterol

hESC: Human embryonic stem cells

HPLC: High-Performance Liquid Chromatography

HuCNS-SC: human central nervous system

HuVECs: Human Umbilical Vein Endothelial Cells

Hx: Hypoxia

IC₅₀: Half maximal inhibitory concentration

ICN : Institut Chimie de Nice (Institut of Chemistry of Nice)

IL-8: Interleukine 8

iPSC: Human-induced pluripotent stem cells

IR: infrared reflectance

IRCAN: Institute for Research on Cancer and Aging

Kd: Dissociation constant

LCMS: Liquid Chromatography-Mass Spectrometry

LRAT: lecithin retinol acyltransferase

MAC: membrane attack complex

MeCN: Acetonitrile

MeOH: Methanol

MeST: 5-(methylthio)-4H-1,2,4-triazol-3-amine

MLA: age-related maculopathy

MW: microwave

n.c.: no conversion

n.d.: not determined

n.i.: not isolated

NMR: Nuclear Magnetic Resonance

Nrf-2: Nuclear factor E2-related factor

NV: new vessels

OCT: optical coherence tomography

o.n.: overnight

ORT: outer retinal tubulation

PDGF: platelet-derived growth factor

PDGF-R: Platelet Derived Growth Factor Receptor

PDR: proliferative diabetic retinopathy

PIGF: placenta growth factor

PPAR: peroxisome proliferator-activated receptor

qPCR: quantitative polymerase chain reaction

RBP4: retinol 4

RCC: renal cell carcinoma

RDH: retinol dehydrogenase

RNP: ribonucleoproteins

ROS: reactive oxygen species

RPE: retinal pigment epithelium

RPE65: retinal pigment epithelium-specific 65

SAR: Structure–activity relationship

SC: stem cells

sFLT-1: VEGF receptor

siRNA: Small interfering RNA

SM: starting material

S_NAr: Aromatic nucleophilic substitution

r.t.: room temperature

T: Temperature

TAP: Treatment of AMD with Photodynamic Therapy

TP: tempol

TTR: transthyretin

VA: Visual acuity

VEGF: Vascular endothelial growth factor

VEGF-R: Vascular Endothelial Growth Factor Receptor

Vg: vector genomes

VIP: Verteporfin In Photodynamic Therapy

THF: Tetrahydrofuran

TLC: Thin Layer Chromatography

t_R: Retention time

UMR : Unité Mixte de Recherche

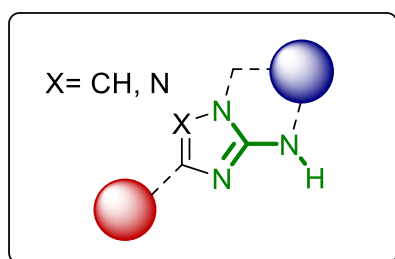
U.V.: Ultra-Violet

GENERAL INTRODUCTION

Exudative age-related macular degeneration (AMD) is characterized by the neo-vascularization of the choroid mediated by the vascular endothelial growth factor A (VEGF-A) and by inflammation. Currently, only symptomatic treatments exist, which rely on humanized monoclonal antibodies (mAbs) and recombinant fusion glycoprotein targeting pro-angiogenic factors. However, 30% of the patients are insensitive to this therapy: no means are available to predict their degree of response. Other problems were highlighted as the side effects (retinal atrophy), the only delay progression to blindness, the stressful formulation by intravitreal injections. In addition, this approach targets only neo-vascularization mediated by VEGF, but it does not target the inflammation process. Inflammation and angiogenesis are integrated processes, and several cytokines are pro-inflammatory and pro-angiogenic. This Ph.D. project aims to concomitantly tackle these two phenomena by targeting the ERL⁺ CXCL cytokines signaling pathway. Besides, this cytokine CXC family is precisely involved both in the early stage of the pro-angiogenic signal and in the inflammatory development.

Chapter 1 presents AMD as one of the major eye diseases. First, a description of pathogenesis, development, and characteristics has been broached. Second, a study of several strategies against atrophic AMD is depicted. A particular emphasis is given to the potential treatments currently in clinical trials or in a late research phase. Finally, the same study is performed for exudative AMD treatments including those currently on the market (anti-VEGF) and those currently tested in clinical or research phase with a particular focus on VEGF, PDGF, angiopoietin 2, and several miscellaneous targets.

Chapter 2 introduces our therapeutic target, the ERL⁺ CXC cytokine subfamily, and is focused on the CXCL chemokines context as well as on the known CXCR1/2 antagonists. Based on two hit compounds already synthesized and validated by our group both *in vitro* and *in vivo*, the design of a new pharmacophore is depicted. Indeed, this Ph.D. deals with the development of new series of CXCR1/2 inhibitors with optimized physicochemical properties. Besides, in this document, the study of four new series based on the same pharmacophore is reported, they feature in their scaffold an imidazole or a triazole ring.



Pharmacophore of this Ph.D.

Chapter 3 is devoted to the study of the two series based on imidazole ring. We will describe different synthetic pathways explored during this work, namely: aza-Hantzsch, S_NAr , Riley oxidation, and pyrimidinium pathways, with a particular emphasis on the encountered difficulties and how they were managed and scientifically addressed.

Chapter 4 deals with the two triazoles series with the modulations studied on the two aromatic parts linked to the central triazole core. Based on an original and straightforward synthetic pathway, 63 benzyl analogues, and 14 *1H*-1,2,4-triazole intermediates have been synthesized. The structure-activity relationships of these series have been studied using: (i) cell viability XTT assays on retinal and endothelial cells, (ii) migration assays in a Boyden chamber allowing to block the cell migration associated with ELR⁺ CXCL-CXCR1/2 interaction, (iii) qPCR assays, (iv) immunoblotting assays, (v) ROS study and (vi) an *in vivo* zebrafish neovascular AMD model (*in vivo* angiogenesis study),

Lastly, chapter 5 will be devoted to annexe projects developed in parallel during my Ph.D. thesis: (i) transfer of biamidines to biguanides and (ii) the pharmacological study of a new anti-cancer agent active *in vivo*: NRPa-308.

Chapter 1. EXUDATIVE AGE-RELATED MACULAR DEGENERATION
(AMD): EVOLUTION OF THE DIFFERENT TREATMENTS

1.1 INTRODUCTION

The increase in life expectancy results in the emergence of new age-related pathologies, among them age-related macular degeneration (AMD), the leading cause of blindness in the elderly.¹ AMD constitutes a major health problem worldwide as no therapeutic curing options exist.

AMD is a degenerative disease mainly affecting people over 65, associated with the aging of the macula¹, and results in an irreversible loss of central vision. Although this pathology is generally bilateral, its progression rate may not be necessarily the same in both eyes. The early AMD stage, age-related maculopathy (MLA), can evolve towards two main advanced forms: the atrophic (dry) or the exudative (neovascular or wet) AMD.² This disease aggravation may occur within few months to several years and depends on various factors (demographic, environmental, genetic, and phenotypic risks), which remains not fully understood yet. Moreover, the mechanisms underlying these two advanced forms differ strongly, rendering the development of a global treatment challenging.

1.1.1 The complexity of the eye's anatomy

The eye is the central organ of the visual system, responsible for the phototransduction mechanism characterized by the capture of light, its switch into a cellular signal, and its transmission to the brain by the optic nerve.^{3,4}

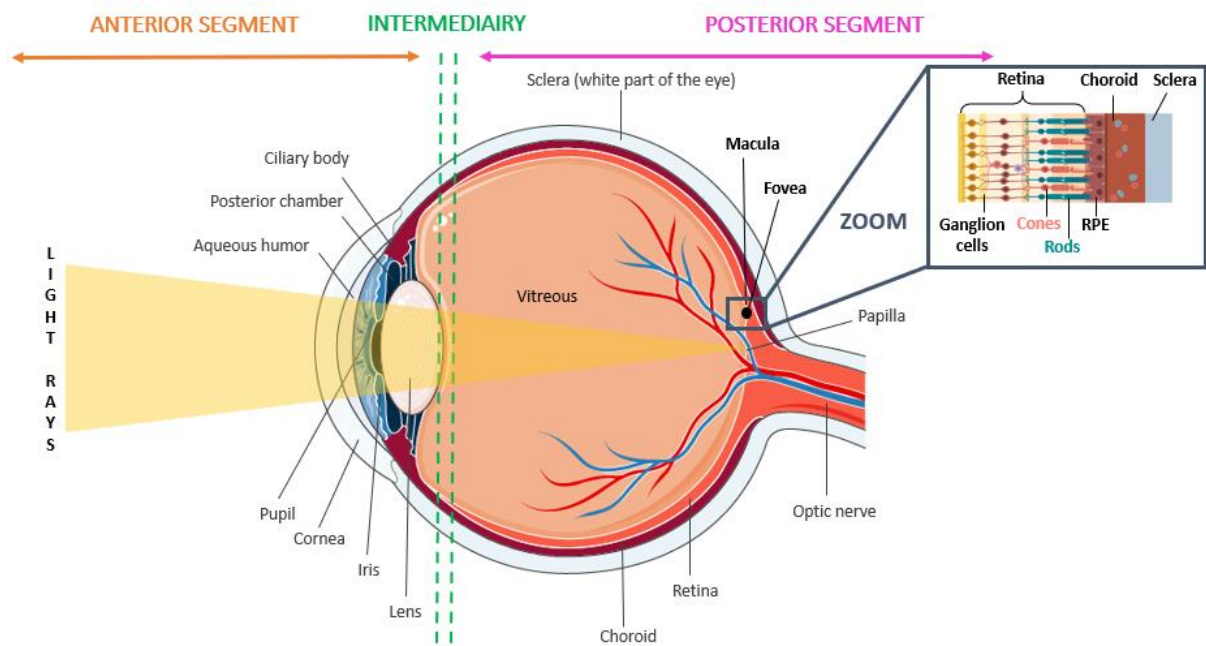


Figure 1-1: Eye's anatomy.

The eyeball is divided into two segments corresponding to different compartments and envelopes with distinct functions: (i) the anterior segment includes the ciliary body, the cornea, the iris, the aqueous humor, the lens, and (ii) the posterior segment including the choroid, the retina, and the optic nerve. Several envelopes protect the eye globe around the vitreous body and maintain the eye's shape, including the sclera, a white resistant fibrous tissue protecting the eye (Figure 1-1).⁴

The cornea is responsible for the transmission of light to the lens. The iris is known to act as a diaphragm by controlling the size of the pupil and focusing the light on the retina.⁵ In coordination with the lens,⁶ the iris acts as a natural zoom to converge the light rays. On the other hand, the choroid is a highly vascularized and pigmented membrane allowing the retina nourishment.⁷ The retina is considered as the photographic film, composed of sensory cells, called cones (for colorful vision during daytime) and rods (for black and white vision during twilight and night), able to catch the light and to transform it into nervous impulses.⁸ Finally, the **macula**, part of the retina center, is another key element of the posterior segment,⁹ responsible for the clarity of the vision and the perception of colors. Encompassing the highest concentration of photoreceptor, the macula, therefore, allows maximum visual acuity (VA).¹⁰ Its center is characterized by a small depression, called the fovea (Figure 1-1).

1.1.2 The different eye diseases

A large number of eye's pathologies affecting the vision have been reported, estimated at 45 million blind people worldwide. There are two main categories of ocular pathologies: on the one hand, the general diseases affecting the entire eye, and on the other hand, specific pathologies restricted to one compartment/membrane of the eye. However, very few diseases affect for more than 50% of the European population and are responsible for global visual in the elderly: glaucoma, cataracts, and AMD (Figure 1-2). Indeed, AMD is the most important since it affects 26% of the population over 65, closely followed by glaucoma (20.5%) and cataracts (20%).¹¹ AMD is considered to be one of the leading causes of central vision loss in patients over 65 years due to severe retinal damages. Glaucoma results in an irreversible neurodegeneration that primarily damages the optic nerve and usually occurs after fluid build-up, causing increased pressure in the eye. Moreover, cataracts is a slow-growing eye disease in which the lens becomes cloudy, causing opacity or loss of transparency and can affect one or both eyes.¹² Finally, cataract can be treated with surgery, glaucoma can be treated with eye drops, laser, or surgery, while AMD is incurable.

INCIDENCE IN EUROPE OF AMD, GLAUCOMA AND CATARACTS

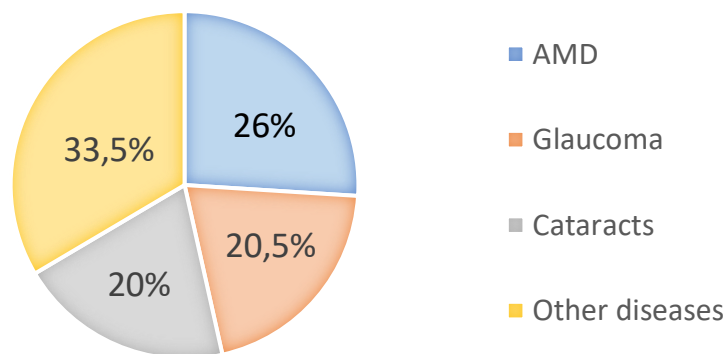


Figure 1-2: Incidence in Europe of the different eyes' diseases affected people over 65 years old.¹³

1.2 PATHOGENESIS, DEVELOPMENT AND CHARACTERISTICS OF AMD

1.2.1 Pathogenesis

AMD covers different types of lesions altering the macula; depending on the grade of the disease, AMD results in a progressive visual loss. No symptoms appeared at its early stage; conversely, the advanced stages lead to wavy vision. Patients complain mainly of a decrease in central visual acuity predominant in near vision combined with metamorphopsia (distorted perception of straight lines and wavy images) and possibly the presence of a scotoma (dark spot), rendering diverse daily activities, such as reading and driving, problematic and even impossible (Figure 1-3).¹⁰

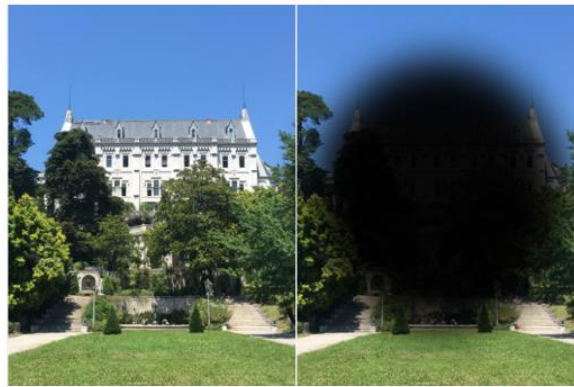


Figure 1-3: How people's vision is affected by AMD.

Among the tests to diagnose AMD, one can mention the Amsler's grid (allowing control of the central vision abnormalities generated by a fluid in the subretinal space)¹⁴ and the ETDRS scale (Early Treatment Diabetic Retinopathy Study), currently in clinical trial to evaluate the visual acuity, and based on expressing the number of letters correctly read.¹⁵ In addition, clinicians monitor morphological changes in the retina/retinal pigment epithelium (RPE)/choroid by fundus exam, color fundus photography¹⁶, fundus autofluorescence (FAF)¹⁷, optical coherence tomography (OCT)¹⁸ and infrared reflectance (IR)¹⁹. AMD diagnosis is primarily achieved through these various ocular-imaging techniques that allowed to establish a classification system for early forms of AMD as well as refining the classification of late AMD (Figure 1-4).²⁰

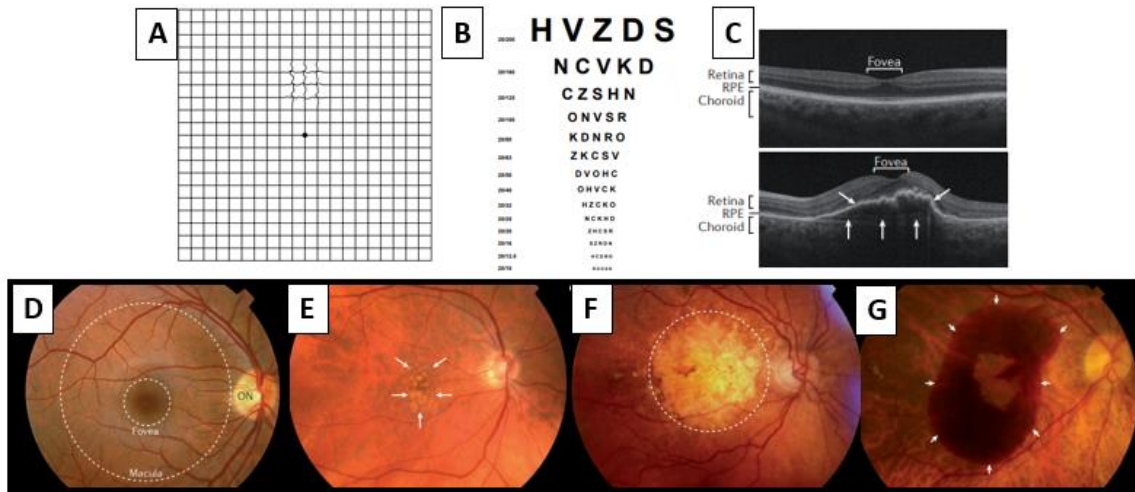


Figure 1-4: Diagnostics methods for visual acuity analysis. (A) Amsler's grid.¹⁹ (B) ETDRS scale.²⁰ (C) Retina diagram by optical coherence tomography: normal retina (top) and a retina with pigmented epithelium detachment (bottom). (D) Normal retina and macula. (E) Early stage. (F) Atrophic stage. (G) Exudative stage.²¹

AMD can be described with different grades or stages, depending on its severity or evolution²² (Figure 1-5). First, early-stage known as age-related maculopathy (MLA),²³ is characterized by the presence of insoluble extracellular lipid-rich aggregates and β -amyloid peptides accumulating in the retina/subretinal space. These aggregates are called drusen. AMD aggravation is associated with the formation of miliary drusens, small asymptomatic white spots in the perimacular region (diameter less than 63 μm), or with the presence of larger drusen ($\geq 125 \mu\text{m}$ in diameter).^{24,25} These drusen are considered as a prognostic marker for the evolution of the disorders to the late AMD forms.²⁶ However, the lesions affecting the macula are non-symptomatic and have no functional repercussion, even if it may induce in some cases a relative decrease in visual capacities or the presence of pigmentary abnormalities.²⁷

The advanced (late) stage is characterized by the impaired central vision.²⁸ Furthermore, the risk of an unfavorable progression in patients suffering from early bilateral or unilateral lesions was assessed at 26.4% and 6.3%, respectively.²² Moreover, atrophic AMD can be considered as a risk factor or even a precursor condition of exudative AMD, which is less common and affects only 10% to 15% of patients but it is responsible for 90% of acute blindness²⁹. Typical symptoms in late-stage disease include decreased night vision and progressive loss of central vision.³⁰ Loss of vision is attributed to: (i) macular drop out of RPE and photoreceptors, termed geographic atrophy (GA) or to (ii) subretinal hemorrhage induced by the invasion of RPE and/or retina by abnormal blood vessels. This last symptom is called exudative AMD since it involves choroidal neovascularization (CNV).³¹ However, these two late forms

differ strongly, and are classified according to the presence or absence of blood vessels, in the retina in a disruptive manner.^{32,33} According to this classification, the atrophic form does not present blood vessels in opposition to the exudative form which is characterized by neovascularization under the RPE.²⁹ Both forms are not mutually exclusive: the dry form can eventually develop CNV, and patients with CNV may display some degree of atrophy after a few years.³⁴

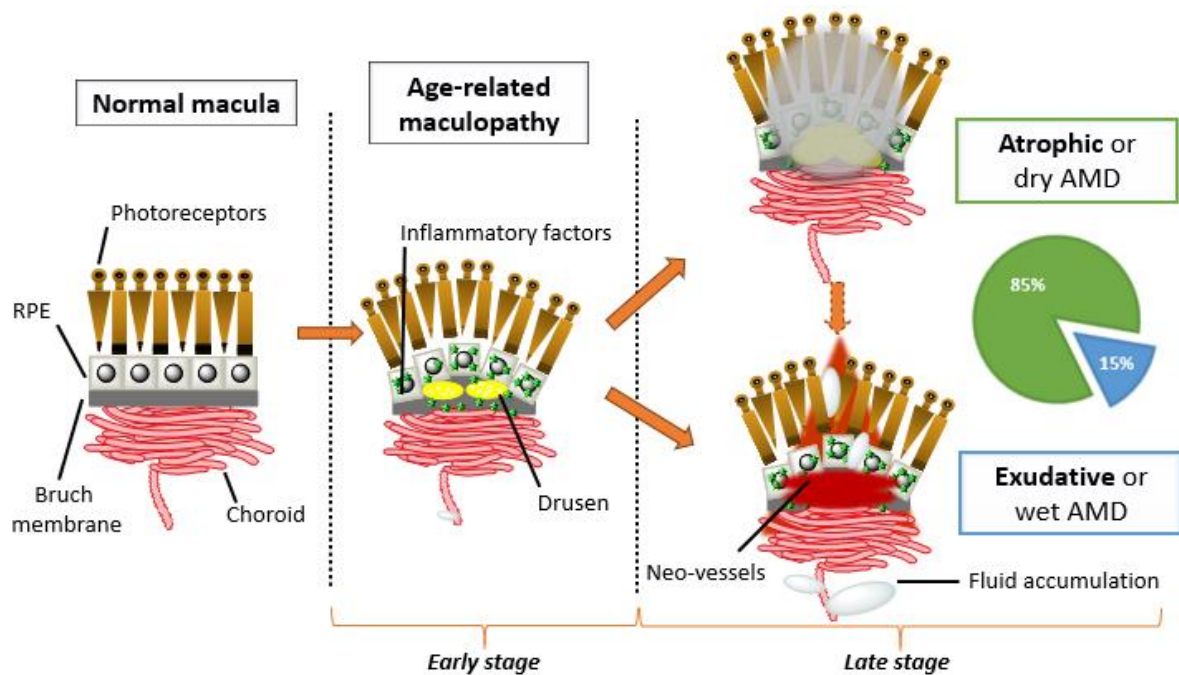


Figure 1-5: Different stages of the AMD disease.

1.2.2 Epidemiology and Risks factors of AMD

As explained before, AMD is the leading cause of severe visual loss in persons older than 65 years.¹ Indeed, after 75 years, one in four people are affected by this disease and one in two people over the age of 80 years. Interestingly, its prevalence is higher in women than in men at 65–69 years.³⁵ In 2015, approximately 67 million people in the EU were affected by any type of AMD with severe visual loss.³⁶ Besides, due to the increase in the global population size and mean population age, this number is expected to increase by 15% by 2050.³⁷

In Europe the annual incidence for stage III (late AMD) is 1.4 cases per 1000 individuals over 50 years old, then 0.5 cases per 1000 individuals under 70, and finally 6.7 cases per 1000 individuals over 70 years old (Figure 1-6).³⁵

GLOBAL PREVALENCE IN EUROPE ACCORDING THE DIFFERENT STAGES OF AMD

■ MLA (stages I, II) ■ late AMD (stage III) ■ nAMD (stage III) ■ GA (stage III)

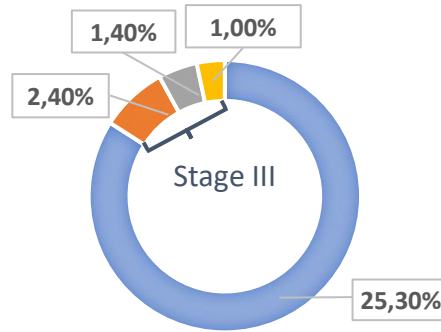


Figure 1-6: Prevalence in Europe for all ages (from < 64 years to >75 years). *MLA: Age-related maculopathy. nAMD: neovascular AMD. GA: geographic atrophy.*

Several risk factors have been identified. First, demographic and environmental risks may be highly (age and smoking) or occasionally (body mass index (BMI), gender, education) related to the AMD progression. Genetic factors (*e.g.* in the complement factor) are also involved in the aggravation of the disease as well as phenotypic factors, including drusen or pigment abnormalities. Of note, molecular factors (High-Density Lipoprotein Cholesterol (HDL-C), Docosahexaenoic acid (DHA), eicosapentaenoic acid (EPA), zeaxanthin or lutein) are excluded from prediction models but could be interesting because they are easily measured in blood.³⁸

1.2.3 AMD characteristics

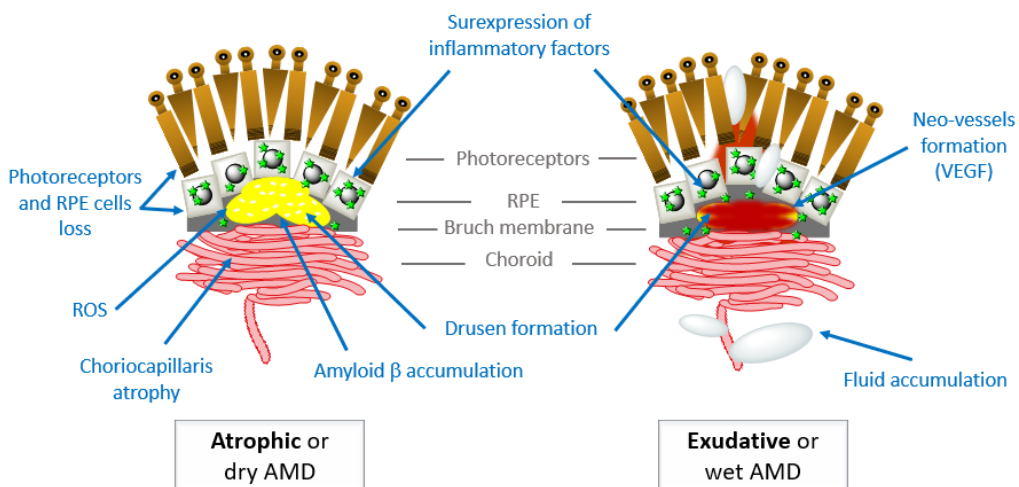


Figure 1-7: Strategies and targeted elements for AMD treatment.

In both atrophic and exudative AMD forms, some common characteristics have been reported to be responsible for the disease progression. In particular, chronic inflammation may be a key player in AMD evolution through different pathways, including endothelial dysfunction in choroidal vessels, development of basal deposit and drusen, and degeneration of Bruch's membrane.

Some other factors, such as accumulation of amyloid β and reactive oxygen species (ROS) have been defined as causes of disease progression and degeneration. Unfortunately, their mechanism of action in the progression of AMD is only partially known and requires studies. Of course, the main difference concerns the exudative form, whose angiogenesis phenomenon is observed, leading to a fluid accumulation under the RPE and to its subsequent destruction. (Figure 1-7).

1.2.3.1 Atrophic form

The atrophic AMD form, also known as dry or geographic atrophy (GA), corresponds to 85% of the late-stage form.³⁹ The main common symptom is a vision blurring with vision loss affecting, in general, both eyes, but sometimes only one eye.

This form is characterized by progressive dysfunction of the RPE, photoreceptors degeneration, choriocapillaris, inflammation, and peripapillary atrophy (Figure 1-8).^{40,41} These disorders are caused by the thickening of the Bruch's membrane (BrM) due to the accumulation of drusen.⁴²⁻⁴⁴ This accumulation of lipids primarily interferes with the fluid efflux of RPE through the BrM, thus stressing the RPE.⁴⁵ The drusen's emergence and their growth occur slowly over years, but they are responsible for the RPE cell death and the synaptic dysfunction. Aging correlated with the formation of these drusens allows for biochemical and anatomical changes that occur in BrM. Subsequently, these physical deformities result in decreased nutrient flow through BrM⁴⁶ and are also associated with mild to moderate retinal degeneration and vision loss. Thus, areas of hypopigmentation of the RPE monolayer are observed in the macula. However, the precise formation of drusens in the AMD pathogenicity has not been fully elucidated.^{47,48} Interestingly, even if most of late AMD starts as the atrophic form, 10-20% of individuals suddenly turn into the exudative form. Unfortunately, no mechanistic model explains this conversion.⁴⁹

Currently, atrophic AMD form remains incurable. However, several strategies are under investigation to decrease the formation of drusen and/or avoid RPE disorders. The current symptomatic treatments include the targeting of (i) the visual cycle with the A2E (*N*-retinylidene-*N*-retinylethanolamine) formation, Amyloid β ($A\beta$) protein aggregates, and drusens apparition⁵⁰; (ii) the choroid's atrophy

stimulated by drusen's multiplication and choriocapillaris (CC) atrophy^{51,52}; (iii) the loss of photoreceptor cells and RPE; (iv) the oxidative stress with neuroprotection agents⁵³; (v) the inflammation^{54,55} (Figure 1-8). Although some treatments have reached the clinical trials stage (phase 1 & 2), and many other therapeutic options are currently under investigation, the lack of global comprehension in the AMD's aggravation mechanisms currently impairs the emergence of an efficient curing treatment.

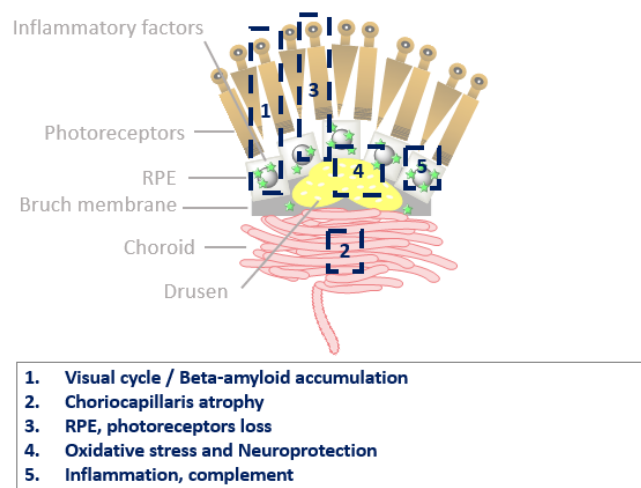


Figure 1-8: Current therapeutic targets for the treatment of atrophic AMD.

1.2.3.2 Exudative form

The exudative form is characterized by neovascularization and choroidal proliferation, responsible for a decrease of the visual acuity (VA). The formation of these new choroidal vessels (CNV)⁵⁶ is mediated by vascular endothelial growth factor (VEGF) and also by local inflammatory cytokines, such as tumor necrosis factor-alpha (TNF-alpha) or NF-κB.⁵⁷⁻⁵⁹ These neovessels can be described as visible (CNV) or occult (OCNV) and have a variable location compared to the fovea (extrafoveal, juxtafoveal, subfoveal). They can be also formed from the macular retina, which can secondarily establish contacts with the choroid network (angiomatous retinal proliferation), namely chorioretinal anastomoses.

CNV commonly is categorized into these three major types: (i) **Extrafoveal**, CNV is located between 200 μm and 2500 μm from the geometric center of the foveal avascular zone, (ii) **Juxtafoveal**, CNV is confined to an area up to 199 μm from the geometric center of the foveal avascular zone (this area

may include portions of the foveal avascular zone) and, (iii) **Subfoveal**, CNV is directly beneath the geometric center of the foveal avascular zone.

These new vessels, unlike normal vessels, tend to be very fragile and induce tissue extravasation of lipids, plasma or blood, the reason for the name wet AMD. Subsequently, this neovascularization will cross the BrM and develop under the pigment epithelium or in the subretinal space, namely under the macula, thus causing significant retinal detachment responsible for the decrease in visual acuity, metamorphopsia, subretinal hemorrhages, and the formation of a central scotoma. These morphological anomalies quickly damage the macula. Degeneration of the photoreceptors is then observed, leading to cell death. The ultimate evolution is the appearance of a fibrous scar, called disciform.¹⁰

The exudative AMD form emerges abruptly; its most frequent complications is a rapid destruction of photoreceptors, responsible for a severe decrease in VA and a permanent central scotoma. Its evolution can be very fast, causing a loss of central vision in a few weeks or months, and rapidly progresses to blindness if untreated.⁵⁶ The exudative AMD form is considered more severe than the atrophic form, due to the irreversible prognosis. Nevertheless, this neovascular form can be treated with a laser treatment or using anti-angiogenic therapies to avoid the formation of the new vessels.⁶⁰

In fact, in the exudative AMD form, the abnormal overexpression of VEGF is one of the key players involved in the CNV and resulting in the RPE damage induction. Normally, the VEGF plays a physiological role in the development and trophic maintenance of the choriocapillaris⁶¹ and in protecting retinal neurons from apoptosis in ischemic conditions. Conversely, the high level of this growth factor involves the formation of angiogenic germs, and it is responsible for the activation, survival and proliferation of the new vessels (NV).

Therefore, several studies suggest that the production and the activity of the angiogenic factor VEGF would not be sufficient to increase the vascularization but requires the action of other angiogenic factors combined with a reduction in the activity of the antagonistic factors.⁶² Indeed, there is a consortium of pro-angiogenic factors but also pro-inflammatory factors which undoubtedly affect the progression of AMD.⁶³ Even if some benefits with antiangiogenic treatments are observed (see part 1.4 Exudative (wet) AMD treatments), they are not efficient in the long term and patients have to resume the treatments.

1.3 ATROPHIC (DRY) AMD TREATMENTS

Several organelles of the eye macula have been targeted to propose therapeutic options towards atrophic AMD treatment (Figure 1-8), all of them having been developed during the past 15 years (Figure 1-9).

Each strategy presented shows the importance of the administration mode. For example, in the visual cycle, administration to patients as an oral capsule. In the same idea, another interesting point is an administration by eye drop in the case of MC-1101, OT-551 or tansospirone, considered a real challenge. This is very relevant to point out, as this type of formulation is less frightening for patients than intraocular injections, intravenous or subcutaneous injections present in most cases.

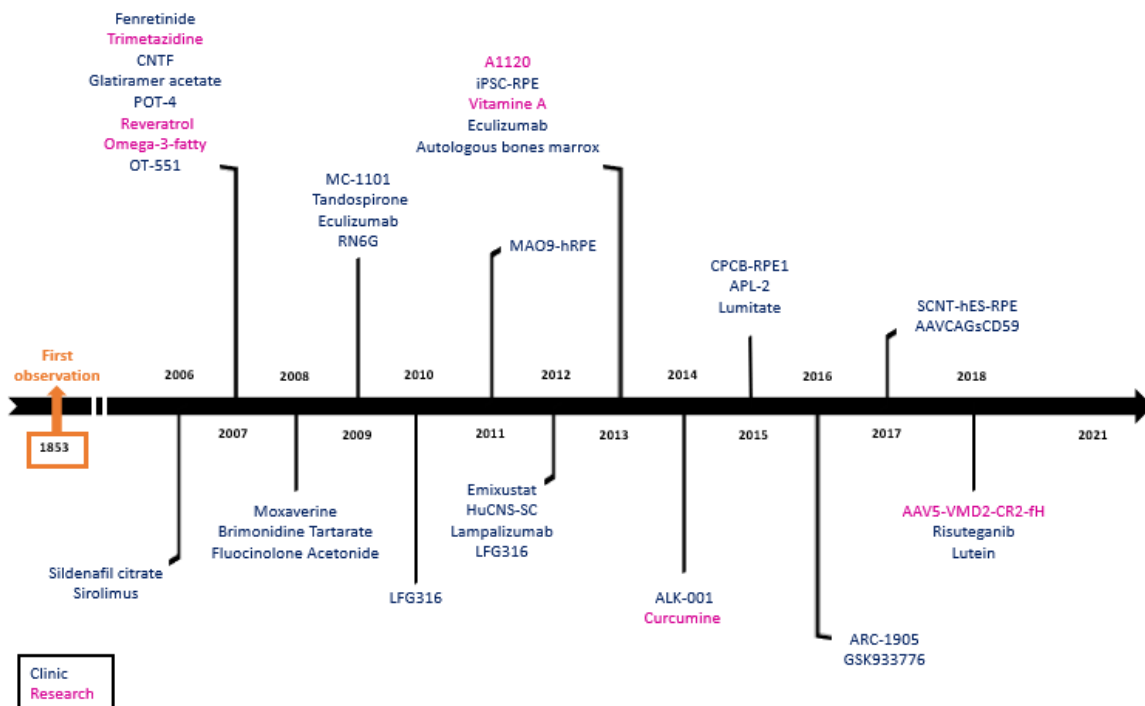


Figure 1-9: Timeline of therapeutic agents developed against atrophic AMD.

1.3.1 Visual cycle

The molecular base of the visual cycle is well known for years. Basically, when light reaches the photoreceptors cells, retinal 11-*cis* undergoes a photochemical reaction and converts into its more stable all-*trans* isomer. After a reduction of the retinal in all-*trans* retinol in photoreceptor cells, this

one undergoes esterification by lecithin retinol acyltransferase (LRAT) in RPE cells. Subsequently, all-*trans* retinyl ester is isomerized, and the ester bond is hydrolysed by retinal pigment epithelium-specific 65 (RPE65) to form 11-*cis* retinol. Finally, this retinol is oxidized from 11-*cis* retinol to 11-*cis* retinal by 11-*cis* retinol dehydrogenase (RDH), then it migrates back to the photoreceptors, ready to start another cycle. However, in the case of atrophic AMD, this cycle is altered. Thus, in RPE cells, retinal all-*trans* isomer is converted, to a dimeric form: the *N*-retinylidene-*N*-retinylethanolamine (A2E) which aggregates and constitutes lipofuscin, a major aggravating factor in AMD (Figures 1-10, 1-11).⁶⁴⁻⁶⁶ In this perspective, deceleration of the visual cycle turn-over was proposed as a therapeutic option.⁶⁴ To date, four small-sized organic molecules have been developed to interfere with this mechanism.

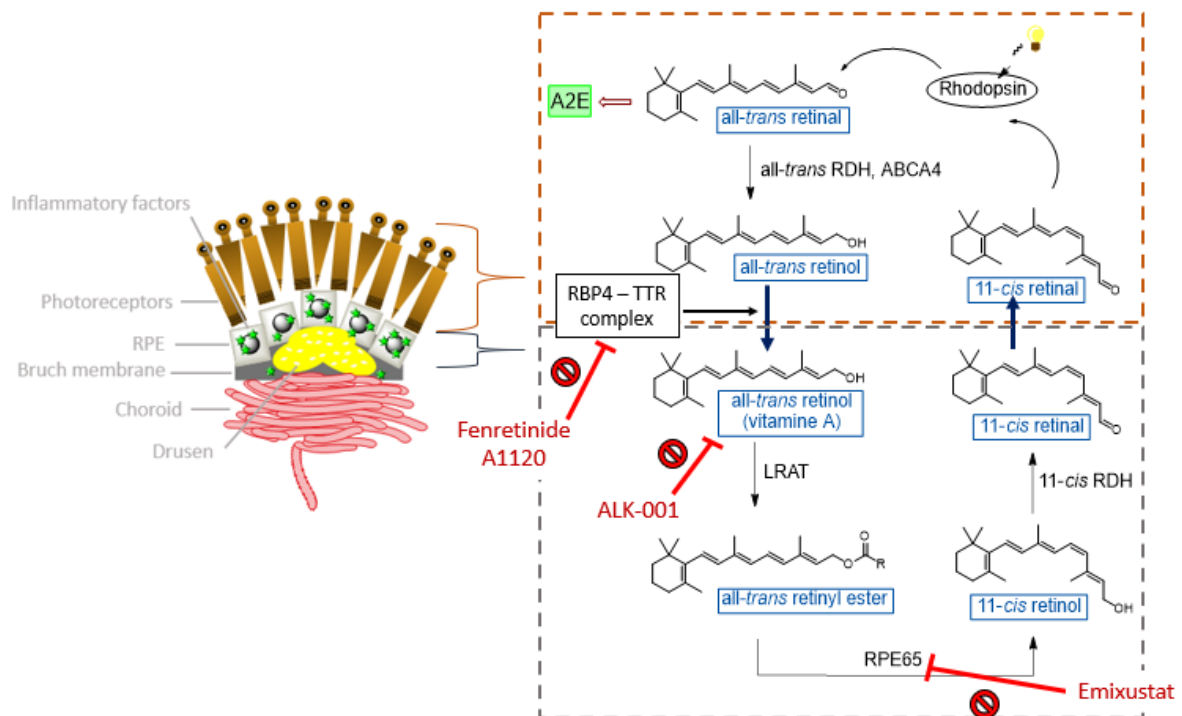


Figure 1-10: Visual cycle in the retina with AMD disease. A2E : *N*-retinylidene-*N*-retinylethanolamine ; ABCA4 : ATP-Binding Cassette Subfamily A Member 4 ; LRAT : lecithin retinol acyltransferase ; RBP4 : retinol 4 ; RDH : retinol dehydrogenase ; RPE65 : retinal pigment epithelium-specific 65 ; TTR : transthyretin.

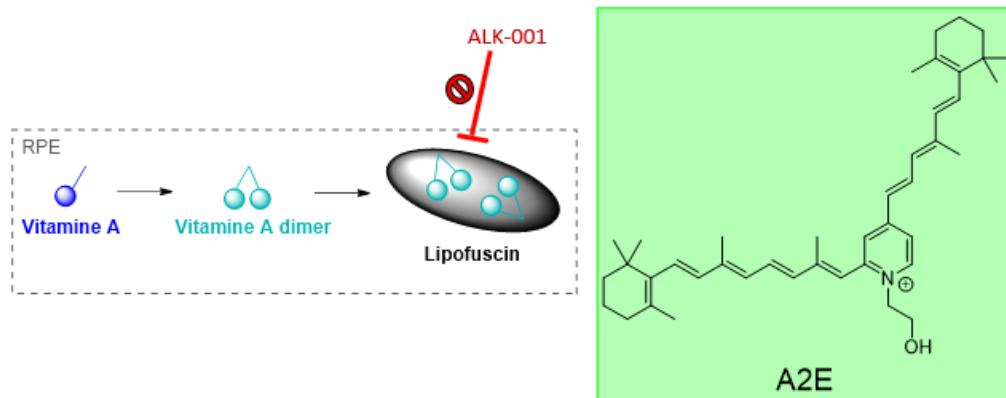
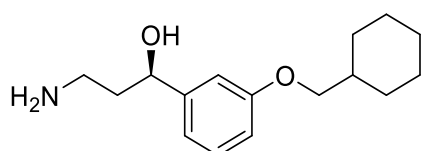
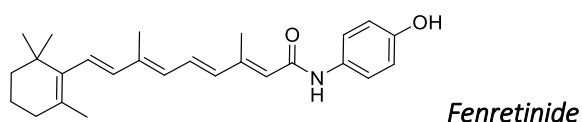


Figure 1-11: Lipofuscin obtention in RPE.

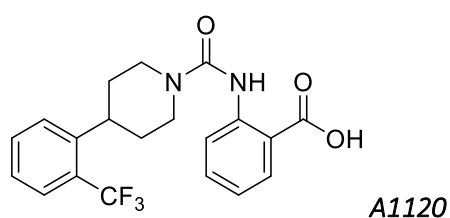


Emixustat or ACU-4429

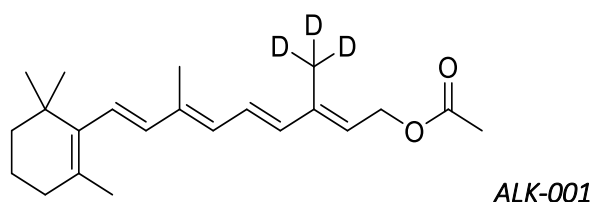
Emixustat (Acucela, Inc., Kubota Vision Inc.; Otsuka Pharmaceutical Co., Ltd., 2012) was the first small-sized modulator of the visual cycle.^{67,68} This molecule inhibits the enzyme catalyzing the transformation of all-*trans* retinyl ester into 11-*cis*-retinol, the RPE65. Emixustat binds the retinoid site of RPE65 with its hydroxyl group, and this molecule inhibits *in vitro* this isomerase within an IC₅₀ of 4.4 nM.⁶⁹ In turn, emixustat induces the deceleration of the visual cycle and the reduction of A2E accumulation. Moreover, the binding affinity of (*R*)-emixustat with RPE65 is higher compare to (*S*)-emixustat.⁷⁰ The emixustat dose-effect correlations have been evaluated in a phase 2/3 study (SEATTLE, NCT01802866, 2013-2017)^{71,72} with different amounts of the drug (2.5 to 10 mg) given to patients during 24 months. However, it resulted in a non-reduction of the growth rate of GA in AMD whatever the dose. A phase 1 and two phases 2 studies (NCT02130531, 2014-2016; NCT01002950, 2009-1014; NCT03033108, 2017-2019)⁷³⁻⁷⁵ have been also performed aiming at evaluating the safety, the tolerability and the pharmacokinetics/pharmacodynamics of emixustat given in different doses level to atrophic AMD patients (2, 5, 7, or 10 mg) for 90 days. The drug was well tolerated when given daily for 2 weeks (phase 1 trial), and⁶⁸ at this level emixustat displayed a reversible dose-response effect (in phase 2 trial). Two doses were interrupted (7 and 10 mg) due to side effects in their groups, but for 7 mg and 5 mg, two patients (in each group) showed a decrease in VA compare to the placebo group.⁷⁶ Of note, this molecule is already used in Stargardt macular dystrophy (*in vivo* studies)⁷⁷, a pathology sharing with dry AMD the presence of lipofuscin.



Another target is the interaction between transthyretin (TTR) and retinol 4 (RBP4), which is in charge of the all-*trans* retinol transport from the photoreceptors to the RPE.^{78,79} Thus a RBP4 antagonist mimicking vitamin A⁸⁰, the Fenretinide (ReVision Therapeutics, Inc.), inhibits the TTR-RBP4 complex formation with an IC₅₀ of 56 nM.^{81,82} A phase 2 study (NCT00429936, 2007-2010)⁸³ implemented to evaluate the efficacy of this molecule (100 mg during 24 months) in atrophic AMD, has demonstrated a reduction in the growth of GA lesions and a decrease in neovascularization. This result suggests that fenretinide may prevent the evolution of the AMD from its dry to its wet form.⁸⁰

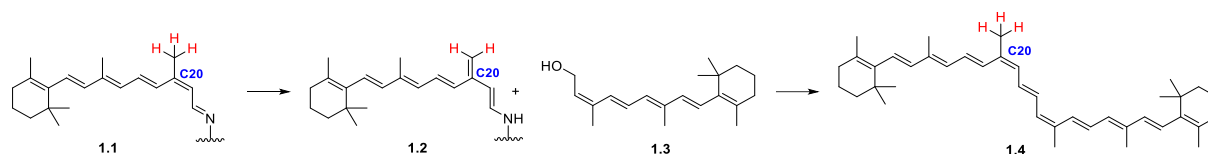


A1120 is another small molecule impeding the interaction between RBP4 and TTR, with a high affinity for RBP4 ($K_i = 8.3$ nM), leading to the subsequent blockade of the RBP4-TTR complex formation. A1120 causes retinol orientation changes after binding to it and, leads downstream to the blockade of lipofuscin's formation (proved *in vivo* in an *Abca4* mouse model)⁸¹. Remarkably, the scaffold of this molecule differs strongly from this of vitamin A, suggesting an original interaction with its molecular target.⁸¹ The inhibition of TTR-RBP4 complex formation showed an IC₅₀ of 14.8 nM for A1120, which is a better result than fenretinide.⁸¹ To date, this molecule has not reached the trial stage for the atrophic AMD treatment.



ALK-001, or C20-D3-vitamin A, is a deuterated derivative of vitamin A, which prevents A2E by vitamin A replacement.⁸⁴ A pre-clinical study revealed that ALK-001 could slow down the vitamin A dimerization (Scheme 1-1) due to an isotopic effect.⁶⁶ ALK-001 was developed by Alkeus Pharmaceuticals, Inc. to slow down vision loss in atrophic AMD and Stargardt disease.⁶⁶ After a phase 1 study (NCT02230228, 2014-2015)⁸⁵ to evaluate the safety and pharmacokinetics in 40 healthy

patients, a phase 3 study (SAGA, NCT03845582, 2019-2020)⁸⁶ was recently recruiting 300 AMD patients to evaluate its potential benefits.



Scheme 1-1: Vitamin A dimerization. *Dimerization occurs after cleavage of a C-H bond in position C20.*

Table 1-1: Drugs targeting the visual cycle.

Drugs	Structure	Target	Clinic or Research	Formulation	Ref.
Emixustat		RPE65	1, 2	Oral (Tablet)	NCT01802866 ⁷¹ NCT02130531 ⁷³ NCT01002950 ⁷⁴ NCT03033108 ⁷⁵
Fenretinide		RBP4	2	Oral capsules	NCT00429936 ⁸³
A1120		RBP4	R	-	-
ALK-001		Vit. A	1	Oral capsules	NCT02230228 ⁸⁵ NCT03845582 ⁸⁶

1.3.2 Amyloid β ($A\beta$)

The amyloid β accumulation in drusen, in particular the amyloid peptides $A\beta_{1-40}$ ($A\beta_{40}$) and $A\beta_{1-42}$ ($A\beta_{42}$) could be responsible for AMD aggravation.^{50,87} Indeed, $A\beta$ participates in the inflammatory induction, and it inhibits in turn the complement factor I (CFI) activity, responsible for the alternative

complement cascade.⁸⁸ Thus, its elimination – or reduction – may constitute a therapeutic option for atrophic AMD treatment.

RN6G

RN6G (also called PF-04382923) is an anti-amyloid- β monoclonal antibody developed by Pfizer, which binds and traps A β in the retinal periphery and reduces in mice the accumulation of toxic species in the macula.^{87,89} Two phases 1 studies (NCT01003691, 2009-2013; NCT00877032, 2009-2015)^{90,91} have been completed to assess the optimal dose of RN6G; however, in both cases, no improvement in visual acuity (BCVA assays) has been reported. In addition, a phase 2 study (NCT01577381, 2012-2016)⁹² demonstrated also no improvements in BCVA neither in ocular lesions (GA).

GSK933776

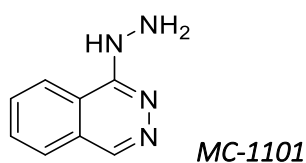
GSK933776 is a fully-humanized mouse anti-human A β immunoglobulin G1 which will bind to the A β N-terminal end.⁹³ This drug, developed by GlaxoSmithKline, designed to restore the CFI bioactivity has been proved active *in vivo*.⁸⁸ It was initially used in the treatment of the Alzheimer’s Disease. In the case of AMD treatment, two studies have been performed: a phase 1 study (NCT02033668, 2014-2017)⁹⁴ to evaluate the pharmacokinetic and different forms of the formulation by intravenous injection or subcutaneous injection of GSK933776 (200 mg) and a phase 2 study (NCT01342926, 2011-2017)⁹⁵. This latter showed no improvement in GA enlargement rate and VA. Moreover, no correlation was observed between GA enlargement rate and the CFI variations.⁹⁶

Table 1-2: Drugs targeting β -Amyloid.

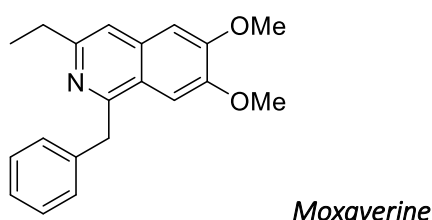
Drugs	Structure	Clinic or Research	Formulation	Ref.
RNG6	Monoclonal antibody	1	Intravenous	NCT01003691 ⁹⁰
				NCT00877032 ⁹¹
		2		NCT01577381 ⁹²
GSK933776	Monoclonal antibody	1	Intravenous or subcutaneous injection	NCT02033668 ⁹⁴
		2		NCT01342926 ⁹⁵

1.3.3 Choriocapillaris (CC) atrophy

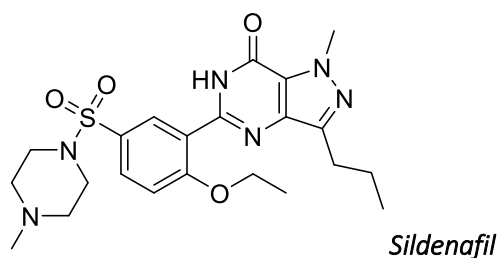
CC ensures in the RPE the nutrients intake and the removal of waste;⁹⁷ its alteration induces ocular hypoxia. This hypoxia may be potentially responsible for drusen multiplication may be an aggravating factor for AMD. In line with this consideration, vasodilators have been proposed to counteract this atrophy.^{51,52}



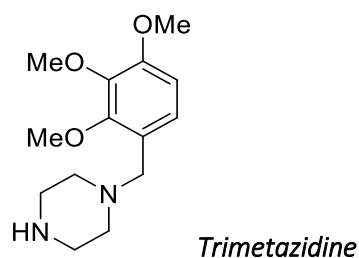
Hydralazine (so-called MC-1101, or Apresoline® hydrochloride; MacuCLEAR Inc.)⁹⁸ is an antihypertensive, anti-inflammatory, antioxidant and vasodilating agent, FDA approved in 1997 by the FDA to treat high blood pressure.⁹⁹ In addition, on an animal model of an ocular hypertensive rabbit, MC-1101 proved to increase the choroidal blood flow in the macula.^{53,100} Furthermore, the authors demonstrated that hydralazine increases the choroidal blood flow and in animal models (rats and rabbits), antioxidant action and suppression of atrophic AMD were observed.¹⁰⁰ In humans, two phases 1 studies (NCT01013376, 2009; NCT01922128, 2013-2014)^{101,102} and a phase 2/3 study (NCT01601483, 2012-2014)¹⁰³ dealing with the hydralazine safety profile (including AMD patients), and its optimal use (dose and administration mode). These assays proved (including for patients suffering atrophic AMD) that no adverse effects (cardiovascular effects, ocular toxicity, and no effect on the blood-eye barrier) when the drug was given by topical mode (1% in an ophthalmic solution).



Moxaverine (Kollateral forte®) is a papaverine derivative developed by Ursapharm, is a phosphodiesterase inhibitor exerting a vasodilator effect that was also studied for the enhancement of the choroidal blood flow.¹⁰⁴ This molecule was initially used for the peripheral microcirculatory impairment treatment.¹⁰⁵ Moxaverine has been assayed in a clinical trial phase 2/3 (NCT00709449, 2008-2009)¹⁰⁶ as an intravenous infusion at the dose of 150 mg, demonstrating an increase of the choroidal blood flow in patients suffering AMD and glaucoma.¹⁰⁴

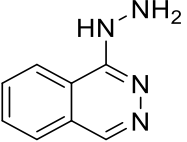
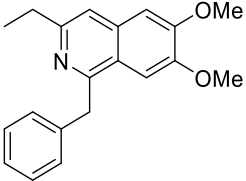
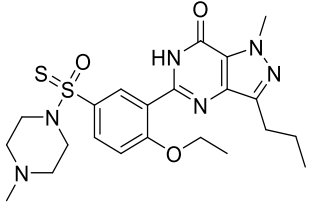
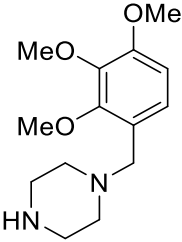


Sildenafil citrate (Viagra®), developed by Pfizer, is a phosphodiesterase type-5 inhibitor marketed for the treatment of erectile dysfunction.¹⁰⁷ A small pilot phase 2 study (NCT01830790, 2013-2015)¹⁰⁸ including 10 AMD patients (exudative and atrophic) evaluated its effects (100 mg) on the increase of the choroid thickness, since the choroid being thinner in AMD patients. The authors reported that choroid thickness increased in both AMD forms (6.7-11.9% for atrophic AMD and 10.1-11.5% for exudative AMD from 1 to 3 h).¹⁰⁹ However, because of insufficient support to complete the recruitment, this trial was closed prematurely. In 2019, a study with 23 subjects, including 15 AMD patients, showed an increase of choroid thickness from 6.0% to 9.0% (1-3 h) after the administration of a sildenafil oral dose of 100 mg. Nevertheless, in the older subjects the choroid thickness is thinner at the beginning with a smaller increase after treatment suggesting that with age, sildenafil will have a weaker vascular response.¹¹⁰



Trimetazidine (TMZ), Vastarel®, is a piperazine derivative developed by Servier designed to inhibit the oxidation of fatty acids and glucose.¹¹¹ First, this therapeutic agent has been used for anti-ischaemic properties (1981)¹¹². However, TMZ also prevents microvascular abnormalities in the choroid and retina. Moreover, its protecting effects have been validated in glaucoma and degenerative myopia; this drug improves the sensitivity to contrast and the visual acuity (20 mg, twice a day of TMZ during 6 months) of patients.¹¹³ Nonetheless, a human study, carried out for its use at the dose of 35 mg, twice daily over 3–5 years) in exudative and atrophic forms of AMD, failed to demonstrate a clinical benefit on CNV for these patients,¹¹⁴ even if a possible preventive effect to delay atrophy has been suggested.

Table 1-3: Drugs targeting choriocapillaris atrophy.

Drugs	Structure	Clinic or Research	Formulation	Ref.
MC-1101		1 2/3 1	Eye drops	NCT01013376 ¹⁰¹ NCT01601483 ¹⁰³ NCT01922128 ¹⁰²
Moxaverine		2/3	Intravenous infusion	NCT00709449 ¹⁰⁶
Sildenafil		2	Oral	NCT01830790 ¹⁰⁸
Trimetazidine		-	-	-

1.3.4 RPE and photoreceptors loss: Stem cells (SC)

The discovery of stem cells and their implication in tissues regeneration led to the emergence of new therapy options in numerous diseases. In atrophic AMD, three types of SC have been studied to regenerate the RPE and to produce cytokines (growth promoters), allowing the maintenance of the choriocapillaris and the retina¹¹⁵: SC issued from fibroblasts (iPSC), SC from the central nervous system (HuCNS) and SC resulting from fertilization (hESC) (Figure 1-12).

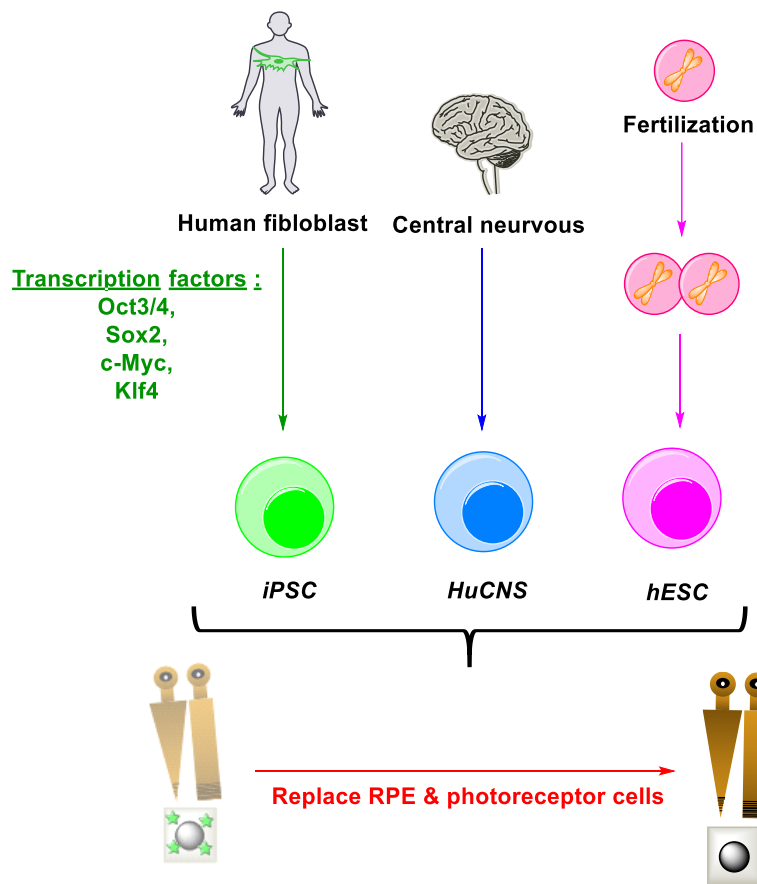


Figure 1-12: Stem cells therapy for the regeneration of RPE and photoreceptor cells.

Human-induced pluripotent stem cells (iPSC)

Human-induced pluripotent stem cells (iPSC) are obtained from adult human fibroblasts, resulting from the activation of a set of transcription factors including Oct3/4, Sox2, c-Myc and Klf4. These cells are characterized by the presence in their membrane of a sodium and potassium ion transport channel¹¹⁶. They have similarities with native RPEs in terms of membrane potential, polarized secretion of VEGF and gene expression.¹¹⁷ iPSCs can be used to generate pigmented epithelial cells in the outer retina to replace or regenerate the defective ones. Moreover, these cells can produce growth factors and supporting cytokines (brain-derived neurotrophic factor for supportive paracrine effect in the macula)¹¹⁷. These iPSC cells may be sub-retinal grafted in AMD patients, as shown in a transplantation study carried out on a hereditary degenerative rat retina model (RCS rat).¹¹⁸ A more recent *in vitro* study (2016) was also carried out against atrophic AMD to understand its mechanisms through a RPE-iPSC-RPE SC of AMD compare to normal RPE-iPSC-RPE. AMD model shows a different disease phenotype than the normal model and higher ROS formation under oxidative stress. Among others, an underlying pathway is involved in the disease: SIRT1/PGC-1 α .¹¹⁹ Another trial is ongoing (NCT02464956, 2015)¹²⁰. To be able to study and better understand AMD on cells, a study

(NCT03372746, 2017-2019)¹²¹ was carried out to establish a bank of samples. These samples can be differentiated into ocular cells (transformation of skin, blood into iPSCs).

Human embryonic stem cells (hESC)

The transplantation of human embryonic stem cells (hESC) has been assayed in atrophic AMD to replace damaged RPEs based on the MA09-hRPE model (hESC-RPE cell line). Once grafted, the SC proliferated without senescence nor apoptosis.^{122,123} A 1/2 phase study (NCT01344993, 2011-2017)¹²⁴ demonstrated the survival of the transplant over 12 months, without abnormal proliferation nor side effects for the patients.^{122,123} A recent complete study (NCT02463344, 2015-2020)¹²⁵ aimed at evaluating the long-term (5 years) safety and tolerability of MA09-hRPE in atrophic AMD patients, will report conclusions shortly.

CPCB-RPE1 is a subretinal human implant, composed of hESC-RPEs precultured on a biocompatible, mesh-supported submicron parylene C membrane.¹²⁶ Their use *in vivo*, in mini pigs eyes, was performed in 2016 and the safety of the subretinal implantation has been subsequently proved.¹²⁶ A phase 1/2 study (NCT02590692, 2015-2020)¹²⁷ is currently ongoing to observe the damages of the RPE/photoreceptor complex after a CPCB-RPE1 implant in atrophic AMD patients.

Human central nervous system (HuCNS-SC)

The stem cells issued from the human central nervous system (HuCNS-SC) have been used to prevent degeneration of the photoreceptors in Royal College of Surgeons rats, an animal known for inherited retinal degeneration.¹²⁸ The HuCNS-SCs survive over a minimum of eight months after their transplantation into the subretinal space; they minimize long-term vision loss and preserve photoreceptors, and they can.^{129,130} In humans, thanks to a safety profiles appearing from a phase 1/2 study (NCT01632527, 2012-2015)¹³¹ of HuCNS-SC in atrophic AMD patients, a complementary phase 2 (RADIANT, NCT02467634, 2015-2016)¹³² has been implemented one year later, by StemCells, Inc.. The authors concluded the maintains or improvement of BCVA and contrast sensitivity (CS), increasing the central subfield thickness, the macular volume and the decrease in the growth rate of GA in the treated eye compared to the control eye.¹³³ Finally, a study to evaluate the long-term safety and the possible benefits for patients (NCT02137915, 2014-2016)¹³⁴ was terminated early due to financial reasons, despite no safety issues observed.

Table 1-4: Stem cells against atrophic AMD.

Drugs	Origin	Goal	Clinic or Research	Formulation	Ref.
iPSC	Human fibroblast	RPE cells regeneration	not yet recruiting	Transplantation	NCT02464956 ¹²⁰
hESC	Central nervous	Replace RPE cells	1/2	Transplantation	NCT01344993 ¹²⁴ NCT02463344 ¹²⁵ NCT02590692 ¹²⁷
HuCNS-SC	Fertilization	Photoreceptors regeneration	2	Transplantation	NCT01632527 ¹³¹ NCT02467634 ¹³² NCT02137915 ¹³⁴

1.3.5 Oxidative stress

Recent evidence suggests that mitochondrial damages and oxidative stresses in RPE are key players in AMD, even if the damages mechanism is not fully understood yet.¹³⁵ Indeed, RPE cells are exposed to chronic oxidative stress due to their oxygen requirements and to their exposure to products resulting from the peroxidation of lipids derived from external photoreceptors.¹³⁶ At the RPE cells' level, a set of ROS and/or free radicals are produced, such as superoxide, hydrogen peroxide, hydroxyl radicals.¹³⁷ This accumulation is also associated with an overproduction of lipofuscin and beta-amyloid peptides.¹³⁸ These damages to the RPE induce in turn apoptosis of photoreceptors. Furthermore, oxidative stresses are closely related to inflammation, which is also responsible for the development of AMD lesions. Moreover, inflammatory stimuli increase the production of reactive oxygen intermediates and reduce the bioavailability of antioxidants, initiating thereby a vicious circle.¹³⁹ To summarize, oxidative stresses lead to the aggravation of the disease, and their downregulation may lead to potential therapeutic options (Figure 1-13).¹⁴⁰ In line with this, compounds with anti-oxidative properties or aimed at interfering with the production of ROS have been proposed as potential treatments for AMD patients.

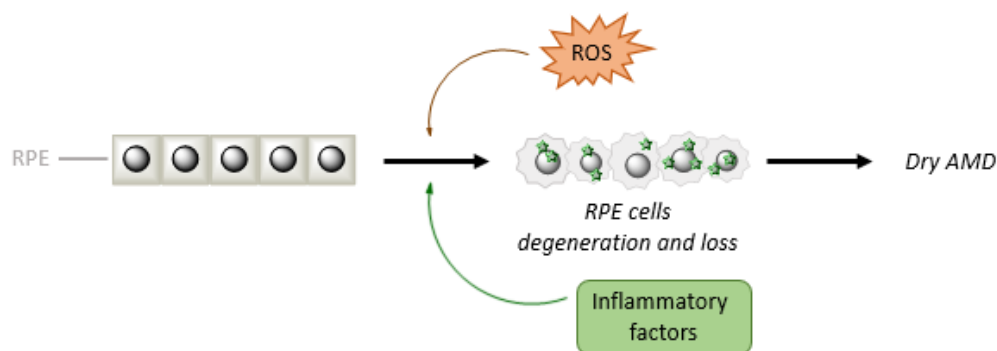
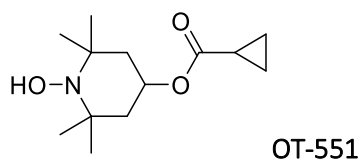


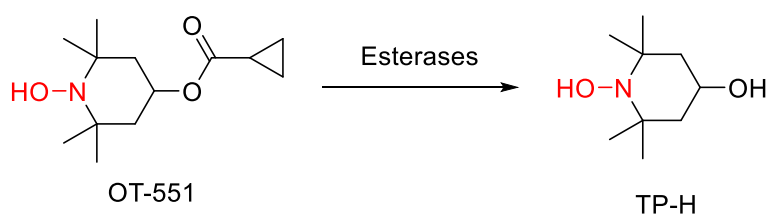
Figure 1-13: AMD progression due to ROS and inflammatory factors.

1.3.5.1 Small-sized molecules

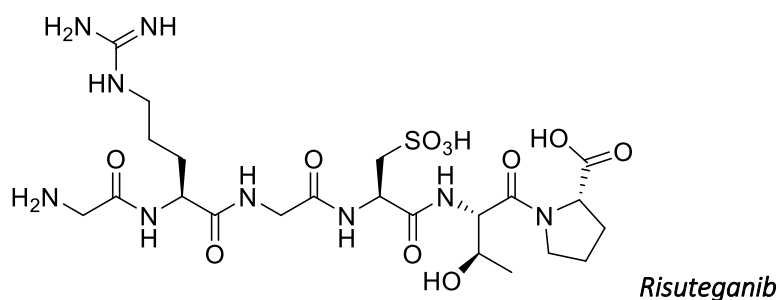


OT-551, developed by Othera Pharmaceuticals, is a derivative of the well-known radicals' quencher TEMPO. Delivered by eye drops, this lipophilic prodrug of tempol (TP) has the remarkable capacity to penetrate the cornea towards the back of the eye to reach the macula. The surrounding esterases then convert OT-551 into its corresponding acid TP-H (Scheme 1-2) making it an interesting candidate for the treatment of ocular disease, preserving VA.¹⁴¹ A non-direct mechanism of action of OT-551 was shown to downregulate through multiple pathways the activation of Nuclear factor E2-related factor (Nrf-2), overexpressed in inflammatory disease. As the consequence, OT-551 may act as an anti-oxidant and anti-inflammatory factor.¹⁴¹

A phase 2 study (NCT00306488, 2006-2011)¹⁴², with 11 participants, reported an improvement (mean change: for study eyes +0.2, 13.3 letters and for fellow eyes -11.3, 7.6 letters) in BCVA for patients treated with OT-511 (0.45% concentration eye drops, three times a day, during 24 months) and the prodrug was well-tolerated. However, these positive results have been counterbalanced by the fact that the administration mode allowed no benefits for other AMD markers (lesions size, retinal sensitivity and drusen area).¹⁴³ Moreover, another phase 2 study (OMEGA, NCT00485394, 2007-2010)¹⁴⁴, not proved this VA improvement for 198 participants after 18 months (same dose and administration mode).¹⁴⁵ These divergent studies may suggest that OT-551 is not an adequate treatment according to this administration mode.



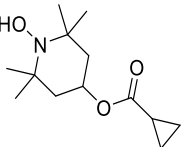
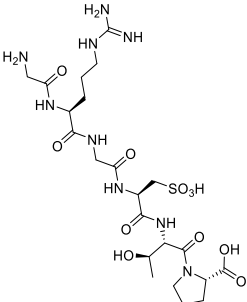
Scheme 1-2: OT-551 transformation in the eye. *The prodrug has the ability to penetrate the cornea compare to TP-H, then OT-551 can be transformed in TP-H in the retina thanks to esterases.*



Risuteganib (ALG-1001, Luminite®), developed by Allegro Ophthalmics, is a small pseudo peptide targeting the integrin heterodimers ($\alpha_v\beta_3$, $\alpha_v\beta_5$, $\alpha_5\beta_1$, and $\alpha_M\beta_2$) involved in angiogenesis, vascular leakage and inflammation. However, targeting $\alpha_v\beta_3$ and $\alpha_v\beta_5$ heterodimers, induce also an oxidative stress action; moreover, in mice, their inhibitions reduced AMD and diabetic macular edema (DME) angiogenesis.^{146,147}

A phase 2 study (NCT03626636, 2018-2019)¹⁴⁸ evaluated the safety profile and the efficacy of risuteganib in atrophic AMD patients. It concluded to an improvement in BCVA, characterized by a gain of Early Treatment Diabetic Retinopathy Study (ETDRS) letters, to measure VA; however, no longer-term studies have been reported.¹⁴⁶

Table 1-5: Drugs targeting oxidative stress.

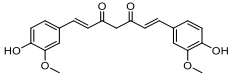
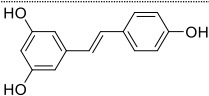
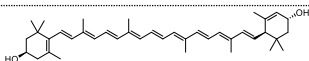
Drugs	Structure	Target	Clinic or Research	Formulation	Ref.
OT-551		Nrf-2, ROS	2	Eye drops	NCT00485394 ¹⁴⁴ NCT00306488 ¹⁴²
Risuteganib		integrin heterodimers	2	Intravitreal injection	NCT03626636 ¹⁴⁸

1.3.5.2 Nutritional supplements

In the absence of a curative treatment, lifestyles and nutritional supplements have also been proposed to slow down the disease's progression.¹⁴⁹ Thus, two studies dealing with the use of nutritional

supplements (vitamins C, β -carotene and minerals such as zinc and copper) have been carried out by Bausch & Lomb, Inc: Age-Related Eye Disease Study 1 (AREDS1)¹⁵⁰ and Age-Related Eye Disease Study 2 (AREDS2)¹⁵¹. These supplements downregulate AMD progression (20% with antioxidant vs 28% without) and vision impairment (19%) after 5 years.¹⁵² In another study (TOZTAL, 2007) based on the supplements in Taurine, Omega-3 Fatty Acids, Zinc, Antioxidant, Lutein showed, no change in VA.¹⁵³ Other dietary supplements have also been studied such as curcumin^{154–156} or resveratrol¹⁵⁷ with no conclusive result yet. To conclude, nutrient supplementation is a part of research in the prevention of AMD but, further research is needed to demonstrate the effectiveness of supplements.¹⁵⁸

Table 1-6: Supplement drugs.

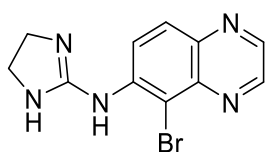
Drugs	Structure
Curcumin	
Resveratrol	
Lutein	

1.3.6 Neuroprotection

Neuroprotective factors protect RPE and photoreceptors cells from oxidative stress damages.⁵³

CNTF

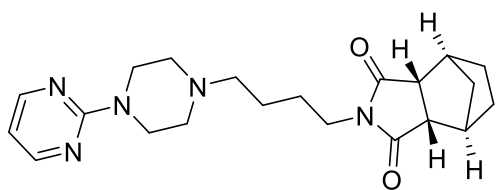
The ciliary neurotrophic factor (CNTF), developed by Neurotech Pharmaceuticals, is a cytokine belonging to the IL-6 family. In a set of neurodegenerative disorders, this survival factor is reported to delay the symptoms' aggravation. In the specific cases of ocular diseases, CNTF improves the survival of the photoreceptors and the RPE cells; in animals suffering retinitis pigmentosa, CNTF proved to slow down the retinal degeneration.^{159,160} In humans, CNTF secreted by modified human retinal pigment epithelium cells, trapped in a polymer implant (NT-501), maybe surgically implemented into the vitreous of the eye.¹⁶¹ For patients suffering atrophic AMD, a phase 2 study (NCT00447954, 2007-2016)¹⁶² evaluated the safety and efficacy of CNTF in this implant. The encapsulated cells remain active after 24 months, and positive pharmacokinetic results with continuous delivery of CNTF secreted by the implant have been observed.



Brimonidine Tartrate

Brimonidine tartrate (Alphagan®), developed by Allergan, Inc., is a small-sized 2-imidazoline, α 2-adrenergic receptor agonist⁸⁹, used for the treatment of ocular hypertension and glaucoma (FDA approved in 1996).^{163,164} Brimonidine has been well described to reduce intraocular pressure (IOP).¹⁶⁵ This therapeutic agent prevents also RPE and photoreceptors cells apoptosis, by allowing the release of neurophins such as brain-derived neurotrophic factor (BDNF), CNTF and basic fibroblast growth factor (b-FGF) are prevented.¹⁶⁶

This molecule was administered as an intravitreal biodegradable implant for clinical studies. Allergen performed two phases 2 studies (NCT00658619, 2008-2018; BEACON, NCT02087085, 2014-2019)^{167,168} to evaluate its safety and efficacy. Thus, injecting 200 or 400 μ g of brimonidine for 24 months demonstrated a change in the size of the lesions with smaller GA lesions, especially for patients with larger lesions. In the BEACON study, an intravitreal implant of brimonidine (400 μ g) applicate every three months through month 21, showed a reduction of the GA lesions after 30 months.¹⁶⁹

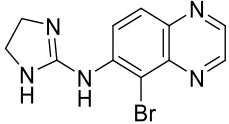
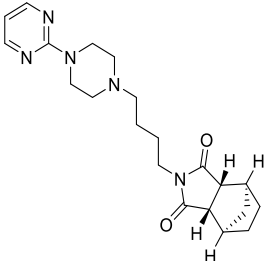


Tandospirone

Tandospirone (AL-8309B, Sediel®), developed by Alcon Laboratories, Inc., is a 1A serotonin agonist⁵³, used as anti-oxidant and anti-depressant. In the external retina, this molecule slows down the activation of microglia and the deposition of different complement proteins such as C3, factor B, factor H and MAC.¹⁷⁰ This will preserve in turn RPE cells and photoreceptors from oxidative stress and prevents retinal cells apoptosis.^{89,171} Interestingly, tandospirone may be given to patients thanks to eye's drops.

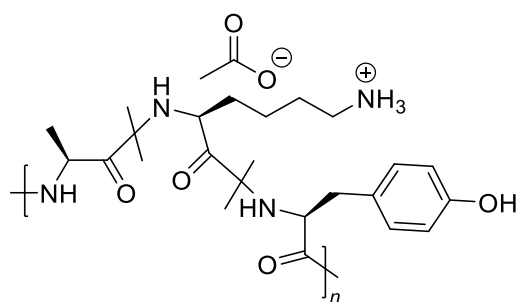
A phase 3 study (GATE, NCT00890097, 2009-2014)¹⁷² did not point out any safety concerns for the use of tandospirone, but there was a lack of efficacy since no changes in the GA lesions growth were reported compared to untreated patients.¹⁷³

Table 1-7: Drugs targeting neuroprotection.

Drugs	Structure	Target	Clinic or Research	Formulation	Ref.
CNTF	Protein	Photo and RPE cells	2	intravitreal injections (Implant: NT-501)	NCT00447954 ¹⁶²
Brimonidine		Photo and RPE cells	2	intravitreal injections (Implant)	NCT00804921 ¹⁷⁴ NCT00864838 ¹⁷⁵ NCT00658619 ¹⁶⁷ NCT02087085 ¹⁶⁸
Tandospirone		Photo and RPE cells	3	Eye drops	NCT00890097 ¹⁷²

1.3.7 Inflammatory pathways

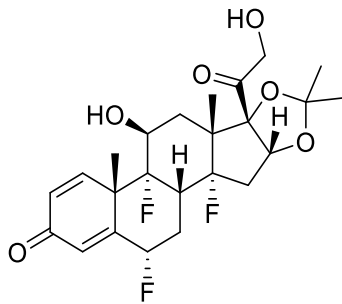
Many daily stressors, such as UV radiation, oxidation, infection result in a chronic low-grade inflammation, which is a relevant parameter for several age-related degenerative diseases,^{176,177} including AMD.¹⁷⁸ In AMD, chronic inflammation may induce endothelial dysfunction in choroidal vessels, development of basal deposit and drusen, degeneration of Bruch's membrane. In addition, AMD is associated also with the increase of the permeability of the vessel wall, the leakage into the surrounding interstitial tissue and edema, the activation of blood-borne inflammatory cells, and the involvement of the complement system, which all are conventional inflammation hallmarks.¹⁷⁹



Glatiramer acetate

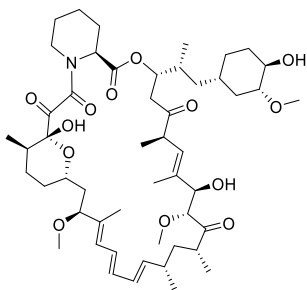
Glatiramer acetate (Copaxone[®]), developed by Teva Pharmaceutical, is a four amino acid (Glu-Ala-Tyr-Lys) polymer mimicking myelin, currently used in multiple sclerosis (FDA approved in 1996).¹⁸⁰ By an

unclear mechanism of action, glatiramer acetate suppresses the inflammatory response, as the pro-inflammatory T cells are feigned into Th2 cytokines (anti-inflammatory or regulatory cells).^{181,182} In 2007, a phase 2/3 study (NCT00466076, unknown status)¹⁸³ and a phase 1 study (NCT00541333, 2007-2013)¹⁸⁴ assessed its efficacy and safety for its use as a preventive treatment to block the conversion of dry AMD to wet AMD; at the endpoint, both studies highlighted a decrease in the area of drusen.¹⁸⁵



Flucinolone acetonide

Flucinolone Acetonide (Iluvien®), is a lipophilic corticosteroid developed by Alimera Sciences,¹⁸⁶ currently used in the treatment of DME (FDA approved in 1963).¹⁸⁷ In a phase 2 study (NCT00695318, 2008-2015)¹⁸⁸ flucinolone acetonide (0.2 or 0.5 µg/day) demonstrated only a slight improvement in the size of GA after 24 months.



Sirolimus

Sirolimus (rapamycin, Rapamune®) is a well known natural macrocycle with several therapeutic activities. This is an inhibitor of the mammalian target of rapamycin (mTOR),¹⁸⁹ initially used as an immunosuppressant to prevent graft rejects (first agreement by FDA in 1999, given in the case of renal transplantation).¹⁹⁰ Sirolimus was given in association with Lidocaine (Phase 2, NCT01675947, 2012-2015)¹⁹¹ but this trial was stopped for safety concerns. A phase 1/2 study (SIRGA, NCT0071249, 2008-2013)¹⁹², complemented by a phase 1/2 study (SIRGA2, NCT01445548, 2011-2019)¹⁹³ were evaluated the safety and efficacy of sirolimus formulation; unfortunately, side effects of retinal atrophy and/or RPE were observed without beneficial effects for patients.¹⁹⁴ Thus, the use of sirolimus remains questionable for AMD treatment, and additional studies are needed.

Complement cascade

An important part of inflammatory treatment passed by the complement system, a group of proteins able to stimulate inflammation and opsonization during the immune response. Three distinct biochemical pathways leading to cells swelling¹⁹⁵ exist: classical, alternative and lectin pathway (Figure 1-14). This terminal cell lysis step is induced by the membrane attack complex (MAC) formation thanks to the complex formed including C5b, C6, C7, C8 and C9. MAC also acts at the level of the CC loss and, possibly, for the drusen formation.¹⁹⁶ In atrophic AMD, the alternative pathway of the complement cascade may be targeted.

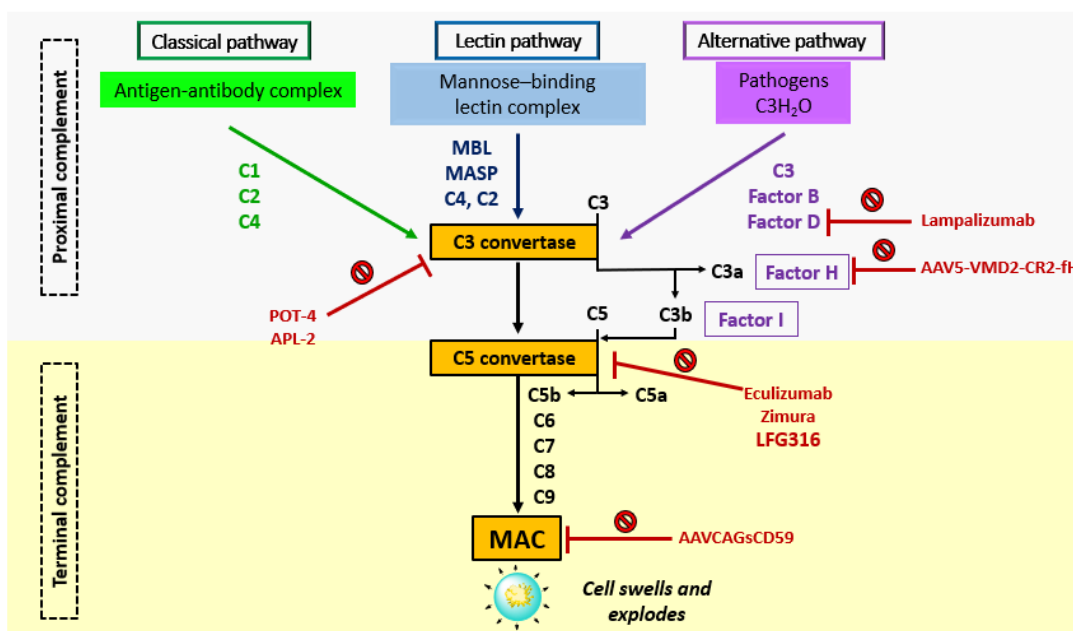


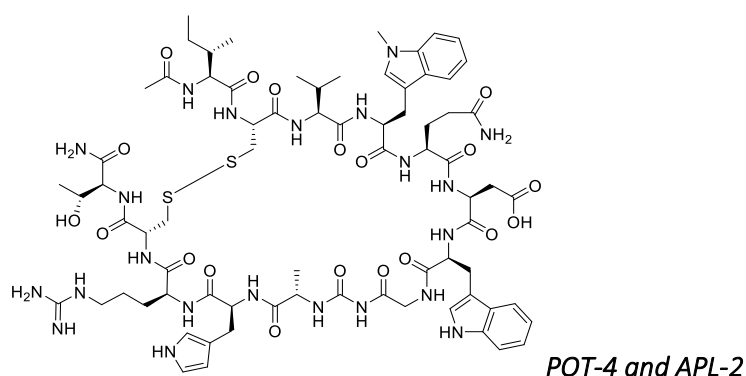
Figure 1-14: The complement cascade.

*MBL: mannose binding lectin; MASP: MBL-associated serine protease; MAC: Membrane attack complex. Alternative pathway: linkage of Factor B with hydrolysed C₃, then cleavage by Factor D to form C₃ convertase. C₃ convertase to cleave and active complement C₃ for C₃a and C₃b conversion. Factor H to intervene over C₃/C₅ dissociation and Factor I to inactive C₃b. C₅ convertase to cleave and active complement C₅ for C₅a and C₅b conversion. C₅b, C₆, C₇, C₈ and C₉ allows the MAC formation.*¹⁹⁵

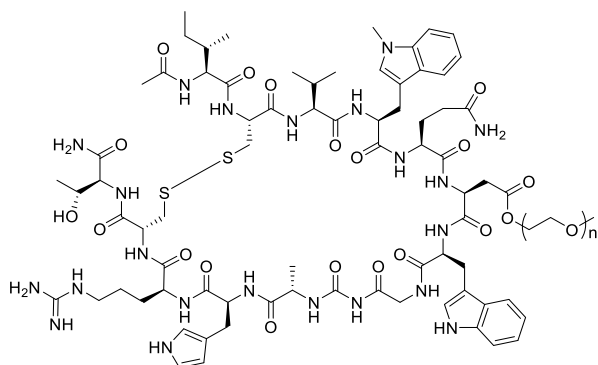
Lampalizumab

Lampalizumab (FCFD4514S) is an antigen-binding (Fab) fragment from monoclonal antibody with an anti-inflammatory activity developed by Genentech, Inc. from Hoffmann-LaRoche to target the factor D. Two phases 2 studies (MAHALO, NCT01229215, 2010-2016; NCT02288559, 2014-2019)^{197,198} evaluated its safety: the drug was given by intravitreal injection during 18 months and 24 weeks at the

dose of 10 mg. Great benefits for patients have been reported, since authors reported an average reduction by 20% of the lesion's progression, which reached 44% for a subgroup of CFI risk-allele carriers.¹⁹⁹ This study also pointed out that patients suffering from outer retinal tubulation (ORT) in atrophic AMD treated with lampalizumab have lesions that grow more slowly than those of untreated patients.²⁰⁰ An extension of the precedent studies (NCT01602120, 2012-2019)²⁰¹ was performed but was terminated prematurely because of a lack of treatment's efficacy. In addition, phase 3 clinical trials studies (CHROMA, NCT02247479, 2014-2019; SPECTRI, NCT02247531, 2014-2019)^{202,203} were performed to evaluate the efficacy and safety of lampalizumab intravitreal injection (10 mg) during 96 weeks. An extension phase 3 study (OMASPECT, NCT02745119, 2016-2019)²⁰⁴ was terminated in 2019 and tarnished the former results since no significant reduction in geographic atrophy have been observed by comparison with a placebo group. Roche, therefore, announced the termination of the study in 2017.²⁰⁵



POT-4 or AL-78898A is a 13 amino acids cyclic peptide derived from compstatin, a C3-targeted complement inhibitor, developed by Potentia Pharmaceuticals. This molecule has been reported to inhibit the conversion of C3 to C3a and C3b, preventing in turn MAC formation, in a comparable way to its parent compound.²⁰⁶ A phase 2 study (NCT01603043, 2012-2014)²⁰⁷ demonstrated product deposits for four patients among seven (57.4%) due to a poor solubility of POT-4.²⁰⁸



APL-2 is a synthetic cyclic peptide conjugated to a PEG polymer developed by Apellis Pharmaceuticals. This molecule has been developed to counteract the solubility concerns of POT-4. APL-2 corresponds to a 40,000 Da PEGylated conjugate of POT-4, which is also able to block the C3 complement protein.²⁰⁹ A phase 2 study (FILLY, NCT02503332, 2015-2019)²¹⁰ was completed to evaluate the safety and tolerability of APL-2 and to demonstrate the relevance of multiple intravitreal injections (every month or every two months). This study evidenced a reduction in the growth of GA lesions.²⁰⁹ Two other studies are currently ongoing: a phase 1 study (NCT03777332, 2018-2019, active, not recruiting)²¹¹ and a phase 3 study (NCT03525600, 2018-2020, recruiting)²¹².

Eculizumab

Eculizumab (Soliris®), developed by Alexion Pharmaceuticals, is a monoclonal antibody that targets the C5 complement protein and prevents its conversion into C5a and C5b. Eculizumab has been approved by FDA in 2007 to treat atypical hemolytic uremic syndrome and paroxysmal nocturnal hemoglobinuria.²¹³ A phase 2 study (COMPLETE, NCT00935883, 2009-2017)^{214–216} evaluated the effects intravenous injection of eculizumab against atrophic AMD (600 mg or 900 mg). Normal-luminance and low-luminance visual acuities were analyzed throughout this study, without observing any significant results on the GA's growth rate or on the drusen volume reduction.

Tesidolumab

Tesidolumab (LFG316) is a fully-human IgG1 antibody developed by Novartis, that targets the complement protein C5 and has the same mode of action than ecluzumab.²⁰⁹ A phase 1 study (NCT01255462, 2010-2012)²¹⁷ showed the safety and tolerability of tesidolumab (doses up to 5 mg) in patients suffering advanced AMDs. Next, two phases 2 studies (NCT01527500, 2012-2019; NCT02515942, 2015-2019)^{218,219} evaluated tesidolumab multiple-dose intravitreal injections (12 injections every 28 days). However, while little gain was observed in VA, no improvement in GA lesion size was reported.

Avacincaptad pegol or ARC1905 or Zimura®

Avacincaptad pegol (ARC-1905, Zimura®), a 40 kDa PEG-conjugated aptamer,²²⁰ is another inhibitor of C5 complement protein developed by Ophthotech which can be used in both AMD types (atrophic and exudative). A phase 1 study (NCT00950638, 2009-2017)²²¹ proved the safety of avacincaptad pegol up to a dose of 2 mg. Recently (late 2020), a phase 2 study (NCT02686658, 2016-2020)²²² was initiated to evaluate the safety and tolerability of intravitreal injections of avacincaptad in GA secondary atrophic AMD patients.

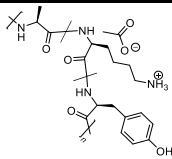
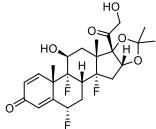
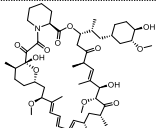
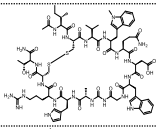
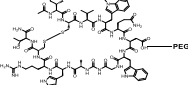
AAV5-VMD2-CR2-fH

AAV5-VMD2-CR2-fH (AAV5-VMD2-mCherry) is an adeno-associated virus gene, coding for an inhibitor of C3a, complement proteins in the eye. In 2018, a study on a mouse model identified a secretion of CR2-fH in RPE cells after injection of AAV5-VMD2-CR2-fH. Moreover, a reduction in the production of C3a associated with CNV was observed. This study shows the potential role of the alternative pathway of complement in the treatment of AMD.²²³

AAVCAGsCD59 or HMR59

AAVCAGsCD59 is an adeno-associated viral vector serotype 2 expressing sCD59 developed by Hemera Biosciences. AAVCAGsCD59 allows normal retinal cells to increase the soluble form of CD59 expression (sCD59), which protects the retinal cells of central vision by inhibiting MAC, complement-mediated cell lysis terminal step. A phase 1 study (NCT03144999, 2017-2019)²²⁴ is ongoing to measure intraocular inflammation, evaluate VA, observe GA zone change, the GA rate of growth, the drusens volume in atrophic AMD patient's eyes and the incidence of the conversion of dry AMD to wet AMD.

Table 1-8: Drugs targeting inflammation.

Drugs	Structure	Target	Clinic or Research	Formulation	Ref.
Glatiramer acetate		Inflammation	1, 2, 3	Injection	NCT00466076 ¹⁸³ NCT00541333 ¹⁸⁴
Fluocinolone Acetonide		Inflammation	2	Injection	NCT00695318 ¹⁸⁸
Sirolimus		mTOR	2	Intravitreal/ Subconjunctival injection	NCT01675947 ¹⁹¹ NCT0071249 ¹⁹² NCT01445548 ¹⁹³
Lampalizumab	antigen-binding (Fab) fragment from monoclonal antibody	Factor D	3	Intravitreal	NCT01602120 ²⁰¹ NCT02288559 ¹⁹⁸
POT-4		C3	2	Intravitreal	NCT01603043 ²⁰⁷
APL-2		C3	2	Intravitreal	NCT02503332 ²¹⁰ NCT03777332 ²¹¹ NCT03525600 ²¹²
Eculizumab	monoclonal antibody	C5	2	Intravenous	NCT00935883 ²¹⁴
Tesidolumab	fully human IgG1, monoclonal antibody	C5	2	Intravitreal	NCT01255462 ²¹⁷ NCT01527500 ²¹⁸ NCT02515942 ²¹⁹
Avacincaptad pegol	PEGylated nucleic acid aptamer	C5	1 2	Intravitreal	NCT00950638 ²²¹ NCT02686658 ²²²
AAV5-VMD2-CR2-fH	ocular gene therapy product	Factor H	R	Intravitreal injection	-
AAVCAGsCD5 9	ocular gene therapy product	MAC	1	Intravitreal injection	NCT03144999 ²²⁴

Despite intensive researches towards the treatment of atrophic AMD, no curing option emerged, and only three molecules reached clinical trials phase 3 (ALK-001, tandospirone and lampalizumab); the poor knowledge on the exact mechanism of the atrophic AMD remains poorly understood, which delay

the emergence of a viable therapeutic option. However, the survey of the literature depicted above points out inflammation as a target of utmost interest, since it is a common denominator of both AMD forms. By a marked contrast, the strategy consisting in targeting amyloid β accumulation with monoclonal antibodies (RN6G and GSK933776) showed no beneficial effect. Last, there are not sufficient and convergent results yet, to consider the use of SC to replace and/or regenerate cells damaged by the disease, as a promising outcome. Therefore, today, only lifestyle improvement is used to delay disease progression.

1.4 EXUDATIVE (WET) AMD TREATMENTS

Exudative AMD has been reported for the first time in the 1850s, and the first therapeutic option, the laser photocoagulation therapy, was found more than a century later. Fortunately, new therapies and drugs validations against this disease are constantly accelerating since the beginning of the 21st century as illustrated in Figure 1-15. These can be divided into two main families, the phototherapies and the anti-angiogenic treatments. New molecular targets have been recently disclosed, and they pave the way for the development of new drugs.

Similarly to the atrophic treatments, the formulation mode is a real challenge. The marketed drugs are administered by intravitreal injections, invasive and stressful for the patient. But, some new therapies use the administration of eye drops in the case of tyrosine kinase or squalamine inhibitors, which are less invasive.

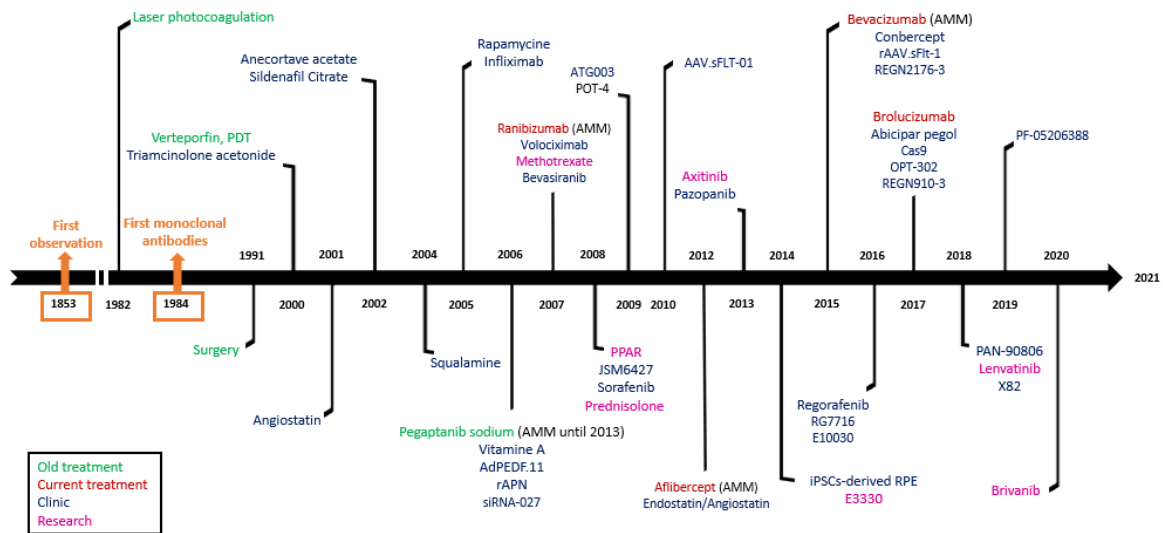


Figure 1-15: Evolution of exudative AMD treatments.

1.4.1 Phototherapies

Laser photocoagulation

Historically, the laser photocoagulation, developed in the late 1980s, was the first therapeutic option against exudative AMD.²²⁵ This treatment aims at preserving the VA after the new choroidal vessels appearance in the in the juxtafoveolar or extrafoveolar regions. It is a non-selective treatment, which consists of the destruction of the new vasculature responsible for the formation of a fibroglial scar and for the destruction of the surrounding neuroretin. Practically, a laser beam is focalized on the RPE, generating locally an increase in temperature inducing neovascularization destruction (Figure 1-16). Different lasers are clinically used, including Argon Blue-green and Argon Green only, Krypton Red and Yellow, and the tuneable Dye Laser.²²⁵

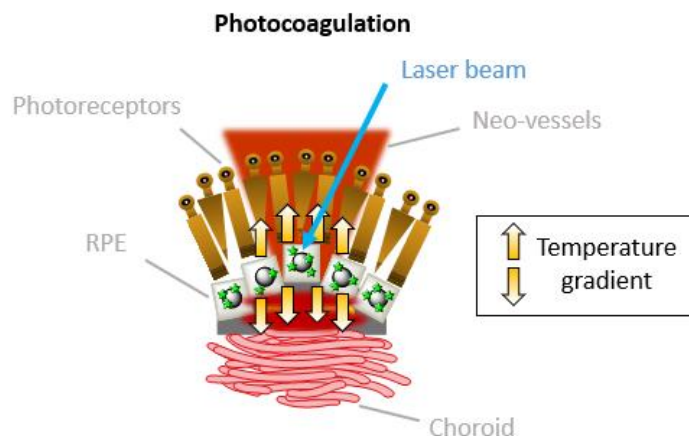
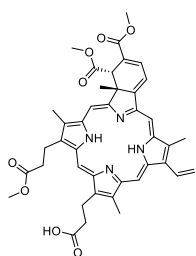


Figure 1-16: Laser photocoagulation mode of action.

The Macular Photocoagulation Studies (MPS, NCT00000158)²²⁶, a phase 3 clinical trial, initiated in the 1970s with a 5-years follow-up, recruited patients with extrafoveal choroidal neovascularization, and demonstrated significant effectiveness of the treatment with the Argon Blue-Green Laser Photocoagulation method. On the other hand, a visual decompensation and loss of VA were observed, as well as some immediate or delayed side effects like scar enlargement or scotoma. This therapy was well tolerated by patients, and photocoagulation after 5 years allowed a benefit on the vision stabilization.²²⁷



Photodynamic therapy (PDT)

Photodynamic therapy (PDT) has been originally used to treat cancers,²²⁸ but Novartis Pharma S.A.S. proposed its use in the 2000s for treating choroidal neovascular membrane, and developed verteporfin (Visudyne®) a photo-sensitizing agent, active against the retro-foveal neovessels. Visudyne® is administered as an intravenous infusion (over 10 min. at a dose of 6 mg/m² of body surface area), then, the laser beam is used for 15 min to target the specific lesion area without affecting the surrounding tissues.²²⁹

Verteporfin is a monoacid derivative of benzoporphyrin (BPD-MA, chlorin type). The drug was prepared as a mixture of two regioisomers (BPD-MA_C **1.5** and BPD-MA_D **1.6**, Figure 1-17), and does not

present apparent cytotoxicity perhaps due to its relatively limited lifetime in the body ($t_{1/2} = 5-6$ h) that reduces the risk of photosensitivity reactions.²²⁹ The therapy process consists of both verteporfin administration by injection and a non-thermal red light at a wavelength of 689 nm (diode laser).^{230,231} Once activated, this drug can transfer its energy to oxygen molecules to form singlet oxygen, which in turn creates damages and lesions on the surrounding tissues (Figure 1-18). For many years, this treatment has been studied through various clinical cases.²³²

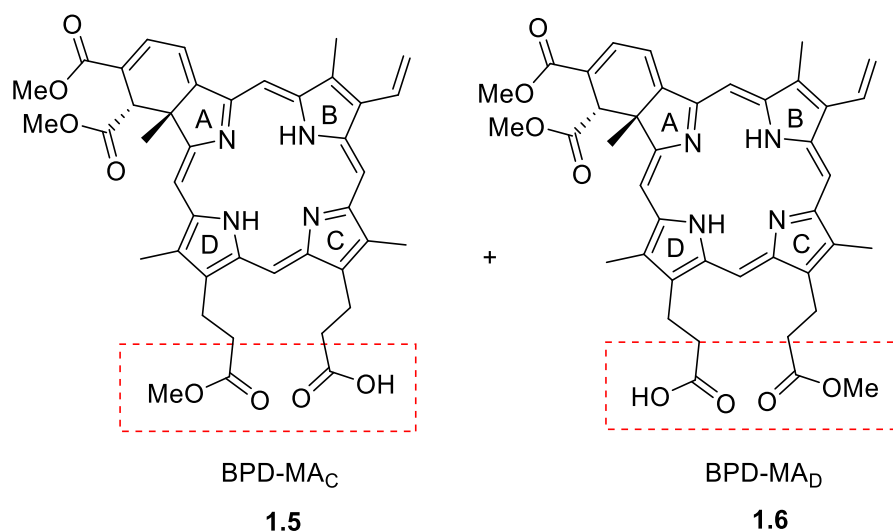


Figure 1-17: Verteporfin as a racemic mixture of two regioisomers.

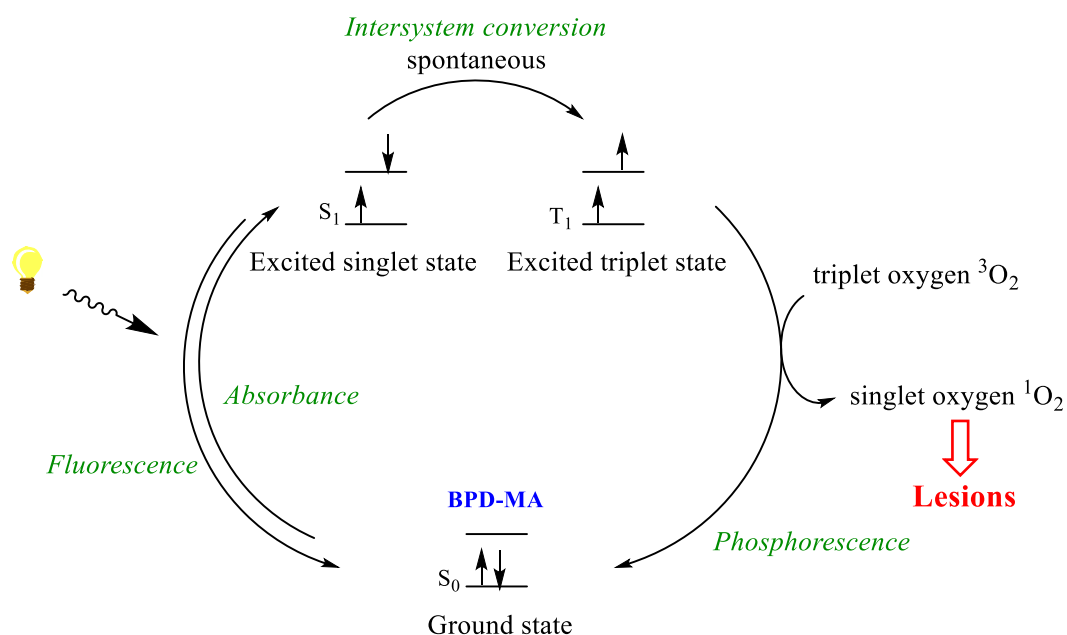


Figure 1-18: Mechanism of PDT.

Two studies were performed to evaluate the verteporfin-PDT effects on lesions and VA in exudative AMD patients: Treatment of Age-related Macular Degeneration with Photodynamic Therapy (TAP) and Verteporfin In Photodynamic Therapy (VIP). Both studies showed that small lesions respond better to this treatment than larger ones; moreover, VA has been maintained thanks to PDT/verteporfin treatment.²³³ Visudyne® was approved by FDA in 2002²³⁴ (approved by French HAS in 2000²³⁵) for its use against choroidal exudative AMD. An extension was obtained from the French HAS in 2002 for occult retrofoveal choroidal neovascularization. Currently, Visudyne is used as a second-line treatment, after the failure of anti-VEGF drugs.²³⁶

1.4.2 Anti-VEGF drugs

Angiogenesis is one of the major key markers of the progression from dry AMD to wet AMD. Thus, taking advantage of the breakthrough of the antiangiogenic drugs for cancer therapy, new AMD therapeutic options emerged in the 1980s. A particular emphasis has been dedicated to research on VEGF, which is the main target to tackle pathologic proangiogenesis signaling pathway. Anti-VEGF agents were initially developed as anti-tumor drugs,²³⁷ but they are nowadays commonly used against exudative AMD.^{238,239} Different VEGF-A isoforms exist: some of them exerting pro-angiogenic effects (VEGF-A₂₀₆, VEGF-A₁₈₉, VEGF-A₁₆₅ and VEGF-A₁₂₁), while others are anti-angiogenic (VEGF-A_{186b}, BEGF-A_{165b}, VEGF-A_{121b}). The most relevant pro-angiogenic isoform in cancers and retinopathies is VEGF-A₁₆₅. These two pathologies are associated with a high over-expression of this isoform, which has therefore been considered as the major therapeutic target to tackle AMD angiogenesis.

1.4.2.1 Marketed drugs

Currently, five molecules have been approved for the palliative treatment of wet AMD, all of them being large size biologics.

Pegaptanib sodium (Macugen®)

Pegaptanib sodium (Macugen®, developed by Pfizer) is a short (28-base) RNA oligonucleotide PEGylated aptamer, which specifically targets VEGF-A₁₆₅²⁴⁰ (IC₅₀ = 750–1400 pM)²⁴¹. The key study VISION (VEGF Inhibition Study in Ocular Neovascularization) explored the intravitreal use of

pegaptanib sodium (0.3; 1 or 3 mg every six weeks) for VEGF inhibition in subfoveal CNV.²⁴² Thanks to pegaptanib sodium, the patients suffering of exudative AMD has better VA. The drug was approved by FDA in 2004 (0,3 mg injectable solution)²⁴³ and was marketed in France from 2006 for the treatment of wet AMD. However, pegaptanib sodium induces side effects such as endophthalmitis, traumatic injury to the lens and retinal detachment associated with VA loss, rendering its use questionable.²⁴⁴ Thus, anti-VEGFs with greater visual acuity efficacy replaced pegaptanib sodium, which was withdrawn from the market in 2013 in France²⁴⁵).

Ranibizumab (Lucentis®)

Ranibizumab (Lucentis®), also called rhuFab V2, was developed by Novartis Pharma. This is a recombinant humanized monoclonal antibody of 48 kDa Fab and targeting all VEGF-A isoforms with an IC₅₀ of 88–1140 pM.²⁴¹ The most relevant study is a phase 3 clinical trial (MARINA, NCT00056836, 2003-2014; NCT01442064, 2011-2012; NCT00379795, 2006-2017) exploring its use by intravitreal injection (0.5 mg monthly) to exudative AMD patients^{246–248}. This 2-years study demonstrated (i) the prevention in vision loss, (ii) an average VA improvement and (iii) the angiographic lesions reduction. Little adverse effects have been reported (intraocular inflammation for 8-14.6%, phakic eyes for 5.1-7.2% patients, and endophthalmitis for 1%, were among the most relevant).²⁴⁹

On the other hand, the ANCHOR study (NCT00061594, 2003-2014)²⁵⁰ compared the use of ranibizumab vs photodynamic therapy (PDT) with verteporfin. This study undoubtedly established that ranibizumab improves the VA of 1 year in average, and exhibits superior beneficial effects than PDT. In addition, few low ocular adverse effects were observed (intraocular inflammation for 8-9.3%, rhegmatogenous retinal detachment for 0.7%, endophthalmitis for 0.7%, ...).²⁵¹ The long term (7-8 years) prognosis of these treatments has been summarized by the SEVEN-UP study, which concluded that one third of the patients demonstrated good visual outcomes, whereas another third had poor outcomes.²⁵² Next, different drug administration protocols have been studied for 0.5 mg: HARBOR (13.5 mean number injections showing an improvement in BCVA)²⁵³ and TREX-AMD (13 and 10.1 mean number injections showing visual gain)²⁵⁴.

Ranibizumab was FDA-approved in 2006 and marketed in 2007 in France for the treatment of wet AMD under the brand name Lucentis® (injectable solutions of 0.5 mg/month). Importantly, this drug is also used to treat neovascularization secondary choroid for high myopia (MF), diabetic macular edema (MDG), macular edema secondary to retinal vein branch occlusion (OBVR) or central retinal vein (OVCR).²⁵⁵

Aflibercept (Eylea®)

Aflibercept was developed by Bayer HealthCare under the brand name of Eylea®. This is a dimeric recombinant fusion glycoprotein, composed by fragments of the VEGF receptors 1 and 2 extracellular domains with an IC₅₀ of 16–90 pM.²⁴¹ These domains are fused thanks to the Fc fusion protein (115 kDa) region of human immunoglobulin gamma 1 (IgG1).²⁵⁶

Phase 3 studies comparing ranibizumab and aflibercept (VIEW1/2, NCT00509795, 2007-2012; NCT00637377, 2008-2014)^{257,258} proved that aflibercept intravitreal doses (0.5 mg to 2 mg) administered every 2 months (after 3 initial monthly doses) show similar efficacy and safety than monthly ranibizumab (0.5 mg) treatment. This lower injection frequency brought indisputable improvements for the patient, such as in terms of risk reduction for the patients' eyes and reduced monitoring.²⁵⁹

Aflibercept was FDA-approved in 2011 and marketed in France in 2012 to treat wet AMD (injectable solution of 2 mg/month). Interestingly, aflibercept is also used in combination with fluoropyrimidine-based chemotherapy, for adult patients with colorectal cancer metastatic (MA in 2005); in metastatic breast cancer, in combination with paclitaxel (MA in 2007) and several other cancers.²³⁶ Moreover, it was a treatment for macular edema following retinal vein occlusion (RVO), macular edema (DME) and diabetic retinopathy (DR) in patients with DME.²⁶⁰

Bevacizumab (Avastin®)

Bevacizumab or rhumAb was developed by Roche. This is a recombinant humanized full-length 149 kDa monoclonal antibody directed toward all VEGF-A isoform²⁹² with an IC₅₀ of 500–1476 pM.²⁴¹ This mAb has been marketed in 2004 (Avastin®) for the treatment of metastatic colorectal cancer and other neoplastic diseases.²⁶³

The five years of study CATT (comparison of age-related macular degeneration treatments trials) study comparing the use of ranibizumab vs bevacizumab, showed that these drugs have similar effects on VA.^{264,265} A phase 3 study (GEFAL, NCT01170767, 2010-2019)^{266,267} compared ranibizumab and bevacizumab to evaluate the efficacy in clinical terms on the VA of patients with exudative AMD.^{267,268} These results led to its marketing authorization in France (2015) for the treatment of exudative AMD; however, its use is not approved by the FDA in the USA due to a potential risk of contamination observed for about 20 Americans cases (eye infections)²⁶⁹. To date, this drug is administrated at the concentration of 25 mg /mL by intravenous infusion.²⁷⁰

Brolucizumab (ESBA 1008, RTH 258, Beovu®)

Brolucizumab (Beovu®) was developed by Novartis. This is a relatively low molecular weight (26 kDa) humanized single-chain antibody fragment, that inhibits all isoforms of VEGF-A ($IC_{50} = 0.49$ nM).^{271,272}

Recently, four clinical trials (one phase 2 trial in 2018: NCT02507388 and three phases 3 trials in 2019 and 2020: NCT03930641, NCT03954626, NCT03386474)^{273–276} were completed and showed the safety of 6 mg of brolucizumab in exudative AMD patients. Moreover, the two phases 3 trials HAWK (NCT02307682, 2019)²⁷⁷ and HARRIER (NCT02434328, 2019)²⁷⁸ compared the effects of brolucizumab vs aflibercept.²⁷⁹ These studies differ only in the doses intravitreally administered to patients: two doses of brolucizumab (3 mg and 6 mg) and a dose of 2 mg aflibercept for HAWK; 6 mg of brolucizumab vs a dose of 2 mg of aflibercept for HARRIER. Overall, these studies demonstrated that at 6 mg, brolucizumab is an interesting anti-VEGF drug with efficacy, safety and solubility that can be compared to the 3 anti-VEGF currently used as treatment against wet AMD (ranibizumab, aflibercept and bevacizumab). Moreover, HAWK and HARRIER show that brolocizuanb may be a more durable agent compare to other anti-VEGF, which allows high molar doses; and this might allow fewer injections to patients. These results show that brolucizumab might be preferred over aflibercept. Brolucizumab was recently approved in the US (FDA) for the treatment of exudative AMD (2019) and its authorization is in progress in France.²⁸⁰ This drug is currently used for the treatment of exudative AMD, diabetic macular edema and macular edema secondary to retinal vein occlusion.

Currently, among the five anti-VEGF treatments which have been approved for the treatment of wet-AMD from 2006 to 2019, four have been marketed (Table 1-9). All these drugs share the same mode of administration, which is intravitreal injection. This allows a rapid and focused action, even if this process might be traumatic for some patients.²⁸¹ Nevertheless, these treatments are not curative, since they only slow down the progression of the disease to blindness. Last, ranibizumab and bevacizumab have similar effects on VA after 1/2 years, and similar side effects.^{264,282} Injection price discrepancies are nevertheless of note, bevacizumab being significantly more economic.

Table 1-9: Marked anti-VEGF drugs.

Drugs	Structure	Target	Visual acuity efficiency in phase 3	Formulation	Prices (US; France)	Ref.
Pegaptanib	Aptamer (50 kDa)	VEGF-A 165	-	Intravitreal injections (0.3 mg / 6 weeks)	\$5,300 per 5 doses	VISION ²⁴²
Ranibizumab	Monoclonal Antibody, Fab Fragment (48 kDa)	All isoforms of VEGF- A	+	Intravitreal injections (0.5 mg /month)	\$2,023 per dose; 738 euros /monthly dose	NCT00056836 ²⁴⁶ NCT01442064 ²⁴⁷ NCT00379795 ²⁴⁸ NCT00061594 ²⁵⁰
Aflibercept	Fusion Protein (115 kDa)	All isoforms of VEGF- A + PIGF	+	Intravitreal injections (2 mg /month)	\$1,940.90 per dose; 730 euros /monthly dose	NCT00509795 ²⁵⁷ NCT00637377 ²⁵⁸
Bevacizumab	Monoclonal Antibody (149 kDa)	All isoforms of VEGF- A	+	Intravitreal injections (1.25 mg)	\$55 per dose; 100 euros per dose	NCT01170767 ²⁶⁶
Brolucizumab	Monoclonal Antibody (26 kDa)	All isoforms of VEGF- A	+	Intravitreal injections (6 mg /month for the first three doses, followed by 6 mg / 8-12 weeks)	\$1,940.90 per dose	NCT02507388 ²⁷³ NCT03930641 ²⁷⁴ NCT03954626 ²⁷⁵ NCT03386474 ²⁷⁶ NCT02307682 ²⁷⁷ NCT02434328 ²⁷⁸

1.4.2.2 Future trends

In addition of anti-VEGF treatments present in the market, several drugs were explored in clinic thanks to currently active research.

1.4.2.2.1 Proteins drugs

Conbercept (KH-902; Lumitin)

Conbercept (also called KH-902) is developed by Chengdu Kanghong Biotech Co., Ltd. (Sichuan, China). This is a recombinant fusion protein similar to aflibercept except for the VEGF2 domain 4 present in conbercept which is larger.²⁸³ It is composed of the second Ig domain of VEGFR-1, the third and fourth Ig domains of VEGFR-2 and the constant region (Fc) of human IgG1. Like aflibercept, conbercept blocks all isoforms of VEGF A, VEGF B and PlGF but with a higher affinity than bevacizumab and ranibizumab ($IC_{50} = 7\text{--}15\text{ pM}$)²⁸⁴. Moreover, this mAbs exerts doubly superior bioactivity for VEGF inhibition compared to ranibizumab.²⁸⁵

Thanks to animal studies (rats and mouse models)²⁸⁴, conbercept reached several clinical studies in phase 1 (HOPE, NCT01242254, 2010-2014)^{283,286}, 2 (AURORA, NCT01157715, 2010-2014)^{287,288}, 3 (PHOENIX, NCT01436864, 2011-2014)²⁸⁹ and 4 (RELIANCE, NCT02577107, 2015-2017)²⁹⁰ but has not yet obtained marketing authorization in the United States and France (but this drug is approved by the China Food and Drug Administration in 2013,)^{285,291,292}

Abicipar pegol

Abicipar pegol (or AGN-150998) is a recombinant protein of the DARPIn family (Designed Ankyrin Repeat Protein) developed by Allergan. It is a small 34 kDa protein formed from the repeat of an ankyrin structure. This recombinant protein has a greater affinity than ranibizumab ($K_d = 2\text{ pM}$ vs 46 pM) for all the VEGF-A isoforms ($IC_{50} = 17\text{ pM}$).²⁹³ In 2018, Allergan demonstrated that abicipar pegol has also a longer length of action than ranibizumab and bevacizumab.²⁹⁴

Phase 1 studies (NCT02859766, 2016-2018; PINE, NCT03335852, 2017-2018)^{295,296} evaluated the safety and pharmacokinetics of abicipar pegol in exudative AMD, without results posted yet. Phase 2 studies (CYPRESS, NCT02181517, 2014-2016 / BAMBOO, NCT02181504, 2014-2017)^{297,298} has been implemented in Japan and in the US to compare the effects of three monthly intravitreal injections of

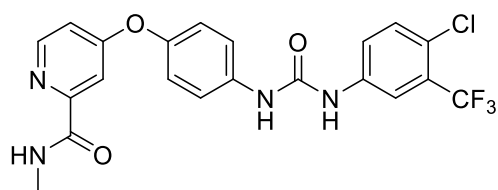
abicipar (1 or 2 mg) or five monthly intravitreal injections of ranibizumab (0.5 mg). This study established that abicipar pegol allows not only an improvement in VA but also induces a decrease in the thickness of the retina.²⁹³ In addition, a phase 2 stage 3 study (REACH, NCT01397409, 2011-2019)²⁹⁹, demonstrated that abicipar pegol reduces the number of the injection compared to ranibizumab treatment (3 against 5), while improving the BCVA and the thickness of the central retina (CRT) and devoid of serious side effects.³⁰⁰ Two phases 3 studies are currently ongoing with a larger dose (2 mg) of abicipar pegol comparing to ranibizumab at different injection times (CDER, NCT02462928, 2015-2019 et SEQUOIA, NCT02462486, 2015-2019)^{301,302} Moreover, a phase 2 study is also ongoing to evaluate the safety and effect of the drug in AMD patients (NCT03539549, 2018-2020)³⁰³.

OPT-302

All the above-mentioned drugs are directed towards VEGF-A, but AMD is also characterized by abnormally elevated levels of other growth factors such as VEGF-C and D (and their corresponding receptors VEGFR 2 and 3), which are also key players in the hypervascularization. Moreover, VEGF-C is reported as a potent inducer of vascular permeability or leakage. Thus, blocking simultaneously VEGF-A, C and D could stop the angiogenesis and vascular leakage occurring in wet AMD. In line with these considerations, OPT-302 has been developed by Ophthea. This is a soluble form of VEGFR-3 (the transmembrane receptor for VEGF-D), including the 1–3 extracellular domains of VEGFR 3 and the Fc fragment of human IgG1. OPT-302 is designed to bind and consequently neutralize the activity of VEGF-C and D. The safety, pharmacokinetics and pharmacodynamics of OPT-302 have been evaluated thanks to the phase 1 trial (NCT02543229, 2015-2017)^{304,305} when given at the dose of 2 mg, *via* an intravitreal injection alone or in combination with ranibizumab (0.5 mg). Then, a phase 2 study (NCT03345082, 2017-2020)³⁰⁶ was carried out to compare two doses of OPT-302 (2 mg and 0.5 mg) in combination with ranibizumab (0.5 mg). This trial revealed that the combined therapy induces a better VA, a decrease in macular thickness with OP-302-ranibizumab association compared to the use of ranibizumab alone. Moreover, this strategy allows a longer delay between two successive injections (every 4 weeks).

1.4.2.2.2 Small-sized molecules

Another anti-angiogenic strategy consists in targeting growth factor receptors with small-sized molecules. Indeed, these receptors exert intracellular tyrosine kinase activities on several substrates and are involved in numerous signaling pathways involved in proliferation, cell growth, apoptosis, angiogenesis and cellular motricity. These growth factors receptors have been extensively studied for more than two decades as relevant targets in oncology for the development of “targeted therapies”.

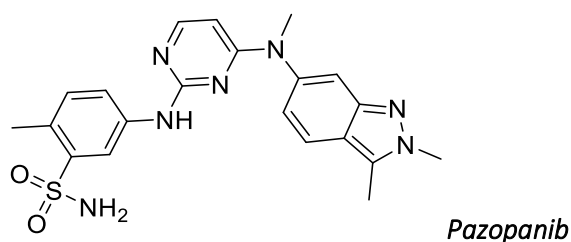


Sorafenib

Sorafenib (BAY 43-9006, Nexavar[®]), is a poly-specific inhibitor of Raf, PDGF, VEGF receptor kinases and c Kit, developed by Bayer with low nanomolar IC₅₀ (among them 26, 90, 20 nM for VEGFR-1, 2-, 3-).³⁰⁷ This molecule has been initially FDA approved for hepatocellular carcinoma, renal cell carcinoma, and thyroid carcinoma in 2005³⁰⁸ and marketed for hepatocellular carcinoma in 2006 in France.³⁰⁹

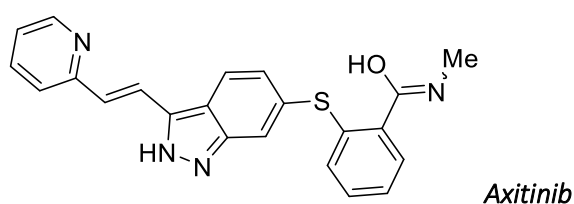
An *in vitro* study was performed to block three specific targets involved in angiogenesis: VEGF, PIGF and PDGF. By treating RPE cells with sorafenib and exposing them to white light, these factors were reduced. In contrast, the absence of sorafenib treatment led to an increase of VEGF, PIGF and PDGF in the same conditions, highlighting the beneficial role of sorafenib.³¹⁰

Out of formal clinical studies, some studies have been performed on isolated cases of patients for sorafenib in association with anti-VEGF: a study was implemented in 2008 to monitor the effects of a treatment combining sorafenib (200 mg, 3 times a week for 5 weeks) and ranibizumab for two cases. This study showed that in combination or alone, sorafenib allows VA improvement and a resolution of the intraretinal fluid without serious adverse effects. However, to definitively validate these results, another clinical study would be necessary with a larger recruitment of AMD patients.³¹¹ Another study led on a single case was performed in 2008 to observe bevacizumab injection (1.25 mg twice) in combination with oral sorafenib (400 mg twice daily). A VA improvement and a decrease in the retina thickness were observed. A longer-term study would be required for sorafenib use.³¹²



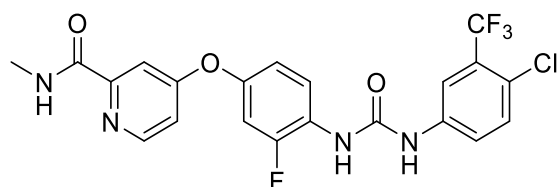
Pazopanib (Votrient®) is another small-sized inhibitor that target VEGFR-1, -2, -3 (IC₅₀= 7, 15, 2 nM), platelet-derived growth factor (PDGFR- α , - β ; IC₅₀= 73, 215 nM)³¹³ and stem cell growth factor (c-Kit). This molecule has been approved by FDA in 2009 for the treatment of the renal cell carcinoma and of the soft tissue sarcoma (in combination with chemotherapy).³¹⁴

GSK led several studies on the oral administration of pazopanib to evaluate its safety, tolerability, efficacy, absorption, pharmacodynamics or pharmacokinetics for exudative AMD: phase 1 studies (NCT00463320, 2007-2012; NCT00659555, 2008-2017; NCT01154062, 2010-2017; NCT01051700, 2010-2017; NCT01072214, 2010-2017)³¹⁵⁻³¹⁹ and phase 2 studies (NCT00612456, 2008-2017; NCT00733304, 2008-2017; NCT01134055, 2010-2018)³²⁰⁻³²², (NCT01362348, 2011-2017)³²³. The results of these phase 1 studies showed that pazopanib was well tolerated with improvement in BCVA, central retinal lesion thickness, and central retinal thickness.³²⁴ However, a phase 2 study³²³ was stopped because of a lack of efficacy.³²⁵ Finally, another phase 2 study³²² compared the effects of pazopanib given in eye drops *versus* intravitreal injections of ranibizumab. This study revealed that pazopanib drops were well tolerated; however, after using pazopanib drops for one year, no greater therapeutic improvement has been observed and the number of intravitreal injections of ranibizumab could not be reduced.³²⁶ Of note, administration by eye drops (2 to 5 mg/mL) would be a more acceptable mode of administration for patients compared to intravitreal injections.



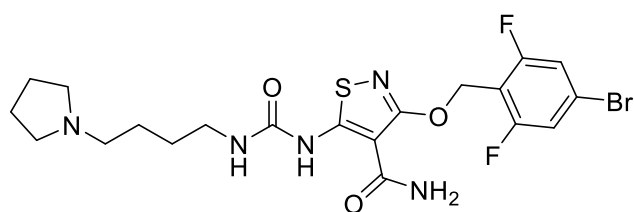
Axitinib (Inlyta®) is a small-sized bispecific inhibitor of VEGFR, PDGFR and fibroblast growth factor receptor (FGFR), colony-stimulating factor receptor, developed by Pfizer. This molecule appeared more potent in inhibiting kinases than some reference compounds such as pazopanib and sorafenib. Indeed, axitinib inhibits VEGFR-1, -2, -3 with IC₅₀ ranging between 0.1 nM to 0.3 nM, and inhibits PDGF-R, FGFR with IC₅₀ ranging between 1.6 nM to more than 1000 nM for PDGF, FGFR, colony-stimulating factor.³²⁷ FDA approved its use in 2012 for renal cell carcinoma.³²⁸ *In vitro* and *in vivo* studies on a mouse model

of AMD demonstrated that oral administration of axitinib enabled 70.1% inhibition of choroidal neovascularization (CNV) lesions and significant regression of established CNV.^{329,330} Axitinib could be used in combination with other anti-VEGFs in the treatment of exudative AMD but more research is needed to determine its safety, the minimum dose needed or the effectiveness of the treatment on the long term.³³⁰



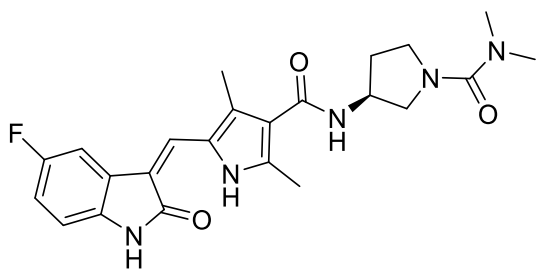
Regorafenib

Regorafenib (Stivarga®) is a small-sized kinases inhibitor developed by Bayer, which remarkably inhibits VEGFR-1, -2, -3 (IC₅₀= 13, 4, 46 nM), PDGFR (IC₅₀= 22 nM).³³¹ This drug has been approved by FDA for the treatment of metastatic colorectal cancer (CRC), of gastrointestinal stromal tumor (GIST) in 2012, and of hepatocellular carcinoma (HCC) in 2017.³³² In the case of AMD, a phase 2 clinical trial (DREAM, NCT02222207, 2014-2016)³³³ terminated in 2016 evaluated its use in an ophthalmic oily suspension in eye drops. However, this study was prematurely terminated due to a lack of efficacy compared to current treatments, potentially due to an unsatisfactory diffusion of the molecule in the back of the eye.³³⁴



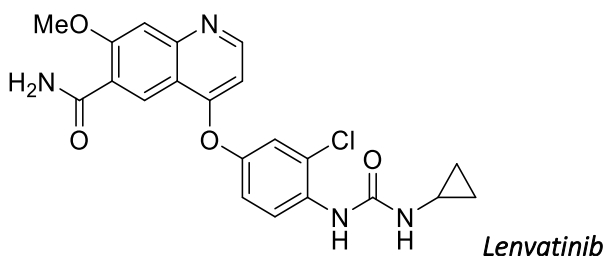
PAN-90806

PAN-90806, is a VEGF-R2 inhibitor (IC₅₀= 1.27 nM) specifically developed by PanOptica, Inc. for the treatment of exudative AMD and other neovascular eye diseases, exerting an antiangiogenic effect.³³⁵ PAN-90806 is an interesting molecule due to its topical administration by eye drops.³³⁶ A phase 1 study (NCT02022540, 2013-2016)³³⁷ completed in 2016 to evaluate the safety and tolerability of PAN-90806 as monotherapy or in association with ranibizumab showed a biological positive response of PAN-90806 for 45-50% of patients. After these phase 1 outcomes, a recent phase 1/2 (NCT03479372, 2018-2019)³³⁸ is ongoing to determinate the quantity dose of PAN-90806 administered orally.



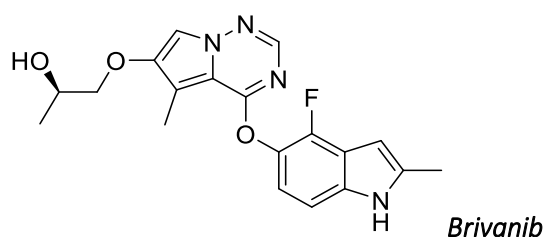
Vorolanib

Vorolanib (X82 or CM-082) is a kinase inhibitor derived from sunitinib (anti-cancer agent), with anti-VEGFR ($IC_{50} = 0.052 \mu\text{M}$) and anti-PDGFR ($IC_{50} = 0.26 \mu\text{M}$) activities.^{339,340} Tyrogenex, Inc. initiated two phases 1/2 study (NCT01674569, 2012-2018)³⁴¹ to evaluate the use of vorolanib in combination therapy with ranibizumab, and a phase 2 study (NCT02348359, 2015-2018)²¹⁸ in which vorolanib was given in combination with one of the three anti-VEGF (ranibizumab, aflibercept and bevacizumab). For the patients who completed these studies (25 participants, 71%), the authors reported the maintenance or the improvement of the VA, as well as a reduction of the average thickness of the central subfield (SD), except in one case. Unfortunately, this positive result is counterbalanced by undesirable side effects including diarrhea, nausea, fatigue, and transaminase elevation, which led to the discontinuation of the treatment for some patients (17%). Thus, additional studies are needed to evaluate the balance between safety and efficacy.³³⁹

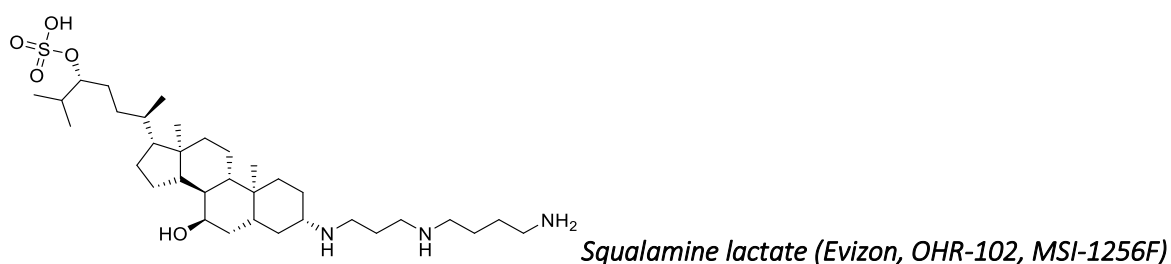


Lenvatinib

Lenvatinib (E7080 or Lenvima®) is developed by Eisai Inc. and FDA approved in 2015 for differentiated thyroid cancer (DTC), renal cell carcinoma (RCC) and hepatocellular carcinoma (HCC).³⁴³ This is a kinase inhibitor³⁴⁴ that targets VEGFR-1, -2, -3, fibroblast growth factor receptor (FGFR1), and platelet-derived growth factor receptor (PDGFR) with an IC_{50} of $22 \mu\text{M}$.³⁴⁵ The drug is interesting by its capacity to penetrate the blood-retina barrier to the retina. Furthermore, thanks to *in vivo* zebrafish model, lenvatinib ($5 \mu\text{M}$ or $10 \mu\text{M}$) inhibited angiogenesis without malformation after 48 h.³⁴⁶ Finally, lenvatinib also stop CNV in a neovascular AMD mouse model (10 mg/day), confirming its interest in exudative AMD treatment.



Brivanib alaninate (BMS-582664) is an orally available inhibitor of FGFR and VEGFR ($IC_{50} = 34 \text{ nM}$)³⁴⁷, with a marked specificity against VEGFR2 and FGFR1,³⁴⁸ developed initially by Bristol-Myers Squibb to treat hepatocellular carcinoma. Studies on mouse and zebrafish models have shown that brivanib is also an inhibitor of proliferation, migration, tubule formation of choroidal microvascular endothelial cells and angiogenesis as observed with lenvatinib.³⁴⁹ These recent results (published in 2020), requires more in-depth studies such as the analysis of brivanib metabolism in the mouse body, the mechanisms of CNV reduction by brivanib or the analysis of others VEGFR/FGFR.



Squalamine, developed by Genaera Corporation and Ohr Pharmaceutical, is a small natural steroid with a steroid-polyamine motive,³⁵⁰ isolated from the liver of sharks of the genus *Squalus*. This drug binds calmodulin once absorbed in the cell, which blocks VEGF signal transduction (antiangiogenic action). This aminosterol is positively charged on the amine functions, which allows electrostatic bonding to the negatively charged cell membrane. As a result, the cell migration process is blocked and consequently angiogenesis.³⁵¹

Three phases 2 studies (NCT00089830, 2004-2007; NCT00333476, 2006-2007; NCT00094120, 2004-2008)³⁵²⁻³⁵⁴ and a phase 3 study (NCT00139282, 2005-2007)³⁵⁵ were terminated to evaluate the safety and efficacy of squalamine lactate (40 mg/infusion/week during 4 weeks). These studies were stopped because the vision improvement does not happen as quickly compare to the treatments competing with squalamine.

A phase 2 study (IMPACT, NCT01678963, 2012-2015)³⁵⁶ compared squalamine (0.2% ophthalmic solution) used in combination with ranibizumab vs the use of ranibizumab alone. The combination therapy allowed an improvement in VA for 42% of patients, compared to 28% for patients receiving ranibizumab alone. This improvement was dependent on the size and type of lesions.³⁵⁷ A phase 3

study (MAKO, NCT02727881, 2016-2017)³⁵⁸ was initiated with a 0.2% ophthalmic solution of squalamine injected twice a day, in combination with a monthly injection of ranibizumab. This study showed a lack of effectiveness of visual acuity gain after nine months.³⁵⁹

1.4.2.2.3 siRNA target: Bevasiranib and siRNA-027

Another antiangiogenic strategy consists in the blockade of VEGF-A production thanks to small interfering RNAs (siRNA), which may induce the inhibition of genes coding for this growth factor. Indeed, siRNAs interact thanks to their two strands of RNA which break down mRNA and if they interact with certain cells, they would block the production of VEGF.³⁶⁰ However, these agents block the synthesis of new VEGF but do not eliminate pre-existing VEGF, rendering the combinational use of a conventional anti-VEGF agent necessary.³⁶⁰

Bevasiranib

Bevasiranib, developed by OPKO Health, Inc, is a siRNA-based anti-angiogenic agent targeting VEGF.³⁶⁰ Bevasiranib showed safety and efficacy profiles with intravitreal injections in pre-clinical mouse models and clinical studies (phase 1 and 2, without literature data). Thus, the first siRNA tested in phase 3, was assayed against exudative AMD in association with ranibizumab in a phase 3 trial (COBALT, NCT00499590, 2017-2019)³⁶¹; nevertheless, this clinical trial was interrupted due to a lack of efficacy for this combination therapy.

siRNA-027 or AGN211745

siRNA-027 or AGN211745, developed by Allergan to suppress CNV and retinal neovascularization by reducing the levels of VEGF-R1-mRNA (IC₅₀= 50 pM).³⁶²

It was studied in two clinical trials completed in 2008 (Phase1/2, NCT00363714)³⁶³ and 2015 (Phase 2, NCT00395057)³⁶⁴. In the first study, single intravitreal injections were given to patients while the second studied a co-administration with ranibizumab. These studies were terminated prematurely due to a lack of efficacy in phase 2 without safety issues.³⁶⁵

1.4.2.2.4 Gene therapies

OXB-201 or RetinoStat®

OXB-201 (RetinoStat®), developed by Oxford BioMedica, corresponds to the lentiviral vector. The infection by a lentivirus (equine infectious anemia virus, EIAV) leads to the expression of two 20-kDa proteins, whose C-terminal fragment is derived from type XVIII collagen (endostatin) for the first and derived from plasminogen for the second (angiostatin). These two proteins exert an anti-angiogenic action by blocking endothelial cell proliferation and migration. Moreover, endostatin and angiostatin induce endothelial cell apoptosis and cell cycle arrest but thanks to the topic subretinal administration, no dose-limiting effects were observed in a dose-escalation assay. Endostatin and angiostatin expressions in the eye may reduce fluorescein angiographic leakage; however, in the context of exudative AMD, subretinal and/or intraretinal fluid was not removed reliably.³⁶⁶ This treatment is also used in cancers, diabetic retinopathy in addition to macular degeneration.

A phase 1 study (GEM, NCT01301443)³⁶⁷, completed in 2017, assayed the use of RetinoStat® when administrated by single subretinal injection with various doses until maximally tolerated dose (MTD). This study showed that EIAV subretinal injections were safe and well-tolerated with reproducible, sustained transgene expression. Moreover, endostatin and angiostatin allowed the fluorescein angiographic leakage reduction but, subretinal/intraretinal fluid is not eliminated in exudative AMD patients.³⁶⁶

Genome surgery using Cas9 ribonucleoproteins (RNPs)

Cas9 (clustered, regularly interspaced, short palindromic repeat)/Cas (CRISPR-associated) ribonucleoproteins (RNPs) can be delivered to human stem and primary cells, as well as to mice to modify target genes.^{368,369} RNP Cas9 was administered in an *in vivo* study (2017) by subretinal injection into RPE cells in adult mice for a potential local treatment of AMD.³⁷⁰ The first results show that CNV is reduced in treated animals and that in RPE the target site has undergone mutagenesis. But other studies need to be done to verify the initial theories supported by this study such as on large animal models or non-human primates.

rAAV.sFlt-1

rAAV.sFlt-1 is a recombinant adeno-associated virus (rAAV2) vector encoded with the naturally occurring VEGF inhibitor known as soluble VEGFR1 receptor or sFLT-1. A phase 1/2 study (NCT01494805)³⁷¹, developed by Lions Eye Institute, Perth, Western Australia and Adverum

Biotechnologies, Inc., in which rAAV.sFlt-1 was administered by subretinal injection at low or high dose (1×10^{10} and 1×10^{11} vector genomes (vg) rAAV.sFlt-1) was completed in 2017. This study showed a well tolerate and demonstrated a favorable safety after injection of rAAV.sFLT-1 in phase 1.³⁷²

AAV.sFLT-01

AAV.sFLT-01 is an adeno-associated viral (AAV) vector similar to rAAV.sFlt-1 with part of the sFLT1 grafted onto an Fc fragment as the synthesized receptor protein, which allows it to be stabilized. A phase 1 study (NCT01024998)³⁷³, developed by Genzyme, a Sanofi Company, where AAV.sFLT-01 was administered by intravitreal injection was completed in 2018 despite the treatment seemed safe and well-tolerated at all doses tested (2×10^{10} , 2×10^{11} , 6×10^{11} and 2×10^{12} vector genomes (vg) AAV2-sFLT01).³⁷⁴ To identify the sources of expression variability, the anti-permeability activity and the potential effect of the basic anti-AAV2 serum antibodies, more detailed studies must be developed.

1.4.3 Anti-PDGFs

Angiogenesis induction is a pivotal step in the progression of macular degeneration. Several studies have reported that an upregulation of PDGF (platelet-derived growth factor) occurs when anti-VEGF therapy is used in the wet AMD. This up-regulation induces the formation of a protective layer of pericytes to cover the neovascular complex, promoting in turn a resistance to anti-VEGF therapies.³⁷⁵ Hence, it is important to consider pretreatment with an anti-PDGF to avoid the apparition of resistance to anti-VEGF therapies. So, this strategy can improve the sensitivity and vulnerability of the neovascular complex to anti-VEGF therapies and other VEGF therapies that can be used in complement. This strategy generally improves visual outcomes.³⁷⁶

Pegleranib or E10030 (Fovista®)

Pegleranib is a 29-nucleotides modified DNA PEGylated aptamer of 40 kDa substituted by 2'-fluoro- and 2'-O-methyl-,²²⁰ developed by Ophthotech. This is an PDGF antagonist, which blocks its interaction with its receptor, namely: PDGFR- β .³⁷⁷ Several trials have been performed to study its use in combination with the anti-VEGF ranibizumab: the phase 1 study (NCT00569140, 2007-2010)³⁷⁸, the phase 2 study (NCT01089517, 2010-2017)³⁷⁹ resulted in an improvement in BCVA and the phase 3

clinical studies (NCT01940900, 2013-2018 & NCT01944839, 2013-2018)^{380,381}, still ongoing.³⁸² These trials investigated the average variations in BCVA and demonstrated an improvement of VA. Moreover, another phase 3 study (NCT01940887, 2013-2020)³⁸³ was compared pegleranib with other anti-VEGF agents (aflibercept and bevacizumab) in wet AMD patients is underway.

Rinucumab or REGN2176-3

Rinucumab is a monoclonal antibody developed by Regeneron directed towards PDGF as pegleranib. A phase 1 study (NCT02061865, 2014-2015)³⁸⁴ demonstrated the maintenance of a VA without serious adverse effects. Then in a subsequent phase 2 study, rinucumab was assayed in combination with aflibercept (CAPELLA, NCT02418754, 2015-2017)³⁸⁵; however, this trial showed no benefit of the combination compared to aflibercept in monotherapy.

1.4.4 Angiopoietin 2 inhibitors

Angiopoietin-2 is a cytokine involved in angiogenesis and inflammatory processes. It is a Tie-2 receptor-ligand found in endothelial cells and fibroblasts.³⁸⁶ The angiopoietin (ANG) -Tie1/2 signaling pathway is necessary for the development of blood and lymphatic vessels. It plays an important role in the maturation of blood vessels, that result from VEGF-induced endothelial germination.³⁸⁷ In addition, this pathway controls also vascular permeability, inflammation and pathological angiogenic responses in adult tissues.³⁸⁸ Therefore, the activity of deregulated angiopoietin contributes to various pathological conditions, including cancer and AMD, where angiogenesis is promoted by overexpression of growth factors. In fact, Ang-2 is regulated *via* the binding of VEGF to TIE2 endothelial cell receptors.³⁸⁷ This interaction improves retinal neovascularization mediated by VEGF but does not by itself stimulates endothelial cells or proliferation *in vitro*. Angiopoietin-1 appears to play a maturation role and may have potential therapeutic benefit through its inhibition of inflammatory pathways.³⁸⁹

However, the molecular mechanisms resulting from the activation of the Ang-Tie signaling pathway are not fully understood. A better understanding is essential for the implementation of future therapies.

Faricimab or RG7716

Faricimab, or RG7716, is a related human monoclonal antibody developed by Roche. In a mouse model, a combined therapy targeting simultaneously VEGF-A and ANG2 was tested by intravitreal injections of faricimab to show the effectiveness in CNV.³⁹⁰ A phase 1 study (NCT01941082, 2013-2016)³⁹¹ and phase 2 study (AVENUE, NCT02484690, 2015-2019)³⁹² have already demonstrated the potential of this mAb which improves the VA. Recently, two phases 3 studies (LUCERNE, NCT03823300 and TENAYA, NCT03823287, 2019-2020)^{393,394} were initiated to compare combination treatments with aflibercept.

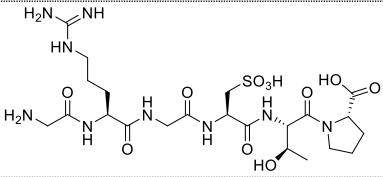
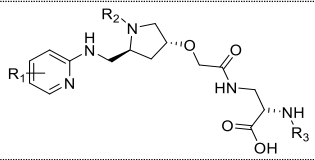
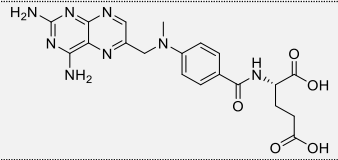
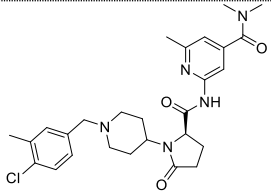
Nesvacumab or REGN910-3

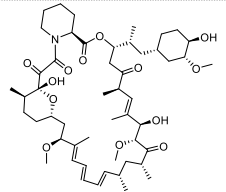
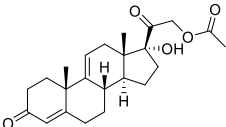
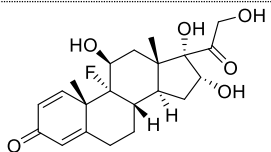
Nesvacumab, or REGN910-3, is a monoclonal antibody developed by Regeneron Pharmaceuticals, which, specifically targets ANG2. A phase 1 study (NCT01997164, 2013-2016)³⁹⁵ has been completed to evaluate its efficacy and safety when administrated in combination with aflibercept against exudative AMD and Diabetic Macular Edema (DME). A phase 2 study (ONYX, NCT02713204, 2016-2019)³⁹⁶ was performed to compare the therapeutic effects of nesvacumab vs aflibercept intravitreal injections showing inconclusive results.

1.4.5 Miscellaneous targets

Many studies have been performed to consider a pathway that does not specifically inhibit angiogenesis but other targets, such as PPAR, integrin receptors, anti-immune or anti-inflammatory pathways (mTOR, TNF- α , complement cascade, ...).³⁹⁷ Indeed, the inflammatory axis is responsible for the exudative form of AMD. These studies are summarized in table 1-10. Multiple structures have been explored ranging from small molecules to monoclonal antibodies and the majority has been studied for both types of AMD. Furthermore, except for Anecortave acetate studied in phase 3 clinical trial in 2012,³⁹⁸ all these drugs did not go beyond phase 2, showing a lack of efficacy and tolerance in healthy patients. Some of these studies have even obtained very recent results, at the end of 2020,³⁹⁹⁻⁴⁰⁴ or are still in progress.⁴⁰⁵

Table 1-10: Different target studied for exudative AMD.

Drugs	Structure	Target	Clinic	Formulation	Ref.
Triple combination therapy	Verteporfin - Ranibizumab - Dexamethasone	Multiple components	2	PDT, Intravitreal injections	NCT02287298 ⁴⁰⁶
PPAR inhibitors ⁴⁰⁷⁻⁴⁰⁹	Nuclear transcription factors	PPAR receptors	R	-	-
ALG-1001		Integrin receptors	1/2	Intravitreal injections	NCT01749891 ⁴¹⁰
JSM6427		Integrin $\alpha 5\beta 1$	1	Intravitreal injections	NCT00536016 ⁴¹¹
Volociximab	Monoclonal Antibody	Integrin $\alpha 5\beta 1$	1	Intravitreal injections	NCT00782093 ⁴¹²
ATG003	Mecamylamine	Nicotinic acetylcholine receptor (nAChR)	2	Eye drops	NCT00607750 ¹¹⁶ NCT00414206 ¹¹⁷
AdPEDF.11	Adenoviral PEDF	PEDF	1	Intravitreal injections	⁴¹⁵
Methotrexate ^{416,417}		Antifolate drug	R	Intravitreal injections	
ALK4290		CCL11	2	Oral	NCT03558061 ¹²¹ NCT03558074 ¹²²

Sirolimus		mTOR	2	Intravitreal injections	NCT00304954 ¹²³ NCT00712491 ⁴¹⁹ NCT02357342 ⁴²⁰ NCT02732899 ¹²⁶
Anecortave acetate		Inflammatory	3	Intravitreal injections	NCT00299507 ³⁹⁸ NCT00346866 ⁴²²
Triamcinolone		Inflammatory	2	Intravitreal Injections	NCT00464347 ⁴²³ NCT00211419 ⁴²⁴
Infliximab	Monoclonal Antibody	TNF- α	1	Intravitreal injections	NCT00304954 ⁴¹⁸
Tesidolumab	Monoclonal Antibody	C5	2	Intravitreal injections	NCT01255462 ²¹⁷ NCT01535950 ⁴⁰¹ NCT01624636 ⁴⁰²
Avacincaptad pegol	Aptamer	C5	1 2	Intravitreal injections	NCT00709527 ⁴²⁵ NCT03362190 ⁴²⁶
POT-4 / APL-2	Cyclic peptide	C3	2 / 1/2	Intravitreal injections	NCT00473928 ⁴²⁷ NCT01157065 ⁴²⁸ NCT02461771 ⁴⁰³ NCT03465709 ⁴⁰⁴
AAVCAGsCD59	Ocular gene therapy product	MAC	1 (Active, not recruiting)	Intravitreal injections	NCT03585556 ⁴⁰⁵

1.4.6 Stem cell transplant

Human-induced pluripotent stem cells (iPSC)

iPSC was tested in *in vivo* assays (mouse and rat models) to evaluate the tumorigenic potential of hiPSC-derived RPE in exudative AMD disease and this study showed no tumours during 6–12 months of monitoring.⁴²⁹ iPSC was first subretinally transplanted in exudative AMD patients in 2014 by Riken (Kobe, Japan)⁴³⁰, to replace or regenerate the dead or dying RPE. No side effects were observed and the vision loss was stabilized.¹¹⁷

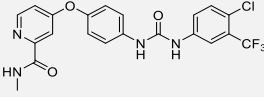
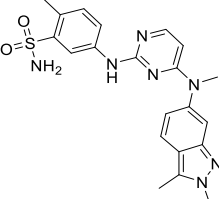
Human embryonic stem cells (hESC)

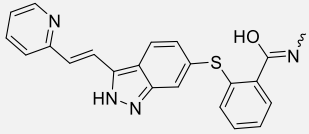
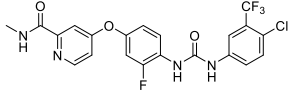
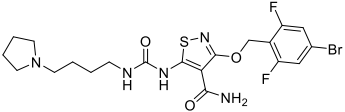
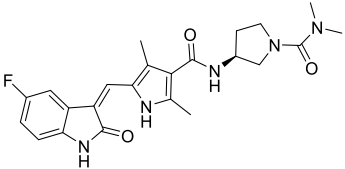
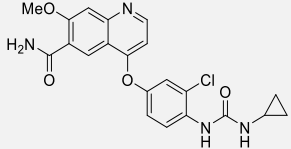
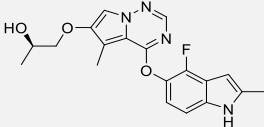
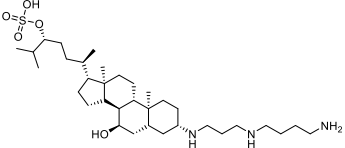
The implantation of **PF-05206388** (retinal pigment epithelium-derived from human embryonic stem cells) in wet AMD patients has been recently studied (2019). A phase 1 study (NCT01691261, 2012-2019)¹⁴⁴ and a four-year study (NCT03102138, 2017-2019)¹⁴⁵ developed by Moorfields Eye Hospital NHS Foundation Trust have been initiated to replace RPE.

Exudative AMD is currently one of the major causes of blindness, and is globally responsible for 90% of vision loss.⁴³³ Anti-VEGF therapies are effective over several years, based on humanized monoclonal antibodies (mAbs), as ranibizumab, bevacizumab, brolocizumab or dimeric recombinant fusion glycoprotein as aflibercept and combercept. But only 30% of the patients present a durable response to this treatment, that suggest the redundancy of alternative pro-angiogenic signaling pathways. In the same angiogenic strategy, the future trend focus on VEGF, PDGF or ANG2, resume in table 1-11. The non-response to anti-VEGF treatment explained by only the presence of inflammatory factor without VEGF factors in the eye. Some drugs were studied to block the inflammatory and/or integrin pathway (Table 1-10). As in the atrophic form, SC is currently ongoing as an interesting approach in the context of AMD, but these studies have been initiated too recently in the exudative part to be able to conclude the treatment efficacy. Other patients also refuse to take the treatment, because of the stress and discomfort caused by intravitreal injections. It should be possible to predict the response to treatment in patients, and research is currently ongoing in this direction.

This introductory chapter is the subject of a review currently in preparation: Fabre, M., et al. "Recent advances in age-related macular degeneration therapies: a review".

Table 1-11: All drugs studying for exudative AMD.

Drugs	Structure	Target	Clinic	Formulation	Ref.
Conbercept		all isoforms of VEGF A, + VEGF B + PIGF	1	Intravitreal injections	NCT01242254 ²⁸⁶
			2		NCT01157715 ²⁸⁷
			3		NCT01436864 ²⁸⁹
			4		NCT02577107 ²⁹⁰
Abicipar pegol	DARpin	VEGF	1	Intravitreal injections	NCT02859766 ²⁹⁵
					NCT03335852 ²⁹⁶
			2		NCT02181517 ²⁹⁷
					NCT02181504 ²⁹⁸
					NCT01397409 ²⁹⁹
			3		NCT02462928 ³⁰¹
	NCT02462486 ³⁰²				
	NCT03539549 ³⁰³				
OPT-302	soluble form of VEGFR-3	VEGF C and D	2b	Intravitreal injections	NCT02543229 ³⁰⁴ NCT03345082 ³⁰⁶
Sorafenib		Raf, PDGF, VEGF receptor kinases and c Kit	R	Eye drops	-
Pazopanib		VEGFR, PDGFR	1	Eye drops	NCT00463320 ³¹⁵
					NCT00659555 ³¹⁶
					NCT01154062 ³¹⁷
					NCT01051700 ³¹⁸
					NCT01072214 ³¹⁹
	NCT00612456 ³²⁰				
	NCT00733304 ³²¹				
	NCT01134055 ³²²				

Axitinib		VEGFR, PDGFR, FGFR and colony-stimulating factor receptor	R	Eye drops	-
Regorafenib		VEGFR, PDGFR	2	Eye drops	NCT02222207 ³³³
PAN-90806		VEGF-R2	1 1/2	Eye drops	NCT02022540 ³³⁷ NCT03479372 ³³⁸
Vorolanib		VEGFR, PDGFR	2		NCT01674569 ³⁴¹ NCT02348359 ³⁴²
Lenvatinib		VEGFR, PDGFR and FGFR	R		-
Brivanib		VEGFR2 and FGFR1	R		-
Squalamine		VEGF + PDGF	3	Eye drops	NCT00089830 ³⁵² NCT00333476 ³⁵³ NCT00094120 ³⁵⁴ NCT00139282 ³⁵⁵ NCT01678963 ³⁵⁶
Bevasiranib	Small interfering RNA	siRNA	3	Intravitreal injections	NCT00499590 ³⁶¹
siRNA-027		siRNA		Intravitreal injections	NCT00363714 ³⁶³ NCT00395057 ³⁶⁴

RetinoStat	Lentivirus expressing endostatin/angiostatin	Gene therapy (VEGF)	1	Subretinal Injections	GEM STUDY ³⁶⁶
Cas9	ribonucleoproteins	Gene therapy (VEGF)	R	Subretinal injections	-
rAAV.sFLT-1	AAV expressing sFLT	Gene therapy (VEGF)	1/2	Subretinal injections	NCT01494805 ^{371,372}
AAV2.sFLT01	AAV expressing sFLT	Gene therapy (VEGF)	1	Intravitreal injections	NCT01024998 ^{373,374}
Pegleranib	PEGylated aptamer	PDGF	1 2 3	Intravitreal injections	NCT00569140 ³⁷⁸ NCT01089517 ³⁷⁹ NCT01940900 ⁹⁶ NCT01944839 ⁹⁷ NCT01940887 ³⁸³
Rinucumab	Monoclonal Antibody	PDGF	1 2	Intravitreal injections	NCT02061865 ³⁸⁴ NCT02418754 ³⁸⁵
Faricimab	Monoclonal Antibody	ANG2	1 2 3	Intravitreal injections	NCT01941082 ³⁹¹ NCT02484690 ³⁹² NCT03823300 ¹⁰⁶ NCT03823287 ¹⁰⁷
Nesvacumab	Fully human antibody	ANG2	1 2	Intravitreal injections	NCT01997164 ³⁹⁵ NCT02713204 ³⁹⁶
iPSC	Human fibroblast	RPE cells	-	Implant	-
PF-05206388	Stem cell	RPE cells	1	Implant	NCT01691261 ⁴³¹ NCT03102138 ⁴³²

Chapter 2. DEVELOPMENT OF DUAL ANTIANGIOGENIC /ANTI-
INFLAMMATORY COMPOUNDS TARGETING THE CXCR1/2 RECEPTORS

This Ph.D. thesis focuses on exudative AMD because this form represents 90% of patients with vision loss.⁴³³ This disease is characterized by exacerbated angiogenesis dependent on the overexpression of the VEGF and by severe inflammation.⁵⁷⁻⁵⁹ Both inflammation and angiogenesis induce in turn the neo-vascularization of the retro-foveal choroid. As mentioned in chapter 1, the only available treatments are anti-VEGF therapies, consisting on intra-vitreal injection of mAbs. However, anti-VEGF injections delay progression to blindness, but 30% of the patients are insensitive or present a transient response to these agents. We hypothesized that these anti-VEGF therapies failures due to the redundancy of pro-angiogenic factors and to the activation of alternative signaling pathways. Moreover, anti-VEGF/PDGF/PIGF therapies do not avoid inflammation, which also characterizes AMD. In addition, this anti-VEGF strategy is not viable for long term treatment, since (i) it is a palliative rather than curative approach, and (ii) the chronic use of anti-VEGF-agents may induce retinal atrophy⁴³⁴ because VEGF is implicated in the neuroprotection of retinal neuronal cells and in the maintenance of the retinal pigment epithelium.

By the way, inflammation and angiogenesis, are integrated processes: inflammatory conditions induce tissue hypoxia and pro-angiogenic factors expression, and angiogenesis may increase the inflammation.⁴³⁵ Thus, the cytokines, initially discovered as mediators of inflammation,⁴³⁶ are also involved in pro-angiogenic processes.⁴³⁷ We have focused our attention on the ERL⁺ CXCL cytokine subclass (including CXCL 1, 2, 3, 5, 6, 7, 8), which exhibits pro-angiogenic/pro-inflammatory properties.^{438,439} The leading member of this cytokine family, interleukin 8 (IL-8) is abundantly secreted where and when VEGF is produced, and the molecular factors involved in VEGF expression stimulate also IL-8 expression.⁴⁴⁰ The ERL⁺ CXCL exert their activity upon the stimulation of their receptors, CXCR1 and CXCR2, two heptahelical G-protein coupled receptors.⁴⁴¹ The stimulation of CXCR1/2 results in the activation of pathways mediated by protein kinases C, phospholipase C and PI3K/AKT/mTOR, RAS/RAF/MEK/ERK and NF-κB pathways.⁴³⁶

In this context, the **inhibition of the ERL⁺ CXCL cytokines signaling pathway by small molecules** has been proposed as a promising strategy to increase potency and pharmacologic properties (pharmacokinetic and pharmacodynamic) and to target the exudative AMD specifically including the angiogenesis and inflammatory phenomena.

2.1 CXCL CHEMOKINE FAMILY AND THEIR RECEPTORS

Chemokines are small proteins of 8 to 12 kDa, involved essentially in the immune and/or inflammatory response. They are also involved in the coordination of the leukocytes migration, in the inflammation regulation and angiogenesis.^{442,443} They are differentiated into four different families, according to the number of amino acids between the two first cysteines in their N-terminal position :

- i) CXC corresponds to two cysteines separated by one amino acid other than cysteine. This family includes 7 receptors CXCR and 17 ligands CXCL;
- ii) CC corresponds to two first adjacent cysteines. This family includes 10 receptors CCR and 28 ligands CCL;
- iii) CX₃C corresponds to two cysteines separated by three amino acids other than cysteine. This family includes only one member, Fractalkine and one receptor CX₃CR1;
- iv) C corresponding to 2 single cysteines. This family includes two members only: Lymphotactine α & β and one receptor XCR1 (Figure 2-1).⁴³⁸

This Ph.D. project focuses on the **CXC family** and their G-protein-coupled receptors (GPCRs), CXCR owning seven transmembrane domains.⁴⁴¹ Moreover, this family can be subdivided into two types depending on the presence or absence of the so-called ELR pattern, which corresponds to a N-terminal glutamate-leucine-arginine motif. ELR⁺ CXCL (1, 2, 3, 5, 6, 7, 8, 15) have pro-inflammatory and pro-angiogenic properties, whereas ELR⁻ CXCL (4, 9, 10, 11, 12, 13, 16, 17) have anti-inflammatory and anti-angiogenic properties (Figure 2-1).^{438,439} Thus, the **ELR⁺ CXCL chemokines** positively regulate the angiogenesis and the chemotaxis of neutrophils and endothelial cells⁴³⁸, which are over-regulated in AMD. In this context, we propose to inhibit their two receptors, namely CXCR1 and CXCR2, to counteract their multiple interactions with CXCL6 and CXCL8 (for CXCR1), and with CXCL1-3 and CXCL 5-8 (for CXCR2). Importantly, the leading member of this CXCL subclass is CXCL8 or Interleukin-8 (IL-8).⁴⁴⁰

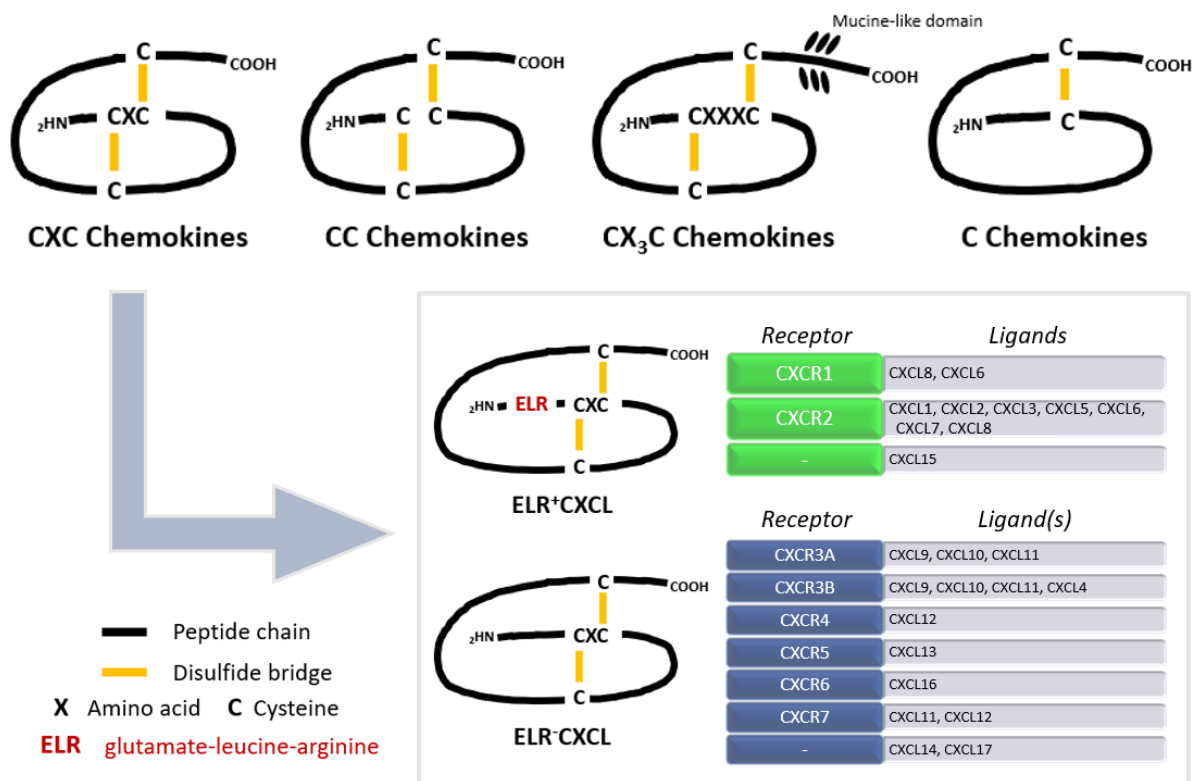


Figure 2-1: Structure of Chemokine families.

2.2 CXCR1/2 KNOWN ANTAGONISTS

Small-sized CXCR1/2 antagonists have already been designed and synthesized for their use in chronic obstructive pulmonary diseases (COPD), asthma, cystic fibrosis and cancer. Among them, eight compounds reached the clinical trial stage (Figure 2-2, 2-3, 2-4, 2-5).^{436,444} These molecules may be classified in four distinct families:

The **phenol-containing diaryl ureas** family⁴⁴⁵ is a group of molecules consisting in an urea flanked by a phenol motive and an aryl moiety. This series of compounds has been originally developed by GlaxoSmithKline, and the first-in-class compound is SB225002, (1-(2-bromophenyl)-3-(2-hydroxy-4-nitrophenyl)urea). This is the first non-peptidic potent and selective antagonist of the CXCL8-CXCR2 interaction ($IC_{50} = 22$ nM).⁴⁴⁶ Several SB225002 derivatives, including various electron-donating or electron-withdrawing groups on the phenol or the aromatic ring (in green and blue, Figure 2-2) have been studied. In particular, the presence of a sulfonamide function adjacent to the phenol shows a major improvement in the inhibiting potency, and a decrease of the clearance in rat models.⁴⁴⁷ The most relevant compounds of this series are danirixin and elubrixin evaluated in clinical trials. These

compounds target the interaction between the receptor CXCR2 and its ligands CXCL1 and CXCL8 (IC_{50} of 0.5-40 nM) with a marked selectivity over CXCR1 ($IC_{50} > 150$ nM).^{436,445} In continuation, phase 1 or 2 clinical trials have been performed for the treatment of COPD.⁴³⁶ For danirixin, two phases 2 studies showed no improvements compared to placebo with an unfavorable benefit-risk profile and a lack of efficacy.⁴⁴⁸ For elubrixin (SB656933), phase 1 clinical trials showed safety and well-tolerated in healthy subjects.

Phenol-containing diarylureas (8)

CXCR2 selective

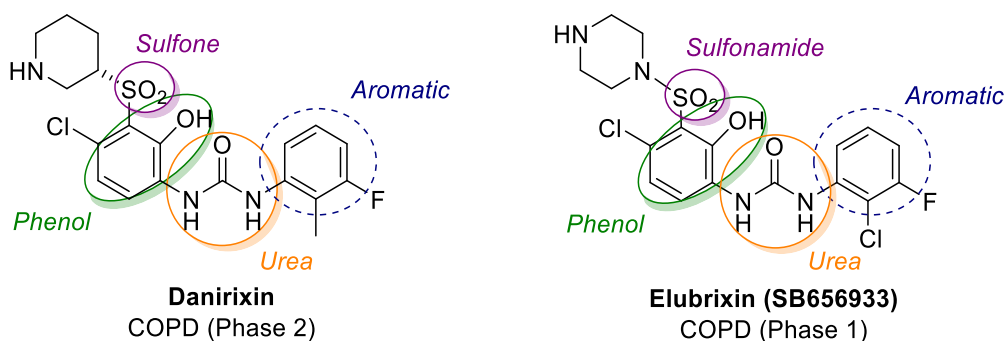


Figure 2-2: CXCR1/2 inhibitors of the phenol-containing diarylureas family tested in clinical studies.

Another structural modification consists in the replacement of the urea by 3-amino-4-(propylamino)cyclobut-3-ene-1,2-dione (squaramide) as bioisosteric functional group. This *N,N'*-diarylsquaramides family includes three compounds developed by Merck Sharp & Dohme Corp.⁴⁴⁹ These molecules feature a phenol substituted by *N,N*-dimethylacetamide and two aromatic rings (furan or benzene). Navarixin displays strong CXCL8-CXCR1 and CXCL8-CXCR2 antagonisms, with respective values of $IC_{50} = 36$ nM and $IC_{50} = 2.6$ nM. A phase 2 trial was initiated for COPD, asthma and psoriasis but the clinical study was stopped due to a warning decreased number of neutrophils.⁴⁴⁴

***N, N'*-diarylsquaramides family (3)**

CXCR1/2 bi-selective

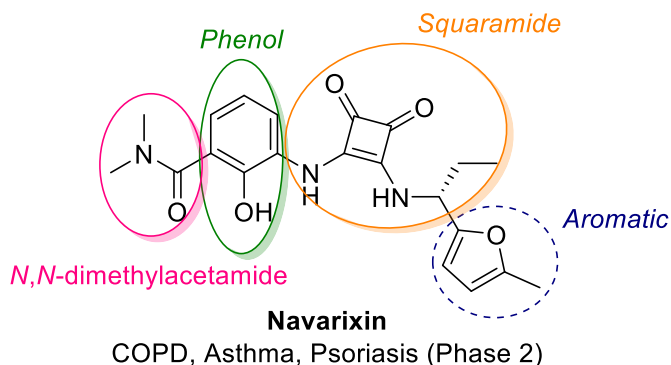


Figure 2-3: CXCR1/2 inhibitors of the *N, N'*-diarylsquaramides family tested in clinical studies.

Next, **reparixin** or *(R)*(-)-2-(4-isobutylphenyl)propionylmethansulfonamide, developed by Dompé Farmaceutici S.p.A, is a selective CXCL8-CXCR1 antagonist ($IC_{50} = 1$ nM) over CXCR2 ($IC_{50} = 100$ nM). Six analogues of reparixin presenting the same *(R)*-*N*-(1-phenethyl)acethyl methylsulfonamide motif (in orange, Figure 2-4) with various substituted aromatic parts (in blue, Figure 2-4) and the presence of nitrogen or oxygen between the carbonyl and the sulfone (in green, Figure 2-4). They are also CXCL8 inhibitors binding CXCR1 and CXCR2 with efficiencies ranging from 2.1-34 nM. Reparixin was assayed in different treatments in phase 2 such as metastatic breast cancer, kidney transplantation, lung transplantation and in phase 3 for pancreatic islet transplantation in type-1 diabetes. Besides, another compound, **ladarixin** was used for bullous Pemphigoid in phase 2 and type-1 diabetes (not yet recruiting).⁴³⁶

Reparixin-derived family (7)

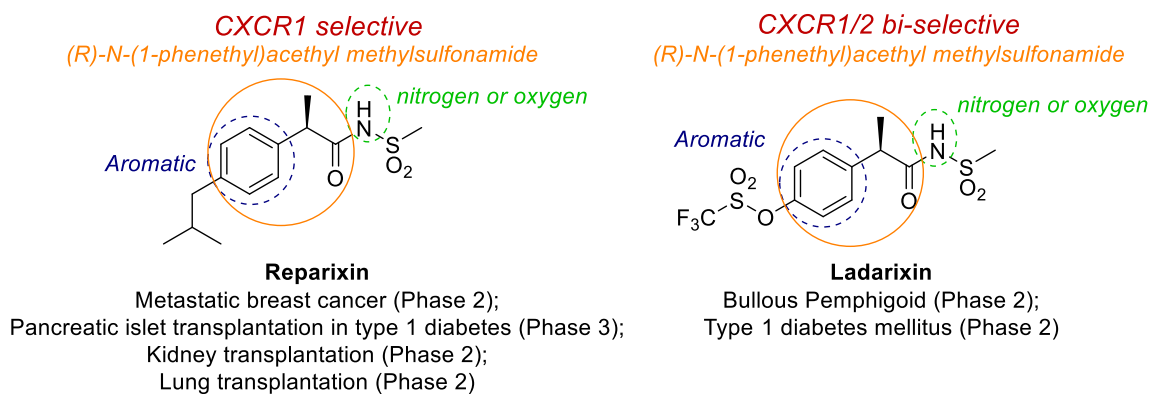


Figure 2-4: CXCR1/2 inhibitors of the reparixin family tested in clinical studies.

Finally, the **2-thiobenzylpyrimidine** family, developed by AstraZeneca, is composed of 15 members including AZD5069 ($IC_{50} = 0.8$ nM), AZD8309 or SX-682 which all selectively inhibit the interaction between CXCL8 and CXCR2. For each member, a 2-thiobenzylpyrimidine motif is present (in orange, Figure 2-5). Phase 1 or 2 studies were terminated for asthma, COPD and were initiated in the case of bronchiectasis, head/neck cancer and rheumatoid arthritis for AZD5069. A phase 1 study is currently ongoing with SX-682 for metastatic melanoma.⁴³⁶

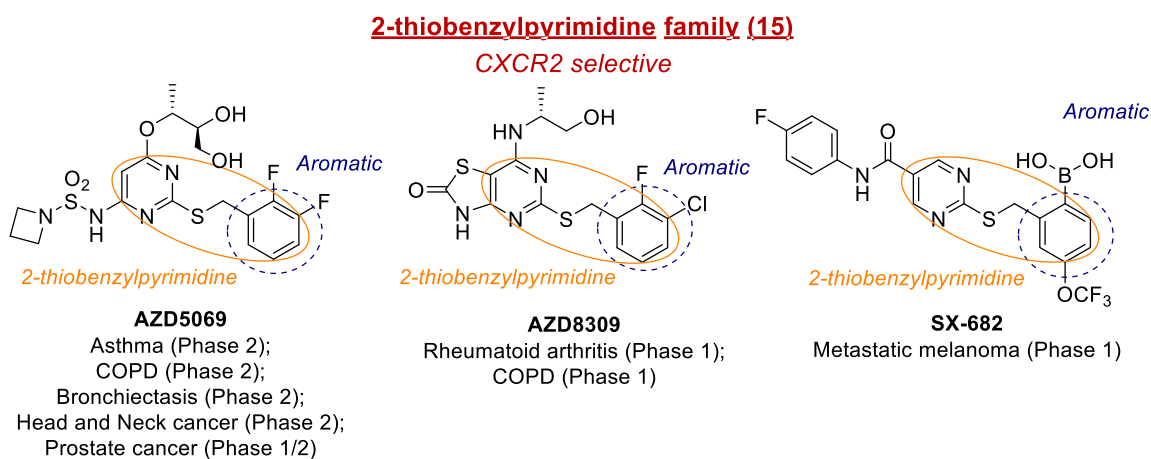


Figure 2-5: CXCR1/2 inhibitors of the 2-thiobenzylpyrimidine family tested in clinical studies.

2.3 PROOFS OF CONCEPT OF CXCR1/2 ANTAGONISTS EFFECTS IN ANGIOGENIC PATHOLOGIES

In the two last decades, the search for new CXCR1 and CXCR2 has been mainly focused on the development of drugs targeting pulmonary diseases as asthma or COPD. Several molecules have been also studied in clinical trials as anti-tumor agents: reparixin (phase 1: 2013-2015; phases 2: 2013-2020, 2015-2020)^{450,451}, navarixin (phase 2: 2018-2021; not yet recruiting), AZD5069 (phases 1/2: 2015-2019; 2015-2020; 2017-2020) and SX-682 (phases 1/2: 2017-2020; 2020-2021; recruiting) (Figure 2-6).

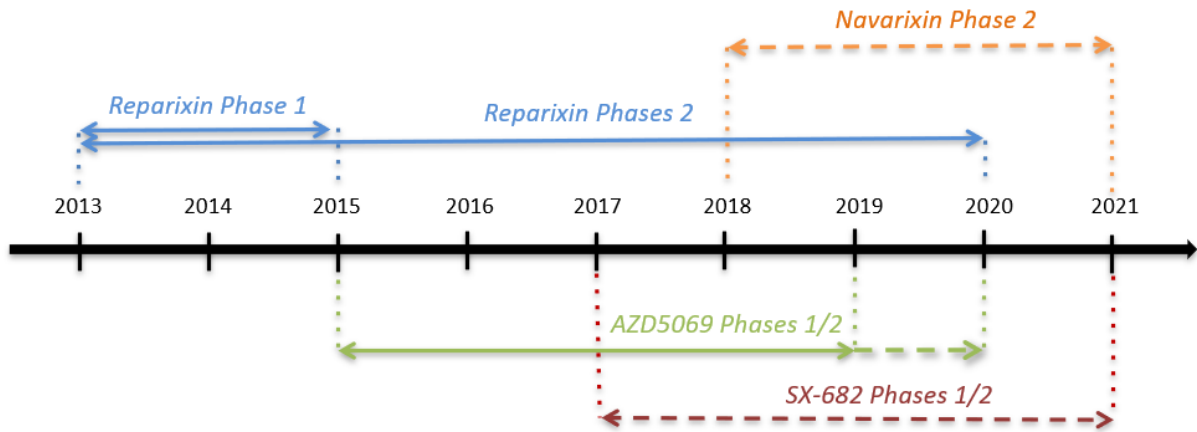


Figure 2-6: Know CXCR1/2 antagonists in clinical trial for cancer.

Before these studies, the Pagès team, a specialized group in cancer and angiogenesis, established in 2012-2014, a correlation between ELR⁺ CXCL cytokines decrease and renal cancer cell growth inhibition, *in vitro* and *in vivo*.^{437,452} Overall, the inhibition of the interaction between ELR⁺ CXCL and their receptors CXCR1/2 (expressed on endothelial cells and neutrophils/macrophages) promotes at the same time the reduction of neutrophils/macrophages attraction and endothelial/cancer cells proliferation (Figure 2-7).⁴³⁷ For these reasons, the Benhida and Pagès groups were interested to apply this strategy in cancerology, for which inflammation and angiogenesis are well-known hallmarks. Another pathology that could be targeted by this strategy, and which is the subject of this Ph.D. is the **exudative AMD**.

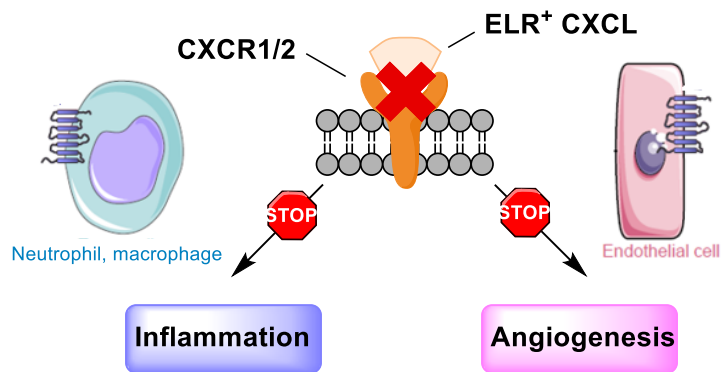


Figure 2-7: ELR⁺ CXCL pathway.

2.3.1 In cancers

Pagès group demonstrated in a pioneering work, that the binding of cytokines ELR⁺ CXCL to their chemokine receptors CXCR1 and CXCR2 stimulates kidney cancer cells proliferation, tumor inflammation and angiogenesis (Figure 2-7)⁴⁵³. The treatment of mice tumors three times a week with 200 µg of the CXCR2-selective competitive antagonist SB225002^{446,454} induces a significant decrease in blood vessels formation and inhibits cell proliferation.⁴⁵³ However, the cell viability EC₅₀ of SB225002 is greater than 90 micromolar on cancer cells (Breast, Kidney, AML, MDS, CML), which greatly limits its applications.⁴⁵³

In the continuation of this work, our group at the ICN Institute designed and synthesized new series of diarylurea family for biological studies. After several rounds of derivatizations, the urea was functionalized on one side with a benzothiazole. Then, after a rationalization of the structure activity relationships, two compounds have been identified, namely **MCK133** and **MCK140**. These molecules present an IC₅₀ between 2 and 10 micromolar against various cancer cells (Breast, Kidney, Head and Neck, AML, MDS, CML) which was a real improvement compared to the activity of the parent compound SB225002. Moreover, *in vivo*, **MCK140** has shown significant tumor growth inhibition on xenografted mice with a clear reduction in the tumor volume and weight compared to the control (Figure 2-8, A-B).

Besides, **MCK140** has shown a better effectiveness in inhibiting the ELR⁺ CXCL7-CXCR2 pathway compared to the reference CXCR2 antagonist danirixin. This observation was performed thanks to a migration assay after 24 hours in HuVEC cells (Human Umbilical Vein Endothelial Cells) by Boyden chamber using 1 or 2.5 µM of **MCK140** and 5 µM of danirixin (Figure 2-8, C).^{435,455}

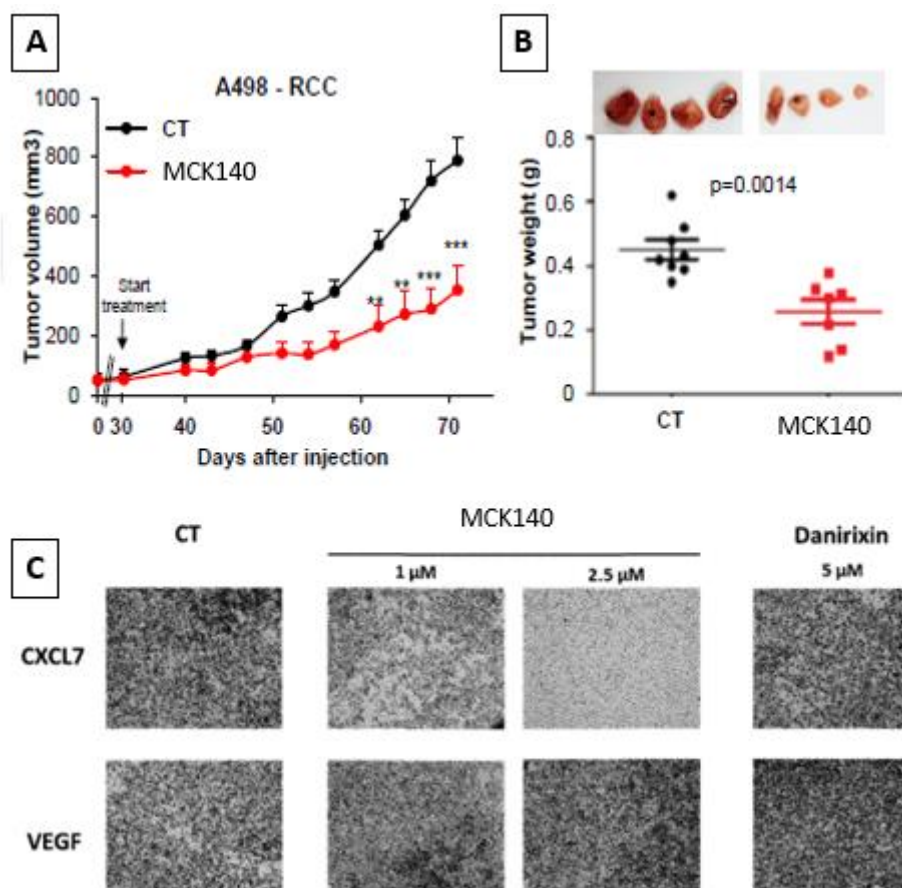


Figure 2-8: Structures of **MCK133/MCK140** and tumor growth inhibition in renal cell carcinoma (RCC) with **MCK140** thanks to CXCL-CXCR2 antagonist effect. *Human A-498 Kidney Cancer Cells. (A) The tumor volume was measured twice weekly. The results are presented as the means \pm sd. (B) Tumor weights at the end of the experiment. (C) CXCL7 or VEGF-dependent HuVEC migration was analyzed using Boyden chamber assays in the presence/absence of **MCK140** or danirixin.^{435,455}

2.3.2 In AMD

Arylurea are already used in applications for ocular pathologies related to an angiogenic context. For example, they have been used to treat posterior segment disorders in the case of exudative AMD, macular degeneration, proliferative diabetic retinopathy (PDR)⁴⁵⁶, cancers and inflammatory diseases (such as COPD or cystic fibrosis).^{436,457}

The two lead compounds **MCK133** and **MCK140** have been assayed *in vivo* in a model of AMD induced by eye cornea laser burn. These experiments have been performed in collaboration with Iris Pharma, a world-class CRO dedicated to ophthalmology. They consist in burning the mice cornea with a laser beam followed by 3 weeks intraperitoneally daily treatment of 0.15 mg of **MCK133** or **MCK140**. After 15 days, an angiography (to observe the ocular vascularity) points out that treated animals have a lower angiogenesis compared to the untreated animals (Figure 2-9).

These preliminary results also highlighted the limits of these inhibitors. They underline the need of new compounds with an optimized efficacy and with improved solubility to allow the administration of higher dosages. The possibility of administration by eye drops – the least intrusive for patients – is also an ideal goal to pursue.

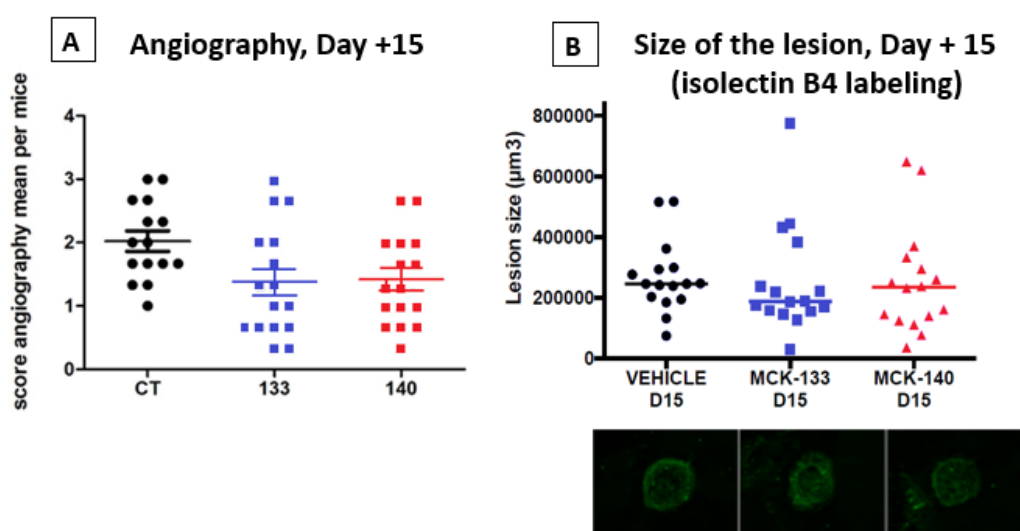


Figure 2-9: Angiography of **MCK133** and **MCK140** in exudative AMD model.¹ (A) Angiography after 15 days. (B) Size of the lesion after 15 days.

2.4 DESIGN OF NEW SERIES OF CXCR1/2 ANTAGONISTS

2.4.1 Rationale

2.4.1.1 Predicted pharmacophore

In the continuation of the above reported studies, the goal of my Ph.D. project, which is a part of ANR program, was to **develop a new family of small-sized molecules** specifically designed for the treatment of AMD. A particular emphasis has been given to the isosteric replacement of the urea motif of SB225602, **MCK133** and **MCK140** (Figure 2-10). Thus, we seek for new molecular scaffolds to simultaneously enhance efficacy and solubility properties by scaffold hopping. A potential pharmacophore was predicted by the team, with a specific motif as cyclic bio-isostere of urea: a 2-

¹ Unpublished results

aminoimidazole or a 3,5-diamino-1,2,4-triazole. Indeed, these heterocycles present structural similarities with the urea in terms of geometry with similar bond angles ($115\text{-}125^\circ$ for urea motif while $121\text{-}131^\circ$ corresponding of outside angle and $103\text{-}113^\circ$ corresponding to inside angle for our new pharmacophore), presence of lone pairs and hydrogen bond donors, and electronic density repartition. (in green, Figure 2-10). This 5-membered heterocycle would require to be joined to two aromatic moieties to ensure the structural similarities with the diarylurea family and to complete the potential pharmacophore.

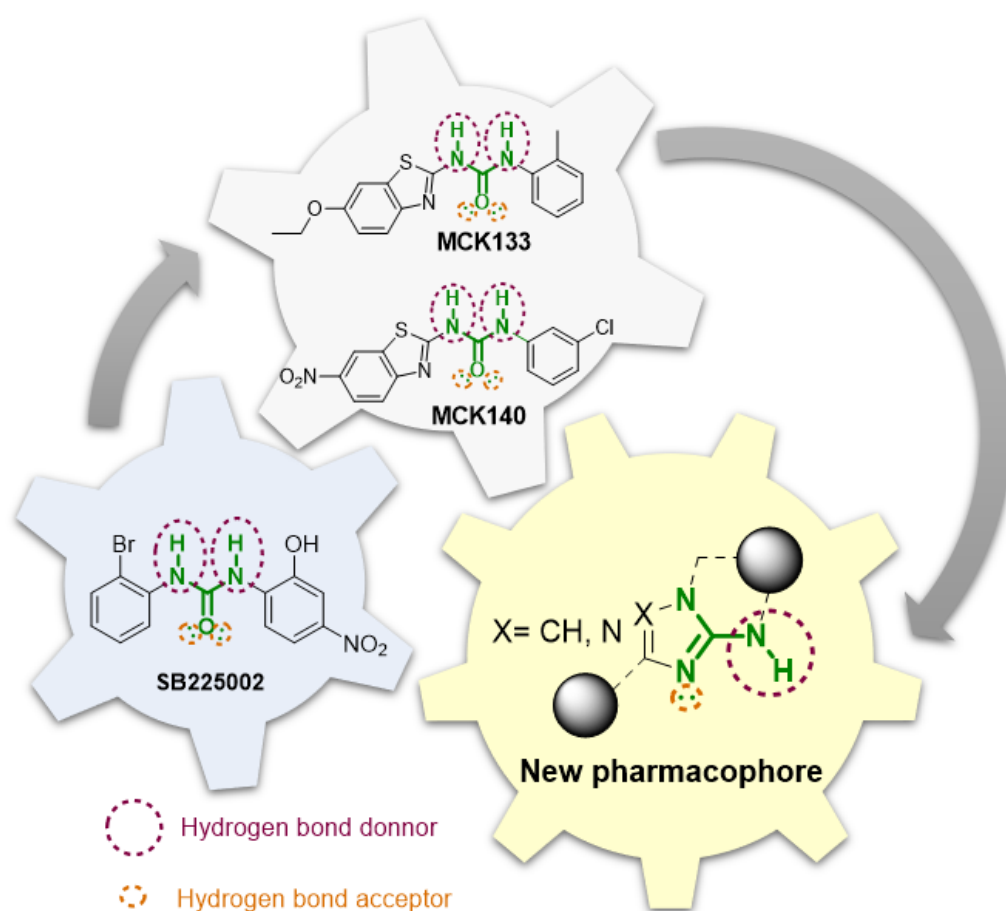


Figure 2-10: Scaffold hopping from the diarylurea to the new predicted pharmacophore

2.4.2 Envisaged series

Our predicted pharmacophores can be declined in four different series, two belonging to the 2-aminoimidazole series (series A and B) and two belonging to the 3,5-diamino-1,2,4-triazole series (series C and D) (Figure 2-11). However, all these series present similarities in their scaffolds elements,

namely the aminoazole (in green, Figure 2-11), flanked by two aryl moieties (in blue and red, Figure 2-11). My objectives were to attempt the synthesis of these four series and to create analogues thereof in order to define the structure-activity relationships.

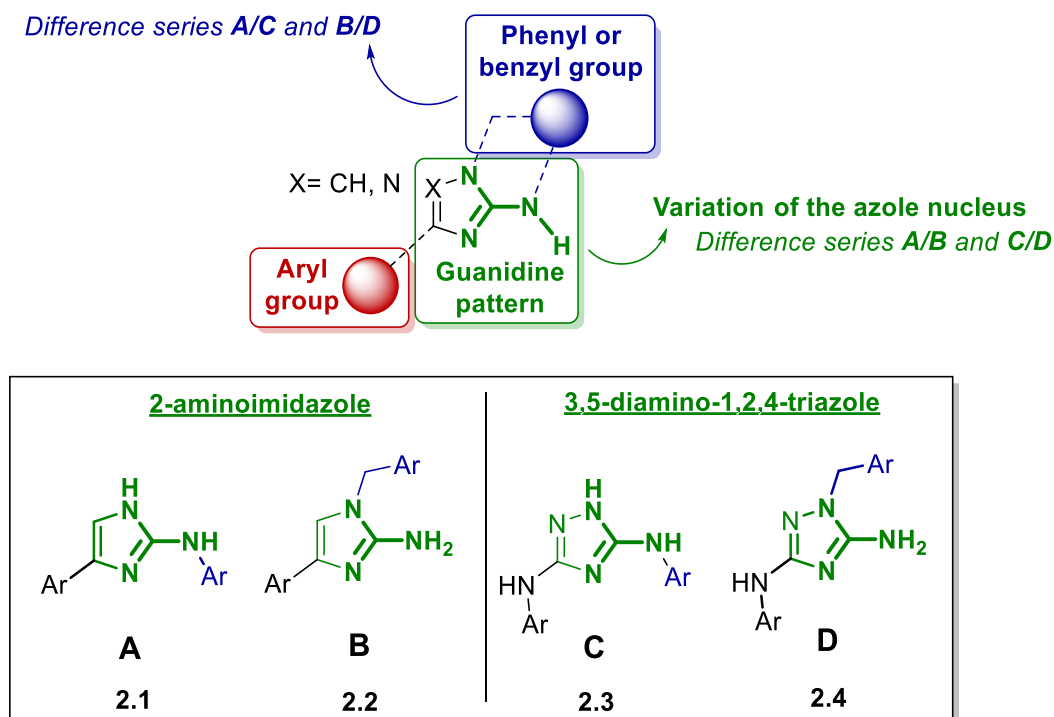


Figure 2-11: Declination of the predicted pharmacophore and different series envisaged.

Practically, the synthetic development of the two imidazole series (A and B) is presented in chapter 3, whereas the triazole derivatives of series C and D are the object of chapter 4.

2.4.3 Structural properties and similarities of the predicted pharmacophores and diuretics

The diuretics series is characterized by an urea with two hydrogen bond donors (the nitrogens) and acceptors (the oxygen) (Figure 2-10). The urea motif is basic, with pK_b of 13.9. Whereas imidazoles and 1,2,4-triazoles are ubiquitous 5-membered aromatic heterocycles both presenting two nitrogen atoms at positions 1 and 3 of the ring. We can observe a weak basic character with a pK_b-imidazole of 7.0, pK_a-imidazole of 14.9⁴⁵⁸ and pK_a-1,2,4-triazole of 10.⁴⁵⁹ These features lead to partially charged molecules in water and therefore are beneficial for the overall polarity and solubility properties. Finally, thanks to similar structural properties, these two nuclei can correspond to our chosen pharmacophore.

Chapter 3. SYNTHESIS OF THE IMIDAZOLE SERIES

The 2-aminoimidazole derivatives possess, in addition to the imidazole core, two aryl groups at defined positions: a phenyl on the extra-cyclic nitrogen, keeping the N-1 free (series A) or a benzyl directly on the intra-cyclic nitrogen, keeping the extra-cyclic nitrogen free (series B). The synthetic routes towards these series A and B are described in this chapter.

3.1 *N*, PHENYL-1*H*-IMIDAZOL-2-AMINE SYNTHESIS (SERIES A)

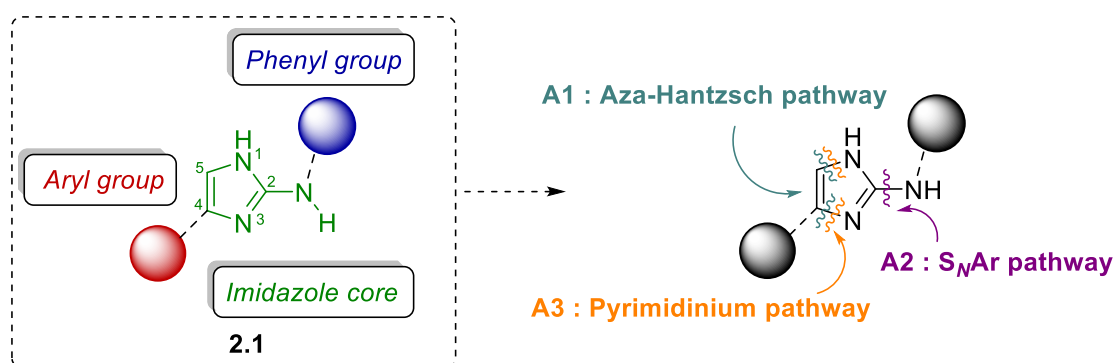


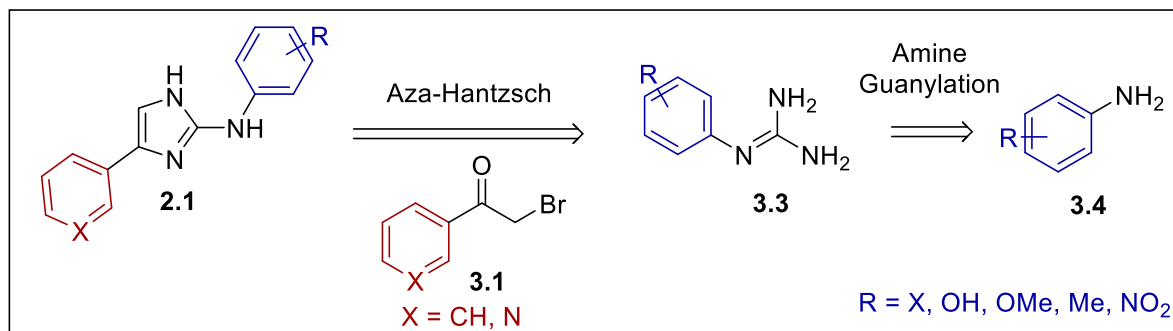
Figure 3-1: Compounds of series A and main retrosynthesis disconnections.

The first target molecule was *N*-phenyl-1*H*-imidazol-2-amine **2.1**, which includes a phenyl on the extra-cyclic nitrogen (in blue, Figure 3-1) and an aryl in position C-4 of the imidazole (in red, Figure 3-1). Three synthetic pathways have been envisaged and attempted to synthesize the molecule **2.1**. The first concerns an aza-Hantzsch reaction from a guanidine intermediate (A1 pathway), the second involves a nucleophilic aromatic substitution (S_NAr) of a thiomethyl derivative by aniline (A2 pathway) and the last requires a nucleophilic addition of hydrazine on a pyrimidinium protected imidazole formed by cyclocondensation and S_NAr (A3 pathway) (Figure 3-1).

3.1.1 A1: Aza-Hantzsch pathway: Unexpected product

The desired imidazole would be obtained through aza-Hantzsch reaction between aryl guanidines **3.3** and bromoacetophenone **3.1a** or chloroacetophenone **3.2a** following a procedure described in the literature by Mahboobi et al.,⁴⁶⁰ then confirmed by Capua et al.⁴⁶¹. Thus, aminoimidazole **2.1** can be

synthesized starting from phenylguanidine **3.3a** and pyridyl-bromoacetophenone **3.1b**. The guanidine intermediates can be obtained from anilines **3.4** through arylguanidine synthesis (Scheme 3-1).

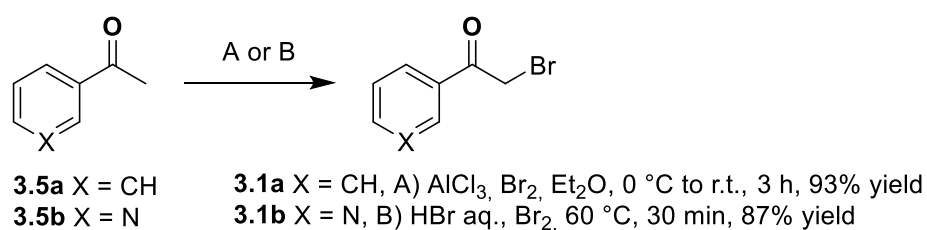


Scheme 3-1: Retrosynthesis of pathway A1.

3.1.1.1 Bromination

The bromination has been carried out by following two procedures depending on the aromatic ring.

- i. The bromination of acetophenone **3.5a** has been carried out with bromine using aluminium chloride catalytic activation in ether at 0 °C for 3 hours to afford product **3.1a** in 93% yield.⁴⁶²
- ii. The synthesis of pyridyl-bromoacetophenone **3.5b** was performed by bromination based on Dornow's work in 1951⁴⁶³ with bromine in aqueous hydrogen bromide solution at 60 °C for 30 minutes to isolate 87% yield of **3.1b** (Scheme 3-2).



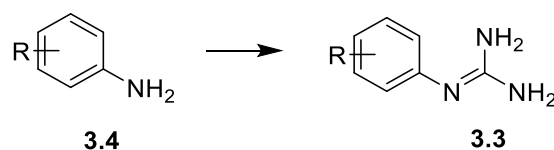
Scheme 3-2: Bromination reactions.

3.1.1.2 Guanidine formation

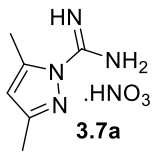
3.1.1.2.1 Literature survey

Several methods for arylguanidine syntheses have been described and they are listed in the table 3-1. The first pathway requires the addition of substituted anilines **3.4** on cyanamide **3.6** in acidic conditions, to obtain a variety of arylguanidines in 36-98% yield.⁴⁶⁴⁻⁴⁶⁸ The second method, based on Scott et al. work in 1953,⁴⁶⁹ was performed with 3,5-dimethylpyrazole guanidine nitrate **3.7a** and aniline **3.4a** or aminophenol **3.4b** to obtain phenylguanidine **3.3a** in 96% yield or hydroxyphenylguanidine **3.3b** in 76% yield. Scott conditions (2 hours of reaction) are shorter than the substitutions on cyanamide **3.6**. Moreover, the use of neat conditions simplifies the purification process.

Table 3-1: State of the art of guanylation synthesis.



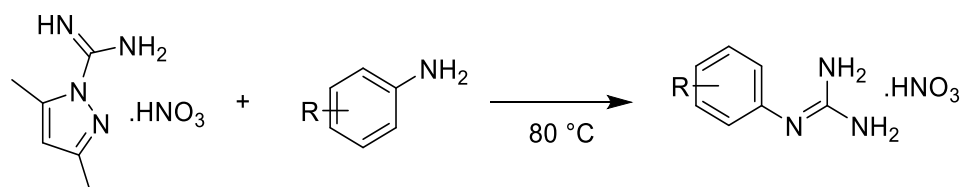
entry	R	Conditions	Yield , %	Limitations	Ref.
1	R=H; 3-OMe; 2-Me-5-Cl	H ₂ NCN 3.6 , HNO ₃ conc., EtOH, 90 °C	82	✓ Good yield	Ha, H. et al. (2008) ⁴⁶⁴
2	<i>Ortho</i> : R=H, Me, CF ₃ , Et, OMe, OCHF ₂ , OEt <i>Meta</i> : R=H, Me, CF ₃ , COMe, NHSO ₂ NH ₂ , OMe <i>Para</i> : H, F, Cl, Me, Et, OMe	H ₂ NCN 3.6 , HNO ₃ , EtOH/H ₂ O, reflux, o.n.	30–98	* Long time treatment (o.n. at 4 °C) * Low yield for phenylguanidine (30% yield)	Diab, S. et al. (2014) ⁴⁶⁵
3	R=H; 4-OMe; 4-tBu; 4-CF ₃ ; CO ₂ Me	H ₂ NCN 3.6 , Sc(OYTf ₃) (10mol%), H ₂ O, 100 °C, 1-2 d	63-88	✓ Moderate to good yield * Long-time reaction	Tsubokura, K. et al. (2014) ⁴⁶⁶
4	R=H.HCl	H ₂ NCN 3.6 , EtOH, Reflux, 40 h	guanidine picrate (69) + aniline HCl (15)	* Still aniline in end * phenylguanidine salt formation * Possible hydrolysatation of cyanamide	Horwitz, J. P. et al. (1958) ⁴⁶⁷
5	R=2-Me, 5-NO ₂	H ₂ NCN 3.6 , HCl, m-cresol/H ₂ O, 100 °C, 10 h	82	✓ Good yield ✓ NO ₂ substituent * Non-common solvent	Ciufolini, M. et al. (2006) ⁴⁶⁸

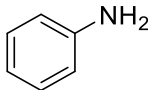
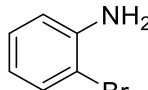
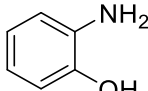
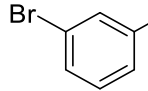
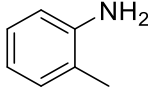
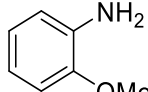
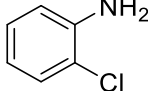
6	R=H	 <p>3.7a</p> <p>reflux, 2h or H₂O, reflux, 1 day</p>	79 or 96	<p>✓ Solvent-free, short-time reaction</p> <p>✓ Good yield</p> <p>* Loss of several 10 eq. or 5eq. of aniline (but can be recovered in Et₂O after treatment)</p> <p>* Need a big dilution of aniline in water to have a dissolution</p>	Scott, F. L. et al. (1953) ⁴⁶⁹
---	-----	---	----------	--	---

3.1.1.2.2 Synthesis

Surprisingly, in our hands, the direct substitution of anilines **3.4** by cyanamide **3.6** failed. By a marked contrast, the use of the Scott conditions⁴⁶⁹ led to the desired products in 54-92% yield (Table 3-2). All these reactions were performed with aniline **3.4** in neat conditions at 75-80 °C for 1.5 hours to 2 days. In the case of aminophenol **3.4b**, water was used as a solvent with less equivalent of aminophenol **3.4b**, due to its high melting point of 190 °C, to obtain hydroxyphenylguanidine **3.3b** in 54% yield.

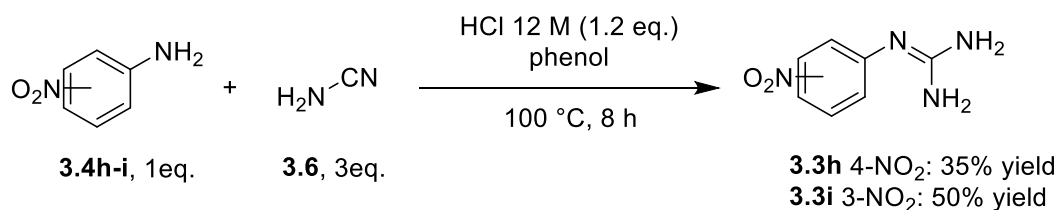
Table 3-2: Aryl guanidine synthesis with Scott method.



entry	Aniline	Time (h)	Yield (%)	entry	Aniline	Time (h)	Yield (%)
1 ^a	 3.4a	2	92 (3.3a)	5 ^a	 3.4e	48	96 (3.3e)
2 ^b	 3.4b	24	54 (3.3b)	6 ^a	 3.4f	16	71 (3.3f)
3 ^a	 3.4c	1.5	82 (3.3c)	7 ^a	 3.4g	24	80 (3.3g)
4 ^a	 3.4d	16	92 (3.3d)				

^aFree-solvent reaction with 10 eq. of aniline. ^bReaction in water with 5.0 eq. of aniline.

Unfortunately, nitroanilines **3.4h-i** were not soluble in water and their high melting point (114-147 °C) led us to use another method, using in phenol as solvent. Thus, we added hydrochloric acid on cyanamide **3.6** at 100 °C for 8 hours.⁴⁶⁸ After purification by silica gel flash chromatography (CH₂Cl₂/MeOH, 10/0 then 9/1), the nitrophenylguanidine **3.3h** and **3.3i** were obtained with 35% and 50% yield respectively (Scheme 3-3). All these guanidines were directly used in the next aza-Hantzsch step.

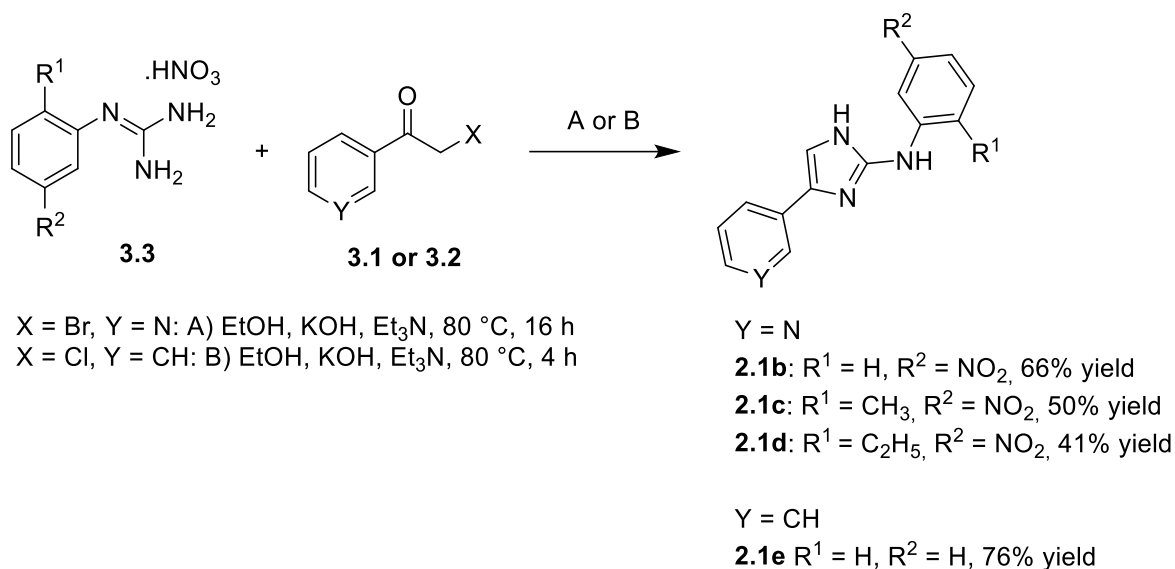


Scheme 3-3: Aryl guanidine synthesis from Ciufolini et al. method.

3.1.1.3 Aza-Hantzsch

3.1.1.3.1 Literature survey

In 2009, Mahboobi et al.⁴⁶⁰ synthesized different imidazoles with aryl group substituted in the extra-cyclic nitrogen and with a pyridine ring in position C-4 of the imidazole, starting from the substituted-guanidine **3.4** and bromoacetophenone **3.1**. This reaction was conducted in basic media in ethanol, at 80 °C to obtain four required products **2.1b-d** in 41-76% yield (Scheme 3-4). Moreover, Capua et al.⁴⁶¹ confirmed, the work of Mahboobi et al., synthesizing several triaryl-substituted imidazoles **2.1** in the same conditions, starting from substituted-guanidine **3.3** and chloroacetophenone **3.2**.



Scheme 3-4: Examples of aza-Hantzsch reaction in the literature.

3.1.1.3.2 Methodological study

A variety of conditions were screened for the aza-Hantzsch reaction (Table 3-3). Unfortunately, product **3.8** was obtained instead expected product **2.1** (see below).

First, we demonstrated the requirement of using a base (entries 1, 2), then the Mahboobi et al. conditions were applied after freebasing of guanidine **3.3a**. The addition of triethylamine and pyridyl-bromoacetophenone **3.1b** at room temperature overnight led only to a partial conversion (entry 3). LCMS showing a major polar peak with two mass compounds inside: the product **3.8a** and a side-product, expected to be 1,3-diphenylguanidine **3.9**. Unfortunately, the product **3.8a** was not isolated due to its very high polarity (no migration on silica gel using CH₂Cl₂/MeOH, 9/1 as mobile phase).

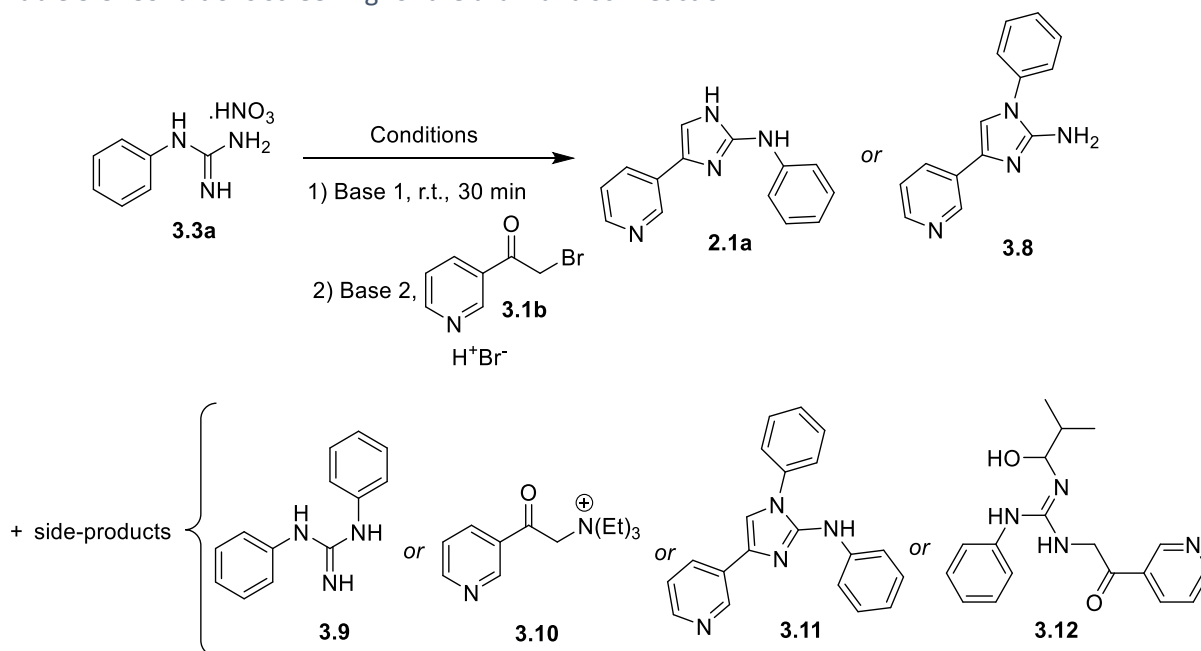
To overcome these problems, we attempted two procedures: (i) the introduction of a strong base to freebase guanidine **3.3a** first, followed by the introduction of (pyridyl)-bromoacetophenone **3.1b** with a weak base to catch salt; (ii) the introduction of a single strong base: to identify if the reaction requires the guanidine freebasing or weak to the salt catching.

- i. However, the use of the first approach did not reach the desired product:
 - The utilisation of a strong base (KOH or ^tBuOK) with a weak base (Et₃N or NaHCO₃) led to a mixture of product **3.8a** in mixture with side-products **3.9** or possible *N,N,N*-triethyl-2-oxo-2-(pyridin-3-yl)ethan-1-aminium **3.10** (entries 3-7).
 - The replacement by only strong bases (KOH or NaH) led to degradation (entry 8).

- The introduction of a Lewis acid (AlCl_3) instead of the base did not give conversion (entry 9).
- ii. The second approach is divided by:
 - The utilisation of only a strong base in various solvents led to a partial conversion of 53% with $t\text{BuOK}$ in dioxane (entries 11).
 - The replacement by weak bases Et_3N in ethanol led to a mixture of product **3.8a** with side product, expected to correspond to *N*-1-diphenyl-4-(pyridin-3-yl)-1H-imidazol-2-amine **3.11** (entry 13). In isopropanol, the product **3.8a** was formed with side product, expected to correspond to 2-(1-hydroxy-2-methylpropyl)-1-(2-oxo-2-(pyridin-3-yl)ethyl)-3-phenyl-guanidine **3.12** (entry 14). Finally, in dioxane, by increasing the equivalents number of Et_3N up to 5.5, the product **3.8a** has been isolated in 30% yield (entry 15).

Of note, our results showed an advantage to use guanidine **3.3a** in a salt form rather than as free base to avoid the formation of 1,3-diphenylguanidine **3.9**.

Table 3-3: Conditions screening for the aza-Hantzsch reaction.



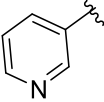
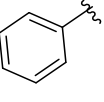
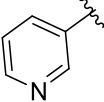
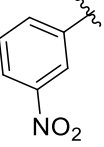
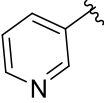
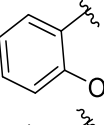
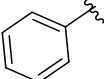
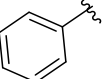
entry	Base 1	Base 2	Solvent	T (°C)	Reaction time (h)	Conversion ^b (Yield), %
1	-	-	EtOH	80	16	n.c.
2	-	-	iPrOH	80	16	n.c.
3	KOH (1 eq.)	Et ₃ N (3 eq.)	EtOH	80	16	n.d. (mixture of 3.8a and side products 3.9)
4	^t BuOK (1 eq.)	Et ₃ N (2-3 eq.)	EtOH	r.t. to 80	16	Mixture of 3.8a (38%) and side product 3.10 (38%)
5	KOH (1 eq.)	NaHCO ₃ (3 eq.)	EtOH	80	16	n.d. (mixture of 3.8a and side products 3.9)
6	KOH (1 eq.)	Et ₃ N (2-3 eq.)	nBuOH	110 (MW)	1-3	Traces of 3.8a
7	KOH (1 eq.)	Et ₃ N (2-3 eq.)	DMF	r.t. to 150	72	Mixture of 3.8a , 3.9 (38%), side product 3.10 (28%) and possible degradation (34%)
8	KOH (1 eq.)	NaH (2 eq.)	Dioxane	r.t. to 80	24	Mixture of 3.8a , 3.9 (25%) and degradation (75%)
9	KOH (1 eq.)	AlCl ₃	Dioxane	80	72	n.c.
10	^t BuOK (1-4 eq.)	-	EtOH			n.c.
11	^t BuOK (1-3 eq.)	-	Dioxane	r.t.	48	Mixture of 3.8a (53%) and 3.3a (47%)
12	KOH (1-3 eq.)	-	DMF	r.t.	72	n.c.
13	-	Et ₃ N (3 eq.)	EtOH	80	16	n.d. (mixture of 3.8a and side-products 3.11)
14	-	Et ₃ N (2-3 eq.)	iPrOH	80	24	Mixture of 3.8a (39%) and side product 3.12 (61%)
15	-	Et ₃ N (5.5 eq.)	Dioxane	r.t.	5.5	n.d., 30% yield ^c (3.8a)

^aReaction and conditions: **3.3a** (1.0 mmol), **3.1b** (1.0 mmol), solvent (8 mL). ^bCalculate by the ratio between products and reagent **3.3a**. Reaction followed by LCMS (D.A.D.) ^cIsolated yield. MW: microwave irradiation. n.d.: not determined. n.c.: no conversion.

The best conditions (Et₃N, 5.5 eq., in dioxane at room temperature for 5.5 hours) were applied to the synthesis of three arylguanidines **3.8a-b**, **e-f**: unsubstituted, substituted by an electron-withdrawing group (3-NO₂),⁴⁶⁰ and by an electron donor group (2-OMe) (Table 3-4).

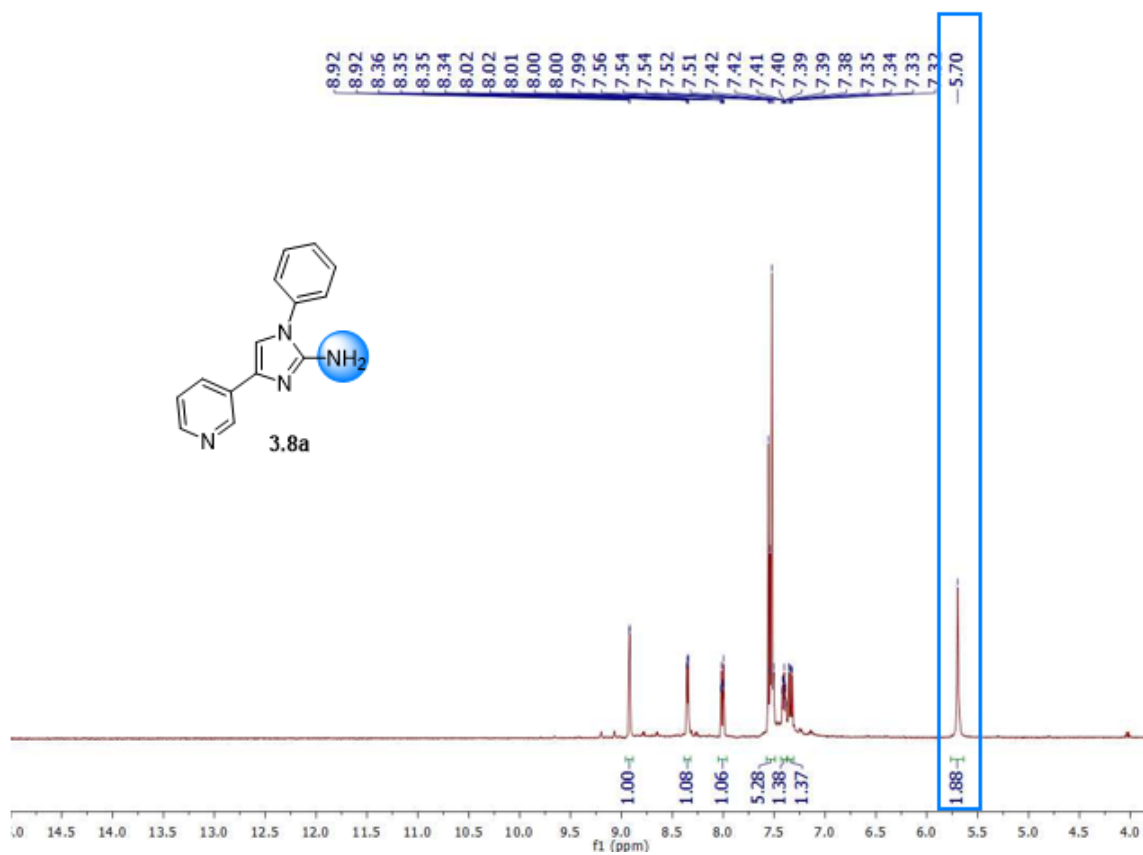
Importantly, we observed discrepancies with the product described in the literature. Indeed, the aza-Hantzsch product in the literature⁴⁶⁰ was described as *N*-(3-nitrophenyl)-4-(pyridin-3-yl)-1*H*-imidazol-2-amine **2.1**. However, we obtained a regioisomer, 1-(3-nitrophenyl)-4-(pyridin-3-yl)-1*H*-imidazol-2-amine **3.8** with intra-cyclic nitrogen substitution (Table 3-4).

Table 3-4: *N*, phenyl-1*H*-imidazol-2-amine obtained.

Entry	R ¹	R ²	Yield (%)
1			16 (3.8a)
2			54 (3.8b)
3			26 (3.8c)
4			18 (3.8d)

The careful examination of ¹H NMR of **2.1**,⁴⁶⁰ revealed some anomalies, notably for the description of both intra- and extra-cyclic nitrogen, described at 6.0 ppm. Furthermore, Capua et al.⁴⁶¹ publication described the triaryl-substituted imidazole as substituted by aryl groups in intra- and extra-cyclic nitrogen positions and by a phenyl ring in C-4 **3.13** (in the place of pyridine ring), hence the regioselectivity problem was not applicable. However, one example of 1*H*-diaryl-substituted imidazole **2.1e**, described in extra-cyclic nitrogen and C-4 positions with a shift characterization at 4.90 ppm explaining the exchange of the 2 NH (N-1, N²) groups with D₂O. However, a previous work of Little and Webber in 1994⁴⁷⁰, on the imidazole formation, showed a shift of the proton carried by intra-cyclic nitrogen at 12 ppm whereas the extra-cyclic nitrogen would correspond to 7.07 ppm. Likewise, an imidazole protected by a Boc group had a shift of NH at 10.32 – 10.5 ppm.⁴⁷¹ Finally, in 2016, Iwata et al.⁴⁷² explained that starting from a guanidine with methyl fumaraldehyde **3.14** under basic conditions (Et₃N (1.0 eq.), NaOMe, MeOH) at room temperature will form the imidazole with the free extra-cyclic nitrogen (*in situ* reaction, non-isolated product).

Similarly, we obtained the characteristic shift at 6.0 ppm corresponding to 1,4-diaryl-1*H*-imidazol-2-amine **3.8** with unsubstituted extra-cyclic nitrogen and substituted intra-cyclic nitrogen (Figure 3-2). Even if R¹ is a phenyl or pyridine ring or if we introduce different groups, the same shift at 6 ppm has been noted. In the literature, the unsubstituted intra-cyclic nitrogen of an imidazole should be more de-shielded. This hypothesis will be demonstrated in the later in the manuscript



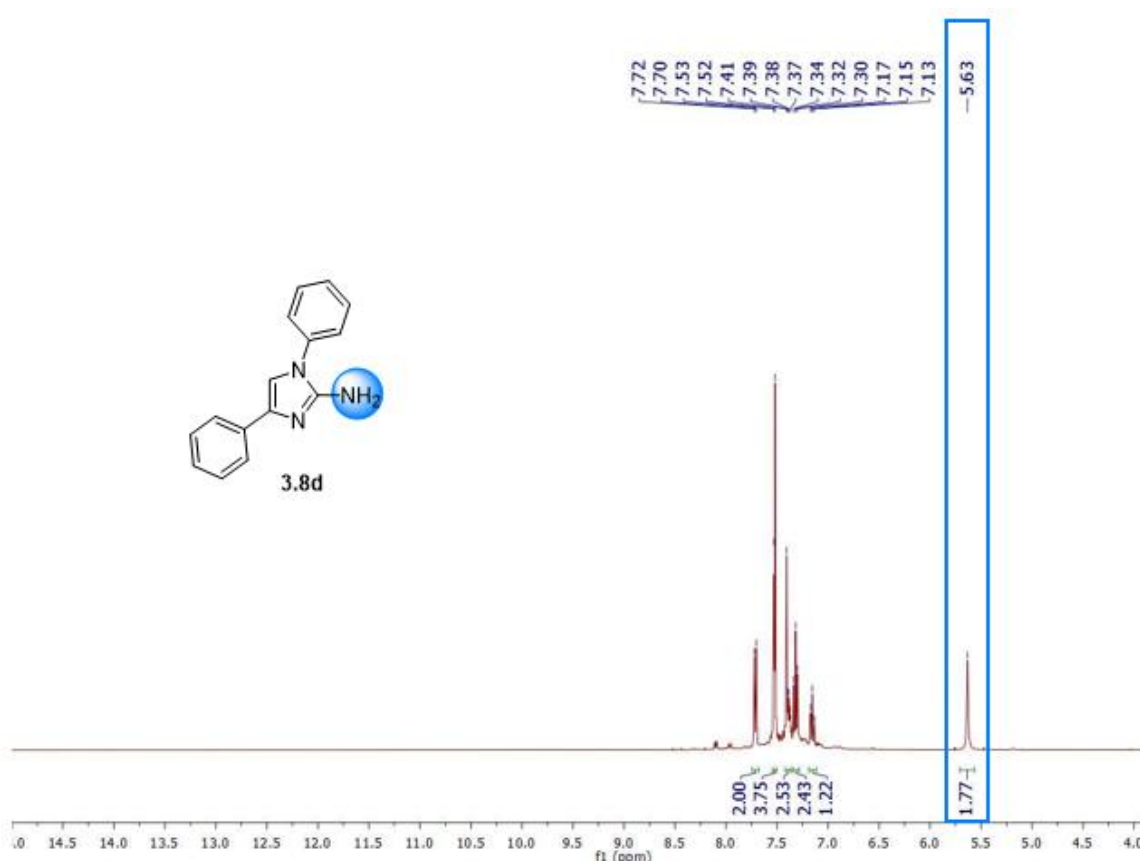
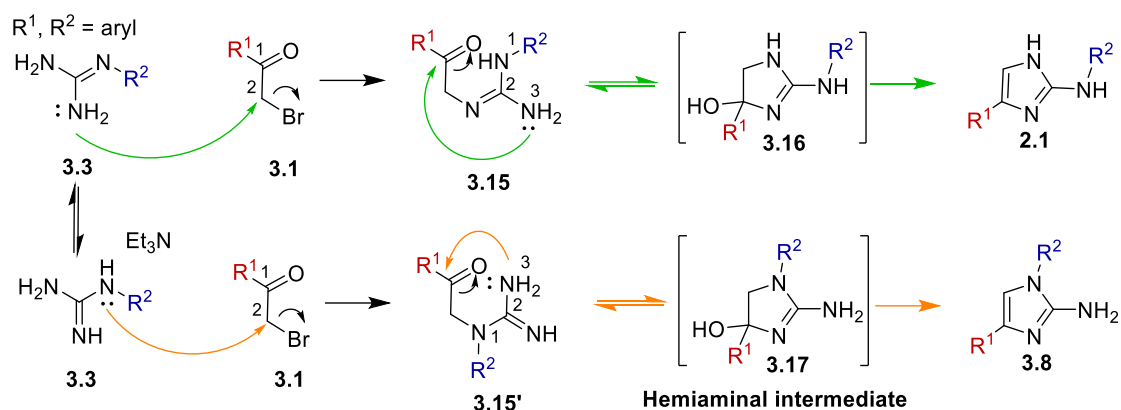


Figure 3-2: ¹H NMR of 1-(3-nitrophenyl)-4-(pyridin-3-yl)-1*H*-imidazol-2-amine **3.8a** and 1,4-diphenyl-1*H*-imidazol-2-amine **3.8d** with the unsubstituted extra-cyclic nitrogen.

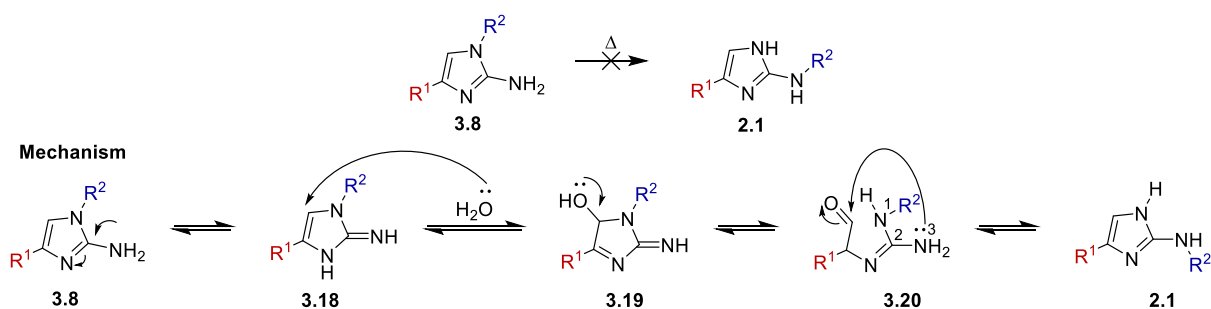
This result can be explained by the proposed mechanism of the aza-Hantzsch reaction depicted in Scheme 3-5. We hypothesized that the first step is the nucleophilic substitution to carbon C-2 of **3.1** by guanidine **3.3** to form **3.15**. Then, the second nucleophilic addition occurs by the nitrogen N-3 of guanidine **3.15** to generate the hemiaminal **3.16**. This hemiaminal **3.16** undergoes water dehydration to access to the desired regioisomer *N*-phenyl-4-(aryl)-2,3-dihydro-1*H*-imidazol-2-amine **2.1** (green path, Scheme 3-5). However, the nitrogen N-1 of guanidine **3.3**, despite its steric hindrance, will produce the first nucleophilic substitution to attain guanidine intermediate **3.15'**. After the second nucleophilic addition to form **3.17** and dehydration, the undesired regioisomer 1-phenyl-4-(aryl)-2,3-dihydro-1*H*-imidazol-2-amine **3.8** has been reached (orange path, Scheme 3-5). This configuration was explained by the pKa of phenyl guanidine of 9.70² deprotonated by triethylamine (pKa = 10.78) rendering this nitrogen N-1 of **3.3** more available to produce the nucleophilic substitution.

² Values was predicted with the ChemAxon calculator



Scheme 3-5: Supposed mechanism of the desired regioisomer *N*-aryl-2-aminoimidazole **2.1** and undesired regioisomer 1-aryl-2-aminoimidazole **3.8**.

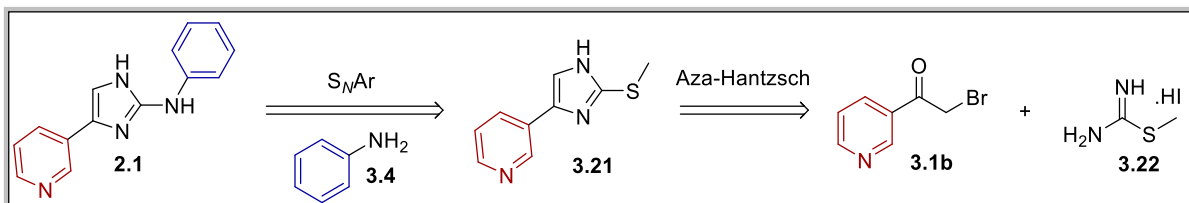
In the end, a Dimroth rearrangement was attempted at 125 °C to transfer R^2 group from the intra-cyclic nitrogen to the extra-cyclic one. The mechanism proceeds *via* the nucleophilic addition of a water molecule to the electrophilic carbon C-5 of **3.18** to form an hemiaminal intermediate **3.19**, and subsequent ring-opening. Secondly, by nucleophilic addition of the N^2 on the electrophilic carbon of carbonyl **3.20**, the desired imidazole **2.1** was formed (Scheme 3-6). Nevertheless, the degradation of the product **3.8** was observed without conversion into the desired imidazole.



Scheme 3-6: Supposed mechanism of Dimroth rearrangement.

3.1.2 A2: S_NAr pathway

Another straightforward pathway consisting of aza-Hantzsch reaction from pyridyl-bromoacetophenone **3.1b** and methyl carbamimidothioate hydroiodide **3.22**, after *S*-methylation, to obtain thiomethyl imidazole pyridine **3.21**, as key intermediate bearing a thiomethyl leaving group. Then, this leaving group can be substituted by aniline through an aromatic nucleophilic substitution (S_NAr) (Scheme 3-7).



Scheme 3-7: Retrosynthesis through 2-(methylthio)-4-pyridin-1H-imidazole **3.21**.

3.1.2.1 Literature survey

First, in 2010, Laufer et al.⁴⁷³ developed a synthesis on *N*-Benzylidene-4-(4-fluorophenyl)-2-methylthio-1H-imidazol-1-amine **3.24** by introducing a protective group, phenylmethanimine on the nitrogen of imidazole. The product was obtained in 81% yield with sodium bicarbonate in acetonitrile at 75 °C for 3 hours. In 2017, Laufer et al.⁴⁷⁴ reproduced the conditions by replacing the solvent by a THF/H₂O: 4/1 mixture at reflux and without phenylmethanimine group to isolate the same desired product **3.21b** in 50% yield (and a range of 15-65% yield for various alkyl or aryl group).

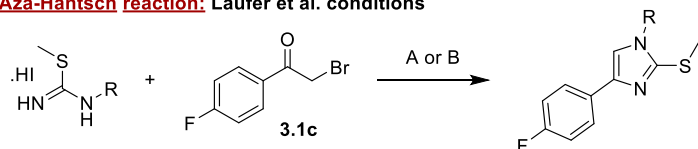
Concerning the S_NAr , several conditions exist, and they depend on the leaving group. In the case of thiomethyl, Li et al.⁴⁷⁵ developed a method in 2-propanol at 80 °C for 2 hours to isolate **3.27** in 80% yield.

In the case of methylsulfinyl, three conditions were performed.

- i. By using a strong base, from 1-methyl-2-(methylsulfonyl)-5-nitro-1H-imidazole **3.28** in sodium hydride allowed to isolated **3.29** in a low 11% yield (Sudarsanam et al. conditions).⁴⁷⁶
- ii. By using a weak base, from the substitution of benzoimidazole **3.30** by methyl sulfonamide with an excess of aniline **3.4a** (5 equivalents) and triethylamine at 120 °C for 2 hours to obtain *N*-phenyl-1H-benzo[*d*]imidazol-2-amine **3.31** in 69% yield (Lan et al. conditions).⁴⁷⁷
- iii. By using microwave irradiation, from the addition of the aniline **3.4a** on imidazopyridine in acetonitrile at 160 °C under microwave irradiation for 40 min to obtain **3.33** in 24% (Lukasik et al. conditions).⁴⁷⁸

At last, in the case of phenylsulfinyl, D'Sidocky et al. described a method from a substituted imidazole **3.34** and primary amine **3.35**, using a strong base, *n*-BuLi, in dioxane/hexane at 0 °C for 30 min to isolate **3.36** in 40% yield.⁴⁷⁹

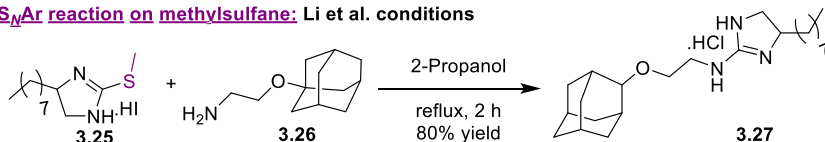
Aza-Hantzsch reaction: Laufer et al. conditions



3.23 R = Phenylmethanimine
3.22 R = H

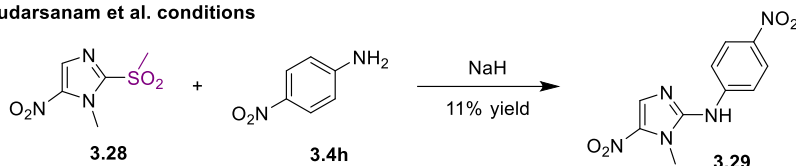
3.24 R = Phenylmethanimine, A) NaHCO₃, CH₃CN, 75 °C, 3 h, 81%
3.21b R = H, B) NaHCO₃, THF/H₂O, reflux, 45 min, 50%

S_NAr reaction on methylsulfane: Li et al. conditions

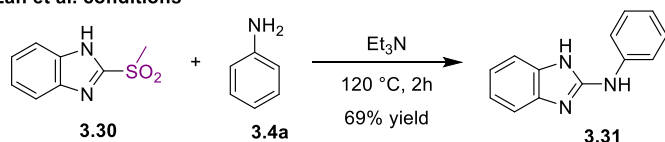


S_NAr reaction on methylsulfonyl:

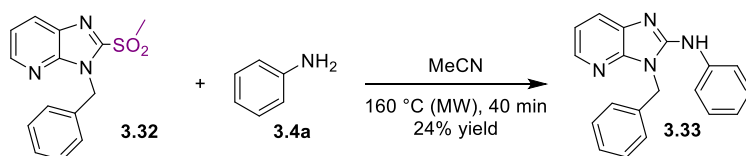
Sudarsanam et al. conditions



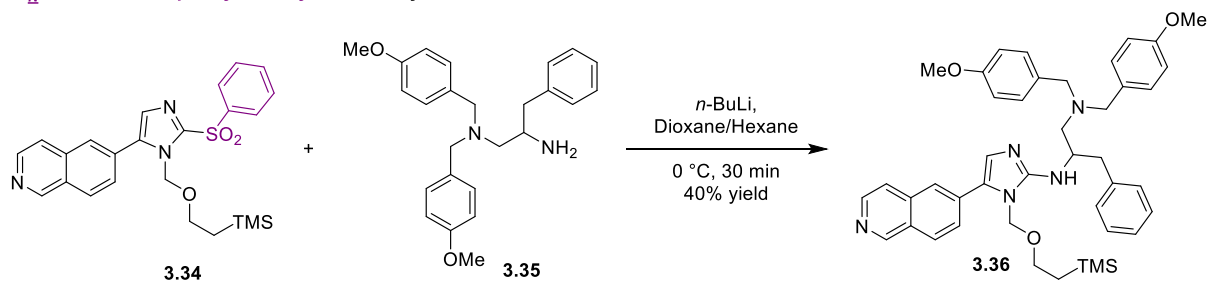
Lan et al. conditions



Lukasik et al. conditions



S_NAr reaction on phenylsulfonyl: D'Sidocky et al. conditions



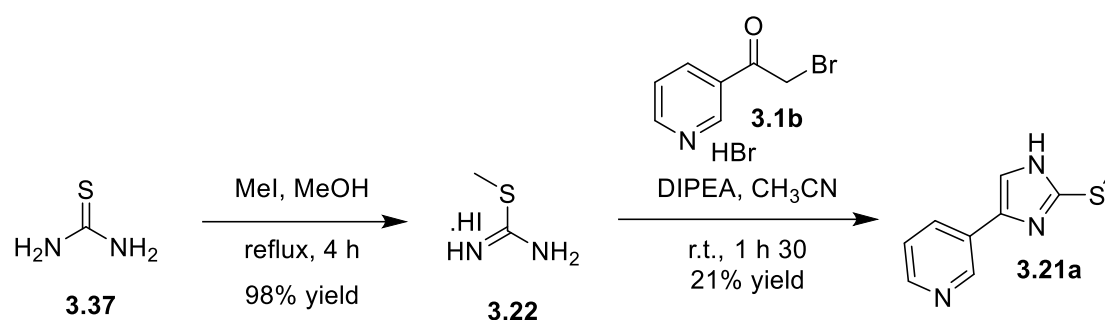
Scheme 3-8: State of the art for pathway A2.

3.1.2.2 Methodological study

Firstly, the methylation of thiourea **3.37** was performed with iodomethane in refluxing methanol⁴⁸⁰, leading quantitatively to **3.22**, 98% (Table 3-5). The second step of the aza-Hantzsch reaction to isolate

thiomethyl imidazolepyridine **3.21**, never characterized before, was based on the work of Laufer et al. of 2017.⁴⁷⁴ We replaced 4-fluoro phenyl **3.21b** with pyridine ring to isolate **3.21a** in 19%. We tried to optimize these conditions by taking the first condition of Laufer et al.⁴⁷³ with sodium bicarbonate in acetonitrile at 80 °C to isolate only 1% of **3.21a**. However, changing the base with DIPEA at room temperature led to 21% of **3.21a**.

Table 3-5: Screening conditions for aza-Hantzsch reaction in pathway A2.



entry	Base	Solvent	T (°C)	Reaction time (h)	Yield ^b
1	NaHCO ₃ (3eq.)	THF/H ₂ O	80	1.5	19% yield
2	NaHCO ₃ (3eq.)	CH ₃ CN	75	16	1% yield
3	DIPEA (4eq.)	CH ₃ CN	r.t.	1.5	21% yield
4	Et ₃ N	EtOH	r.t. to 80	48	n.d. (mixture of 3.21a and side product)
5	DBU	CH ₃ CN	r.t.	1.5	n.d. (mixture of 3.21a and side product)
6	-	Pyridine	50		n.c.

^aReaction and conditions: **3.22** (1.0 mmol), **3.1b** (1.0 mmol), bases (3.0 mmol), solvent (2-3 mL).

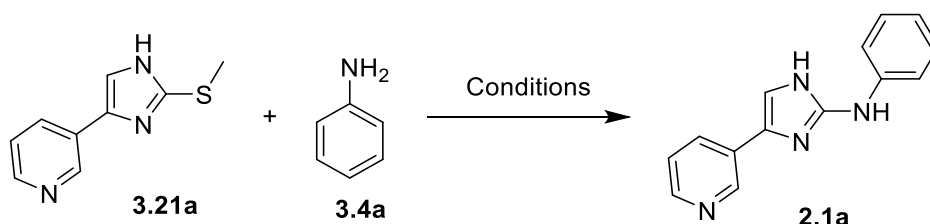
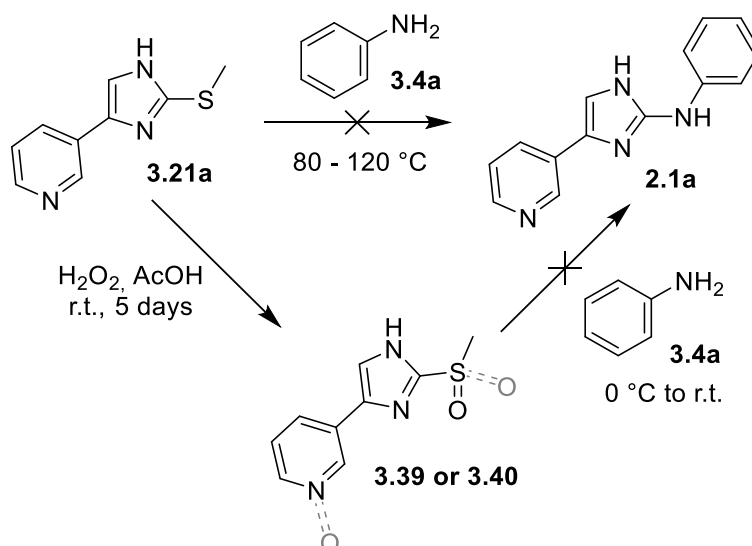
^bReaction followed by LCMS (D.A.D.). n.d.: not determined. n.c.: no conversion.

First, following Li et al. protocol⁴⁷⁵ aromatic nucleophilic substitution using thiomethyl as leaving group was tried with **3.21a** at 80 °C, in isopropanol or in aniline **3.4a** as solvent, without observing conversion (Table 3-6, entries 1-2). The same result had been noted based on an adapted procedure from D'Sidocky et al.,⁴⁷⁹ using *n*-BuLi in dioxane (entry 3).

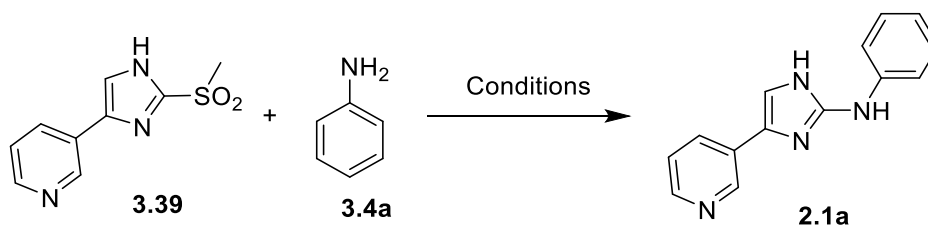
Secondly, we attempted to oxidize the sulphur atom to sulfone to create a better leaving group. A similar protocol of Lan et al. or Lankasik et al. with a methylsulfonyl group was attempted.^{477,478} To that end, two sulfur oxidation conditions were tested: (i) using *m*-CPBA in dichloromethane, that lead to

the detection of mono-oxidized and di-oxidized products and, (ii) using 2 equivalents of hydrogen peroxide in glacial acetic acid, which shows after two days 55% mono-oxidized product **3.38** and 42% di-oxidized product **3.39**; after five days 88% of di-oxidized **3.39** has been observed by LCMS. It is believed that the sulfoxide oxidation to sulfone is more difficult to achieve, which could explain the easy access to sulfoxide. This last method allows obtaining 36% yield of the di-oxidized product **3.39**. This product **3.39** is then used following the same methods of D'Sidocky et al.⁴⁷⁹ with *n*-BuLi in dioxane but, only traces of the product **2.1a** were then observed. We hypothesized that the second oxidation carried out not on sulphur to reach 3-(2-(methylsulfonyl)-1*H*-imidazol-4-yl)pyridine **3.39** but could have been on the nitrogen of the pyridine to lead 3-(2-(methylsulfinyl)-1*H*-imidazol-4-yl)pyridine 1-oxide **3.40** (entry 4).

Table 3-6: Screening conditions for S_NAr reaction in pathway A2.



entry	Base	Solvent	T (°C)	Reaction time (h)	Conversion ^b (Yield), %
1	-	iPrOH	80	24	n.c.
2	-	-	80 - 120	24	n.c.
3	<i>n</i> -BuLi	Dioxane	0 to r.t.	48	n.c.



4	<i>n</i> -BuLi	Dioxane	0 to r.t.	48	n.d. (traces of 2.1a)
---	----------------	---------	-----------	----	-------------------------------

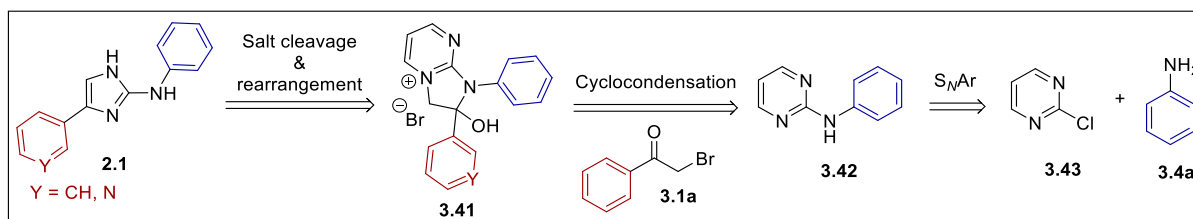
^aReaction and conditions: **3.21a** or **3.39** (1.0 mmol), **3.4a** (1.8 mmol), bases (1.8 mmol), solvent (2 mL).

^bCalculate by the ratio between products and reagents **3.21a** or **3.39**. Reaction followed by LCMS (D.A.D.). n.d.: not determined. n.c.: no conversion.

Finally, due to unsatisfactory results, pathway A2 was abandoned to concentrate our efforts on pathway 3 to reach our pharmacophore.

3.1.3 A3: Pyrimidinium pattern pathway

The last pathway relies on the use of a pyrimidinium salt **3.41**, a **protected aminoimidazole pattern**. After cleavage and rearrangement, the desired substituted aminoimidazole **2.1e** can be reached. The straightforward synthesis starts with the S_NAr of chloropyrimidine **3.43** by aniline **3.4a** to form amino-pyrimidine **3.42** in order to introduce our aryl on extra-cyclic nitrogen of imidazole. Then, a cyclocondensation has been achieved with bromoacetophenone **3.1a** to form 2-hydroxy-1,2-diphenyl-2,3-dihydro-1*H*-imidazo [1,2-*a*] pyrimidin-4-ium bromide salt **3.41**, a key intermediate and allowing the second aryl introduction. The last step is the nucleophilic addition of hydrazine, followed by the cleavage of a pyrimidinium salt leading to the *N*²-substituted aminoimidazole product **2.1** (Scheme 3-9).⁴⁸¹

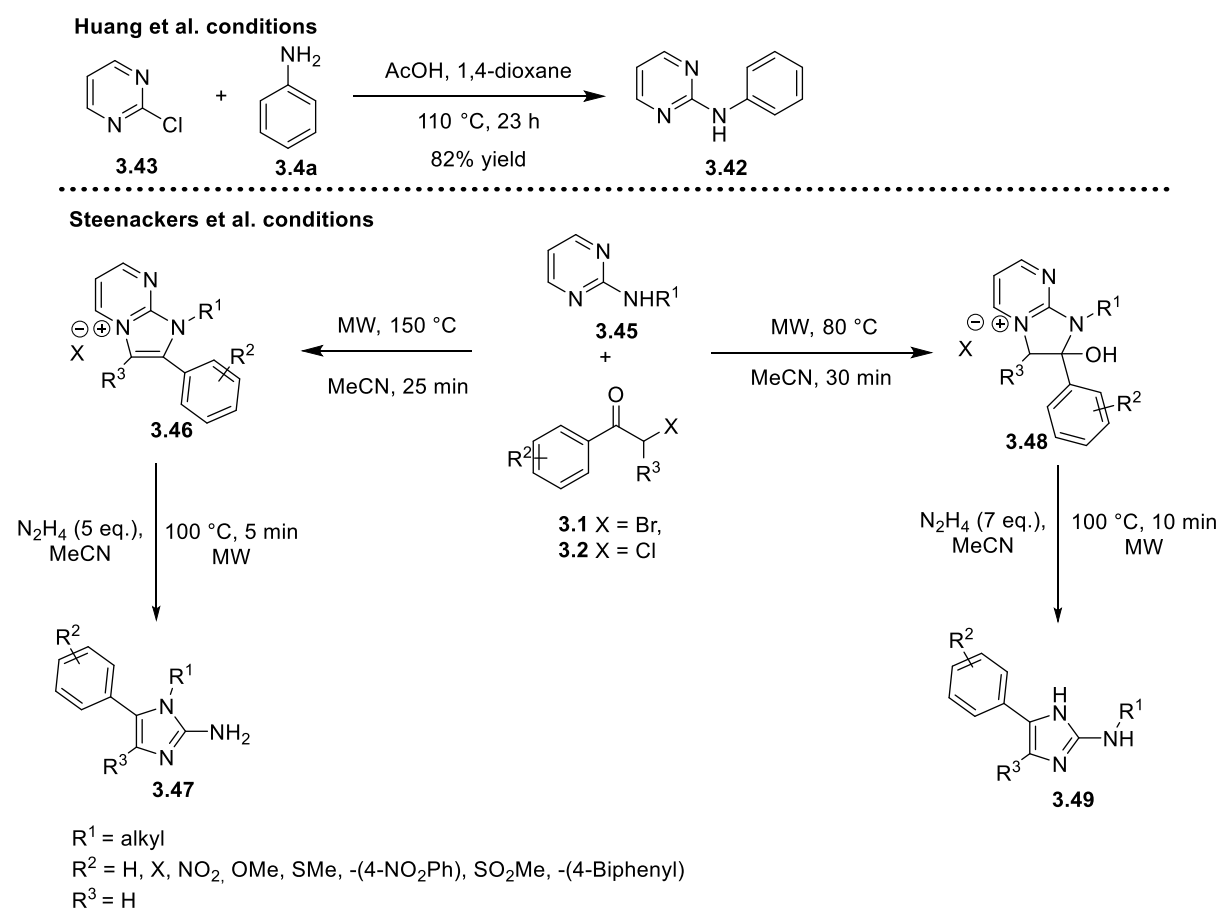


Scheme 3-9: Retrosynthesis from chloro-pyrimidine starting.

3.1.3.1 Literature survey

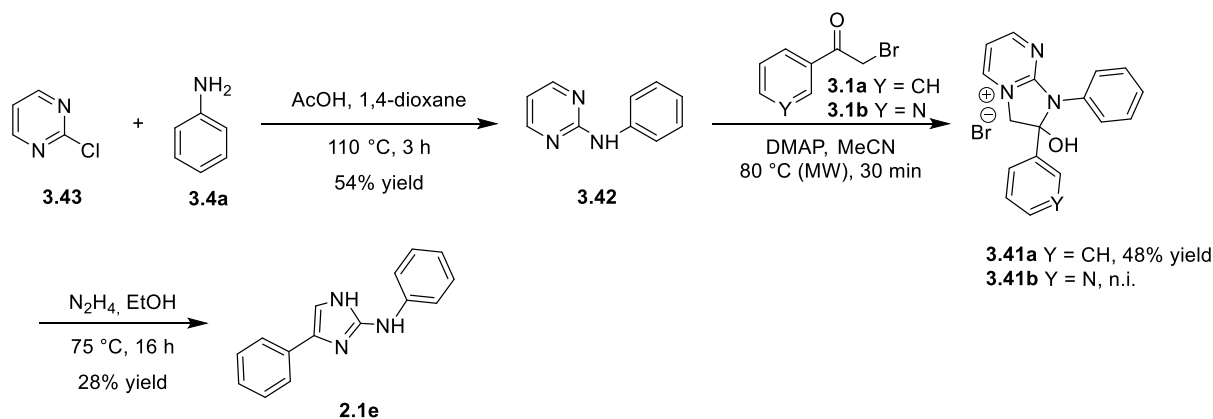
The S_NAr first step was widely developed, foremost in 2011 by Delvos et al.⁴⁸² with the use of an *o*-tolylzinc (II) agent bromide **3.44** in acetonitrile for 5 hours at room temperature with 87% yield. Then, methods based on the Buchwald-Hartwig amination gave **3.42** in 44% yield (developed by the Hao et al.⁴⁸³ in 2012 and 88% yield in 2014 by Shaw et al.⁴⁸⁴). Another simple method was developed under acetic acid and dioxane conditions in 2014 by Huang et al.⁴⁸⁵ at 110 °C for 23 hours in 82% yield (Scheme 3-10).

The pyrimidinium salt formation **3.41**, is based on the publication of Steenackers et al.,⁴⁸¹ which has shown two pathways to isolate intra-cyclic substituted aminoimidazole **3.47** or extra-cyclic substituted aminoimidazole **3.49**. These pathways dependent on the hydroxy group at position 2 of the salt, obtained or not thanks to temperature changes in a microwave (80 °C to keep it and 150 °C to not). The last nucleophilic addition of hydrazine is similar in both cases but, the elimination of water allowed the rearrangement to isolate N^2 -substituted aminoimidazole **3.49** (Scheme 3-10, yield not disclosed).



Scheme 3-10: State of the art of A3 pathway.

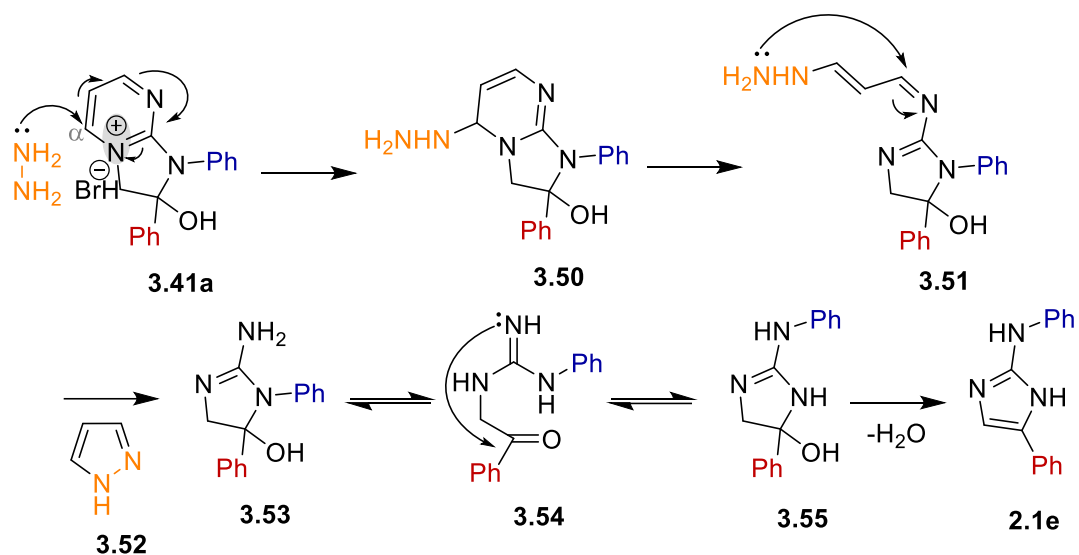
3.1.3.2 Synthesis



Scheme 3-11: Synthesis of *N*,4-diphenyl-1*H*-imidazol-2-amine **2.1e**. n.i.: not isolated.

The Huang et al. conditions⁴⁸⁵ were reproduced for chlorine substitution (S_NAr) with aniline in total conversion for 3 hours leading after purification to **3.42** in 54% yield. Then, the next cyclisation was performed at 80 °C for 30 minutes by microwave irradiation following the Steenackers et al.⁴⁸¹ protocol allowing to isolate 2-hydroxy pyrimidinium **3.41**. In the case of bromoacetophenone **3.1a**, product **3.41a** was easily recovered by filtration of the precipitate appearing upon cooling down of the reaction mixture. Unfortunately, no conversion to the desired product **3.41b** was observed in the case of pyridyl-bromoacetophenone **3.1b**, limiting the reproducibility of this reaction for the pyridine group in *N*-2-aminoimidazole **2.1a**. **3.41a** was directly mixed with hydrazine hydrate in ethanol at 75 °C overnight to obtain our desired amino imidazole of series A **2.1e** (Scheme 3-11).

The mechanism of this last step corresponds to the nucleophilic addition of hydrazine on electrophilic carbon in α position of the positive nitrogen of **3.41a**, depleted in electrons by the presence of this positive nitrogen. The second free nucleophilic amine of hydrazine attacks another electrophilic carbon to eliminate 1-*H*-pyrazole **3.52**. In this way, the unprotected aminoimidazole will undergo a rearrangement similarly to Dimroth rearrangement by water elimination to isolate **2.1e** (Scheme 3-12).



Scheme 3-12: Mechanism of pyrimidinium salt **3.41a** cleavage.

Finally, ^1H NMR analysis allowed to confirm the isolation of extra-cyclic nitrogen substituted aminoimidazole **2.1e** and not its intra-cyclic nitrogen substituted regioisomer **3.8d** such as in pathway A1. Indeed, the nitrogen N-1 of imidazole was observed at 10.85 ppm (in pink, Figure 3-3) and the extra-cyclic nitrogen N^2 linked to phenyl at 8.74 ppm (in green, Figure 3-3). This result is in contradiction to Capua et al. publication⁴⁶¹ which explained that both intra- and extra-cyclic nitrogen were exchangeable in D_2O at 4.90 ppm.

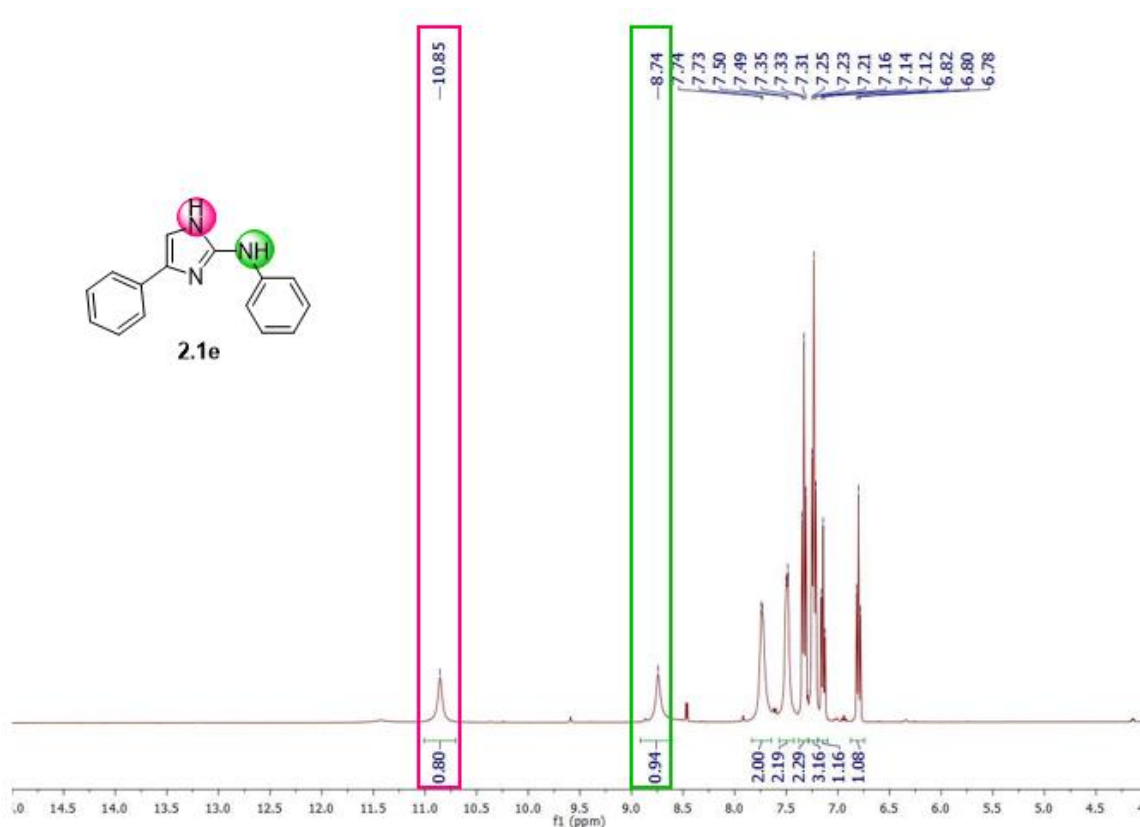


Figure 3-3: ^1H NMR of *N*,4-diphenyl-1*H*-imidazol-2-amine **2.1e**.

To summarize, thanks to isolation and NMR analysis in paths A1 and A3, both regioisomers intra-cyclic nitrogen substituted imidazole **3.8a-d** and extra-cyclic nitrogen substituted imidazole **2.1e** have been identified. Unfortunately, pathway A3 was not applicable for pyridyl derivative of **2.1a**.

3.2 1-BENZYL-1*H*-IMIDAZOL-2-AMINE SYNTHESIS (SERIES B)

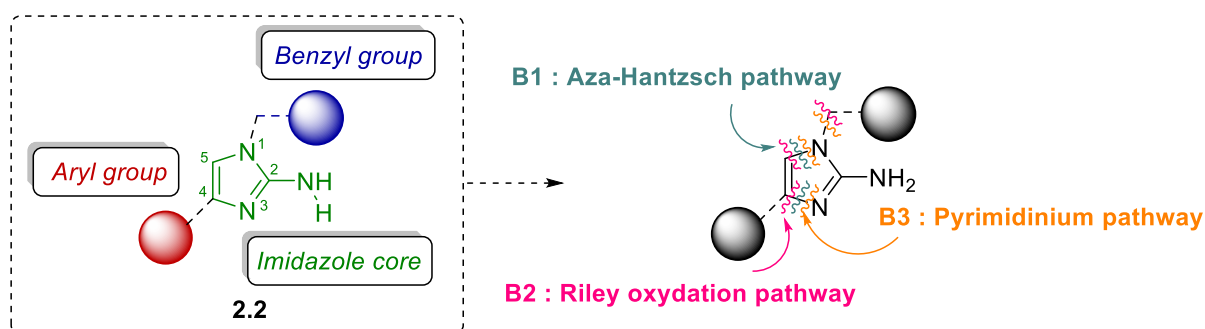
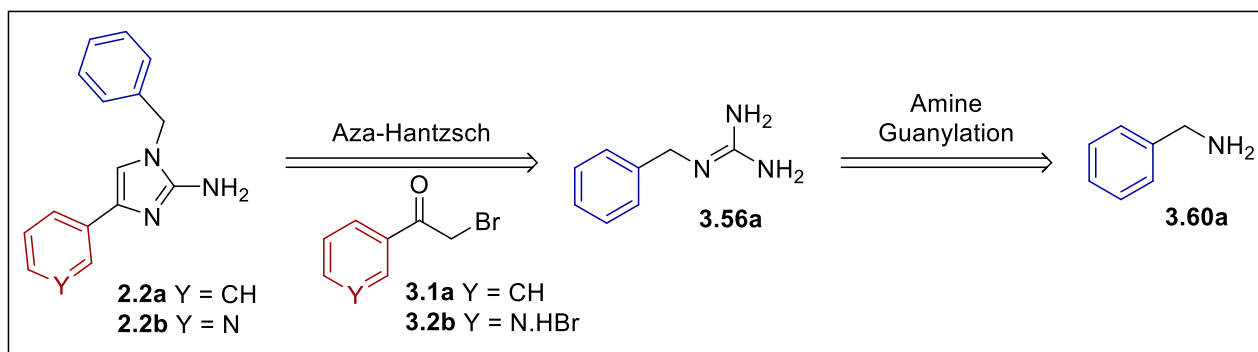


Figure 3-4: Compounds of series B and main retrosynthesis disconnections.

The introduction of benzyl group on the intra-cyclic nitrogen of 1*H*-imidazol-2-amine substituted by an aryl allow to reach the pharmacophore *via* the compound **2.2** (Figure 3-4). This series of 1-benzyl-2-aminoimidazole starting from benzylamines has been designed to increase the flexibility of the aminoimidazole and potentially increase the water solubility properties. Three pathways have been attempted: (i) aza-Hantzsch reaction from benzylguanidine **3.56** intermediate (B1 pathway), (ii) through 2-oxo-2-(pyridin-3-yl)acetaldehyde **3.57**, product of Riley's oxidation, to undergo cyclocondensation and benzylation steps (B2 pathway), and (iii) through 1*H*-imidazo pyrimidinium **3.59** key intermediate allowing the imidazole liberation by hydrazine addition similar to A3 pathway (B3 pathway, Figure 3-4).

3.2.1 B1: Aza-Hantzsch pathway

The formation of these products would be carried out in two steps, reproducing the path A1 strategy. First, the formation of benzylguanidine **3.56** is synthesized, then, this intermediate is cyclized through an aza-Hantzsch reaction with a 2-bromo-1- (pyridin-3-yl) ethan-1-one **3.1b** (Scheme 3-13).



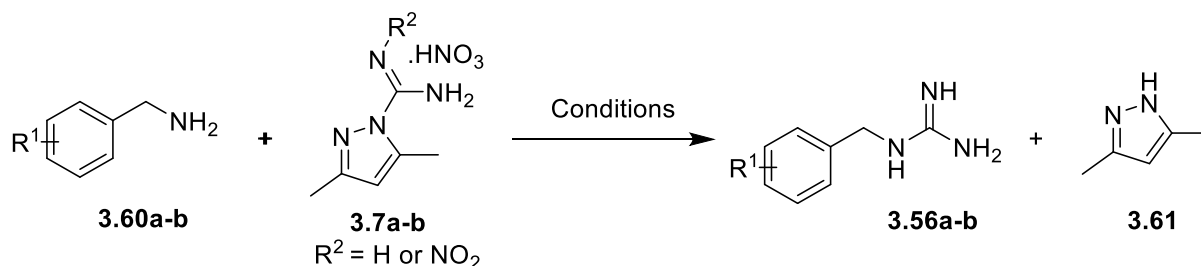
Scheme 3-13: Retrosynthesis of pathway B1.

3.2.1.1 Literature survey

The first step consists on the guanylation of benzylamines **3.60** from the 3,5-dimethylpyrazole guanidine salt **3.7a-b**. Three methods have been tested: (i) in methanol at room temperature for 12 hours to isolate 100% yield (conditions already used in path A1^{469,486}), (ii) in basic medium with

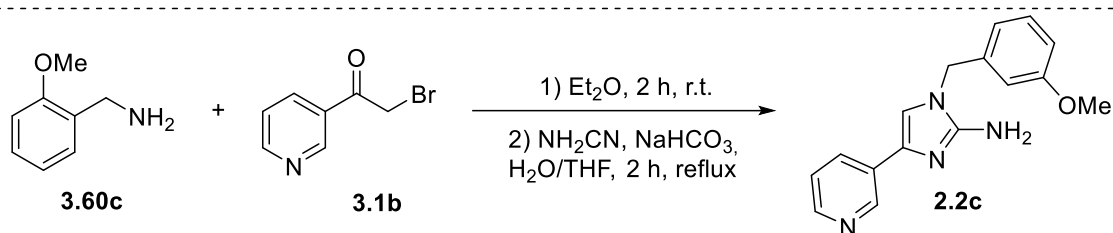
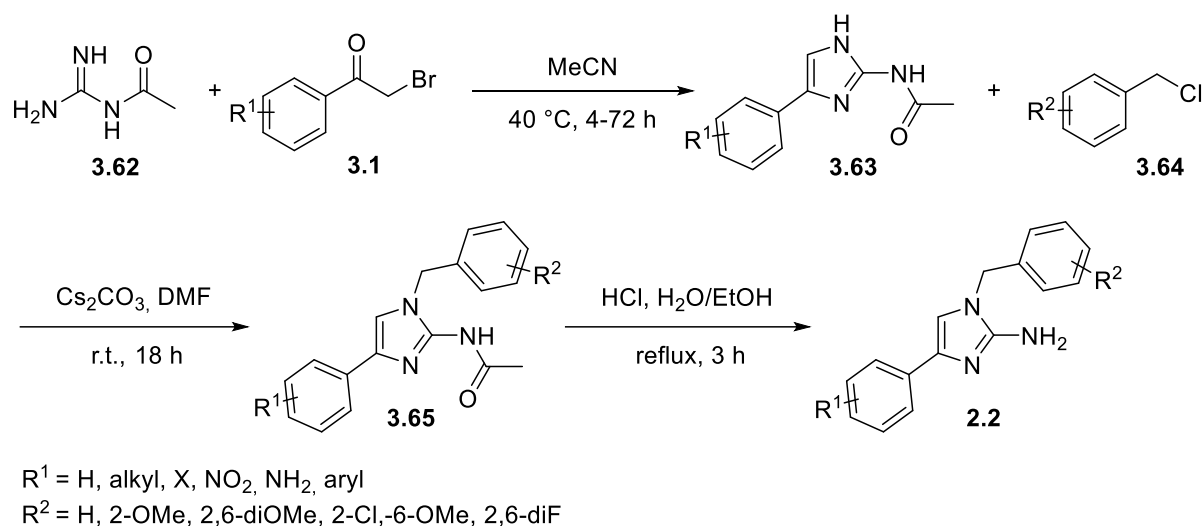
triethylamine insertion at 60 °C in thermic (98% yield), and (iii) triethylamine insertion at 90 °C in microwave activation (67% yield)⁴⁸⁷ (Table 3-7).

Table 3-7: State of the art of benzylamine guanylation.



entry	R ¹ , R ²	Conditions	Yield, %	limitation	Ref.
1	R ¹ = 4-OMe, R ² = NO ₂	MeOH, r.t., 12 h	100	✓ Good yield * Long-time reaction * Guanidine different	Castillo-Meléndez, J. A. et al. (2004) ⁴⁸⁶
2	R ¹ = H, R ² = H	Et ₃ N, MeCN, 60 °C, 24 h	98	✓ Good yield * Long-time reaction	Solodenko, W. et al. (2006) ⁴⁸⁷
3	R ¹ = H, R ² = H	Et ₃ N, THF, 90 °C (MW), 10 min	67	✓ Only 10min * Less quantity (MW)	Solodenko, W. et al. (2006) ⁴⁸⁷

This type of molecule **2.2** has been already described with a phenyl ring or pyridine ring **2.2c** in position C-4 of the imidazole.^{488,489} This method starts by an aza-Hantzsch reaction to form *N*-(1*H*-imidazol-2-yl)acetamide **3.63**, followed by the insertion of a benzyl group in position N-1, and by the final elimination of an acetamide group. Another method consists in introducing the benzyl group by nucleophilic substitution of bromoacetophenone **3.1a** by benzylamine **3.60**, followed by nucleophilic addition of amine over the carbon of cyano group leading to aminoimidazole **2.2** (Figure 3-14, yield not disclosed).



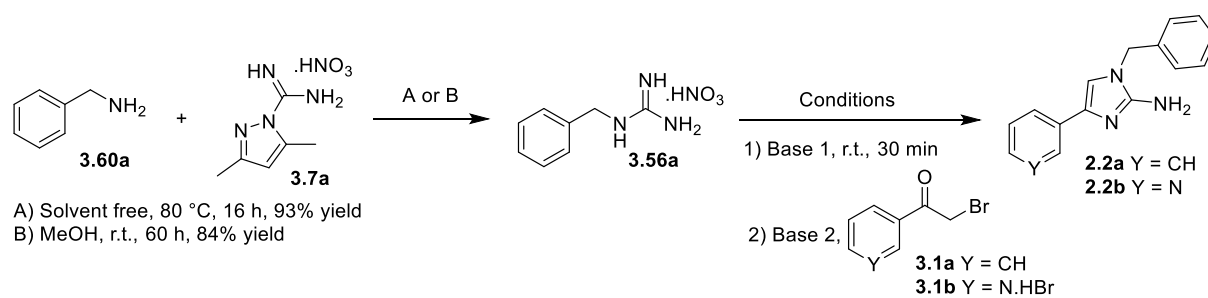
Scheme 3-14: State of the art of pathway B1: Amberg et al. conditions.⁴⁸⁹

3.2.1.2 Methodological study

Two conditions were explored to synthesize benzyl guanidine **3.56**: (i) first, the Scott et al. condition⁴⁶⁹ consists in an amidine transfer using 10.0 equivalents of benzylamine **3.60a** in 3,5-dimethylpyrazole guanidine nitrate **3.7a** at reflux to isolate product **3.56a** in 93% yield and, (ii) second, Castillo-Meléndez et al.⁴⁸⁶ conditions, which proceeds in methanol at room temperature for 60 hours to reach **3.56a** in 84% yield.

Various conditions were tested to obtain our desired product **2.2** (aza-Hantzsch reaction). According to the Mahboobi et al. conditions⁴⁶⁰, potassium hydroxide was added to benzyl guanidine nitrate **3.56** in ethanol and mixed for 30 minutes at room temperature before addition of triethylamine at reflux in pyridyl-bromoacetophenone **3.1b**. Similarly, conditions with potassium carbonate in DMF did not allow the conversion. Finally, using 5.5 equivalents of triethylamine in dioxane at room temperature, only freebase form of benzyl guanidine **3.56** and pyridyl-bromoacetophenone **3.1b** or bromoacetophenone **3.1a** were detected in LCMS (Table 3-8).

Table 3-8: Conditions screening for the aza-Hantzsch reaction.



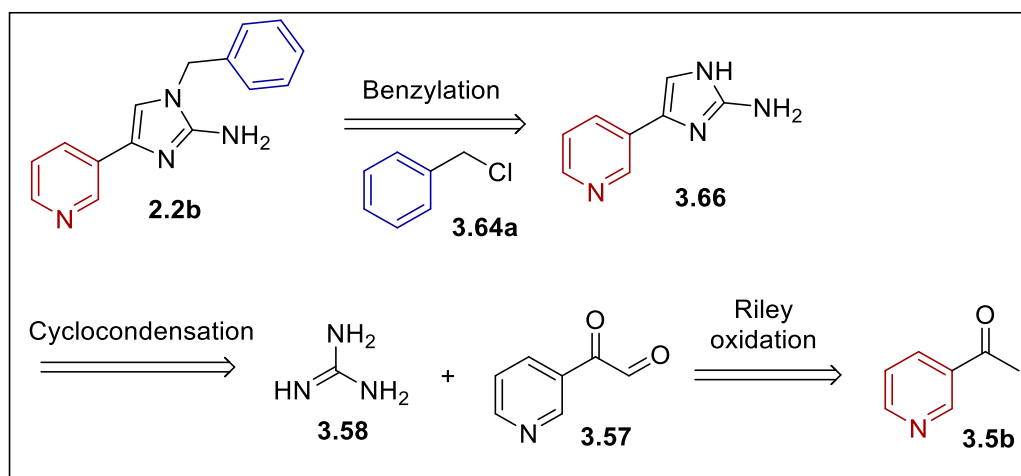
entry	Y	Base 1	Base 2	Solvent	T (°C)	Reaction time (h)	Conversion ^b (Yield), %
1	N	KOH	Et ₃ N (2 eq.)	EtOH	80	16	n.c.
2	N	KOH	K ₂ CO ₃ (3 eq.)	DMF	reflux	16	n.c.
3	N	-	Et ₃ N (5.5 eq.)	Dioxane	r.t.	36	n.c.
4	CH	-	Et ₃ N (5.5 eq.)	Dioxane	r.t.	36	n.c.

^aReaction and conditions: **3.56a** (1.0 mmol), **3.1** (1.0 mmol), bases (3.0 or 5.5 mmol), solvent (2 mL).

^bCalculate by the ratio between products and reagent **3.56a**. Reaction followed by LCMS (D.A.D.). n.c.: no conversion.

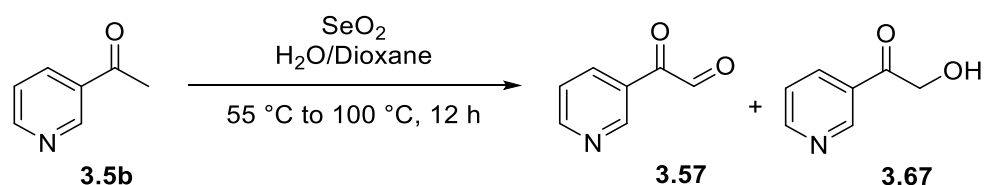
3.2.2 B2: Riley oxidation pathway

The Riley oxidation pathway allow the oxidation of 1-(pyridin-3-yl)ethan-1-one **3.5b** to form **3.57**, 2-oxo-2-(pyridin-3-yl)acetaldehyde. Then, a cyclocondensation⁴⁹⁰ with guanidine **3.58**, followed by benzylation with benzyl chloride **3.64a** could lead to the desired product **2.2b** (Scheme 3-15).



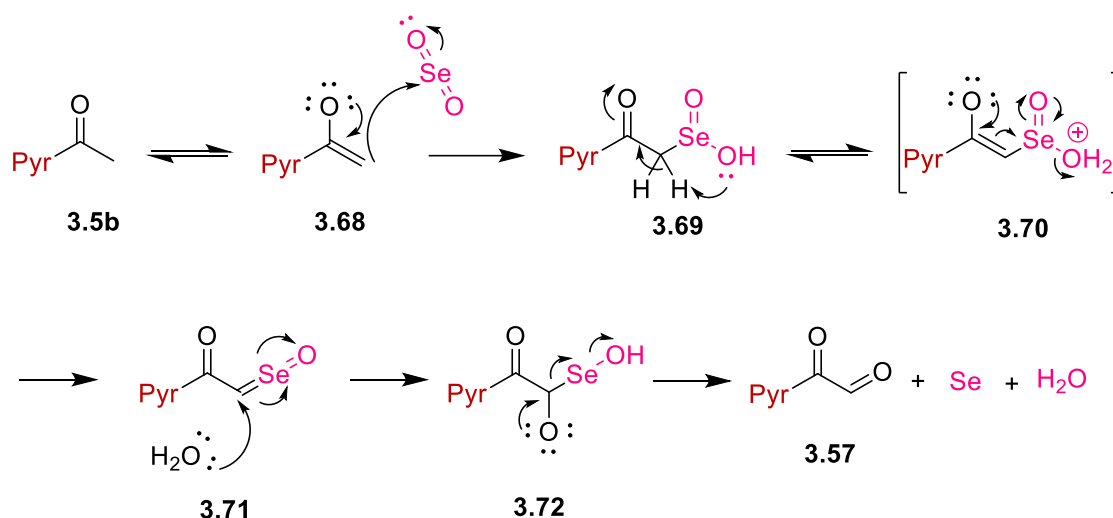
Scheme 3-15: Retrosynthesis of pathway B2.

Riley oxidation was performed according to the procedure patented by Congreve et al. in 2011⁴⁹¹, and involving the use of selenium dioxide in a mixture of water/dioxane: 1/33 at 55 °C for 6 hours, followed by the addition of water and heating at reflux for 12 hours. According to this, we observed after the complete dissolution of selenium dioxide, a red coloration of the solution. Water was added at 100 °C until the disappearance of 1-(pyridin-3-yl)ethan-1-one **3.5b** (Scheme 3-16).



Scheme 3-16: Riley oxidation.

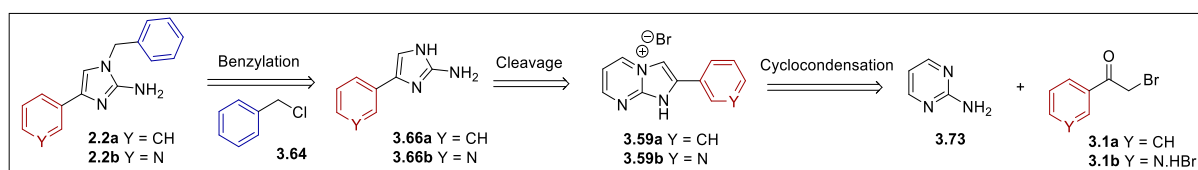
Selenium dioxide oxidizes a carbon in α position of a carbonyle. This proceeds by attack of the enol **3.68** to the selenium atom, followed by hydrolysis. Selenium is reduced to selenium zero, and it precipitates as a black solid and can be therefore removed by filtration (Scheme 3-17). However, we observed a mixture of two oxidation products that can correspond to **3.57** and **3.67** in proportion 2.5:1 by ¹H NMR.



Scheme 3-17: Mechanism of Riley oxidation.

3.2.3 B3: Pyrimidinium pathway

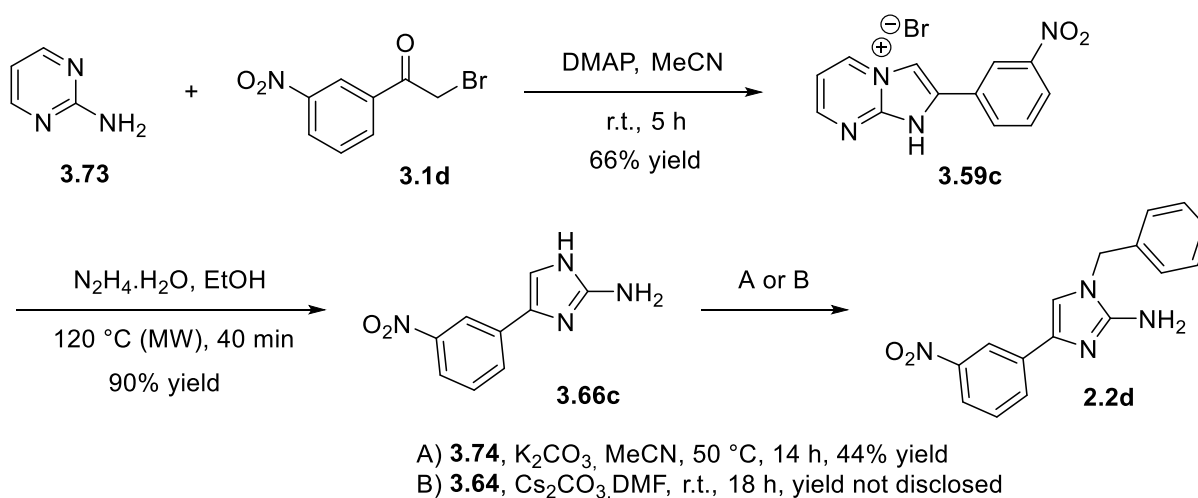
To reproduce the A3 path, we choose to develop the protected imidazole in the form of pyrimidinium salt **3.59** by cyclocondensation of pyrimidin-2-amine **3.73** and bromoacetophenone **3.1**. Then protecting group was removed releasing 1-*H*-pyrazole **3.52** and 2-aminoimidazole **3.66**. The last benzylation step leads to molecule **2.2**, which is our pharmacophore (Scheme 3-18).



Scheme 3-18: Retrosynthesis of pathway B3.

3.2.3.1 Literature survey

Zidar et al. developed a synthesis using 3-nitroacetophenone **3.1d** and pyrimidin-2-amine **3.73** to isolate **3.59c** in 66% yield. Then this intermediate was cyclized in **3.66c** in 90% yield and the final benzylation, using benzyl bromide **3.74**, K_2CO_3 in acetonitrile at 50 °C for 14 h afforded **2.2d** in 44% yield (Figure 3-19).^{492,493} Another benzylation method was described by Amberg et al. using benzyl chloride **3.64**, Cs_2CO_3 in DMF at room temperature for 18 hours (yield not disclosed)⁴⁸⁹ and will be explored widely in chapter 4.

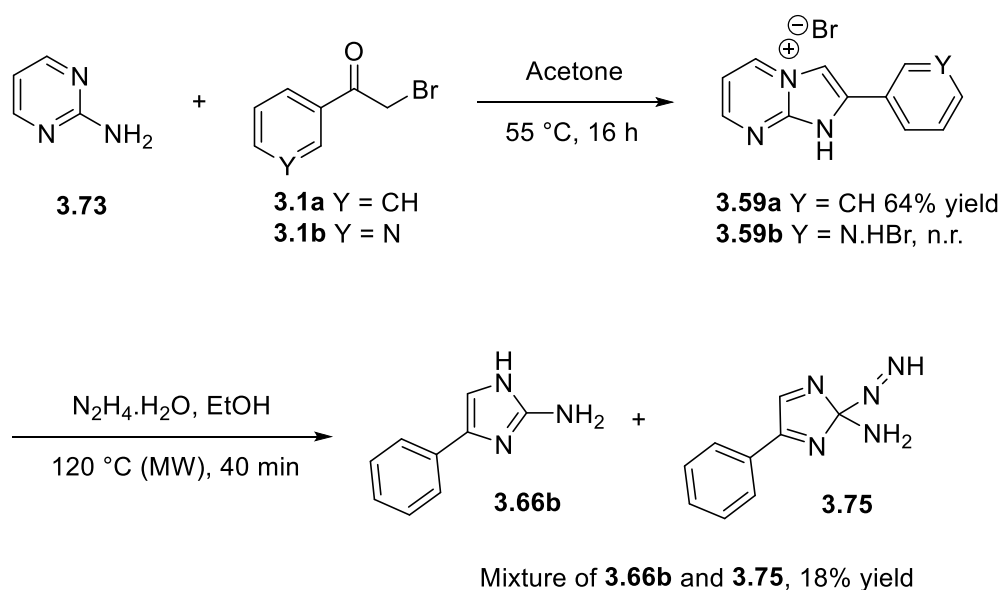


Scheme 3-19: State of the art of pathway B3.^{492,493}

3.2.3.2 Methodological study

The exploration of this pathway was performed for N^3 -pyridine ring in C-2 of imidazopyrimidinium **3.59b**. The reaction was first assayed overnight in acetone at 55 °C - but these condition doesn't led to the expected 2-(pyridin-3-yl)-1*H*-imidazo[1,2-*a*]pyrimidin-4-ium bromide **3.59b**. In a recent paper of 2019,⁴⁹⁴ an example of this pyrimidinium salt formation with N^3 -pyridine ring in C-2 of imidazopyrimidinium has been described in ethanol at 100 °C for 3 hours in only 4% yield. Conversely, with phenyl ring, the cyclisation occurs when using a bromoacetophenone **3.1a** and afforded the expected product **3.59a** in 64% yield.

Next, **3.59a** was treated with 40% of hydrazine hydrate at 120 °C for 30 minutes under microwave activation to obtain a mixture of product **3.66b** and side product, expected to be 2-diazenyl-4-phenyl-2*H*-imidazol-2-amine **3.75** (Scheme 3-20 after purification (CH₂Cl₂/MeOH, 10/0 then 9/1)). Indeed, LCMS shows two mass compounds: the product **3.66b** and the supposed side-product **3.75**. No investigation was performed and the pathway B3 was abandoned.



Scheme 3-20: Our work in pathway B3.

To conclude, we observed that with a phenyl ring, the desired extra-cyclic substituted 2-aminoimidazole **2.1e** was obtained in 28% yield after 3 steps (pathway A3). Unfortunately, imidazole carrying the pyridyl ring could not be obtained with our desired regioisomer for series A. We have also demonstrated that starting from an aryl guanidine by an aza-Hantzsch reaction, the regioisomer intra-

cyclic nitrogen substituted 2-aminoimidazole **3.8a-d** will be favored compared to the extra-cyclic nitrogen substituted **2.1**.

Regarding series B, the imidazole precursor is also difficult to form, and unsatisfactory results have been realized. These pathways were then discarded in favour of the development of the triazoles series in order to get the pharmacophore.

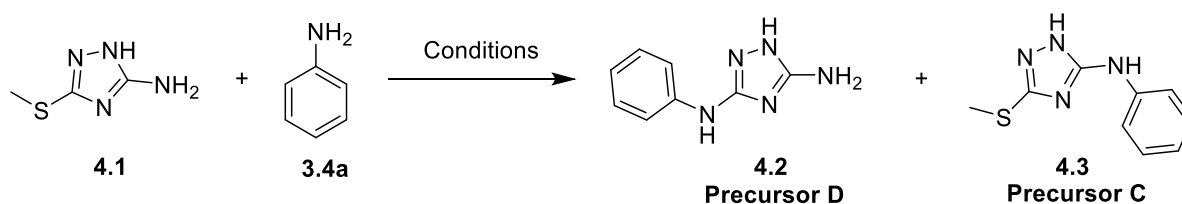
Chapter 4. SYNTHESIS OF THE TRIAZOLE SERIES

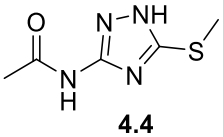
Two series of triazole derivatives have been developed: series C encompasses a phenyl ring linked to the extra-cyclic nitrogen of the 2-amino-1,2,4-triazole core, whereas series D (encompasses a benzyl substituent linked to the intra-cyclic nitrogen of the 2-amino-1,2,4-triazole core.

4.1 S_NAr APPROACH (SERIES C & D)

We first aimed to adapt the Li et al. conditions⁴⁷⁵ described in pathway A2 (Chapter 3) for the substitution of a thiomethylimidazole **3.21** by aniline **3.4a** to the S_NAr on a 3-thiomethyltriazole **4.1**. Therefore, various conditions have been tested for the substitution of 5-(methylthio)-1,2,4-triazolidine-3-amine (MeST) **4.1** with aniline **3.4a** (Table 4-1). In neat conditions, a minimum of 150 °C was necessary to obtain the product **4.2** (entry 5), which is quite unstable (degradation begins after 1 day). To speed up the reaction, microwave activation was applied, leading to 21% conversion of **4.2** and the apparition of a side product: **4.3** (9%) (entry 6). Besides, this unexpected product represents an interesting precursor of the series C. However, the increase of the temperature to 155 °C led to worst conversion rates (15% and 6%, entry 7), and at 170 °C, only degradation was observed (entry 8). Likewise, the increase of the number of equivalents of the aniline **3.4a** led to only 4% of **4.2** and 2% of **4.3** (entry 9). Moreover, no conversion was observed in dioxane, DMF, or acid medium, even at 150 °C (entries 10-13).

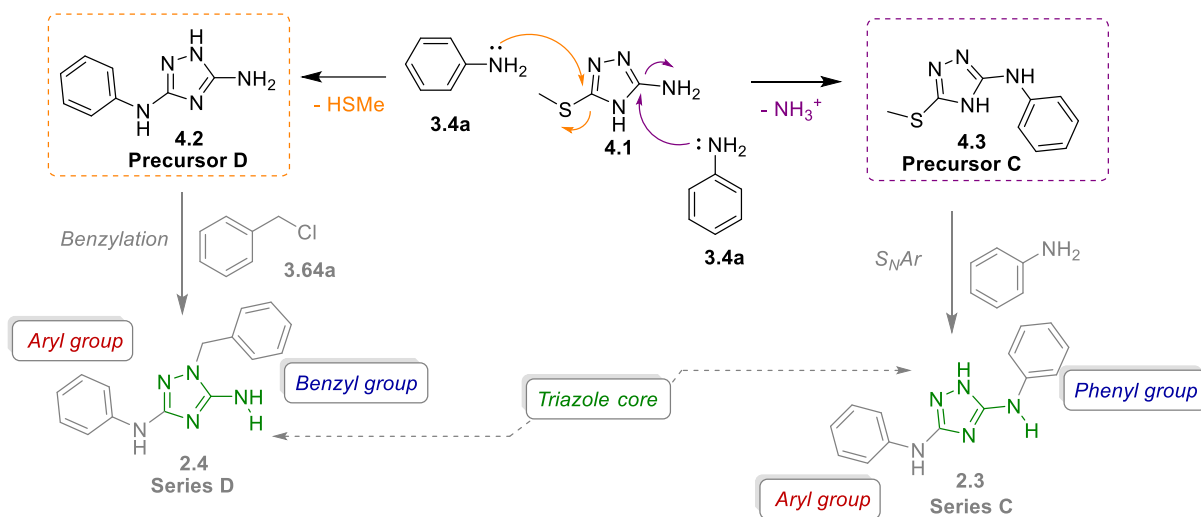
Table 4-1: Conditions for the synthesis of precursors C and D.



Entry	Eq. 4.1:3.4a	Conditions	T (°C)	Reaction time (h)	Conversion ^a , %		
					4.1	4.2	4.3
1	1:5	Neat	100 - 130	24	n.c.		
2	1:5	Solvent-free, KF (2.5 eq.)	100 - 130	24 - 120	n.c.		
3	1:5	Et ₃ N (5.0 eq.), Solvent-free	100 - 130	24 - 48	n.c.		
4	1:2	EtOH	140 (MW)	1.30	n.c.		
5	1:1	Solvent free	150	16	84	16	-
6	1:1	Solvent free	150 (MW)	1	70	21	9
7	1:1	Solvent free	155 (MW)	1	79	15	6
8	1:1	Solvent-free	170 (MW)	15 min.	degradation		
9	1:5	Solvent free	150 (MW)	1	94	4	2
10	1:1	Dioxane	150 (MW)	1	n.c.		
11	1:1	DMF	150 (MW)	1	n.c.		
12	1:1	AcOH	150	24	 <p style="text-align: center;">4.4</p>		
13	1:1	HCl in dioxane (1.0 eq.)	100 - 120	24			

^aCalculate by the ratio between products **4.2** or **4.3** and reagent **4.1**. Reaction followed by LCMS (D.A.D.). MW: microwave reaction. n.c.: no conversion.

We propose that at high temperature, two nucleophilic aromatic substitutions are possible *via* (i) substitution of thiomethyl group by aniline **3.4a** as already described (in orange, Scheme 4-1) and (ii) substitution of the amino group at position 3 of the triazole (in purple, Scheme 4-1). In general, this substitution was described with halogen as a leaving group.⁴⁹⁵ Thiomethyl group seems to react slower.



Scheme 4-1: Mechanism and supposed reaction to obtain series C & D.

Face to these problems, we moved to the synthesis of series D.

4.2 1-BENZYL- N^3 -1H-1,2,4-TRIAZOLE-3,5-DIAMINE (SERIES D)

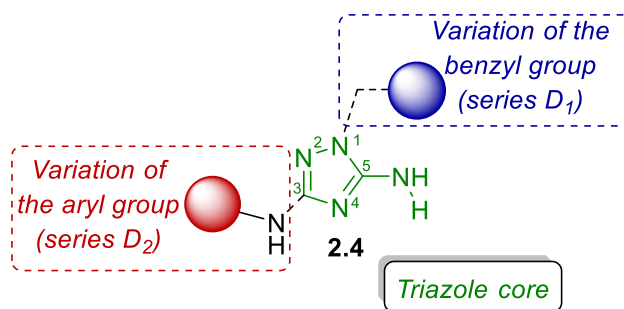


Figure 4-1: SAR prediction of series D.

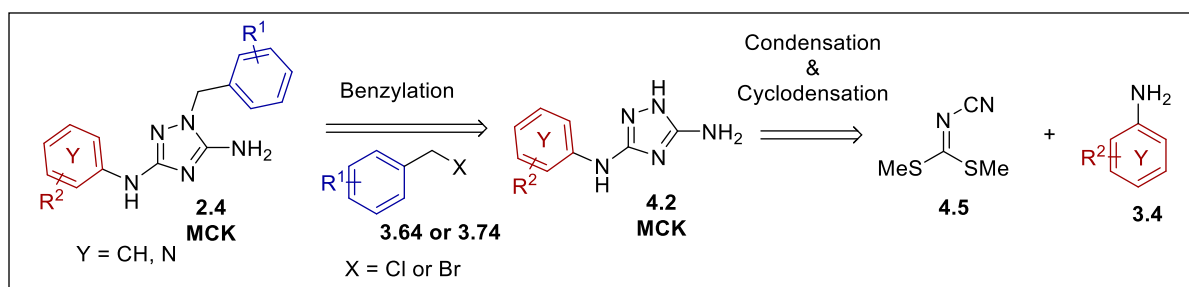
Series D constitutes the main family of compounds of this Ph.D. thesis. These compounds consist of a triazole core substituted with

- i) a benzyl substituent at N-1, which introduces flexibility to the molecule. This benzyl group was further substituted with various groups in series D₁;
- ii) an aryl group linked to the amine on the position 3 of the triazole ring, which modulated by the addition of different substituents in series D₂.

The preparation of these two subseries aims to decipher the SAR around our pharmacophore (Figure 4-1).

To synthesize the benzyl-1,2,4-triazole **2.4**, three steps were needed. A first condensation step of dimethyl cyanodithioimidocarbonate **4.5** with aniline **3.4a, h-i, n-s** or aminopyridine **3.4j-m** resulted in the formation of imidates **4.6**. The resulting compounds were cyclized into the corresponding 5-amino-1*H*-[1,2,4]-triazole derivatives **4.2** in the presence of hydrazine hydrate in ethanol under reflux. Finally, the benzylation step was performed with benzyl chloride **3.64** or benzyl bromide **3.74** in the presence of a base at room temperature (Scheme 4-2), resulting in the desired compounds.

It is to note that all molecules that were evaluated in biological assays are named “**MCK**” compounds followed by a number for this thesis.



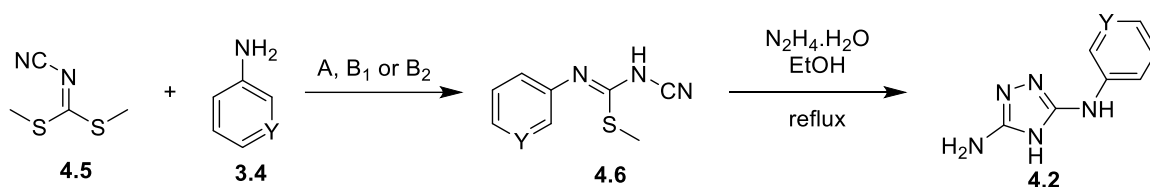
Scheme 4-2: Retrosynthesis of triazole series.

4.2.1 1*H* 1,2,4-triazole intermediates

4.2.1.1 Literature survey

The desired *N*³-phenyl-1*H*-1,2,4-triazole-3,5-diamine **MCK243** has been already described and synthesized in two steps (Scheme 4-3)⁴⁹⁶⁻⁴⁹⁹. After condensation of dimethyl cyanocarbonimidodithioate **4.5** with aniline **3.4**, the reaction mixture is treated with hydrazine to perform the triazole cyclization.

This first step has been already described for the *N*⁴-pyridine ring **4.6b** and *N*³-pyridine ring **4.6c** using sodium hydrate, with or without DMAP, in DMF to obtain product **4.6b-c** in good yield (84% in both cases)⁵⁰⁰⁻⁵⁰³. The cyclization was described for *N*³-pyridine ring by the treatment of hydrazine with 70% yield⁴⁹⁹ for **MCK245** with the phenyl group, but it has not been described for *N*⁴-pyridine ring **MCK244** (Scheme 4-3).



A: EtOH, 80 °C

B₁: NaH, DMAP, DMF, r.t.; B₂: NaH, DMF, r.t.

Y = CH: **4.6a** 71-85% yield (step 1, method A), **MCK243** 92% yield (step 2)

Y = N⁴: **4.6b** 84% yield (step 1, method B₁), **4.6b** 67% yield (step 1, method B₂), (step 2 not described)

Y = N³: **4.6c** 84% yield (step 1, method B₁), **4.6c** 64% yield (step 1, method B₂), **MCK245** 70% yield (step 2)

Scheme 4-3: 1H-1,2,4-triazole-3,5-diamine synthesis described in the literature.

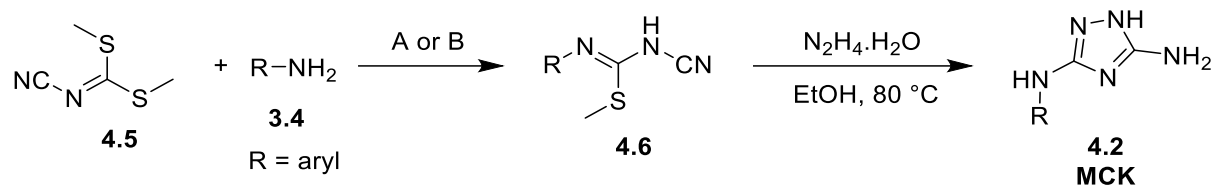
4.2.1.2 Synthesis

Starting from dimethyl cyanocarbonylimidodithioate **4.5** and the **substituted-aniline 3.4** in ethanol at 80 °C, as described in the literature,⁴⁹⁷ the carbamimidothioic acid, *N*-cyano-*N*-phenyl-methyl ester intermediate **4.6a** was obtained with 60% yield. A cyclization step with hydrazine hydrate allowed to reach the product **MCK243** with 96% yield. A series of 1H-1,2,4-triazoles **MCK265-266/285-287/302-304** was synthesized from substituted anilines **3.4n-r** with yields in the range of 24-69% over two steps after cyclization.

From the **pyridyl group**, 1H-1,2,4-triazoles **MCK244-247** were obtained as described in table 4-2, with sodium hydride, with or without DMAP, in DMF or THF for the first step. In THF the product precipitate before its reprotonation *via* NH₄Cl treatment. Sodium hydride is required to obtain **4.6b-e**, as the nitro-substituted and ester-substituted compounds **4.6k-m**. A reaction test for *N*²-pyridine **4.6d** allowed to show that the presence of DMAP decreases the reaction time, but no significant difference in reaction yield was observed.

All these molecules were used in the last benzylation step without needing purifications, except **MCK246**. Moreover, after hydrolysis by LiOH in water/THF 4-((5-amino-1H-1,2,4-triazol-3-yl)amino)benzoic acid **MCK305** was obtained in 26% yield.

Table 4-2: Two-step synthesis of 1*H*-1,2,4-triazole formation **MCK243-247/265-266/285-287/302-305**.



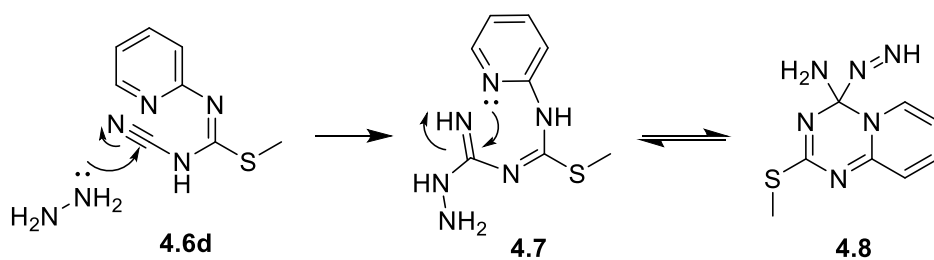
A: EtOH, 80 °C

B: NaH, DMF or THF, r.t.

R	Step 1 ^a	Step 2 ^a	R	Step 1 ^a	Step 2 ^a
	4.6a (60%)	MCK243 (96%)		4.6h (48%)	MCK285 (94%)
	4.6b (39%)	MCK244 (83%)		4.6i (44%)	MCK286 (91%)
	4.6c (64%)	MCK245 (73%)		4.6j (59%)	MCK287 (96%)
	4.6d (41%)	MCK246 (36%)		4.6k (16%)	MCK302 (78%)
	4.6e (72%)	MCK247 (90%)		4.6l (72%)	MCK303 (90%)
	4.6f (24%)	MCK265 (99%)		4.6m (n.i.)	MCK304 (91% over 2 steps)
	4.6g (73%)	MCK266 (95%)		-	MCK305 (26%) ^b

^aThe yields obtained are indicated in brackets. ^bThe product was obtained by hydrolysis. n.i.: not isolated.

Moreover, in the case of *N*²-pyridine **MCK246**, a purification was needed after the cyclization step due to another product formed, which explains the lower yield (36%). A hypothesis could be either a lack of reactivity of intermediate **4.7** to cyclize or an undesired cyclization in **4.8**, 4-diazenyl-2-(methylthio)-3,4-dihydro-2*H*-pyrido[1,2-*a*][1,3,5]triazin-4-amine (Figure 4-4). But further analysis is necessary to confirm their structures.



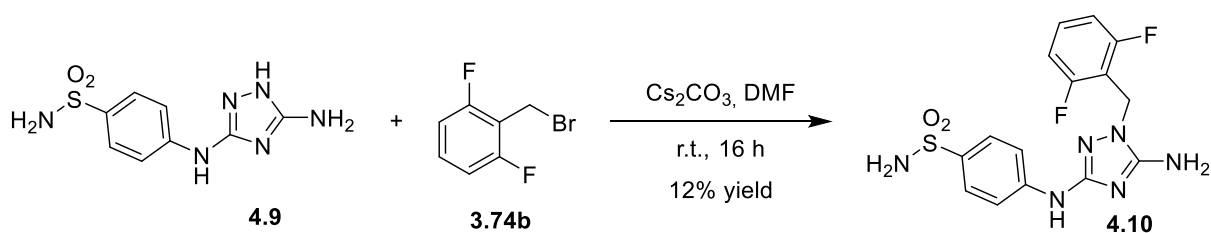
Scheme 4-4: Mechanism of hypothetical formation of **4.7** methyl-*N'*-(hydrazinyl(imino)methyl)-*N*-(pyridin-2-yl)carbamiimidothioate or **4.8** 4-diazenyl-2-(methylthio)-3,4-dihydro-2*H*-pyrido[1,2-*a*][1,3,5]triazin-4-amine.

4.2.2 Benzyl-1,2,4-triazole: First results

To reach our predicted pharmacophore, a benzylation step is required at intra-cyclic nitrogen in position N-1.

4.2.2.1 Literature survey

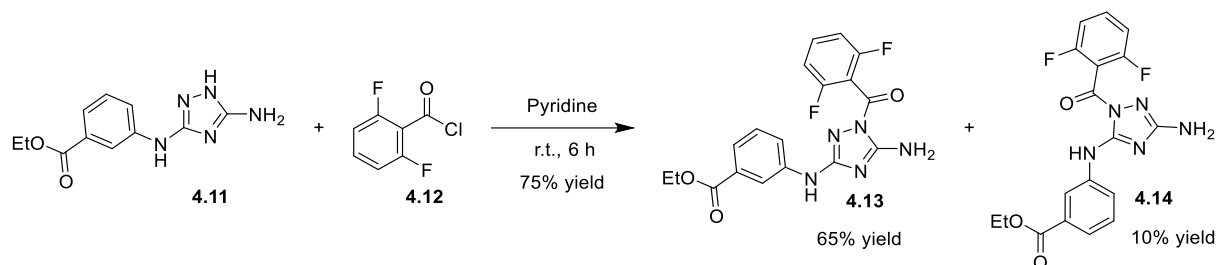
The benzylation at position 1 of a 1,2,4-triazole was described only once in the literature, starting from 4-((5-amino-1*H*-1,2,4-triazol-3-yl)-amino) benzenesulfonamide **4.9** and 2-(bromomethyl)-1,3-difluorobenzene **3.74b** with cesium carbonate in DMF at room temperature to obtain **4.10** with 12% yield (Scheme 4-5).⁵⁰⁴



Scheme 4-5: 4-((5-amino-1-(2,6-difluorobenzyl)-1*H*-1,2,4-triazol-3-yl)amino)benzenesulfonamide **4.10** formation.

A benzoylation step to obtain a similar compound with carbonyl in the place of methylene group has been described by Malerich et al..⁵⁰⁵ This reaction was performed in pyridine at room temperature for

6 hours, affording two regioisomers **4.13** with 65% yield and **4.14** with 10% yield. In this work, the separation of these two products by silica gel flash chromatography was very challenging.

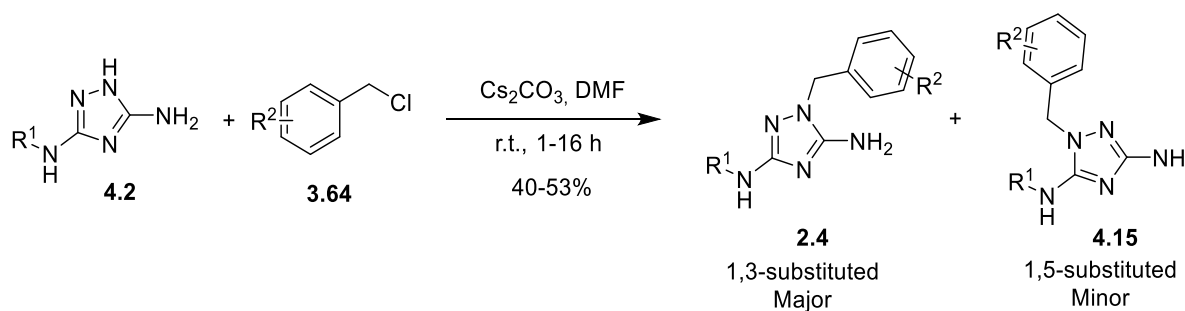


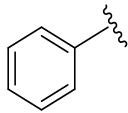
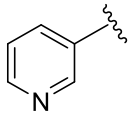
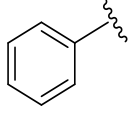
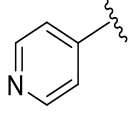
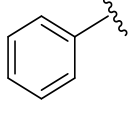
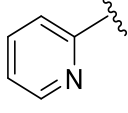
Scheme 4-6: Example of the Malerich group's conditions.

4.2.2.2 Synthetic approach to identify the preferred aryl group of the molecule

To obtain **2.4**, the first reactions were performed according to the protocol described in the literature (item 4.2.2.1) using benzyl chloride **3.64** with cesium carbonate in DMF. This afforded a mixture of two regioisomers **2.4** and **4.15**, in variable ratios with conversion rates ranging between 40% and 53%. This reaction has been tested with four substrates: $R^1 = \text{Ph}$, 2-pyr, 3-pyr and 4-pyr (Table 4-3).

Table 4-3: Ratio of the regioisomers resultant from the benzylation step.



R ¹	R ²	Ratio regioisomer ^a	R ¹	R ²	Ratio regioisomer ^a
	H	3 :1		H	9 :1
	2-Me	8 :2		H	9 :1
	2,6-F	3 :1		H	4 :2 :1

^aDetermined by HPLC analysis.

In the case of a phenyl substituent in position 3 of the triazole (**MCK243**), three groups were introduced at R², leading to different ratios between the regioisomers in favor to the 1,3-isomer (3:1 for R² = H or 2,6-difluoro and 8:2 for 2-methyl). The separation of these regioisomers by silica gel flash chromatography was done with the eluent system CH₂Cl₂/THF isocratic 1/1. The major products were isolated with 13-30% yield for major isomers **MCK249-250**, **MCK256**, and 5-7% yield for minor isomers **MCK248/MCK257** (Scheme 4-2). This fairly low isolated yield could be explained by a poor chromatography separation efficiency, resulting in a fraction mixture of **2.4** and **4.15**, but also the presence of **4.2** as well as the dibenzylated product **4.16**.

The pyridine-substituted triazoles **MCK244-246** showed a better conversion towards the major regioisomer (ratio 9:1), except for *N*²-pyridine. The separation method was performed by silica gel flash chromatography with a CH₂Cl₂/MeOH, 9/1 as eluent. But the major regioisomers from **MCK253-255** led to low isolated yield (2-16%), and only traces of the minor regioisomer **MCK252** was observed. Moreover, **MCK255** was obtained after 2 hours with 2% yield but, prolonging the reaction to 3 days, a nitrogen substitution of pyridine ring **MCK251** was noted with 26% yield.

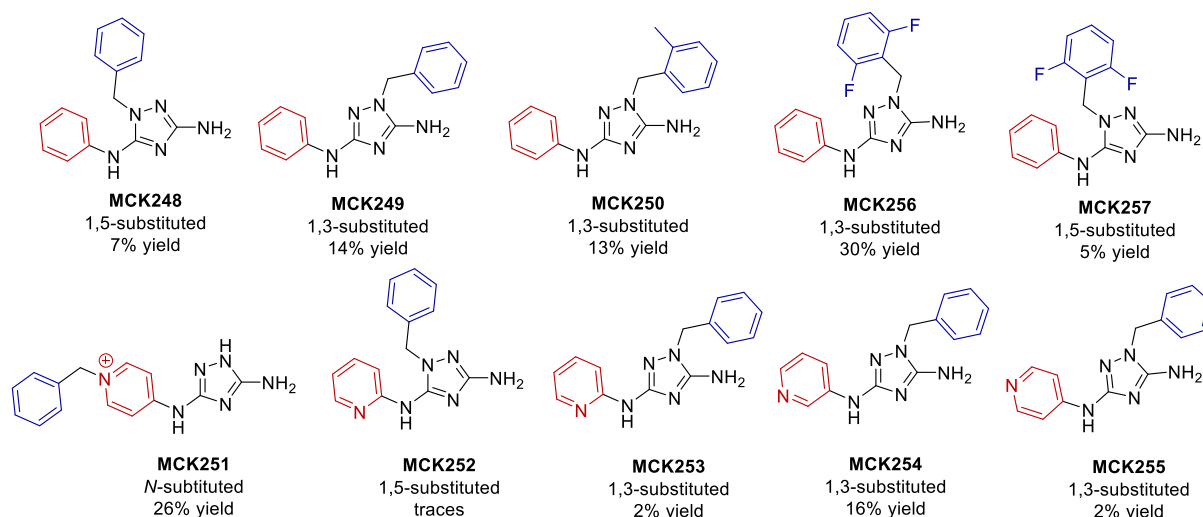
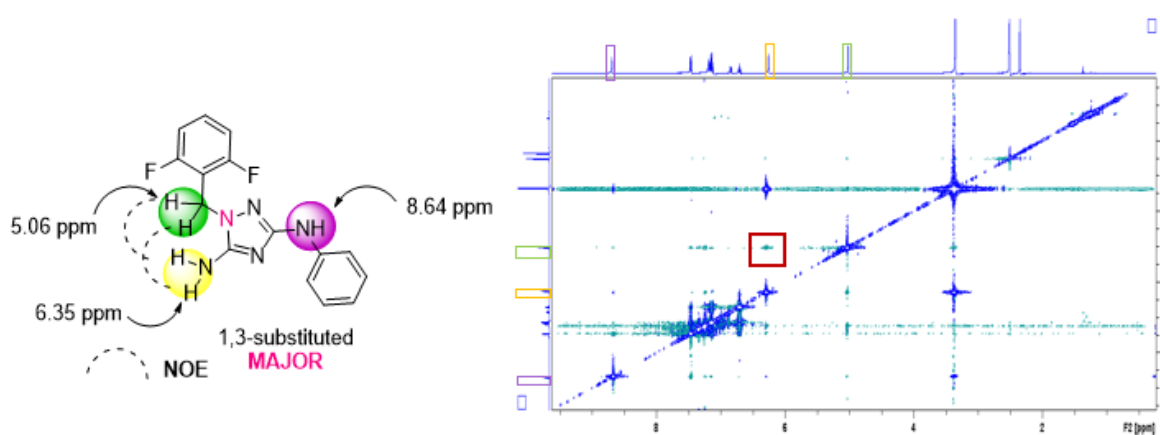


Figure 4-2: Scope of benzyl derivatives **MCK248-257**.

4.2.2.3 Chemical characterization

4.2.2.3.1 NMR and HPLC

The characterization of the regioisomers **MCK256** and **MCK257** was carried out using NMR and HPLC analyses. We observed a difference in the chemical shift of the amino group in position 3 in ^1H NMR, with a signal at 6 ppm for the major product **MCK256**, but at 5 ppm for the minor product **MCK257**. Through NOESY analysis, a significant correlation between the amino group in position 3 and the methylene of the benzyl is observed for the major product **MCK256** (Figure 4-3). Similarly, we observed a correlation between the NH at position 3 and the methylene of the benzyl for **MCK257** (Figure 4-3). The peaks are closed to each other in HPLC but not overlapping, allowing us to distinguish both regioisomers: t_R : 8.22 min for major **MCK256** and t_R : 7.68 min for minor **MCK257**.



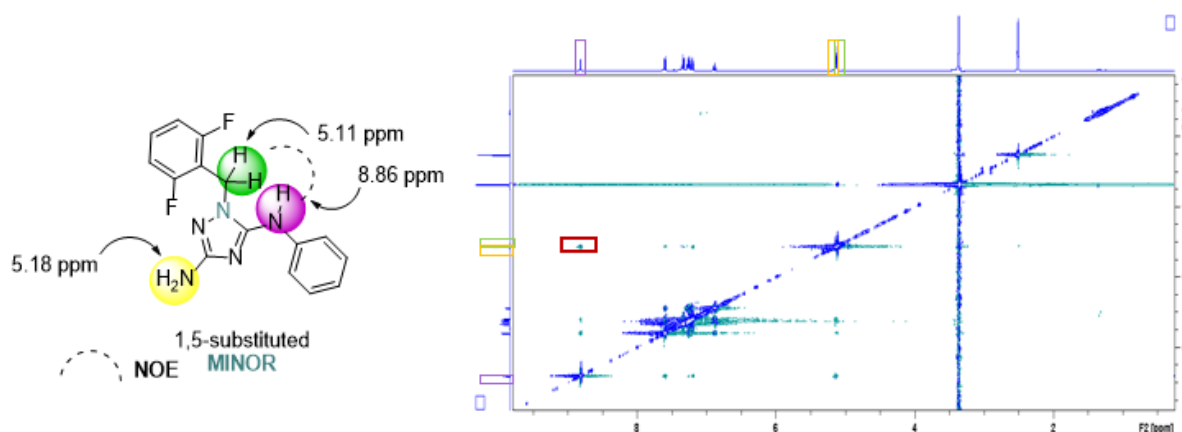


Figure 4-3: ^1H NMR and NOESY spectra supporting the characterization of the regioisomers **MCK256** and **MCK257**.

4.2.2.3.2 Crystallization studies

The two regioisomers **MCK256** and **MCK257** were crystallized to confirm their structure. Multiple solvent systems were tested: methanol in pentane, toluene or ether, which didn't lead to the desired crystals. The same result was observed with ethanol in pentane or only DMSO but, ethyl acetate in pentane gave great crystals (Figure 4-4). **MCK256** and **MCK257** crystals confirmed the identification of the major (1,3) and the minor (1,5) regioisomers.



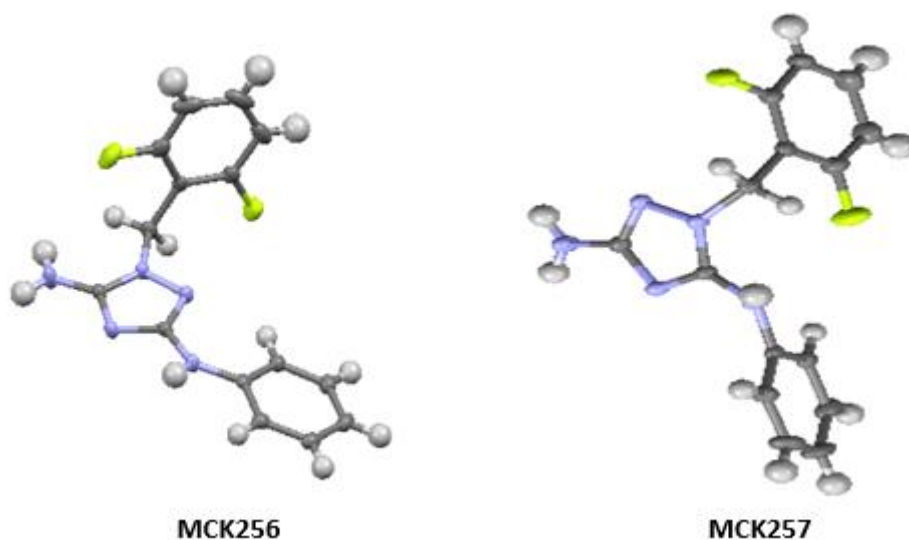
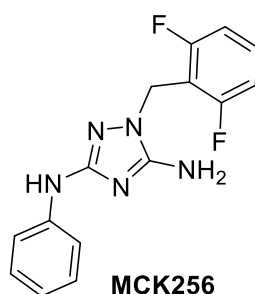


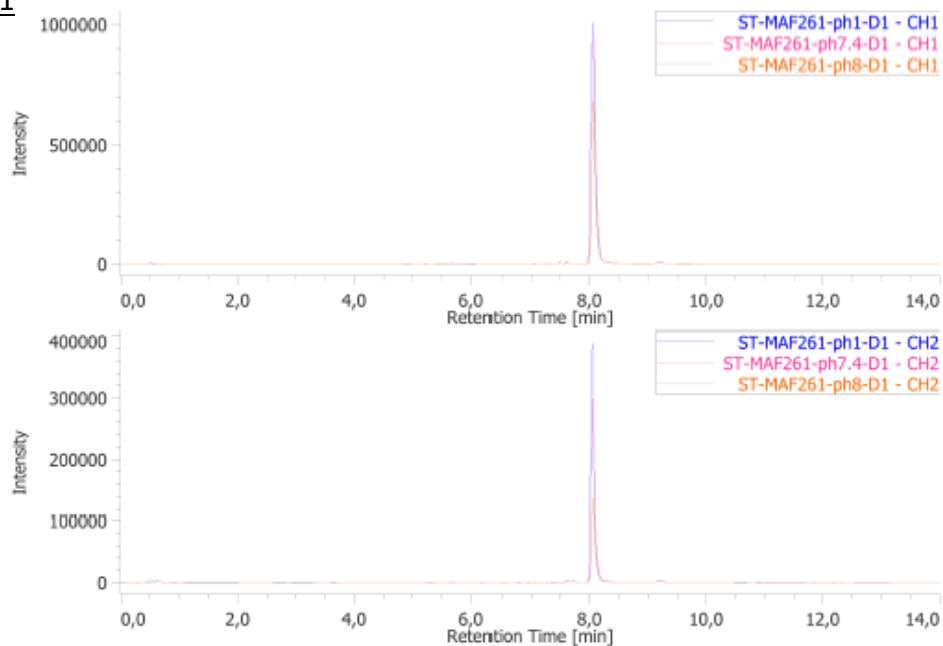
Figure 4-4: X-ray crystal structure of **MCK256** and **MCK257** showing the major and minor regioisomers.

4.2.2.3.3 Stability assay

The stability in solutions at different pHs was studied to correlate with the pH of the different compartments of the body. For this study, **MCK256** was chosen as a model and showed to be stable at acidic, physiologic, and basic conditions (pH 0.9, 7.4, 8.4, respectively) after 14 days in the corresponding aqueous buffers ($C=1,7 \times 10^{-3}$ M) with 5% DMSO (Figure 4-5). HPLC analysis showed no decomposition peak, but the decrease in the peak intensity might be related to the precipitation of the compound in the respective aqueous solutions.



Day 1



Day 14

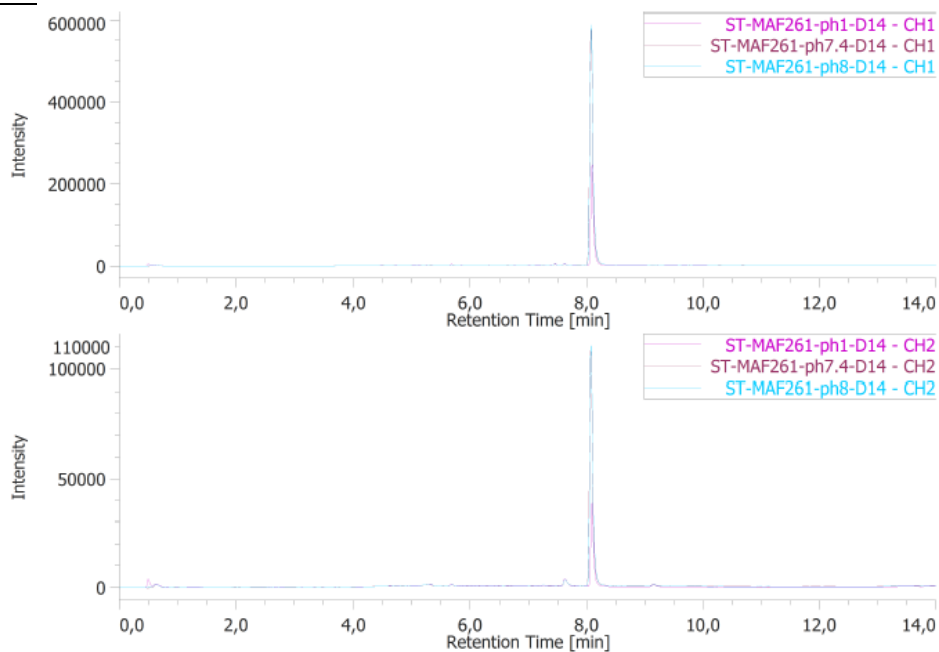


Figure 4-5: Stability assay of **MCK256** monitored by HPLC (CH1 = 254 nm and CH2 = 280 nm) at t_0 and after 14 days.

4.2.2.4 Biological evaluation

The biological assays were carried out by the Pagès team from the IRCAN in Nice. I had the chance to participate in the cytotoxicity assay to evaluate their viability but also, I observed how to perform

migration assay by Boyden chamber. At first, we studied the viability and anti-proliferative effect on several cell lines (keratinocytes cells; fibroblastes cells; carcinoma cells, RCC or TFE3; retinal cells, ARPE and endothelial cells, TIME) when cultured in the presence of different concentrations of our molecules. Second, to inhibit ELR⁺ CXCL-CXCR1/2 interaction so as to block exudative AMD. This group is specialized in angiogenesis, particularly in cancer, and some tests are performed over cancer cell lines. Our intermediate 1H-1,2,4-triazole compounds **MCK243-247** were also tested to understand if the benzyl group is necessary and which aryl group can show activity.

4.2.2.4.1 Cytotoxicity assay

Cytotoxicity assays were performed to evaluate the viability of different cell lines when cultured in the presence of compounds (**MCK243-256**) at a simple dose (10 μ M). Different lines were assayed:

- i) in cancer cells (RCC), 786 and A498 to analyze the activity of MCK in carcinoma cancer and,
- ii) in keratinocytes and fibroblasts cells to evaluate their viability and proliferation in healthy cells.

All the compounds were tested upon 48 h incubation and showed no significant effect. An exception for **MCK250** has an anti-proliferative effect on healthy keratinocyte cells due to a proliferation's decrease than 50%.

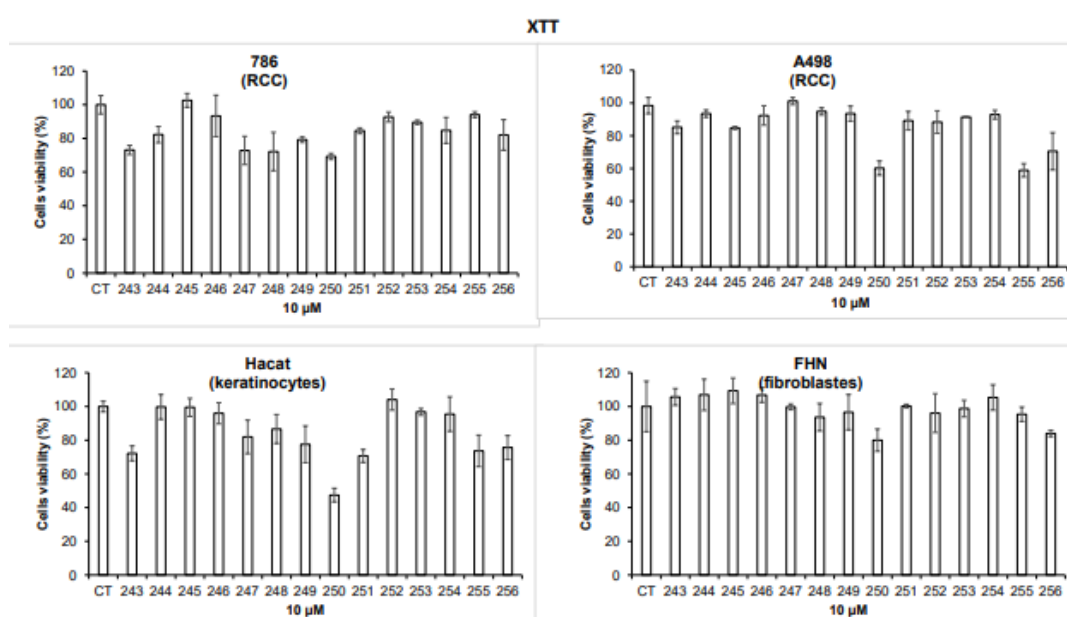
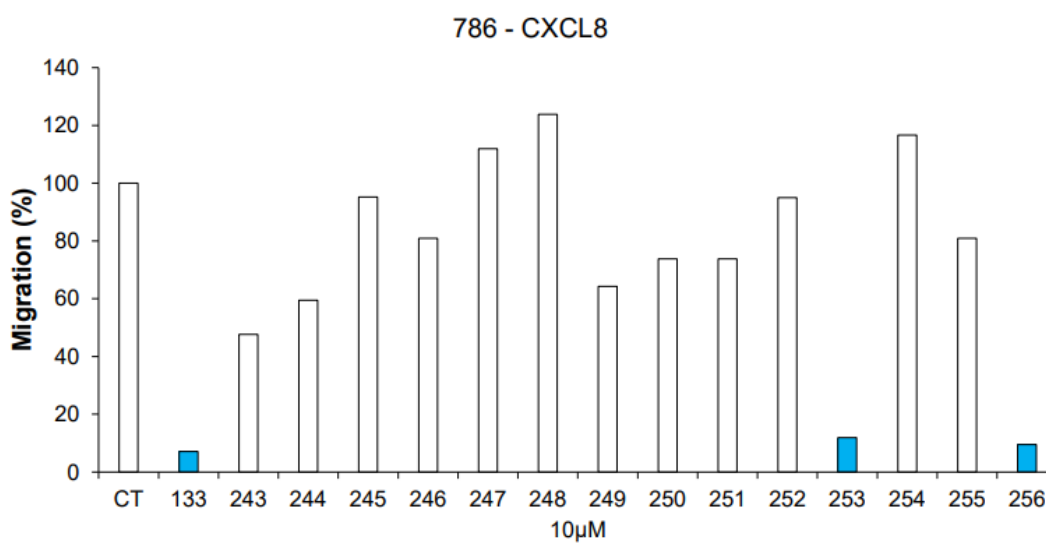
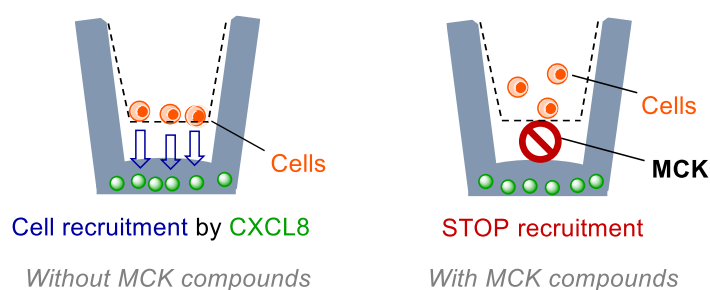


Figure 4-6: First cellular viability in carcinoma cells (RCC) and health cells (keratinocytes and fibroblastes). *Values not released.*

4.2.2.4.2 Migration assay (Boyden chamber)

The Boyden chamber assay allows to observe cell migrations. These migrations are stimulated by cytokines and can be modulated under the action of CXCR antagonists. Thus, a decrease in cell migration in the presence of our compounds means that the CXCR1/2 receptors are antagonized (functional tests). The migration assay was performed after 24 h over the carcinoma cancer cell line (786, RCC) with the cytokine CXCL8 for fourteen compounds **MCK243-256**. The reference molecule is the previously presented lead compound (**MCK133**), produced by the group, showing migration inhibition of more than 80% (10 μ M). Two of the compounds **MCK253** and **MCK256** show a similar result with the same migration inhibition of more than 80% (10 μ M).



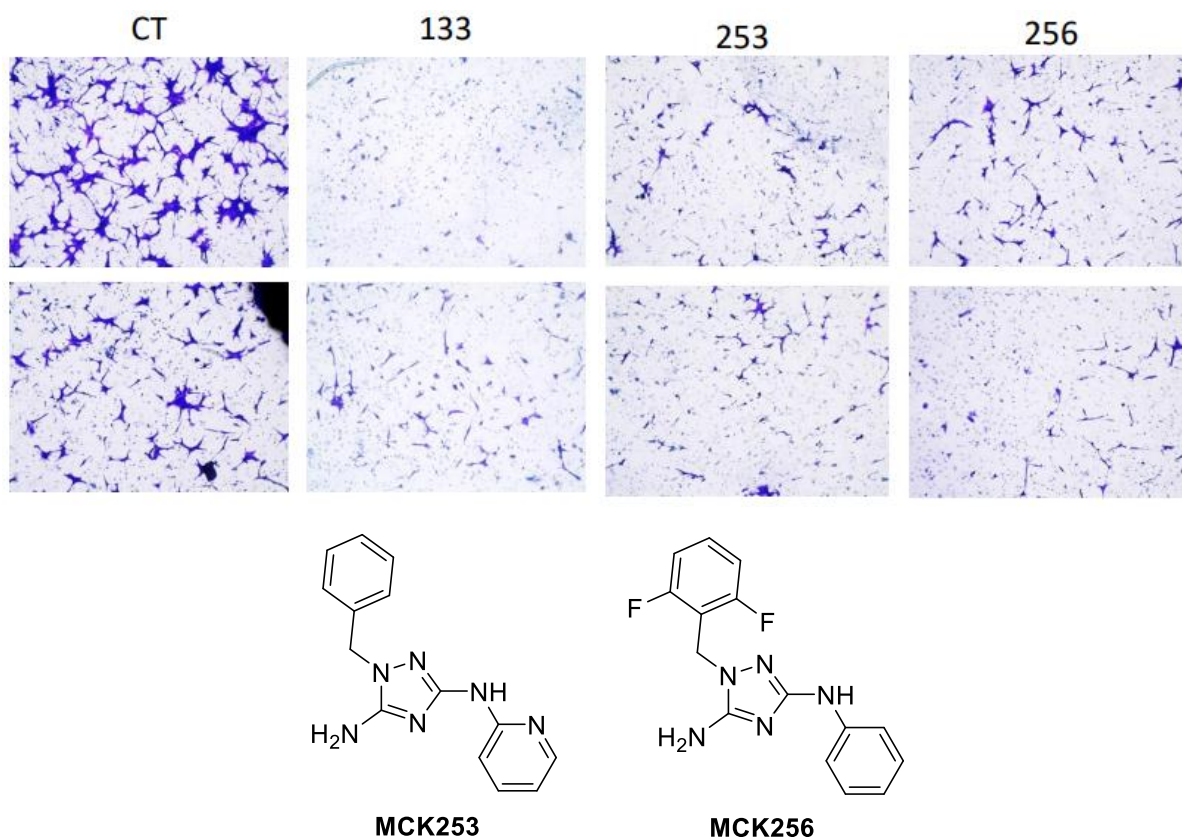


Figure 4-7: Migration test by Boyden chamber on 786 RCC cells after 24 h treatment with 10 μM of the indicated compounds relative to a DMSO control.

The benzene and N^2 -pyridine ring seem to show an inhibition of CXCL8 and are the basis of our series D_1 for the following synthesis by varying the groups on the benzyl at different positions. Indeed, we can observe that unsubstituted benzyl **MCK253** and 2,6-difluoro substituted benzyl **MCK256** show similar results of inhibitions.

Unfortunately, the Boyden chamber assays could not be reproducible during the time of this thesis due to a technical problem.

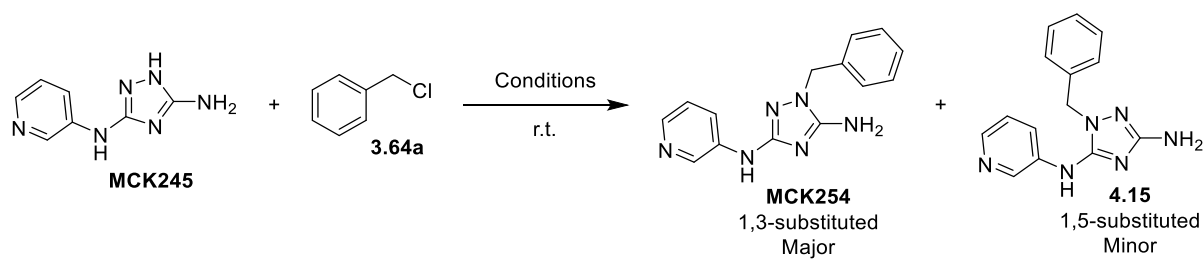
4.2.3 Series D_1 : functionalization with different benzyl groups

4.2.3.1 Optimization of benzylation conditions and synthesis

A conditions screening was performed with N^3 -pyridine-1*H*-1,2,4-triazole **MCK245** and benzyl chloride **3.64a** as a model substrate. First, was studied the solvent effects by using dioxane, acetonitrile, THF or water. In our hands, we observed the formation of the two expected regioisomers in DMF only

(conversion rate: 80%). No reaction occurred obtained when using the other solvents (Table 4-4, entries 2-5). We also explored the nature of the base. In particular, we focused our interest on the nature of the counter cation by using various carbonate: cesium, potassium, or lithium. We do not observe conversion with lithium carbonate, whereas 10% conversion was obtained with potassium carbonate (Table 4-4, entries 8-9). Thus, the conversion is higher with cesium carbonate. Indeed, the attack of the lone pair of the triazole will be facilitated with the larger and softest cesium counter-cation. Moreover, Cs₂CO₃ increased solubility in DMF compared to potassium carbonate. We also studied the use of strong bases were, like potassium hydroxide or sodium hydride, which led to higher amounts of by-products. Finally, ^tBuOK showed a good conversion of 90%. Additional studies with some aryl modulations have been performed to compared Cs₂CO₃ and ^tBuOK (Table 4-5).

Table 4-4: Screening condition for benzylation of *N*³-pyridine 1*H*-1,2,4-triazole diamine.



entry	Solvent	Conversion ^b , %	entry	Bases	Conversion ^b , %
Base: Cs ₂ CO ₃			Solvent: DMF		
1	DMF	80	1	Cs ₂ CO ₃	80
2	Dioxane	n.c.	7	-	n.c.
3	Acetonitrile	n.c.	8	Li ₂ CO ₃	n.c.
4	THF or THF/DMF	n.c.	9	K ₂ CO ₃	10
5	H ₂ O/DMF	n.c.	10	KOH	70
			11	NaH	80
			12	^t BuOK	90

^aReagents and conditions: Bases (1.2 eq.), *N*³-pyridinetriazole **MCK245** (1.0 eq.), Benzyl chloride **3.64a** (1.0 eq.); ^bGlobal conversion from **MCK245** into the mixture of regioisomers **MCK254** and **4.15** observed by HPLC. n.c: no conversion.

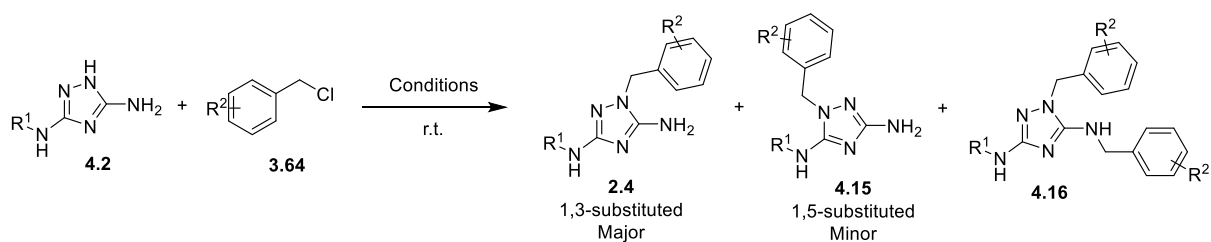
In some case (*e.g.* phenyl ring as R¹ and hydrogen as R²), these optimized conditions (^tBuOK in DMF) led to a significant improvement of the conversion rates. Furthermore, the ratio towards the major/minor isomers is higher, but not significant, towards **MCK249** regioisomer with ^tBuOK (9/1),

compared to 8/2 with Cs₂CO₃. In the case of *N*²-pyridine, using this condition, the conversion was improved from 10% up to 79%; moreover, also reduces the reaction time from 16 h to 1-2 h. Besides, the conversion only leads to **MCK253**, allowing to increase the yield from 2% to 37%. Furthermore, by LCMS and HPLC studies, a side-product **4.16** corresponding to *N*⁵-1-dibenzyl-*N*³-(aryl)-1*H*-1,2,4-triazole-3,5-diamine has been observed.

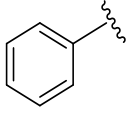
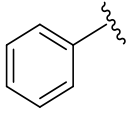
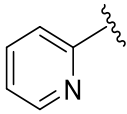
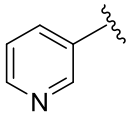
The addition of ^tBuOK as base allowed the direct deprotonation of the amine N-1 **4.2**. This can be predicted by calculation;³ the p*K*_b values are 13.45 for N-1 and 14.05 for N-5 **4.2**, and experimentally attested by a change in the color (from clear purple to deep red). Conversely, the use of Cs₂CO₃ induces slow reaction kinetics (coloration of the solution: deep purple). Finally, no deprotonation occurred with Li₂CO₃ (no color change due to the weakness of the base).

The benzylation step was performed by the dropwise addition of halobenzyl derivatives (**3.64** or **3.74**) into the deprotonated N-1 **4.2**. The corresponding reaction leads to a mixture of two regioisomers: **MCK249** (major) and **MCK248** (minor) (Table 4-5). These conditions in hand, we synthesized a series of derivatives with selected electro-withdrawing or electron-donating groups (halogen, methoxy, methyl, nitro, trifluoromethyl, or cyano) on the benzyl group. We also studied the modification of the methylene link by an ethylene or an ethan-1-one group. Hence, these derivatives were obtained from the two 1*H*,1,2,4-triazole intermediates **MCK243** and **MCK246**. Besides, two different separation system conditions were noted.

Table 4-5: Conversion survey for the benzylation step.



³ Values was predicted with the ChemAxon calculator

entry	R ¹	R ²	Cs ₂ CO ₃		^t BuOK	
			Conversion ^b , %	Ratio Maj./Min.	Conversion ^b , %	Ratio Maj./Min.
1		H	44-69	8/2	68-74	9/1
2		2-Me	45-56	8/2	78-80	9/1
3		H	10 ^c	3/7	79	10/0
4		H	80	n.d.	90	n.d.

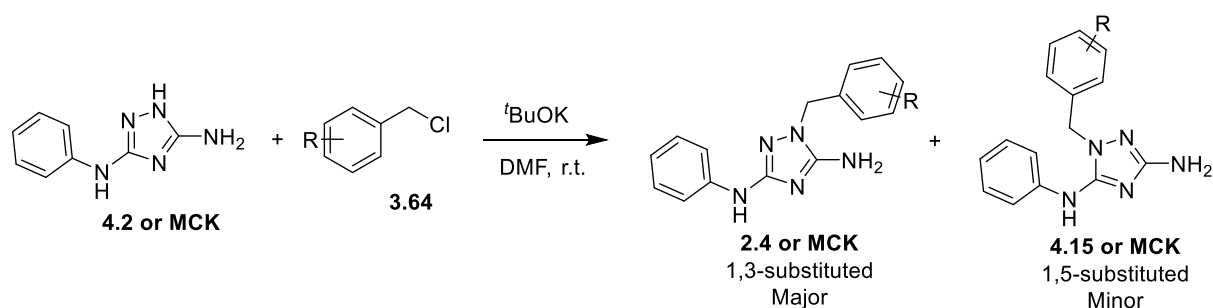
^aReagents and conditions: Bases (1.0 - 1.2 eq.), triazole intermediate **4.2** (1.0 eq.), R²-Benzyl chloride **3.64** (1.0 eq.) in DMF at r.t. for 2 h; ^bGlobal conversion from **4.2** into the mixture of regioisomers **2.4** and **4.15** observed by HPLC. ^cResult after 16 h. n.d.: not determined.

We usually observed conversion rates close to 80%; however, the isolated yields in purified products were low because of difficult separation. We tried to optimize our separation condition to obtain preferentially 1,3-substituted major regioisomer.

First, the separation method developed before was used (in 4.2.2 First results). This method consisted of using a mixture of CH₂Cl₂/THF as eluent for chromatography to separate easily R¹ phenyl ring and using a mixture of CH₂Cl₂/MeOH for purifying R¹ N²-pyridyl ring. However, even with these purification systems and with the optimized base (^tBuOK), yields of pure products remain low (5-30% yield for major while 3-7% yield for minor). It has been noted that the yields are higher for the N²-pyridyl subseries due to a higher conversion to our desired regioisomer **2.4**, 20-56% yield.

Next, we tested an improvement in the purification procedure base on a reverse-phase gel chromatography system with H₂O/CH₃CN as solvent (Table 4-6). After optimization steps, greater isolation of 1,3-substituted **2.4** was obtained for R¹ phenyl ring: from 7-22% to 30-50%. Moreover, the global yields increased from 7-22% yield to 38-57%. It is also to underline that in these conditions, we were able to isolate some minor compound, which was not possible before, as **MCK338** and **MCK339**.

Table 4-6: Isolated yield of the optimization separation method.

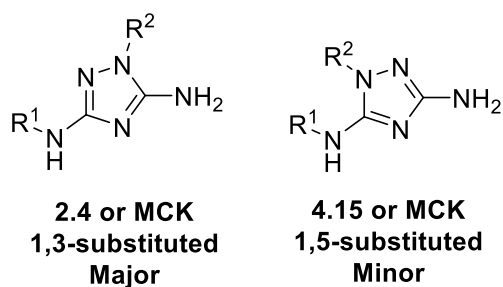


entry	R	Normal Phase ($\text{CH}_2\text{Cl}_2/\text{THF}$)		Reverse phase ($\text{H}_2\text{O}/\text{CH}_3\text{CN}$)	
		Maj.	Min.	Maj.	Min.
1	H	14 ^a (MCK249)	7 ^a (MCK248)	50 ^b (MCK249)	7 ^b (MCK248)
2	2-Me	13 ^a (MCK250)	n.i.	46 ^b (MCK250)	n.i.
3	4-isopropyl	14 ^b (MCK263)	3 ^b (MCK262)	28 ^b (MCK263)	12 ^b (MCK262)
4	3-Br	22 ^b (MCK264)	n.i.	30 ^b (MCK264)	10 ^b (MCK 339)
5	4-Me	7 ^b (MCK271)	n.i.	38 ^b (MCK271)	n.i.
6	3-CF ₃	15 ^b (MCK273)	1 ^b (n.d.)	41 ^b (MCK273)	11 ^b (MCK 338)

^aReagents and conditions: (a) **MCK243** (1.0 eq.), R-benzyl chloride (1.0 eq.), Cs_2CO_3 (1.0 eq.) in DMF, 0°C to r.t.; (b) **MCK243** (1.0 eq.), R-benzyl chloride (1.0 eq.), $t\text{BuOK}$ (1.0 eq.) in DMF, 0°C to r.t.. n.i.: not isolated, n.d.: not described.

These various improvements enabled us to obtain 40 molecules for the first D₁ series in addition to the previous 10 optimized compounds (4.2.2 First results), summarized in table 4-7.

Besides, the low yields obtained are comparable to those reported in the literature with similar regioisomery problems. Indeed, we saw that the only molecule described, **4.10** had a yield of 12%⁵⁰⁴. Moreover, 1-benzyl-1H-1,2,4-triazole mono or di-amino substituted have a range of 14-36% yield^{506,507}.

Table 4-7: Series D₁ products.

Compound ^a	R ¹	R ²	Compound ^a	R ¹	R ²
Phenyl series			Pyridine series		
1,3-substituted					
MCK249 (50%) ^d	Ph	benzyl	MCK253 (37%) ^c	N ² -pyridyl	benzyl
MCK250 (46%) ^d	Ph	2-methylbenzyl	MCK254 (16%) ^b	N ³ -pyridyl	benzyl
MCK256 (30%) ^b	Ph	2,6-difluorobenzyl	MCK255 (19%) ^c	N ⁴ -pyridyl	benzyl
MCK261 (8%) ^b	Ph	3-methoxybenzyl	MCK258 (45%) ^c	N ² -pyridyl	3-methoxybenzyl
MCK263 (28%) ^d	Ph	4-isopropylbenzyl	MCK259 (20%) ^c	N ² -pyridyl	2,6-difluorobenzyl
MCK264 (30%) ^d	Ph	3-bromobenzyl	MCK269 (53%) ^c	N ² -pyridyl	2-methylbenzyl
MCK267 (21%) ^c	Ph	4-benzonitrile	MCK270 (56%) ^c	N ² -pyridyl	4-isopropylbenzyl
MCK268 20%) ^c	Ph	2,6-dichlorobenzyl	MCK276 (25%) ^c	N ² -pyridyl	3-bromobenzyl
MCK271 (38%) ^d	Ph	4-methylbenzyl	MCK278 (7%) ^c	N ² -pyridyl	2,6-dichlorobenzyl
MCK272 (18%) ^c	Ph	4-chlorobenzyl	MCK279 (25%) ^c	N ² -pyridyl	4-methylbenzyl
MCK273 (41%) ^d	Ph	3-(trifluoromethyl)benzyl	MCK280 (17%) ^c	N ² -pyridyl	4-chlorobenzyl
MCK274 (5%) ^c	Ph	3,5-difluorobenzyl	MCK281 (12%) ^c	N ² -pyridyl	4-benzonitrile
MCK275 (8%) ^c	Ph	3-nitrobenzyl	MCK282 (41%) ^c	N ² -pyridyl	3-(trifluoromethyl)benzyl
MCK277 (7%) ^c	Ph	2,4-difluorobenzyl	MCK283 (29%) ^c	N ² -pyridyl	3,5-difluorobenzyl
MCK288 (5%) ^c	Ph	4-nitrobenzyl	MCK284 (46%) ^c	N ² -pyridyl	2,4-difluorobenzyl

MCK297 (14%) ^d	Ph	2-nitrobenzyl	MCK289 (21%) ^c	N ² -pyridyl	2-nitrobenzyl
MCK298 (20%) ^d	Ph	3,4,5-trimethoxybenzyl	MCK290 (24%) ^c	N ² -pyridyl	4-nitrobenzyl
MCK299 (33%) ^d	Ph	phenylethan-1-one	MCK292 (20%) ^c	N ² -pyridyl	3-nitrobenzyl
MCK301 (9%) ^d	Ph	phenethyl	MCK293 (16%) ^c	N ² -pyridyl	3,4,5-trimethoxybenzyl
1,5-substituted			MCK294 (15%) ^c	N ² -pyridyl	phenylethan-1-one
MCK248 (7%) ^d	Ph	benzyl	MCK295 (12%) ^c	N ² -pyridyl	(3-nitrophenyl)ethan-1-one
MCK257 (5%) ^c	Ph	2,6-difluorobenzyl	MCK296 (9%) ^d	N ² -pyridyl	phenethyl
MCK260 (1%) ^c	Ph	3-methoxybenzyl	1,5-substituted		
MCK262 (3%) ^c	Ph	4-isopropylbenzyl	MCK252 (traces) ^b	N ² -pyridyl	benzyl
MCK300 (3%) ^d	Ph	phenethyl			
MCK338 (11%) ^d	Ph	3-(trifluoromethyl)benzyl			
MCK339 (10%) ^d	Ph	3-bromobenzyl			

^aIsolated yields are indicated in brackets. ^bCs₂CO₃, CH₂Cl₂/THF for R¹ phenyl or CH₂Cl₂/MeOH for R¹ N-pyridyl separation method. ^c ^tBuOK, CH₂Cl₂/THF for R¹ phenyl or CH₂Cl₂/MeOH for R¹ N-pyridyl separation method. ^d ^tBuOK, H₂O/CH₃CN separation method.

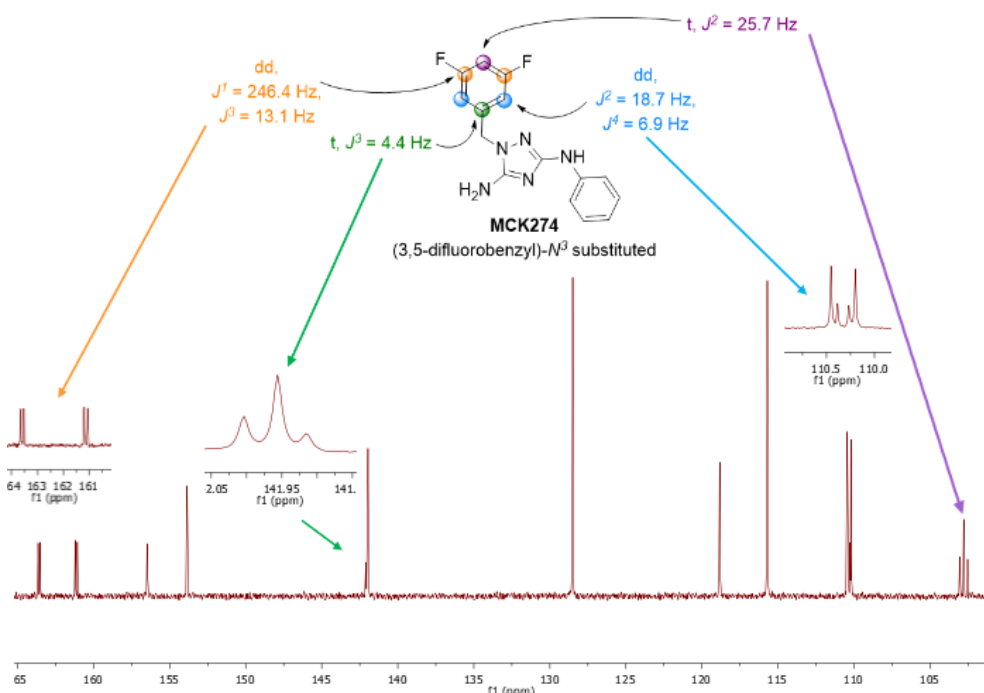
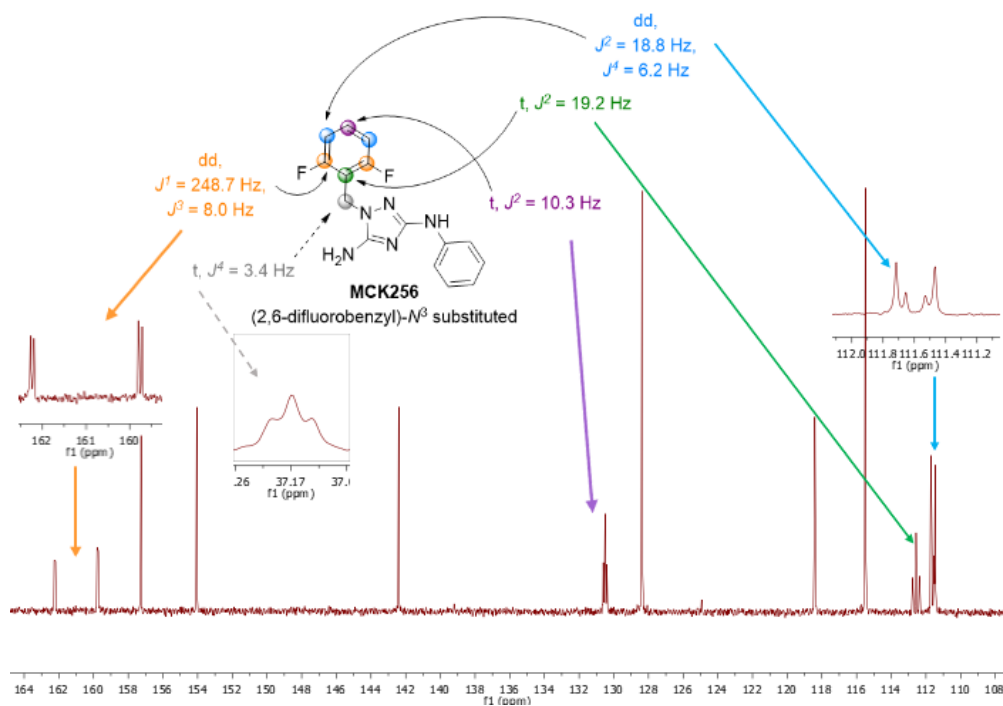
4.2.3.2 Chemical characterization of fluoro compounds

The ¹³C of the 2,6-difluoro and 3,5-difluoro compounds (**MCK256** and **MCK274**) showed (Figure 4-8):

- a doublet of doublet for the two carbons substituted with both fluorine in J¹ and J³ (in orange);
- a doublet of doublet for the two CH in β position of fluor with J² and J⁴ (in blue);
- a triplet for the quaternary carbon, respectively J², J³ (in green);
- a triplet for the CH which couples with the fluorines, respectively J³ and J² (in purple);
- also, for 2,6-difluoro **MCK256**, we can see a triplet for CH₂, which sees the fluors in J⁴ (in grey).

These carbon analyses were confirmed by 2D NMR: HSQC, HMBC, proton decoupled from fluorine, carbon decoupled from fluorine, and carbon coupled to fluorine and the proton. In the latter, we could confirm the carbon equivalence. A doubt arises for the carbon carrying the proton, which in uncoupled

carbon does not show any link with fluorine except if we consider the frequency equal to 0 Hz. However, no correlation exists, of course, to 2,4-difluoro product **MCK277** with five doublet of doublet and one triplet in a different position depending of the coupling constant between the carbon and fluorine. All the J constants are reported with corresponding peak of ^{13}C NMR in Figure 4-8. Thanks to this study, the positions of the fluor were confirmed by fluorine-carbon couplings. Thus, allowed the most comprehensive analysis of the ^{13}C NMR.



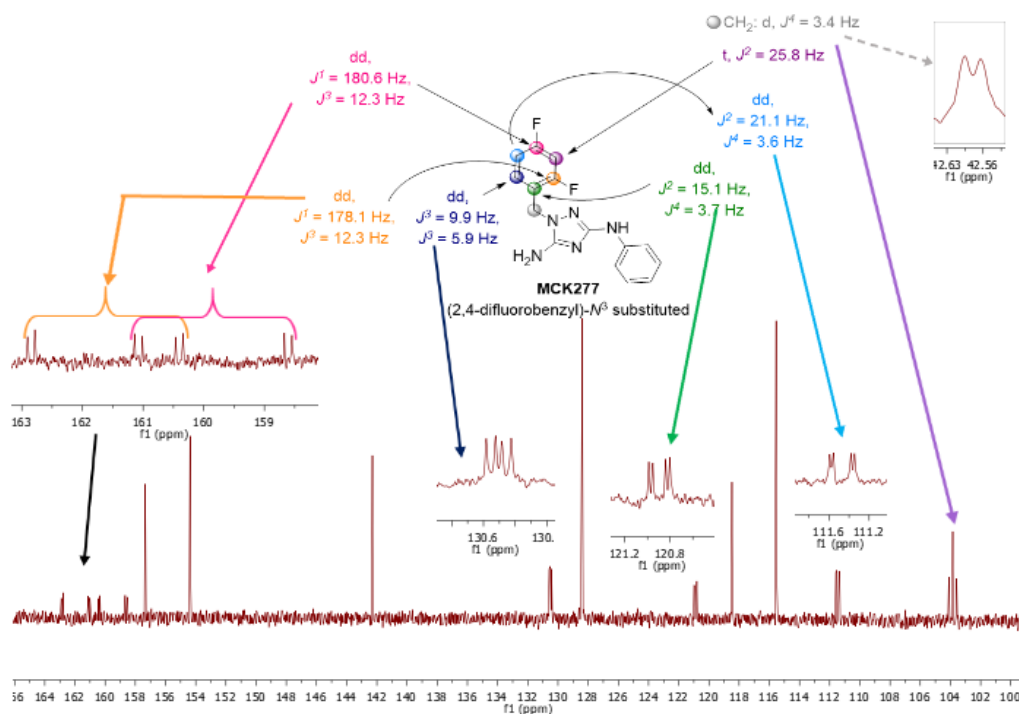


Figure 4-8: ^{13}C NMR (coupling of F, decoupling of H) data supporting to fluoro compounds **MCK256**, **MCK274** and **MCK277**.

4.2.3.3 Biological evaluation

4.2.3.3.1 Cytotoxicity assay

We assessed the cytotoxicity of the newly synthesized compounds on ARPE cells to evaluate the biological effects of the benzyl group modulations. All the compounds were tested at 2.5, 10, and 25 μM upon 48 h incubation (Table 4-8). Above all, **MCK250**, **MCK263-265**, and **MCK272-273** showed interesting results and have been selected to be also assayed at 50 μM . Then the cases of **MCK263-265** and **MCK272-273** report a proliferation's decrease by more than 50%, which represents significant anti-proliferative effects.

Table 4-8: Cell viability by XTT assays on ARPE cells after 48 hours of treatment at 2.5, 10, 25, and 50 μM of the indicated compound compared to the DMSO control.

Compounds	% cell viability in ARPE cells			
	2.5 μM	10 μM	25 μM	50 μM
MCK133	99.0 \pm 0.0	43.6 \pm 7.0	54.4 \pm 0.0	58.0 \pm 9.8
MCK140	25.4 \pm 5.5	13.5 \pm 3.4	4.6 \pm 3.9	6.2 \pm 3.3
MCK243	118.9 \pm 2.9	94.0 \pm 5.5	106.9 \pm 0.0	n.d.
MCK244	121.8 \pm 3.5	91.8 \pm 8.1	90.1 \pm 5.5	n.d.
MCK245	114.7 \pm 7.4	99.7 \pm 4.4	115.0 \pm 5.4	n.d.
MCK246	116.7 \pm 4.4	102.4 \pm 0.0	108.1 \pm 0.0	n.d.
MCK247	74.3 \pm 7.2	95.0 \pm 1.9	93.4 \pm 5.4	n.d.
MCK248	74.2 \pm 7.4	82.0 \pm 1.2	70.2 \pm 2.7	n.d.
MCK249	82.1 \pm 2.9	90.5 \pm 8.7	66.6 \pm 1.9	n.d.
MCK250	101.8 \pm 4.1	83.7 \pm 0.0	77.7 \pm 0.0	73.2 \pm 0.0
MCK251	107.6 \pm 7.4	101.3 \pm 4.2	116.8 \pm 5.2	n.d.
MCK252	101.6 \pm 3.5	92.8 \pm 3.1	86.8 \pm 0.0	n.d.
MCK253	132.8 \pm 0.0	85.4 \pm 0.0	117.5 \pm 0.0	n.d.
MCK254	134.7 \pm 5.2	97.9 \pm 6.5	91.7 \pm 2.8	n.d.
MCK255	133.7 \pm 7.2	114.7 \pm 0.0	100.9 \pm 0.0	n.d.
MCK256	124.5 \pm 3.1	99.0 \pm 0.0	108.0 \pm 0.0	n.d.
MCK257	92.8 \pm 1.9	109.4 \pm 9.2	103.1 \pm 4.1	n.d.
MCK258	100.3 \pm 5.5	98.8 \pm 2.3	101.8 \pm 3.0	n.d.
MCK259	105.8 \pm 9.8	101.6 \pm 2.2	113.0 \pm 0.0	n.d.
MCK260	103.9 \pm 0.0	99.4 \pm 0.0	97.3 \pm 0.0	n.d.
MCK261	109.4 \pm 6.4	99.1 \pm 9.7	93.9 \pm 2.6	n.d.
MCK262	128.3 \pm 5.7	102.2 \pm 7.6	108.7 \pm 4.0	n.d.
MCK263	123.5 \pm 0.0	84.0 \pm 0.0	58.3 \pm 4.8	38.0 \pm 4.8
MCK264	118.0 \pm 0.0	65.7 \pm 4.0	79.2 \pm 1.5	49.9 \pm 0.0
MCK265	116.0 \pm 7.3	54.5 \pm 8.3	50.3 \pm 9.6	32.6 \pm 6.8
MCK266	132.1 \pm 0.0	96.0 \pm 0.0	126.8 \pm 0.0	n.d.
MCK267	95.2 \pm 4.5	97.2 \pm 0.0	74.3 \pm 6.1	n.d.
MCK268	206.9 \pm 8.0	95.9 \pm 5.8	98.1 \pm 6.1	n.d.
MCK269	111.2 \pm 0.0	108.4 \pm 0.0	112.1 \pm 9.0	n.d.
MCK270	113.2 \pm 0.0	115.2 \pm 0.0	116.2 \pm 0.0	n.d.
MCK271	119.4 \pm 2.0	106.8 \pm 0.0	95.1 \pm 7.7	n.d.
MCK272	109.8 \pm 8.6	93.8 \pm 5.9	65.6 \pm 4.0	35.7 \pm 3.3

MCK273	116.4 ± 2.0	69.1 ± 4.9	56.0 ± 9.1	27.4 ± 5.3
MCK274	133.6 ± 0.0	91.2 ± 0.0	89.2 ± 9.5	n.d.
MCK275	134.4 ± 0.0	80.7 ± 0.0	80.4 ± 0.0	n.d.
MCK276	122.6 ± 0.0	86.3 ± 0.0	119.6 ± 0.0	n.d.
MCK277	106.4 ± 0.0	97.7 ± 5.9	90.1 ± 3.6	n.d.
MCK278	95.3 ± 0.0	84.8 ± 0.0	94.1 ± 2.3	n.d.
MCK279	112.8 ± 0.0	87.9 ± 0.0	109.0 ± 8.5	n.d.
MCK280	106.6 ± 0.0	102.5 ± 0.0	110.2 ± 0.0	n.d.
MCK281	115.0 ± 0.0	95.7 ± 7.1	106.7 ± 0.0	n.d.
MCK282	113.1 ± 0.0	92.8 ± 2.3	109.5 ± 1.8	n.d.
MCK283	108.8 ± 0.0	90.8 ± 0.0	99.8 ± 0.0	n.d.
MCK284	111.8 ± 0.0	77.2 ± 5.8	94.9 ± 0.0	n.d.
MCK285	140.4 ± 0.0	91.7 ± 5.2	84.8 ± 0.0	n.d.
MCK286	136.2 ± 0.0	121.6 ± 0.0	80.6 ± 0.0	n.d.

The assay is based on the cleavage of the yellow tetrazolium salt XTT to form an orange formazan dye only by metabolic active cells (viable cells). n.d.: not determined.

MCK250, **MCK263-265**, and **MCK272-273** have also been tested *via* cell viability XTT assay on the TIME cells, corresponding to endothelial cells at 12.5, 25, and 50 µM for 48 h. A strong anti-proliferative effect has been noted for **MCK264-265** and **MCK272-273** (Table 4-9).

Table 4-9: Cell viability by XTT assays on TIME cells after 48 hours of treatment at 12.5, 25 and 50 µM of the indicated compound compared to the DMSO control.

Compounds	% cell viability in TIME cells		
	12.5 µM	25 µM	50 µM
MCK133	76.0 ± 9.4	69.3 ± 0.0	57.8 ± 2.8
MCK140	5.2 ± 1.5	7.3 ± 4.2	6.5 ± 2.8
MCK250	99.2 ± 3.0	89.7 ± 7.9	80.2 ± 5.3
MCK263	89.1 ± 3.5	68.0 ± 3.8	102 ± 4.9
MCK264	87.8 ± 7.2	72.9 ± 6.0	39.5 ± 2.1
MCK265	82.0 ± 6.6	61.1 ± 3.6	31.5 ± 3.5
MCK272	70.4 ± 4.2	76.5 ± 4.2	29.5 ± 3.6
MCK273	71.5 ± 0.0	71.4 ± 3.5	31.2 ± 1.3

The assay is based on the cleavage of the yellow tetrazolium salt XTT to form an orange formazan dye only by metabolic active cells (viable cells).

In addition, the anti-proliferative effects of our compounds have also been assayed on TFE3 cells (CXCR1⁺ and CXCR2⁺ kidney cancer). Compared to the reference compounds, **MCK133** and **MCK140**, whose have inhibition activity on cancer cells, no cytotoxicity has been observed with our new derivatives. The most relevant effects on ARPE cells have been reported with **MCK263-265** and **MCK272-273**, in 38-52%, except for **MCK250** with the nearly equivalent percentage of 73% (Figure 4-9).

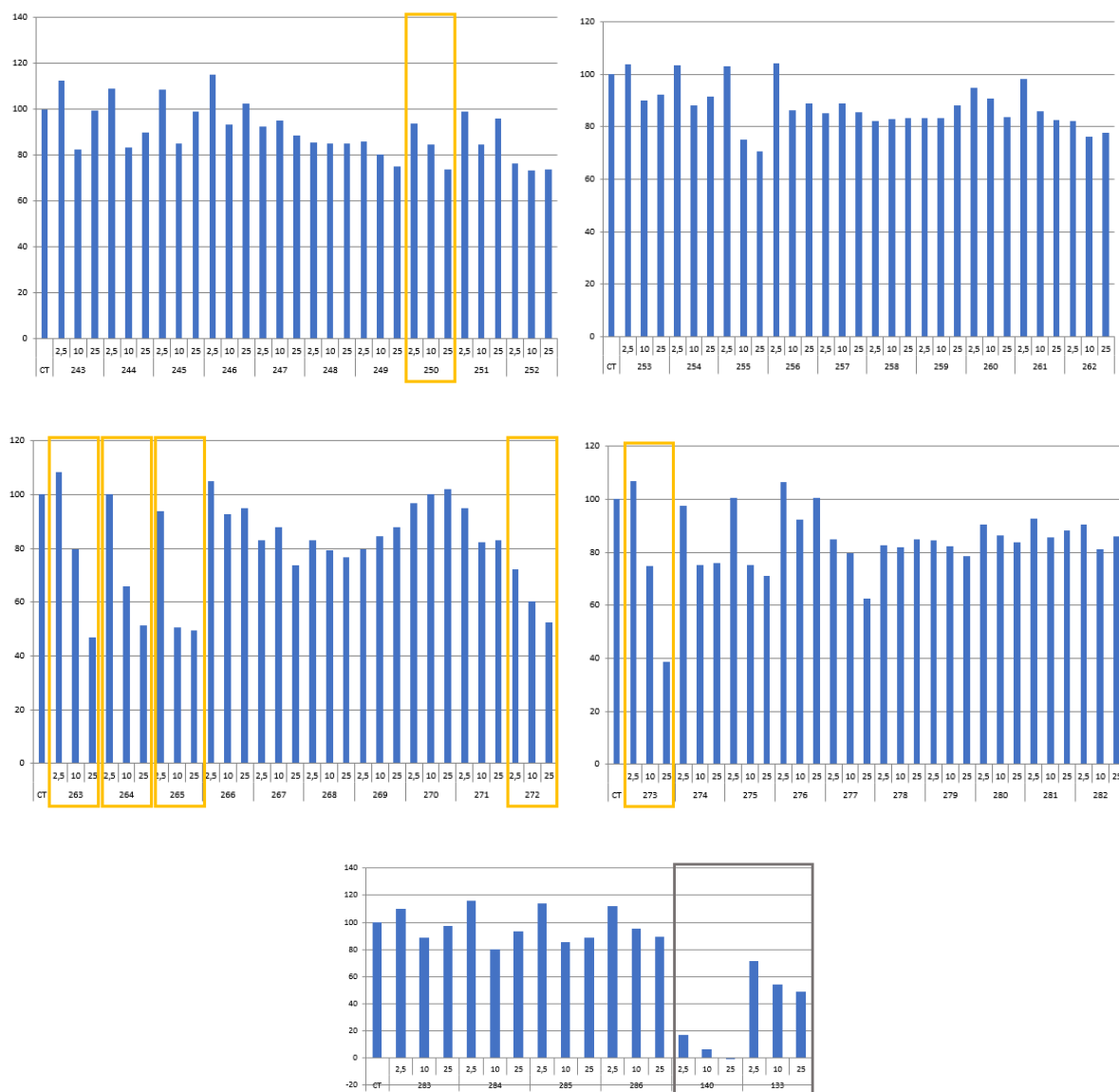
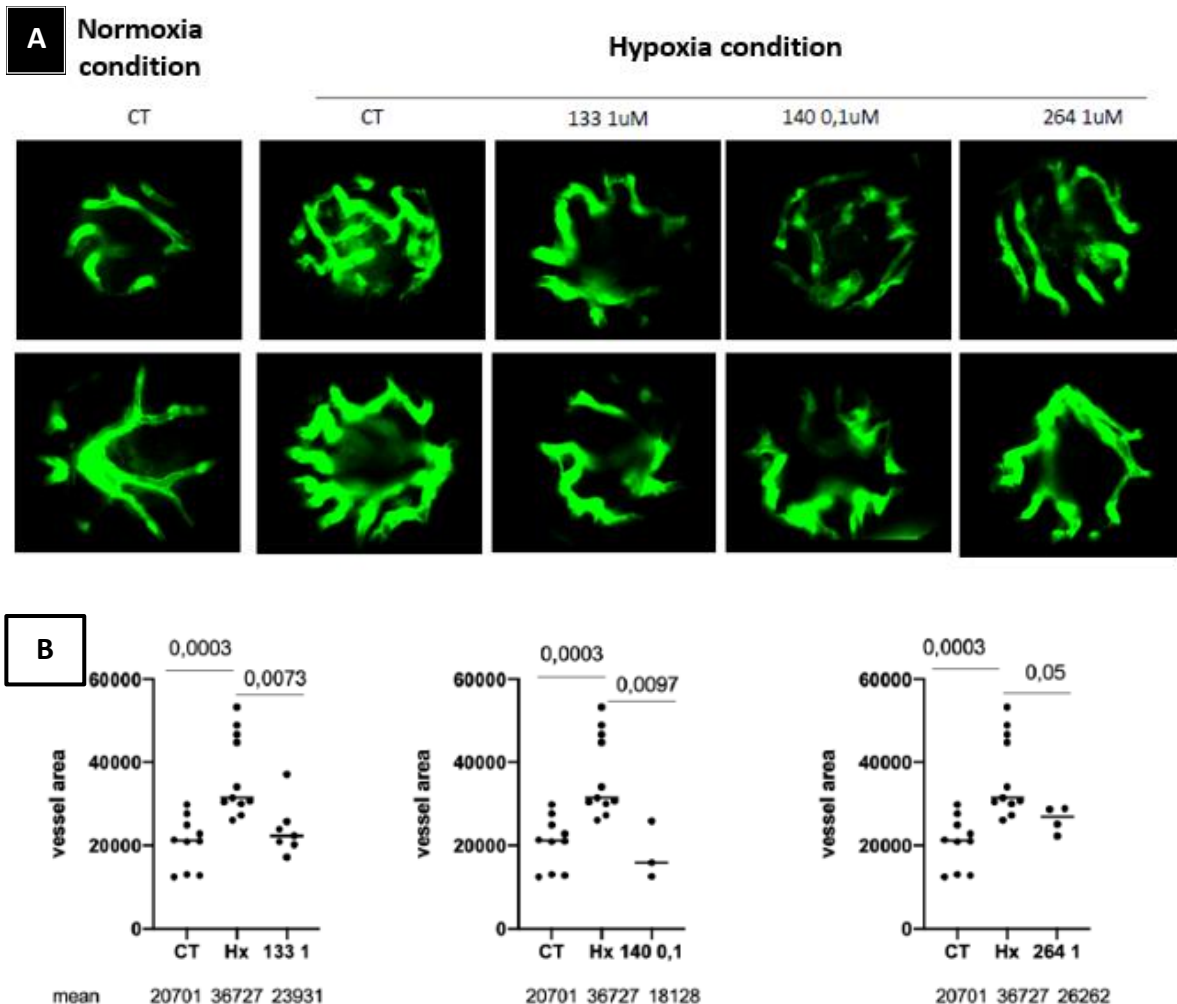


Figure 4-9: Cell viability on TFE3 cells after 48 hours of treatment at 2.5, 5, and 25 μM of the indicated compound compared to the DMSO control. The assay is based on the cleavage of the yellow tetrazolium salt XTT to form an orange formazan dye only by metabolic active cells (viable cells).

4.2.3.3.2 ZebraFish

We studied our compound *in vivo* in a zebrafish model. These microscopic animals are transgenic and express the GFP (green fluorescent protein) into their blood vessel cells constitutively. Thus, allowing easy visualization of their vascularization in different organs. In hypoxic conditions, the pro-angiogenic potency may be therefore quantified: under hypoxia (Hx), the vessel area increases above 40000 nm² compared to CT below 20000 nm² in normoxia (Figure 4-10, B-C). Thus, we can test the anti-angiogenic potential of our newly synthesized compounds, which can be directly dissolved in the aquarium at a final concentration of 0.1 or 1 μM. After 48 h, the environment in the zebrafish eye was analyzed (Figure 4-10, A) by fluorescence analyses. Thanks to the first cytotoxicity tests, **MCK264** was chosen to evaluate its anti-angiogenic activity.



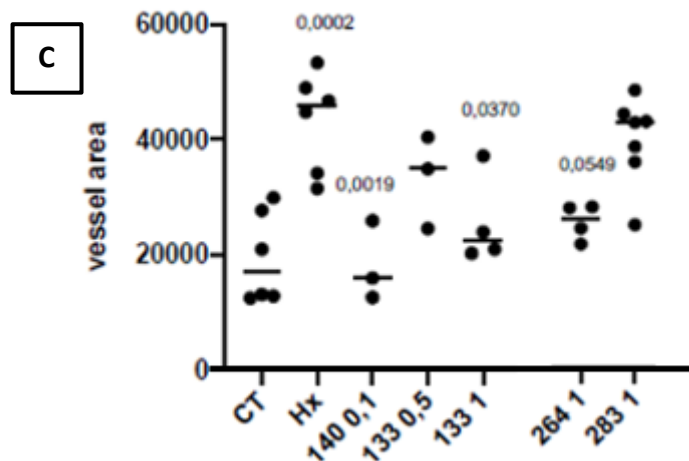


Figure 4-10: ZebraFish in eyes with 5% hypoxia after 48 h. CT: Control. Hx: under hypoxia. The line is the median, and the points are the fish, the quantification of the vessel area for each fish.

With our reference compounds (**MCK133** and **MCK140**), the vessel area decreases widely; however, in this case, the anti-angiogenic effect may be related to toxicity. The toxicity value that kills zebrafish in hypoxia of **MCK140** is above 0.25 μM , so **MCK140** was injected at 0.1 μM , compare to the toxicity value of **MCK133**, above 2.5 μM . **MCK283** is considered as a negative control due to no effect in decreasing vessel area, even if we increase the concentration from 1 to 5 μM . Finally, **MCK264** has an efficient effect by decreasing vessel area, close to the CT in normoxia condition, without revealed toxicity effect against zebrafish. A toxicity assay has been performed with increasing doses confirming the toxic effect of **MCK140** with $\text{EC}_{50} = 1 \mu\text{M}$ compared to **MCK264** with $\text{EC}_{50} = 10 \mu\text{M}$.

In conclusion, **MCK264** has a clear anti-angiogenic effect *in vivo* without toxicity.

4.2.3.3.3 Western blot assay

The inflammatory axis is induced by ERK/AKT signaling pathway activation in AMD. Endothelial cells (TIME cells) were stimulated with CXCL8 to induced activation of ERK pathway (p-ERK). MCK molecules were added to CXCL8 stimulation to determine if the reversion of this ERK pathway occurs or not: if MCK are active, there is a decreased of ERK pathway (p-ERK).

Table 4-10: Results of western blot assays on MCK243-305 in TIME cells.

Compounds ^a	Block pERK ^b	Compounds ^a	Block pERK ^b	Compounds ^a	Block pERK ^a
MCK133 ^c	0				
MCK243	n.y.d.	MCK264	n.y.d.	MCK285	0
MCK244	n.y.d.	MCK265	1	MCK286	0
MCK245	n.y.d.	MCK266	n.y.d.	MCK287	0
MCK246	n.y.d.	MCK267	n.y.d.	MCK288	0
MCK247	n.y.d.	MCK268	n.y.d.	MCK289	0
MCK248	n.y.d.	MCK269	n.y.d.	MCK290	0.5
MCK 249	n.y.d.	MCK270	n.y.d.	MCK292	0.5
MCK250	n.y.d.	MCK271	n.y.d.	MCK293	0
MCK251	n.y.d.	MCK272	n.y.d.	MCK294	0
MCK252	n.y.d.	MCK273	0	MCK295	1
MCK253	0	MCK274	0	MCK296	0
MCK254	n.y.d.	MCK275	0	MCK297	1
MCK255	n.y.d.	MCK276	1	MCK298	1
MCK256	0	MCK277	0	MCK299	1
MCK257	n.y.d.	MCK278	1	MCK300	1
MCK258	n.y.d.	MCK279	0.5	MCK301	0
MCK259	n.y.d.	MCK280	1	MCK302	1
MCK260	n.y.d.	MCK281	1	MCK303	1
MCK261	n.y.d.	MCK282	1	MCK304	1
MCK262	n.y.d.	MCK283	0	MCK305	0
MCK263	n.y.d.	MCK284	1		

^aMCK = 2.5 μM. ^bResults corresponding to 0 for no effective/no decrease, 0.5 for effective/weak decrease and 1 for effective/decrease. ^cMCK133 as reference. n.y.d.: not yet determined.

A decrease of ERK signaling pathway has been highlighted for **MCK265, MCK276, MCK278, MCK280-282, MCK284, MCK295, MCK297-300, and MCK 302-304** in TIME cells. Three of these compounds corresponding to intermediates and major regioisomers, three of the phenyl ring series and seven of *N*²-pyridine ring series.

In contrast, no effective effect in the decrease of ERK signaling pathway has been observed for **MCK273-275, MCK277, MCK283, MCK285-289, MCK293-294, MCK296, MCK301, and MCK305**. Another point is the no effective effect for **MCK253** and **MCK256**, which had shown interesting results in the Boyden chamber test (presented above).

4.2.3.3.4 Quantitative polymerase chain reaction (qPCR) assay

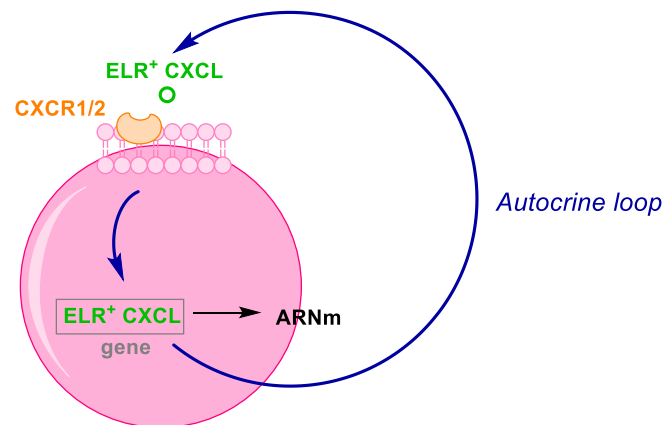


Figure 4-11: Autocrine loop of ELR⁺ CXCL -CXCR1/2.

ELR⁺ CXCL will bind to CXCR1/2 receptors allowing the induction of CXCL transcription (ELR⁺ CXCL mRNA increased) and increase in turn ELR⁺ CXCL expression and subsequent secretion to form an autocrine loop (Figure 4-11). The amount of mRNA transcript can be measured thanks to a quantitative polymerase chain reaction (qPCR). This evaluation allows to measurement of **ELR⁺ CXCL expression from a CXCL1 mRNA sample**. The same results were obtained with other ELR⁺ CXCL (CXCL2/5/8). Indeed, we can conclude CXCL-CXCR1/2 inhibition thanks to MCK antagonists owing to the decrease of mRNA.

Table 4-11: CXCL1 inhibition in TIME or ARPE cells.

Compounds ^a	qPCR ^b		Compounds ^a	qPCR ^b		Compounds ^a	qPCR ^b	
	TIME	ARPE		TIME	ARPE		TIME	ARPE
MCK243	0.5	0	MCK264	1	1	MCK285	0	0
MCK244	0	0	MCK265	0.5	1	MCK286	0	0
MCK245	0	0	MCK266	n.y.d.	0	MCK287	n.y.d.	n.y.d.
MCK246	0	0	MCK267	n.y.d.	0	MCK288	n.y.d.	n.y.d.
MCK247	0	0	MCK268	n.y.d.	0	MCK289	n.y.d.	n.y.d.
MCK248	0	0	MCK269	n.y.d.	0	MCK290	0	0
MCK 249	0	0	MCK270	n.y.d.	0	MCK292	0	0
MCK250	0	0	MCK271	n.y.d.	n.y.d.	MCK293	n.y.d.	0
MCK251	n.y.d.	0	MCK272	1	1	MCK294	n.y.d.	0
MCK252	n.y.d.	0.5	MCK273	1	0.5	MCK295	n.y.d.	0
MCK253	n.y.d.	0.5	MCK274	0	0	MCK296	n.y.d.	0
MCK254	n.y.d.	0.5	MCK275	0	0	MCK297	n.y.d.	0
MCK255	n.y.d.	0	MCK276	0	0	MCK298	n.y.d.	0.5
MCK256	n.y.d.	0	MCK277	0.5	0	MCK299	n.y.d.	0
MCK257	n.y.d.	0.5	MCK278	0	0	MCK300	n.y.d.	0
MCK258	n.y.d.	0	MCK279	0	0	MCK301	n.y.d.	0.5
MCK259	n.y.d.	1	MCK280	0	0	MCK302	n.y.d.	0
MCK260	n.y.d.	0	MCK281	0	0	MCK303	n.y.d.	0
MCK261	n.y.d.	0	MCK282	1	1	MCK304	n.y.d.	0
MCK262	n.y.d.	0.5	MCK283	0	0.5	MCK305	n.y.d.	0.5
MCK263	0.5	1	MCK284	0	0			

^aMCK = 2.5 μM. ^bResults corresponding to 0 for no effective/no decrease, 0.5 for effective/weak decrease and 1 for effective/decrease. n.y.d.: not yet determined.

For TIME cells, a weak decrease was observed for **MCK243**, **MCK263**, **MCK265**, **MCK277**, and inhibition of CXCL1-CXCR1/2 interaction effect for **MCK264**, **MCK272**, **MCK273**, **MCK282**, translating a better effect for phenyl ring (except **MCK282** corresponding to *N*²-pyridine ring). It has been interesting to note the weak decrease of mRNA for intermediates 1*H*-amino-1,2,4-triazole (**MCK243** and **MCK265**).

For ARPE cells, a weak decrease of mRNA was observed for **MCK252-254**, **MCK257**, **MCK262**, **MCK273**, **MCK283**, **MCK298**, **MCK301**, and **MCK305**, corresponding to both major and minor products, without intermediates this time. Besides, a substantial decrease of mRNA will be noted for the same MCK as in TIME cells (**MCK259**, **MCK263-265**, **MCK272**, and **MCK282**).

This last test was carried out in a broader choice of MCK, showing the weak effect of *N*²-pyridine group in position N-4 of 1,2,4-triazole (in both regioisomers major and minor), except for **MCK282**. Whereas an effective result was noted for phenyl modulation in position N-4 of 1,2,4-triazole in the case of major regioisomer.

4.2.3.3.5 Reactive Oxygen Species (ROS) assay

In the late stages of AMD, the number of Reactive Oxygen Species (ROS) increases significantly.¹³⁷ An evaluation based on a measure of ROS cytometry has been explored. ARPE cells were treated with hydrogen peroxide to induced ROS +/- MCK. Finally, DCFDA (2',7'-dichlorofluorescein diacetate) was added as a dye to measure ROS species. So we can follow if ROS disappears thanks to MCK inhibitors.

Table 4-12: Results of ROS assays on MCK246-292 in ARPE-H₂O₂ cells.

Compounds ^a	ROS ^b	Compounds ^a	ROS ^b	Compounds ^a	ROS ^b
MCK243	n.y.d.	MCK264	1	MCK285	1
MCK244	n.y.d.	MCK265	1	MCK286	1
MCK245	n.y.d.	MCK266	1	MCK287	1
MCK246	0.5	MCK267	0	MCK288	1
MCK247	0	MCK268	1	MCK289	1
MCK248	1	MCK269	1	MCK290	1
MCK 249	1	MCK270	0	MCK292	0
MCK250	0	MCK271	1	MCK293	0
MCK251	0	MCK272	0.5	MCK294	0
MCK252	0	MCK273	n.y.d.	MCK295	0
MCK253	0	MCK274	0.5	MCK296	0
MCK254	0	MCK275	0.5	MCK297	0
MCK255	0	MCK276	0	MCK298	0
MCK256	0	MCK277	0	MCK299	0
MCK257	1	MCK278	0	MCK300	0
MCK258	0	MCK279	0	MCK301	0
MCK259	0	MCK280	0	MCK302	0
MCK260	1	MCK281	0	MCK303	0
MCK261	1	MCK282	0	MCK304	0
MCK262	1	MCK283	0	MCK305	0
MCK263	0.5	MCK284	0		

^aMCK = 5 μM. ^bResults corresponding to 0 for no effective/no decrease, 0.5 for effective/weak decrease and 1 for effective/decrease. n.y.d.: not yet determined.

First, a weak ROS decrease has been observed for **MCK246**, **MCK263**, **MCK272**, and **MCK274-275**. Secondly, a positive ROS decrease for **MCK248-249**, **MCK257**, **MCK260-262**, **MCK264-266**, **MCK268-269**, **MCK271** and **MCK285-290**. Finally, **MCK247**, **MCK250-256**, **MCK258-259**, **MCK267**, **MCK270**, **MCK276-284** and **MCK292-305** do not show disappearance of ROS.

In general, the MCKs with ROS decrease corresponds to phenyl group in position N-4 of 1,2,4-triazole, such as proton (**MCK248-249**), 3-bromo (**MCK264**), 4-chloro (**MCK272**) or 4-isopropyl (**MCK262-263**). Five intermediates also present a ROS decrease (e.g. **MCK265** with 3,4-dichloro substitution). Of note, two compounds (**MCK289-290**), substituted with *N*²-pyridyl modification in position N-4 and nitro groups in benzyl part, show ROS decrease.

By contrast, most compounds without ROS disappearance have a *N*²-pyridyl group in position N-4 of 1,2,4-triazole or has an ethyl or oxo modulation in place of methylene group.

Overall, phenyl ring in N-4 of 1,2,4-triazole and some intermediates 1*H*-1,2,4-triazole are more effective on the ROS decrease. Research is still ongoing regarding other MCKs.

In summary, in each biological evaluation, a correlation of activity was observed for **MCK263**, **MCK264**, and **MCK265**. We do not reproduce the positive result discovered for **MCK256** or **MCK253** earlier in Boyden chamber. However, we can explain it by studying cancer cells and not in the retina or endothelial cells.

To conclude, **MCK264** has presented a better activity and was chosen for the next D₂ series. Moreover, **MCK265**, corresponding to an intermediate 1*H*-1,2,4-triazole with 3,4-dichlorophenyl in position N-4, will be chosen to mix both effects of 3,4-dichloro for one side of phenyl in N-4 and 3-bromo or 4-isopropyl (**MCK263**) in another side of benzyl in N-1.

4.2.3.4 Dockings

Recently in 2020, a publication of the cryo-electron microscopy structures of CXCL8-activated human CXCR2 in complex with Gi protein has been published.⁵⁰⁸ Thanks to this model, docking studies were carried out to verify the binding on our Lead MCK with CXCR2 (Figure 4-12). Several MCK were chosen, the reference compound **MCK140** and **MCK263-265**, **MCK283** representing the amino-1,2,4-triazole

family. The higher vinardo score, the more binding is important. The vinardo score corresponds to the energies sum of predicted interaction between molecule and target.

In a green circle, three of our molecules have a high binding with CXCR2, between 8.75 to 9.5, compared to **MCK265** (red circle, Figure 4-12) below 7.75. This docking shows the necessity of the benzyl part contributing to confirm our pharmacophore represented by two aryl modulation in each part of the triazole core. Indeed, despite the good biological result of the intermediate 1*H*-1,2,4-triazole **MCK265** presented before, its vinardo score is weaker. In contrast, **MCK283** presents a high vinardo score without *in vitro* and *in vivo* effect in exudative AMD models (showing the limits of the predictive model). Finally, **MCK263-264** showed a clear antagonist effect of the interaction CXCL8-CXCR2, confirming a precedent positive effect to inhibit ELR⁺ CXCL-CXCR1/2 in exudative AMD models.

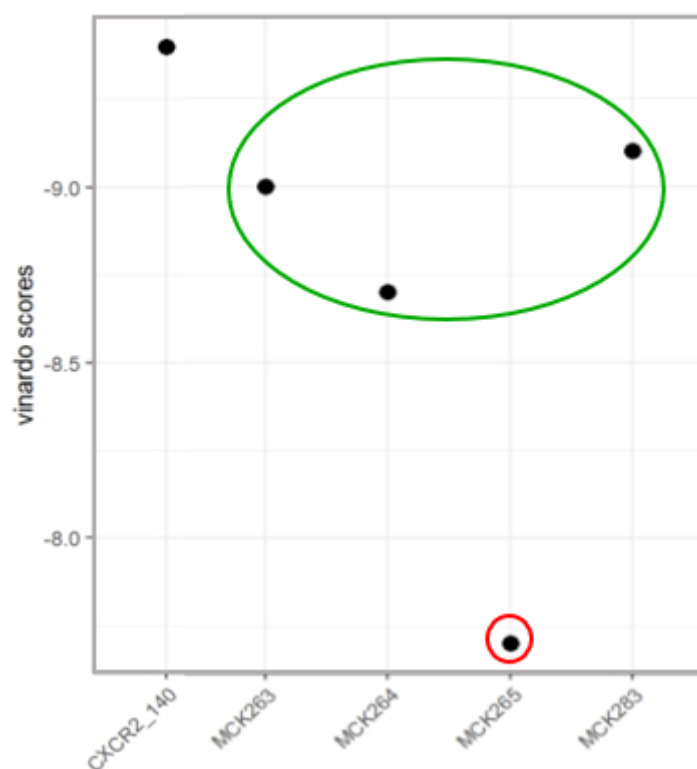


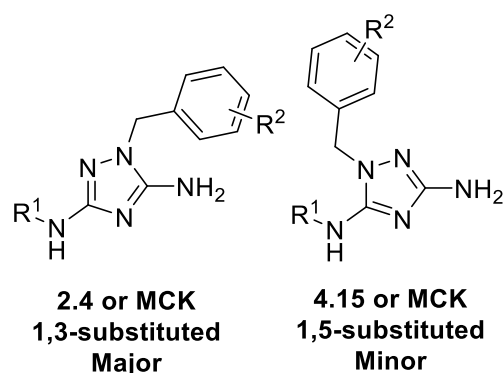
Figure 4-12: Docking of the **MCK263-265** and **MCK283** structures with cryo-electron microscopy structures of CXCR2.

4.2.4 Series D₂: functionalization of R¹ group

The subseries D₁ corresponded to the functionalization by various benzyl group in the position N-1 of the 1,2,4-triazole allowed to observe the positive biological evaluation of **MCK264**. Thus, 3-bromobenzyl substitution was chosen to perform the second series of compounds D₂: functionalization of R¹ group. Thanks to the results of these both functionalizations, the SARs of our pharmacophore will be highlighted.

The aryl part R¹ was modulated by various phenyls substituted with methyl, methoxy, halogen, nitro or ester mainly in position 4 and by changing with a pyridine ring in positions 3 or 4. Thanks to optimized conditions (^tBuOK in DMF) with purification by reverse-phase gel chromatography (H₂O/CH₃CN as solvent system), a range of thirteen new **MCK340-352** was isolated in 14-42% yields for 1,3-substituted 2-amino-1,3,4-triazole and 1-11% yields for 1,5-substituted 2-amino-1,3,4-triazole, allowing a yield of reaction until 50%. The reaction was also tested with nitro substituted group, but the isolated product corresponding to a mixture of major and minor regioisomers. Moreover, due to the interesting results obtained with **MCK263** and **MCK265**, compound **MCK350** was synthesised with 4-isopropylbenzyl part in one hand and 3,4-dichloro substitution in aryl part in the other hand. The biological assays are underways.

Table 4-13: Series D₂ products.



Compound	R ¹	R ²
1,3-substituted		
MCK340 (19%)	4-methoxybenzene	3-Br
MCK342 (35%)	4-methylbenzene	3-Br
MCK344 (42%)	4-chlorobenzene	3-Br
MCK346 (32%)	4-bromobenzene	3-Br
MCK348 (20%)	4-benzoate	3-Br
MCK349 (22%)	3,4-dichlorobenzene	3-Br
MCK350 (42%)	3,4-dichlorobenzene	4-isopropyl
MCK351 (29%)	N ³ -pyridyl	3-Br
MCK352 (14%)	N ⁴ -pyridyl	3-Br
1,5-substituted		
MCK341 (11%)	4-methylbenzene	3-Br
MCK343 (6%)	4-chlorobenzene	3-Br
MCK345 (1%)	4-bromobenzene	3-Br
MCK347 (2%)	benzoate	3-Br

^aThe isolated yields are indicated in brackets.

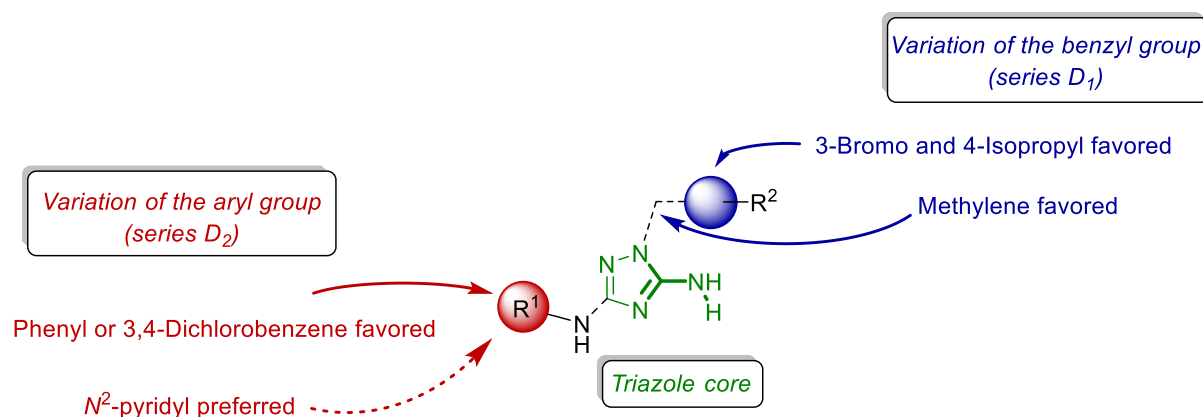
GENERAL CONCLUSION AND PERSPECTIVES

Exudative age-related macular degeneration (Exudative AMD) is a pathology mainly diagnosed in the elderly population, which leads to severe visual complications and blindness within few years. It is characterized by the neo-vascularization of the retro-foveolar choroid and a high inflammatory environment. The pathogenesis of AMD involves complex biological factors and remains poorly understood and treatment insufficiently effective. Currently, only symptomatic anti-VEGF (Vascular endothelial growth factor) treatments exist, which only delay blindness and 30% of the patients are insensitive to this therapy.

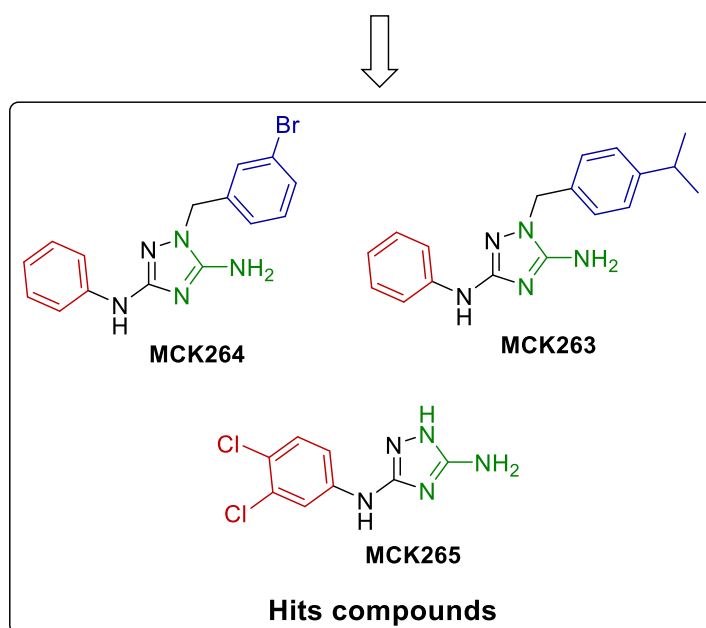
Angiogenesis and inflammation are two integrated processes allowing AMD development and progression. The blockage of the ERL⁺ CXCL cytokines signaling pathway and their CXCR1/2 receptors allow to tackle these two processes simultaneously. Our team has already selected two hit compounds, namely **MCK133** and **MCK140**, exhibiting anti-angiogenic and anti-inflammatory effects *in vitro* and *in vivo* in exudative AMD models. Based on these preliminary results and inspired by the chemical structure of the hit compounds, new bioactive molecules with new scaffolds have been designed and synthesized. They encompass an azole core and two aryl moieties to enhance their activity and their physicochemical properties. Precisely, four new series of compounds have been explored in this Ph.D. thesis: two with an imidazole core and two with a triazole core.

The three first series are: (i) *N*, aryl-1*H*-imidazol-2-amine (series A), (ii) 1-benzyl-4-aryl-1*H*-imidazol-2-amine (series B) and (iii) *N*,3-diaryl-1*H*-1,2,4-triazol-5-amine (series C). These series did not lead to conclusive results due to different problems in the synthetic pathways. Moreover, a structure revision of a series of compounds presented in the literature has been highlighted, namely the formation of 1,4-diaryl-2-aminoimidazoles **3.8** in the described conditions, instead of the claimed regioisomers 2-arylamino-4-arylimidazole **2.1** (series A).

Conversely, series D allowed us to develop a straightforward synthesis towards 1-benzyl-*N*³-1*H*-1,2,4-triazole-3,5-diamines, a scaffold encompassing our pharmacophore. Two main modifications of this scaffold have been studied by successive modulations introduced at the benzyl group (series D₁) and at the R¹ aryl group (series D₂). In addition, two types of triazole regioisomers (1,3- and 1,5-) have been obtained and their physicochemical properties and yields have been compared. In total, these series of molecules account for 63 fully characterized analogues, never described before. Moreover, 14 intermediates containing the 1*H*-1,2,4-triazole core have been obtained and fully characterized. To evaluate the efficiency of these series on angiogenesis and inflammation in exudative AMD models, all compounds have been tested in different biological assays including cytotoxicity, migration assay, western blot, qPCR, ROS production as well as on an *in vivo* zebrafish model.



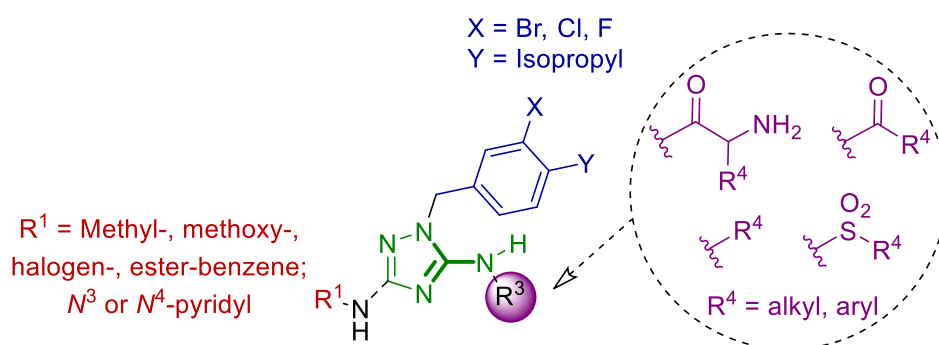
SAR determined during this Ph.D. thesis



Overall, from these results, two analogues **MCK263** and **MCK264**, corresponding to 4-isopropyl and 3-bromobenzyl derivatives, respectively, show the best activities to inhibit the ELR⁺ CXCL-CXCR1/2 interaction. In addition, several points of SAR have been deduced. First, the *N*²-pyridine is preferred compared to *N*³- or *N*⁴-pyridine in Boyden chamber assay. But the phenyl ring is favored in comparison of *N*²-pyridine due to no effect in decreasing vessel area through *in vivo* zebrafish assay on the analogue **MCK283**. The same result was observed in qPCR and ROS assays. Second, no activity improvement has been noticed by changing the methylene group by an ethyl or an ethan-1-one. Third, concerning the R¹ aryl part, the evaluation of 14 intermediates (1*H*-1,2,4-triazoles) particularly highlights the 3,4-dichlorobenzene group, with **MCK265** showing the best activities. In parallel, dockings studies confirmed the importance of the benzyl part. Promising compounds have already been synthesized composed of these favored substituents with 3-bromobenzyl or 4-isopropyl on one side and 3,4-dichlorobenzene group on the other, **MCK349** and **MCK350**.

The short-term perspectives of this Ph.D. thesis are the evaluation of D₂ series in exudative AMD models. In parallel, another *in vitro* assay is currently being implemented to evaluate the anti-angiogenic effect of MCKs. Next, the *in vivo* evaluation in zebrafish exudation AMD model will be extended to other interesting compounds of D₁ or D₂ Series.

Besides, to increase the molecular diversity and to improve the physicochemical properties, we would like to substitute the extra-cyclic nitrogen in series D₃ by various groups such as (i) amino acids by a simple peptide coupling, (ii) alkyl by direct substitution or aryl by metal-catalyzed *N*-arylation, and (iii) acyl or sulfonyl by a simple acylation or sulfonylation. With this last modification, the SAR will be complete. Furthermore, the mode of action can be deeply studied using biochemical tools already developed in our group, *i.e.*, biotin and fluorescence labelling in order to identify and validate the molecular target.



Perspectives: Substitution of amine group (series D₃)

As follow up, the activity of the lead compound (*e.g.* **MCK264**) will be evaluated *in vivo* in a rodent neovascular AMD model (mice, rats).

Finally, a galenic study of our leads MCKs using several formulations is envisaged towards different mode of administration, *e.g.*, topical administration in the eye (established collaboration, L. Demange and C. Charrueau). Moreover, to get further insight on the potentiating effect of anti-VEGF therapy by our lead compounds, we plan to test our MCKs in combination with anti-VEGF antibodies, brolucizumab (latest FDA approved treatment with high molar doses for fewer injections to patients) towards a curative therapy of exudative AMD. We also plan to evaluate the potency of the most active compounds in other cancer and non-cancer models (uveal melanoma, polyarthritis, etc).

Publications

- Fabre, M. *et al.* Synthesis, 3D-structure and stability analyses of NRPa-308, a new promising anti-cancer agent. *Bioorganic Med. Chem. Lett.* **29**, 126710 (2019)⁵⁰⁹ ;
- Fabre, M. *et al.* "Mild biamidine transfer conditions for the synthesis of aliphatic biguanides", submitted.
- Fabre, M., *et al.* "Recent advances in age-related macular degeneration therapies: a review", in preparation.

Chapter 5. ANNEXE PROJECTS

During this thesis, I had the chance to participate in two different annexe projects. The first project consisted in the synthesis of biguanides compounds, a topic well developed in the group⁴, developed with another Ph.D. student Rostyslav Bardovskyi. The second project concerned the stability studies on a potential anticancer agent NRPa-308.

5.1 BIAMIDINE TRANSFER IN BIGUANIDES COMPOUNDS

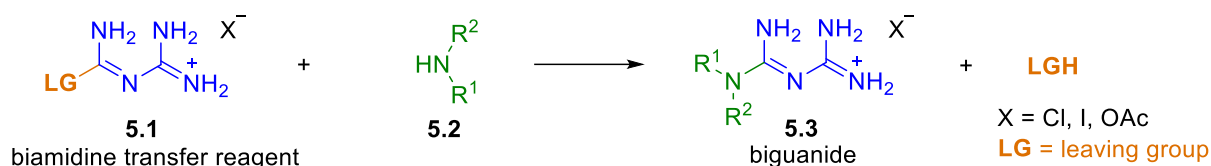
5.1.1 Introduction

Biguanides are a class of compounds of interest with wide applications in catalysis, superbase chemistry, as organometallic ligands and with a broad range of bioactivities such as antidiabetic (metformin), antimalarial, antiseptic (chlorhexidine), antiviral, and more recently anticancer.⁵¹⁰ Indeed, the biguanide function displays attractive properties of strong organic basicity, Lewis basicity and represents a potential pharmacophore related to its particular structure with 5 heteroatoms and 5 H-bonds sites modulated through several tautomeric forms. Meanwhile, these features render the synthesis and isolation of the biguanide derivatives sometimes tricky, with highly polar compounds and potential undesired complexation properties.^{511,512} The transformation of an amine to the corresponding biguanide derivative is particularly interesting. Precedents in the literature are scarce and basically rely on mixing an amine and cyanoguanidine in harsh conditions at temperatures above 100 °C (even neat) in the presence of hydrochloric acid.⁵¹²⁻⁵¹⁵ The conversion of aliphatic amines is especially demanding, and some improvements have been proposed recently such as the replacement of HCl by iron trichloride⁵¹⁶ or the use of silylamines.^{517,518} Nevertheless, conditions remain harsh and prolonged heating is still necessary.⁵¹⁹ Alternatively, the pre-activation of cyanoguanidine has been described through the use of *N*-(diaminomethylene)-1*H*-pyrazole-1-carboximidamide hydrochloride (**5.1a**)^{511,520-524} or *S*-methylguanylisothiuronium iodide (**5.1b**)^{511,525} as biamidine transfer reagents. However, these conditions suffer from low or moderate isolation yields, long reaction times and/or harsh conditions, and no general protocol exists for this transformation, especially for aliphatic amines. In this context, the purpose of this study has been to compare exhaustively the conditions and reagents used for the transfer of a biamidine group, propose new ones, and identify the problems related to this transformation. Mild high-yielding and straightforward reaction conditions suitable for various

⁴ "Synthetic accesses to biguanide compounds." Grytsai, O. Ronco, C. Benhida, R. Beilstein Journal of Chemistry (2021), accepted

amines have been developed, including a biological media compatible protocol in water. The study of the scope and limitations has demonstrated broad applicability for the synthesis of diverse biguanides in very smooth conditions.

5.1.2 Results and discussion



Scheme 5-1: Biguanide formation with biamidine transfer reagents.

The conversion of amines into monosubstituted biguanides consists of the addition of a biamidine group to the amine. This can be achieved either by direct addition of the amine to cyanoguanidine, which requires harsh reaction conditions or by using a biamidine transfer reagent. The latter comprises a biamidine moiety linked to a leaving group to allow the transfer by addition-elimination (Scheme 5-1). As the nature of the leaving group was predicted to have a major influence on the reactivity, six potential reagents with different leaving groups were synthesized (Figure 5-1). From those, only **5.1a** and **5.1b** were described to produce biguanides whereas **5.1e** is a new molecule. Shortly, reagents **5.1a**, **5.1c** and **5.1e** were synthesized by addition of a heterocycle to cyanoguanidine in the presence of hydrochloric acid in water under reflux or at 80 °C for 3-24 hours with 65%, 44% and 25% yields respectively.⁵²⁶ S-methyl derivative **5.1b** was prepared from 2-imino-4-thiobiuret and methyl iodide in 91% yield.⁵²⁷ Phenolic derivate **5.1d** was obtained from cyanoguanidine dihydrochloride in phenol as solvent at 70 °C for 3 hours in 33% yield.⁵²⁸ Finally, *N*-guanyl-*O*-methylisourea hydroacetate (**5.1f**) was synthesized in two steps from cyanoguanidine in methanol under reflux for 2 hours in the presence of copper acetate monohydrate, then the product was released from the copper complex following hydrogen sulphide treatment, with a 46% overall yield.⁵²⁹ These procedures provided after suitable washings the pure desired biamidine derivatives as salt form.

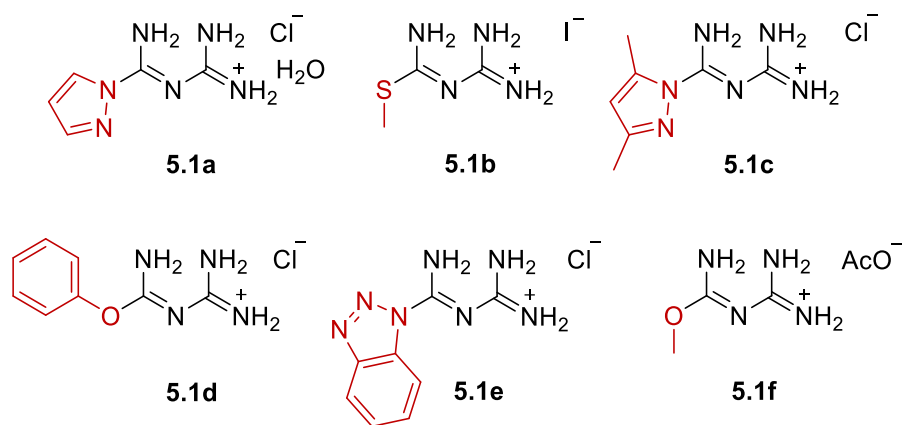


Figure 5-1: Synthesized biamidine transfer reagents.

With these reagents **5.1a-f** in hand, we screened different reaction conditions on a model transformation of UV-absorbing benzylamine to the corresponding benzylbiguanide (Figure 5-1). Reagent *N*-amidinopyrazole-1-carboxamide hydrochloride **5.1a** was first used to compare the effect of additives and solvent nature on the conversion. The temperature was set up to 25 °C in DMF as the aim was to develop mild conditions. The addition of DIPEA to the reaction did not have a significant effect compared to the control experiment without additive, whereas the addition of 1.0 equivalent of hydrochloric acid, triflic acid or trifluoroacetic acid prevented the reaction (entries 1-3). Performing the reaction in the presence of copper acetate also did not show any improvement (entry 4). As a result, additive-free conditions were chosen, which led to the most efficient and cleanest reaction mixtures.

Table 5-1: Effect of additives and solvent.

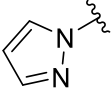
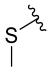
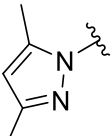
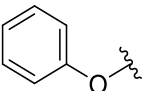
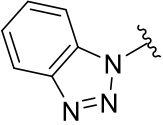
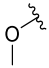
Entry	Reagent	Solvent	Additive	Equivalent	Conversion ^d (%)
1	5.1a	DMF	-	-	19
2	5.1a	DMF	DIPEA	1.1	18
3	5.1a	DMF	HCl	1	0
4	5.1a	DMF	Cu(OAc) ₂	0.1	15
5	5.1a	AcOH	-	-	0
6	5.1a	Acetone	-	-	0,5 ^c
7	5.1a	NMP	-	-	5
8	5.1a	DMA	-	-	7
9	5.1a	Acetonitrile	-	-	32 ^c
10	5.1a	EtOH	-	-	40
11	5.1a	MeOH	-	-	45
12	5.1a	Pyridine	-	-	51
13	5.1a	H ₂ O	-	-	53
14	5.1a	Pyridine	-	-	67 ^b
15	5.1b	Pyridine	-	-	53 ^b
16	5.1b	Pyridine/Toluene:1/1	-	-	64 ^b
17	5.1b	Pyridine/Toluene:1/9	-	-	58 ^b

^aAll reactions were performed with 0.8 mmol of benzylamine, 0.88 mmol of the corresponding reagent in 4 mL of solvent, stirred for 6 hours at 25 °C and monitored by HPLC ($\lambda = 254$ nm). ^bAll reactions were performed with 0.5 mmol of benzylamine, 0.55 mmol of the corresponding reagent in 1 mL of solvent, stirred for 5 hours at 25 °C and monitored by HPLC ($\lambda = 254$ nm). ^cSolubility issues with the formation of a suspension. ^dCalculate by the ratio between product and benzylamine. Determined by HPLC analysis.

Then a solvent survey with a variety of polar solvents was carried out (Table 5-1). Alcohols proved more beneficial than DMF, with respective conversions of 40% and 45% for ethanol and methanol after 6 hours, compared to 19% in DMF. However, the most preferable solvents were pyridine and water, which showed higher solubility properties than alcohols, and demonstrated conversions of 51% and 53% respectively, (entries 1, 10-13). Pyridine showed the highest conversion rate and the easiest product recovery by direct precipitation from the reaction mixture and short washings. For their part, water conditions are attractive as bio-compatible protocol using a green nontoxic solvent.

For the next optimization step, we selected pyridine as a solvent and increased the reagent concentration from 0.20 to 0.50 mmol of reagent per mL of solvent, leading to an increase of the conversion from 51% to 67% (entries 12, 14). The reagent *S*-methyl-guanylisothiuronium iodide **5.1b** proved to be somewhat less efficient in pyridine (entry 15), while the addition of toluene as a co-solvent led to conversion improvement (entries 16,17). As for reagent **5.1a**, the product was not observed because of reagent insolubility in pyridine/toluene mixtures. Overall, the conditions of entry 14 and 16, respectively reagent **5.1a** in pyridine and reagent **5.1b** in pyridine/toluene 1/1, turned out to be the best and were selected for the next optimization stages.

Table 5-2: Comparison of the biamidine transfer reagents in pyridine and water.

	R	Conversion ^b (%)	
		Pyridine	H ₂ O
5.1a		48	50
5.1b		43	15
5.1c		26	20
5.1d		17	28
5.1e		34	0
5.1f		0	1

^aAll reactions were performed with 0.8 mmol of benzylamine, 0.88 mmol of the corresponding reagent in 4 mL of solvent, stirred for 5 hours at 25 °C and monitored by HPLC ($\lambda = 254$ nm). ^bCalculate by the ratio between product and benzylamine. Determined by HPLC analysis.

The performance of the different biamidine transfer reagents **5.1a-f** was screened in the two optimal solvents: water and pyridine (Table 5-2). As expected, reagent **5.1f** allowed the formation of only traces of product as it contains a poor leaving group methoxy. Benzotriazole derivative **5.1e** showed a moderate conversion in pyridine but only traces of product in water. The most reactive compound proved to be **5.1d**, but its reactivity led to concomitant degradation in the solvent and the overall

conversion was low. Decreasing the temperature to enhance the stability of **5.1d** allowed to reach 60% conversion, but only after unacceptable 7 days. Compound **5.1c** is an analogue of pyrazole derivative **5.1a** with two methyl groups, which surprisingly showed significantly diminished conversion efficacy. S-methyl derivative **5.1b** demonstrated good conversion in pyridine whereas low in water. As a result, this survey revealed the best results for **5.1a** in both solvents, as well as **5.1b** in pyridine. It is also worth noting that reactions using **5.1a** are easier to workup and purify than with **5.1b**. In addition, they avoid the release of toxic, flammable and strong odoring gas methanethiol.

Finally, we studied the influence of concentration, temperature and equivalents of reactants on the formation of benzylbiguanide hydrochloride (Table 5-3). Increasing the concentration of **5.1a** from 0.2 mol/L to 1.0 mol/L had a great influence, enhancing the yield from 51% to 73%. Further concentrating of **5.1a** was not possible because of its saturation threshold in pyridine. Next, we moved the number of equivalents of benzylamine at a constant concentration of 1.0 mol/L of **5.1a**. At 1.0 eq. of benzylamine, we observed 1% of side products from self-condensation or condensation with product leading to polyguanidines formation. Increased amounts of benzylamine eliminated the presence of side products and led to higher yields. A good compromise was found with the use of 1.5 eq. of amine. As the product is a salt, the excess of amine could be easily removed by simple washings. With the optimized conditions, we explored the effect of temperature increase on the conversions with **5.1a** in pyridine and with **5.1b** in pyridine/toluene 1/1 mixture. We found for both reagents 40 °C to be the optimal temperature, given the conversion and the formation of low amounts of side products. Overheating reaction mixture over 40 °C promoted the formation of undesired products (~ 5%), whereas at 25 °C the conversion was clean but required a longer reaction time of up to 2 days. Eventually, optimized conditions proved to be the use of 1.5 eq. at a concentration of 1.0 mol/L at 40 °C.

Table 5-3: Effect of concentration, equivalents of amine and temperature.

Reagent	Solvent	Eq. of amine	Concentration (mol/L) ^b	Temperature (°C)	Time (h)	Conversion ^c (%)
5.1a	Pyridine	1.0	0.2	25	6	51
5.1a	Pyridine	1.0	0.5	25	6	68
5.1a	Pyridine	1.0	1.0	25	6	73
5.1a	Pyridine	1.0	1.0	25	3	52
5.1a	Pyridine	1.1	1.0	25	3	56
5.1a	Pyridine	1.2	1.0	25	3	59
5.1a	Pyridine	1.5	1.0	25	3	65
5.1a	Pyridine	2.0	1.0	25	3	68
5.1a	Pyridine	1.0	1.0	25	5	64
5.1a	Pyridine	1.0	1.0	30	5	83
5.1a	Pyridine	1.0	1.0	40	5	91
5.1a	Pyridine	1.0	1.0	50	5	92
5.1b	Pyridine/toluene 1/1	1.0	1.0	25	5	70
5.1b	Pyridine/toluene 1/1	1.0	1.0	30	5	75
5.1b	Pyridine/toluene 1/1	1.0	1.0	40	5	86
5.1b	Pyridine/toluene 1/1	1.0	1.0	50	5	91

^aAll reactions were monitored by HPLC ($\lambda = 254$ nm). ^bConcentration in mol of reagent dissolved per L of solvent. ^cCalculate by the ratio between product and amidine transfer reagent **5.1a** or **5.1b**. Determined by HPLC analysis.

To study the scope and limitations of the conditions developed (**5.1a** in pyridine, **5.1a** in water and **5.1b** in pyridine/toluene 1/1), several alkyl and dialkyl amines, substituted benzylamines, L-phenylalanine and aniline were used as substrates (Table 5-4). Alkyl and dialkyl amines were converted to the corresponding biguanides with excellent conversions (91-99% after 6 h) and good to excellent isolated yields (69-96%) for both **5.1a**-based methods. Only the reactions with butylamine and hexylamine were slower (12-24 h) due to steric hindrance. Different substituted benzylamines were also isolated in good yields 70-95%, without significant effect of the substitution pattern on the conversion. The formation of phenylbiguanide proved less efficient however and the protocol in water

is clearly preferred with 68% isolated yield after 22h reaction, compared to 44% after 6 days in pyridine. Likewise, mainly for solubility reasons, the protocol in water was the most efficient to convert L-phenylalanine to its biguanide analogue in 53% isolated yield (for this substrate, the procedure was modified with the addition of 1.0 eq. of DIPEA and 1.0 eq. of amino acid). Generally, despite good conversion rates with *S*-methyl derivative **5.1b**, the workup and isolation often were less direct than with **5.1a**, often requiring chromatography methods to afford the biguanides with high purity. Adding the necessity to consider the use of a gas trap to deal with methanethiol evolution, the reagent **5.1b** appears not to be preferable for this reaction. Contrarily, *N*-(diaminomethylene)-1*H*-pyrazole-1-carboximidamide hydrochloride **5.1a** is facile to work with, providing products are hydrochloride salts in high yields and purity after simple workup.

Table 5-4: Scope and limitations of the conditions developed on a panel of amines.

Amine	Pyridine			H ₂ O			Pyridine/toluene - 1/1		
	Time (h)	Conversion (%) ^c	Isolated yield (%)	Time (h)	Conversion (%) ^c	Isolated yield (%)	Time (h)	Conversion (%) ^c	Isolated yield (%)
Benzylamine	6	99	93	6	97	96	6	95	82
4-chlorobenzylamine	6	94	86	6	96	75	6	97	n.d.
4-methylbenzylamine	6	96	87	6	95	70	6	98	n.d.
4-nitrobenzylamine	6	99	90	6	98	93	6	97	n.d.
4-methoxybenzylamine	6	95	95	6	96	82	6	98	n.d.
Ethylamine	6	99	75	12	97	82	6	98	n.d.
Butylamine	24	95	86	12	96	77	6	98	54
Hexylamine	24	98	86	12	97	92	6	98	n.d.
Morpholine	6	96	83	6	97	91	6	97	82
<i>N</i> -methylpiperazine	6	99	83	6	97	96	6	96	97
<i>N</i> -methylbenzylamine	6	98	69	22	96	96	6	91	n.d.
Aniline	144	44	nd	22	71	68	6	0,1	n.d.
L-phenylalanine ^b	96	0	nd	24	94	53	6	10	n.d.

^aAll reactions were performed with 8.25 mmol of amine, 5.50 mmol of the corresponding reagent in 5.5 mL of the corresponding solvent at 40 °C and monitored by HPLC ($\lambda = 254$ nm). ^bReaction performed with 5.50 mmol of L-phenylalanine, 5.50 mmol of corresponding reagent and 5.50 mmol of DIPEA in 5.5 mL of the corresponding solvent, stirred for 24 hours at 40 °C and monitored by HPLC ($\lambda = 254$ nm). n.d.: not determined. ^cCalculate by the ratio between product and biguanide transfer reagent **5.1a** or **5.1b**. Determined by HPLC analysis.

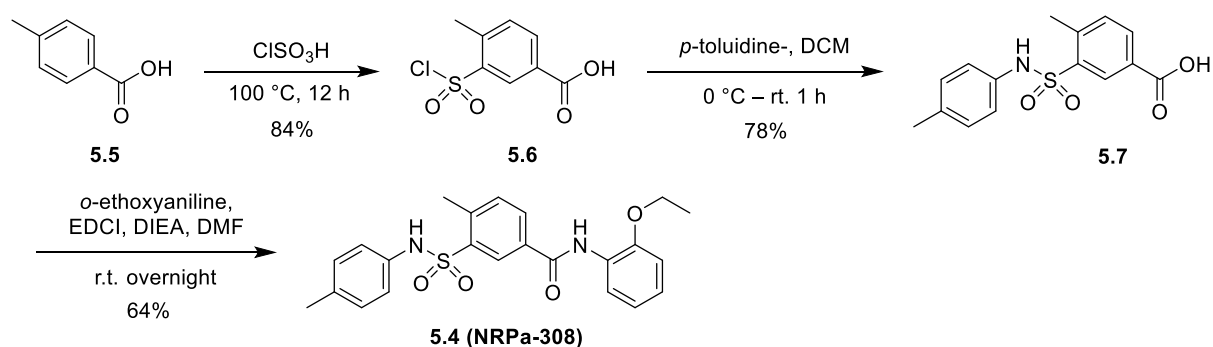
5.1.3 Conclusions

In summary, we have led a methodological study on the use of biamidine transfer reagents to convert amines into the corresponding guanidines. We have proposed and compared 6 potential reagents and concluded that *N*-(diaminomethylene)-1*H*-pyrazole-1-carboximidamide hydrochloride (**5.1a**) is the best in terms of both efficiency and practicability. Moreover, we have shown that the choice of solvent, concentration and temperature are key parameters. The optimal conditions were achieved either in water or pyridine, affording the smooth transformation of various amines into biguanides with high yields up to 96%. The method with pyridine showed fast workup, requiring only a washing step but is not applicable for amino acids or arylamines. The procedure in water showed very good efficiency for all tested amines under biological medium suitable conditions (water, no additive, temperature range: 25-40 °C). As a result, this protocol will be compatible with sensitive or bio-inspired substrates like peptides, aminosugars or amine-bearing nucleotide analogues.

This project allowed the writing of a first-authored article: Fabre, M. *et al.* "Mild biamidine transfer conditions for the synthesis of aliphatic biguanides", submitted.

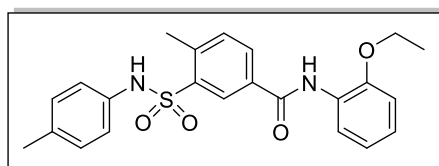
5.2 STABILITY ANALYSES OF NRPA-308

NRPa-308 (**5.4**) is an anticancer agent antagonizing Neuropilin-1, a multi-partners transmembrane receptor overexpressed in numerous tumours. A three steps synthesis without intermediate purification was previously developed within the group. After a first chlorosulfonylation step from 4-methylbenzoic acid **5.5** at 100 °C for 12 hours, 3-(chlorosulfonyl)-4-methylbenzoic acid **5.6** was obtained in 84% yield. This crude product was directly reacted in the sulfonylation of amine with *p*-toluidine at 0 °C in dichloromethane for one hour to afford the bi-aryl sulfonamide **5.7** in 78% yield. 4-methyl-3-(*N*-(*p*-tolyl)sulfamoyl)benzoic acid **5.7** was reacted with *o*-ethoxyaniline in the presence of EDCI as coupling agent and diisopropylethylamine as base in an addition/elimination reaction to afford the final amide **5.4** after overnight reaction at room temperature. This final step afforded NRPa-308 in 64% yield (42% overall yield after three steps (Scheme 5-2)).



Scheme 5-2: NRPa-308 synthesis.

The group reported formerly that the anti-proliferative activities of NRPa-308 show strong dependence with the incubation times with tumor cells (Figure 5-2). Thus, our purpose was to unambiguously demonstrate that these anti-proliferative effects are solely due to NRPa-308, and not to one of its potential metabolites / degradation products. Therefore, stability studies *in vitro* and *in cellulo* have been performed to address this question.



5.4 (NRPa-308)

NRPa-308 anti-proliferative activity :

IC₅₀ (48h) MDA-MB231 : 4.9 μM **IC₅₀ (72h)** MDA-MB231 : 0.2 μM
 BT549 : 2.1 μM BT549 : 0.1 μM

Sunitinib anti-proliferative activity :

IC₅₀ (48h) MDA-MB231 : 2.6 μM **IC₅₀ (72h)** MDA-MB231 : 3.7 μM
 BT549 : 2.2 μM BT549 : 3.5 μM

Figure 5-2: Structure of NRPa-308, and its antiproliferative activity against two breast cancer cell lines (MDA-MB-231 and BT549) measured after 48 h and 72 h treatment and compared to these of the marketed drug Sunitinib®. These values have been reported in ref.⁵³⁰

First, the chemical stability of NRPa-308 was assayed by HPLC analysis at three different pH acid, medium and basic (0.9, 7.4 and 8.4) and two temperatures (25 °C and 37 °C) to study its ionisation state in order to know its stability in human body. After 16 days, the compound proved fully stable under all these conditions (Figure 5-3).

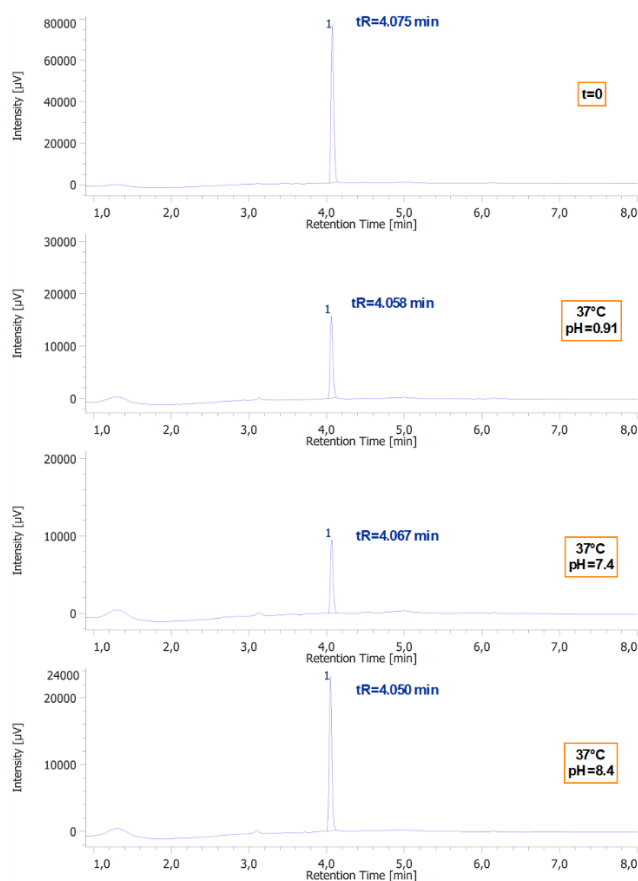


Figure 5-3: Chromatograms showing the stability of NRPa-308 in aqueous buffers at pH 0.9, 7.4 and 8.4 after 16 days incubation at 37 °C.

Next, we studied the stability of NRPa-308 in cellular culture media, in presence of malignant cells. To this end, MDA-MB-231 and BT-549 breast cancer cells were cultured in the presence of 2 μmol of NRPa-308 for three days, and the HPLC analyses of the supernatant revealed that NRPa-308 was still largely the main compound detected, indicating a high stability of compound NRPa-308 in the extracellular medium (Figure 5-4).

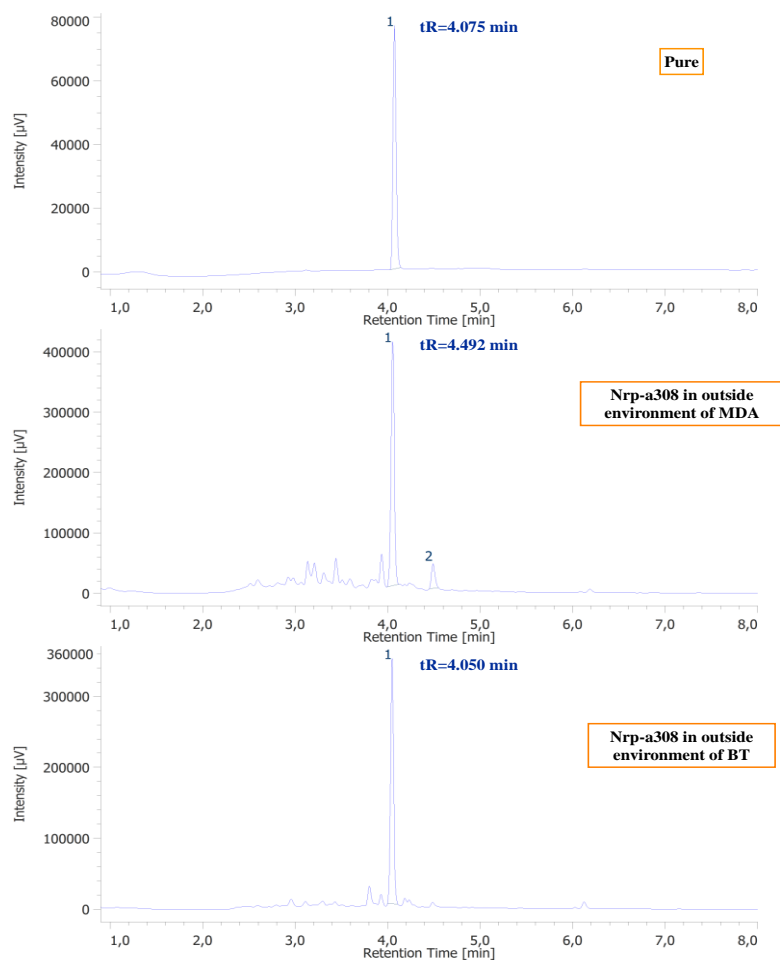


Figure 5-4: Stability of NRPa-308 in outside environment of MDA and BT after three days incubation at 37 $^{\circ}\text{C}$.

Then, the cells were washed and lysed with methanol. The lysates were extracted with $\text{CHCl}_3/\text{MeOH}$, 9/1, v/v and the extracts were quantitatively analysed by HPLC. In both cases, NRPa-308 proved fully stable, with no other peak detected (Figure 5-5). In addition, the quantitative dosage revealed a significant accumulation of NRPa-308 in cells, with respectively $5.14 \pm 0.06 \cdot 10^{-9}$ mol and $1.40 \pm 0.01 \cdot 10^{-9}$ mol calculated in MDA-MB231 and BT549 cells, after three days.

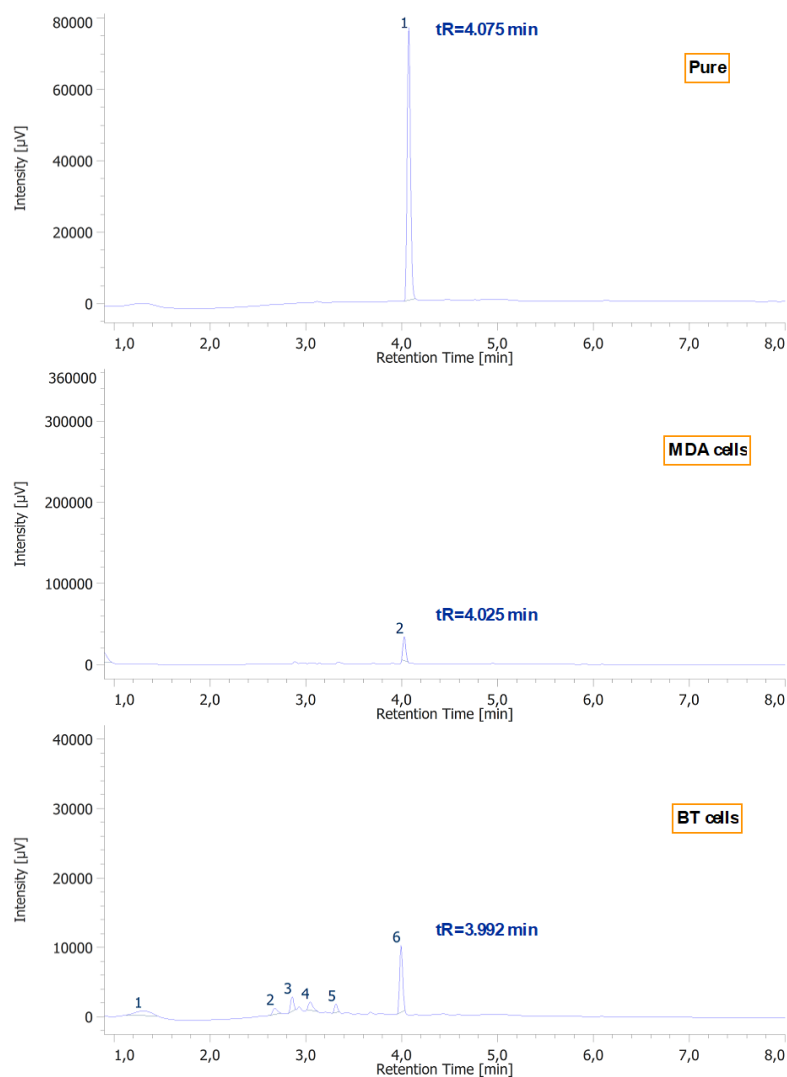


Figure 5-5: Chromatograms showing the metabolism of NRPa-308 in MDA-MB231 and BT549 cells after three days incubation at 37 °C.

In summary, these short stability studies confirmed us that the measured *in vitro* antiproliferative activities (Figure 5-2), are the result of the effect of compound NRPa-308 and are not due to one of its metabolites or degradation products.

This project allows the publication of an article in 2019 (Fabre, M. *et al.* Synthesis, 3D-structure and stability analyses of NRPa-308, a new promising anti-cancer agent. *Bioorganic Med. Chem. Lett.* **29**, 126710 (2019)).⁵⁰⁹

EXPERIMENTAL PART

General.

All the commercially available products from chemical providers were used without purification. Solvents were purchased from Sigma Aldrich. All chemicals were purchased from Aldrich, Fisher or Alfa Aesar. All the chemical reactions were monitored simultaneously by LCMS, HPLC and thin-layer chromatography (TLC, Merck silica gel 60 F254 plates) and visualized both by UV radiation (254 & 365 nm) and by spraying with a relevant staining agent followed by subsequent warming with a heat gun. Column chromatography was performed on a CombiFlash Rf+, TELEDYNE Isco, using prepacked column (CHROMABOND Flash, SiOH 40-63 μm , MACHEREY NAGEL or CHROMABOND Flash, C₁₈ec 40-63 μm , MACHEREY NAGEL or POLYGOPREP 60-30 C₁₈, MACHEREY NAGEL). All NMR spectra (¹H, ¹³C, ¹⁹F) were recorded on Bruker Advance Spectrometers (200 or 400 MHz). ¹H NMR (200 and 400 MHz), ¹³C{¹H} NMR (50 and 101 MHz) and ¹⁹F{¹H} (188 and 377 MHz) spectra were obtained with samples dissolved in CDCl₃ and DMSO-*d*₆ with the solvent residual signals as internal references: CHCl₃ (¹H = 7.26 ppm, ¹³C = 77.16) and DMSO-*d*₆ (¹H = 2.50 ppm, ¹³C = 39.52). Chemical shifts (δ) are given in ppm to the nearest 0.01 (¹H) or 0.1 ppm (¹³C). The coupling constants (*J*) are given in Hertz (Hz). The signals are reported as follows: chemical shift, multiplicity (s = singlet, d = doublet, t = triplet, m = multiplet, dd = doublet of doublets, br s = broad singlet), coupling constants (*J*) and integration. Dye syntheses were performed in a Branson 5510 ultrasound bath. Mass spectra (ESI-MS) were recorded on a ThermoFisher LCQ advantage ion trap mass spectrometer hyphenated with an Agilent 1100 HPLC or an Agilent iQ single quadrupole mass spectrometer hyphenated with an Agilent 1260 infinity HPLC. HRMS was carried out on a Thermo Q-exactive Focus mass spectrometer hyphenated to Thermo Vanquish UHPLC system including degasser, binary pump, autosampler and multiwavelength detector. Separation was done on a Thermo scientific Hypersil GOLD (150mm x 2.1mm, 1.9 μm) at 0.2 ml/min. Gradient starts at 90/10 water (0.1% formic acid)/ acetonitrile (0.1% formic acid) to 98% acetonitrile (0.1% formic acid) in 15 minutes, and then kept for two minutes. Mass spectrometry was used in Electrospray ionization in switch mode (alternate positive/negative scan) using the following parameters: spray voltage was 3.7kV (pos mode) and 2.7kV (neg mode); capillary temperature: 320 °C; sheath gas: 30 a.u.; Auxiliary gas: 15 a.u.; probe heater temperature: 350 °C. Microwaves experiments were performed in CEM Discover 201A15 with a puissance of 150 Watts. Melting points were achieved over system Kofler type WME Heizbank nr. 7563 (44-266 °C). The purity of compounds was further assayed by HPLC analysis on a JASCO PU-2089 apparatus with Supelco analytical column Ascentis Express C18, 100mm x 46mm 5 μm . Eluent A: water with 1‰ formic acid, Eluent B: CH₃CN with 1‰ formic acid. Four different methods were used which are described as follows: Method 1: 100% A over 2 min, 100% A to 60% A over 5 min, 60% A for 3 min then from 60% A to 100% A over 1 min (11 min in

total). Method 2: 100% A over 2 min, 100% A to 60% A over 8 min, 60% A for 4 min then from 60% A to 100% A over 1 min (15 min in total)). Method 3: 95% A over 2 min, 95% A to 50% A over 8 min, 50% A for 4 min, from 50% A to 40% A over 6.5 min, 40% A for 6 min, from 40% A to 95% for 2 min then 95% A for 2.5 min (30 min in total)). Method 4: 95% A over 2 min, 95% A to 50% A over 8 min, 50% A for 8 min, from 50% A to 95% A over 0.5 min, then 95% A for 0.5 min (20 min in total)). For chapter 5, the reactions were followed by HPLC analysis on a JASCO PU-2089 apparatus with the following method 5: EC 125/4 NUCEODUR HILIC, 5 μ m. UV-detection: 254 and 280 nm. Eluent A: water with 0.1 M of TEAB buffer pH = 7. Eluent B: CH₃CN: 20% A over 1 min, 20% A to 60% A over 12 min, 60% A for 6 min then from 60% A to 20% A over 0.5 min (20 min in total).

CHAPTER 3

General procedure for the formation of guanidine (I):

Method A: 3,5-dimethyl-1-guanylpirazole nitrate (1.0 eq.) was dissolved in aniline (10.0 eq.) and the solution was heated at 80 °C. After cooling down, diethylether was added to the reaction mixture. The precipitate that formed was filtered and washed with diethylether to afford the corresponding guanidine nitrate.

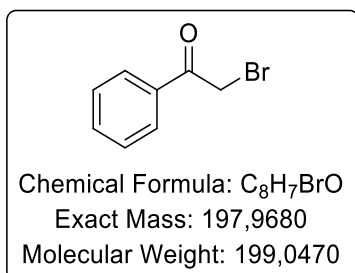
Method B: 3,5-dimethyl-1-guanylpirazole nitrate (1.0 eq.) was dissolved in water and aniline (5.0 eq.) was added. The mixture reaction was heated at 80 °C. After cooling down, diethylether was added to the reaction mixture. The precipitate that formed was filtered and washed with diethylether to afford the corresponding guanidine nitrate.

Method C: Aniline (1.0 eq.) and cyanamide (3.0 eq.) were dissolved in phenol, then 12 M aq. HCl solution (1.2 eq.) was added dropwise to the mixture reaction. The solution was heated at 100 °C, then cooled down to r.t. and quenched with water and basified with NaOH 2.5 M. The mixture was extracted with ethyl acetate, washed with water, dried over magnesium sulfate and the solvents were evaporated under reduced pressure. Purification by silica gel flash chromatography (CH₂Cl₂/MeOH, 10/0 then 9/1) afforded the corresponding guanidine nitrate.

General procedure for the formation of *N*, phenyl-1*H*-imidazol-2-amine (II):

To a solution of corresponding guanidine nitrate (1.0 eq.) with triethylamine (2.4 eq.) in dioxane (0.12 M) were added triethylamine (3.1 eq.) and 2-bromo-1-(pyridin-3-yl)ethan-1-one hydrogen bromide or 2-bromo-1-phenylethan-1-one (1.0 eq.). The reaction mixture was stirred at r.t. (from 3 h to 16 h). Dioxane was removed under reduced pressure and the crude material was purified by silica gel column chromatography (CH₂Cl₂/MeOH, 100/0 then 90/10) to afford the pure corresponding *N*, phenyl-1*H*-imidazol-2-amine.

3.1a: 2-bromo-1-phenylethan-1-one

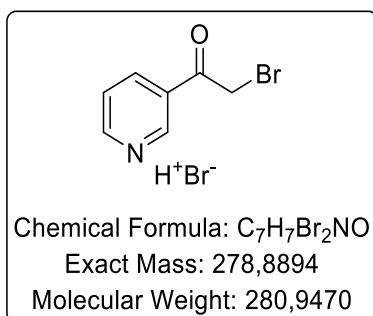


Characterization: 2-bromo-1-phenylethan-1-one

Acetophenone (1.94 mL, 16.7 mmol) and AlCl₃ (cat.) were dissolved in Et₂O (13 mL) and cooled to 0 °C. Bromine (0.86 mL, 16.7 mmol) was added dropwise to the mixture reaction, then the solution was allowed to warm to r.t. and stirred for 3 h. Water was added and the mixture was extracted with Et₂O, washed with water, dried over MgSO₄ and the solvent was evaporated. The crude product (3.085 g, 15.6 mmol, 93% yield) was afforded as a green solid.

Green solid, 3.085 g, 15.6 mmol, 93% yield. ¹H NMR (400 MHz, DMSO-*d*₆) δ 8.03 – 7.98 (m, 2H, Ar), 7.71 – 7.66 (m, 1H, Ar), 7.56 (dd, *J* = 8.4, 7.1 Hz, 2H, Ar), 4.95 (s, 2H, CH₂). LCMS: *t*_R = 9.71 min. [M+H]⁺ = 199.00. Data in accordance with the literature.⁵³¹

3.1b: 2-bromo-1-(pyridin-3-yl)ethan-1-one hydrogen bromide

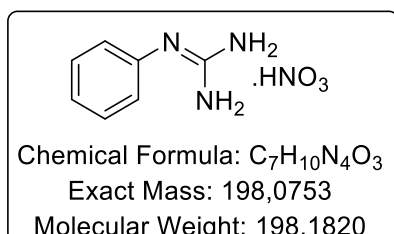


Characterization: 2-bromo-1-(pyridin-3-yl)ethan-1-one hydrogen bromide

3-Acetylpyridine (1.1 mL, 10 mmol) was dissolved in HBr 40% w/w (2mL) and was heated to 45 °C before addition dropwise bromine (0.52 mL, 10 mmol). The reaction mixture was gradually warmed up to 60 °C until solubilization, then a precipitate was formed, which was filtered and washed with ether to afford the title compound as a white solid (2.49 g, 8.86 mmol, 88% yield).

White solid, 2.49 g, 8.86 mmol, 88% yield. ^1H NMR (400 MHz, Acetone- d_6) δ 9.50 (s, 1H), 9.26 (d, J = 8.2 Hz, 1H), 9.19 (d, J = 5.7 Hz, 1H), 8.46 (dd, J = 8.1, 5.7 Hz, 1H), 5.10 (s, 2H). LCMS: t_R = 2.73 min. $[\text{M}+\text{H}]^+ = 199.93$. Data in accordance with the literature.⁴⁶⁸

3.3a: 1-phenylguanidine nitrate

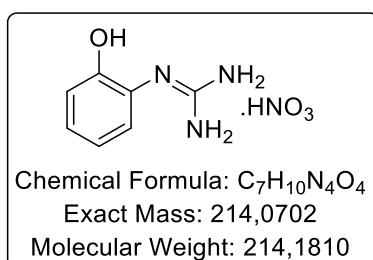


Characterization: 1-phenylguanidine nitrate

The general procedure for the formation of guanidine (I, method A) was followed using 3,5-dimethyl-1-guanylpyrazole nitrate (1 g, 4.97 mmol) and aniline (4.54 mL, 49.7 mmol) as reagents for 2 h.

White solid, 529.1 mg, 3.92 mmol, 79% yield. R_f ($\text{CH}_2\text{Cl}_2/\text{MeOH}, 9/1, v/v$) = 0.33. ^1H NMR (400 MHz, DMSO- d_6) δ 9.55 (s, 1H), 7.46 (t, J = 7.8 Hz, 2H), 7.37 – 7.28 (m, 5H), 7.27 – 7.22 (m, 2H). LCMS: t_R = 1.57, 1.85 min. $[\text{M}+\text{H}]^+ = 136.133$. Data in accordance with the literature.⁴⁶⁹

3.3b: 1-(2-hydroxyphenyl)guanidine

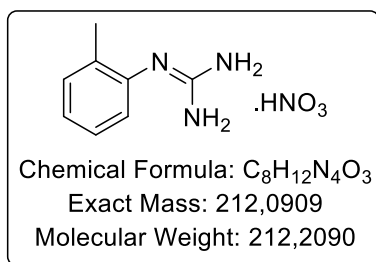


Characterization: 1-(2-hydroxyphenyl)guanidine

The general procedure for the formation of guanidine (I, method B) was followed using 3,5-dimethyl-1-guanylpyrazole nitrate (1 g, 4.97 mmol) and 2-aminophenol (2 mL, 24.85 mmol) as reagents in water (45 mL) for 24 h.

Brown solid, 404.7 mg, 2.67 mmol, 54% yield. R_f ($\text{CH}_2\text{Cl}_2/\text{MeOH}, 9/1, v/v$) = 0.1. ^1H NMR (400 MHz, DMSO- d_6) δ 7.16 (m, 9H), 7.04 – 6.91 (m, 1H). LCMS: t_R = 1.80, 1.86 min. $[\text{M}+\text{H}]^+ = 152.07$. Data in accordance with the literature.⁵³²

3.3c : 1-(*o*-tolyl)guanidine

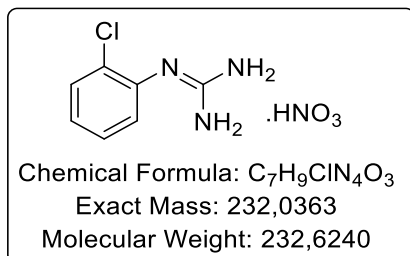


Characterization: 1-(*o*-tolyl)guanidine

The general procedure for the formation of guanidine (I, method A) was followed using 3,5-dimethyl-1-guanylpyrazole nitrate (3 g, 14.91 mmol) and *o*-toluidine (15.84 mL, 149.1 mmol) as reagents for 1 h 30.

Purple solid, 2.60 g, 12.27 mmol, 82% yield. R_f (CH₂Cl₂/MeOH,9/1, v/v) = 0.18. ¹H NMR (400 MHz, DMSO-*d*₆) δ 9.19 (s, 1H, NH), 7.38 – 7.33 (m, 1H), 7.32 – 7.27 (m, 2H), 7.23 – 7.18 (m, 1H), 7.17 (s, 1H), 2.20 (s, 3H, CH₃). LCMS: t_R = 1.93 min. [M+H]⁺ = 150.07. Data in accordance with the literature.⁵³³

3.3d: 1-(2-chlorophenyl)guanidine

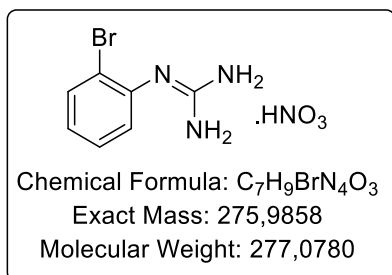


Characterization: 1-(2-chlorophenyl)guanidine

The general procedure for the formation of guanidine (I, method A) was followed using 3,5-dimethyl-1-guanylpyrazole nitrate (3 g, 14.91 mmol) and 2-chloroaniline (15.68 mL, 149.1 mmol) as reagents for 16 h.

Purple solid, 3.17 g, 13.66 mmol, 92% yield. R_f (CH₂Cl₂/MeOH,9/1, v/v) = 0.16. ¹H NMR (400 MHz, DMSO-*d*₆) δ 9.46 (d, *J* = 3.0 Hz, 1H, NH), 7.66 – 7.59 (m, 1H), 7.43 (d, *J* = 1.5 Hz, 2H), 7.35 (s, 4H). LCMS: t_R = 2.60, 3.40 min. [M+H]⁺ = 170.07. Data in accordance with the literature.⁵³⁴

3.3e: 1-(2-bromophenyl)guanidine

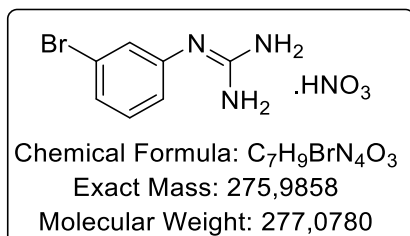


Characterization: 1-(2-bromophenyl)guanidine

The general procedure for the formation of guanidine (I, method A) was followed using 3,5-dimethyl-1-guanylpyrazole nitrate (1 g, 4.97 mmol) and 2-bromoaniline (5.56 mL, 49.7 mmol) as reagents for 2 days.

Grey solid, 1.02 mg, 4.79 mmol, 90% yield. R_f (CH₂Cl₂/MeOH,9/1, v/v) = 0.14. ¹H NMR (400 MHz, DMSO-*d*₆) δ 9.54 (s, 1H), 7.51 – 7.29 (m, 8H). ¹³C NMR (101 MHz, DMSO-*d*₆) δ 156.1, 133.5 (2C), 130.0, 129.9, 129.2, 122.0. LCMS: *t*_R = 2.35, 3.35 min. [M+H]⁺ = 214.07, 216.07.

3.3f: 1-(3-bromophenyl)guanidine

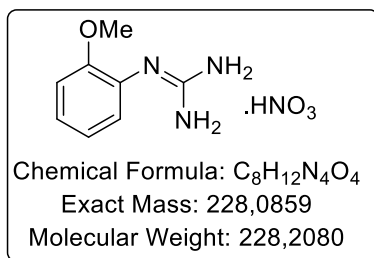


Characterization: 1-(3-bromophenyl)guanidine

The general procedure for the formation of guanidine (I, method A) was followed using 3,5-dimethyl-1-guanylpyrazole nitrate (1 g, 4.97 mmol) and 3-bromoaniline (5.35 mL, 49.7 mmol) as reagents for 16 h.

Purple solid, 754.5 mg, 3.54 mmol, 71% yield. R_f (CH₂Cl₂/MeOH,9/1, v/v) = 0.16. ¹H NMR (400 MHz, DMSO-*d*₆) δ 9.73 (s, 1H), 7.49 (d, *J* = 20.9 Hz, 6H), 7.39 (t, *J* = 7.8 Hz, 1H), 7.32 – 7.20 (m, 1H). LCMS: *t*_R = 2.68, 3.48 min. [M+H]⁺ = 214.07, 216.07. Data in accordance with the literature.⁵³⁵

3.3g: 1-(2-methoxyphenyl)guanidine

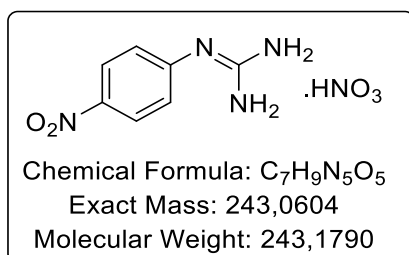


Characterization: 1-(2-methoxyphenyl)guanidine

The general procedure for the formation of guanidine (I, method A) was followed using 3,5-dimethyl-1-guanylpurazole nitrate (1 g, 4.97 mmol) and *m*-anisidine (5.6 mL, 49.7 mmol) as reagents for 24 h.

Grey solid, 907.2 mg, 3.98 mmol, 80% yield. *R_f* (CH₂Cl₂/MeOH, 9/1, v/v) = 0.18. ¹H NMR (400 MHz, DMSO-*d*₆) δ 9.64 (s, 1H, NH), 7.51 – 7.28 (m, 4H), 6.87 (dd, *J* = 8.4, 2.4 Hz, 1H), 6.80 (dd, *J* = 4.5, 2.1 Hz, 2H), 3.77 (s, 3H, OCH₃). LCMS: *t_R* = 2.67, 3.42 min. [M+H]⁺ = 166.07. Data in accordance with the literature.⁵³⁶

3.3h: 1-(4-nitrophenyl)guanidine

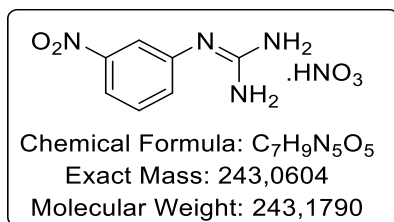


Characterization: 1-(4-nitrophenyl)guanidine

The general procedure for the formation of guanidine (I, method C) was followed using cyanamide (4.56 g, 108.70 mmol), 4-nitroaniline (5 g, 36.23 mmol) and HCl 12M (3.68 mL, 44.20 mmol) as reagents for 8 h.

Yellow solid, 2.28 g, 12.65 mmol, 35% yield. ¹H NMR (400 MHz, Chloroform-*d*) δ 8.17 (d, *J* = 8.9 Hz, 2H), 7.02 (d, *J* = 8.9 Hz, 2H), 4.25 (s, 4H). LCMS: *t_R* = 2.68, 3.42 min. [M+H]⁺ = 181.07. Data in accordance with the literature.⁵³⁷

3.3i : 1-(3-nitrophenyl)guanidine

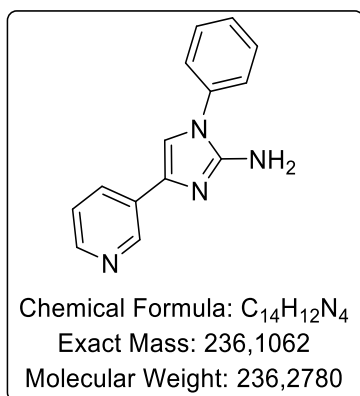


Characterization: 1-(3-nitrophenyl)guanidine

The general procedure for the formation of guanidine (I, method C) was followed using cyanamide (1.43 g, 43.47 mmol), 3-nitroaniline (2 g, 14.49 mmol) and HCl 12M (1.47 mL, 17.68 mmol) as reagents for 8 h.

Yellow solid, 65.7 mg, 3.65 mmol, 50% yield. ¹H NMR (400 MHz, DMSO-*d*₆) δ 7.67 – 7.59 (m, 1H, CH_{Ar}), 7.55 (t, *J* = 2.2 Hz, 1H, CH_{Ar}), 7.41 (t, *J* = 8.1 Hz, 1H, CH_{Ar}), 7.25 – 7.13 (m, 1H, CH_{Ar}), 5.65 (s, 3H, NH, NH₂), 3.40 (s, 1H, NH). LCMS: *t*_R = 2.67, 3.41 min. [M+H]⁺ = 181.07. Data in accordance with the literature.⁵³⁷

3.8a: 1-phenyl-4-(pyridin-3-yl)-1H-imidazol-2-amine

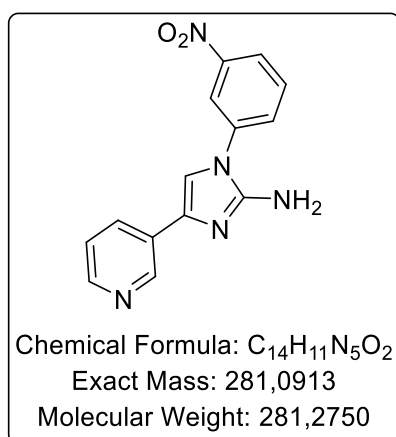


Characterization: 1-phenyl-4-(pyridin-3-yl)-1H-imidazol-2-amine

The procedure for the formation of *N*, phenyl-1H-imidazol-2-amine (II) was followed using guanidine nitrate **3.3a** (113 mg, 0.57 mmol), 2-bromo-1-(pyridin-3-yl)ethan-1-one hydrogen bromide (159 mg, 0.57 mmol) and triethylamine as reagents for 3 h. After evaporation of dioxane under reduced pressure, water was added. The mixture reaction was extracted with ethyl acetate, washed with water, dried over magnesium sulfate and the solvents were evaporated under reduced pressure. Purification by silica gel flash chromatography (CH₂Cl₂/MeOH, 100/0 then 90/10) afforded the titled imidazole **3.8a** as a yellow solid (21.8 mg, 0.092 mmol, 16% yield).

Yellow solid, 21.8 mg, 0.092 mmol, 16% yield. R_f (CH₂Cl₂/MeOH,9/1, v/v) =0.51. ¹H NMR (400 MHz, DMSO-*d*₆) δ 8.92 (d, *J* = 1.6 Hz, 1H, CH_{Pyr}), 8.35 (dd, *J* = 4.7, 1.5 Hz, 1H, CH_{Pyr}), 8.01 (dt, *J* = 7.9, 1.9 Hz, 1H, CH_{Pyr}), 7.57 – 7.49 (m, 5H, CH_{Ph}), 7.40 (ddd, *J* = 8.5, 5.6, 2.2 Hz, 1H, CH_{im}), 7.34 (dd, *J* = 7.7, 5.0 Hz, 1H, CH_{Pyr}), 5.70 (s, 2H, NH₂). ¹³C NMR (101 MHz, DMSO-*d*₆) δ 149.0, 146.7, 145.4, 136.9, 133.5, 130.6, 130.3, 129.6 (2C), 127.1, 124.1 (2C), 123.5, 112.7. LCMS: *t*_R = 2.80, 5.30 min. [M+H]⁺ = 237.20. Data in accordance with the literature.⁵³⁸

3.8b 1-(3-nitrophenyl)-4-(pyridin-3-yl)-1H-imidazol-2-amine

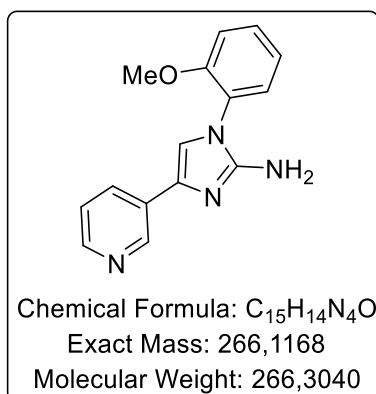


Characterization: 1-(3-nitrophenyl)-4-(pyridin-3-yl)-1H-imidazol-2-amine

The procedure for the formation of *N*, phenyl-1H-imidazol-2-amine (II) was followed using guanidine nitrate **3.3i** (656.7 mg, 2.70 mmol), 2-bromo-1-(pyridin-3-yl)ethan-1-one hydrogen bromide (759 mg, 2.70 mmol) and triethylamine as reagents for 5 h. Purification by silica gel flash chromatography (CH₂Cl₂/MeOH, 100/0 then 90/10) afforded the titled imidazole **3.8b** as a yellow solid (409.7 mg, 1.46 mmol, 54% yield).

Yellow solid, 409.7 mg, 1.46 mmol, 54% yield. ¹H NMR (400 MHz, DMSO-*d*₆) δ 8.93 (d, *J* = 2.1 Hz, 1H), 8.44 – 8.30 (m, 2H), 8.23 (dd, *J* = 8.2, 2.0 Hz, 1H), 8.02 (ddd, *J* = 10.4, 8.1, 2.1 Hz, 2H), 7.82 (t, *J* = 8.1 Hz, 1H), 7.73 (s, 1H), 7.36 (dd, *J* = 7.9, 4.7 Hz, 1H), 5.97 (s, 2H, NH₂). ¹³C NMR (101 MHz, DMSO-*d*₆) δ 149.2, 148.3, 147.0, 145.5, 137.8, 134.2, 131.1, 130.8, 130.4, 130.0, 123.5, 121.5, 118.8, 112.4. LCMS: *t*_R = 2.67, 3.82 min. [M+H]⁺ = 282.13. HPLC (λ₂₅₄): Purity 96.9%, (λ₂₈₀): Purity 95.8%; *t*_R: 5.375 min (method 1). Data recorded are in accordance to the reported⁴⁶⁰ describing *N*-(3-nitrophenyl)-4-(pyridin-3-yl)-1H-imidazol-2-amine.

3.8c: 1-(2-methoxyphenyl)-4-(pyridin-3-yl)-1H-imidazol-2-amine

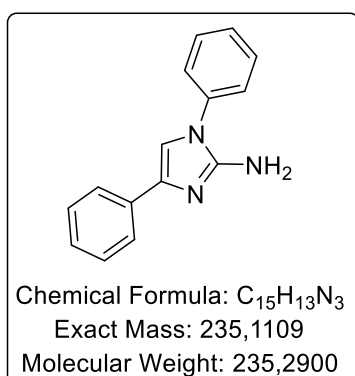


Characterization: 1-(2-methoxyphenyl)-4-(pyridin-3-yl)-1H-imidazol-2-amine

The procedure for the formation of *N*, phenyl-1H-imidazol-2-amine (II) was followed using guanidine nitrate **3.3g** (410.5 g, 1.80 mmol), 2-bromo-1-(pyridin-3-yl)ethan-1-one hydrogen bromide (505.9 mg, 1.80 mmol) and triethylamine as reagents for 16 h. Purification by silica gel flash chromatography (CH₂Cl₂/MeOH, 100/0 then 90/10) afforded the titled imidazole **3.8c** as a brown solid (125 mg, 0.47 mmol, 26% yield).

Brown solid, 125 mg, 0.47 mmol, 26% yield. ¹H NMR (400 MHz, Chloroform-*d*) δ 8.92 (dd, *J* = 2.3, 0.9 Hz, 1H), 8.43 (dd, *J* = 4.8, 1.6 Hz, 1H), 7.99 (dt, *J* = 7.9, 1.9 Hz, 1H), 7.41 (td, *J* = 7.9, 0.8 Hz, 1H), 7.27 (ddd, *J* = 7.9, 4.9, 0.9 Hz, 1H), 7.07 (s, 1H), 7.02 (ddd, *J* = 7.9, 1.9, 1.0 Hz, 1H), 6.98 – 6.92 (m, 2H), 4.58 (s, 2H), 3.85 (s, 3H). ¹³C NMR (101 MHz, Chloroform-*d*) δ 160.9, 148.2, 147.6, 146.3, 137.7, 134.9, 131.6, 130.9, 130.1, 123.6, 116.8, 113.9, 112.2, 110.6, 55.7.

3.8d: 1,4-diphenyl-1H-imidazol-2-amine

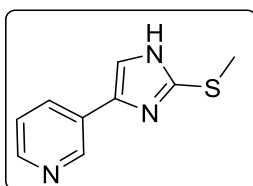


Characterization: 1,4-diphenyl-1H-imidazol-2-amine

The procedure for the formation of *N*, phenyl-1*H*-imidazol-2-amine (II) was followed using guanidine nitrate **3.3a** (250 mg, 1.26 mmol), 2-bromo-1-phenylethan-1-one (250 mg, 1.26 mmol) and triethylamine as reagents for 3 h. After evaporation of dioxane under reduced pressure, water was added. The mixture reaction was extracted with ethyl acetate, washed with water, dried over magnesium sulfate and the solvents were evaporated under reduced pressure. Purification by silica gel flash chromatography (CH₂Cl₂/MeOH, 100/0 then 90/10) afforded the titled imidazole as a brown solid **3.8d** (54.4 mg, 0.231 mmol, 18% yield).

Brown solid, 54.4 mg, 0.231 mmol, 18% yield. *R_f* (CH₂Cl₂/MeOH, 9/1, v/v) = 0.59. ¹H NMR (400 MHz, DMSO-*d*₆) δ 7.71 (d, *J* = 7.3 Hz, 2H, CH_{Ph}), 7.52 (d, *J* = 4.3 Hz, 4H, CH_{Ph}), 7.39 (d, *J* = 9.0 Hz, 3H, CH_{im}, CH_{Ph}), 7.32 (t, *J* = 7.7 Hz, 2H, CH_{Ph}), 7.15 (t, *J* = 7.4 Hz, 1H, CH_{Ph}), 5.63 (s, 2H, NH₂). ¹³C NMR (101 MHz, DMSO-*d*₆) δ 148.6, 137.1, 136.4, 134.6, 129.6 (2C), 128.3 (2C), 126.8, 125.7, 123.9 (2C), 123.8 (2C), 111.5. LCMS: *t_R* = 8.12 min. [M+H]⁺ = 236.13. Data in accordance with the literature.⁵³⁹

3.21: 3-(2-(methylthio)-2,3-dihydro-1*H*-imidazol-4-yl)pyridine

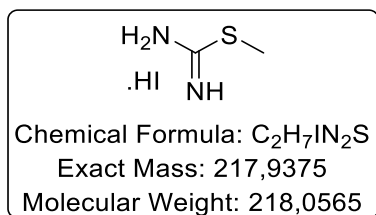


Characterization: 3-(2-(methylthio)-1*H*-imidazol-4-yl)pyridine

Methyl carbamimidothioate hydrogen iodide (1 g, 4.59 mmol), 2-bromo-1-(pyridin-3-yl)ethan-1-one hydrogen bromide (1.29 g, 4.59 mmol) and DIPEA (3.12 mL, 18.36 mmol) were stirred in acetonitrile (43 mL) at r.t. for 1 h 30. After evaporation of acetonitrile under reduced pressure, water was added. The mixture reaction was extracted with CH₂Cl₂, washed with water, dried over magnesium sulfate and the solvents were evaporated under reduced pressure. Purification by silica gel flash chromatography (CH₂Cl₂/MeOH, 10/0 then 9/1) afforded the titled compound as a brown oil (180.3 mg, 0.944 mmol, 21% yield).

Brown oil, 180.3 mg, 0.944 mmol, 21% yield. ¹H NMR (400 MHz, DMSO-*d*₆) δ 12.49 (s, 1H, NH), 8.99 – 8.84 (m, 1H, CH_{pyr}), 8.36 (dd, *J* = 4.8, 1.7 Hz, 1H, CH_{pyr}), 8.06 (d, *J* = 7.9 Hz, 1H, CH_{pyr}), 7.73 (s, 1H, CH_{imidazole}), 7.35 (dd, *J* = 7.9, 4.8 Hz, 1H, CH_{pyr}), 2.56 (s, 3H, SCH₃).

3.22: methyl carbamimidothioate hydrogen iodide

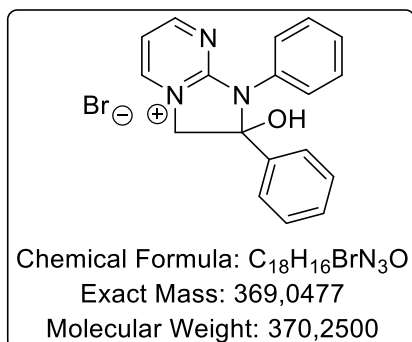


Characterization: methyl carbamimidothioate hydrogen iodide

Methyl iodide (3.43 mL, 55.2 mmol) was added dropwise to a solution of thiourea (3 g, 39.4 mmol) in methanol (30 mL) at 0 °C, then mixture reaction was heated at reflux temperature for 4 h. The solvent was evaporated to afford the titled compound as a yellow solid (8.42 g, 38.63 mmol, 98% yield).

Yellow solid, 8.42 g, 38.63 mmol, 98% yield. ¹H NMR (400 MHz, DMSO-*d*₆) δ 8.85 (s, 4H, NH, NH₂, HI), 2.56 (s, 3H, CH₃). Data in accordance with the literature.⁴⁸⁰

3.41: 2-(hydroxy(phenyl)methyl)-1-phenyl-2,3-dihydro-1H-imidazo[1,2-a]pyrimidin-4-ium bromide



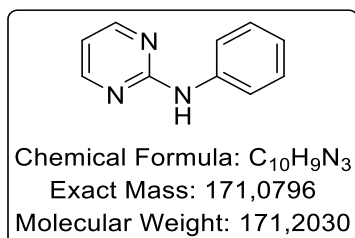
Characterization: 2-(hydroxy(phenyl)methyl)-1-phenyl-2,3-dihydro-1H-imidazo[1,2-a]pyrimidin-4-ium bromide

N-phenylpyrimidin-2-amine (200 mg, 1.17 mmol) was dissolved in CH₃CN with DMAP (7 mg, 0.06 mmol). Then 2-bromo-1-phenylethan-1-one (278 mg, 1.4 mmol) was added to the solution. The reaction mixture was stirred at 80 °C for 30 min under microwave irradiation. After cooling down, a precipitate formed, which was filtered and washed with acetone to afford the compound as a white solid (417.8 mg, 1.13 mmol, 48% yield).

White solid, 417.8 mg, 1.13 mmol, 48% yield. R_f (CH₂Cl₂/MeOH,9/1, v/v) = 0.2. M.p. = 230-232 °C. ¹H NMR (400 MHz, DMSO-*d*₆) δ 9.04 (dd, *J* = 28.2, 5.5 Hz, 2H), 8.44 (s, 1H), 7.77 (d, *J* = 7.4 Hz, 2H), 7.48 (t, *J* = 5.5 Hz, 1H), 7.33 (hept, *J* = 5.8, 4.5 Hz, 8H), 5.22 – 4.90 (m, 2H). ¹³C NMR (101 MHz, DMSO-*d*₆) δ

167.6, 154.3, 148.3, 137.8, 133.3, 129.0, 128.9 (2C), 128.1 (3C), 127.2 (2C), 127.0 (2C), 112.7, 92.2, 63.5. LCMS: $t_R = 2.43, 3.65$ min. $[M+H]^+ = 290.13$.

3.42: *N*-phenylpyrimidin-2-amine

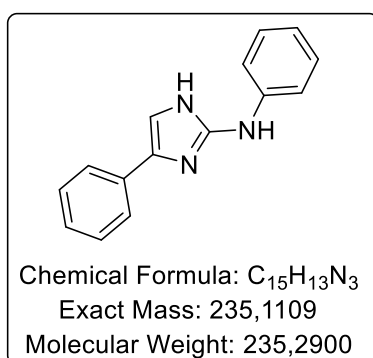


Characterization: *N*-phenylpyrimidin-2-amine

Chloropyrimidine (2 g, 17.5 mmol) was dissolved in AcOH and 1,4-dioxane with aniline (2.4 mL, 26.3 mmol). The reaction mixture was stirred at 110 °C for 3 h. Solvents were removed under reduced pressure and the crude material was purified by silica gel flash chromatography (CH/EtOAc, 10/0 then 50/50) to afford the titled compound as a yellow solid (1.6 g, 9.41 mmol, 54% yield).

Yellow solid, 1.6 g, 9.41 mmol, 54% yield. R_f (CH/EtOAc, 1/1, v/v) = 0.4. ¹H NMR (200 MHz, DMSO-*d*₆) δ 9.62 (s, 1H, NH), 8.47 (d, $J = 4.8$ Hz, 2H, CH_{pyr}), 7.76 (dt, $J = 8.1, 1.1$ Hz, 2H, CH_{Ph}), 7.27 (dd, $J = 8.6, 7.2$ Hz, 2H, CH_{Ph}), 7.00 – 6.88 (m, 1H, CH_{Ph}), 6.82 (t, $J = 4.8$ Hz, 1H, CH_{pyr}). LCMS: $t_R = 10.50$ min. $[M+H]^+ = 172.13$. Data in accordance with the literature.⁵⁴⁰

2.1e: *N*,4-diphenyl-1*H*-imidazol-2-amine



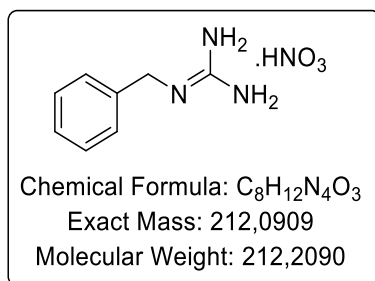
Characterization: *N*,4-diphenyl-1*H*-imidazol-2-amine

2-(hydroxy(phenyl)methyl)-1-phenyl-2,3-dihydro-1*H*-imidazo[1,2-*a*]pyrimidin-4-ium bromide (439 mg, 1.19 mmol) was dissolved in EtOH, then N₂H₄·H₂O (4 mL, 0.083 mmol) was added. The reaction mixture was stirred at 75 °C for 3 days. EtOH was removed under reduced pressure and the crude

material was purified by silica gel flash chromatography (CH₂Cl₂/MeOH, 10/0 then 90/10) to afford the titled compound as a yellow solid (77 mg, 0.328 mmol, 28% yield).

Yellow solid, 77 mg, 0.328 mmol, 28% yield. R_f (CH₂Cl₂/MeOH,9/1, v/v) =0.6. M.p. = 176-178 °C. ¹H NMR (400 MHz, DMSO-*d*₆) δ 10.85 (s, 1H, NH_{im}), 8.74 (s, 1H, NH_{ph}), 7.82 – 7.66 (m, 2H), 7.56 – 7.43 (m, 2H), 7.33 (t, *J* = 7.6 Hz, 2H), 7.28 – 7.19 (m, 3H), 7.18 – 7.11 (m, 1H), 6.80 (tt, *J* = 7.3, 1.2 Hz, 1H). ¹³C NMR (101 MHz, DMSO-*d*₆) δ 158.0, 145.3, 142.6, 128.8 (2C), 128.5, 128.4, 125.6, 124.8, 123.8, 121.4, 119.2, 118.9, 115.4 (2C). LCMS: *t*_R = 2.38, 3.33 min. [M+H]⁺ = 236.20. HPLC (λ254): Purity 96.980%, (λ280): Purity 98.184%; *t*_R: 5.90 min (method 1).

3.56: 1-benzylguanidine

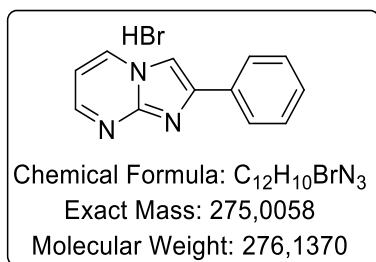


Characterization: 1-benzylguanidine

The general procedure for the formation of guanidine (I, method A) was followed using 3,5-dimethyl-l-guanylpurazole nitrate (1 g, 4.97 mmol) and benzylamine (5.46 mL, 49.7 mmol) as reagents for 16 h.

White solid, 992.4 mg, 4.64 mmol, 93% yield. R_f (CH₂Cl₂/MeOH,9/1, v/v) = 0.44. ¹H NMR (400 MHz, DMSO-*d*₆) δ 7.85 (s, 1H, NH), 7.44 – 7.35 (m, 2H, CH_{Ar}), 7.35 – 7.26 (m, 3H, CH_{Ar}), 7.12 (s, 4H, NH, NH₂, HNO₃), 4.36 (s, 2H, CH₂). ¹³C NMR (101 MHz, DMSO-*d*₆) δ 156.7, 137.1, 128.6, 127.5, 127.2, 44.0. LCMS: *t*_R = 3.63 min. [M+H]⁺ =150.06. Data in accordance with the literature.⁵⁴¹

3.59: 2-phenylimidazo[1,2-a]pyrimidine bromide



Characterization: 2-phenylimidazo[1,2-a]pyrimidine bromide

Aminopyrimidine (2 g, 21.05 mmol) was dissolved in acetone with 2-bromo-1-phenylethan-1-one (2.07 mg, 10.5 mmol). The reaction mixture was stirred at 60 °C overnight. A precipitate was formed, filtered and washed with acetone and diethylether to obtain the compound as a grey solid (3.71 g, 13.47 mmol, 64% yield).

Grey solid, 3.71 g, 13.47 mmol, 64% yield. R_f (CH₂Cl₂/MeOH,9/1, v/v) =0.7. ¹H NMR (200 MHz, DMSO-*d*₆) δ 9.36 (dd, *J* = 6.7, 1.8 Hz, 1H), 9.02 (dd, *J* = 4.4, 1.8 Hz, 1H), 8.83 (s, 1H), 8.01 (dt, *J* = 5.8, 1.7 Hz, 2H), 7.71 – 7.53 (m, 3H), 7.50 – 7.36 (m, 1H). LCMS: *t*_R = 6.76 min. [M+H]⁺ = 196.27. Data in accordance with the literature.⁵⁴²

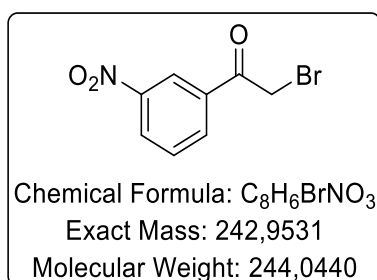
CHAPTER 4

General procedure for the formation of carbamimidothioic acid:

Method A: To a solution of aniline (1.0 eq.) in ethanol was added dimethylcyanodithioimidocarbonate (1.6 eq.) and the mixture was heated at 80 °C overnight. The precipitate was filtered, washed with cold ethanol and diethylether to obtain a solid.

Method B: To a solution of aminopyridine (1.0 eq.) in dry DMF or THF was added dimethylcyanodithioimidocarbonate (1.3 eq.), NaH 60% in mineral oil (1.6 eq.), with or without DMAP at 0 °C. The reaction mixture was stirred at r.t.. The solution was cooled down to 0°C and aq. NH₄Cl solution was added until pH 7 and extracted with CH₂Cl₂/MeOH:1/1. The precipitate was filtered, washed with diethylether to obtain a solid.

3.1d: 2-bromo-1-(3-nitrophenyl)ethan-1-one

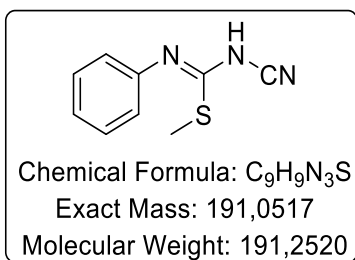


Characterization: 2-bromo-1-(3-nitrophenyl)ethan-1-one

3-Nitroacetophenone (4 g, 24.24 mmol) and AlCl₃ (cat.) was dissolved in Et₂O (30 mL) and cooled down to 0°C. Bromine (1.25 mL, 24.24 mmol) was added dropwise to the mixture reaction, then the solution was warmed to r.t. and stirred for 3 h. Water was added to quench the reaction and the mixture was extracted with Et₂O, washed with water, dried over MgSO₄. The solvent were evaporated under pressure to afford the product as a white solid (3.597 g, 14.86 mmol, 61% yield).

White solid, 3.597 g, 14.86 mmol, 61% yield. ¹H NMR (400 MHz, DMSO-*d*₆) δ LCMS: *t*_R = 9.74min. [M-H]⁺ = 242.3. Data in accordance with the literature.⁵⁴³

4.6a: Carbamimidothioic acid, N-cyano-N'-phenyl, methyl ester

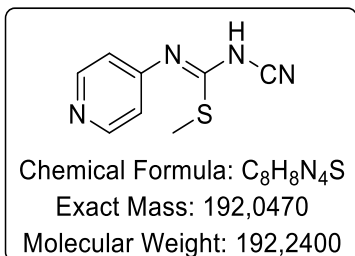


Characterization: Carbamimidothioic acid, N-cyano-N'-phenyl, methyl ester

The general procedure for the carbamimidothioic acid formation (method A) was followed using aniline (0.98 mL, 10.75 mmol) and dimethylcyanodithioimidocarbonate (2.52 g, 17.20 mmol) as reagents in ethanol (30 mL) for 16 h.

White solid, 1.13 g, 5.92 mmol, 55% yield. R_f (CH/EtOAc,6/4, v/v) = 0.23. ¹H NMR (200 MHz, DMSO-*d*₆) δ 10.16 (br. s, 1H, NH), 7.60 – 7.12 (m, 5H, CH_{Ph}), 2.70 (s, 3H, CH₃). LCMS: t_R = 10.14 min. [M+H]⁺ = 192.07. Data in accordance with the literature.⁴⁹⁶

4.6b: Carbamimidothioic acid, N-cyano-N'-(pyridin-4-yl), methyl ester

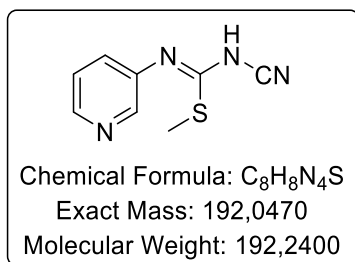


Characterization: Carbamimidothioic acid, N-cyano-N'-(pyridin-4-yl), methyl ester

The general procedure for the carbamimidothioic acid formation (method B) was followed using pyridin-4-amine (1 g, 10.64 mmol), NaH 60% in mineral oil (680 mg, 17.02 mmol), DMAP (320 mg, 2.66 mmol) and dimethylcyanodithioimidocarbonate (2.02 g, 13.83 mmol) as reagents in dry DMF (10 mL) for 16 h.

White solid, 1.79 g, 9.34 mmol, 88% yield. R_f (CH₂Cl₂/MeOH,9/1, v/v) = 0.24. ¹H NMR (200 MHz, DMSO-*d*₆) δ 8.57 (d, J = 7.1 Hz, 2H, CH_{PYR}), 7.81 (d, J = 6.3 Hz, 2H, CH_{PYR}), 2.76 (s, 3H, CH₃). LCMS: t_R = 2.42 min. [M+H]⁺ = 192.93. Data in accordance with the literature.⁵⁰¹

4.6c: Carbamimidothioic acid, *N*-cyano-*N'*-(pyridin-3-yl), methyl ester

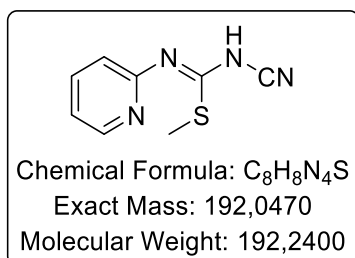


Characterization: Carbamimidothioic acid, *N*-cyano-*N'*-(pyridin-3-yl), methyl ester

The general procedure for the carbamimidothioic acid formation (method B) was followed using pyridin-3-amine (500 mg, 5.32 mmol), NaH 60% in mineral oil (327 mg, 8.51 mmol), DMAP (cat.) and dimethylcyanodithioimidocarbonate (1.01 g, 6.91 mmol) as reagents in dry DMF (4 mL) for 3 h at r.t., 16 h at 50 °C and 1 h at 80 °C.

White-off solid, 650.2 mg, 3.39 mmol, 64% yield. R_f (CH₂Cl₂/MeOH,9/1, v/v) = 0.30. ¹H NMR (200 MHz, DMSO-*d*₆) δ 8.63 (d, *J* = 2.6 Hz, 1H, CH_{pyr}), 8.42 (dd, *J* = 4.8, 1.5 Hz, 1H, CH_{pyr}), 7.97 – 7.84 (m, 1H, CH_{pyr}), 7.43 (dd, *J* = 8.3, 4.7 Hz, 1H, CH_{pyr}), 2.75 (s, 3H, CH₃). LCMS: *t*_R = 3.78 min. [M+H]⁺ = 192.93. Data in accordance with the literature.⁵⁰¹

4.6d: Carbamimidothioic acid, *N*-cyano-*N'*-(pyridin-2-yl), methyl ester

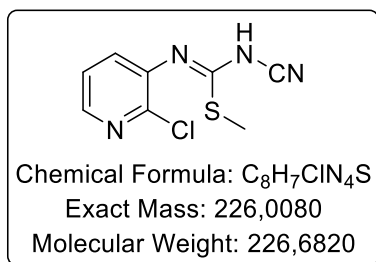


Characterization: Carbamimidothioic acid, *N*-cyano-*N'*-(pyridin-2-yl), methyl ester

The general procedure for the carbamimidothioic acid formation (method B) was followed using pyridin-2-amine (1.00 g, 10.64 mmol), NaH 60% in mineral oil (680 mg, 13.83 mmol) and dimethylcyanodithioimidocarbonate (2.02 g, 17.02 mmol) as reagents in dry DMF (10 mL) for 16 h.

Orange solid, 440 mg, 2.29 mmol, 43% yield. R_f (EtOAc/MeOH,9/1, v/v) = 0.78. M.p. = 114-116 °C. ¹H NMR (400 MHz, DMSO-*d*₆) δ 8.99 – 8.91 (m, 1H, CH_{pyr}), 8.02 (ddd, *J* = 9.0, 7.1, 1.7 Hz, 1H, CH_{pyr}), 7.34 (br. s, 1H, NH), 7.26 – 7.19 (m, 2H, CH_{pyr}), 2.43 (s, 3H, CH₃). ¹³C NMR (101 MHz, DMSO-*d*₆) δ 172.6, 152.8, 150.2, 142.5, 130.1, 122.6, 116.3, 13.1. LCMS: *t*_R = 2.70 min. [M+H]⁺ = 192.93.

4.6e: Carbamimidothioic acid, *N*-cyano-*N'*-(2-chloro, pyridine-3-yl), methyl ester

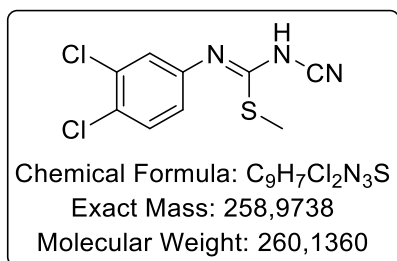


Characterization: Carbamimidothioic acid, *N*-cyano-*N'*-(2-chloro, pyridine-3-yl), methyl ester

The general procedure for the carbamimidothioic acid formation (method B) was followed using 3-amino-2-chloropyridine (1.00 g, 7.81 mmol), NaH 60% in mineral oil (500 mg, 12.5 mmol) and dimethylcyanodithioimidocarbonate (1.48 mg, 10.15 mmol) as reagents in THF (8 mL) for 4 days.

Grey solid, 1.27 mg, 5.64 mmol, 72% yield. R_f (CH₂Cl₂/MeOH, 9/1, v/v) = 0.63. M.p. = 166-168 °C. ¹H NMR (400 MHz, DMSO-*d*₆) δ 10.43 (s, 1H), 8.42 (dd, *J* = 4.7, 1.8 Hz, 1H), 7.97 (dd, *J* = 7.8, 1.8 Hz, 1H), 7.54 (dd, *J* = 7.8, 4.7 Hz, 1H), 2.68 (s, 3H). ¹³C NMR (101 MHz, DMSO-*d*₆) δ 172.2, 148.8, 147.9, 138.8, 131.3, 123.9, 114.3, 14.6. LCMS: t_R = 4.68 min. [M-H]⁺ = 224.93.

4.6f: Carbamimidothioic acid, *N*-cyano-*N'*-3,4-dichlorophenyl), methyl ester

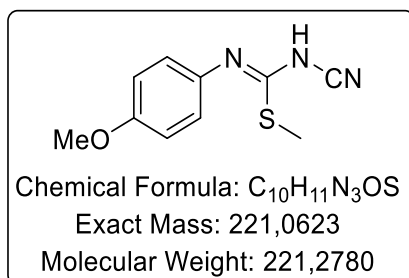


Characterization: Carbamimidothioic acid, *N*-cyano-*N'*-3,4-dichlorophenyl), methyl ester

The general procedure for the carbamimidothioic acid formation (method A) was followed using 3,4-dichloroaniline (1.00 g, 6.21 mmol) and dimethylcyanodithioimidocarbonate (1.45 g, 9.93 mmol) as reagents in ethanol (30 mL) for 4 days.

Grey solid, 390.8 mg, 1.51 mmol, 24% yield. R_f (CH/EtOAc, 6/4, v/v) = 0.18. ¹H NMR (400 MHz, DMSO-*d*₆) δ 10.22 (s, 1H), 7.99 – 7.36 (m, 3H), 2.74 (s, 3H). LCMS: t_R = 11.63 min. [M-H]⁺ = 257.93; 259.87. Data in accordance with the literature.⁵⁴⁴

4.6g: Carbamimidothioic acid, *N*-cyano-*N'*-(4-methoxyphenyl), methyl ester

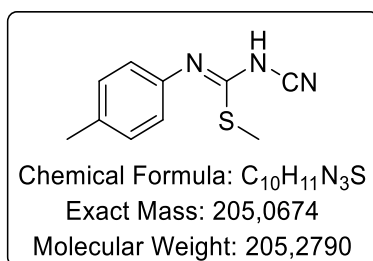


Characterization: Carbamimidothioic acid, *N*-cyano-*N'*-(4-methoxyphenyl), methyl ester

The general procedure for the carbamimidothioic acid formation (method A) was followed using 4-methoxyaniline (1.00 g, 8.12 mmol) and dimethylcyanodithioimidocarbonate (1.19 g, 8.12 mmol) as reagents in ethanol (30 mL) for 24 h.

Grey solid, 1.31 mg, 5.95 mmol, 73% yield. R_f (CH/EtOAc,6/4, v/v) = 0.22. ¹H NMR (400 MHz, DMSO-*d*₆) δ 10.16 (s, 1H), 7.42 – 7.25 (m, 2H), 7.07 – 6.85 (m, 2H), 3.75 (s, 3H), 2.66 (s, 3H). LCMS: *t*_R = 10.20 min. [M+H]⁺ = 220.20. Data in accordance with the literature.⁴⁹⁶

4.6h: Carbamimidothioic acid, *N*-cyano-*N'*-(4-methylphenyl), methyl ester

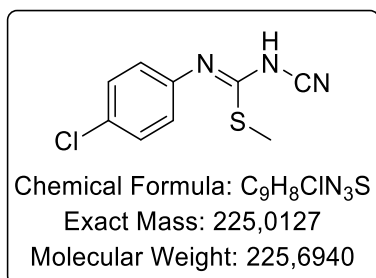


Characterization: Carbamimidothioic acid, *N*-cyano-*N'*-(4-methylphenyl), methyl ester

The general procedure for the carbamimidothioic acid formation (method A) was followed using *p*-toluidine (1.00 g, 9.34 mmol) and dimethylcyanodithioimidocarbonate (1.50 g, 10.27 mmol) as reagents in ethanol (10 mL) for 16 h.

White solid, 925.1 mg, 4.51 mmol, 48% yield. R_f (CH/EtOAc,6/4, v/v) = 0.31. ¹H NMR (400 MHz, DMSO-*d*₆) δ 10.10 (s, 1H), 7.30 (d, *J* = 8.1 Hz, 2H), 7.20 (d, *J* = 8.2 Hz, 2H), 2.67 (s, 3H), 2.30 (s, 3H). LCMS: *t*_R = 10.54 min. [M+H]⁺ = 206.07. Data in accordance with the literature.⁵⁴⁵

4.6i: Carbamimidothioic acid, *N*-cyano-*N'*-(4-chlorophenyl), methyl ester

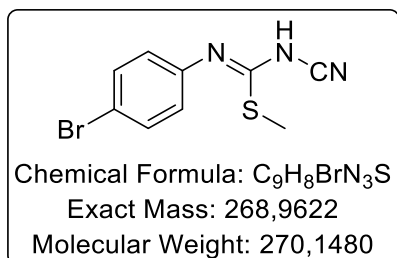


Characterization: Carbamimidothioic acid, *N*-cyano-*N'*-(4-chlorophenyl), methyl ester

The general procedure for the carbamimidothioic acid formation (method A) was followed using 4-chloroaniline (1.00 g, 7.89 mmol) and dimethylcyanodithioimidocarbonate (1.26 g, 8.62 mmol) as reagents in ethanol (10 mL) for 24 h.

White solid, 789.1 mg, 3.51 mmol, 44% yield. R_f (CH/EtOAc, 6/4, v/v) = 0.29. ¹H NMR (400 MHz, DMSO-*d*₆) δ 10.18 (s, 1H), 7.71 – 7.28 (m, 4H), 2.72 (s, 3H). LCMS: t_R = 10.84 min. [M+H]⁺ = 226.00. Data in accordance with the literature.⁵⁴⁶

4.6j: Carbamimidothioic acid, *N*-cyano-*N'*-(4-bromophenyl), methyl ester

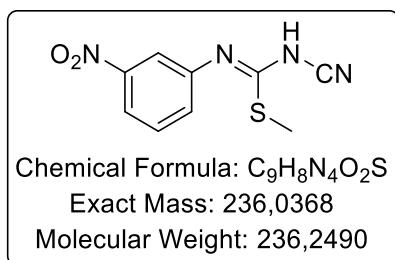


Characterization: Carbamimidothioic acid, *N*-cyano-*N'*-(4-bromophenyl), methyl ester

The general procedure for the carbamimidothioic acid formation (method A) was followed using 4-bromoaniline (1.00 g, 5.88 mmol) and dimethylcyanodithioimidocarbonate (940 mg, 6.47 mmol) as reagents in ethanol (10 mL) for 3 days.

White solid, 942.5 mg, 3.49 mmol, 59% yield. R_f (CH/EtOAc, 1/1, v/v) = 0.22. M.p. = 190-192 °C. ¹H NMR (400 MHz, DMSO-*d*₆) δ 10.17 (s, 1H), 7.59 (d, *J* = 8.4 Hz, 2H), 7.43 (d, *J* = 8.4 Hz, 2H), 2.72 (s, 3H). ¹³C NMR (101 MHz, DMSO-*d*₆) δ 170.1, 136.6, 131.6 (2C), 125.9 (2C), 118.5, 114.5, 14.9. LCMS: t_R = 10.99 min. [M+H]⁺ = 270.00; 271.93.

4.6k: Carbamimidothioic acid, *N*-cyano-*N'*-(3-nitrophenyl), methyl ester

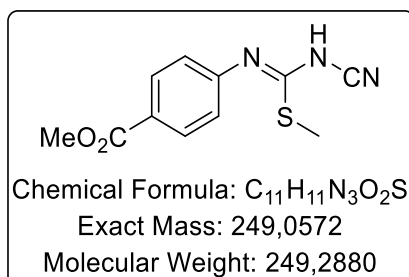


Characterization: Carbamimidothioic acid, *N*-cyano-*N'*-(3-nitrophenyl), methyl ester

The general procedure for the carbamimidothioic acid formation (method B) was followed using 3-nitroaniline (1.00 g, 7.24 mmol), NaH 60% in mineral oil (460 mg, 11.59 mmol) and dimethylcyanodithioimidocarbonate (1.38 g, 9.42 mmol) as reagents in THF (30 mL) at 70 °C for 2 days.

Brown solid, 270 mg, 1.14 mmol, 16% yield. R_f (CH/EtOAc, 1/1, v/v) = 0.24. ¹H NMR (200 MHz, DMSO-*d*₆) δ 10.41 (s, 1H), 8.41 (t, *J* = 2.2 Hz, 1H), 8.08 (ddd, *J* = 8.2, 2.3, 1.0 Hz, 1H), 7.98 (ddd, *J* = 8.2, 2.2, 1.1 Hz, 1H), 7.69 (t, *J* = 8.2 Hz, 1H), 2.79 (s, 3H). LCMS: *t*_R = 10.46 min. [M+H]⁺ = 237.00. Data in accordance with the literature.⁵⁴⁷

4.6l: Carbamimidothioic acid, *N*-cyano-*N'*-(4-methylbenzoate), methyl ester

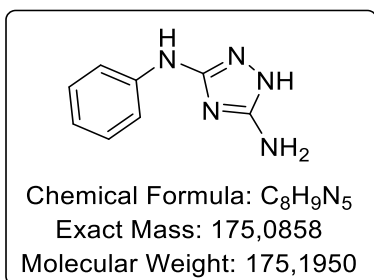


Characterization: Carbamimidothioic acid, *N*-cyano-*N'*-(4-methylbenzoate), methyl ester

The general procedure for the Carbamimidothioic acid formation (method B) was followed using methyl 4-aminobenzoate (1.00 g, 6.62 mmol), NaH 60% in mineral oil (420 mg, 10.60 mmol) and dimethylcyanodithioimidocarbonate (1.26 g, 8.61 mmol) as reagents in THF (30 mL) at 70 °C for 2 days.

Yellow solid, 1.19 g, 4.77 mmol, 72% yield. R_f (CH/EtOAc, 1/1, v/v) = 0.24. M.p. = 178-180 °C. ¹H NMR (200 MHz, DMSO-*d*₆) δ 10.17 (s, 1H), 8.02 – 7.80 (m, 2H), 7.57 – 7.37 (m, 2H), 3.82 (s, 3H), 2.62 (s, 3H). LCMS: *t*_R = 10.31 min. [M+H]⁺ = 249.93.

MCK243: *N*³-phenyl-1*H*-1,2,4-triazole-3,5-diamine

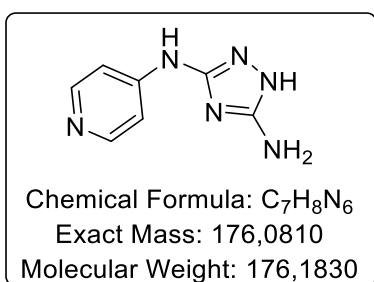


Characterization: *N*³-phenyl-1*H*-1,2,4-triazole-3,5-diamine

To a solution of carbamimidothioic acid, *N*-cyano-*N'*-phenyl, methyl ester (1.05 g, 5.51 mmol) in ethanol was added N₂H₄·H₂O (0.34 mL, 10.99 mmol), then the solution was warmed at 75 °C overnight. The precipitate was filtered and washed with diethyl ether to obtain a white solid (922.8 mg, 5.27 mmol, 96% yield).

White solid, 922.8 mg, 5.27 mmol, 96% yield. R_f (CH₂Cl₂/MeOH,9/1, v/v) =0.28. M.p. = 160-162 °C. ¹H NMR (400 MHz, DMSO-*d*₆) δ 11.04 (br. s, 1H, NH), 8.60 (s, 1H, NH), 7.49 (d, *J* = 7.7 Hz, 2H, CH_{Ph}), 7.15 (t, *J* = 7.9 Hz, 2H, CH_{Ph}), 6.71 (t, *J* = 7.3 Hz, 1H, CH_{Ph}), 5.82 (s, 2H, NH₂). ¹³C NMR (400 MHz, DMSO-*d*₆) δ 157.7, 155.6, 142.6, 128.4 (2C), 118.3, 115.5 (2C). LCMS: *t*_R = 5.44 min. [M+H]⁺ = 176.13. HPLC (λ₂₅₄): Purity 99.6%; HPLC (λ₂₈₀): Purity 96.7%; *t*_R: 4.73 min (method 1). Data in accordance with the literature.⁴⁹⁸

MCK244: *N*³-(pyridin-4-yl)-1*H*-1,2,4-triazole-3,5-diamine

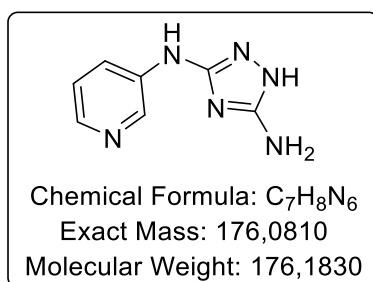


Characterization: *N*³-(pyridin-4-yl)-1*H*-1,2,4-triazole-3,5-diamine

To a solution of carbamimidothioic acid, *N*-cyano-*N'*-(pyridin-4-yl), methyl ester (81.1 mg, 0.422 mmol) in ethanol (1 mL) was added N₂H₄·H₂O (0.03 mL, 0.833 mmol), then the solution was warmed at 75 °C overnight. The precipitate was filtered and washed with diethyl ether to obtain a grey solid (61.6 mg, 0.35 mmol, 83% yield).

Grey solid, 61.6 mg, 0.35 mmol, 83% yield. Rf (CH₂Cl₂/MeOH,9/1, v/v) =0.28. M.p. = 270 °C. ¹H NMR (400 MHz, DMSO-*d*₆) δ 11.35 (s, 1H, NH), 9.23 (s, 1H, NH), 8.10 (d, *J* = 5.8 Hz, 2H, CH_{pyr}), 7.32 (d, *J* = 5.8 Hz, 2H, CH_{pyr}), 5.92 (s, 2H, NH₂). ¹³C NMR (101 MHz, DMSO-*d*₆) δ 156.5, 155.8, 149.1, 148.2 (2C), 110.3 (2C). LCMS: *t*_R = 2.10 min. [M+H]⁺ = 177.13. HPLC (λ₂₅₄): Purity 94.4%; HPLC (λ₂₈₀): Purity 99.1%; *t*_R: 0.59 min (method 1).

MCK245: *N*³-(pyridin-3-yl)-1*H*-1,2,4-triazole-3,5-diamine

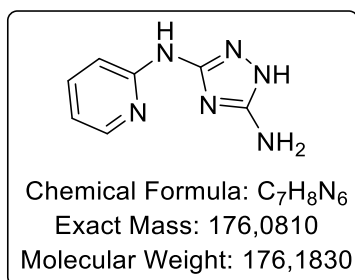


Characterization: *N*³-(pyridin-3-yl)-1*H*-1,2,4-triazole-3,5-diamine

To a solution of carbamimidothioic acid, *N*-cyano-*N'*-(pyridin-3-yl), methyl ester (650 mg, 3.39 mmol) in ethanol (8 mL) was added N₂H₄·H₂O (0.21 mL, 6.77 mmol), then the solution was warmed at 75 °C overnight. The precipitate was filtered and washed with diethyl ether to obtain a grey solid (435.9 mg, 2.48 mmol, 73% yield).

Grey solid, 435.9 mg, 2.48 mmol, 73% yield. Rf (CH₂Cl₂/MeOH,9/1, v/v) =0.10. M.p. = 210 °C. ¹H NMR (400 MHz, DMSO-*d*₆) δ 11.27 (br. s, 1H, NH), 8.89 (s, 1H, NH), 8.64 (d, *J* = 2.6 Hz, 1H, CH_{pyr}), 7.97 – 7.91 (m, 2H, CH_{pyr}), 7.17 (dd, *J* = 8.3, 4.7 Hz, 1H, CH_{pyr}), 5.91 (s, 2H, NH₂). ¹³C NMR (400 MHz, DMSO-*d*₆) δ 157.6, 155.6, 139.3, 139.1, 137.9, 123.3, 121.4. LCMS: *t*_R = 2.15 min. [M+H]⁺ = 177.20. HPLC (λ₂₅₄): Purity 99.9%; *t*_R: 4.73 min (method 1). Data in accordance with the literature.⁵⁴⁸

MCK246: *N*³-(pyridin-2-yl)-1*H*-1,2,4-triazole-3,5-diamine

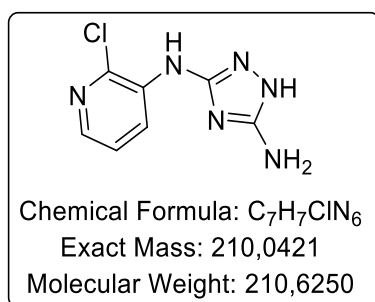


Characterization: *N*³-(pyridin-2-yl)-1*H*-1,2,4-triazole-3,5-diamine

To a solution of carbamimidothioic acid, *N*-cyano-*N'*-(pyridin-2-yl), methyl ester (426 mg, 2.22 mmol) in ethanol (6 mL) was added $\text{N}_2\text{H}_4\cdot\text{H}_2\text{O}$ (0.35 mL, 10.87 mmol), then the solution was warmed at 75 °C for 2 days. After evaporation, the precipitate was filtered and washed with diethyl ether. Purification by silica gel flash chromatography ($\text{CH}_2\text{Cl}_2/\text{MeOH}$, 10/0 then 90/10) afforded the titled compound as a yellow solid (327.4 mg, 1.86 mmol, 36% yield).

Yellow solid, 327.4 mg, 1.86 mmol, 36 % yield. Rf ($\text{CH}_2\text{Cl}_2/\text{MeOH}$, 9/1, v/v) = 0.25. M.p. = 212-214 °C. ^1H NMR (400 MHz, $\text{DMSO}-d_6$) δ 10.92 (s, 1H, NH), 8.25 (s, 1H, NH), 7.81 (d, J = 7.6 Hz, 1H, CH_{pyr}), 7.68 (d, J = 7.1 Hz, 1H, CH_{pyr}), 6.77 (d, J = 42.1 Hz, 2H, CH_{pyr}), 6.22 (s, 2H, NH_2). ^{13}C NMR (101 MHz, $\text{DMSO}-d_6$) δ 156.1, 154.1, 153.7, 146.7, 138.9, 115.51, 110.6. LCMS: t_{R} = 2.00 min. $[\text{M}+\text{H}]^+$ = 177.20. HPLC (λ_{254}): Purity 97.1%; HPLC (λ_{280}): Purity 100%; t_{R} : 0.62 min (method 1).

MCK247: *N*³-(2-chloropyridin-3-yl)-1*H*-1,2,4-triazole-3,5-diamine

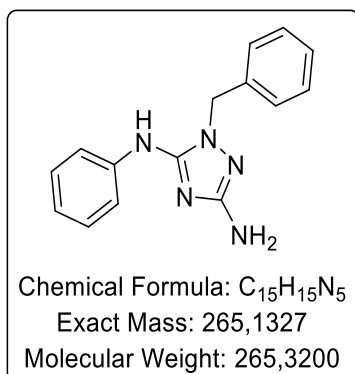


Characterization: *N*³-(2-chloropyridin-3-yl)-1*H*-1,2,4-triazole-3,5-diamine

To a solution of carbamimidothioic acid, *N*-cyano-*N'*-(2-chloro, pyridine-3-yl), methyl ester (1.27 mg, 5.64 mmol) in ethanol (20 mL) was added $\text{N}_2\text{H}_4\cdot\text{H}_2\text{O}$ (0.56 mL, 11.29 mmol), then the solution was warmed at 75 °C for 24 h. After evaporation of solvent, the precipitate was filtered and washed with diethyl ether to obtain a white solid (1.07 mg, 5.09 mmol, 90% yield).

White solid, 44.7 mg, 0.213 mmol, 19% yield. Rf ($\text{CH}_2\text{Cl}_2/\text{MeOH}$, 9/1, v/v) = 0.34. M.p. = 210-212 °C. ^1H NMR (400 MHz, $\text{DMSO}-d_6$) δ 11.48 (br. s, 1H, NH), 8.50 (d, J = 8.4 Hz, 1H, CH_{pyr}), 7.84 (d, J = 4.5 Hz, 1H, CH_{pyr}), 7.56 (br. s, 1H, NH), 7.32 (dd, J = 8.2, 4.6 Hz, 1H, CH_{pyr}), 6.05 (s, 2H, NH_2). ^{13}C NMR (101 MHz, $\text{DMSO}-d_6$) δ 156.4, 155.8, 138.9, 136.8, 135.4, 124.2, 123.5. LCMS: t_{R} = 4.48 min. $[\text{M}+\text{H}]^+$ = 211.07. HPLC (λ_{254}): Purity 100%; HPLC (λ_{280}): Purity 99.3%; t_{R} : 1.78 min (method 1).

MCK248: 1-benzyl-N⁵-phenyl-1H-1,2,4-triazole-3,5-diamine

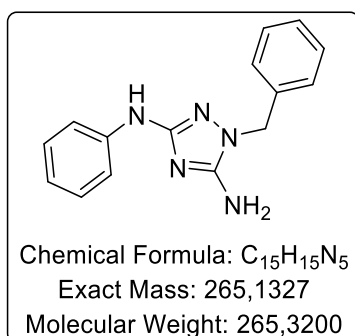


Characterization: 1-benzyl-N⁵-phenyl-1H-1,2,4-triazole-3,5-diamine

N³-phenyl-1H-1,2,4-triazole-3,5-diamine (200 mg, 1.14 mmol) was dissolved in degassed DMF, then Cs₂CO₃ (447 mg, 1.37 mmol) was added. Benzyl chloride (0.14 mL, 1.26 mmol) was added and the reaction mixture was stirred at r.t. overnight. Cs₂CO₃ was filtered and DMF was evaporated under reduced pressure. Purification by silica gel flash chromatography (CH₂Cl₂/THF, 10/0 then 5/5) afforded the titled compound as a brown solid (20.9 mg, 0.0786 mmol, 7% yield) along with the N³-benzylated regioisomer.

Brown solid, 20.9 mg, 0.0786 mmol, 7% yield. R_f (CH₂Cl₂/THF, 1/1, v/v) = 0.69. M.p. = 166-168 °C. ¹H NMR (400 MHz, DMSO-*d*₆) δ 8.81 (s, 1H, NH), 7.59 (d, *J* = 7.7 Hz, 2H, CH_{Ar}), 7.34 (t, *J* = 7.3 Hz, 2H, CH_{Ar}), 7.29 – 7.22 (m, 3H, CH_{Ar}), 7.22 – 7.17 (m, 2H, CH_{Ar}), 6.88 (t, *J* = 7.3 Hz, 1H, CH_{Ar}), 5.14 (s, 2H, NH₂), 5.11 (s, 2H, CH₂). ¹³C NMR (101 MHz, DMSO-*d*₆) δ 160.7, 150.2, 141.1, 137.6, 128.6 (2C), 128.4 (2C), 127.2, 127.2 (2C), 120.5, 116.9 (2C), 48.7. LCMS: *t*_R = 9.56 min. [M+H]⁺ = 266.07. HPLC (λ₂₅₄): Purity 97.7%; HPLC (λ₂₈₀): Purity 96.8%; *t*_R: 7.73 min (method 1).

MCK249: 1-benzyl-N³-phenyl-1H-1,2,4-triazole-3,5-diamine

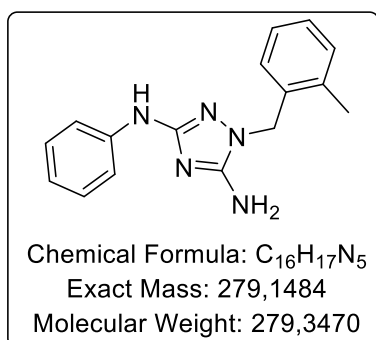


Characterization: 1-benzyl-N³-phenyl-1H-1,2,4-triazole-3,5-diamine

*N*³-phenyl-1*H*-1,2,4-triazole-3,5-diamine (150 mg, 0.857 mmol) was dissolved in degassed DMF (1 mL), then potassium *tert*-butoxide (96 mg, 0.857 mmol) was added. Benzyl chloride (0.12 mL, 0.857 mmol), dissolved in degassed DMF (1 mL), was added dropwise and the reaction mixture was stirred at 0 °C for 1 h, then at r.t. for an additional 1 h. Water was added to the mixture reaction and was extracted with ethyl acetate, washed with water, dried over magnesium sulfate and the solvents were evaporated under reduced pressure. Purification by reversed-phase chromatography (H₂O/CH₃CN, 10/0 then 60/40) afforded the titled compound as a white solid (119 mg, 0.449 mmol, 50%) along with the *N*₅-benzylated regioisomer (15.9 mg, 0.06 mmol, 7%).

White solid, 119 mg, 0.449 mmol, 50% yield. R_f (CH₂Cl₂/THF, 1/1, v/v) = 0.54. M.p. = 136-138 °C. ¹H NMR (400 MHz, DMSO-*d*₆) δ 8.67 (s, 1H, NH), 7.46 (d, *J* = 7.8 Hz, 2H, CH_{Ar}), 7.34 (t, *J* = 7.3 Hz, 2H, CH_{Ar}), 7.29 – 7.21 (m, 3H, CH_{Ar}), 7.14 (t, *J* = 7.9 Hz, 2H, CH_{Ar}), 6.70 (t, *J* = 7.3 Hz, 1H, CH_{Ar}), 6.29 (s, 2H, NH₂), 5.03 (s, 2H, CH₂). ¹³C NMR (101 MHz, DMSO-*d*₆) δ 157.1, 154.1, 142.4, 137.6, 128.4 (2C), 128.4 (2C), 127.2 (2C), 127.2, 118.4, 115.5 (2C), 48.7. LCMS: *t*_R = 9.65 min. [M+H]⁺ = 266.07. HPLC (λ₂₅₄): Purity 99.4%; HPLC (λ₂₈₀): Purity 97.9%; *t*_R: 8.25 min (method 1).

MCK250: 1-(2-methylbenzyl)-*N*³-phenyl-1*H*-1,2,4-triazole-3,5-diamine

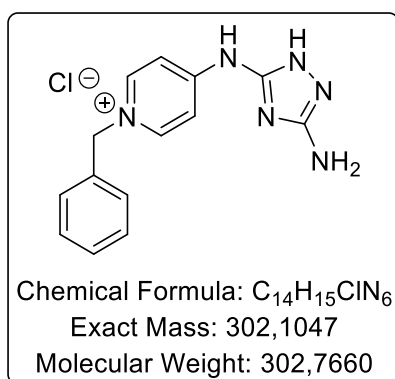


Characterization: 1-(2-methylbenzyl)-*N*³-phenyl-1*H*-1,2,4-triazole-3,5-diamine

*N*³-phenyl-1*H*-1,2,4-triazole-3,5-diamine (150 mg, 0.857 mmol) was dissolved in degassed DMF, then potassium *tert*-butoxide (96 mg, 0.857 mmol) was added. 2-Methylbenzyl chloride (150 mg, 1.07 mmol) was added and the reaction mixture was stirred at r.t. for 2 h. Water was added to the mixture reaction and was extracted with ethyl acetate, washed with water, dried over magnesium sulfate and the solvents were evaporated under reduced pressure. Purification by reversed-phase chromatography (H₂O/CH₃CN, 10/0 then 60/40) afforded the titled compound as a brown solid (111 mg, 0.398 mmol, 46% yield).

Brown solid, 111 mg, 0.398 mmol, 46% yield. Rf (CH₂Cl₂/THF,1/1, v/v) =0.51. M.p. = 156-158 °C. ¹H NMR (400 MHz, DMSO-*d*₆) δ 8.67 (s, 1H, NH), 7.48 – 7.41 (m, 2H, CH_{Ar}), 7.14 (ddd, *J* = 15.8, 13.8, 7.6 Hz, 5H, CH_{Ar}), 6.82 (d, *J* = 6.8 Hz, 1H, CH_{Ar}), 6.68 (t, *J* = 7.3 Hz, 1H, CH_{Ar}), 6.23 (s, 2H, NH₂), 4.99 (s, 2H, CH₂), 2.33 (s, 3H, CH₃). ¹³C NMR (101 MHz, DMSO-*d*₆) δ 157.1, 154.3, 142.4, 135.8, 135.4, 129.9, 128.4 (2C), 126.9, 126.6, 125.8, 118.4, 115.5 (2C), 46.9, 18.7. LCMS: *t*_R = 10.10 min. [M+H]⁺ = 280.13. HPLC (λ₂₅₄): Purity 99.5%; HPLC (λ₂₈₀): Purity 98.5%; *t*_R: 8.78 min (method 1).

MCK251: 4-((3-amino-1H-1,2,4-triazol-5-yl)amino)-1-benzylpyridin-1-ium chloride

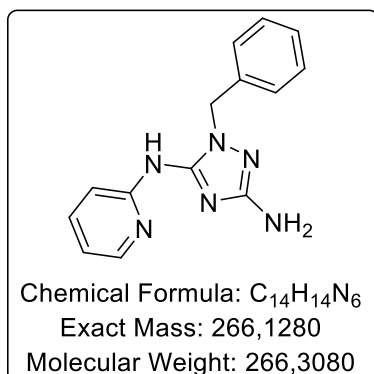


Characterization: 4-((3-amino-1H-1,2,4-triazol-5-yl)amino)-1-benzylpyridin-1-ium chloride

N³-(pyridin-4-yl)-1H-1,2,4-triazole-3,5-diamine (1 g, 5.68 mmol) was dissolved in degassed DMF, then Cs₂CO₃ (2.22 g, 6.80 mmol) was added. Benzyl chloride (0.72 mL, 6.25 mmol) was added and the reaction mixture was stirred at r.t. for 2 days. Cs₂CO₃ was filtered and DMF was evaporated under reduced pressure. Purification by silica gel flash chromatography (CH₂Cl₂/MeOH, 10/0 to 8/2) afforded the desired compound as white solid (442.6 mg, 1.47 mmol, 26% yield).

White solid, 442.6 mg, 1.47 mmol, 26% yield. Rf (CH₂Cl₂/MeOH,9/1, v/v) =0.10. M.p. = 254 °C. ¹H NMR (400 MHz, DMSO-*d*₆) δ 12.09 (s, 1H, NH), 11.26 (s, 1H, NH), 8.69 (d, *J* = 37.6 Hz, 2H, CH_{Ar}), 8.34 (s, 1H, CH_{Ar}), 7.47 – 7.34 (m, 6H, CH_{Ar}), 6.29 (s, 2H, NH₂), 5.53 (s, 2H, CH₂). ¹³C NMR (101 MHz, DMSO-*d*₆) δ 156.1, 154.8, 152.9, 135.4, 129.1 (4C), 128.8, 128.1 (4C), 60.3. LCMS: *t*_R = 2.52; 3.76 min. [M+H]⁺ = 267.13. HPLC (λ₂₅₄): Purity = 99.1%; HPLC (λ₂₈₀): Purity = 98.1%; *t*_R: 5.29 min (method 1).

MCK252: 1-benzyl-*N*⁵-(pyridin-2-yl)-1*H*-1,2,4-triazole-3,5-diamine

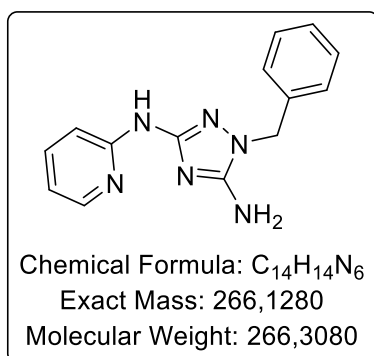


Characterization: 1-benzyl-*N*⁵-(pyridin-2-yl)-1*H*-1,2,4-triazole-3,5-diamine

*N*³-(pyridin-2-yl)-1*H*-1,2,4-triazole-3,5-diamine (560 mg, 3.2 mmol) was dissolved in degassed DMF, then Cs₂CO₃ (1.18 g, 3.2 mmol) was added. Benzyl chloride (0.39 mL, 3.2 mmol) was added and the reaction mixture was stirred at r.t. overnight. Cs₂CO₃ was filtered and DMF was evaporated under reduced pressure. Purification by silica gel flash chromatography (CH₂Cl₂/MeOH, 10/0 then 95/5) afforded the titled compound as a yellow solid (4.9 mg, 0.018 mmol, 0.6% yield) along with the *N*₃-benzylated regioisomer.

Yellow solid, 4.9 mg, 0.018 mmol, 0.6% yield. R_f (CH₂Cl₂/MeOH:9/1, v/v) = 0.69. M.p. = 162 °C. ¹H NMR (400 MHz, DMSO-*d*₆) δ 9.60 (s, 1H, NH), 8.17 (d, *J* = 4.5 Hz, 1H, CH_{Ar}), 7.80 (d, *J* = 8.4 Hz, 1H, CH_{Ar}), 7.66 (t, *J* = 7.8 Hz, 1H, CH_{Ar}), 7.30 (t, *J* = 7.2 Hz, 2H, CH_{Ar}), 7.23 (t, *J* = 7.3 Hz, 1H, CH_{Ar}), 7.20 – 7.15 (m, 2H, CH_{Ar}), 6.91 – 6.85 (m, 1H, CH_{Ar}), 5.16 (s, 2H, CH₂), 5.15 (s, 2H, NH₂). ¹³C NMR (101 MHz, DMSO-*d*₆) δ 160.82, 153.9, 148.7, 147.6, 137.8, 137.4, 128.3 (2C), 127.4 (2C), 127.2, 116.4, 110.5, 49.1. LCMS: *t*_R = 2.73; 6.37 min. [M+H]⁺ = 267.13. HPLC (λ₂₅₄): Purity 99.6%; *t*_R: 5.45 min (method 1).

MCK253: 1-benzyl-*N*³-(pyridin-2-yl)-1*H*-1,2,4-triazole-3,5-diamine

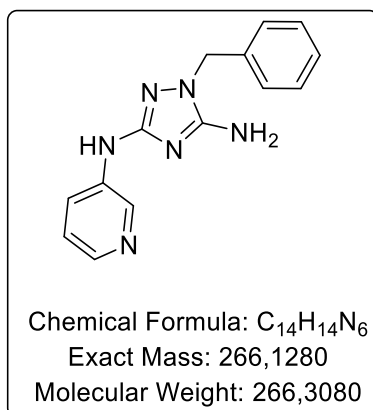


Characterization: 1-benzyl-*N*³-(pyridin-2-yl)-1*H*-1,2,4-triazole-3,5-diamine

*N*³-(pyridin-2-yl)-1*H*-1,2,4-triazole-3,5-diamine (250 mg, 1.42 mmol) was dissolved in degassed DMF (10 mL), then potassium tert-butoxide (159 mg, 1.42 mmol) was added at 0 °C. Benzyl chloride (0.16 mL, 1.42 mmol), dissolved in degassed DMF (5 mL), was added dropwise and the reaction mixture was stirred at r.t. for 2 h. Water was added to the mixture reaction and was extracted with ethyl acetate, washed with water, dried over magnesium sulfate and the solvents were evaporated under reduced pressure. Purification by silica gel flash chromatography (CH₂Cl₂/MeOH, 10/0 then 9/1) afforded the titled compound as a yellow solid (140 mg, 0.526 mmol, 37% yield).

Yellow solid, 16.4 mg, 0.062 mmol, 2% yield. R_f (CH₂Cl₂/MeOH:9/1, v/v) = 0.61. M.p. = 204 °C. ¹H NMR (400 MHz, DMSO-*d*₆) δ 9.48 (s, 1H, NH), 8.16 – 8.11 (m, 1H, CH_{Pyr}), 7.83 (d, *J* = 8.5 Hz, 1H, CH_{Pyr}), 7.64 – 7.57 (m, 1H, CH_{Pyr}), 7.35 (t, *J* = 7.3 Hz, 2H, CH_{Ph}), 7.30 – 7.20 (m, 3H, CH_{Ph}), 6.80 – 6.72 (m, 1H, CH_{Pyr}), 6.47 (s, 2H, NH₂), 5.06 (s, 2H, CH₂). ¹³C NMR (101 MHz, DMSO-*d*₆) δ 155.8, 154.4, 154.3, 147.6, 137.6, 137.4, 128.4 (2C), 127.2, 127.2 (2C), 114.9, 109.5, 48.7. LCMS: *t*_R = 2.71; 6.42 min. [M+H]⁺ = 267.13. HPLC (λ₂₅₄): Purity 98.8%; HPLC (λ₂₈₀): Purity 95.6%; *t*_R: 5.55 min (method 1).

MCK254: 1-benzyl-*N*³-(pyridin-3-yl)-1*H*-1,2,4-triazole-3,5-diamine



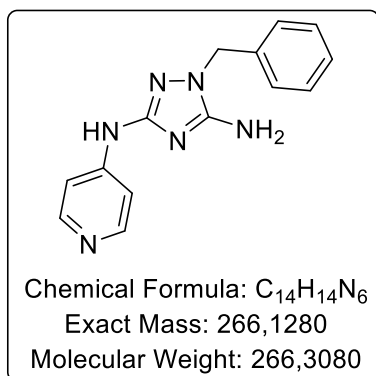
Characterization: 1-benzyl-*N*³-(pyridin-3-yl)-1*H*-1,2,4-triazole-3,5-diamine

*N*³-(pyridin-3-yl)-1*H*-1,2,4-triazole-3,5-diamine (50 mg, 0.284 mmol) was dissolved in degassed DMF, then Cs₂CO₃ (92 mg, 0.284 mmol) was added. Benzyl chloride (0.03 mL, 0.284 mmol) was added and the reaction mixture was stirred at r.t. overnight. Cs₂CO₃ was filtered and DMF was evaporated under reduced pressure. Purification by silica gel flash chromatography (CH₂Cl₂/MeOH, 10/0 then 9/1) afforded the titled compound as a brown solid (12.5 mg, 0.047 mmol, 17% yield).

Brown solid, 12.5 mg, 0.047 mmol, 17% yield. R_f (CH₂Cl₂/MeOH, 9/1, v/v) = 0.12. M.p. = 140 °C. ¹H NMR (400 MHz, DMSO-*d*₆) δ 8.97 (s, 1H, NH), 8.64 (d, *J* = 2.3 Hz, 1H, CH_{Ar}), 7.93 (dd, *J* = 12.0, 3.5 Hz, 2H, CH_{Ar}), 7.35 (t, *J* = 7.3 Hz, 2H, CH_{Ar}), 7.30 – 7.24 (m, 3H, CH_{Ar}), 7.18 (dd, *J* = 8.3, 4.6 Hz, 1H), CH_{Ar}, 6.37 (s,

2H, NH₂), 5.04 (s, 2H, CH₂). ¹³C NMR (101 MHz, DMSO-*d*₆) δ 156.5, 154.1, 139.2, 138.7, 137.7, 137.3, 128.2 (2C), 127.1 (2C), 127.0, 123.1, 121.3, 48.5. LCMS: *t*_R = 2.69; 4.92 min. [M+H]⁺ = 267.20. HPLC (λ₂₅₄): Purity 97.6%; HPLC (λ₂₈₀): Purity 97.1%; *t*_R: 5.21 min (method 1).

MCK255: 1-benzyl-N³-(pyridin-4-yl)-1H-1,2,4-triazole-3,5-diamine

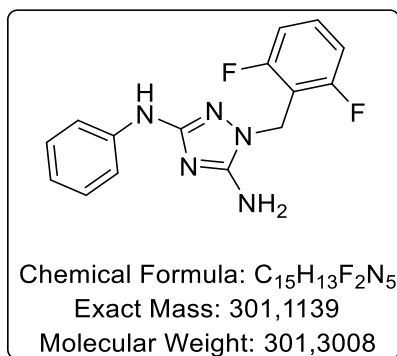


Characterization: 1-benzyl-N³-(pyridin-4-yl)-1H-1,2,4-triazole-3,5-diamine

N³-(pyridin-4-yl)-1H-1,2,4-triazole-3,5-diamine (200 mg, 1.14 mmol) was dissolved in degassed DMF (8 mL), then potassium *tert*-butoxide (130 mg, 1.14 mmol) was added at 0 °C. Benzyl chloride (0.13 mL, 1.14 mmol), dissolved in degassed DMF (4 mL), was added dropwise and the reaction mixture was stirred at r.t. for 6 h. Water was added to the mixture reaction and was extracted with ethyl acetate, washed with water, dried over magnesium sulfate and the solvents were evaporated under reduced pressure. Purification by silica gel flash chromatography (H₂O/CH₃CN, 10/0 then 70/30) afforded the titled compound as a white solid (58.5 mg, 0.220 mmol, 19%).

White solid, 58.5 mg, 0.220 mmol, 19% yield. R_f (CH₂Cl₂/MeOH, 9/1, v/v) = 0.21. M.p. = 206-208 °C. ¹H NMR (400 MHz, DMSO-*d*₆) δ 9.35 (s, 1H, NH), 8.18 (d, *J* = 6.3 Hz, 2H, CH_{Ar}), 7.40 – 7.36 (m, 2H, CH_{Ar}), 7.34 (d, *J* = 7.5 Hz, 2H, CH_{Ar}), 7.30 – 7.22 (m, 3H, CH_{Ar}), 6.42 (s, 2H, NH₂), 5.06 (s, 2H, CH₂). ¹³C NMR (101 MHz, DMSO-*d*₆) δ 156.1, 154.3, 149.5 (2C), 148.1, 137.3, 128.4 (2C), 127.3 (2C), 127.3, 110.3 (2C), 48.8. LCMS: *t*_R = 2.80; 3.90 min. [M+H]⁺ = 267.20. HPLC (λ₂₅₄): Purity 100%; HPLC (λ₂₈₀): Purity 100%; *t*_R: 5.1 min (method 1).

MCK256: 1-(2,6-difluorobenzyl)-N³-phenyl-1H-1,2,4-triazole-3,5-diamine

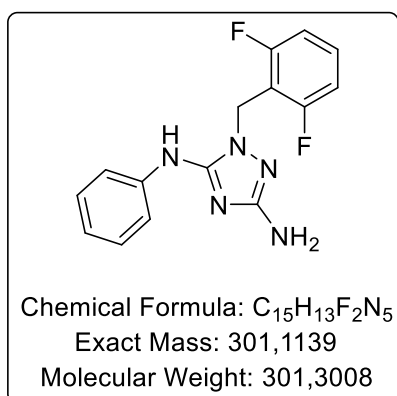


Characterization: 1-(2,6-difluorobenzyl)-N³-phenyl-1H-1,2,4-triazole-3,5-diamine

N³-phenyl-1H-1,2,4-triazole-3,5-diamine (500 mg, 2.86 mmol) was dissolved in degassed DMF, then Cs₂CO₃ (930 mg, 2.86 mmol) was added. 2,6-Difluorobenzyl chloride (463 mg, 2.86 mmol) was added and the reaction mixture was stirred at r.t. overnight. Cs₂CO₃ was filtered and DMF was evaporated under reduced pressure. Purification by silica gel flash chromatography (CH₂Cl₂/THF, 10/0 then 5/5) afforded the titled compound as a white-off solid (257 mg, 0.851 mmol, 30% yield) along with the N₅-benzylated regioisomer (46.9 mg, 0.155 mmol, 5% yield).

White-off solid, 257 mg, 0.851 mmol, 30% yield. R_f (CH₂Cl₂/THF, 1/1, v/v) = 0.40. M.p. = 154-156 °C. ¹H NMR (400 MHz, DMSO-*d*₆) δ 8.64 (s, 1H, NH), 7.42 (dd, *J* = 13.6, 8.0 Hz, 3H, CH_{Ar}), 7.11 (td, *J* = 8.0, 5.1 Hz, 4H, CH_{Ar}), 6.69 (t, *J* = 7.3 Hz, 1H, CH_{Ar}), 6.35 (s, 2H, NH₂), 5.06 (s, 2H, CH₂). ¹³C NMR (101 MHz, DMSO-*d*₆) δ 160.9 (dd, *J* = 248.7, 8.0 Hz, 2C), 157.2, 154.0, 142.4, 130.5 (t, *J* = 10.3 Hz), 128.3 (2C), 118.4, 115.4 (2C), 112.5 (t, *J* = 19.2 Hz), 111.6 (dd, *J* = 18.8, 6.2 Hz, 2C), 37.1 (t, *J* = 3.4 Hz). ¹⁹F NMR (376 MHz, DMSO-*d*₆) δ -114.67 (2F). LCMS: *t*_R = 10.20 min. [M+H]⁺ = 302.13. HPLC (λ₂₅₄): Purity 98.3%; HPLC (λ₂₈₀): Purity 99.5%; *t*_R: 8.22 min (method 1).

MCK257: 1-(2,6-difluorobenzyl)-N⁵-phenyl-1H-1,2,4-triazole-3,5-diamine

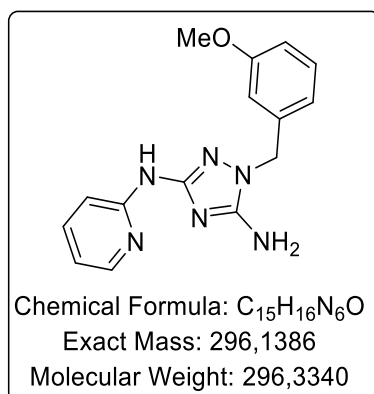


Characterization: 1-(2,6-difluorobenzyl)-N⁵-phenyl-1H-1,2,4-triazole-3,5-diamine

*N*³-phenyl-1*H*-1,2,4-triazole-3,5-diamine (500 mg, 2.86 mmol) was dissolved in degassed DMF, then Cs₂CO₃ (930 mg, 2.86 mmol) was added. 2,6-Difluorobenzyl chloride (463 mg, 2.86 mmol) was added and the reaction mixture was stirred at r.t. overnight. Cs₂CO₃ was filtered and DMF was evaporated under reduced pressure. Purification by silica gel flash chromatography (CH₂Cl₂/THF, 10/0 then 6/4) afforded the titled compound as a white solid (46.9 mg, 0.155 mmol, 5% yield) along with the *N*₃-benzylated regioisomer (257 mg, 0.851 mmol, 30% yield).

White solid, 46.9 mg, 0.155 mmol, 5% yield. R_f (CH₂Cl₂/THF, 1/1, v/v) = 0.65. M.p. = 240-242 °C. ¹H NMR (400 MHz, DMSO-*d*₆) δ 8.86 (s, 1H, NH), 7.59 (d, *J* = 7.7 Hz, 2H, CH_{Ar}), 7.42 (ddd, *J* = 15.0, 8.4, 6.7 Hz, 1H, CH_{Ar}), 7.29 – 7.22 (m, 2H, CH_{Ar}), 7.09 (t, *J* = 8.0 Hz, 2H, CH_{Ar}), 6.92 – 6.84 (m, 1H, CH_{Ar}), 5.18 (s, 2H, NH₂), 5.11 (s, 2H, CH₂). ¹³C NMR (101 MHz, DMSO-*d*₆) δ 160.9 (dd, *J* = 248.3, 8.0 Hz, 2C), 160.7, 150.0, 141.1, 130.48 (t, *J* = 10.3 Hz), 128.6 (2C), 120.4, 116.8 (2C), 112.64 (t, *J* = 19.1 Hz), 111.6 (dd, *J* = 18.8, 6.2 Hz, 2C), 37.21 (t, *J* = 3.4 Hz). ¹⁹F NMR (376 MHz, DMSO-*d*₆) δ -114.99 (2F). LCMS: *t*_R = 9.77 min. [M+H]⁺ = 302.07. HPLC (λ₂₅₄): Purity 95.3%; HPLC (λ₂₈₀): Purity 97.5%; *t*_R: 7.68 min (method 1).

MCK258: 1-(3-methoxybenzyl)-*N*³-(pyridin-2-yl)-1*H*-1,2,4-triazole-3,5-diamine

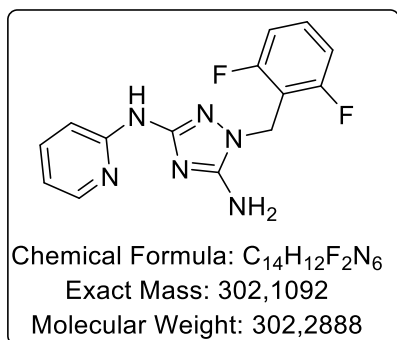


Characterization: 1-(3-methoxybenzyl)-*N*³-(pyridin-2-yl)-1*H*-1,2,4-triazole-3,5-diamine

*N*³-(pyridin-2-yl)-1*H*-1,2,4-triazole-3,5-diamine (200 mg, 1.14 mmol) was dissolved in degassed DMF (10 mL), then potassium *tert*-butoxide (127 mg, 1.14 mmol) was added. 3-Methoxybenzyl chloride (0.17 mL, 1.14 mmol), dissolved in degassed DMF (5 mL), was added dropwise and the reaction mixture was stirred at 0 °C for 3 h. Water was added to the mixture reaction and was extracted with ethyl acetate, washed with water, dried over magnesium sulfate and the solvents were evaporated under reduced pressure. Purification by silica gel flash chromatography (CH₂Cl₂/MeOH, 10/0 then 90/10) afforded the titled compound as a yellow solid (151.2 mg, 0.51 mmol, 45% yield).

Yellow solid, 151.2 mg, 0.51 mmol, 45% yield. Rf (CH₂Cl₂/MeOH:9/1, v/v) = 0.34. M.p. = 206 °C. ¹H NMR (400 MHz, DMSO-*d*₆) δ 10.51 (s, 1H, NH), 8.24 – 8.18 (m, 1H, CH_{Ar}), 7.89 (d, *J* = 8.5 Hz, 1H, CH_{Ar}), 7.70 – 7.62 (m, 1H, CH_{Ar}), 7.26 (dd, *J* = 8.9, 7.6 Hz, 1H, CH_{Ar}), 6.88 – 6.77 (m, 4H, CH_{Ar}), 6.70 (s, 2H, NH₂), 5.08 (s, 2H, CH₂), 3.72 (s, 3H, CH₃). ¹³C NMR (101 MHz, DMSO-*d*₆) δ 159.3, 155.6, 154.3, 154.1, 147.6, 138.8, 137.9, 129.5, 119.3, 114.9, 113.1, 112.4, 109.5, 54.9, 48.7. LCMS: *t*_R = 2.67; 4.03 min. [M+H]⁺ = 297.07. HPLC (λ₂₅₄): Purity 97.8%; *t*_R: 5.78 min (method 1).

MCK259: 1-(2,6-difluorobenzyl)-*N*³-(pyridin-2-yl)-1*H*-1,2,4-triazole-3,5-diamine

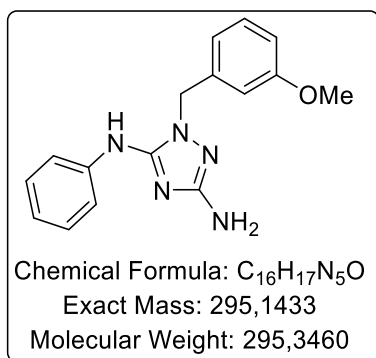


Characterization: 1-(2,6-difluorobenzyl)-*N*³-(pyridin-2-yl)-1*H*-1,2,4-triazole-3,5-diamine

*N*³-(pyridin-2-yl)-1*H*-1,2,4-triazole-3,5-diamine (250 mg, 1.42 mmol) was dissolved in degassed DMF (10 mL), then potassium *tert*-butoxide (159 mg, 1.42 mmol) was added at 0 °C. 2,6-Difluorobenzyl chloride (230 mg, 1.42 mmol), dissolved in degassed DMF (5 mL), was added dropwise and the reaction mixture was stirred at r.t. for 1 h 30. Water was added to the mixture reaction and was extracted with ethyl acetate, washed with water, dried over magnesium sulfate and the solvents were evaporated under reduced pressure. Purification by silica gel flash chromatography (CH₂Cl₂/MeOH, 10/0 then 9/1) afforded the titled compound as a white solid (87.8 mg, 0.291 mmol, 20% yield).

White solid, 87.8 mg, 0.291 mmol, 20% yield. Rf (CH₂Cl₂/MeOH:9/1, v/v) = 0.56. M.p. >260 °C. ¹H NMR (400 MHz, DMSO-*d*₆) δ 9.69 (s, 1H, NH), 8.16 – 8.08 (m, 1H, CH_{Ar}), 7.73 (d, *J* = 8.4 Hz, 1H, CH_{Ar}), 7.57 (ddd, *J* = 8.8, 7.2, 2.0 Hz, 1H, CH_{Ar}), 7.43 (ddd, *J* = 15.0, 8.5, 6.6 Hz, 1H, CH_{Ar}), 7.12 (t, *J* = 7.9 Hz, 2H, CH_{Ar}), 6.74 (ddd, *J* = 7.2, 4.9, 1.0 Hz, 1H, CH_{Ar}), 6.56 (s, 2H, NH₂), 5.10 (s, 2H, CH₂). ¹³C NMR (101 MHz, DMSO-*d*₆) δ 160.9 (dd, *J* = 248.9, 7.9 Hz, 2C), 155.7, 154.2, 154.2, 147.5, 137.5, 130.5 (t, *J* = 10.4 Hz), 114.8, 112.3 (t, *J* = 19.3 Hz), 111.6 (dd, *J* = 18.8, 6.1 Hz, 2C), 109.3, 37.44 – 37.1 (m). ¹⁹F NMR (376 MHz, DMSO-*d*₆) δ -114.67 (2F). LCMS: *t*_R = 2.48; 3.80 min. [M+H]⁺ = 303.07. HPLC (λ₂₅₄): Purity 99.8%; HPLC (λ₂₈₀): Purity 95.3%; *t*_R: 5.53 min (method 1).

MCK260: 1-(3-methoxybenzyl)-*N*⁵-phenyl-1*H*-1,2,4-triazole-3,5-diamine

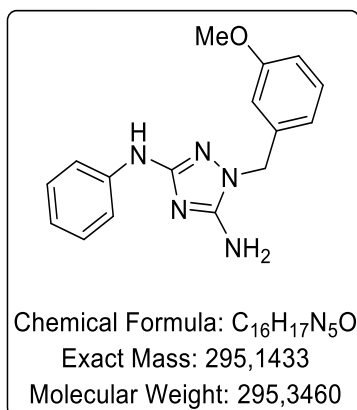


Characterization: 1-(3-methoxybenzyl)-*N*⁵-phenyl-1*H*-1,2,4-triazole-3,5-diamine

*N*³-phenyl-1*H*-1,2,4-triazole-3,5-diamine (250 mg, 1.43 mmol) was dissolved in degassed DMF (10 mL), then potassium *tert*-butoxide (159 mg, 1.43 mmol) was added. 3-Methoxybenzyl chloride (0.22 mL, 1.43 mmol), dissolved in degassed DMF (5 mL), was added dropwise and the reaction mixture was stirred at 0 °C for 30 min, then at r.t. for 4 h. Water was added to the mixture reaction and was extracted with ethyl acetate, washed with water, dried over magnesium sulfate and the solvents were evaporated under reduced pressure. Purification by silica gel flash chromatography (CH₂Cl₂/THF, 10/0 then 40/60) afforded the titled compound as a white solid (3 mg, 0.0102 mmol, 0.7% yield) along with the *N*₃-benzylated regioisomer.

White solid, 3 mg, 0.0102 mmol, 0.7% yield. *R*_f (CH₂Cl₂/THF, 1/1, v/v) = 0.74. M.p. = 130-132 °C. ¹H NMR (400 MHz, DMSO-*d*₆) δ 8.78 (s, 1H, NH), 7.58 (d, *J* = 7.7 Hz, 2H, CH_{Ar}), 7.24 (t, *J* = 7.6 Hz, 3H, CH_{Ar}), 6.87 (t, *J* = 7.3 Hz, 1H, CH_{Ar}), 6.83 (dd, *J* = 8.2, 1.8 Hz, 1H, CH_{Ar}), 6.77 – 6.71 (m, 2H, CH_{Ar}), 5.11 (s, 2H, NH₂), 5.09 (s, 2H, CH₂), 3.70 (s, 3H, OCH₃). ¹³C NMR (101 MHz, DMSO-*d*₆) δ 160.6, 159.2, 150.2, 141.1, 139.1, 129.5, 128.6 (2C), 120.4, 119.2, 116.8 (2C), 113.0, 112.2, 55.0, 48.6. LCMS: *t*_R = 9.82 min. [M+H]⁺ = 296.07. HPLC (λ₂₅₄): Purity 90.7%; HPLC (λ₂₈₀): Purity 92.4%; *t*_R: 7.75 min (method 2).

MCK261: 1-(3-methoxybenzyl)-*N*³-phenyl-1*H*-1,2,4-triazole-3,5-diamine

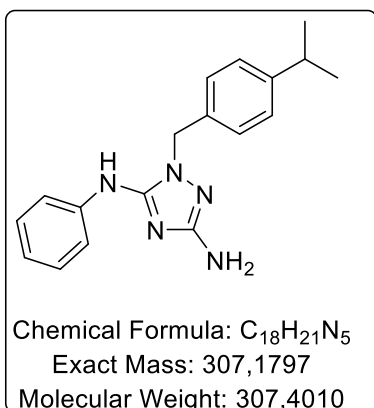


Characterization: 1-(3-methoxybenzyl)-*N*³-phenyl-1*H*-1,2,4-triazole-3,5-diamine

*N*³-phenyl-1*H*-1,2,4-triazole-3,5-diamine (250 mg, 1.43 mmol) was dissolved in degassed DMF (10 mL), then potassium *tert*-butoxide (159 mg, 1.43 mmol) was added. 3-Methoxybenzyl chloride (0.22 mL, 1.43 mmol), dissolved in degassed DMF (5 mL), was added dropwise and the reaction mixture was stirred at 0 °C for 30 min, then at r.t. for 4 h. Water was added to the mixture reaction and was extracted with ethyl acetate, washed with water, dried over magnesium sulfate and the solvents were evaporated under reduced pressure. Purification by silica gel flash chromatography (CH₂Cl₂/THF, 10/0 then 40/60) afforded the titled compound as a white solid (33.7 mg, 0.114 mmol, 8% yield) along with the *N*₅-benzylated regioisomer.

White solid, 33.7 mg, 0.114 mmol, 8% yield. R_f (CH₂Cl₂/THF, 1/1, v/v) = 0.69. M.p. = 106-108 °C. ¹H NMR (400 MHz, DMSO-*d*₆) δ 8.69 – 8.64 (m, 1H, NH), 7.46 (d, *J* = 7.7 Hz, 2H, CH_{Ar}), 7.25 (td, *J* = 7.5, 1.3 Hz, 1H, CH_{Ar}), 7.14 (t, *J* = 7.9 Hz, 2H, CH_{Ar}), 6.86 – 6.78 (m, 3H, CH_{Ar}), 6.70 (t, *J* = 7.3 Hz, 1H, CH_{Ar}), 6.27 (s, 2H, NH₂), 5.03 – 4.94 (m, 2H, CH₂), 3.72 (s, 3H, CH₃). ¹³C NMR (101 MHz, DMSO-*d*₆) δ 159.2, 157.1, 154.1, 142.3, 139.1, 129.4, 128.4 (2C), 119.4, 118.3, 115.5 (2C), 113.2, 112.3, 54.9, 48.5. LCMS: *t*_R = 9.71 min. [M+H]⁺ = 296.00. HPLC (λ₂₅₄): Purity 96.7%; *t*_R: 8.18 min (method 2).

MCK262: 1-(4-isopropylbenzyl)-*N*⁵-phenyl-1*H*-1,2,4-triazole-3,5-diamine

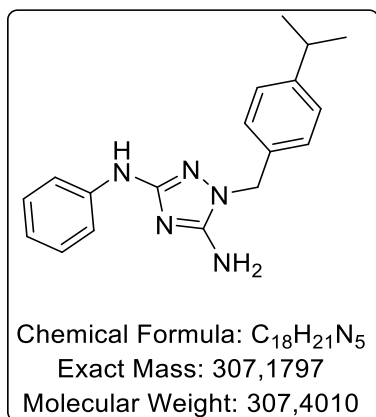


Characterization: 1-(4-isopropylbenzyl)-*N*⁵-phenyl-1*H*-1,2,4-triazole-3,5-diamine

*N*³-phenyl-1*H*-1,2,4-triazole-3,5-diamine (250 mg, 1.43 mmol) was dissolved in anhydrous DMF (1 mL), then potassium *tert*-butoxide (160 mg, 1.43 mmol) was added. 4-Isopropylbenzyl chloride (0.22 mL, 1.43 mmol), dissolved in anhydrous CH₂Cl₂ (1 mL), was added dropwise and the reaction mixture was stirred at 0 °C for 1 h and at r.t. for 2 h. Water was added to the mixture reaction and the solvents were evaporated under reduced pressure. Purification by reversed-phase chromatography (H₂O/CH₃CN, 10/0 then 45/55) afforded the titled compound as a white solid (51.8 mg, 0.169 mmol, 12% yield) along with the *N*₃-benzylated regioisomer.

White solid, 51.8 mg, 0.169 mmol, 12% yield). *R*_f (CH₂Cl₂/THF, 1/1, v/v) = 0.81. M.p. = 146 °C. ¹H NMR (400 MHz, DMSO-*d*₆) δ 8.78 (s, 1H, NH), 7.59 (d, *J* = 7.7 Hz, 2H, CH_{Ar}), 7.27 – 7.21 (m, 2H, CH_{Ar}), 7.19 (d, *J* = 8.1 Hz, 2H, CH_{Ar}), 7.11 (d, *J* = 8.1 Hz, 2H, CH_{Ar}), 6.87 (t, *J* = 7.3 Hz, 1H, CH_{Ar}), 5.09 (s, 2H, NH₂), 5.07 (s, 2H, CH₂), 2.84 (p, *J* = 6.9 Hz, 1H, CH), 1.16 (d, *J* = 6.9 Hz, 6H, CH₃). ¹³C NMR (101 MHz, DMSO-*d*₆) δ 160.6, 150.0, 147.4, 141.1, 134.9, 128.6 (2C), 127.2 (2C), 126.2 (2C), 120.4, 116.8 (2C), 48.4, 33.1, 23.8 (2C). LCMS: *t*_R = 11.15 min. [M+H]⁺ = 308.07. HPLC (λ₂₅₄): Purity 91.1%; *t*_R: 9.47min (method 2).

MCK263: 1-(4-isopropylbenzyl)-*N*³-phenyl-1*H*-1,2,4-triazole-3,5-diamine

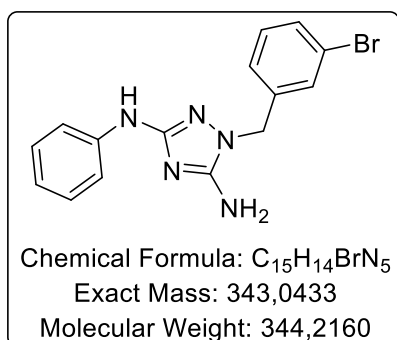


Characterization: 1-(4-isopropylbenzyl)-*N*³-phenyl-1*H*-1,2,4-triazole-3,5-diamine

*N*³-phenyl-1*H*-1,2,4-triazole-3,5-diamine (250 mg, 1.43 mmol) was dissolved in anhydrous DMF (1 mL), then potassium *tert*-butoxide (160 mg, 1.43 mmol) was added. 4-Isopropylbenzyl chloride (0.22 mL, 1.43 mmol), dissolved in anhydrous CH₂Cl₂ (1 mL), was added dropwise and the reaction mixture was stirred at 0 °C for 1 h and at r.t. for 2 h. Water was added to the mixture reaction and the solvents were evaporated under reduced pressure. Purification by reversed-phase chromatography (H₂O/CH₃CN, 10/0 then 45/55) afforded the titled compound as a white solid (122 mg, 0.397 mmol, 28% yield) along with the *N*₅-benzylated regioisomer.

White solid, 122 mg, 0.397 mmol, 28% yield. R_f (CH₂Cl₂/THF, 1/1, v/v) = 0.79. M.p. = 140-142 °C. ¹H NMR (400 MHz, DMSO-*d*₆) δ 8.66 (s, 1H, NH), 7.47 (d, *J* = 7.8 Hz, 2H, CH_{Ar}), 7.17 (dq, *J* = 15.6, 8.2 Hz, 6H, CH_{Ar}), 6.70 (t, *J* = 7.3 Hz, 1H, CH_{Ar}), 6.27 (s, 2H, NH₂), 4.98 (s, 2H, CH₂), 2.84 (hept, *J* = 6.9 Hz, 1H, CH), 1.16 (s, 6H, CH₃). ¹³C NMR (101 MHz, DMSO-*d*₆) δ 157.0, 154.0, 147.3, 142.3, 135.0, 128.4 (2C), 127.3 (2C), 126.2 (2C), 118.3, 115.5 (2C), 48.4, 33.1, 23.9 (2C). LCMS: *t*_R = 11.15 min. [M+H]⁺ = 308.07. HPLC (λ₂₅₄): Purity 97.3%; *t*_R: 9.82 min (method 2).

MCK264: 1-(3-bromobenzyl)-*N*³-phenyl-1*H*-1,2,4-triazole-3,5-diamine

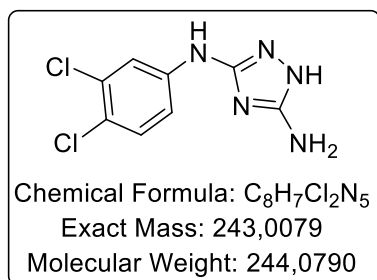


Characterization: 1-(3-bromobenzyl)-*N*³-phenyl-1*H*-1,2,4-triazole-3,5-diamine

*N*³-phenyl-1*H*-1,2,4-triazole-3,5-diamine (150 mg, 0.857 mmol) was dissolved in anhydrous DMF (1 mL), then potassium *tert*-butoxide (96 mg, 0.857 mmol) was added. 3-Bromobenzyl bromide (225 mg, 0.857 mmol), dissolved in anhydrous CH₂Cl₂ (1 mL), was added dropwise and the reaction mixture was stirred at 0 °C for 1 h and at r.t. for an additional 1 h. Water was added to the mixture reaction and the solvents were evaporated under reduced pressure. Purification by reversed-phase chromatography (H₂O/CH₃CN, 10/0 then 45/55) afforded the titled compound as a purple solid (89 mg, 0.259 mmol, 30% yield) along with the *N*₅-benzylated regioisomer.

Purple solid, 89 mg, 0.259 mmol, 30% yield. R_f (CH₂Cl₂/THF, 1/1, v/v) = 0.56. M.p. = 108-110 °C. ¹H NMR (400 MHz, DMSO-*d*₆) δ 8.69 (s, 1H, NH), 7.46 (q, *J* = 6.2, 5.5 Hz, 4H, CH_{Ar}), 7.32 (t, *J* = 7.8 Hz, 1H, CH_{Ar}), 7.25 (d, *J* = 7.7 Hz, 1H, CH_{Ar}), 7.14 (t, *J* = 7.7 Hz, 2H, CH_{Ar}), 6.71 (t, *J* = 7.3 Hz, 1H, CH_{Ar}), 6.34 (s, 2H, NH₂), 5.04 (s, 2H, CH₂). ¹³C NMR (101 MHz, DMSO-*d*₆) δ 157.2, 154.2, 142.2, 140.3, 130.6, 130.0, 128.4 (2C), 126.3, 121.6, 118.4, 115.5 (2C), 48.0. LCMS: *t*_R = 10.75 min. [M+H]⁺ = 244.00; 246.00. HPLC (λ₂₅₄): Purity 99.4%; HPLC (λ₂₈₀): Purity 96.7%; *t*_R: 8.85 min (method 2).

MCK265: *N*³-(3,4-dichlorophenyl)-1*H*-1,2,4-triazole-3,5-diamine

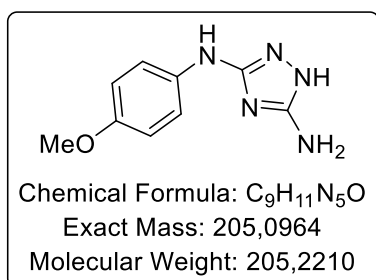


Characterization: *N*³-(3,4-dichlorophenyl)-1*H*-1,2,4-triazole-3,5-diamine

To a solution of carbamimidothioic acid, *N*-cyano-*N'*-(3,4-dichlorophenyl), methyl ester (250 mg, 0.965 mmol) in ethanol (10 mL) was added N₂H₄·H₂O (0.1 mL, 1.93 mmol), then the solution was warmed at 75 °C for 3 h. The precipitate was filtered and washed with diethyl ether to obtain a grey solid (232 mg, 0.95 mmol, 99% yield).

Grey solid, 232 mg, 0.95 mmol, 99% yield. R_f (CH₂Cl₂/MeOH, 9/1, v/v) = 0.34. M.p. = 210-212 °C. ¹H NMR (400 MHz, DMSO-*d*₆) δ 11.28 (s, 1H, NH), 9.10 (s, 1H, NH), 7.92 (s, 1H, CH_{Ar}), 7.36 (q, *J* = 8.9 Hz, 2H, CH_{Ar}), 5.96 (s, 2H, NH₂). ¹³C NMR (101 MHz, DMSO-*d*₆) δ 157.2, 155.5, 142.6, 130.7, 130.1, 119.0, 116.2, 115.8. LCMS: *t*_R = 9.32 min. [M+H]⁺ = 244.00. HPLC (λ₂₅₄): Purity 99.4%; HPLC (λ₂₈₀): Purity 96.5%; *t*_R: 7.37 min (method 1).

MCK266: *N*³-(4-methoxyphenyl)-1*H*-1,2,4-triazole-3,5-diamine

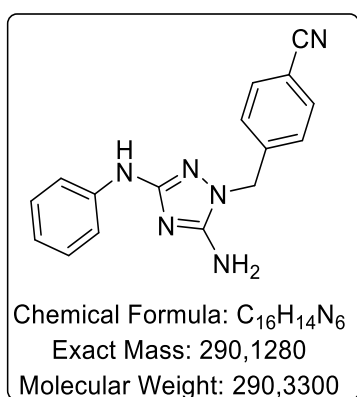


Characterization: *N*³-(4-methoxyphenyl)-1*H*-1,2,4-triazole-3,5-diamine

To a solution of carbamimidothioic acid, *N*-cyano-*N'*-(4-methoxyphenyl), methyl ester (1 g, 4.52 mmol) in ethanol (30 mL) was added N₂H₄·H₂O (0.45 mL, 9.05 mmol), then the solution was stirred at 75 °C for 4 h. The precipitate was filtered and washed with diethyl ether to obtain a grey solid (873.3 mg, 4.28 mmol, 95% yield).

Grey solid, 873.3 mg, 4.28 mmol, 95% yield. R_f (CH₂Cl₂/MeOH,9/1, v/v) = 0.24. ¹H NMR (400 MHz, DMSO-*d*₆) δ 11.14 (s, 1H, NH), 8.35 (s, 1H, NH), 7.41 (d, *J* = 8.6 Hz, 2H, CH_{Ar}), 6.76 (d, *J* = 8.6 Hz, 2H, CH_{Ar}), 5.84 (s, 2H, NH₂), 3.66 (s, 3H, OCH₃). ¹³C NMR (101 MHz, DMSO-*d*₆) δ 158.2, 155.4, 152.0, 136.3, 116.6 (2C), 113.8 (2C), 55.2. LCMS: *t*_R = 2.45, 3.30 min. [M+H]⁺ = 206.07. HPLC (λ₂₅₄): Purity 99.3%; HPLC (λ₂₈₀): Purity 96.3%; *t*_R: 4.86 min (method 1). Data in accordance with the literature.⁴⁹⁸

MCK267: 1-(4-cyanobenzyl)-*N*³-phenyl-1*H*-1,2,4-triazole-3,5-diamine



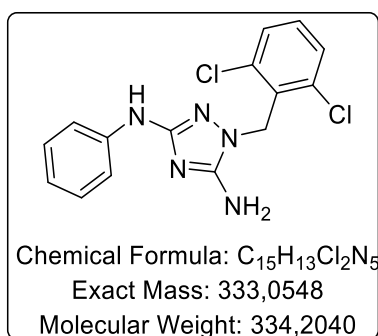
Characterization: 1-(4-cyanobenzyl)-*N*³-phenyl-1*H*-1,2,4-triazole-3,5-diamine

*N*³-phenyl-1*H*-1,2,4-triazole-3,5-diamine (250 mg, 1.43 mmol) was dissolved in degassed DMF (10 mL), then potassium *tert*-butoxide (159 mg, 1.43 mmol) was added. 4-Cyanobenzyl chloride (217 mg, 1.43 mmol), dissolved in degassed DMF (5 mL), was added dropwise and the reaction mixture was stirred at 0 °C for 30 min, then at r.t. for 3 h. Water was added to the mixture reaction and was extracted with

ethyl acetate, washed with water, dried over magnesium sulfate and the solvents were evaporated under reduced pressure. Purification by silica gel flash chromatography (CH₂Cl₂/THF, 10/0 then 50/50) afforded the titled compound as a grey solid (88.1 mg, 0.304 mmol, 21% yield).

Grey solid, 88.1 mg, 0.304 mmol, 21% yield. R_f (CH₂Cl₂/THF, 1/1, v/v) = 0.48. M.p. = 178-180 °C. ¹H NMR (400 MHz, DMSO-*d*₆) δ 8.71 (s, 1H, NH), 7.83 (d, *J* = 8.1 Hz, 2H, CH_{Ar}), 7.45 (d, *J* = 8.0 Hz, 2H, CH_{Ar}), 7.38 (d, *J* = 8.1 Hz, 2H, CH_{Ar}), 7.14 (t, *J* = 7.8 Hz, 2H, CH_{Ar}), 6.71 (t, *J* = 7.3 Hz, 1H, CH_{Ar}), 6.35 (s, 2H, NH₂), 5.14 (s, 2H, CH₂). ¹³C NMR (101 MHz, DMSO-*d*₆) δ 157.4, 154.4, 143.3, 142.2, 132.4 (2C), 128.4 (2C), 127.9 (2C), 118.7, 118.5, 115.5 (2C), 109.9, 48.3. LCMS: *t*_R = 9.90 min. [M+H]⁺ = 291.07. HPLC (λ₂₅₄): Purity 97.3%; *t*_R: 8.09 min (method 2).

MCK268: 1-(2,6-dichlorobenzyl)- *N*³-phenyl-1*H*-1,2,4-triazole-3,5-diamine

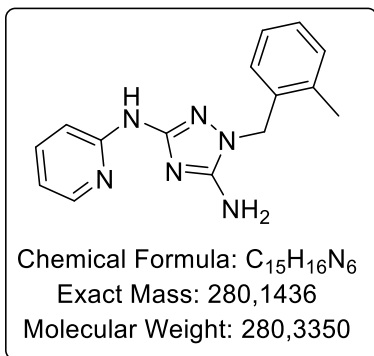


Characterization: 1-(2,6-dichlorobenzyl)- *N*³-phenyl-1*H*-1,2,4-triazole-3,5-diamine

*N*³-phenyl-1*H*-1,2,4-triazole-3,5-diamine (250 mg, 1.43 mmol) was dissolved in degassed DMF (10 mL), then potassium *tert*-butoxide (159 mg, 1.43 mmol) was added. 2,6-Dichlorobenzyl chloride (276 mg, 1.43 mmol), dissolved in degassed DMF (5 mL), was added dropwise and the reaction mixture was stirred at 0 °C for 30 min, then at r.t. for 3 h. Water was added to the mixture reaction and was extracted with ethyl acetate, washed with water, dried over magnesium sulfate and the solvents were evaporated under reduced pressure. Purification by silica gel flash chromatography (CH₂Cl₂/THF, 10/0 then 50/50) afforded the titled compound as a brown solid (93.3 mg, 0.028 mmol, 20% yield).

Brown solid, 93.3 mg, 0.028 mmol, 20% yield. R_f (CH₂Cl₂/THF, 8/2, v/v) = 0.57. M.p. = 206-208 °C. ¹H NMR (400 MHz, DMSO-*d*₆) δ 8.61 (s, 1H, NH), 7.51 (d, *J* = 8.0 Hz, 2H, CH_{Ar}), 7.43 – 7.33 (m, 3H, CH_{Ar}), 7.07 (t, *J* = 7.9 Hz, 2H, CH_{Ar}), 6.66 (t, *J* = 7.3 Hz, 1H, CH_{Ar}), 6.37 (s, 2H, NH₂), 5.16 (s, 2H, CH₂). ¹³C NMR (101 MHz, DMSO-*d*₆) δ 157.1, 154.0, 142.4, 135.6 (2C), 131.7, 130.4, 128.5 (2C), 128.2 (2C), 118.2, 115.4 (2C), 44.6. LCMS: *t*_R = 10.31 min. [M+H]⁺ = 334.00. HPLC (λ₂₅₄): Purity 100%; HPLC (λ₂₈₀): Purity 96.9%; *t*_R: 8.78 min (method 2).

MCK269: 1-(2-methylbenzyl)-N³-(pyridin-2-yl)-1H-1,2,4-triazole-3,5-diamine

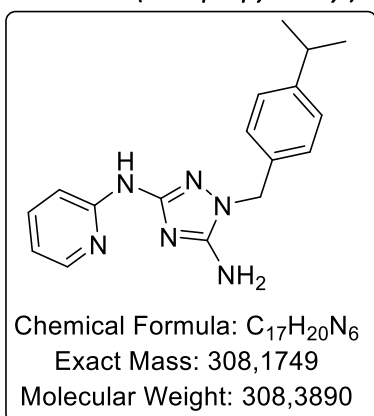


Characterization: 1-(2-methylbenzyl)-N³-(pyridin-2-yl)-1H-1,2,4-triazole-3,5-diamine

N³-(pyridin-2-yl)-1H-1,2,4-triazole-3,5-diamine (250 mg, 1.42 mmol) was dissolved in degassed DMF (10 mL), then potassium *tert*-butoxide (159 mg, 1.42 mmol) was added at 0 °C. 2-Methylbenzyl chloride (0.19 mL, 1.42 mmol), dissolved in degassed DMF (5 mL), was added dropwise and the reaction mixture was stirred at r.t. for 3 h. Water was added to the mixture reaction and was extracted with ethyl acetate, washed with water, dried over magnesium sulfate and the solvents were evaporated under reduced pressure. Purification by silica gel flash chromatography (CH₂Cl₂/MeOH, 10/0 then 9/1) afforded the titled compound as a yellow solid (210.9 mg, 0.753 mmol, 53% yield).

Yellow solid, 210.9 mg, 0.753 mmol, 53% yield. R_f (CH₂Cl₂/MeOH:95/5, v/v) = 0.44. M.p. = 256-258 °C. ¹H NMR (400 MHz, DMSO-*d*₆) δ 10.09 (s, 1H, NH), 8.17 (d, *J* = 3.8 Hz, 1H, CH_{Ar}), 7.84 (d, *J* = 8.5 Hz, 1H, CH_{Ar}), 7.71 – 7.55 (m, 1H, CH_{Ar}), 7.16 (dq, *J* = 12.8, 7.0 Hz, 3H, CH_{Ar}), 6.90 – 6.75 (m, 2H, CH_{Ar}), 6.56 (s, 2H, NH₂), 5.07 (s, 2H, CH₂), 2.35 (s, 3H, CH₃). ¹³C NMR (101 MHz, DMSO-*d*₆) δ 155.6, 154.5, 154.2, 147.6, 137.7, 135.5, 135.3, 129.9, 127.0, 126.4, 125.8, 114.9, 109.5, 47.0, 18.6. LCMS: *t*_R = 2.53; 3.64 min. [M+H]⁺ = 281.07. HPLC (λ₂₅₄): Purity 99.9%; HPLC (λ₂₈₀): Purity 97.4%; *t*_R: 5.85 min (method 1).

MCK270: 1-(4-isopropylbenzyl)-N³-(pyridin-2-yl)-1H-1,2,4-triazole-3,5-diamine

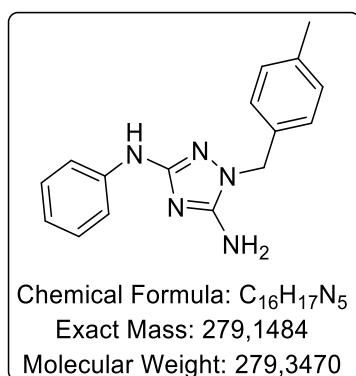


Characterization: 1-(4-isopropylbenzyl)-N³-(pyridin-2-yl)-1H-1,2,4-triazole-3,5-diamine

*N*³-(pyridin-2-yl)-1*H*-1,2,4-triazole-3,5-diamine (250 mg, 1.42 mmol) was dissolved in degassed DMF (10 mL), then potassium *tert*-butoxide (159 mg, 1.42 mmol) was added at 0 °C. 4-Isopropylbenzyl chloride (0.16 mL, 1.42 mmol), dissolved in degassed DMF (5 mL), was added dropwise and the reaction mixture was stirred at r.t. for 3 h. Water was added to the mixture reaction and was extracted with ethyl acetate, washed with water, dried over magnesium sulfate and the solvents were evaporated under reduced pressure. Purification by silica gel flash chromatography (CH₂Cl₂/MeOH, 10/0 then 9/1) afforded the titled compound as a yellow solid (244.1 mg, 0.792 mmol, 56% yield).

Yellow solid, 244.1 mg, 0.792 mmol, 56% yield. R_f (CH₂Cl₂/MeOH:95/5, v/v) = 0.46. M.p. = 190 °C. ¹H NMR (400 MHz, DMSO-*d*₆) δ 10.11 (s, 1H, NH), 8.20 – 8.14 (m, 1H, CH_{Ar}), 7.86 (d, *J* = 8.5 Hz, 1H, CH_{Ar}), 7.68 – 7.57 (m, 1H, CH_{Ar}), 7.26 – 7.11 (m, 4H, CH_{Ar}), 6.82 – 6.74 (m, 1H, CH_{Ar}), 6.59 (s, 2H, NH₂), 5.04 (s, 2H, CH₂), 2.85 (hept, *J* = 6.8 Hz, 1H, CH), 1.17 (d, *J* = 6.9 Hz, 6H, CH₃). ¹³C NMR (101 MHz, DMSO-*d*₆) δ 155.5, 154.2, 154.1, 147.5, 147.4, 137.8, 134.7, 127.2 (2C), 126.3 (2C), 114.9, 109.5, 48.5, 33.1, 23.8 (2C). LCMS: *t*_R = 7.42 min. [M+H]⁺ = 309.07. HPLC (λ₂₅₄): Purity %; HPLC (λ₂₈₀): Purity 98.1%; *t*_R: 7.15 min (method 1).

MCK271: 1-(4-methylbenzyl)- *N*³-phenyl-1*H*-1,2,4-triazole-3,5-diamine

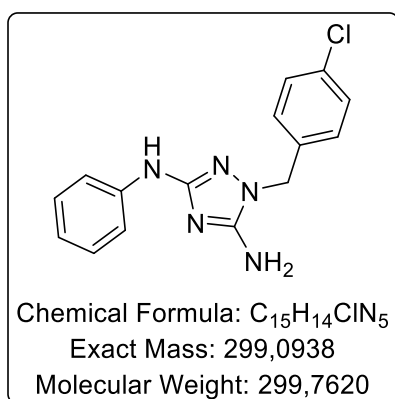


Characterization: 1-(4-methylbenzyl)- *N*³-phenyl-1*H*-1,2,4-triazole-3,5-diamine

*N*³-phenyl-1*H*-1,2,4-triazole-3,5-diamine (250 mg, 1.43 mmol) was dissolved in degassed DMF (10 mL), then potassium *tert*-butoxide (159 mg, 1.43 mmol) was added. 4-Methylbenzyl chloride (0.19 mL, 1.43 mmol), dissolved in degassed DMF (5 mL), was added dropwise and the reaction mixture was stirred at 0 °C for 30 min, then at r.t. for 2 h. Water was added to the mixture reaction and was extracted with ethyl acetate, washed with water, dried over magnesium sulfate and the solvents were evaporated under reduced pressure. Purification by silica gel flash chromatography (CH₂Cl₂/THF, 10/0 then 50/50) afforded the titled compound as a purple solid (28 mg, 0.100 mmol, 7% yield).

Purple solid, 28 mg, 0.100 mmol, 7% yield. Rf (CH₂Cl₂/THF,1/1, v/v) = 0.56. M.p. = 116-118 °C. ¹H NMR (400 MHz, DMSO-*d*₆) δ 8.70 (s, 1H, NH), 7.45 (d, *J* = 7.7 Hz, 2H, CH_{Ar}), 7.14 (s, 6H, CH_{Ar}), 6.72 (t, *J* = 7.3 Hz, 1H, CH_{Ar}), 6.37 (s, 2H, NH₂), 4.97 (s, 2H, CH₂), 2.26 (s, 3H, CH₃). ¹³C NMR (101 MHz, DMSO-*d*₆) δ 156.3, 153.5, 142.1, 136.3, 134.4, 128.8 (2C), 128.4 (2C), 127.2 (2C), 118.5, 115.5 (2C), 48.5, 20.6. LCMS: *t*_R = 9.82 min. [M+H]⁺ = 280.00. HPLC (λ₂₅₄): Purity 99.7%; HPLC (λ₂₈₀): Purity 95.0%; *t*_R: 8.61 min (method 2).

MCK272: 1-(4-chlorobenzyl)- N³-phenyl-1H-1,2,4-triazole-3,5-diamine

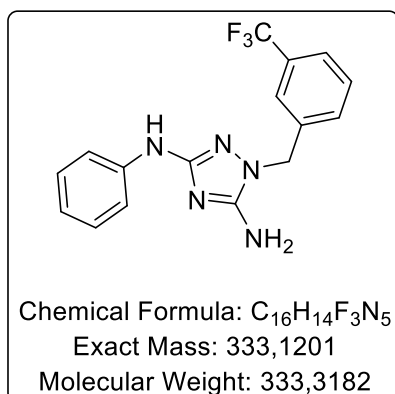


Characterization: 1-(4-chlorobenzyl)- N³-phenyl-1H-1,2,4-triazole-3,5-diamine

N³-phenyl-1H-1,2,4-triazole-3,5-diamine (250 mg, 1.43 mmol) was dissolved in degassed DMF (10 mL), then potassium *tert*-butoxide (159 mg, 1.43 mmol) was added. 4-Chlorobenzyl chloride (230 mg, 1.43 mmol), dissolved in degassed DMF (5 mL), was added dropwise and the reaction mixture was stirred at 0 °C for 30 min, then at r.t. for 2 h. Water was added to the mixture reaction and was extracted with ethyl acetate, washed with water, dried over magnesium sulfate and the solvents were evaporated under reduced pressure. Purification by silica gel flash chromatography (CH₂Cl₂/THF, 10/0 then 40/60) afforded the titled compound as a purple solid (76.9 mg, 0.257 mmol, 18% yield).

Purple solid, 76.9 mg, 0.257 mmol, 18% yield. Rf (CH₂Cl₂/THF,1/1, v/v) = 0.47. M.p. = 156-158 °C. ¹H NMR (400 MHz, DMSO-*d*₆) δ 8.69 (s, 1H, NH), 7.43 (dd, *J* = 14.6, 8.1 Hz, 4H, CH_{Ar}), 7.26 (d, *J* = 8.1 Hz, 2H, CH_{Ar}), 7.14 (t, *J* = 7.8 Hz, 2H, CH_{Ar}), 6.71 (t, *J* = 7.3 Hz, 1H, CH_{Ar}), 6.34 (s, 2H, NH₂), 5.03 (s, 2H, CH₂). ¹³C NMR (101 MHz, DMSO-*d*₆) δ 157.0, 154.0, 142.2, 136.5, 131.8, 129.1 (2C), 128.4 (2C), 128.3 (2C), 118.4, 115.5 (2C), 48.0. LCMS: *t*_R = 10.63 min. [M+H]⁺ = 300.07. HPLC (λ₂₅₄): Purity 99.7%; HPLC (λ₂₈₀): Purity 98.5%; *t*_R: 8.98 min (method 2).

MCK273: *N*³-phenyl-1-(3-(trifluoromethyl)benzyl)-1*H*-1,2,4-triazole-3,5-diamine

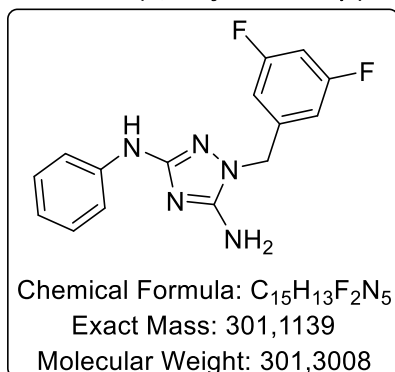


Characterization: *N*³-phenyl-1-(3-(trifluoromethyl)benzyl)-1*H*-1,2,4-triazole-3,5-diamine

*N*³-phenyl-1*H*-1,2,4-triazole-3,5-diamine (250 mg, 1.43 mmol) was dissolved in anhydrous DMF (1 mL), then potassium *tert*-butoxide (160 mg, 1.43 mmol) was added. 3-(Trifluoromethyl)benzyl chloride (0.22 mL, 1.43 mmol), dissolved in anhydrous CH₂Cl₂ (1 mL), was added dropwise and the reaction mixture was stirred at 0 °C for 1 h and at r.t. for 2 h. Water was added to the mixture reaction and the solvents were evaporated under reduced pressure. Purification by reversed-phase chromatography (H₂O/CH₃CN, 10/0 then 45/55) afforded the titled compound as a yellow solid (197.1 mg, 0.592 mmol, 41% yield) along with the *N*₅-benzylated regioisomer.

Yellow solid, 197.1 mg, 0.592 mmol, 41% yield. R_f (CH₂Cl₂/THF,1/1, v/v) = 0.71. M.p. = 118-120 °C. ¹H NMR (400 MHz, DMSO-*d*₆) δ 8.69 (s, 1H, NH), 7.68 – 7.57 (m, 3H, CH_{Ar}), 7.54 (d, *J* = 7.6 Hz, 1H, CH_{Ar}), 7.45 (d, *J* = 7.8 Hz, 2H, CH_{Ar}), 7.14 (t, *J* = 7.9 Hz, 2H, CH_{Ar}), 6.71 (t, *J* = 7.3 Hz, 1H, CH_{Ar}), 6.35 (s, 2H, NH₂), 5.13 (s, 2H, CH₂). ¹³C NMR (101 MHz, DMSO-*d*₆) δ 157.3, 154.2, 142.2, 139.0, 131.4, 129.5 (2C), 129.2, 128.9, 128.4 (2C), 124.0-123.8 (m), 118.5, 115.5 (2C), 48.1. ¹⁹F NMR (376 MHz, DMSO-*d*₆) δ -61.11 (3F). LCMS: *t*_R = 10.58 min. [M+H]⁺ = 334.07. HPLC (λ₂₅₄): Purity 98.1%; *t*_R: 9.59 min (method 2).

MCK274: 1-(3,5-difluorobenzyl)- *N*³-phenyl-1*H*-1,2,4-triazole-3,5-diamine

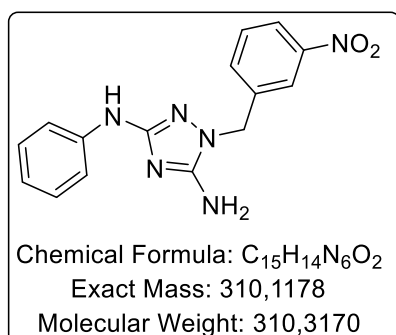


Characterization: 1-(3,5-difluorobenzyl)- *N*³-phenyl-1*H*-1,2,4-triazole-3,5-diamine

*N*³-phenyl-1*H*-1,2,4-triazole-3,5-diamine (250 mg, 1.43 mmol) was dissolved in degassed DMF (10 mL), then potassium *tert*-butoxide (159 mg, 1.43 mmol) was added. 3,5-Difluorobenzyl chloride (230 mg, 1.43 mmol), dissolved in degassed DMF (5 mL), was added dropwise and the reaction mixture was stirred at 0 °C for 30 min, then at r.t. for 3 h. Water was added to the mixture reaction and was extracted with ethyl acetate, washed with water, dried over magnesium sulfate and the solvents were evaporated under reduced pressure. Purification by silica gel flash chromatography (CH₂Cl₂/THF, 10/0 then 50/50) afforded the titled compound as a purple solid (20.1 mg, 0.066 mmol, 5% yield).

Purple solid, 20.1 mg, 0.066 mmol, 5% yield. R_f (CH₂Cl₂/THF, 1/1, v/v) = 0.61. M.p. = 146-148 °C. ¹H NMR (400 MHz, DMSO-*d*₆) δ 8.82 (s, 1H, NH), 7.46 (d, *J* = 8.0 Hz, 2H, CH_{Ar}), 7.16 (t, *J* = 7.9 Hz, 3H, CH_{Ar}), 6.94 (d, *J* = 6.5 Hz, 2H, CH_{Ar}), 6.74 (t, *J* = 7.3 Hz, 1H, CH_{Ar}), 6.54 (s, 2H, NH₂), 5.09 (s, 2H, CH₂). ¹³C NMR (101 MHz, DMSO-*d*₆) δ 162.36 (dd, *J* = 246.4, 13.1 Hz, 2C), 156.4, 153.8, 142.0, 141.96 (t, *J* = 4.4 Hz), 128.5 (2C), 118.8, 115.7 (2C), 110.3 (dd, *J* = 18.7, 6.9 Hz, 2C), 102.79 (t, *J* = 25.7 Hz), 47.9. ¹⁹F NMR (376 MHz, DMSO-*d*₆) δ -109.66 (2F). LCMS: *t*_R = 10.13 min. [M+H]⁺ = 302.07. HPLC (λ₂₅₄): Purity 98.4%; *t*_R: 8.88 min (method 2).

MCK275: 1-(3-nitrobenzyl)-*N*³-phenyl-1*H*-1,2,4-triazole-3,5-diamine

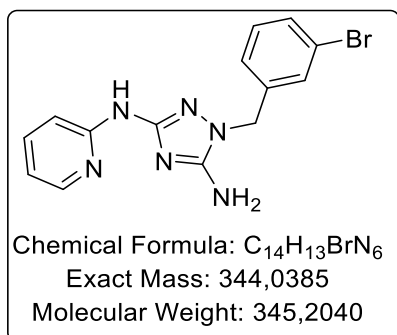


Characterization: 1-(3-nitrobenzyl)-*N*³-phenyl-1*H*-1,2,4-triazole-3,5-diamine

*N*³-phenyl-1*H*-1,2,4-triazole-3,5-diamine (250 mg, 1.43 mmol) was dissolved in degassed DMF (10 mL), then potassium *tert*-butoxide (159 mg, 1.43 mmol) was added. 3-Nitrobenzyl bromide (307 mg, 1.43 mmol), dissolved in degassed DMF (5 mL), was added dropwise and the reaction mixture was stirred at 0 °C for 30 min, then at r.t. for 3 h. Water was added to the mixture reaction and was extracted with ethyl acetate, washed with water, dried over magnesium sulfate and the solvents were evaporated under reduced pressure. Purification by silica gel flash chromatography (CH₂Cl₂/THF, 10/0 then 50/50) afforded the titled compound as a yellow solid (37.3 mg, 0.120 mmol, 8% yield).

Yellow solid, 37.3 mg, 0.120 mmol, 8% yield. R_f ($\text{CH}_2\text{Cl}_2/\text{THF}, 1/1, v/v$) = 0.51. M.p. = 180-182 °C. ^1H NMR (400 MHz, $\text{DMSO}-d_6$) δ 9.12 (s, 1H, NH), 8.24 – 8.12 (m, 2H, CH_{Ar}), 7.76 (d, J = 7.7 Hz, 1H, CH_{Ar}), 7.69 (t, J = 7.8 Hz, 1H, CH_{Ar}), 7.43 (d, J = 7.7 Hz, 2H, CH_{Ar}), 7.26 – 7.15 (m, 2H, CH_{Ar}), 6.82 (t, J = 7.3 Hz, 1H, CH_{Ar}), 5.25 (s, 2H, CH_2). ^{13}C NMR (101 MHz, $\text{DMSO}-d_6$) δ 149.4, 148.9, 147.8, 139.7, 137.8, 134.3, 130.2, 128.9 (2C), 122.8, 122.5, 120.9, 116.6 (2C), 48.6. LCMS: t_R = 9.77 min. $[\text{M}+\text{H}]^+$ = 311.07. HPLC (λ_{254}): Purity 98.0%; HPLC (λ_{280}): Purity 95.3%; t_R : 8.61 min (method 2).

MCK276: 1-(3-bromobenzyl)- N^3 -(pyridin-2-yl)-1H-1,2,4-triazole-3,5-diamine

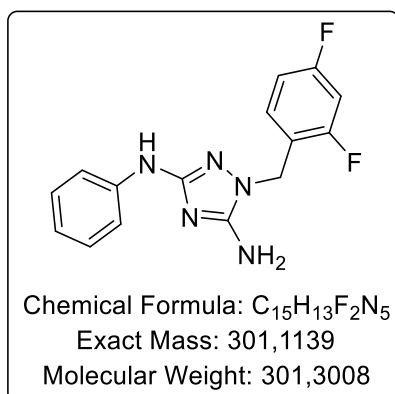


Characterization: 1-(3-bromobenzyl)- N^3 -(pyridin-2-yl)-1H-1,2,4-triazole-3,5-diamine

N^3 -(pyridin-2-yl)-1H-1,2,4-triazole-3,5-diamine (250 mg, 1.42 mmol) was dissolved in degassed DMF (10 mL), then potassium *tert*-butoxide (159 mg, 1.42 mmol) was added at 0 °C. 3-Bromobenzyl bromide (352 mg, 1.42 mmol), dissolved in degassed DMF (5 mL), was added dropwise and the reaction mixture was stirred at r.t. for 2 h. Water was added to the mixture reaction and was extracted with ethyl acetate, washed with water, dried over magnesium sulfate and the solvents were evaporated under reduced pressure. Purification by silica gel flash chromatography ($\text{CH}_2\text{Cl}_2/\text{MeOH}$, 10/0 then 9/1) afforded the titled compound as a yellow solid (121.9 mg, 0.352 mmol, 25% yield).

Yellow solid, 121.9 mg, 0.352 mmol, 25% yield. R_f ($\text{CH}_2\text{Cl}_2/\text{MeOH}:9/1, v/v$) = 0.50. M.p. = 232-234 °C. ^1H NMR (400 MHz, $\text{DMSO}-d_6$) δ 9.97 (s, 1H, NH), 8.18 (ddd, J = 4.9, 2.0, 0.9 Hz, 1H, CH_{Ar}), 7.84 (dt, J = 8.6, 1.0 Hz, 1H, CH_{Ar}), 7.63 (ddd, J = 8.8, 7.2, 2.0 Hz, 1H, CH_{Ar}), 7.54 – 7.43 (m, 2H, CH_{Ar}), 7.33 (t, J = 7.8 Hz, 1H, CH_{Ar}), 7.25 (dt, J = 7.8, 1.3 Hz, 1H, CH_{Ar}), 6.79 (ddd, J = 7.2, 4.9, 1.1 Hz, 1H, CH_{Ar}), 6.62 (s, 2H, NH_2), 5.10 (s, 2H, CH_2). ^{13}C NMR (101 MHz, $\text{DMSO}-d_6$) δ 155.8, 154.4, 154.1, 147.6, 140.1, 137.8, 130.7, 130.1, 129.9, 126.3, 121.6, 115.0, 109.5, 48.0. LCMS: t_R = 7.40 min. $[\text{M}+\text{H}]^+$ = 345.07; 347.07. HPLC (λ_{254}): Purity 99.4%; t_R : 6.55 min (method 1).

MCK277: 1-(2,4-difluorobenzyl)-N³-phenyl-1H-1,2,4-triazole-3,5-diamine

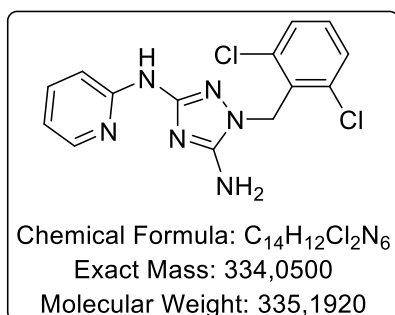


Characterization: 1-(2,4-difluorobenzyl)-N³-phenyl-1H-1,2,4-triazole-3,5-diamine

N³-phenyl-1H-1,2,4-triazole-3,5-diamine (250 mg, 1.43 mmol) was dissolved in degassed DMF (10 mL), then potassium *tert*-butoxide (159 mg, 1.43 mmol) was added. 2,4-Difluorobenzyl chloride (232 mg, 1.43 mmol), dissolved in degassed DMF (5 mL), was added dropwise and the reaction mixture was stirred at 0 °C for 30 min, then at r.t. for 3 h. Water was added to the mixture reaction and was extracted with ethyl acetate, washed with water, dried over magnesium sulfate and the solvents were evaporated under reduced pressure. Purification by silica gel flash chromatography (CH₂Cl₂/THF, 10/0 then 50/50) afforded the titled compound as a brown solid (30.4 mg, 0.101 mmol, 7% yield).

Brown solid, 30.4 mg, 0.101 mmol, 7% yield. R_f (CH₂Cl₂/THF, 1/1, v/v) = 0.55. M.p. = 74-76 °C. ¹H NMR (400 MHz, DMSO-*d*₆) δ 8.68 (s, 1H, NH), 7.48 – 7.41 (m, 2H, CH_{Ar}), 7.26 (ddd, *J* = 10.4, 9.3, 2.5 Hz, 1H, CH_{Ar}), 7.20 – 7.04 (m, 4H, CH_{Ar}), 6.70 (t, *J* = 7.3 Hz, 1H, CH_{Ar}), 6.33 (s, 2H, NH₂), 5.06 (s, 2H, CH₂). ¹³C NMR (101 MHz, DMSO-*d*₆) δ 161.9 (dd, *J* = 178.1, 12.3 Hz), 159.5 (dd, *J* = 180.6, 12.3 Hz), 157.3, 154.3, 142.2, 130.5 (dd, *J* = 9.9, 5.9 Hz), 128.4 (2C), 120.9 (dd, *J* = 15.1, 3.7 Hz), 118.4, 115.5 (2C), 111.4 (dd, *J* = 21.1, 3.6 Hz), 103.8 (t, *J* = 25.8 Hz), 42.5 (d, *J* = 3.4 Hz). ¹⁹F NMR (376 MHz, DMSO-*d*₆) δ -111.47, -113.80. LCMS: *t*_R = 10.34 min. [M+H]⁺ = 302.07. HPLC (λ₂₅₄): Purity 98.3%; *t*_R: 8.55 min (method 2).

MCK278: 1-(2,6-dichlorobenzyl)-N³-(pyridin-2-yl)-1H-1,2,4-triazole-3,5-diamine

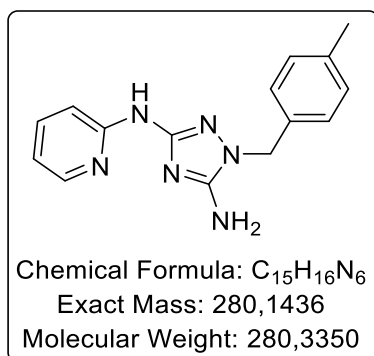


Characterization: 1-(2,6-dichlorobenzyl)-N³-(pyridin-2-yl)-1H-1,2,4-triazole-3,5-diamine

*N*³-(pyridin-2-yl)-1*H*-1,2,4-triazole-3,5-diamine (250 mg, 1.42 mmol) was dissolved in degassed DMF (10 mL), then potassium *tert*-butoxide (159 mg, 1.42 mmol) was added at 0 °C. 2,6-Dichlorobenzyl chloride (274 mg, 1.42 mmol), dissolved in degassed DMF (5 mL), was added dropwise and the reaction mixture was stirred at r.t. for 3 h. Water was added to the mixture reaction and was extracted with ethyl acetate, washed with water, dried over magnesium sulfate and the solvents were evaporated under reduced pressure. Purification by silica gel flash chromatography (CH₂Cl₂/MeOH, 10/0 then 9/1) afforded the titled compound as a white solid (30.9 mg, 0.093 mmol, 7% yield).

White solid, 30.9 mg, 0.093 mmol, 7% yield. *R*_f (CH₂Cl₂/MeOH:9/1, v/v) = 0.42. M.p. > 60 °C. ¹H NMR (400 MHz, DMSO-*d*₆) δ 9.57 (s, 1H, NH), 8.11 (dd, *J* = 5.0, 1.8 Hz, 1H, CH_{Ar}), 7.72 – 7.66 (m, 1H, CH_{Ar}), 7.52 (dq, *J* = 5.7, 2.9, 1.9 Hz, 3H, CH_{Ar}), 7.39 (dd, *J* = 8.7, 7.4 Hz, 1H, CH_{Ar}), 6.72 (ddd, *J* = 7.2, 4.8, 1.0 Hz, 1H, CH_{Ar}), 6.57 (s, 2H, NH₂), 5.20 (s, 2H, CH₂). ¹³C NMR (101 MHz, DMSO-*d*₆) δ 155.6, 154.2, 154.2, 147.5, 137.4, 135.6 (2C), 131.5, 130.5, 128.6 (2C), 114.8, 109.3, 44.7. LCMS: *t*_R = 2.57; 2.08min. [M+H]⁺ = 335.00. HPLC (λ₂₅₄): Purity 97.2%; *t*_R: 6.26 min (method 1).

MCK279: 1-(4-methylbenzyl)-*N*³-(pyridin-2-yl)-1*H*-1,2,4-triazole-3,5-diamine



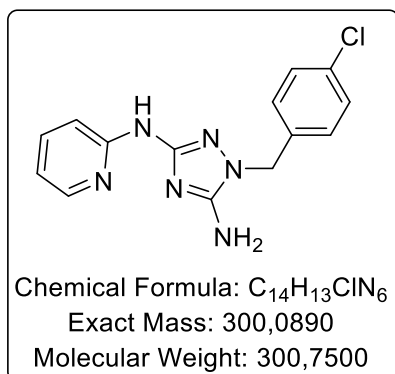
Characterization: 1-(4-methylbenzyl)-*N*³-(pyridin-2-yl)-1*H*-1,2,4-triazole-3,5-diamine

*N*³-(pyridin-2-yl)-1*H*-1,2,4-triazole-3,5-diamine (250 mg, 1.42 mmol) was dissolved in degassed DMF (10 mL), then potassium *tert*-butoxide (159 mg, 1.42 mmol) was added at 0 °C. 4-Methylbenzyl chloride (0.19 mL, 1.42 mmol), dissolved in degassed DMF (5 mL), was added dropwise and the reaction mixture was stirred at r.t. for 2 h. Water was added to the mixture reaction and was extracted with ethyl acetate, washed with water, dried over magnesium sulfate and the solvents were evaporated under reduced pressure. Purification by silica gel flash chromatography (CH₂Cl₂/MeOH, 10/0 then 9/1) afforded the titled compound as a yellow solid (99.9 mg, 0.357 mmol, 25% yield).

Yellow solid, 99.9 mg, 0.357 mmol, 25% yield. *R*_f (CH₂Cl₂/MeOH:9/1, v/v) = 0.52. M.p. = 210-212 °C. ¹H NMR (400 MHz, DMSO-*d*₆) δ 10.03 (s, 1H, NH), 8.23 – 8.13 (m, 1H, CH_{Ar}), 7.85 (d, *J* = 8.5 Hz, 1H, CH_{Ar}),

7.63 (td, $J = 8.8, 8.1, 1.9$ Hz, 1H, CH_{Ar}), 7.15 (s, 4H, CH_{Ar}), 6.78 (ddd, $J = 7.2, 4.9, 1.1$ Hz, 1H, CH_{Ar}), 6.56 (s, 2H, NH₂), 5.03 (s, 2H, CH₂), 2.27 (s, 3H, CH₃). ¹³C NMR (101 MHz, DMSO-*d*₆) δ 155.5, 154.2, 154.2, 147.5, 137.8, 136.3, 134.3, 128.9 (2C), 127.2 (2C), 114.9, 109.5, 48.5, 20.6. LCMS: $t_R = 2.45; 3.95$ min. $[M+H]^+ = 281.07$. HPLC (λ_{254}): Purity 99.5%; HPLC (λ_{280}): Purity 97.1%; t_R : 6.13 min (method 1).

MCK280: 1-(4-chlorobenzyl)-*N*³-(pyridin-2-yl)-1*H*-1,2,4-triazole-3,5-diamine

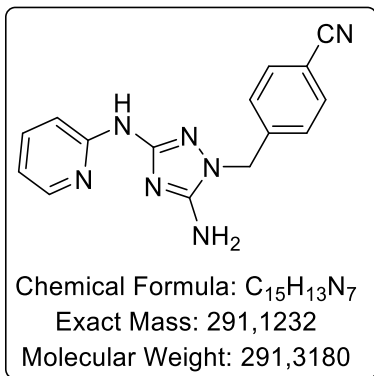


Characterization: 1-(4-chlorobenzyl)-*N*³-(pyridin-2-yl)-1*H*-1,2,4-triazole-3,5-diamine

*N*³-(pyridin-2-yl)-1*H*-1,2,4-triazole-3,5-diamine (250 mg, 1.42 mmol) was dissolved in degassed DMF (10 mL), then potassium *tert*-butoxide (159 mg, 1.42 mmol) was added at 0 °C. 4-Chlorobenzyl chloride (229 mg, 1.42 mmol), dissolved in degassed DMF (5 mL), was added dropwise and the reaction mixture was stirred at r.t. for 2 h. Water was added to the mixture reaction and was extracted with ethyl acetate, washed with water, dried over magnesium sulfate and the solvents were evaporated under reduced pressure. Purification by silica gel flash chromatography (CH₂Cl₂/MeOH, 10/0 then 9/1) afforded the titled compound as a yellow solid (70.9 mg, 0.236 mmol, 17% yield).

Yellow solid, 70.9 mg, 0.236 mmol, 17% yield. R_f (CH₂Cl₂/MeOH, 9/1, v/v) = 0.47. M.p. = 230-232 °C. ¹H NMR (400 MHz, DMSO-*d*₆) δ 9.72 (s, 1H, NH), 8.15 (ddd, $J = 4.9, 1.9, 0.9$ Hz, 1H, CH_{Ar}), 7.83 (d, $J = 8.5$ Hz, 1H, CH_{Ar}), 7.62 (ddd, $J = 8.8, 7.2, 2.0$ Hz, 1H, CH_{Ar}), 7.49 – 7.36 (m, 2H, CH_{Ar}), 7.26 (d, $J = 8.5$ Hz, 2H, CH_{Ar}), 6.77 (ddd, $J = 7.2, 4.9, 1.0$ Hz, 1H, CH_{Ar}), 6.54 (s, 2H, NH₂), 5.07 (s, 2H, CH₂). ¹³C NMR (101 MHz, DMSO-*d*₆) δ 155.8, 154.4, 154.1, 147.6, 137.7, 136.4, 131.8, 129.1 (2C), 128.4 (2C), 114.9, 109.5, 48.0. LCMS: $t_R = 2.50 ; 3.49$ min. $[M+H]^+ = 301.13$. HPLC (λ_{254}): Purity 98.4%; t_R : 6.47 min (method 1).

MCK281: 4-((5-amino-3-(pyridin-2-ylamino)-1H-1,2,4-triazol-1-yl)methyl)benzonitrile

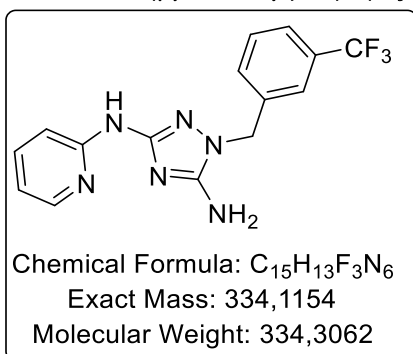


Characterization: 4-((5-amino-3-(pyridin-2-ylamino)-1H-1,2,4-triazol-1-yl)methyl)benzonitrile

*N*³-(pyridin-2-yl)-1H-1,2,4-triazole-3,5-diamine (250 mg, 1.42 mmol) was dissolved in degassed DMF (10 mL), then potassium *tert*-butoxide (159 mg, 1.42 mmol) was added at 0 °C. 4-(Chloromethyl)benzonitrile (220 mg, 1.42 mmol), dissolved in degassed DMF (5 mL), was added dropwise and the reaction mixture was stirred at r.t. for 2 h. Water was added to the mixture reaction and was extracted with ethyl acetate, washed with water, dried over magnesium sulfate and the solvents were evaporated under reduced pressure. Purification by silica gel flash chromatography (CH₂Cl₂/MeOH, 10/0 then 9/1) afforded the titled compound as a yellow solid (49.8 mg, 0.171 mmol, 12% yield).

Yellow solid, 49.8 mg, 0.171 mmol, 12% yield. R_f (CH₂Cl₂/MeOH:9/1, v/v) = 0.47. M.p. = 242 °C. ¹H NMR (400 MHz, DMSO-*d*₆) δ 10.07 (s, 1H, NH), 8.20 – 8.15 (m, 1H, CH_{Ar}), 7.84 (d, *J* = 8.2 Hz, 3H, CH_{Ar}), 7.63 (ddd, *J* = 8.8, 7.2, 2.0 Hz, 1H, CH_{Ar}), 7.40 (d, *J* = 8.3 Hz, 2H, CH_{Ar}), 6.79 (ddd, *J* = 7.2, 4.9, 1.0 Hz, 1H, CH_{Ar}), 6.65 (s, 2H, NH₂), 5.21 (s, 2H, CH₂). ¹³C NMR (101 MHz, DMSO-*d*₆) δ 155.9, 154.6, 154.1, 147.6, 143.1, 137.8, 132.4 (2C), 127.9 (2C), 118.7, 115.0, 110.0, 109.5, 48.4. LCMS: *t*_R = 2.68 ; 4.46 min. [M+H]⁺ = 292.07. HPLC (λ₂₅₄): Purity 99.8%; *t*_R: 5.26 min (method 1).

MCK282: *N*³-(pyridin-2-yl)-1-(3-(trifluoromethyl)benzyl)-1H-1,2,4-triazole-3,5-diamine

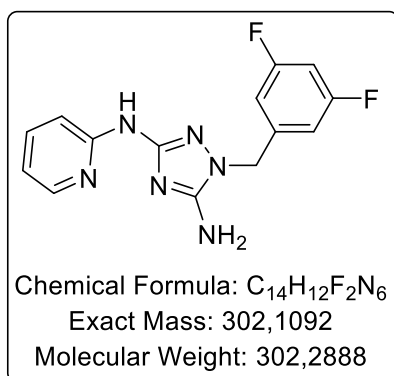


Characterization: *N*³-(pyridin-2-yl)-1-(3-(trifluoromethyl)benzyl)-1H-1,2,4-triazole-3,5-diamine

*N*³-(pyridin-2-yl)-1*H*-1,2,4-triazole-3,5-diamine (250 mg, 1.42 mmol) was dissolved in degassed DMF (10 mL), then potassium *tert*-butoxide (159 mg, 1.42 mmol) was added at 0 °C. 3-(Trifluoromethyl)benzyl chloride (0.22 mL, 1.42 mmol), dissolved in degassed DMF (5 mL), was added dropwise and the reaction mixture was stirred at r.t. for 2 h. Water was added to the mixture reaction and was extracted with ethyl acetate, washed with water, dried over magnesium sulfate and the solvents were evaporated under reduced pressure. Purification by silica gel flash chromatography (CH₂Cl₂/MeOH, 10/0 then 9/1) afforded the titled compound as a white solid (194.7 mg, 0.583 mmol, 41% yield).

White solid, 194.7 mg, 0.583 mmol, 41% yield. R_f (CH₂Cl₂/MeOH:9/1, v/v) = 0.42. M.p. = 248-250 °C. ¹H NMR (400 MHz, DMSO-*d*₆) δ 9.86 (s, 1H, NH), 8.23 – 8.12 (m, 1H, CH_{Ar}), 7.84 (d, *J* = 8.5 Hz, 1H, CH_{Ar}), 7.69 – 7.58 (m, 4H, CH_{Ar}), 7.54 (d, *J* = 7.8 Hz, 1H, CH_{Ar}), 6.78 (ddd, *J* = 7.3, 4.9, 1.0 Hz, 1H, CH_{Ar}), 6.62 (s, 2H, NH₂), 5.19 (s, 2H, CH₂). ¹³C NMR (101 MHz, DMSO-*d*₆) δ 155.9, 154.5, 154.1, 147.6, 138.8, 137.7, 131.4, 129.6, 129.1 (q, *J* = 31.5 Hz), 124.1 (q, *J* = 272.2 Hz), 124.1 (q, *J* = 3.8 Hz), 123.8 (q, *J* = 3.9 Hz), 115.0, 109.5, 48.2. ¹⁹F NMR (376 MHz, DMSO-*d*₆) δ -61.12 (3F). LCMS: *t*_R = 4.00 min. [M+H]⁺ = 335.07. HPLC (λ₂₅₄): Purity 99.7%; HPLC (λ₂₈₀): Purity 99.3%; *t*_R: 6.75 min (method 1).

MCK283: 1-(3,5-difluorobenzyl)-*N*³-(pyridin-2-yl)-1*H*-1,2,4-triazole-3,5-diamine

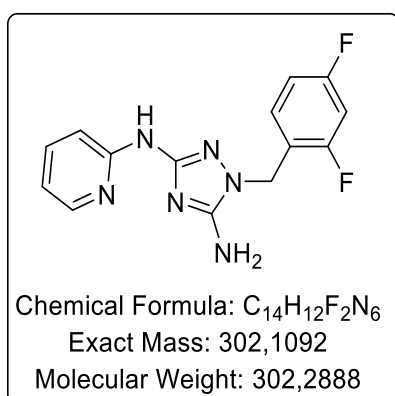


Characterization: 1-(3,5-difluorobenzyl)-*N*³-(pyridin-2-yl)-1*H*-1,2,4-triazole-3,5-diamine

*N*³-(pyridin-2-yl)-1*H*-1,2,4-triazole-3,5-diamine (250 mg, 1.42 mmol) was dissolved in degassed DMF (10 mL), then potassium *tert*-butoxide (159 mg, 1.42 mmol) was added at 0 °C. 3,5-Difluorobenzyl chloride (232 mg, 1.42 mmol), dissolved in degassed DMF (5 mL), was added dropwise and the reaction mixture was stirred at r.t. for 2 h. Water was added to the mixture reaction and was extracted with ethyl acetate, washed with water, dried over magnesium sulfate and the solvents were evaporated under reduced pressure. Purification by silica gel flash chromatography (CH₂Cl₂/MeOH, 10/0 then 9/1) afforded the titled compound as a yellow solid (124.8 mg, 0.413 mmol, 29% yield).

Yellow solid, 124.8 mg, 0.413 mmol, 29% yield. R_f ($\text{CH}_2\text{Cl}_2/\text{MeOH}:9/1$, v/v) = 0.45. M.p. = 258 °C. ^1H NMR (400 MHz, $\text{DMSO}-d_6$) δ 10.08 (s, 1H, NH), 8.25 – 8.15 (m, 1H, CH_{Ar}), 7.85 (d, J = 8.5 Hz, 1H, CH_{Ar}), 7.64 (ddd, J = 8.8, 7.2, 2.0 Hz, 1H, CH_{Ar}), 7.17 (tt, J = 9.4, 2.4 Hz, 1H, CH_{Ar}), 6.97 – 6.89 (m, 2H, CH_{Ar}), 6.80 (ddd, J = 7.2, 4.9, 1.0 Hz, 1H, CH_{Ar}), 6.66 (s, 2H, NH_2), 5.13 (s, 2H, CH_2). ^{13}C NMR (101 MHz, $\text{DMSO}-d_6$) δ 162.3 (dd, J = 246.4, 13.1 Hz, 2C), 155.9, 154.5, 154.1, 147.6, 141.9 (t, J = 9.0 Hz), 137.88, 115.07, 110.2 (d, J = 6.8, 18.7 Hz, 2C), 109.5, 102.8 (t, J = 25.7 Hz), 47.9. ^{19}F NMR (376 MHz, $\text{DMSO}-d_6$) δ -109.58 (2F). LCMS: t_R = 2.66; 4.80 min. $[\text{M}+\text{H}]^+$ = 303.13. HPLC (λ_{254}): Purity 98.7%; t_R : 6.03 min (method 1).

MCK284: 1-(2,4-difluorobenzyl)- N^3 -(pyridin-2-yl)-1H-1,2,4-triazole-3,5-diamine



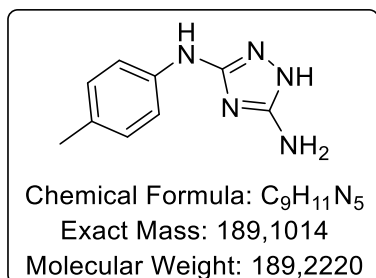
Characterization: 1-(2,4-difluorobenzyl)- N^3 -(pyridin-2-yl)-1H-1,2,4-triazole-3,5-diamine

N^3 -(pyridin-2-yl)-1H-1,2,4-triazole-3,5-diamine (250 mg, 1.42 mmol) was dissolved in degassed DMF (10 mL), then potassium *tert*-butoxide (159 mg, 1.42 mmol) was added at 0 °C. 2,4-Difluorobenzyl chloride (232 mg, 1.42 mmol), dissolved in degassed DMF (5 mL), was added dropwise and the reaction mixture was stirred at r.t. for 2 h. Water was added to the mixture reaction and was extracted with ethyl acetate, washed with water, dried over magnesium sulfate and the solvents were evaporated under reduced pressure. Purification by silica gel flash chromatography ($\text{CH}_2\text{Cl}_2/\text{MeOH}$, 10/0 then 9/1) afforded the titled compound as a yellow solid (199.3 mg, 0.660 mmol, 46% yield).

Yellow solid, 199.3 mg, 0.660 mmol, 46% yield. R_f ($\text{CH}_2\text{Cl}_2/\text{MeOH}:9/1$, v/v) = 0.40. M.p. > 60 °C. ^1H NMR (400 MHz, $\text{DMSO}-d_6$) δ 9.92 (s, 1H, NH), 8.20 – 8.12 (m, 1H, CH_{Ar}), 7.82 (d, J = 8.5 Hz, 1H, CH_{Ar}), 7.62 (ddd, J = 8.8, 7.2, 2.0 Hz, 1H, CH_{Ar}), 7.27 (ddd, J = 10.5, 9.3, 2.5 Hz, 1H, CH_{Ar}), 7.17 (td, J = 8.6, 6.6 Hz, 1H, CH_{Ar}), 7.08 (td, J = 8.6, 2.6 Hz, 1H, CH_{Ar}), 6.78 (ddd, J = 7.2, 4.9, 1.0 Hz, 1H, CH_{Ar}), 6.60 (s, 2H, NH_2), 5.12 (s, 2H, CH_2). ^{13}C NMR (101 MHz, $\text{DMSO}-d_6$) δ 161.9 (dd, J = 182.2, 12.2 Hz), 159.5 (dd, J = 184.6, 12.3 Hz), 155.9, 154.5, 154.1, 147.0, 137.7, 130.4 (dd, J = 9.9, 5.9 Hz), 120.66 (dd, J = 15.1, 3.7 Hz), 114.9, 111.5 (dd, J = 21.3, 3.6 Hz), 109.5, 103.9 (t, J = 25.7 Hz), 42.7 (d, J = 2.8 Hz). ^{19}F NMR (376 MHz,

DMSO-*d*₆) δ -111.33, -113.74. LCMS: t_R = 2.73; 6.94 min. $[M+H]^+$ = 303.13. HPLC (λ_{254}): Purity 97.1%; t_R : 5.60 min (method 1).

MCK285: *N*³-(4-methylphenyl)-1*H*-1,2,4-triazole-3,5-diamine

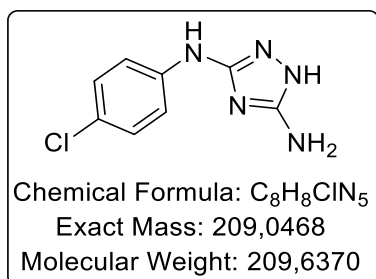


Characterization: *N*³-(4-methylphenyl)-1*H*-1,2,4-triazole-3,5-diamine

To a solution of carbamimidothioic acid, *N*-cyano-*N*'-(4-methylphenyl), methyl ester (900 mg, 4.39 mmol) in ethanol (15 mL) was added N₂H₄·H₂O (0.44 mL, 8.78 mmol), then the solution was stirred at 75 °C for 1 h. The precipitate was filtered and washed with diethyl ether to obtain a white solid (780.2 mg, 4.13 mmol, 94% yield).

White solid, 780.2 mg, 4.13 mmol, 94% yield. R_f (CH₂Cl₂/MeOH,9/1, v/v) = 0.32. ¹H NMR (400 MHz, DMSO-*d*₆) δ 10.99 (s, 1H, NH), 8.45 (s, 1H, NH), 7.38 (d, J = 8.4 Hz, 2H, CH_{Ar}), 6.96 (d, J = 8.3 Hz, 2H, CH_{Ar}), 5.77 (s, 2H, NH₂), 2.18 (s, 3H, CH₃). ¹³C NMR (101 MHz, DMSO-*d*₆) δ 157.8, 155.6, 140.1, 128.8 (2C), 126.6, 115.5 (2C), 20.2. LCMS: t_R = 6.86 min. $[M+H]^+$ = 190.13. HPLC (λ_{254}): Purity 100%; t_R : 4.92 min (method 1). Data in accordance with the literature.⁴⁹⁷

MCK286: *N*³-(4-chlorophenyl)-1*H*-1,2,4-triazole-3,5-diamine



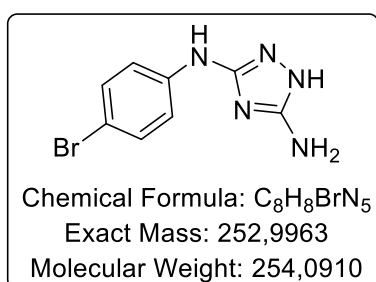
Characterization: *N*³-(4-chlorophenyl)-1*H*-1,2,4-triazole-3,5-diamine

To a solution of carbamimidothioic acid, *N*-cyano-*N*'-(4-chlorophenyl), methyl ester (740 mg, 3.29 mmol) in ethanol (15 mL) was added N₂H₄·H₂O (0.33 mL, 6.54 mmol), then the solution was stirred at

75 °C for 1 h. The precipitate was filtered and washed with diethyl ether to obtain a white solid (628.2 mg, 3.01 mmol, 91% yield).

White solid, 628.2 mg, 3.01 mmol, 91% yield. R_f ($\text{CH}_2\text{Cl}_2/\text{MeOH}, 9/1, v/v$) = 0.32. ^1H NMR (400 MHz, $\text{DMSO}-d_6$) δ 11.18 (s, 1H, NH), 8.82 (s, 1H, NH), 7.51 (d, J = 8.9 Hz, 2H, CH_{Ar}), 7.19 (d, J = 8.8 Hz, 2H, CH_{Ar}), 5.88 (s, 2H, NH_2). ^{13}C NMR (101 MHz, $\text{DMSO}-d_6$) δ 157.6, 155.4, 141.5, 128.1 (2C), 121.5, 116.9 (2C). LCMS: t_R = 7.88 min. $[\text{M}+\text{H}]^+ = 210.13$. HPLC (λ_{254}): Purity 100%; HPLC (λ_{280}): Purity 99.86%; t_R : 5.58 min (method 1). Data in accordance with the literature.⁵⁴⁹

MCK287: N^3 -(4-bromophenyl)-1H-1,2,4-triazole-3,5-diamine

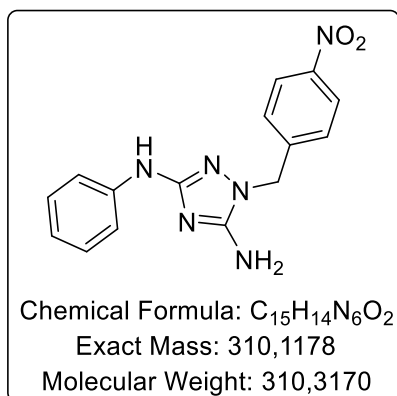


Characterization: N^3 -(4-bromophenyl)-1H-1,2,4-triazole-3,5-diamine

To a solution of carbamimidothioic acid, N -cyano- N' -4,6-dimethylpyrimidine, methyl ester (850 mg, 3.15 mmol) in ethanol (5 mL) was added $\text{N}_2\text{H}_4 \cdot \text{H}_2\text{O}$ (0.31 mL, 6.29 mmol), then the solution was stirred at 75 °C for 4 h. The precipitate was filtered and washed with diethyl ether to obtain a white solid (763.8 mg, 3.019 mmol, 96% yield).

White solid, 763.8 mg, 3.019 mmol, 96% yield. R_f ($\text{CH}_2\text{Cl}_2/\text{MeOH}, 95/5, v/v$) = 0.26. ^1H NMR (400 MHz, $\text{DMSO}-d_6$) δ 10.75 (s, 1H, NH), 8.85 (s, 1H, NH), 7.47 (d, J = 8.9 Hz, 2H, CH_{Ar}), 7.30 (d, J = 8.8 Hz, 2H, CH_{Ar}), 5.87 (s, 2H, NH_2). ^{13}C NMR (101 MHz, $\text{DMSO}-d_6$) δ 157.40, 155.64, 141.93, 131.03 (2C), 117.46 (2C), 109.23. LCMS: t_R = 8.47 min. $[\text{M}+\text{H}]^+ = 254.07; 256.07$. HPLC (λ_{254}): Purity 100%; HPLC (λ_{280}): Purity 98.3%; t_R : 5.93 min (method 1). Data in accordance with the literature.⁵⁴⁹

MCK288: 1-(4-nitrobenzyl)-*N*³-phenyl-1*H*-1,2,4-triazole-3,5-diamine

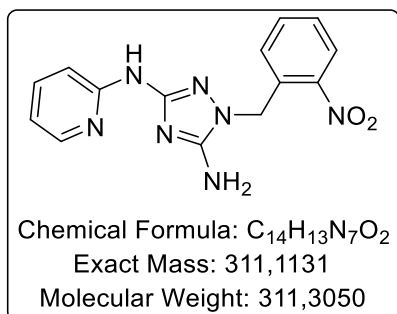


Characterization: 1-(4-nitrobenzyl)-*N*³-phenyl-1*H*-1,2,4-triazole-3,5-diamine

*N*³-phenyl-1*H*-1,2,4-triazole-3,5-diamine (250 mg, 1.43 mmol) was dissolved in degassed DMF (10 mL), then potassium *tert*-butoxide (159 mg, 1.43 mmol) was added. 4-Nitrobenzyl bromide (307 mg, 1.43 mmol), dissolved in degassed DMF (5 mL), was added dropwise and the reaction mixture was stirred at 0 °C for 30 min, then at r.t. for 3 h. Water was added to the mixture reaction and was extracted with ethyl acetate, washed with water, dried over magnesium sulfate and the solvents were evaporated under reduced pressure. Purification by silica gel flash chromatography (CH₂Cl₂/THF, 10/0 then 50/50) and second purification by silica gel flash chromatography (CH₂Cl₂/THF, iso 50/50) afforded the titled compound as a yellow solid (21.1 mg, 0.068 mmol, 5% yield).

Yellow solid, 21.1 mg, 0.068 mmol, 5% yield. R_f (CH₂Cl₂/THF, 1/1, v/v) = 0.32. M.p. = 168-170 °C. ¹H NMR (400 MHz, DMSO-*d*₆) δ 8.72 (s, 1H, NH), 8.24 (d, *J* = 8.8 Hz, 2H, CH_{Ar}), 7.50 – 7.39 (m, 4H, CH_{Ar}), 7.21 – 7.08 (m, 2H, CH_{Ar}), 6.71 (t, *J* = 7.3 Hz, 1H, CH_{Ar}), 6.37 (s, 2H, NH₂), 5.19 (s, 2H, CH₂). ¹³C NMR (101 MHz, DMSO-*d*₆) δ 157.4, 154.4, 146.7, 145.4, 142.2, 128.4 (2C), 128.2 (2C), 123.6 (2C), 118.5, 115.5 (2C), 48.1. LCMS: *t*_R = 10.18 min. [M+H]⁺ = 311.13. HPLC (λ₂₅₄): Purity 97.2%; *t*_R: 8.41 min (method 2).

MCK289: 1-(2-nitrobenzyl)-*N*³-(pyridin-2-yl)-1*H*-1,2,4-triazole-3,5-diamine

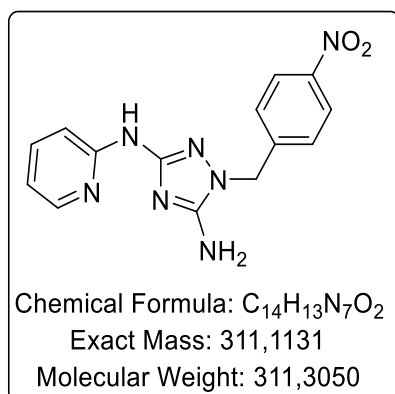


Characterization: 1-(2-nitrobenzyl)-*N*³-(pyridin-2-yl)-1*H*-1,2,4-triazole-3,5-diamine

*N*³-(pyridin-2-yl)-1*H*-1,2,4-triazole-3,5-diamine (250 mg, 1.42 mmol) was dissolved in degassed DMF (10 mL), then potassium *tert*-butoxide (159 mg, 1.42 mmol) was added at 0 °C. 2-Nitrobenzyl bromide (305 mg, 1.42 mmol), dissolved in degassed DMF (5 mL), was added dropwise and the reaction mixture was stirred at 0 °C for 1 h, then at r.t. for 4 h. Water was added to the mixture reaction and was extracted with ethyl acetate, washed with water, dried over magnesium sulfate and the solvents were evaporated under reduced pressure. Purification by silica gel flash chromatography (CH₂Cl₂/MeOH, 10/0 then 9/1) afforded the titled compound as a yellow solid (94.1 mg, 0.303 mmol, 21% yield).

Yellow solid, 94.1 mg, 0.303 mmol, 21% yield. R_f (CH₂Cl₂/MeOH:9/1, v/v) = 0.22. M.p. = 262 °C. ¹H NMR (400 MHz, DMSO-*d*₆) δ 9.76 (s, 1H, NH), 8.20 – 8.10 (m, 2H, CH_{Ar}), 7.84 (d, *J* = 8.5 Hz, 1H, CH_{Ar}), 7.74 (t, *J* = 7.2 Hz, 1H, CH_{Ar}), 7.59 (ddd, *J* = 14.3, 10.4, 4.5 Hz, 2H, CH_{Ar}), 6.98 (d, *J* = 7.6 Hz, 1H, CH_{Ar}), 6.84 – 6.73 (m, 1H, CH_{Ar}), 6.56 (s, 2H, NH₂), 5.46 (s, 2H, CH₂). ¹³C NMR (101 MHz, DMSO-*d*₆) δ 156.2, 154.9, 154.1, 147.6, 147.3, 137.6, 134.2, 133.2, 128.5, 128.1, 124.9, 115.0, 109.6, 46.7. LCMS: *t*_R = 2.68; 6.32 min. [M+H]⁺ = 312.13. HPLC (λ₂₅₄): Purity 98.6%; *t*_R: 5.23 min (method 1).

MCK290: 1-(4-nitrobenzyl)-*N*³-(pyridin-2-yl)-1*H*-1,2,4-triazole-3,5-diamine

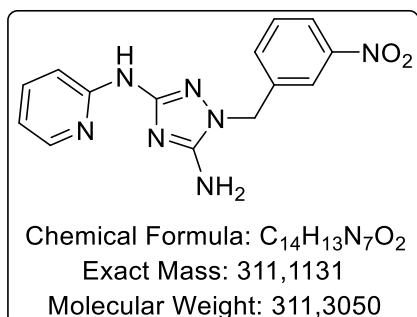


Characterization: 1-(4-nitrobenzyl)-*N*³-(pyridin-2-yl)-1*H*-1,2,4-triazole-3,5-diamine

*N*³-(pyridin-2-yl)-1*H*-1,2,4-triazole-3,5-diamine (250 mg, 1.42 mmol) was dissolved in degassed DMF (10 mL), then potassium *tert*-butoxide (159 mg, 1.42 mmol) was added at 0 °C. 4-Nitrobenzyl bromide (305 mg, 1.42 mmol), dissolved in degassed DMF (5 mL), was added dropwise and the reaction mixture was stirred at 0 °C for 1 h, then at r.t. for 4 h. Water was added to the mixture reaction and was extracted with ethyl acetate, washed with water, dried over magnesium sulfate and the solvents were evaporated under reduced pressure. Purification by silica gel flash chromatography (CH₂Cl₂/MeOH, 10/0 then 9/1) afforded the titled compound as a yellow solid (107.3 mg, 0.345 mmol, 24% yield).

Yellow solid, 107.3 mg, 0.345 mmol, 24% yield. Rf (CH₂Cl₂/MeOH:9/1, v/v) = 0.28. M.p. = 246 °C. ¹H NMR (400 MHz, DMSO-*d*₆) δ 10.26 (s, 1H, NH), 8.28 – 8.22 (m, 2H, CH_{Ar}), 8.22 – 8.17 (m, 1H, CH_{Ar}), 7.85 (d, *J* = 8.5 Hz, 1H, CH_{Ar}), 7.64 (ddd, *J* = 8.8, 7.2, 2.0 Hz, 1H, CH_{Ar}), 7.48 (d, *J* = 8.7 Hz, 2H, CH_{Ar}), 6.80 (ddd, *J* = 7.2, 4.9, 1.0 Hz, 1H, CH_{Ar}), 6.72 (s, 2H, NH₂), 5.27 (s, 2H, CH₂). ¹³C NMR (101 MHz, DMSO-*d*₆) δ 156.0, 154.6, 154.0, 147.6, 146.7, 145.1, 137.9, 128.2 (2C), 123.7 (2C), 115.0, 109.6, 48.2. LCMS: *t*_R = 2.69; 6.36 min. [M+H]⁺ = 312.13. HPLC (λ₂₅₄): Purity 98.8%; *t*_R: 5.43 min (method 1).

MCK292: 1-(3-nitrobenzyl)-N³-(pyridin-2-yl)-1H-1,2,4-triazole-3,5-diamine

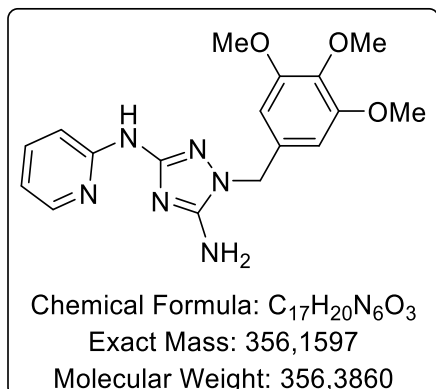


Characterization: 1-(3-nitrobenzyl)-N³-(pyridin-2-yl)-1H-1,2,4-triazole-3,5-diamine

N³-(pyridin-2-yl)-1H-1,2,4-triazole-3,5-diamine (250 mg, 1.42 mmol) was dissolved in degassed DMF (10 mL), then potassium *tert*-butoxide (159 mg, 1.42 mmol) was added at 0 °C. 3-Nitrobenzyl chloride (305 mg, 1.42 mmol), dissolved in degassed DMF (5 mL), was added dropwise and the reaction mixture was stirred at r.t. for 3 h. Water was added to the mixture reaction and was extracted with ethyl acetate, washed with water, dried over magnesium sulfate and the solvents were evaporated under reduced pressure. Purification by silica gel flash chromatography (CH₂Cl₂/MeOH, 10/0 then 9/1) afforded the titled compound as a yellow solid (89 mg, 0.286 mmol, 20% yield).

Yellow solid, 89 mg, 0.286 mmol, 20% yield. Rf (CH₂Cl₂/MeOH:9/1, v/v) = 0.32. M.p. = 266 °C. ¹H NMR (400 MHz, DMSO-*d*₆) δ 9.92 (s, 1H, NH), 8.21 – 8.12 (m, 3H, CH_{Ar}), 7.85 (dt, *J* = 8.5, 1.0 Hz, 1H, CH_{Ar}), 7.73 – 7.67 (m, 2H, CH_{Ar}), 7.66 – 7.60 (m, 1H, CH_{Ar}), 6.79 (ddd, *J* = 7.2, 4.9, 1.0 Hz, 1H, CH_{Ar}), 6.66 (s, 2H, NH₂), 5.24 (s, 2H, CH₂). ¹³C NMR (101 MHz, DMSO-*d*₆) δ 156.0, 154.5, 154.1, 147.8, 147.6, 139.6, 137.7, 134.0, 130.1, 122.3, 121.9, 115.0, 109.5, 48.0. LCMS: *t*_R = 6.86 min. [M+H]⁺ = 312.07. HPLC (λ₂₅₄): Purity 99.5%; HPLC (λ₂₈₀): Purity 99.1%; *t*_R: 5.80 min (method 1).

MCK293.2: *N*³-(pyridin-2-yl)-1-(3,4,5-trimethoxybenzyl)-1*H*-1,2,4-triazole-3,5-diamine

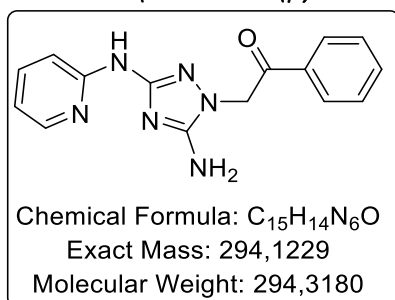


Characterization: *N*³-(pyridin-2-yl)-1-(3,4,5-trimethoxybenzyl)-1*H*-1,2,4-triazole-3,5-diamine

*N*³-(pyridin-2-yl)-1*H*-1,2,4-triazole-3,5-diamine (250 mg, 1.42 mmol) was dissolved in degassed DMF (10 mL), then potassium *tert*-butoxide (159 mg, 1.42 mmol) was added at 0 °C. 5-(Chloromethyl)-1,2,3-trimethoxybenzene (307 mg, 1.42 mmol), dissolved in degassed DMF (5 mL), was added dropwise and the reaction mixture was stirred at 0 °C for 1 h, then at r.t. for 4 h. Water was added to the mixture reaction and was extracted with ethyl acetate, washed with water, dried over magnesium sulfate and the solvents were evaporated under reduced pressure. Purification by silica gel flash chromatography (CH₂Cl₂/MeOH, 10/0 then 9/1) afforded the titled compound as a yellow solid (79.8 mg, 0.224 mmol, 16% yield).

Yellow solid, 79.8 mg, 0.224 mmol, 16% yield. R_f (CH₂Cl₂/MeOH:9/1, v/v) = 0.36. M.p. = 248-250 °C. ¹H NMR (400 MHz, DMSO-*d*₆) δ 9.34 (s, 1H, NH), 8.13 (ddd, *J* = 4.9, 2.0, 0.9 Hz, 1H, CH_{Ar}), 7.87 (d, *J* = 8.5 Hz, 1H, CH_{Ar}), 7.60 (ddd, *J* = 8.8, 7.3, 2.0 Hz, 1H, CH_{Ar}), 6.76 (ddd, *J* = 7.2, 4.9, 1.1 Hz, 1H, CH_{Ar}), 6.65 (s, 2H, NH₂), 6.43 (s, 2H, CH_{Ar}), 4.95 (s, 2H, CH₂), 3.73 (s, 6H, OCH₃), 3.62 (s, 3H, OCH₃). ¹³C NMR (101 MHz, DMSO-*d*₆) δ 155.7, 154.3, 154.2, 152.8 (2C), 147.6, 137.5, 136.7, 132.8, 114.8, 109.9, 104.9 (2C), 59.9, 55.8 (2C), 48.9. LCMS: *t*_R = 2.72; 6.38 min. [M+H]⁺ = 357.00. HPLC (λ₂₅₄): Purity 99.4%; *t*_R: 5.34 min (method 1).

MCK294: 2-(5-amino-3-(pyridin-2-ylamino)-1*H*-1,2,4-triazol-1-yl)-1-phenylethan-1-one

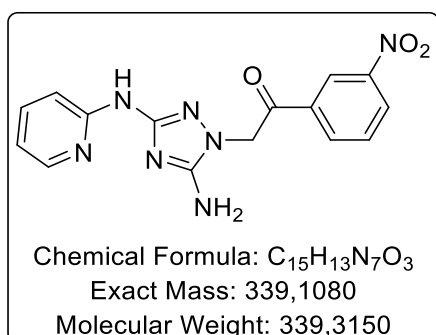


Characterization: 2-(5-amino-3-(pyridin-2-ylamino)-1*H*-1,2,4-triazol-1-yl)-1-phenylethan-1-one

*N*³-(pyridin-2-yl)-1*H*-1,2,4-triazole-3,5-diamine (250 mg, 1.42 mmol) was dissolved in degassed DMF (10 mL), then potassium *tert*-butoxide (159 mg, 1.42 mmol) was added at 0 °C. 2-Bromo-1-phenylethan-1-one (281 mg, 1.42 mmol), dissolved in degassed DMF (5 mL), was added dropwise and the reaction mixture was stirred at 0 °C for 1 h, then at r.t. for 4 h. Water was added to the mixture reaction and was extracted with ethyl acetate, washed with water, dried over magnesium sulfate and the solvents were evaporated under reduced pressure. Purification by silica gel flash chromatography (CH₂Cl₂/MeOH, 10/0 then 9/1) afforded the titled compound as a white solid (60.9 mg, 0.207 mmol, 15% yield).

White solid, 60.9 mg, 0.207 mmol, 15% yield. *R*_f (CH₂Cl₂/MeOH:9/1, v/v) =0.26. M.p. = 260-262 °C. ¹H NMR (400 MHz, DMSO-*d*₆) δ 9.56 (s, 1H), 8.13 (ddd, *J* = 4.9, 2.0, 0.9 Hz, 1H), 8.09 – 7.99 (m, 2H), 7.83 (d, *J* = 8.5 Hz, 1H), 7.77 – 7.66 (m, 1H), 7.64 – 7.54 (m, 3H), 6.76 (ddd, *J* = 7.2, 4.9, 1.0 Hz, 1H), 6.37 (s, 2H), 5.51 (s, 2H). ¹³C NMR (101 MHz, DMSO-*d*₆) δ 193.0, 155.6, 155.5, 154.2, 147.6, 137.5, 134.6, 133.8, 128.8 (2C), 128.0 (2C), 114.8, 109.5, 52.7. LCMS: *t*_R = 2.72; 6.06 min. [M+H]⁺ = 295.13. HPLC (λ₂₅₄): Purity 99.3%; *t*_R: 5.26 min (method 1).

MCK295: 2-(5-amino-3-(pyridin-2-ylamino)-1*H*-1,2,4-triazol-1-yl)-1-(3-nitrophenyl)ethan-1-one

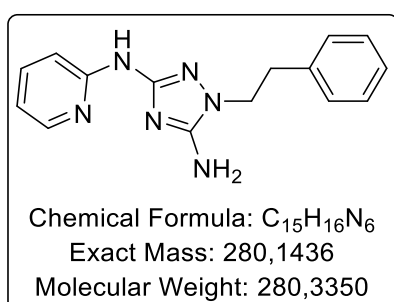


Characterization: 2-(5-amino-3-(pyridin-2-ylamino)-1*H*-1,2,4-triazol-1-yl)-1-(3-nitrophenyl)ethan-1-one

*N*³-(pyridin-2-yl)-1*H*-1,2,4-triazole-3,5-diamine (250 mg, 1.42 mmol) was dissolved in degassed DMF (10 mL), then potassium *tert*-butoxide (159 mg, 1.42 mmol) was added at 0 °C. 2-Bromo-1-(3-nitrophenyl)ethan-1-one (344 mg, 1.42 mmol), dissolved in degassed DMF (5 mL), was added dropwise and the reaction mixture was stirred at 0 °C for 1 h, then at r.t. for 4 h. Water was added to the mixture reaction and was extracted with ethyl acetate, washed with water, dried over magnesium sulfate and the solvents were evaporated under reduced pressure. Purification by silica gel flash chromatography (CH₂Cl₂/MeOH, 10/0 then 9/1) afforded the titled compound as a yellow solid (56.4 mg, 0.166 mmol, 12% yield).

Yellow solid, 56.4 mg, 0.166 mmol, 12% yield. Rf (CH₂Cl₂/MeOH:9/1, v/v) = 0.30. M.p. = 240 °C. ¹H NMR (400 MHz, DMSO-*d*₆) δ 10.22 (s, 1H, NH), 8.74 (t, *J* = 1.9 Hz, 1H, CH_{Ar}), 8.57 – 8.50 (m, 1H, CH_{Ar}), 8.47 (d, *J* = 7.8 Hz, 1H, CH_{Ar}), 8.19 – 8.13 (m, 1H, CH_{Ar}), 7.94 – 7.83 (m, 2H, CH_{Ar}), 7.62 (ddd, *J* = 8.8, 7.1, 2.0 Hz, 1H, CH_{Ar}), 6.79 (ddd, *J* = 7.2, 4.9, 1.0 Hz, 1H, CH_{Ar}), 6.55 (s, 2H, NH₂), 5.66 (s, 2H, CH₂). ¹³C NMR (101 MHz, DMSO-*d*₆) δ 192.0, 155.7, 155.5, 154.1, 148.0, 147.5, 137.8, 135.8, 134.2, 130.7, 127.9, 122.4, 114.9, 109.6, 53.1. LCMS: *t*_R = 2.76; 6.66 min. [M+H]⁺ = 340.07. HPLC (λ₂₅₄): Purity 96.1%; *t*_R: 5.71 min (method 1).

MCK296: 1-phenethyl-N³-(pyridin-2-yl)-1H-1,2,4-triazole-3,5-diamine

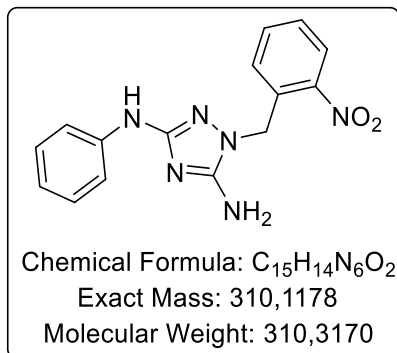


Characterization: 1-phenethyl-N³-(pyridin-2-yl)-1H-1,2,4-triazole-3,5-diamine

N³-(pyridin-2-yl)-1H-1,2,4-triazole-3,5-diamine (250 mg, 1.42 mmol) was dissolved in degassed DMF (10 mL), then potassium tert-butoxide (159 mg, 1.42 mmol) was added at 0 °C. (2-chloroethyl)benzene (mL, 1.42 mmol), dissolved in degassed DMF (5 mL), was added dropwise and the reaction mixture was stirred at 0 °C for 1 h, then at r.t. for 4 h. Water was added to the mixture reaction and was extracted with ethyl acetate, washed with water, dried over magnesium sulfate and the solvents were evaporated under reduced pressure. Purification by reversed-phase chromatography (H₂O/CH₃CN, 10/0 then 60/40) afforded the titled compound as a white solid (11.1 mg, 0.040 mmol, 3% yield).

White solid, 11.1 mg, 0.040 mmol, 3% yield. Rf (CH₂Cl₂/MeOH:9/1, v/v) = 0.38. M.p. = 202 °C. ¹H NMR (400 MHz, DMSO-*d*₆) δ 9.67 (s, 1H, NH), 8.15 (ddd, *J* = 4.9, 2.0, 0.9 Hz, 1H, CH_{Ar}), 7.86 (dt, *J* = 8.4, 1.0 Hz, 1H, CH_{Ar}), 7.64 (ddd, *J* = 8.8, 7.1, 2.0 Hz, 1H, CH_{Ar}), 7.32 – 7.25 (m, 4H, CH_{Ar}), 7.24 – 7.18 (m, 1H, CH_{Ar}), 6.78 (ddd, *J* = 7.2, 4.9, 1.0 Hz, 1H, CH_{Ar}), 6.31 (s, 2H, NH₂), 4.14 – 3.94 (m, 2H, CH₂), 3.12 – 2.90 (m, 2H, CH₂). ¹³C NMR (101 MHz, DMSO-*d*₆) δ 155.3, 154.3, 153.8, 147.5, 138.4, 137.6, 128.8 (2C), 128.2 (2C), 126.2, 114.8, 109.5, 46.4, 34.6. LCMS: *t*_R = 7.01 min. [M+H]⁺ = 281.13. HPLC (λ₂₅₄): Purity 99.8%; HPLC (λ₂₈₂): Purity 99.4%; *t*_R: 5.13 min (method 1).

MCK297: 1-(2-nitrobenzyl)-N³-phenyl-1H-1,2,4-triazole-3,5-diamine

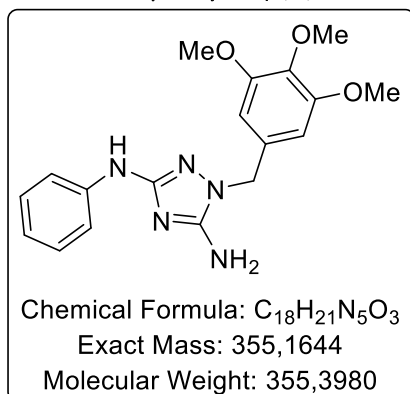


Characterization: 1-(2-nitrobenzyl)-N³-phenyl-1H-1,2,4-triazole-3,5-diamine

N³-phenyl-1H-1,2,4-triazole-3,5-diamine (250 mg, 1.43 mmol) was dissolved in degassed DMF (10 mL), then potassium *tert*-butoxide (159 mg, 1.43 mmol) was added. 2-Nitrobenzyl bromide (307 mg, 1.43 mmol), dissolved in degassed DMF (5 mL), was added dropwise and the reaction mixture was stirred at 0 °C for 30 min, then at r.t. for 3 h. Water was added to the mixture reaction and was extracted with ethyl acetate, washed with water, dried over magnesium sulfate and the solvents were evaporated under reduced pressure. Purification by reversed-phase chromatography (H₂O/CH₃CN, 10/0 then 60/40) afforded the titled compound as a yellow solid (60.9 mg, 0.196 mmol, 14% yield).

Yellow solid, 60.9 mg, 0.196 mmol, 14% yield. R_f (CH₂Cl₂/THF, 1/1, v/v) = 0.57. M.p. = 78-80 °C. ¹H NMR (400 MHz, DMSO-*d*₆) δ 8.76 (s, 1H, NH), 8.14 (dd, *J* = 8.2, 1.3 Hz, 1H, CH_{Ar}), 7.73 (td, *J* = 7.6, 1.3 Hz, 1H, CH_{Ar}), 7.62 – 7.52 (m, 1H, CH_{Ar}), 7.47 (dd, *J* = 8.7, 1.2 Hz, 2H, CH_{Ar}), 7.14 (dd, *J* = 8.6, 7.2 Hz, 2H, CH_{Ar}), 6.99 (dd, *J* = 7.9, 1.3 Hz, 1H, CH_{Ar}), 6.72 (tt, *J* = 7.3, 1.2 Hz, 1H, CH_{Ar}), 6.34 (s, 2H, NH₂), 5.41 (s, 2H, CH₂). ¹³C NMR (101 MHz, DMSO-*d*₆) δ 157.5, 154.6, 147.3, 142.2, 134.2, 133.5, 128.5, 128.4 (2C), 128.2, 124.8, 118.5, 115.6 (2C), 46.6. LCMS: *t*_R = 10.47 min. [M+H]⁺ = 311.07. HPLC (λ₂₈₂): Purity 97.2%; *t*_R: 8.21 min (method 2).

MCK298: N³-phenyl-1-(3,4,5-trimethoxybenzyl)-1H-1,2,4-triazole-3,5-diamine

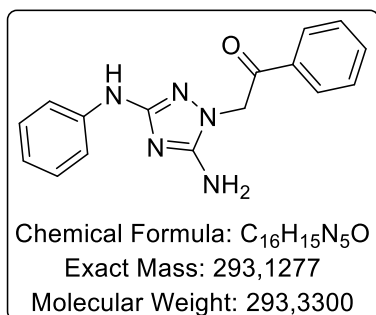


Characterization: *N*³-phenyl-1-(3,4,5-trimethoxybenzyl)-1*H*-1,2,4-triazole-3,5-diamine

*N*³-phenyl-1*H*-1,2,4-triazole-3,5-diamine (250 mg, 1.43 mmol) was dissolved in degassed DMF (10 mL), then potassium *tert*-butoxide (159 mg, 1.43 mmol) was added. 5-(Chloromethyl)-1,2,3-trimethoxybenzene (309 mg, 1.43 mmol), dissolved in degassed DMF (5 mL), was added dropwise and the reaction mixture was stirred at 0 °C for 30 min, then at r.t. for 3 h. Water was added to the mixture reaction and was extracted with ethyl acetate, washed with water, dried over magnesium sulfate and the solvents were evaporated under reduced pressure. Purification by reversed-phase chromatography (H₂O/CH₃CN, 10/0 then 60/40) afforded the titled compound as a white solid (103.5 mg, 0.292 mmol, 20% yield).

White solid, 103.5 mg, 0.292 mmol, 20% yield. R_f (CH₂Cl₂/THF, 1/1, v/v) = 0.48. M.p. = 168-170 °C. ¹H NMR (400 MHz, DMSO-*d*₆) δ 8.65 (s, 1H, NH), 7.49 (dd, *J* = 8.6, 1.2 Hz, 2H, CH_{Ar}), 7.21 – 7.07 (m, 2H, CH_{Ar}), 6.71 (tt, *J* = 7.3, 1.2 Hz, 1H, CH_{Ar}), 6.66 (s, 2H, CH_{Ar}), 6.27 (s, 2H, NH₂), 4.92 (s, 2H, CH₂), 3.74 (s, 6H, CH₃), 3.63 (s, 3H, CH₃). ¹³C NMR (101 MHz, DMSO-*d*₆) δ 157.0, 153.9, 152.7 (2C), 142.4, 136.7, 133.0, 128.4 (2C), 118.4, 115.4 (2C), 105.0 (2C), 59.9, 55.7 (2C), 48.8. LCMS: *t*_R = 9.36 min. [M+H]⁺ = 355.95. HPLC (λ₂₅₄): Purity 99.7%; HPLC (λ₂₈₂): Purity 98.8%; *t*_R: 7.44 min (method 2).

MCK299: 2-(5-amino-3-(phenylamino)-1*H*-1,2,4-triazol-1-yl)-1-phenylethan-1-one

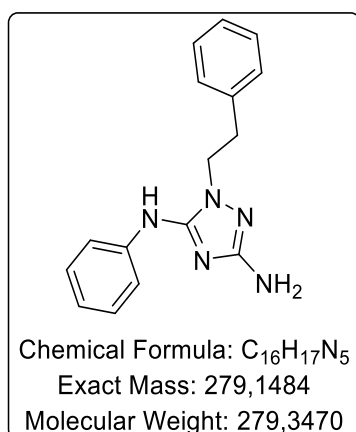


Characterization: 2-(5-amino-3-(phenylamino)-1*H*-1,2,4-triazol-1-yl)-1-phenylethan-1-one

*N*³-phenyl-1*H*-1,2,4-triazole-3,5-diamine (250 mg, 1.43 mmol) was dissolved in degassed DMF (10 mL), then potassium *tert*-butoxide (159 mg, 1.43 mmol) was added. 2-Bromo-1-phenylethan-1-one (283 mg, 1.43 mmol), dissolved in degassed DMF (5 mL), was added dropwise and the reaction mixture was stirred at 0 °C for 30 min, then at r.t. for 2 h. Water was added to the mixture reaction and was extracted with ethyl acetate, washed with water, dried over magnesium sulfate and the solvents were evaporated under reduced pressure. Purification by reversed-phase chromatography (H₂O/CH₃CN, 10/0 then 60/40) afforded the titled compound as a white solid (139.2 mg, 0.475 mmol, 33% yield).

White solid, 139.2 mg, 0.475 mmol, 33% yield. Rf (CH₂Cl₂/THF,1/1, v/v) = 0.50. M.p. = 170-172 °C. ¹H NMR (400 MHz, DMSO-*d*₆) δ 8.65 (s, 1H, NH), 8.09 – 7.99 (m, 2H, CH_{Ar}), 7.70 (t, *J* = 7.4 Hz, 1H, CH_{Ar}), 7.59 (t, *J* = 7.7 Hz, 2H, CH_{Ar}), 7.46 (d, *J* = 7.7 Hz, 2H, CH_{Ar}), 7.13 (t, *J* = 7.9 Hz, 2H, CH_{Ar}), 6.70 (t, *J* = 7.3 Hz, 1H, CH_{Ar}), 6.16 (s, 2H, NH₂), 5.45 (s, 2H, CH₂). ¹³C NMR (101 MHz, DMSO-*d*₆) δ 193.2, 157.0, 155.2, 142.3, 134.6, 133.7, 128.8 (2C), 128.3 (2C), 128.0 (2C), 118.3, 115.5 (2C), 52.6. LCMS: *t*_R = 9.80 min. [M+H]⁺ = 294.07. HPLC (λ₂₅₄): Purity 97.6%; HPLC (λ₂₈₀): Purity 94.2%; *t*_R: 7.73 min (method 2).

MCK300: 1-phenethyl-*N*⁵-phenyl-1*H*-1,2,4-triazole-3,5-diamine

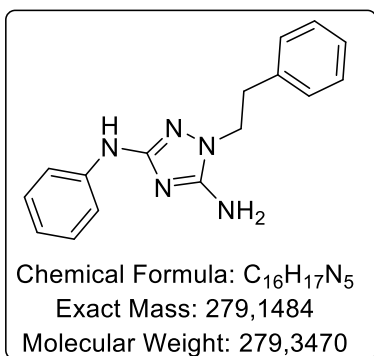


Characterization: 1-phenethyl-*N*⁵-phenyl-1*H*-1,2,4-triazole-3,5-diamine

*N*³-phenyl-1*H*-1,2,4-triazole-3,5-diamine (250 mg, 1.43 mmol) was dissolved in degassed DMF (10 mL), then potassium *tert*-butoxide (159 mg, 1.43 mmol) was added. (2-Chloroethyl)benzene (0.19 mL, 1.43 mmol), dissolved in degassed DMF (5 mL), was added dropwise and the reaction mixture was stirred at 0 °C, then potassium iodide (1.19 g, 7.14 mmol) was added at r.t. for 24 h. Water was added to the mixture reaction and was extracted with ethyl acetate, washed with water, dried over magnesium sulfate and the solvents were evaporated under reduced pressure. Purification by reversed-phase chromatography (H₂O/CH₃CN, 10/0 then 60/40) afforded the titled compound as a white solid (12.7 mg, 0.046 mmol, 3% yield) along with the *N*₃-benzylated regioisomer.

White solid, 12.7 mg, 0.046 mmol, 3% yield. Rf (CH₂Cl₂/THF,1/1, v/v) = 0.57. M.p. = 158-160 °C. ¹H NMR (400 MHz, DMSO-*d*₆) δ 8.48 (s, 1H, NH), 7.50 – 7.44 (m, 2H, CH_{Ar}), 7.31 – 7.14 (m, 7H, CH_{Ar}), 6.88 – 6.81 (m, 1H, CH_{Ar}), 5.11 (s, 2H, NH₂), 4.12 – 4.04 (m, 2H, CH₂), 3.03 – 2.94 (m, 2H, CH₂). ¹³C NMR (101 MHz, DMSO-*d*₆) δ 160.4, 149.6, 141.1, 138.4, 128.7 (2C), 128.4 (2C), 128.2 (2C), 126.2, 120.2, 116.9 (2C), 46.4, 34.8. LCMS: *t*_R = 9.51 min. [M+H]⁺ = 280.07. HPLC (λ₂₅₄): Purity 94.2%; *t*_R: 6.47 min (method 2).

MCK301: 1-phenethyl-*N*³-phenyl-1*H*-1,2,4-triazole-3,5-diamine

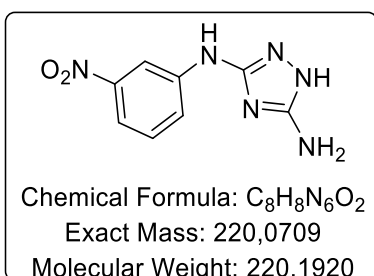


Characterization: 1-phenethyl-*N*³-phenyl-1*H*-1,2,4-triazole-3,5-diamine

*N*³-phenyl-1*H*-1,2,4-triazole-3,5-diamine (250 mg, 1.43 mmol) was dissolved in degassed DMF (10 mL), then potassium *tert*-butoxide (159 mg, 1.43 mmol) was added. (2-chloroethyl)benzene (0.19 mL, 1.43 mmol), dissolved in degassed DMF (5 mL), was added dropwise and the reaction mixture was stirred at 0 °C, then potassium iodide (1.19 g, 7.14 mmol) was added at r.t. for 24 h. Water was added to the mixture reaction and was extracted with ethyl acetate, washed with water, dried over magnesium sulfate and the solvents were evaporated under reduced pressure. Purification by reversed-phase chromatography (H₂O/CH₃CN, 10/0 then 60/40) afforded the titled compound as a white solid (37.6 mg, 0.135 mmol, 9% yield) along with the *N*₅-benzylated regioisomer.

White solid, 37.6 mg, 0.135 mmol, 9% yield. R_f (CH₂Cl₂/THF, 1/1, v/v) = 0.56. M.p. = 160-162 °C. ¹H NMR (400 MHz, DMSO-*d*₆) δ 8.61 (s, 1H, NH), 7.53 – 7.43 (m, 2H, CH_{Ar}), 7.28 (h, *J* = 5.7 Hz, 4H, CH_{Ar}), 7.21 (td, *J* = 6.0, 2.5 Hz, 1H, CH_{Ar}), 7.16 (ddd, *J* = 8.5, 5.7, 2.1 Hz, 2H, CH_{Ar}), 6.77 – 6.65 (m, 1H, CH_{Ar}), 6.06 (s, 2H, NH₂), 4.06 – 3.91 (m, 2H, CH₂), 3.04 – 2.92 (m, 2H, CH₂). ¹³C NMR (101 MHz, DMSO-*d*₆) δ 156.7, 153.5, 142.4, 138.5, 128.8 (2C), 128.4 (2C), 128.2 (2C), 126.2, 118.3, 115.5 (2C), 46.4, 34.6. LCMS: *t*_R = 9.58 min. [M+H]⁺ = 280.07. HPLC (λ₂₅₄): Purity 97.3%; *t*_R: 7.00 min (method 2).

MCK302: *N*³-(3-nitrophenyl)-1*H*-1,2,4-triazole-3,5-diamine

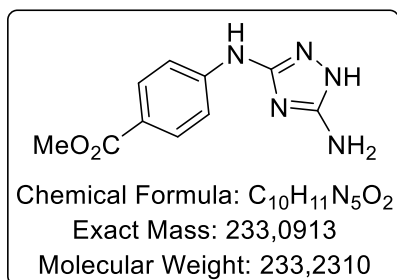


Characterization: *N*³-(3-nitrophenyl)-1*H*-1,2,4-triazole-3,5-diamine

To a solution of carbamimidothioic acid, *N*-cyano-*N'*-(3-nitrophenyl), methyl ester (250 mg, 1.06 mmol) in ethanol (15 mL) was added $\text{N}_2\text{H}_4 \cdot \text{H}_2\text{O}$ (0.10 mL, 2.12 mmol), then the solution was stirred at 75 °C for 3 h. The precipitate was filtered and washed with diethyl ether to obtain a brown solid (181.1 mg, 0.823 mmol, 78% yield).

Brown solid, 181.1 mg, 0.823 mmol, 78% yield. R_f ($\text{CH}_2\text{Cl}_2/\text{MeOH}, 9/1, v/v$) = 0.27. M.p. = 264-266 °C. ^1H NMR (400 MHz, $\text{DMSO}-d_6$) δ 11.35 (s, 1H), 9.31 (s, 1H), 8.60 (t, $J = 2.3$ Hz, 1H), 7.75 (ddd, $J = 8.2, 2.3, 1.0$ Hz, 1H), 7.57 (ddd, $J = 8.1, 2.3, 0.9$ Hz, 1H), 7.43 (t, $J = 8.1$ Hz, 1H), 5.98 (s, 2H). ^{13}C NMR (101 MHz, $\text{DMSO}-d_6$) δ 157.2, 155.5, 148.4, 143.6, 129.5, 121.7, 112.7, 109.1. LCMS: $t_R = 7.84$ min. $[\text{M}+\text{H}]^+ = 221.00$. HPLC (λ_{254}): Purity 97.6%; HPLC (λ_{280}): Purity 97.3%; t_R : 5.10 min (method 1).

MCK303: methyl 4-((5-amino-1*H*-1,2,4-triazol-3-yl)amino)benzoate

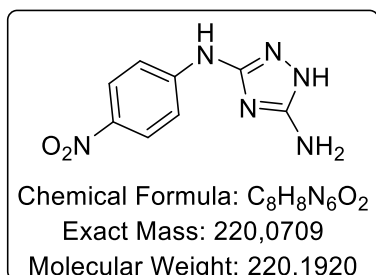


Characterization: methyl 4-((5-amino-1*H*-1,2,4-triazol-3-yl)amino)benzoate

To a solution of carbamimidothioic acid, *N*-cyano-*N'*-(4-methylbenzoate), methyl ester (1.1 g, 4.42 mmol) in ethanol (30 mL) was added $\text{N}_2\text{H}_4 \cdot \text{H}_2\text{O}$ (0.44 mL, 8.86 mmol), then the solution was stirred at 75 °C for 1 day. The precipitate was filtered and washed with diethyl ether to obtain a white solid (929.3 mg, 3.99 mmol, 90% yield).

White solid, 929.3 mg, 3.99 mmol, 90% yield. R_f ($\text{CH}_2\text{Cl}_2/\text{MeOH}, 9/1, v/v$) = 0.33. ^1H NMR (400 MHz, $\text{DMSO}-d_6$) δ 11.33 (s, 1H), 9.27 (s, 1H), 7.84 – 7.73 (m, 2H), 7.61 – 7.52 (m, 2H), 5.94 (s, 2H), 3.77 (s, 3H). ^{13}C NMR (101 MHz, $\text{DMSO}-d_6$) δ 166.2, 157.0, 155.6, 146.9, 130.3 (2C), 118.7, 114.7 (2C), 51.4. LCMS: $t_R = 7.40$ min. $[\text{M}+\text{H}]^+ = 234.07$. HPLC (λ_{254}): Purity 98.5%; HPLC (λ_{280}): Purity 99.1%; t_R : 4.86 min (method 1). Data in accordance with the literature.⁵⁰⁵

MCK304: *N*³-(4-nitrophenyl)-1*H*-1,2,4-triazole-3,5-diamine

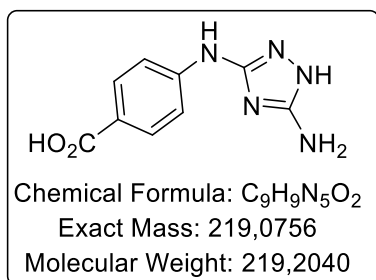


Characterization: *N*³-(4-nitrophenyl)-1*H*-1,2,4-triazole-3,5-diamine

To a solution of carbamimidothioic acid, *N*-cyano-*N*'-(4-nitrobenzoate), methyl ester (2.5g) in ethanol (40 mL) was added N₂H₄·H₂O (1 mL), then the solution was stirred at 75 °C for 4 h. Ethanol was evaporated and the solid was washed with diethyl ether to obtain a red solid (1.456 g, 6.62 mmol, 91% yield (over 2 steps)).

Red solid, 1.456 g, 6.62 mmol, 91% yield (over 2 steps). R_f (CH₂Cl₂/MeOH,95/5, v/v) = 0.29. M.p. > 266 °C. ¹H NMR (400 MHz, DMSO-*d*₆) δ 9.78 (s, 1H, NH), 8.21 – 7.98 (m, 2H, CH_{Ar}), 7.81 – 7.51 (m, 2H, CH_{Ar}), 6.07 (s, 2H, NH₂). ¹³C NMR (101 MHz, DMSO-*d*₆) δ 156.4, 155.8, 148.8, 138.1, 125.4 (2C), 114.7 (2C). LCMS: *t*_R = 8.02 min. [M+H]⁺ = 221.07. HPLC (λ₂₅₄): Purity 97.3%; *t*_R: 4.79 min (method 1).

MCK305: 4-((5-amino-1*H*-1,2,4-triazol-3-yl)amino)benzoic acid



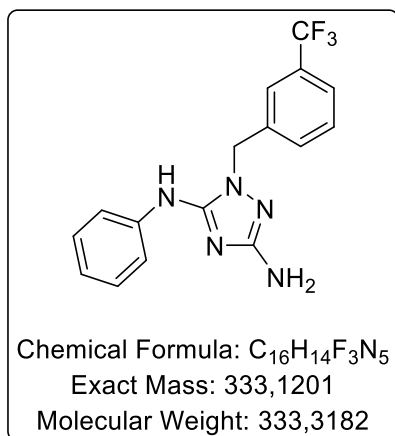
Characterization: 4-((5-amino-1*H*-1,2,4-triazol-3-yl)amino)benzoic acid

To a solution of methyl 4-((5-amino-1*H*-1,2,4-triazol-3-yl)amino)benzoate (450 mg, 1.93 mmol) in H₂O/THF (4/1, 15 mL) was added LiOH·H₂O (138 mg, 3.28 mmol) at r.t.. The solution was heated at 55 °C overnight. The precipitate that formed was filtered and washed with THF to afford an orange solid (111.4 mg, 0.509 mmol, 26% yield).

Orange solid, 111.4 mg, 0.509 mmol, 26% yield. R_f (CH₂Cl₂/MeOH,90/10, v/v) = 0.14. ¹H NMR (400 MHz, DMSO-*d*₆) δ 9.53 (s, 1H), 7.82 (d, *J* = 8.9 Hz, 2H), 7.51 (d, *J* = 8.8 Hz, 2H), 6.83 (s, 2H). ¹³C NMR (101 MHz, DMSO-*d*₆) δ 167.1, 152.8, 152.1, 145.1, 130.6 (2C), 121.5, 115.3 (2C). LCMS: *t*_R = 1.09 min.

$[M+H]^+ = 220.20$. HPLC (λ_{254}): Purity 99.5%; HPLC (λ_{280}): Purity 98.0%; t_R : 3.35 min (method 1). Data in accordance with the literature.⁵⁰⁵

MCK338: *N*⁵-phenyl-1-(3-(trifluoromethyl)benzyl)-1*H*-1,2,4-triazole-3,5-diamine

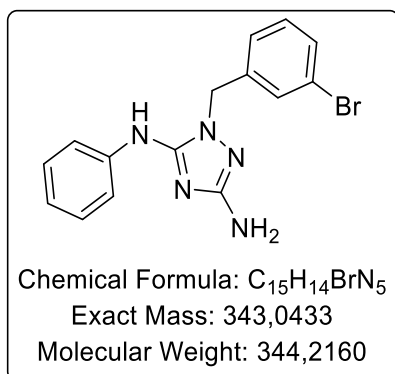


Characterization: *N*⁵-phenyl-1-(3-(trifluoromethyl)benzyl)-1*H*-1,2,4-triazole-3,5-diamine

*N*³-phenyl-1*H*-1,2,4-triazole-3,5-diamine (250 mg, 1.43 mmol) was dissolved in anhydrous DMF (1 mL), then potassium *tert*-butoxide (160 mg, 1.43 mmol) was added at 0 °C. 3-(Trifluoromethyl)benzyl chloride (0.23 mL, 1.50 mmol), dissolved in anhydrous CH₂Cl₂ (1 mL), was added dropwise and the reaction mixture was stirred at 0 °C for 1 h and at r.t. for 2 h. The reaction mixture was quenched with water (1 mL) and the solvents were evaporated under reduced pressure. Purification by reversed-phase chromatography (H₂O/CH₃CN, 10/0 then 45/55) afforded the titled compound as a white solid (51.3 mg, 0.154 mmol, 11% yield) along with the *N*₃-benzylated regioisomer.

White solid, 51.3 mg, 0.154 mmol, 11% yield. R_f (CH₂Cl₂/THF, 1/1, v/v) = 0.83. M.p. = 128-130 °C. ¹H NMR (400 MHz, DMSO-*d*₆) δ 8.85 (s, 1H, NH), 7.68 – 7.60 (m, 2H, CH_{Ar}), 7.60 – 7.55 (m, 3H, CH_{Ar}), 7.49 (d, J = 7.6 Hz, 1H, CH_{Ar}), 7.24 (t, J = 7.9 Hz, 2H, CH_{Ar}), 6.88 (t, J = 7.3 Hz, 1H, CH_{Ar}), 5.23 (s, 2H, NH₂), 5.17 (d, J = 9.4 Hz, 2H, CH₂). ¹³C NMR (101 MHz, DMSO-*d*₆) δ 160.9, 150.4, 140.9, 139.0, 131.3, 129.6, 129.2, 128.9, 128.6 (2C), 124.0, 123.7, 120.6, 117.0 (2C), 48.2. LCMS: t_R = 10.83 min. $[M+H]^+ = 334.16$. HPLC (λ_{280}): Purity 94.5%; t_R : 10.7 min (method 2).

MCK339: 1-(3-bromobenzyl)-N⁵-phenyl-1H-1,2,4-triazole-3,5-diamine

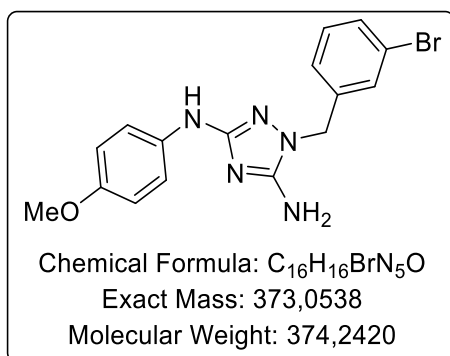


Characterization: 1-(3-bromobenzyl)-N⁵-phenyl-1H-1,2,4-triazole-3,5-diamine

N³-phenyl-1H-1,2,4-triazole-3,5-diamine (150 mg, 0.857 mmol) was dissolved in anhydrous DMF (1 mL), then potassium *tert*-butoxide (96 mg, 0.857 mmol) was added at 0 °C. 3-Bromobenzyl bromide (225 mg, 0.857 mmol), dissolved in anhydrous CH₂Cl₂ (1 mL), was added dropwise and the reaction mixture was stirred at 0 °C for 1 h and at r.t. for an additional 1 h. The reaction mixture was quenched with water (1 mL) and the solvents were evaporated under reduced pressure. Purification by reversed-phase chromatography (H₂O/CH₃CN, 10/0 then 45/55) afforded the titled compound as a white solid (29.5 mg, 0.086 mmol, 10% yield) along with the N₃-benzylated regioisomer.

White solid, 29.5 mg, 0.086 mmol, 10% yield. R_f (CH₂Cl₂/THF, 1/1, v/v) = 0.63. M.p. = 146-148 °C. ¹H NMR (400 MHz, DMSO-*d*₆) δ 8.81 (s, 1H, NH), 7.62 – 7.55 (m, 2H, CH_{Ar}), 7.50 – 7.45 (m, 1H, CH_{Ar}), 7.39 (t, *J* = 1.8 Hz, 1H, CH_{Ar}), 7.31 (t, *J* = 7.8 Hz, 1H, CH_{Ar}), 7.27 – 7.18 (m, 3H, CH_{Ar}), 6.88 (tt, *J* = 7.4, 1.1 Hz, 1H, CH_{Ar}), 5.16 (s, 2H, NH₂), 5.13 (s, 2H, CH₂). ¹³C NMR (101 MHz, DMSO-*d*₆) δ 160.8, 150.3, 140.9, 140.3, 130.6, 130.0, 129.9, 128.6 (2C), 126.2, 121.6, 120.5, 116.9 (2C), 48.0. LCMS: *t*_R = 8.47 min. [M+H]⁺ = 342.30; 343.90. HPLC (λ₂₈₀): Purity 96.5%; *t*_R: 10.5 min (method 3).

MCK340: 1-(3-bromobenzyl)-N³-(4-methoxyphenyl)-1H-1,2,4-triazole-3,5-diamine

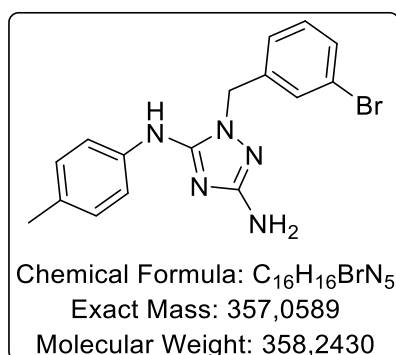


Characterization: 1-(3-bromobenzyl)-N³-(4-methoxyphenyl)-1H-1,2,4-triazole-3,5-diamine

*N*³-(4-methoxyphenyl)-1*H*-1,2,4-triazole-3,5-diamine (250 mg, 1.22 mmol) was dissolved in anhydrous DMF (1 mL), then potassium *tert*-butoxide (137 mg, 1.22 mmol) was added at 0 °C. 3-Bromobenzyl bromide (320 mg, 1.28 mmol), dissolved in anhydrous CH₂Cl₂ (1 mL), was added dropwise and the reaction mixture was stirred at 0 °C for 1 h and at r.t. for 2 h. The reaction mixture was quenched with water (1 mL) and the solvents were evaporated under reduced pressure. Purification by reversed-phase chromatography (H₂O/CH₃CN, 10/0 then 45/55) afforded the titled compound as a beige solid (88.4 mg, 0.237 mmol, 19% yield).

Beige solid, 88.4 mg, 0.237 mmol, 19% yield. R_f (CH₂Cl₂/THF, 1/1, v/v) = 0.35. M.p. = 96-98 °C. ¹H NMR (400 MHz, DMSO-*d*₆) δ 8.43 (s, 1H, NH), 7.47 (ddd, *J* = 7.9, 2.0, 1.1 Hz, 1H, CH_{Ar}), 7.42 (t, *J* = 1.8 Hz, 1H, CH_{Ar}), 7.41 – 7.35 (m, 2H, CH_{Ar}), 7.32 (t, *J* = 7.8 Hz, 1H, CH_{Ar}), 7.24 (dt, *J* = 7.8, 1.4 Hz, 1H, CH_{Ar}), 6.82 – 6.70 (m, 2H, NH₂), 6.28 (s, 2H, CH₂), 5.01 (s, 2H), 3.66 (s, 3H, OCH₃). ¹³C NMR (101 MHz, DMSO-*d*₆) δ 157.6, 154.1, 152.1, 140.4, 136.0, 130.6, 130.0, 129.9, 126.3, 121.5, 116.7 (2C), 113.8 (2C), 55.1, 47.9. LCMS: *t*_R = 8.63 min. [M+H]⁺ = 374.30; 376.40. HPLC (λ₂₅₄): Purity 100%; HPLC (λ₂₈₀): Purity 98.8%; *t*_R: 10.5 min (method 3).

MCK341: 1-(3-bromobenzyl)-*N*⁵-(4-methylphenyl)-1*H*-1,2,4-triazole-3,5-diamine

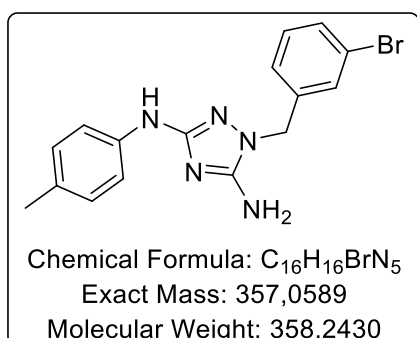


Characterization: 1-(3-bromobenzyl)-*N*⁵-(4-methylphenyl)-1*H*-1,2,4-triazole-3,5-diamine

*N*³-(4-methylphenyl)-1*H*-1,2,4-triazole-3,5-diamine (250 mg, 1.32 mmol) was dissolved in anhydrous DMF (1 mL), then potassium *tert*-butoxide (148 mg, 1.32 mmol) was added at 0 °C. 3-Bromobenzyl bromide (347 mg, 1.39 mmol), dissolved in anhydrous CH₂Cl₂ (1 mL), was added dropwise and the reaction mixture was stirred at 0 °C for 1 h and at r.t. for 2 h. The reaction mixture was quenched with water (1 mL) and the solvents were evaporated under reduced pressure. Purification by reversed-phase chromatography (H₂O/CH₃CN, 10/0 then 45/55) afforded the titled compound as a pale pink solid (47.7 mg, 0.134 mmol, 10% yield) along with the *N*₃-benzylated regioisomer.

Pale pink solid, 47.7 mg, 0.134 mmol, 10% yield. Rf (CH₂Cl₂/THF,1/1, v/v) = 0.54. M.p. = 162-164 °C. ¹H NMR (400 MHz, DMSO-*d*₆) δ 8.70 (s, 1H, NH), 7.47 (dd, *J* = 8.8, 2.1 Hz, 3H, CH_{Ar}), 7.38 (t, *J* = 1.8 Hz, 1H, CH_{Ar}), 7.31 (t, *J* = 7.8 Hz, 1H, CH_{Ar}), 7.22 – 7.18 (m, 1H, CH_{Ar}), 7.08 – 7.02 (m, 2H, CH_{Ar}), 5.14 (s, 2H, NH₂), 5.11 (s, 2H, CH₂), 2.22 (s, 3H, CH₃). ¹³C NMR (101 MHz, DMSO-*d*₆) δ 160.8, 150.5, 140.3, 138.4, 130.6, 130.0, 129.9, 129.2, 129.0 (2C), 126.2, 121.6, 117.1 (2C), 47.9, 20.2. LCMS: *t*_R = 9.06 min. [M+H]⁺ = 357.9; 358.9. HPLC (λ₂₅₄): Purity 99.3%; HPLC (λ₂₈₀): Purity 99.7%; *t*_R: 11.0 min (method 3).

MCK342: 1-(3-bromobenzyl)-N³-(4-methylphenyl)-1H-1,2,4-triazole-3,5-diamine

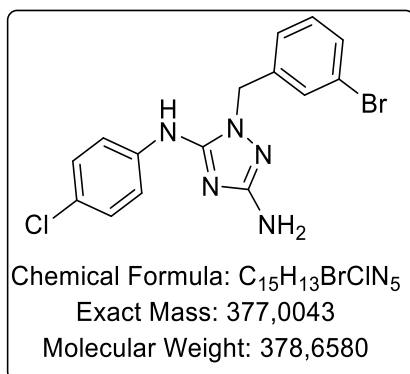


Characterization: 1-(3-bromobenzyl)-N³-(4-methylphenyl)-1H-1,2,4-triazole-3,5-diamine

N³-(4-methylphenyl)-1H-1,2,4-triazole-3,5-diamine (250 mg, 1.32 mmol) was dissolved in anhydrous DMF (1 mL), then potassium *tert*-butoxide (148 mg, 1.32 mmol) was added at 0 °C. 3-Bromobenzyl bromide (347 mg, 1.39 mmol), dissolved in anhydrous CH₂Cl₂ (1 mL), was added dropwise and the reaction mixture was stirred at 0 °C for 1 h and at r.t. for 2 h. The reaction mixture was quenched with water (1 mL) and the solvents were evaporated under reduced pressure. Purification by reversed-phase chromatography (H₂O/CH₃CN, 10/0 then 45/55) afforded the titled compound as a yellow solid (157.4 mg, 0.441 mmol, 33% yield) along with the N₅-benzylated regioisomer.

Yellow solid, 157.4 mg, 0.441 mmol, 33% yield. Rf (CH₂Cl₂/THF,1/1, v/v) = 0.46. M.p. = 86-88 °C. ¹H NMR (400 MHz, DMSO-*d*₆) δ 8.54 (s, 1H, NH), 7.50 – 7.45 (m, 1H, CH_{Ar}), 7.43 (t, *J* = 1.8 Hz, 1H, CH_{Ar}), 7.37 – 7.29 (m, 3H, CH_{Ar}), 7.26 – 7.21 (m, 1H, CH_{Ar}), 7.02 – 6.90 (m, 2H, CH_{Ar}), 6.30 (s, 2H, NH₂), 5.02 (s, 2H, CH₂), 2.18 (s, 3H, CH₃). ¹³C NMR (101 MHz, DMSO-*d*₆) δ 157.4, 154.1, 140.4, 139.8, 130.6, 130.0, 129.9, 128.8 (2C), 126.8, 126.3, 121.5, 115.5 (2C), 47.9, 20.2. LCMS: *t*_R = 9.57 min. [M+H]⁺ = 357.40; 358.40. HPLC (λ₂₅₄): Purity 96.6%; HPLC (λ₂₈₀): Purity 95.1%; *t*_R: 11.5 min (method 3).

MCK343: 1-(3-bromobenzyl)-N⁵-(4-chlorophenyl)-1H-1,2,4-triazole-3,5-diamine

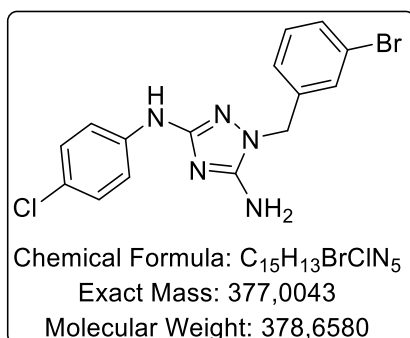


Characterization: 1-(3-bromobenzyl)-N⁵-(4-chlorophenyl)-1H-1,2,4-triazole-3,5-diamine

N³-(4-chlorophenyl)-1H-1,2,4-triazole-3,5-diamine (250 mg, 1.20 mmol) was dissolved in anhydrous DMF (1 mL), then potassium *tert*-butoxide (134 mg, 1.20 mmol) was added at 0 °C. 3-Bromobenzyl bromide (310 mg, 1.26 mmol), dissolved in anhydrous CH₂Cl₂ (1 mL), was added dropwise and the reaction mixture was stirred at 0 °C for 1 h and at r.t. for 2 h. The reaction mixture was quenched with water (1 mL) and the solvents were evaporated under reduced pressure. Purification by reversed-phase chromatography (H₂O/CH₃CN, 10/0 then 45/55) afforded the titled compound as a pale pink solid (22.4 mg, 0.059 mmol, 5% yield) along with the N₃-benzylated regioisomer.

Pale pink solid, 22.4 mg, 0.059 mmol, 5% yield. R_f (CH₂Cl₂/THF, 1/1, v/v) = 0.54. M.p. = 82-84 °C. ¹H NMR (400 MHz, DMSO-*d*₆) δ 9.00 (s, 1H, NH), 7.68 – 7.57 (m, 2H, CH_{Ar}), 7.47 (ddd, *J* = 8.0, 2.1, 1.1 Hz, 1H, CH_{Ar}), 7.38 (t, *J* = 1.8 Hz, 1H, CH_{Ar}), 7.36 – 7.27 (m, 3H, CH_{Ar}), 7.19 (dt, *J* = 7.8, 1.3 Hz, 1H, CH_{Ar}), 5.20 (s, 2H, NH₂), 5.12 (s, 2H, CH₂). ¹³C NMR (101 MHz, DMSO-*d*₆) δ 160.8, 149.8, 140.1, 139.9, 130.6, 130.1, 129.9, 128.4 (2C), 126.2, 124.0, 121.6, 118.4 (2C), 48.0. LCMS: *t*_R = 9.76 min. [M+H]⁺ = 378.4; 380.3. HPLC (λ₂₅₄): Purity 96.4%; HPLC (λ₂₈₀): Purity 98.7%; *t*_R: 11.9 min (method 3).

MCK344: 1-(3-bromobenzyl)-N³-(4-chlorophenyl)-1H-1,2,4-triazole-3,5-diamine

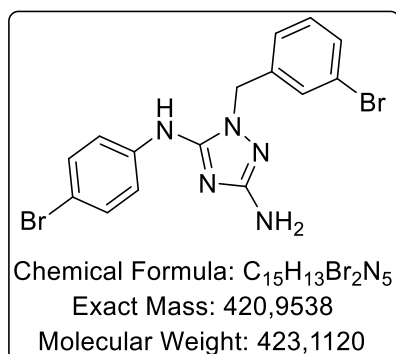


Characterization: 1-(3-bromobenzyl)-N³-(4-chlorophenyl)-1H-1,2,4-triazole-3,5-diamine

*N*³-(4-chlorophenyl)-1*H*-1,2,4-triazole-3,5-diamine (250 mg, 1.20 mmol) was dissolved in anhydrous DMF (1 mL), then potassium *tert*-butoxide (134 mg, 1.20 mmol) was added. 3-Bromobenzyl bromide (310 mg, 1.26 mmol), dissolved in anhydrous CH₂Cl₂ (1 mL), was added dropwise and the reaction mixture was stirred at 0 °C for 1 h and at r.t. for 2 h. The reaction mixture was quenched with water (1 mL) and the solvents were evaporated under reduced pressure. Purification by reversed-phase chromatography (H₂O/CH₃CN, 10/0 then 45/55) afforded the titled compound as an orange solid (197.7 mg, 0.524 mmol, 44% yield) along with the *N*₅-benzylated regioisomer.

Orange solid, 197.7 mg, 0.524 mmol, 44% yield. R_f (CH₂Cl₂/THF,1/1, v/v) = 0.42. M.p. = 124-126 °C. ¹H NMR (400 MHz, DMSO-*d*₆) δ 8.93 (s, 1H NH), 7.53 – 7.45 (m, 3H, CH_{Ar}), 7.43 (t, *J* = 1.8 Hz, 1H, CH_{Ar}), 7.32 (t, *J* = 7.8 Hz, 1H, CH_{Ar}), 7.27 – 7.22 (m, 1H, CH_{Ar}), 7.22 – 7.16 (m, 2H, CH_{Ar}), 6.38 (s, 2H, NH₂), 5.04 (s, 2H, CH₂). ¹³C NMR (101 MHz, DMSO-*d*₆) δ 157.0, 154.3, 141.2, 140.2, 130.6, 130.1, 129.9, 128.2 (2C), 126.3, 121.8, 121.6, 116.9 (2C), 48.0. LCMS: *t*_R = 10.52 min. [M+H]⁺ = 378.4; 380.3. HPLC (λ₂₅₄): Purity 98.5%; HPLC (λ₂₈₀): Purity 98.7%; *t*_R: 12.6 min (method 3).

MCK345: 1-(3-bromobenzyl)-*N*⁵-(4-bromophenyl)-1*H*-1,2,4-triazole-3,5-diamine



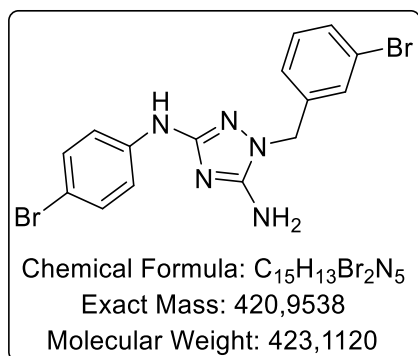
Characterization: 1-(3-bromobenzyl)-*N*⁵-(4-bromophenyl)-1*H*-1,2,4-triazole-3,5-diamine

*N*³-(4-bromophenyl)-1*H*-1,2,4-triazole-3,5-diamine (250 mg, 0.988 mmol) was dissolved in anhydrous DMF (1 mL), then potassium *tert*-butoxide (111 mg, 0.988 mmol) was added at 0 °C. 3-Bromobenzyl bromide (259 mg, 1.04 mmol), dissolved in anhydrous CH₂Cl₂ (1 mL), was added dropwise and the reaction mixture was stirred at 0 °C for 1 h and at r.t. for 2 h. The reaction mixture was quenched with water (1 mL) and the solvents were evaporated under reduced pressure. Purification by reversed-phase chromatography (H₂O/CH₃CN, 10/0 then 45/55) afforded the titled compound as a pink solid (3.5 mg, 0.008 mmol, 1% yield) along with the *N*₃-benzylated regioisomer.

Pink solid (3.5 mg, 0.008 mmol, 1% yield). R_f (CH₂Cl₂/THF,1/1, v/v) = 0.54. M.p. = 76-78 °C. ¹H NMR (400 MHz, DMSO-*d*₆) δ 9.01 (s, 1H, NH), 7.59 – 7.55 (m, 2H, CH_{Ar}), 7.47 (ddd, *J* = 8.0, 2.2, 1.1 Hz, 1H, CH_{Ar}),

7.44 – 7.37 (m, 3H, CH_{Ar}), 7.31 (t, *J* = 7.8 Hz, 1H, CH_{Ar}), 7.19 (dt, *J* = 7.8, 1.3 Hz, 1H, CH_{Ar}), 5.20 (d, *J* = 7.7 Hz, 2H, NH₂), 5.12 (s, 2H, CH₂). ¹³C NMR (101 MHz, DMSO-*d*₆) δ 160.8, 149.8, 140.3, 140.1, 131.3 (2C), 130.6, 130.1, 129.9, 126.2, 121.6, 118.8 (2C), 111.8, 48.1. LCMS: *t*_R = 10.01 min. [M+H]⁺ = 422.3; 424.4. HPLC (λ₂₈₀): Purity 95.1%; *t*_R: 12.2 min (method 3).

MCK346: 1-(3-bromobenzyl)-N³-(4-bromophenyl)-1*H*-1,2,4-triazole-3,5-diamine

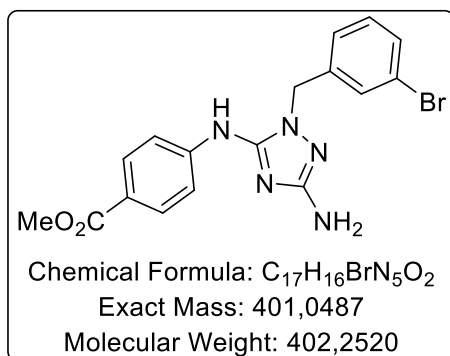


Characterization: 1-(3-bromobenzyl)-N³-(4-bromophenyl)-1*H*-1,2,4-triazole-3,5-diamine

N³-(4-bromophenyl)-1*H*-1,2,4-triazole-3,5-diamine (250 mg, 0.988 mmol) was dissolved in anhydrous DMF (1 mL), then potassium *tert*-butoxide (111 mg, 0.988 mmol) was added at 0 °C. 3-Bromobenzyl bromide (259 mg, 1.04 mmol), dissolved in anhydrous CH₂Cl₂ (1 mL), was added dropwise and the reaction mixture was stirred at 0 °C for 1 h and at r.t. for 2 h. The reaction mixture was quenched with water (1 mL) and the solvents were evaporated under reduced pressure. Purification by reversed-phase chromatography (H₂O/CH₃CN, 10/0 then 45/55) afforded the titled compound as a pink solid (132.4 mg, 0.314 mmol, 32% yield) along with the N₅-benzylated regioisomer.

Pink solid (132.4 mg, 0.314 mmol, 32% yield. R_f (CH₂Cl₂/THF, 1/1, v/v) = 0.42. M.p. = 130-132 °C. ¹H NMR (400 MHz, DMSO-*d*₆) δ 8.94 (s, 1H, NH), 7.50 – 7.45 (m, 1H, CH_{Ar}), 7.45 – 7.41 (m, 3H, CH_{Ar}), 7.35 – 7.28 (m, 3H, CH_{Ar}), 7.26 – 7.21 (m, 1H, CH_{Ar}), 6.38 (s, 2H, NH₂), 5.04 (s, 2H, CH₂). ¹³C NMR (101 MHz, DMSO-*d*₆) δ 156.9, 154.3, 141.6, 140.2, 131.0 (2C), 130.6, 130.1, 129.9, 126.3, 121.6, 117.5 (2C), 109.5, 48.0. LCMS: *t*_R = 10.64 min. [M+H]⁺ = 422.3; 424.2. HPLC (λ₂₅₄): Purity 97.7%; HPLC (λ₂₈₀): Purity 98.8%; *t*_R: 13.0 min (method 3).

MCK347: methyl-4-((3-amino-1-(3-bromobenzyl)-1H-1,2,4-triazol-5-yl)amino)benzoate

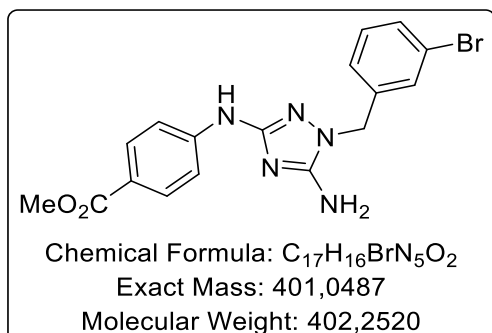


Characterization: methyl-4-((3-amino-1-(3-bromobenzyl)-1H-1,2,4-triazol-5-yl)amino)benzoate

Methyl-4-((5-amino-1H-1,2,4-triazol-3-yl)amino)benzoate (250 mg, 1.07 mmol) was dissolved in anhydrous DMF (1 mL), then potassium *tert*-butoxide (120 mg, 1.07 mmol) was added at 0 °C. 3-Bromobenzyl bromide (280 mg, 1.13 mmol), dissolved in anhydrous CH₂Cl₂ (1 mL), was added dropwise and the reaction mixture was stirred at 0 °C for 1 h and at r.t. for 5 h 30. The reaction mixture was quenched with water (1 mL) and the solvents were evaporated under reduced pressure. Purification by reversed-phase chromatography (H₂O/CH₃CN, 10/0 then 45/55) afforded the titled compound as an off-white solid (9.9 mg, 0.025 mmol, 2% yield) along with the N₃-benzylated regioisomer.

R_f (CH₂Cl₂/THF, 1/1, v/v) = 0.56. M.p. = 100 °C. ¹H NMR (400 MHz, DMSO-*d*₆) δ 9.33 (s, 1H, NH), 7.90 – 7.82 (m, 2H, CH_{Ar}), 7.72 – 7.64 (m, 2H, CH_{Ar}), 7.47 (ddd, *J* = 8.0, 2.1, 1.1 Hz, 1H, CH_{Ar}), 7.39 (t, *J* = 1.8 Hz, 1H, CH_{Ar}), 7.31 (t, *J* = 7.8 Hz, 1H, CH_{Ar}), 7.22 – 7.15 (m, 1H, CH_{Ar}), 5.28 (s, 2H, NH₂), 5.16 (s, 2H, CH₂), 3.80 (s, 3H, CH₃). ¹³C NMR (101 MHz, DMSO-*d*₆) δ 166.0, 161.0, 145.4, 140.0, 130.6 (2C), 130.3 (2C), 130.1, 129.9 (2C), 126.2, 121.6, 115.9 (2C), 51.6, 48.2. LCMS: *t*_R = 8.92 min. [M+H]⁺ = 400.4; 401.8. HPLC (λ₂₈₀): Purity 96.7%; *t*_R = 11.0 min (method 3).

MCK348: methyl-4-((5-amino-1-(3-bromobenzyl)-1H-1,2,4-triazol-3-yl)amino)benzoate

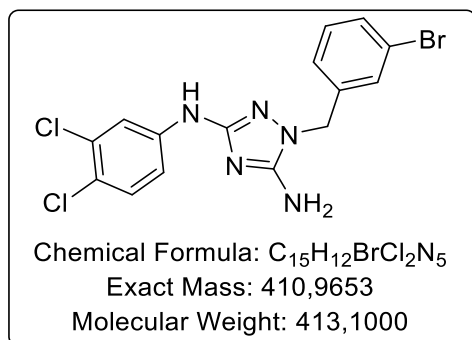


Characterization: methyl-4-((5-amino-1-(3-bromobenzyl)-1H-1,2,4-triazol-3-yl)amino)benzoate

Methyl-4-((5-amino-1*H*-1,2,4-triazol-3-yl)amino)benzoate (250 mg, 1.07 mmol) was dissolved in anhydrous DMF (1 mL), then potassium *tert*-butoxide (120 mg, 1.07 mmol) was added at 0 °C. 3-Bromobenzyl bromide (280 mg, 1.13 mmol), dissolved in anhydrous CH₂Cl₂ (1 mL), was added dropwise and the reaction mixture was stirred at 0 °C for 1 h and at r.t. for 5 h 30. The reaction mixture was quenched with water (1 mL) and the solvents were evaporated under reduced pressure. Purification by reversed-phase chromatography (H₂O/CH₃CN, 10/0 then 45/55) afforded the titled compound as an off-white solid (83.7 mg, 0.209 mmol, 20% yield) along with the *N*₅-benzylated regioisomer.

Rf (CH₂Cl₂/THF,1/1, v/v) = 0.39. M.p. = 182 °C. ¹H NMR (400 MHz, DMSO-*d*₆) δ 9.37 (s, 1H, NH), 7.81 – 7.75 (m, 2H, CH_{Ar}), 7.56 – 7.51 (m, 2H, CH_{Ar}), 7.48 (ddd, *J* = 7.9, 2.1, 1.1 Hz, 1H, CH_{Ar}), 7.44 (t, *J* = 1.8 Hz, 1H, CH_{Ar}), 7.33 (t, *J* = 7.8 Hz, 1H, CH_{Ar}), 7.25 (dt, *J* = 7.8, 1.3 Hz, 1H, CH_{Ar}), 6.45 (s, 2H, NH₂), 5.06 (s, 2H, CH₂), 3.77 (s, 3H, CH₃). ¹³C NMR (101 MHz, DMSO-*d*₆) δ 166.1, 156.5, 154.3, 146.6, 140.1, 130.7, 130.3, 130.1, 130.0 (2C), 126.4, 121.6, 119.0, 114.7 (2C), 51.4, 48.0. LCMS: *t*_R = 9.63 min. [M+H]⁺ = 402.3; 404.3. HPLC (λ₂₈₀): Purity 96.0%; HPLC (λ₂₈₀): Purity 98.1%; *t*_R: 11.6 min (method 3).

MCK349: 1-(3-bromobenzyl)-*N*³-(3,4-dichlorophenyl)-1*H*-1,2,4-triazole-3,5-diamine



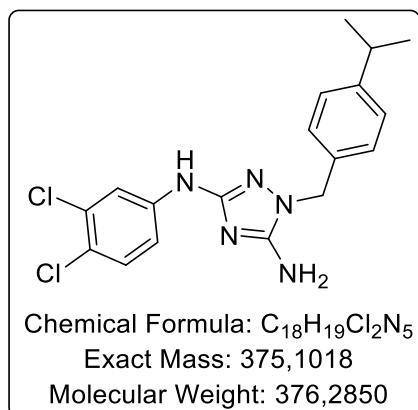
Characterization: 1-(3-bromobenzyl)-*N*³-(3,4-dichlorophenyl)-1*H*-1,2,4-triazole-3,5-diamine

*N*³-(3,4-dichlorophenyl)-1*H*-1,2,4-triazole-3,5-diamine (250 mg, 1.03 mmol) was dissolved in anhydrous DMF (1 mL), then potassium *tert*-butoxide (115 mg, 1.03 mmol) was added at 0 °C. 3-Bromobenzyl bromide (270 mg, 1.08 mmol), dissolved in anhydrous CH₂Cl₂ (1 mL), was added dropwise and the reaction mixture was stirred at 0 °C for 1 h and at r.t. for 16 h. The reaction mixture was quenched with water (1 mL) and the solvents were evaporated under reduced pressure. Purification by reversed-phase chromatography (H₂O/CH₃CN, 10/0 then 45/55) afforded the titled compound as a white solid (93.9 mg, 0.229 mmol, 22% yield).

Rf (CH₂Cl₂/THF,1/1, v/v) = 0.39. M.p. = 150 °C. ¹H NMR (400 MHz, DMSO-*d*₆) δ 9.18 (s, 1H, NH), 7.82 (d, *J* = 2.3 Hz, 1H, CH_{Ar}), 7.49 (ddd, *J* = 7.9, 2.2, 1.1 Hz, 1H, CH_{Ar}), 7.44 (t, *J* = 1.8 Hz, 1H, CH_{Ar}), 7.40 – 7.30

(m, 3H, CH_{Ar}), 7.24 (dt, *J* = 7.8, 1.3 Hz, 1H, CH_{Ar}), 6.45 (s, 2H, NH₂), 5.05 (s, 2H, CH₂). ¹³C NMR (101 MHz, DMSO-*d*₆) δ 156.6, 154.3, 142.3, 140.0, 130.7, 130.7, 130.2, 130.1, 130.0, 126.4, 121.6, 119.4, 116.3, 115.8, 48.0. LCMS: *t*_R = 11.64 min. [M+H]⁺ = 412.3; 414.4. HPLC (λ₂₅₄): Purity 97.7%; HPLC (λ₂₈₀): Purity 96.4%; *t*_R: 15.0 min (method 3).

MCK350: *N*³-(3,4-dichlorophenyl)-1-(4-isopropylbenzyl)-1*H*-1,2,4-triazole-3,5-diamine

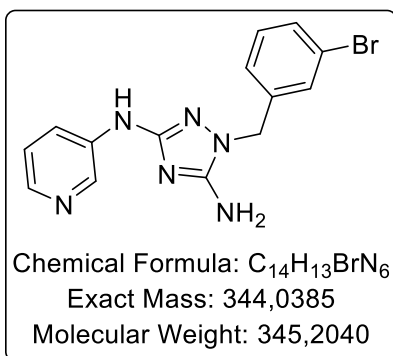


Characterization: *N*³-(3,4-dichlorophenyl)-1-(4-isopropylbenzyl)-1*H*-1,2,4-triazole-3,5-diamine

*N*³-(3,4-dichlorophenyl)-1*H*-1,2,4-triazole-3,5-diamine (250 mg, 1.03 mmol) was dissolved in anhydrous DMF (1 mL), then potassium *tert*-butoxide (115 mg, 1.03 mmol) was added at 0 °C. 4-Isopropylbenzyl chloride (0.18 mL, 1.08 mmol), dissolved in anhydrous CH₂Cl₂ (1 mL), was added dropwise and the reaction mixture was stirred at 0 °C for 1 h and at r.t. for 6 h. The reaction mixture was quenched with water (1 mL) and the solvents were evaporated under reduced pressure. Purification by reversed-phase chromatography (H₂O/CH₃CN, 10/0 then 45/55) afforded the titled compound as an orange solid (162 mg, 0.432 mmol, 42% yield) along with the *N*₅-benzylated regioisomer.

R_f (CH₂Cl₂/THF, 1/1, v/v) = 0.53. M.p. = 138 °C. ¹H NMR (400 MHz, DMSO-*d*₆) δ 9.14 (s, 1H, NH), 7.83 (dd, *J* = 1.8, 1.0 Hz, 1H, CH_{Ar}), 7.45 – 7.30 (m, 2H, CH_{Ar}), 7.26 – 7.11 (m, 4H, CH_{Ar}), 6.38 (s, 2H, NH₂), 4.99 (s, 2H, CH₂), 2.84 (hept, *J* = 6.9 Hz, 1H, CH), 1.16 (d, *J* = 6.9 Hz, 6H, 2CH₃). ¹³C NMR (101 MHz, DMSO-*d*₆) δ 156.3, 154.1, 147.4, 142.4, 134.7, 130.7, 130.2, 127.3 (2C), 126.2 (2C), 119.3, 116.3, 115.8, 48.5, 33.1, 23.8 (2C). LCMS: *t*_R = 12.49 min. [M+H]⁺ = 376.4; 378.4. HPLC (λ₂₅₄): Purity 95.4%; *t*_R: 17.1 min (method 3).

MCK351: 1-(3-bromobenzyl)-N³-(pyridin-3-yl)-1H-1,2,4-triazole-3,5-diamine

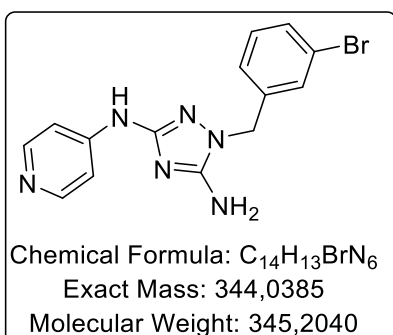


Characterization: 1-(3-bromobenzyl)-N³-(pyridin-3-yl)-1H-1,2,4-triazole-3,5-diamine

N³-(pyridin-3-yl)-1H-1,2,4-triazole-3,5-diamine (250 mg, 1.42 mmol) was dissolved in anhydrous DMF (1 mL), then potassium *tert*-butoxide (159 mg, 1.42 mmol) was added at 0 °C. 3-Bromobenzyl bromide (373 mg, 1.49 mmol), dissolved in anhydrous CH₂Cl₂ (1 mL), was added dropwise and the reaction mixture was stirred at 0 °C for 1 h and at r.t. for 4 h. The reaction mixture was quenched with water (1 mL) and the solvents were evaporated under reduced pressure. Purification by silica gel flash chromatography (CH₂Cl₂/MeOH, 10/0 then 9/1) afforded the titled compound as a brown solid (141.3 mg, 0.411 mmol, 29% yield).

R_f (CH₂Cl₂/MeOH,9/1, v/v) = 0.44. M.p. = 92-94 °C. ¹H NMR (400 MHz, DMSO-*d*₆) δ 8.98 (s, 1H), 8.63 (dd, *J* = 2.7, 0.7 Hz, 1H), 7.94 (dd, *J* = 4.6, 1.5 Hz, 1H), 7.91 (ddd, *J* = 8.4, 2.7, 1.5 Hz, 1H), 7.50 – 7.43 (m, 2H), 7.33 (t, *J* = 7.7 Hz, 1H), 7.25 (dt, *J* = 7.8, 1.4 Hz, 1H), 7.22 – 7.14 (m, 1H), 6.41 (s, 2H), 5.04 (s, 2H). ¹³C NMR (101 MHz, DMSO-*d*₆) δ 156.8, 154.4, 140.1, 139.5, 138.8, 138.0, 130.6, 130.1, 130.0, 126.4, 123.2, 121.1, 121.4, 48.0. LCMS: *t*_R = 6.91 min. [M+H]⁺ = 345.5; 347.4. HPLC (λ₂₅₄): Purity 96.6%; HPLC (λ₂₈₀): Purity 96.5 %; *t*_R: 7.39 min (method 4).

MCK352: 1-(3-bromobenzyl)-N⁴-(pyridin-3-yl)-1H-1,2,4-triazole-3,5-diamine



Characterization: 1-(3-bromobenzyl)-N⁴-(pyridin-3-yl)-1H-1,2,4-triazole-3,5-diamine

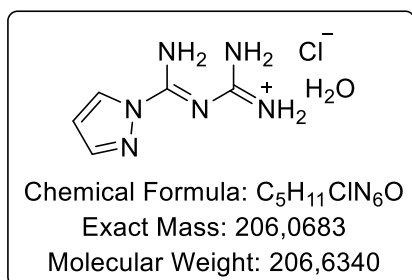
*N*⁴-(pyridin-3-yl)-1*H*-1,2,4-triazole-3,5-diamine (250 mg, 1.42 mmol) was dissolved in anhydrous DMF (1 mL), then potassium *tert*-butoxide (159 mg, 1.42 mmol) was added at 0 °C. 3-Bromobenzyl bromide (373 mg, 1.49 mmol), dissolved in anhydrous DMF (1 mL), was added dropwise and the reaction mixture was stirred at 0 °C for 1 h and at r.t. for 1 h 30. The reaction mixture was quenched with water (1 mL) and the solvents were evaporated under reduced pressure. Purification by reversed-phase chromatography (H₂O/CH₃CN, 10/0 then 45/55) afforded the titled compound as an orange solid (68.7 mg, 0.200 mmol, 14% yield).

R_f (CH₂Cl₂/THF, 1/1, v/v) = 0.72. ¹H NMR (400 MHz, DMSO-*d*₆) δ 9.37 (s, 1H, NH), 8.19 (d, *J* = 6.4 Hz, 2H, CH_{Ar}), 7.49 (ddd, *J* = 7.9, 2.1, 1.2 Hz, 1H, CH_{Ar}), 7.45 (t, *J* = 1.8 Hz, 1H, CH_{Ar}), 7.40 – 7.36 (m, 2H, CH_{Ar}), 7.33 (t, *J* = 7.8 Hz, 1H, CH_{Ar}), 7.25 (dt, *J* = 7.8, 1.3 Hz, 1H, CH_{Ar}), 6.47 (s, 2H, NH₂), 5.07 (s, 2H, CH₂). ¹³C NMR (101 MHz, DMSO-*d*₆) δ 156.2, 154.4, 149.5 (2C), 148.0, 140.0, 130.7, 130.2, 130.0, 126.4, 121.6, 110.3 (2C), 48.1. LCMS: *t*_R = 5.50 min. [M+H]⁺ = 345.5; 347.4. HPLC (λ₂₅₄): Purity 97.7%; HPLC (λ₂₈₀): Purity 100%; *t*_R: 7.22 min (method 4).

CHAPTER 5

Procedures for the synthesis of the biamidine transfer reagents.

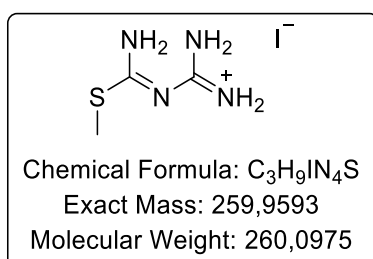
5.1a. *N*-amidinopyrazole-1-carboxamide hydrochloride.



Characterization: *N*-amidinopyrazole-1-carboxamide hydrochloride

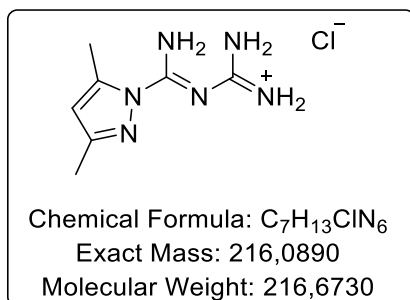
To a solution of pyrazole (20.0 g, 0.294 mol) in water (44 mL) was added hydrochloric acid 37% (25.9 mL, 0.294 mol) and dicyandiamide (24.7 g, 0.294 mol), and the mixture was stirred at 80 °C for 6 h. The resulting colorless solution was cooled to room temperature slowly, and colorless crystals of product appeared. These were filtered, washed with acetone and dried at air. White, crystalline solid (39.5 g, 0.209 mol, 65%). ¹H NMR (400 MHz, DMSO-*d*₆) δ 8.38 (br s, 2H), 8.34 (dd, *J* = 2.8, 0.7 Hz, 1H), 8.28 (br s, 4H), 7.87 (d, *J* = 1.5 Hz, 1H), 6.58 (dd, *J* = 2.8, 1.6 Hz, 1H), 3.44 (s, 2H). Protocol adapted from the literature⁵²⁶ (50%), improved to 65%.

5.1b. *S*-methyl-guanylisothiuronium iodide.



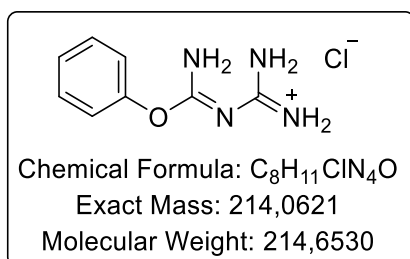
As described.⁵²⁷ Briefly, iodomethane was added dropwise to a suspension of 2-imino-4-thiobiuret (Aldrich) in 100% ethanol while stirring at r.t. The reaction flask was shaken at 37 °C for 2 h. The solvent was removed by evaporation and the residue was washed with cold diethyl ether to give a solid, which was collected by filtration and used without further purification. White, crystalline solid (39.5 g, 0.209 mol, 91%). ¹H NMR (400 MHz, DMSO-*d*₆) δ 7.94 (br s, 4H), 7.58 (br s, 2H), 2.36 (s, 3H).

5.1c. 1-(3,5-dimethylpyrazole-1-carboximidoyl)guanidinium chloride.



To a solution of 3,5-dimethylpyrazole (5.0 g, 52.0 mmol) in water (13 mL) was added hydrochloric acid 37% (4.60 mL, 52.0 mmol) and dicyandiamide (4.37 g, 52.0 mmol), and the mixture was refluxed for 3 h. The solution was evaporated to dryness *in vacuo* and the residue triturated with acetone. White, crystalline solid (4.9 g, 44%). ¹H NMR (400 MHz, DMSO-*d*₆) δ 8.09 (br s, 4H), 8.06 (br s, 2H), 6.18 (s, 1H), 2.44 (s, 3H), 2.19 (s, 3H).

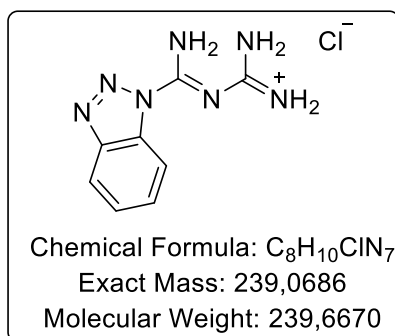
5.1d. *N*-guanyl-*O*-phenylisourea hydrochloride.⁵²⁸



Dicyandiamide dihydrochloride was prepared by mixing 0.1 mol of dicyandiamide with 0.2 mol of 37% aqueous HCl and was cooled to 5 °C. Thereafter 0.2 mol of the acid was added. After 10 min of stirring, a dense crystalline precipitate of dicyandiamide dihydrochloride was obtained. The precipitate was filtered, washed with acetone, and dried *in vacuo* for 10 min. The white, crystalline solid was used in the next step without further purification.

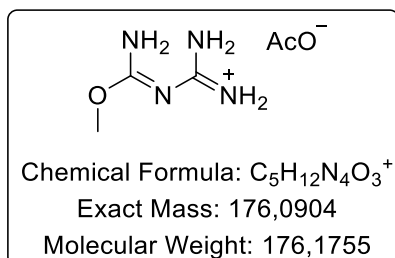
Phenol (53.5 g, 0.568 mol) and dicyandiamide dihydrochloride (16.0 g, 0.102 mol) were stirred at 70 °C for 3 h. The mixture was triturated with toluene and the crude solid was filtered and washed with diethyl ether. The solid was recrystallized from water. White, crystalline solid (7.2 g, 33%). ¹H NMR (400 MHz, DMSO-*d*₆) δ 7.97 (br s, 6H), 7.40 (br s, 2H), 7.23 (br s, 3H).

5.1e. 1-(benzotriazole-1-carboximidoyl)guanidinium chloride.



To a solution of benzotriazole (5.00 g, 4.20 mmol) in water (10.5 mL) was added hydrochloric acid 37% (3.70 mL, 4.2 mmol) and dicyandiamide (3.52 g, 42.0 mmol), and the mixture was refluxed for 24 h. The solution was evaporated to dryness *in vacuo* on and the residue triturated with ethanol, washed with acetone, and dried. White, crystalline solid (2.52 g, 25%). HRMS-ESI(*m/z*): $[M+H]^+$ calc. for $C_8H_{10}N_7^+$, 204.09922; Found: 340.05914. 1H NMR (400 MHz, DMSO- d_6) δ 8.86 (br s, 2H), 8.52 (br s, 2H), 8.46 (br s, 2H), 8.24 (t, $J = 8.3$ Hz, 2H), 7.75 (ddd, $J = 8.3, 7.0, 1.1$ Hz, 1H), 7.59 (ddd, $J = 8.1, 7.0, 1.1$ Hz, 1H). ^{13}C NMR (101 MHz, DMSO- d_6) δ 162.4, 147.8, 145.9, 130.9, 130.1, 126.0, 119.9, 114.8.

5.1f. *N*-guanyl-*O*-methylisourea hydroacetate.⁵²⁹



In methanol (200 mL) was mixed dicyandiamide (43.1 g, 0.51 mol) and $Cu(AcO)_2 \cdot H_2O$ (50 g, 0.25 mol), and the mixture was refluxed for 2 h. After cooling down, the precipitate was filtered off and mixed with 150 mL of distilled water. H_2S was introduced into the suspension until Cu^{2+} is not observed in the solution. CuS was filtered off and water was removed *in vacuo* and treated with isopropanol to give the desired product. White, crystalline solid (40.5 g, 46%). 1H NMR (400 MHz, DMSO- d_6) δ 9.83 (br s, 2H), 7.42 (br s, 4H), 3.63 (s, 3H), 1.66 (s, 3H).

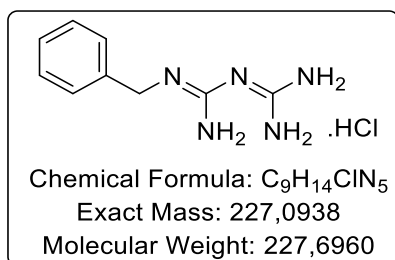
Procedures for the synthesis of the biguanides.

General procedure A: *N*-carbamimidoyl-1*H*-pyrazole-1-carboximidamide (1.14 g, 5.5 mmol, 1.0 eq.) and the corresponding amine (8.25 mmol, 1.5 eq.) were dissolved in pyridine (5.5 mL) and the solution was stirred at 40 °C for 6-24 h. The solution was cooled to room temperature, the precipitate was filtered and washed with diethyl ether to obtain a white powder. In some cases, to promote precipitation, pyridine was evaporated with toluene and triturated with diethyl ether to get a solid product.

General procedure B: *N*-carbamimidoyl-1*H*-pyrazole-1-carboximidamide (1.14 g, 5.5 mmol, 1.0 eq.) and the corresponding amine (8.25 mmol, 1.5 eq.) were dissolved in water (5.5 mL) and the solution was stirred at 40 °C for 6-24 h. Water was evaporated and the residue was triturated with acetone, filtered and washed with acetone and diethyl ether.

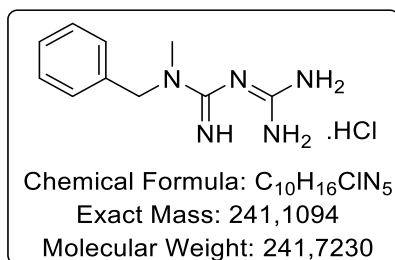
General procedure C: *S*-methyl-guanylisothiuronium iodide (1.43 g, 5.5 mmol, 1.0 eq.) and the corresponding amine (8.25 mmol, 1.5 eq.) were dissolved in a 1/1 pyridine/toluene mixture (5.5 mL) and the solution was stirred at 40 °C for 6 h. The solution was cooled to room temperature, the solvent was removed *in vacuo*, and the residue was triturated with isopropanol, filtered and washed by diethyl ether to obtain a white powder.

5.2a. Benzylbiguanide hydrochloride



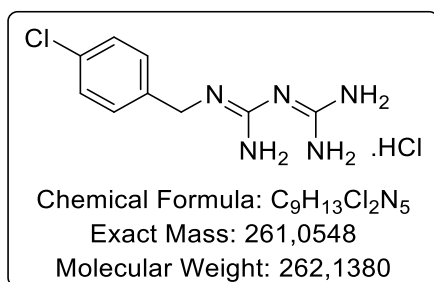
Procedure A: Yield, 93%; **Procedure B:** Yield, 96%; **Procedure C:** (hydroiodide salt) Yield, 82%; HPLC (λ_{254}), t_R : 11.5 min (method 5); ¹H NMR (400 MHz, DMSO-*d*₆) δ 7.96 – 7.74 (s, 1H), 7.42 – 7.21 (m, 5H), 7.01 (s, 6H), 4.35 (d, *J* = 4.8 Hz, 2H). Data in accordance with the literature.⁵¹²

5.2b. 1-benzyl-1-methylbiguanide hydrochloride



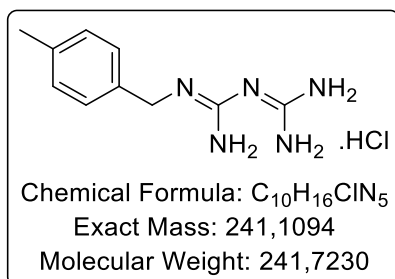
Procedure A: Yield, 69%; **Procedure B:** Yield, 96%; HPLC (λ_{254}), t_R : 10.7 min (method 5); 1H NMR (400 MHz, $DMSO-d_6$) δ 7.41 – 7.32 (m, 4H), 7.28 (t, $J = 6.9$ Hz, 3H), 6.97 (s, 4H), 4.60 (s, 2H), 2.87 (s, 3H). Data in accordance with the literature.⁵¹²

5.2c. 1-(4-chlorobenzyl)biguanide hydrochloride



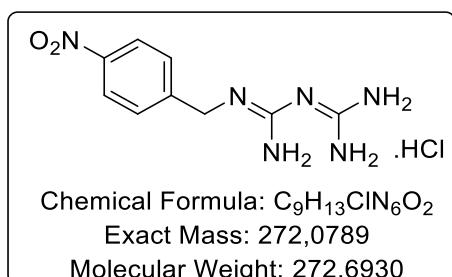
Procedure A: Yield, 86%; **Procedure B:** Yield, 75%; HPLC (λ_{254}), t_R : 11.2 min (method 5); 1H NMR (400 MHz, $DMSO-d_6$) δ 7.89 (br s, 1H), 7.43 – 7.30 (m, 4H), 7.03 (s, 6H), 4.33 (d, $J = 4.2$ Hz, 2H). Data in accordance with the literature.^{550,551}

5.2d. 1-(4-methylbenzyl)biguanide hydrochloride



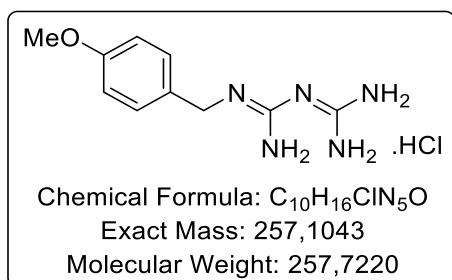
Procedure A: Yield, 87%; **Procedure B:** Yield, 70%; HPLC (λ_{254}), t_R : 10.9 min (method 5); 1H NMR (400 MHz, $DMSO-d_6$) δ 7.82 (br s, 1H), 7.19 (d, $J = 7.9$ Hz, 2H), 7.14 (d, $J = 7.9$ Hz, 2H), 7.01 (br s, 6H), 4.29 (d, $J = 5.9$ Hz, 2H), 2.28 (s, 3H). Data in accordance with the literature.^{551,552}

5.2e. 1-(4-nitrobenzyl)biguanide hydrochloride



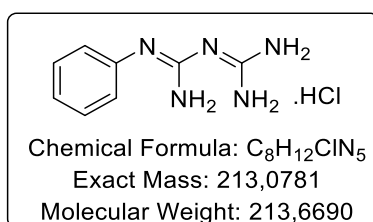
Procedure A: Yield, 90%; **Procedure B:** Yield, 93%; HRMS-ESI(*m/z*): [M+H]⁺ calc. for C₉H₁₃N₆O₂⁺, 237.10945; Found: 237.10876. HPLC (λ₂₅₄), *t*_R: 11.6 min (method 5); ¹H NMR (400 MHz, DMSO-*d*₆) δ 8.21 (d, *J* = 8.7 Hz, 2H), 8.00 (t, *J* = 6.2 Hz, 1H), 7.58 (d, *J* = 8.8 Hz, 2H), 7.07 (s, 6H), 4.50 (d, *J* = 6.1 Hz, 2H). ¹³C NMR (101 MHz, DMSO-*d*₆) δ 160.4, 158.4, 147.3, 146.5, 128.1 (2C), 123.4 (2C), 43.6.

5.2f. 1-(4-methoxybenzyl)biguanide hydrochloride



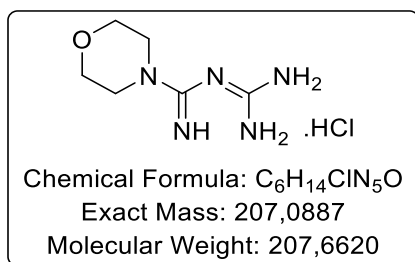
Procedure A: Yield, 95%; **Procedure B:** Yield, 82%; HPLC (λ₂₅₄), *t*_R: 11.6 min (method 5); ¹H NMR (400 MHz, DMSO-*d*₆) δ 7.80 (br s, 1H), δ 7.24 (d, *J* = 8.6 Hz, 1H), 7.01 (s, 4H), 6.89 (d, *J* = 8.6 Hz, 1H), 4.26 (d, *J* = 5.8 Hz, 1H), 3.73 (s, 2H). Data in accordance with the literature.⁵⁵³

5.2g. 1-Phenylbiguanide hydrochloride



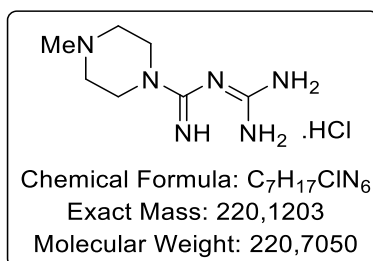
Procedure B: Yield, 68%; HPLC (λ₂₅₄), *t*_R: 12.8 min (method 5); ¹H NMR (200 MHz, DMSO-*d*₆) δ 9.91 (s, 1H), 7.50 – 7.00 (m, 10H). Data in accordance with the literature.⁵¹²

5.2h. Morpholine biguanide hydrochloride



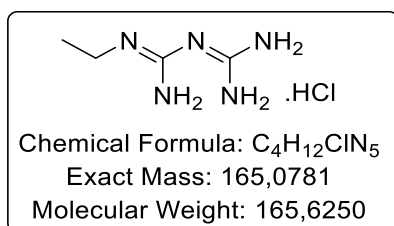
Procedure A: Yield, 83%; **Procedure B:** Yield, 91%; **Procedure C:** (hydroiodide salt) Yield, 82%; HPLC (λ_{254}), t_R : 15.7 min (method 5); ¹H NMR (400 MHz, DMSO-*d*₆) δ 7.39 (s, 2H), 7.02 (s, 4H), 3.58 (d, *J* = 4.6 Hz, 4H), 3.45 (d, *J* = 4.5 Hz, 4H). Data in accordance with the literature.⁵⁵⁴

5.2i. N-methylpiperazine biguanide hydrochloride



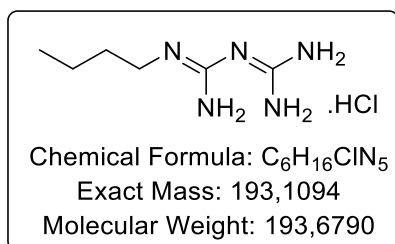
Procedure A: Yield, 83%; **Procedure B:** Yield, 96%; **Procedure C:** (hydroiodide salt) Yield, 97%; HPLC (λ_{254}), t_R : 3.99 min (method 5); ¹H NMR (400 MHz, DMSO-*d*₆) δ 7.35 (s, 2H), 6.96 (s, 4H), 3.44 (t, *J* = 5.0 Hz, 4H), 2.30 (t, *J* = 5.0 Hz, 4H), 2.17 (s, 3H). Data in accordance with the literature.⁵⁵⁵

5.2j. Ethylbiguanide hydrochloride



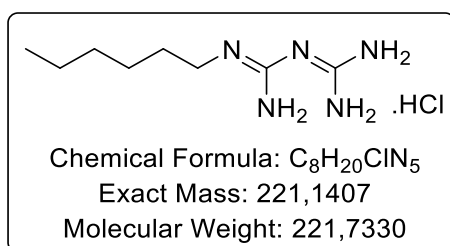
Procedure A: Yield, 75%; **Procedure B:** Yield, 82%; HPLC (λ_{254}), t_R : 15.7 min (method 5); ¹H NMR (400 MHz, DMSO-*d*₆) δ 7.46 (s, 1H), 6.88 (br s, 6H), 3.10 (dt, *J* = 11.4, 5.6 Hz, 2H), 1.05 (t, *J* = 7.2 Hz, 3H). Data in accordance with the literature, described without HCl form.⁵⁵⁶

5.2k. Butylbiguanide hydrochloride



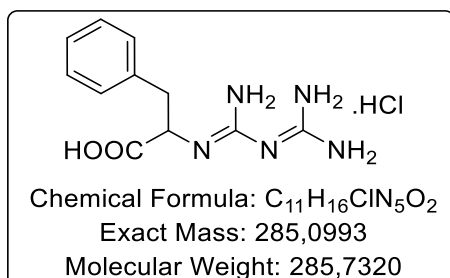
Procedure A: Yield, 86%; **Procedure B:** Yield, 77%; **Procedure C:** (hydroiodide salt) Yield, 54%; HPLC (λ_{254}), t_R : 12.1 min (method 5); ¹H NMR (400 MHz, DMSO-*d*₆) δ 7.50 (t, *J* = 5.6 Hz, 1H), 6.88 (br s, 6H), 3.07 (q, *J* = 6.5 Hz, 2H), 1.42 (p, *J* = 7.1 Hz, 2H), 1.35 – 1.25 (m, 2H), 0.87 (t, *J* = 7.3 Hz, 3H). Data in accordance with the literature.^{516,557}

5.2l. Hexylbiguanide hydrochloride



Procedure A: Yield, 86 %; **Procedure B:** Yield, 92%; HPLC (λ_{254}), t_R : 9.96 min (method 5); ¹H NMR (400 MHz, DMSO-*d*₆) δ 7.58 (br s, 1H), 6.97 (br s, 6H), 3.06 (t, *J* = 7.1 Hz, 2H), 1.52 – 1.34 (m, 2H), 1.26 (d, *J* = 11.2 Hz, 6H), 0.85 (t, *J* = 6.6 Hz, 3H). Data in accordance with the literature, described in free base form.⁵⁵⁸

5.2m. (N-carbamimidoylcarbamimidoyl)phenylalanine



N-carbamimidoyl-1*H*-pyrazole-1-carboximidamide (1.14 g, 5.5 mmol, 1.0 eq.), DIPEA (0.96 mL, 5.50 mmol, 1.0 eq.) and L-phenylalanine (908 mg, 5.50 mmol, 1.0 eq.) were dissolved in water (5.5 mL) and the solution was stirred at 40 °C for 24 h. Water was evaporated and the residue was triturated with

10 mL of ethanol. The precipitate was collected and washed with ethanol and diethyl ether. White, crystalline solid (735 mg, 53%). HRMS-ESI(m/z): $[M+H]^+$ calc. for $C_{11}H_{16}N_5O_2^+$, 250.12985; Found: 250.12911. HPLC (λ_{254}), t_R : 8.5 min (method 5); 1H NMR (400 MHz, $DMSO-d_6$) δ 7.48 (br s, 3H), 7.32 – 7.20 (m, 4H), 7.19 – 6.71 (m, 4H), 4.11 (br s, 1H), 3.18 (br s, 1H), 2.84 (br s, 1H). ^{13}C NMR (101 MHz, $DMSO-d_6$) δ 173.9, 161.9, 159.5, 139.9, 129.0 (2C), 127.8 (2C), 125.7, 59.3, 37.2.

STABILITY ASSAYS

MCK256

HPLC analyses

HPLC analyses were performed on a JASCO PU-2089 apparatus with Supelco analytical column Ascentis Express C18, 100 mm × 46 mm 5 μ. Eluent A: water with 1‰ formic acid. Eluent B: CH₃CN with 1‰ formic acid. Method used: 100% A over 2 min, 100% A to 60% A over 8 min, 60% A for 4 min then from 60% A to 100% A over 1 min (15 min in total).

Chemical stability in buffered solutions.

2 mg of MCK256 was dissolved in 200 μL DMSO and diluted in the corresponding buffer solution, pH 0.9, 7.4 and 8.4 (1.8 mL). These solutions were stored at 25 °C and analysed by HPLC at 0, 1, 2, 7, 9 and 14 days. The areas of the compound peak at 254 nm were reported at the different times and pH.

NRPa-308 Stability assays.

HPLC analyses

HPLC analyses were performed on a JASCO PU-2089 apparatus with Supelco analytical column Ascentis Express C18, 100 mm × 46 mm 5 μ. Eluent A: water with 1‰ formic acid. Eluent B: CH₃CN with 1‰ formic acid. Method used: 0%B to 100%B over 4 min, then 100%B for 4 min (8 min in total).

Chemical stability in buffered solutions.

1 mg of NRP-a308 was dissolved in 200 μL DMSO and diluted in the corresponding buffer solution, pH 0.9, 7.4 and 8.4 (1.8 mL). These solutions were stored at 25 °C or 37 °C and analysed by HPLC at 0, 1, 2, 5, 6, 7, 12 and 16 days. The areas of the compound peak at 280 nm were reported at the different times and pH.

NRPa-308 stability and accumulation in cancer cells.

MDA-MB231 and BT549 cells were purchased from the American Type Culture Collection. Cells were grown in DMEM supplemented with 7 or 10% FCS plus 1% of non-essential amino-acid at 37 °C in a humidified atmosphere containing 5% CO₂ in the presence of 2 μM of NRPa-308. After three days, the supernatant was discarded, the cells were washed with 10mL of PBS from Dutscher and they were then lysed with 1mL of methanol. The methanolic lysates were extracted with CHCl₃/MeOH, 9/1, v/v, dried with MgSO₄ and the solvents were evaporated. The residues were dissolved in 1 mL MeOH and quantitatively analysed by HPLC thanks to a calibration curve.

BIOLOGICAL ASSAYS

Cell viability

XTT

Cells were incubated in a 96-well plate with different effectors for 48 h. Fifty microliters of sodium 3'-[1-phenylaminocarbonyl]-3,4-tetrazolium]-bis(4-methoxy-6-nitro) benzene sulfonic acid hydrate (XTT) reagent was added to each well. The assay is based on the cleavage of the yellow tetrazolium salt XTT to form an orange formazan dye by metabolically active cells. This bio-reduction occurs in viable cells only and is related to NAD(P)H production through glycolysis. Therefore, the amount of formazan dye measured at 490 nm directly correlated with the number of metabolically active cells reflecting cell proliferation and viability. Each assay was performed in quadruplicate.

Migration assay

CXCL8 stimulated chemotaxis assays were monitored using modified Boyden chambers containing polycarbonate membranes (8- μ m pores, Transwell; Corning, Sigma). Cells were seeded onto the upper side of the filters and chambers were placed on 24-well plates containing CXCL8 (50 ng/ml). Cell migration was followed for 24 h at 37 °C in 5% CO₂. Migratory cells on the lower membrane surface were fixed in 3% paraformaldehyde, stained with 0.1% crystal violet.

Zebrafish neovascular AMD model

All animal experiments were approved by the IRCAN Experimental Animal Ethical Committee. Transgenic zebrafishes (fli: EGFP, blood vessels labelled in green) embryos were raised at 28 °C under standard experimental conditions. At the age of 24 hpf, they were incubated in aquarium water containing 0.2 mmol/L 1-phenyl-2-thio-urea (PTU, Sigma). At 48-hpf, they were dechorionated with a pair of sharp-tip forceps and anesthetized with 0.04 mg/mL of tricaine (MS-222, Sigma). Zebrafish embryos were immediately transferred into PTU aquarium water in normoxia (CT) or in 5% oxygen hypoxia in the presence of treatment for 24 and 48 hours. Blood vessel in eyes were analyzed using a fluorescent confocal microscope (Nikon Eclipse 90). The area of blood vessel in retina were quantified by ImageJ software.

Quantitative Real-Time PCR (qPCR) experiments

One microgram of total RNA was used for the reverse transcription, using the QuantiTect Reverse Transcription kit (QIAGEN, Hilden, Germany), with blend of oligo (dT) and random primers to prime first-strand synthesis. SYBR master mix plus (Eurogentec) was used for qPCR. The mRNA level was normalized to 36B4 mRNA.

Immunoblotting

Cells were lysed by Laemmli 1.5x. For 100 mL of Laemmli 1.5x in buffer containing 20% SDS, 100% glycerol, 15 mL of Tris 1M pH 6.8 and 51.25 mL of water at 37 °C. 10 et 50 µg of proteins separated on 10% SDS-PAGE, transferred onto a PVDF membrane and then exposed to the appropriate MCK. Proteins were visualized with the ECL system using horseradish peroxidase-conjugated anti-rabbit or anti-mouse antibodies.

ROS assay

ARPE cells were treated with MCK at 5 µM for 30 min. H₂O₂ was added directly over the cells, without rinsing the medium. Treat cells at 200 µM for 2 h. DCF-DA (2',7'-Dichlorofluorescein diacetate) was added over cells at 10 µM for 30 min. After 30min aspirate the medium, rinse PBS, then trypsinize with 100 µL of 1x trypsin. Stop the trypsin by rinsing in 3-4 mL of PBS and centrifuge at 400 g for 5 min. Resuspend in 200 µL of Facs Buffer (0.5% BSA, 2 mM EDTA). Switch to cytometry Cytoflex. The DCF-DA goes out in the FITC channel.

REFERENCES

1. Gohdes, D. M., Balamurugan, A., Larsen, B. A. & Maylahn, C. Age-related eye diseases: An emerging challenge for public health professionals. *Prev. Chronic Dis.* **2**, 2–7 (2005).
2. Kumar-Singh, R. The role of complement membrane attack complex in dry and wet AMD - From hypothesis to clinical trials. *Exp. Eye Res.* **184**, 266–277 (2019).
3. Forrester, J. V., Dick, A. D., McMenamin, P. G., Roberts, F. & Pearlman, E. Biochemistry and cell biology. in *The Eye* 157-268.e4 (Elsevier, 2016). doi:10.1016/b978-0-7020-5554-6.00004-6.
4. Cholkar, K., Dasari, S. R., Pal, D. & Mitra, A. K. Eye: Anatomy, physiology and barriers to drug delivery. in *Ocular Transporters and Receptors: Their Role in Drug Delivery* 1–36 (Elsevier Ltd., 2013). doi:10.1533/9781908818317.1.
5. Boll, P. F. On the anatomy and physiology of the retina. *Vision Res.* **17**, 1249–1265 (1977).
6. Kuszak, J. R., Zoltoski, R. K. & Tiedemann, C. E. Development of lens sutures. *Int. J. Dev. Biol.* **48**, 889–902 (2004).
7. Nickla, D. L. & Wallman, J. The multifunctional choroid. *Progress in Retinal and Eye Research* vol. 29 144–168 (2010).
8. Mauser, M. W. Exploring the anatomy of your own eye. *Am. Biol. Teach.* **73**, 28–33 (2011).
9. Bird, A. C. & Bok, D. Why the macula? *Eye* **32**, 858–862 (2018).
10. Moschos, M. M., Nitoda, E., Chatziralli, I. P. & Demopoulos, C. A. Age-related macular degeneration: Pathogenesis, genetic background, and the role of nutritional supplements. *J. Chem.* **2014**, (2014).
11. Kocur, I. & Resnikoff, S. Visual impairment and blindness in Europe and their prevention. *Br. J. Ophthalmol.* **86**, 716–722 (2002).
12. Cheng, K. J., Hsieh, C. M., Nepali, K. & Liou, J. P. Ocular Disease Therapeutics: Design and Delivery of Drugs for Diseases of the Eye. *J. Med. Chem.* **63**, 10533–10593 (2020).
13. Prokofyeva, E. & Zrenner, E. Epidemiology of major eye diseases leading to blindness in Europe: A literature review. *Ophthalmic Res.* **47**, 171–188 (2012).
14. Fine, S. L., Berger, J. W., Maguire, M. G. & Ho, A. C. Age-Related Macular Degeneration. *N Engl J Med* **342**, 483–492 (2000).
15. Early Treatment Diabetic Retinopathy Study Design and Baseline Patient Characteristics: ETDRS Report Number 7. *Ophthalmology* **98**, 741–756 (1991).
16. Klein, M. L. *et al.* Retinal Precursors and the Development of Geographic Atrophy in Age-Related Macular Degeneration. *Ophthalmology* **115**, 1026–1031 (2008).
17. Pichi, F., Abboud, E. B., Ghazi, N. G. & Khan, A. O. Fundus autofluorescence imaging in hereditary retinal diseases. *Acta Ophthalmol.* **96**, e549–e561 (2018).
18. Prati, F., Mallus, M. T., Imola, F. & Albertucci, M. Optical coherence tomography (OCT). *Catheter. Cardiovasc. Interv. A Knowledge-Based Approach* **254**, 363–375 (2013).
19. Ly, A., Nivison-Smith, L., Assaad, N. & Kalloniatis, M. Infrared reflectance imaging in age-related

- macular degeneration. *Ophthalmic Physiol. Opt.* **36**, 303–316 (2016).
20. Bowes Rickman, C., Farsiu, S., Toth, C. A. & Klingeborn, M. Dry age-related macular degeneration: Mechanisms, therapeutic targets, and imaging. *Investig. Ophthalmol. Vis. Sci.* **54**, (2013).
 21. Zhang, K., Zhang, L. & Weinreb, R. N. Ophthalmic drug discovery : novel targets and mechanisms for retinal diseases and glaucoma. *Nat. Rev. Drug Discov.* **11**, (2012).
 22. Gheorghe, A., Mahdi, L. & Musat, O. AGE-RELATED MACULAR DEGENERATION. *Rom. J. Ophthalmol.* **59**, 74–77 (2015).
 23. Inana, G. *et al.* RPE phagocytic function declines in age-related macular degeneration and is rescued by human umbilical tissue derived cells. *J. Transl. Med.* **16**, 1–15 (2018).
 24. Mehta, S. Age-Related Macular Degeneration. *Primary Care - Clinics in Office Practice* vol. 42 377–391 (2015).
 25. De Jong, P. T. V. M. Elusive drusen and changing terminology of AMD review-article. *Eye* **32**, 904–914 (2018).
 26. Jonasson, F. *et al.* Prevalence of age-related macular degeneration in old persons: Age, gene/environment susceptibility Reykjavik study. *Ophthalmology* **118**, 825–830 (2011).
 27. Al-Zamil, W. M. & Yassin, S. A. Recent developments in age-related macular degeneration: A review. *Clin. Interv. Aging* **12**, 1313–1330 (2017).
 28. Jong, P. T. V. M. de. Mechanisms of disease Age-Related Macular Degeneration. *new engl J. Med.* **355**, 1474–1485 (2006).
 29. Ambati, J. & Fowler, B. J. Mechanisms of age-related macular degeneration. *Neuron* **75**, 26–39 (2012).
 30. Bird, A. C. & Bird, A. C. Therapeutic targets in age-related macular disease Find the latest version : Review series Therapeutic targets in age-related macular disease. *J. Clin. Invest.* **120**, 3033–3041 (2010).
 31. Sadda, S. R. *et al.* Consensus Definition for Atrophy Associated with Age-Related Macular Degeneration on OCT: Classification of Atrophy Report 3. *Ophthalmology* **125**, 537–548 (2018).
 32. Salvi, S. M., Akhtar, S. & Currie, Z. Ageing changes in the eye. *Postgrad. Med. J.* **82**, 581–587 (2006).
 33. Xu, Q., Cao, S., Rajapakse, S. & Matsubara, J. A. Understanding AMD by analogy: Systematic review of lipid-related common pathogenic mechanisms in AMD, AD, AS and GN. *Lipids Health Dis.* **17**, 1–13 (2018).
 34. Ashraf, M. & Souka, A. A. R. Aflibercept in age-related macular degeneration: Evaluating its role as a primary therapeutic option. *Eye* **31**, 1523–1536 (2017).
 35. Li, J. Q. *et al.* Prevalence, incidence and future projection of diabetic eye disease in Europe: a systematic review and meta-analysis. *Eur. J. Epidemiol.* **35**, 11–23 (2020).
 36. Schachat, A. P. *et al.* Laser Photocoagulation for Juxtafoveal Choroidal Neovascularization: Five-Year Results From Randomized Clinical Trials. *Arch. Ophthalmol.* **112**, 500–509 (1994).
 37. Stevens, G. A. *et al.* Global prevalence of vision impairment and blindness: Magnitude and temporal trends, 1990-2010. *Ophthalmology* **120**, 2377–2384 (2013).

38. Hoyng, C. B. & Lechanteur, Y. T. E. Risk factors for progression of age-related macular degeneration. *40*, 140–170 (2020).
39. Hernández-Zimbrón, L. F. *et al.* Age-Related Macular Degeneration: New Paradigms for Treatment and Management of AMD. *Oxid. Med. Cell. Longev.* **2018**, (2018).
40. Velez-montoya, R. *et al.* Current knowledge and trends in age-related macular degeneration. *Retin. J. Retin. Vit. Dis.* **33**, 1487–1502 (2013).
41. Cheung, L. K. & Eaton, A. Age-related macular degeneration. *Pharmacotherapy* **33**, 838–855 (2013).
42. Crabb, J. W. *et al.* Drusen proteome analysis: An approach to the etiology of age-related macular degeneration. *Proc. Natl. Acad. Sci. U. S. A.* **99**, 14682–14687 (2002).
43. Wang, A. L. *et al.* Autophagy, exosomes and drusen formation in age-related macular degeneration. *Autophagy* **5**, 563–564 (2009).
44. Wang, L. *et al.* Abundant lipid and protein components of drusen. *PLoS One* **5**, 1–12 (2010).
45. Curcio, C. A. & Johnson, M. Structure, Function, and Pathology of Bruch's Membrane. *Anat. Rec. A. Discov. Mol. Cell. Evol. Biol.* **284**, 544–549 (2013).
46. Rudolf, M. *et al.* Prevalence and morphology of druse types in the macula and periphery of eyes with age-related maculopathy. *Investig. Ophthalmol. Vis. Sci.* **49**, 1200–1209 (2008).
47. Hageman, G. S. *et al.* An integrated hypothesis that considers drusen as biomarkers of immune-mediated processes at the RPE-Bruch's membrane interface in aging and age-related macular degeneration. *Prog. Retin. Eye Res.* **20**, 705–732 (2001).
48. Wang, A. L. *et al.* Autophagy and exosomes in the aged retinal pigment epithelium: Possible relevance to drusen formation and age-related macular degeneration. *PLoS One* **4**, (2009).
49. Van Lookeren Campagne, M., Lecouter, J., Yaspan, B. L. & Ye, W. Mechanisms of age-related macular degeneration and therapeutic opportunities. *J. Pathol.* **232**, 151–164 (2014).
50. Zhao, Y. *et al.* Beta-Amyloid Precursor Protein (β APP) Processing in Alzheimer's Disease (AD) and Age-Related Macular Degeneration (AMD). *Mol. Neurobiol.* **52**, 533–544 (2015).
51. Farzdaghi, M. & Ebrahimi, K. Role of the choroid in age-related macular degeneration: A current review. *J. Ophthalmic Vis. Res.* **14**, 78 (2019).
52. Arya, M., Sabrosa, A. S., Duker, J. S. & Waheed, N. K. Choriocapillaris changes in dry age-related macular degeneration and geographic atrophy: a review. *Eye Vis.* **5**, 1–7 (2018).
53. Leung, E. & Landa, G. Update on current and future novel therapies for dry age-related macular degeneration. *Expert Rev. Clin. Pharmacol.* **6**, 565–579 (2013).
54. Biesemeier, A., Taubitz, T., Julien, S., Yoeruek, E. & Schraermeyer, U. Choriocapillaris breakdown precedes retinal degeneration in age-related macular degeneration. *Neurobiol. Aging* **35**, 2562–2573 (2014).
55. Lengyel, I. *et al.* Association of drusen deposition with choroidal intercapillary pillars in the aging human eye. *Investig. Ophthalmol. Vis. Sci.* **45**, 2886–2892 (2004).
56. Guyer, D. R. *et al.* Subfoveal Choroidal Neovascular Membranes in Age-Related Macular Degeneration: Visual Prognosis in Eyes With Relatively Good Initial Visual Acuity. *Arch. Ophthalmol.* **104**, 702–705 (1986).

57. Wong, T. *et al.* The Natural History and Prognosis of Neovascular Age-Related Macular Degeneration. A Systematic Review of the Literature and Meta-analysis. *Ophthalmology* **115**, 116–127 (2008).
58. Masse, H. *et al.* Vue d'ensemble des pratiques médicales dans la DMLA exsudative en France. *J. Fr. Ophtalmol.* **39**, 40–47 (2016).
59. Terasaki, H. *et al.* TNF- α Decreases VEGF Secretion in Highly Polarized RPE Cells but Increases It in Non-Polarized RPE Cells Related to Crosstalk between JNK and NF- κ B Pathways. *PLoS One* **8**, 1–12 (2013).
60. Constable, I., Shen, W. Y. & Rakoczy, E. Emerging biological therapies for age-related macula degeneration. *Expert Opinion on Biological Therapy* vol. 5 1373–1385 (2005).
61. Blaauwgeers, H. G. T. *et al.* Polarized vascular endothelial growth factor secretion by human retinal pigment epithelium and localization of vascular endothelial growth factor receptors on the inner choriocapillaris: Evidence for a trophic paracrine relation. *Am. J. Pathol.* **155**, 421–428 (1999).
62. Marneros, A. G. *et al.* Vascular endothelial growth factor expression in the retinal pigment epithelium is essential for choriocapillaris development and visual function. *Am. J. Pathol.* **167**, 1451–1459 (2005).
63. Wang, H. & Elizabeth Hartnett, M. Regulation of signaling events involved in the pathophysiology of neovascular AMD. *Mol. Vis.* **22**, 189–202 (2016).
64. Waugh, N. *et al.* Treatments for dry age-related macular degeneration and stargardt disease: A systematic review. *Health Technol. Assess. (Rockv).* **22**, 1–167 (2018).
65. Hussain, R. M. *et al.* Pharmacotherapy of retinal disease with visual cycle modulators. *Expert Opin. Pharmacother.* **00**, 1–11 (2018).
66. Saad, L. & Washington, I. Can Vitamin A be Improved to Prevent Blindness due to Age-Related Macular Degeneration, Stargardt Disease and Other Retinal Dystrophies? *Adv. Exp. Med. Biol.* **854**, 355–361 (2016).
67. Kubota, R. *et al.* Safety and effect on rod function of ACU-4429, a novel small-molecule visual cycle modulator. *Retina* **32**, 183–188 (2012).
68. Kubota, R. Y. O., Al-fayoumi, S. & Mallikaarjun, S. PHASE 1, DOSE-RANGING STUDY OF EMIXUSTAT HYDROCHLORIDE (ACU-4429), A NOVEL VISUAL CYCLE MODULATOR, IN HEALTHY VOLUNTEERS. *Retin. J. Retin. Vit. Dis.* **34**, 603–609 (2014).
69. Bavik, C. *et al.* Visual cycle modulation as an approach toward preservation of retinal integrity. *PLoS One* **10**, 1–16 (2015).
70. Zhang, J. *et al.* Molecular pharmacodynamics of emixustat in protection against retinal degeneration. *J. Clin. Invest.* **125**, 2781–2794 (2015).
71. Safety and Efficacy Assessment Treatment Trials of Emixustat Hydrochloride. *ClinicalTrials.gov* <https://clinicaltrials.gov/ct2/show/NCT01802866?term=NCT01802866&cond=AMD&draw=2&rank=1> (2017) doi:NCT01802866.
72. Rosenfeld, P. J. *et al.* Emixustat Hydrochloride for Geographic Atrophy Secondary to Age-Related Macular Degeneration: A Randomized Clinical Trial. *Ophthalmology* **125**, 1556–1567 (2018).
73. Pharmacokinetic and Pharmacodynamic Study of Emixustat in Subjects With Geographic

- Atrophy Associated With Dry Age-Related Macular Degeneration. *ClinicalTrials.gov* <https://clinicaltrials.gov/ct2/show/NCT02130531?term=NCT02130531&cond=AMD&draw=2&rank=1> (2016) doi:NCT02130531.
74. Study of the Safety, Tolerability, Pharmacokinetics and Pharmacodynamics of ACU-4429 in Subjects With Geographic Atrophy. *ClinicalTrials.gov* <https://clinicaltrials.gov/ct2/show/NCT01002950?term=NCT01002950&cond=AMD&draw=2&rank=1> (2014) doi:NCT01002950.
 75. Pharmacodynamic Study of Emixustat Hydrochloride in Subjects With Macular Atrophy Secondary to Stargardt Disease. *ClinicalTrials.gov* <https://clinicaltrials.gov/ct2/show/NCT03033108?term=NCT03033108&cond=AMD&draw=2&rank=1> (2019) doi:NCT03033108.
 76. Dugel, P. U. *et al.* Phase II, randomized, placebo-controlled, 90-day study of emixustat hydrochloride in geographic atrophy associated with dry age-related macular degeneration. *Retina* **35**, 1173–1183 (2015).
 77. Hussain, R. M. *et al.* Stargardt macular dystrophy and evolving therapies. *Expert Opin. Biol. Ther.* **0**, 1 (2018).
 78. Berni, R. & Formelli, F. In vitro interaction of fenretinide with plasma retinol-binding protein and its functional consequences. *FEBS Lett.* **308**, 43–45 (1992).
 79. Malpeli, G., Folli, C. & Berni, R. Retinoid binding to retinol-binding protein and the interference with the interaction with transthyretin. *Biochim. Biophys. Acta - Protein Struct. Mol. Enzymol.* **1294**, 48–54 (1996).
 80. Mata, N. L. *et al.* Investigation of oral fenretinide for treatment of geographic atrophy in age-related macular degeneration. *Retina* **33**, 498–507 (2013).
 81. Dobri, N. *et al.* A1120, a nonretinoid RBP4 antagonist, inhibits formation of cytotoxic bisretinoids in the animal model of enhanced retinal lipofuscinogenesis. *Investig. Ophthalmol. Vis. Sci.* **54**, 85–95 (2013).
 82. Edgar, M., Lichter, J. & Mata, N. L. Compositions and methods for treating ophthalmic conditions cross-reference. (2012) doi:WO2012078525A2.
 83. Study of Fenretinide in the Treatment of Geographic Atrophy Associated With Dry Age-Related Macular Degeneration. *ClinicalTrials.gov* <https://clinicaltrials.gov/ct2/show/NCT00429936?term=Fenretinide&cond=AMD&draw=2&rank=1> (2010) doi:NCT00429936.
 84. Holz, F. G., Strauss, E. C., Schmitz-Valckenberg, S. & Van Lookeren Campagne, M. Geographic atrophy: Clinical features and potential therapeutic approaches. *Ophthalmology* **121**, 1079–1091 (2014).
 85. Phase 1 Safety Study of ALK-001 in Healthy Volunteers. *ClinicalTrials.gov* <https://clinicaltrials.gov/ct2/show/NCT02230228?term=ALK-001&cond=AMD&draw=2&rank=4> (2015) doi:NCT02230228.
 86. Phase 3 Study of ALK-001 in Geographic Atrophy. *ClinicalTrials.gov* <https://clinicaltrials.gov/ct2/show/NCT03845582> (2020) doi:NCT03845582.
 87. Ding, J. D. *et al.* Anti-amyloid therapy protects against retinal pigmented epithelium damage and vision loss in a model of age-related macular degeneration. *Proc. Natl. Acad. Sci. U. S. A.* **108**, 279–287 (2011).

88. Lashkari, K. *et al.* A monoclonal antibody targeting amyloid β (A β) restores complement factor I bioactivity : Potential implications in age-related macular degeneration and Alzheimer ' s disease. *PLoS One* **13**, 1–19 (2018).
89. Damico, F. M. *et al.* New approaches and potential treatments for dry age-related macular degeneration. *Arq Bras Oftalmol.* **75**, 71–75 (2012).
90. Safety And Tolerability Study Of RN6G In Subjects With Advanced Dry, Age-Related Macular Degeneration Including Geographic Atrophy. *ClinicalTrials.gov* <https://clinicaltrials.gov/ct2/show/NCT01003691?term=RN6G&cond=AMD&draw=2&rank=2> (2013) doi:NCT01003691.
91. Safety And Tolerability Study Of RN6G In Patients With Dry, Age-Related Macular Degeneration. *ClinicalTrials.gov* <https://clinicaltrials.gov/ct2/show/NCT00877032?term=RN6G&cond=AMD&draw=2&rank=3> (2015) doi:NCT00877032.
92. Efficacy, Safety And Tolerability Study Of RN6G In Subjects With Geographic Atrophy Secondary to Age-related Macular Degeneration. *ClinicalTrials.gov* <https://clinicaltrials.gov/ct2/show/NCT01577381?term=RN6G&cond=AMD&draw=2&rank=1> (2016) doi:NCT01577381.
93. Andreasen, N. *et al.* First administration of the Fc-attenuated anti- β amyloid antibody GSK933776 to patients with mild Alzheimer's disease: A randomized, placebo-controlled study. *PLoS One* **10**, 1–15 (2015).
94. Pharmacokinetic (PK) Study of GSK933776 in Healthy Volunteers. *ClinicalTrials.gov* <https://clinicaltrials.gov/ct2/show/NCT02033668?term=GSK933776&cond=AMD&draw=2&rank=2> (2017) doi:NCT02033668.
95. Clinical Study to Investigate Safety and Efficacy of GSK933776 in Adult Patients With Geographic Atrophy Secondary to Age-related Macular Degeneration. *ClinicalTrials.gov* <https://clinicaltrials.gov/ct2/show/NCT01342926?term=GSK933776&cond=AMD&draw=2&rank=1> (2017) doi:NCT01342926.
96. Rosenfeld, P. J. *et al.* A Randomized Phase 2 Study of an Anti–Amyloid β Monoclonal Antibody in Geographic Atrophy Secondary to Age-Related Macular Degeneration. *Ophthalmol. Retin.* **2**, 1028–1040 (2018).
97. Booi, J. C., Baas, D. C., Beisekeeva, J., Gorgels, T. G. M. F. & Bergen, A. A. B. The dynamic nature of Bruch's membrane. *Prog. Retin. Eye Res.* **29**, 1–18 (2010).
98. Lewis, P. A. & Woller, W. H. Therapeutic formulation and methods of treatment. (2012) doi:WO2013188217A1.
99. U.S. Food and Drug Administration. *Apresoline hydrochloride*. (1997).
100. Chiou, B. G. Is Dry AMD Treatable ? *Retin. Today* **1101**, 69–71 (2012).
101. A Pilot Study of the Safety of MC-1101 in Both Normal Volunteers and Patients With Early Dry AMD. *ClinicalTrials.gov* <https://clinicaltrials.gov/ct2/show/NCT01013376?term=MC-1101&cond=AMD&draw=2&rank=1> (2009) doi:NCT01013376.
102. Safety Study of a Topical Treatment for Dry Age Related Macular Degeneration. *ClinicalTrials.gov* <https://clinicaltrials.gov/ct2/show/NCT01922128?term=MC-1101&cond=AMD&draw=2&rank=4> (2014).
103. Efficacy and Safety Study of MC-1101 1% TID in the Treatment of Nonexudative Age-Related

- Macular Degeneration. *ClinicalTrials.gov*
<https://clinicaltrials.gov/ct2/show/NCT01601483?term=MC-1101&cond=AMD&draw=2&rank=3> (2014) doi:NCT01601483.
104. Pemp, B. *et al.* The effects of moxaverine on ocular blood flow in patients with age-related macular degeneration or primary open angle glaucoma and in healthy control subjects. *Acta Ophthalmol.* **90**, 139–145 (2012).
 105. Resch, H. *et al.* Effect of systemic moxaverine on ocular blood flow in humans. *Acta Ophthalmol.* **87**, 731–735 (2009).
 106. An Open Study Comparing the Effects of Moxaverine on Ocular Blood Flow in Patients With Age- Related Macular Degeneration, Primary Open Angle Glaucoma and Healthy Control Subjects. *ClinicalTrials.gov*
<https://clinicaltrials.gov/ct2/show/NCT00709449?term=Moxaverine&cond=AMD&draw=2&rank=1> (2009) doi:NCT00709449.
 107. Metelitsina, T. I., Grunwald, J. E., DuPont, J. C., Ying, G. shuang & Liu, C. Effect of viagra on retinal vein diameter in AMD patients. *Exp. Eye Res.* **83**, 128–132 (2006).
 108. Effects of Sildenafil on Choroidal Thickness in AMD. *ClinicalTrials.gov*
<https://clinicaltrials.gov/ct2/show/NCT01830790?term=NCT01830790&draw=2&rank=1> (2015) doi:NCT01830790.
 109. Vuong;, V. S. *et al.* Effect of Sildenafil Citrate on Choroidal Thickness in Age-Related Macular Degeneration. *IOVS, ARVO Journals* **58**, (2017).
 110. Yiu, G. *et al.* Vascular Response to Sildenafil Citrate in Aging and Age-Related Macular Degeneration. *Sci. Rep.* **9**, 1–9 (2019).
 111. Kaszuba-Bartkowiak, K., Nowak, M. S., Jurowski, P. & Goś, R. The role of trimetazidine in the protection of the retina. *Arch. Med. Sci.* **3**, (2007).
 112. Villa, R. F., Benzi, G. & Curti, D. The effect of ischemia and pharmacological treatment evaluated on synaptosomes and purified mitochondria from rat cerebral cortex. *Biochem. Pharmacol.* **30**, 2399–2408 (1981).
 113. Nowak, M. S. *et al.* Protective effect on visual functions of long-term use of trimetazidine in treatment of primary open angle glaucoma and degenerative myopia. *Arch. Med. Sci.* **3**, 152–156 (2007).
 114. Cohen, S. Y. *et al.* Randomized clinical trial france DMLA2: Effect of trimetazidine on exudative and nonexudative age-related macular degeneration. *Retina* **32**, 834–843 (2012).
 115. Nazari, H. *et al.* Stem cell based therapies for age-related macular degeneration: The promises and the challenges. *Prog. Retin. Eye Res.* **48**, 1–39 (2015).
 116. KOKKINAKI, M., SAHIBZADA, N. & GOLESTANEH, N. Human Induced Pluripotent Stem-Derived Retinal Pigment Polarized Vascular Endothelial Growth Factor Secretion , and Gene Expression Pattern Similar to Native RPE. *Stem Cells* **29**, 825–835 (2011).
 117. Bracha, P., Moore, N. A. & Ciulla, T. A. Induced pluripotent stem cell-based therapy for age-related macular degeneration. *Expert Opin. Biol. Ther.* **17**, 1113–1126 (2017).
 118. Surendran, H., Rathod, R. J. & Pal, R. Generation of Transplantable Retinal Pigmented Epithelial (RPE) Cells for Treatment of Age-Related Macular Degeneration (AMD). *Methods Mol. Biol.* (2018) doi:10.1007/7651.

119. Golestaneh, N. *et al.* Repressed SIRT1 / PGC - 1 α pathway and mitochondrial disintegration in iPSC - derived RPE disease model of age - related macular degeneration. *J. Transl. Med.* 1–17 (2016) doi:10.1186/s12967-016-1101-8.
120. Production of iPSC Derived RPE Cells for Transplantation in AMD. *ClinicalTrials.gov* <https://clinicaltrials.gov/ct2/show/NCT02464956?term=iPSC&cond=dry+AMD&draw=2&rank=1> (2015) doi:NCT02464956.
121. Generation of Induced Pluripotent Stem (iPS) Cell Lines From Skin Fibroblast Cells of Participants With Age-Related Macular Degeneration. *ClinicalTrials.gov* <https://clinicaltrials.gov/ct2/show/NCT03372746?term=iPSC&cond=AMD&draw=2&rank=2> (2019) doi:NCT03372746.
122. Schwartz, S. D. *et al.* Embryonic stem cell trials for macular degeneration: A preliminary report. *Lancet* **379**, 713–720 (2012).
123. Schwartz, S. D. *et al.* Human embryonic stem cell-derived retinal pigment epithelium in patients with age-related macular degeneration and Stargardt’s macular dystrophy: Follow-up of two open-label phase 1/2 studies. *Lancet* **385**, 509–516 (2015).
124. Safety and Tolerability of Sub-retinal Transplantation of hESC Derived RPE (MA09-hRPE) Cells in Patients With Advanced Dry Age Related Macular Degeneration. *ClinicalTrials.gov* <https://clinicaltrials.gov/ct2/show/NCT01344993?term=MA09-hRPE&draw=2&rank=6> (2017) doi:NCT01344993.
125. Long Term Follow Up of Sub-retinal Transplantation of hESC Derived RPE Cells in Patients With AMD. *ClinicalTrials.gov* <https://clinicaltrials.gov/ct2/show/NCT02463344?term=NCT02463344&draw=2&rank=1> (2020) doi:NCT02463344.
126. Koss, M. J. *et al.* Subretinal implantation of a monolayer of human embryonic stem cell-derived retinal pigment epithelium : a feasibility and safety study in Yucatán minipigs. *Graefe’s Arch. Clin. Exp. Ophthalmol.* (2016) doi:10.1007/s00417-016-3386-y.
127. Study of Subretinal Implantation of Human Embryonic Stem Cell-Derived RPE Cells in Advanced Dry AMD. *ClinicalTrials.gov* <https://clinicaltrials.gov/ct2/show/NCT02590692?term=NCT02590692&draw=2&rank=1> (2019) doi:NCT02590692.
128. Strauss, O., Stumpffa, S., Mergler, S., Wienrich, M. & Wiederholt, M. The Royal College of Surgeons rat: An animal model for inherited retinal degeneration with a still unknown genetic defect. *Acta Anat. (Basel)*. **162**, 101–111 (1998).
129. McGill, T. J. *et al.* Transplantation of human central nervous system stem cells - neuroprotection in retinal degeneration. *Eur. J. Neurosci.* **35**, 468–477 (2012).
130. McGill, T. J. *et al.* Subretinal transplantation of human central nervous system stem cells stimulates controlled proliferation of endogenous retinal pigment epithelium. *Transl. Vis. Sci. Technol.* **8**, (2019).
131. Study of Human Central Nervous System Stem Cells (HuCNS-SC) in Age-Related Macular Degeneration (AMD). *ClinicalTrials.gov* <https://clinicaltrials.gov/ct2/show/NCT01632527?term=HuCNS-SC&cond=AMD&draw=2&rank=1> (2015) doi:NCT01632527.
132. Study of HUCNS-SC Subretinal Transplantation in Subjects With GA of AMD. *ClinicalTrials.gov* <https://clinicaltrials.gov/ct2/show/NCT02467634?term=HuCNS->

- SC&cond=AMD&draw=2&rank=2 (2016) doi:NCT02467634.
133. StemCells, Inc. Reports Top Line Results for Its Phase I/II Study in Dry Age Related Macular Degeneration Nasdaq:STEM. <https://www.globenewswire.com/news-release/2015/06/26/747839/10139889/en/StemCells-Inc-Reports-Top-Line-Results-for-Its-Phase-I-II-Study-in-Dry-Age-Related-Macular-Degeneration.html>.
 134. Long-Term Follow-up Safety Study of Human Central Nervous System Stem Cells in Subjects With Geographic Atrophy of Age-Related Macular Degeneration. *ClinicalTrials.gov* <https://clinicaltrials.gov/ct2/show/NCT02137915?term=HuCNS-SC&cond=AMD&draw=2&rank=3> (2016) doi:NCT02137915.
 135. Klettner, A. *et al.* Cellular and molecular mechanisms of age-related macular degeneration: From impaired autophagy to neovascularization. *International Journal of Biochemistry and Cell Biology* vol. 45 1457–1467 (2013).
 136. Lipecz, A. *et al.* Microvascular contributions to age-related macular degeneration (AMD): from mechanisms of choriocapillaris aging to novel interventions. *GeroScience* vol. 41 813–845 (2019).
 137. Brown, E. E., DeWeerd, A. J., Ildefonso, C. J., Lewin, A. S. & Ash, J. D. Mitochondrial oxidative stress in the retinal pigment epithelium (RPE) led to metabolic dysfunction in both the RPE and retinal photoreceptors. *Redox Biol.* **24**, 101201 (2019).
 138. Roth, F., Bindewald, A. & Holz, F. G. Keypathophysiologic pathways in age-related macular disease. *Graefe's Arch. Clin. Exp. Ophthalmol.* **242**, 710–716 (2004).
 139. Datta, S., Cano, M., Ebrahimi, K., Wang, L. & Handa, J. T. The Impact of Oxidative Stress and Inflammation on RPE Degeneration in Non-neovascular AMD. *Prog Retin Eye Res.* **60**, 201–2018 (2017).
 140. Woodell, A. & Rohrer, B. A mechanistic review of cigarette smoke and age-related macular degeneration. *Adv. Exp. Med. Biol.* **801**, 301–307 (2014).
 141. Zarling, J. A. *et al.* Nitroxide pharmaceutical development for age-related degeneration and disease. *Front. Genet.* **6**, 1–9 (2015).
 142. OT-551 Antioxidant Eye Drops to Treat Geographic Atrophy in Age-Related Macular Degeneration. *ClinicalTrials.gov* <https://clinicaltrials.gov/ct2/show/NCT00306488?term=OT-551&cond=AMD&draw=2&rank=1> (2011) doi:NCT00306488.
 143. Wong, W. T. *et al.* Treatment of geographic atrophy by the topical administration of OT-551: Results of a phase ii clinical trial. *Investigative Ophthalmology and Visual Science* vol. 51 6131–6139 (2010).
 144. The OMEGA Study: Use of Eye Drops to Treat Geographic Atrophy Associated With Age-Related Macular Degeneration (Dry AMD). *ClinicalTrials.gov* <https://clinicaltrials.gov/ct2/show/NCT00485394?term=NCT00485394&cond=AMD&draw=2&rank=1> (2008) doi:NCT00485394.
 145. Sternberg, P., Rosenfeld, P. J., Slakter, J. S., Koester, J. M. & Reaves, A. Topical OT-551 for Treating Geographic Atrophy: Phase II Results. *Invest. Ophthalmol. Vis. Sci.* **51**, 6416 (2010).
 146. Shaw, L. T. *et al.* Risuteganib—a novel integrin inhibitor for the treatment of non-exudative (dry) age-related macular degeneration and diabetic macular edema. *Expert Opin. Investig. Drugs* 1–7 (2020) doi:10.1080/13543784.2020.1763953.
 147. Friedlander, M. *et al.* Involvement of integrins avB3 and avB5 in ocular neovascular diseases.

- Med. Sci.* **93**, 9764–9769 (1996).
148. A Clinical Trial Designed To Evaluate The Safety And Exploratory Efficacy Of 1.0 Mg Luminate® (Alg-1001) As A Treatment For Non-Exudative Macular Degeneration. *ClinicalTrials.gov* <https://clinicaltrials.gov/ct2/show/NCT03626636?term=Risuteganib&cond=AMD&draw=2&rank=1> (2019) doi:NCT03626636.
 149. Ersoy, L. *et al.* Nutritional risk factors for age-related macular degeneration. *Biomed Res. Int.* **2014**, (2014).
 150. A Randomized, Placebo-Controlled, Clinical Trial of High-Dose Supplementation With Vitamins C and E, Beta Carotene, and Zinc for Age-Related Macular Degeneration and Vision Loss. *Arch Ophthalmol* **119**, 1417–1436 (2001).
 151. Chew, E. Y. *et al.* The Age-Related Eye Disease Study 2 (AREDS2): Study Design and Baseline Characteristics (AREDS2 Report Number 1). *Ophthalmology* **119**, 2282–2289 (2013).
 152. Jones, A. A., Fellow, O. & Eye, C. Age related macular degeneration Should your patients be taking additional. *Clin. Pract.* **36**, 1026–1028 (2007).
 153. Cangemi, F. E. TOZAL Study : An open case control study of an oral antioxidant and omega-3 supplement for dry AMD. *BMC Ophthalmol.* **10**, 1–10 (2007).
 154. Mandal, N. A. *et al.* Free Mandal, Nawajes A, Jagan M R Patlolla, Lixin Zheng, Martin-paul Agbaga, Julie-thu A Tran, Lea Wicker, Anne Kasus-jacobi, Michael H Elliott, Chinthalapally V Rao, and Robert E Anderson. 2009. "Free Radical Biology & Medicine Curcumin Protects Retinal . *Free Radic. Biol. Med.* **46**, 672–679 (2009).
 155. Xie, P. *et al.* Suppression of Experimental Choroidal Neovascularization by Curcumin in Mice. *PLoS One* **7**, (2012).
 156. Meng, Y. & Tao, J. Effect of curcumin on aging retinal pigment epithelial cells. *Drug Des. Devel. Ther.* **9**, 5337–5344 (2015).
 157. Lançon, A., Frazzi, R. & Latruffe, N. Anti-Oxidant, Anti-Inflammatory and Anti-Angiogenic Properties of Resveratrol in Ocular Diseases. *Molecules* (2016) doi:10.3390/molecules21030304.
 158. Evans, J. Antioxidant supplements to prevent or slow down the progression of AMD: A systematic review and meta-analysis. *Eye* **22**, 751–760 (2008).
 159. Li, Y. *et al.* CNTF Induces Regeneration of Cone Outer Segments in a Rat Model of Retinal Degeneration. *PLoS One* **5**, 1–7 (2010).
 160. Do, K. *et al.* CNTF-mediated protection of photoreceptors requires initial activation of the cytokine receptor gp130 in Müller glial cells. *PNAS* (2013) doi:10.1073/pnas.1303604110.
 161. Kauper, K. *et al.* Two-year intraocular delivery of ciliary neurotrophic factor by encapsulated cell technology implants in patients with chronic retinal degenerative diseases. *Investig. Ophthalmol. Vis. Sci.* **53**, 7484–7491 (2012).
 162. A Study of an Encapsulated Cell Technology (ECT) Implant for Patients With Atrophic Macular Degeneration. *ClinicalTrials.gov* <https://clinicaltrials.gov/ct2/show/NCT00447954?term=NT-501&cond=AMD&draw=2&rank=1> (2016) doi:NCT00447954.
 163. Cantor, L. B. The evolving pharmacotherapeutic profile of brimonidine, an α_2 -adrenergic agonist, after four years of continuous use. *Expert Opin. Pharmacother.* **1**, 815–834 (2000).
 164. U.S. Food and Drug Administration. *Alphagan*. (2016).

165. Walters, T. R. Development and use of brimonidine in treating acute and chronic elevations of intraocular pressure: A review of safety, efficacy, dose response, and dosing studies. *Surv. Ophthalmol.* **41**, (1996).
166. Kuno, N. & Fujii, S. Biodegradable intraocular therapies for retinal disorders: Progress to date. *Drugs and Aging* **27**, 117–134 (2010).
167. Safety and Efficacy of Brimonidine Intravitreal Implant in Patients With Geographic Atrophy Due to Age-related Macular Degeneration (AMD). *ClinicalTrials.gov* <https://clinicaltrials.gov/ct2/show/NCT00658619?term=Brimonidine&cond=AMD&draw=2&rank=1> (2018) doi:NCT00658619.
168. A Safety and Efficacy Study of Brimonidine Intravitreal Implant in Geographic Atrophy Secondary to Age-related Macular Degeneration. *ClinicalTrials.gov* <https://clinicaltrials.gov/ct2/show/NCT02087085?term=Brimonidine&cond=AMD&draw=1&rank=2> (2019) doi:NCT02087085.
169. Freeman, W. R. Brimonidine Drug Delivery System for Geographic Atrophy. <https://www.retinalphysician.com/issues/2019/november-2019/brimonidine-drug-delivery-system-for-geographic-at> (2019).
170. Collier, R. J., Wang, Y., Smith, S. S., Martin, E. & Ornberg, R. Complement Deposition and Microglial Activation in the Outer Retina in Light-Induced Retinopathy : Inhibition by a 5-HT 1A Agonist. *Retin. Cell Biol.* 8108–8116 (2011) doi:10.1167/iops.10-6418.
171. Collier, R. J. *et al.* Complement deposition and microglial activation in the outer retina in light-induced retinopathy: Inhibition by a 5-HT 1A Agonist. *Investig. Ophthalmol. Vis. Sci.* **52**, 8108–8116 (2011).
172. Geographic Atrophy Treatment Evaluation. *ClinicalTrials.gov* <https://clinicaltrials.gov/ct2/show/NCT00890097?term=NCT00890097&draw=2&rank=1> (2014).
173. Jaffe, G. J. *et al.* Randomized Trial to Evaluate Tansospirone in Geographic Atrophy Secondary to Age-Related Macular Degeneration: The GATE Study. *Am. J. Ophthalmol.* **160**, 1226–1234 (2015).
174. Effectiveness of Oral Acetazolamide, Brimonidine Tartarate, and Anterior Chamber Paracentesis in Intraocular Pressure (IOP) After Bevacizumab. *ClinicalTrials.gov* <https://clinicaltrials.gov/ct2/show/NCT00804921?term=Brimonidine&cond=AMD&draw=2&rank=4> (2008) doi:NCT00804921.
175. Oral Acetazolamide, Brimonidine Tartarate, and Anterior Chamber Paracentesis for Ocular Hypertension Control After Intravitreal Bevacizumab. *ClinicalTrials.gov* <https://clinicaltrials.gov/ct2/show/NCT00864838?term=Brimonidine&cond=AMD&draw=2&rank=3> (2009) doi:NCT00864838.
176. Whitcup, S. M. *et al.* The role of the immune response in age-related macular degeneration. *Int. J. Inflam.* **2013**, (2013).
177. Wakefield, D. & Lloyd, A. The role of cytokines in the pathogenesis of inflammatory eye disease. *Cytokine* **4**, 1–5 (1992).
178. DAVEY, M. P. & ROSENBAUM, J. T. The Human Leukocyte Antigen Complex and Chronic Ocular Inflammatory Disorders. *ELSEVIER Sci. INC.* **129**, 235–243 (2000).
179. Kauppinen, A., Paterno, J. J., Blasiak, J., Salminen, A. & Kaarniranta, K. Inflammation and its role

- in age-related macular degeneration. *Cell. Mol. Life Sci.* **73**, 1765–1786 (2016).
180. U.S. Food and Drug Administration. *Copaxone*. (2018).
 181. Arnon, R. & Sela, M. The chemistry of the Copaxone drug. *Chem. Isr.* 12–17 (1999) doi:10.1016/0165-2478(96)02506-0.
 182. Yong, V. W. Differential mechanisms of action of interferon- β and glatiramer acetate in MS. *Neurology* **59**, 802–808 (2002).
 183. Copaxone in Age Related Macular Degeneration. *ClinicalTrials.gov* <https://clinicaltrials.gov/ct2/show/NCT00466076?term=Glatiramer+acetate&cond=AMD&draw=2&rank=1> (2007) doi:NCT00466076.
 184. Weekly Vaccination With Copaxone as a Potential Therapy for Dry Age-related Macular Degeneration. *ClinicalTrials.gov* <https://clinicaltrials.gov/ct2/show/NCT00541333?term=Glatiramer+acetate&cond=AMD&draw=2&rank=2> (2013) doi:NCT00541333.
 185. Landa, G., Butovsky, O., Shoshani, J., Schwartz, M. & Pollack, A. Weekly Vaccination with Copaxone (Glatiramer Acetate) as a Potential Therapy for Dry Age-Related Macular Degeneration. *Curr. Eye Res.* **22**, 1011–1013 (2008).
 186. Lemke T., Williams D., R. V. and Z. W. *Foye's Principles of Medicinal Chemistry (6th)*. (2008).
 187. U.S. Food and Drug Administration. *Iluvien*. https://www.accessdata.fda.gov/drugsatfda_docs/label/2017/201923s002lbl.pdf (2016).
 188. Fluocinolone Acetonide Intravitreal Inserts in Geographic Atrophy. *ClinicalTrials.gov* <https://clinicaltrials.gov/ct2/show/NCT00695318?term=Fluocinolone&cond=Geographic+AMD&draw=2&rank=1> (2015) doi:NCT00695318.
 189. Napoli, K. L. & Taylor, P. J. From beach to bedside: History of the development of sirolimus. *Ther. Drug Monit.* **23**, 559–586 (2001).
 190. U.S. Food and Drug Administration. *Rapamune*. https://www.accessdata.fda.gov/drugsatfda_docs/label/2017/021083s059,021110s076lbl.pdf (2017).
 191. Intravitreal Injections of Sirolimus in the Treatment of Geographic Atrophy. *ClinicalTrials.gov* <https://clinicaltrials.gov/ct2/show/NCT01675947?term=Sirolimus&cond=AMD&draw=2&rank=9> (2015) doi:NCT01675947.
 192. Phase 1/2 Study of an Ocular Sirolimus (Rapamycin) Formulation in Patients With Age-Related Macular Degeneration. *ClinicalTrials.gov* <https://clinicaltrials.gov/ct2/show/NCT00712491?term=NCT00712491&draw=2&rank=1> (2013) doi:NCT00712491.
 193. Sirolimus for Advanced Age-Related Macular Degeneration. *ClinicalTrials.gov* <https://clinicaltrials.gov/ct2/show/NCT01445548?term=Sirolimus&cond=AMD&draw=2&rank=5> (2019) doi:NCT01445548.
 194. Petrou, P. A. *et al.* Intravitreal sirolimus for the treatment of geographic atrophy: Results of a phase I/II clinical trial. *Investig. Ophthalmol. Vis. Sci.* **56**, 330–338 (2014).
 195. Boyer, D. S., Schmidt-Erfurth, U., Van Lookeren Campagne, M., Henry, E. C. & Brittain, C. The pathophysiology of geographic atrophy secondary to age-related macular degeneration and the complement pathway as a therapeutic target. *Retina* **37**, 819–835 (2017).

196. Edwards, A. O. *et al.* Complement factor H polymorphism and age-related macular degeneration. *Science* (80-.). **308**, 421–424 (2005).
197. A Study of Safety, Tolerability, and Evidence of Activity of FCFD4514S Administered Monthly or Every Other Month to Patients With Geographic Atrophy. *ClinicalTrials.gov* <https://clinicaltrials.gov/ct2/show/NCT01229215?term=NCT01229215&cond=AMD&draw=2&rank=1> (2016) doi:NCT01229215.
198. A Study of Lampalizumab Intravitreal Injections Administered Every Two Weeks or Every Four Weeks to Participants With Geographic Atrophy. *ClinicalTrials.gov* <https://clinicaltrials.gov/ct2/show/NCT02288559?term=Lampalizumab&draw=2&rank=2> (2019) doi:NCT02288559.
199. Yaspan, B. L. *et al.* Targeting factor D of the alternative complement pathway reduces geographic atrophy progression secondary to age-related macular degeneration. *Sci. Transl. Med.* **9**, 1–13 (2017).
200. Hariri, A., Nittala, M. G. & Sadda, S. R. Outer retinal tubulation as a predictor of the enlargement amount of geographic atrophy in age-related macular degeneration. *Ophthalmology* **122**, 407–413 (2015).
201. An Extension Study to Evaluate the Long-Term Safety of Lampalizumab in Participants With Geographic Atrophy. *ClinicalTrials.gov* <https://clinicaltrials.gov/ct2/show/NCT01602120?term=Lampalizumab&draw=2&rank=3> (2019) doi:NCT01602120.
202. A Study Investigating the Efficacy and Safety of Lampalizumab Intravitreal Injections in Participants With Geographic Atrophy Secondary to Age-Related Macular Degeneration. *ClinicalTrials.gov* <https://clinicaltrials.gov/ct2/show/NCT02247479?term=Lampalizumab&cond=AMD&draw=2&rank=3> (2019) doi:NCT02247479.
203. A Study Investigating the Safety and Efficacy of Lampalizumab Intravitreal Injections in Participants With Geographic Atrophy Secondary to Age-Related Macular Degeneration. *ClinicalTrials.gov* <https://clinicaltrials.gov/ct2/show/NCT02247531?term=Lampalizumab&cond=AMD&draw=2&rank=2> (2019) doi:NCT02247531.
204. Long-Term Safety of Lampalizumab Intravitreal (ITV) Injections in Participants With Geographic Atrophy (GA) Secondary to Age-Related Macular Degeneration (OMASPECT). *ClinicalTrials.gov* <https://clinicaltrials.gov/ct2/show/NCT02745119?term=Lampalizumab&cond=AMD&draw=2&rank=1> (2019) doi:NCT02745119.
205. Roche. Roche provides update on first lampalizumab phase III study for geographic atrophy, an advanced form of age-related macular degeneration. <https://www.roche.com/media/releases/med-cor-2017-09-08b.htm>.
206. Narayanan, R. & Kuppermann, B. D. Corticosteroids and Anti-Complement Therapy in Retinal Diseases. *Springer* (2016) doi:10.1007/164.
207. A Multicenter, Proof-Of-Concept Study Of Intravitreal AL-78898A In Patients With Geographic Atrophy (GA) Associated With Age-Related Macular Degeneration (AMD). *ClinicalTrials.gov* <https://clinicaltrials.gov/ct2/show/NCT01603043?term=AL-78898A&cond=AMD&draw=2&rank=2> (2014) doi:NCT01603043.
208. Park, D. H., Connor, K. M., Lambris, J. D. & Clark, S. J. The Challenges and Promise of

- Complement Therapeutics for Ocular Diseases. *Front. Immunol.* **10**, 1–14 (2019).
209. Kassa, E., Ciulla, T. A., Hussain, R. M. & Dugel, P. U. Complement inhibition as a therapeutic strategy in retinal disorders. *Expert Opin. Biol. Ther.* **19**, 335–342 (2019).
 210. Study of of APL-2 Therapy in Patients Geographic Atrophy. *ClinicalTrials.gov* <https://clinicaltrials.gov/ct2/show/NCT02503332?term=APL-2&cond=AMD&draw=2&rank=6> (2019) doi:NCT02503332.
 211. Study to Evaluate the Safety of Intravitreal APL-2 in Patients Diagnosed With Geographic Atrophy. *ClinicalTrials.gov* <https://clinicaltrials.gov/ct2/show/NCT03777332?term=APL-2&cond=AMD&draw=2&rank=5> (2019) doi:NCT03777332.
 212. Study to Compare the Efficacy and Safety of Intravitreal APL-2 Therapy With Sham Injections in Patients With Geographic Atrophy (GA) Secondary to Age-Related Macular Degeneration. *ClinicalTrials.gov* <https://clinicaltrials.gov/ct2/show/NCT03525600?term=APL-2&cond=AMD&draw=2&rank=3> (2020) doi:NCT03525600.
 213. U.S. Food and Drug Administration. *Soliris*. (2007).
 214. Complement Inhibition With Eculizumab for the Treatment of Non-Exudative Macular Degeneration (AMD). *ClinicalTrials.gov* <https://clinicaltrials.gov/ct2/show/NCT00935883?term=Eculizumab&cond=AMD&draw=2&rank=1> (2017) doi:NCT00935883.
 215. Stetson, P. F. *et al.* OCT minimum intensity as a predictor of geographic atrophy enlargement. *Investig. Ophthalmol. Vis. Sci.* **55**, 792–800 (2014).
 216. Yehoshua, Z. *et al.* Systemic complement inhibition with eculizumab for geographic atrophy in age-related macular degeneration: The COMPLETE study. *Ophthalmology* **121**, 693–701 (2014).
 217. Intravitreal LFG316 in Patients With Advanced Age-related Macular Degeneration. *ClinicalTrials.gov* <https://clinicaltrials.gov/ct2/show/NCT01255462?term=LFG316&cond=AMD&draw=2&rank=4> (2012) doi:NCT01255462.
 218. Intravitreal LFG316 in Patients With Age-related Macular Degeneration (AMD). *ClinicalTrials.gov* <https://clinicaltrials.gov/ct2/show/NCT01527500?term=NCT01527500&cond=AMD&draw=2&rank=1> (2019) doi:NCT01527500.
 219. CLG561 Proof-of-Concept Study as a Monotherapy and in Combination With LFG316 in Subjects With Geographic Atrophy (GA). *ClinicalTrials.gov* <https://clinicaltrials.gov/ct2/show/NCT02515942?term=NCT02515942&cond=AMD&draw=2&rank=1> (2019) doi:NCT02515942.
 220. Park, E. J., Choi, J., Lee, K. C. & Na, D. H. Emerging PEGylated non-biologic drugs. *Expert Opinion on Emerging Drugs* vol. 24 107–119 (2019).
 221. A Study of ARC1905 (Anti-C5 Aptamer) in Subjects With Dry Age-related Macular Degeneration. *ClinicalTrials.gov* <https://clinicaltrials.gov/ct2/show/NCT00950638?term=NCT00950638&cond=AMD&draw=2&rank=1> (2017) doi:NCT00950638.
 222. Zimura in Subjects With Geographic Atrophy Secondary to Dry Age-Related Macular Degeneration. *ClinicalTrials.gov* <https://clinicaltrials.gov/ct2/show/NCT02686658?term=ARC-1905&cond=Geographic+AMD&draw=2&rank=1> (2020) doi:NCT02686658.

223. Schnabolk, G. *et al.* Delivery of CR2-fH Using AAV Vector Therapy as Treatment Strategy in the Mouse Model of Choroidal Neovascularization. *Mol. Ther. - Methods Clin. Dev.* **9**, 1–11 (2018).
224. Treatment of Advanced Dry Age Related Macular Degeneration With AAVCAGsCD59. *ClinicalTrials.gov*
<https://clinicaltrials.gov/ct2/show/NCT03144999?term=NCT03144999&draw=2&rank=1>
 (2019) doi:NCT03144999.
225. L'Esperance, F. A. Clinical Applications of the Organic Dye Laser. *Ophthalmology* **92**, 1592–1600 (1985).
226. National Eye Institute (NEI). Macular Photocoagulation Study (MPS). *ClinicalTrials.gov*
<https://clinicaltrials.gov/ct2/show/NCT00000158?term=MPS&cond=AMD&draw=2&rank=2>
 (2002) doi:NCT00000158.
227. Argon Laser Photocoagulation for Neovascular Maculopathy. *Arch. Ophthalmol.* **109**, 1109 (1991).
228. Saini, R., Lee, N. V., Liu, K. Y. P. & Poh, C. F. Prospects in the application of photodynamic therapy in oral cancer and premalignant lesions. *Cancers (Basel)*. **8**, 1–14 (2016).
229. Houle, J. M. & Strong, A. Clinical pharmacokinetics of verteporfin. *J. Clin. Pharmacol.* **42**, 547–557 (2002).
230. Aveline, B., Hasan, T. & Redmond, R. W. Photophysical and Photosensitizing Properties of Benzoporphyrin Derivative Monoacid Ring a (Bpd-Ma). *Photochem. Photobiol.* **59**, 328–335 (1994).
231. Richter, A. M. *et al.* Photosensitizing potencies of the structural analogues of benzoporphyrin derivative in different biological test systems. *J. Clin. Laser Med. Surg.* **14**, 335–341 (1996).
232. Lim, J. I. Photodynamic therapy for choroidal neovascular disease : photosensitizers and clinical trials. *Ophthalmol. Clin. north Am.* **15**, 473–478 (2002).
233. Blinder, K. J. *et al.* Effect of lesion size, visual acuity, and lesion composition on visual acuity change with and without verteporfin therapy for choroidal neovascularization secondary to age-related macular degeneration: TAP and VIP report no. 1. *Am. J. Ophthalmol.* **136**, 407–418 (2003).
234. U.S. Food and Drug Administration. *Visudyne*. (2002).
235. Haute autorité de santé. *VISUDYNE*. (2006).
236. Haute autorité de santé. *Place dans la stratégie thérapeutique de LUCENTIS, EYLEA et de leurs comparateurs cliniquement pertinents dans la forme néovasculaire (humide) de la dégénérescence maculaire liée à l'âge (DMLA)*. (2017).
237. Senger, D. R. *et al.* Tumor cells secrete a vascular permeability factor that promotes accumulation of ascites fluid. *Science (80-)*. **219**, 983–985 (1983).
238. Kliffen, M., Sharma, H. S., Mooy, C. M., Kerkvliet, S. & De Jong, P. T. V. M. Increased expression of angiogenic growth factors in age-related maculopathy. *Br. J. Ophthalmol.* **81**, 154–162 (1997).
239. Park, Y. G., Rhu, H. W., Kang, S. & Roh, Y. J. New approach of anti-VEGF agents for age-related macular degeneration. *J. Ophthalmol.* **2012**, (2012).
240. Ishida, S. *et al.* VEGF164-mediated inflammation is required for pathological, but not physiological, ischemia-induced retinal neovascularization. *J. Exp. Med.* **198**, 483–489 (2003).

241. Fogli, S. *et al.* Clinical pharmacology of intravitreal anti-VEGF drugs. *Eye* **32**, 1010–1020 (2018).
242. Gragoudas, E. S. *et al.* Pegaptanib for neovascular age-related macular degeneration. *N. Engl. J. Med.* **351**, 2805–2816 (2004).
243. fda & cder. *HIGHLIGHTS OF PRESCRIBING INFORMATION*. www.fda.gov/medwatch.
244. Gragoudas, E. S., Adamis, A. P., Cunningham, E. T., Feinsod, M. & Guyer, D. R. Pegaptanib for neovascular age-related macular degeneration. *Issues Emerg. Health Technol.* 1–4 (2005) doi:10.1016/j.ajo.2005.02.003.
245. Haute autorité de santé. *Macugen*. (2013).
246. A Study to Evaluate rhuFab V2 in Subjects With Minimally Classic or Occult Subfoveal Neovascular Macular Degeneration. *ClinicalTrials.gov* <https://clinicaltrials.gov/ct2/show/NCT00056836?term=NCT00056836&cond=AMD&draw=2&rank=1> (2014) doi:NCT00056836.
247. An Extension Study to Evaluate Safety and Tolerability of Ranibizumab in Macular Edema Secondary to Retinal Vein Occlusion (Cohort 2). *ClinicalTrials.gov* <https://clinicaltrials.gov/ct2/show/NCT01442064?term=NCT01442064&cond=AMD&draw=2&rank=1> (2012) doi:NCT01442064.
248. An Extension Study to Evaluate the Safety and Tolerability of Ranibizumab in Subjects With Choroidal Neovascularization Secondary to AMD or Macular Edema Secondary to RVO. *ClinicalTrials.gov* <https://clinicaltrials.gov/ct2/show/NCT00379795?term=NCT01442064&cond=AMD&draw=2&rank=2> (2017) doi:NCT00379795.
249. Rosenfeld, P. J. *et al.* Ranibizumab for Neovascular Age-Related Macular Degeneration. *N. Engl. J. Med.* **355**, 1419–1431 (2006).
250. A Study to Compare rhuFab V2 With Verteporfin Photodynamic in Treating Subfoveal Neovascular Macular Degeneration - Full Text View - *ClinicalTrials.gov*. <https://clinicaltrials.gov/ct2/show/NCT00061594?term=NCT00061594&cond=AMD&draw=2&rank=1> (2014) doi:NCT00061594.
251. Brown, D. M. *et al.* Ranibizumab versus verteporfin for neovascular age-related macular degeneration. *N. Engl. J. Med.* **355**, 1432–1444 (2006).
252. Rofagha, S., Bhisitkul, R. B., Boyer, D. S., Sadda, S. R. & Zhang, K. Seven-year outcomes in ranibizumab-treated patients in ANCHOR, MARINA, and HORIZON: A multicenter cohort study (SEVEN-UP). *Ophthalmology* **120**, 2292–2299 (2013).
253. Ho, A. C. *et al.* Twenty-four-month efficacy and safety of 0.5 mg or 2.0 mg ranibizumab in patients with subfoveal neovascular age-related macular degeneration. *Ophthalmology* **121**, 2181–2192 (2014).
254. Wykoff, C. C. *et al.* Prospective trial of treat-and-extend versus monthly dosing for neovascular age-related macular degeneration: TREX-AMD 1-year results. *Ophthalmology* **122**, 2514–2522 (2015).
255. Haute autorité de santé. *Ranibizumab*. (2018).
256. Heier, J. S. *et al.* Intravitreal aflibercept (VEGF trap-eye) in wet age-related macular degeneration. *Ophthalmology* **119**, 2537–2548 (2012).
257. Vascular Endothelial Growth Factor VEGF Trap-Eye: Investigation of Efficacy and Safety in Wet

- Age-Related Macular Degeneration(AMD). *ClinicalTrials.gov*
<https://clinicaltrials.gov/ct2/show/NCT00509795?term=NCT00509795&draw=2&rank=1>
 (2012) doi:NCT00509795.
258. Vascular Endothelial Growth Factor (VEGF) Trap-Eye: Investigation of Efficacy and Safety in Wet Age-Related Macular Degeneration (AMD). *ClinicalTrials.gov*
<https://clinicaltrials.gov/ct2/show/NCT00637377?term=NCT00637377&draw=2&rank=1>
 (2014) doi:NCT00637377.
259. Heier, J. S. *et al.* Intravitreal aflibercept (VEGF trap-eye) in wet age-related macular degeneration. *Ophthalmology* **119**, 2537–2548 (2012).
260. U.S. Food and Drug Administration. *EYLEA® (Aflibercept)*. (2018).
261. Al-husein, B. *et al.* REVIEWS THERAPEUTICS Antiangiogenic Therapy for Cancer : An Update. *Pharmacotherapy* **32**, 1095–1111 (2004).
262. Papadopoulos, N. *et al.* Binding and neutralization of vascular endothelial growth factor (VEGF) and related ligands by VEGF Trap, ranibizumab and bevacizumab. *Angiogenesis* **15**, 171–185 (2012).
263. U.S. Food and Drug Administration. *AVASTIN (bevacizumab)*. www.fda.gov/medwatch. (2014).
264. Martin, D. F. *et al.* Ranibizumab and bevacizumab for treatment of neovascular age-related macular degeneration: Two-year results. *Ophthalmology* **119**, 1388–1398 (2012).
265. Maguire, M. G. *et al.* Five-Year Outcomes with Anti-Vascular Endothelial Growth Factor Treatment of Neovascular Age-Related Macular Degeneration: The Comparison of Age-Related Macular Degeneration Treatments Trials. *Ophthalmology* **123**, 1751–1761 (2016).
266. French Evaluation Group Avastin Versus Lucentis. *ClinicalTrials.gov*
<https://clinicaltrials.gov/ct2/show/NCT01170767?term=NCT01170767&draw=2&rank=1>
 (2019) doi:NCT01170767.
267. Kodjikian, L. *et al.* Ranibizumab versus bevacizumab for neovascular age-related macular degeneration: Results from the GEFAL noninferiority randomized trial. *Ophthalmology* **120**, 2300–2309 (2013).
268. French Evaluation Group Avastin Versus Lucentis. *ClinicalTrials.gov*
<https://clinicaltrials.gov/ct2/show/NCT01170767?term=GEFAL&draw=2&rank=1> (2019)
 doi:NCT01170767.
269. Heier, J. S. Ask the doctor: For macular degeneration, which is better, Avastin or Lucentis? - Harvard Health. <https://www.health.harvard.edu/diseases-and-conditions/for-macular-degeneration-which-is-better-avastin-or-lucentis>.
270. Haute autorité de santé. *Recommandation relative à la prise en charge à titre dérogatoire d'Avastin (bevacizumab) dans le cadre d'une recommandation temporaire d'utilisation*. (2018).
271. Yannuzzi, N. A. & Freund, K. B. Brolucizumab: Evidence to date in the treatment of neovascular age-related macular degeneration. *Clin. Ophthalmol.* **13**, 1323–1329 (2019).
272. EMA. Assessment Report Beovu - Brolucizumab. **31**, (2019).
273. Safety and Pharmacokinetics of RTH258 in Subjects With Age-Related Macular Degeneration. *ClinicalTrials.gov*
<https://clinicaltrials.gov/ct2/show/NCT02507388?term=Brolucizumab&cond=AMD&draw=2&rank=8>
 (2018) doi:NCT02507388.

274. Study of the Safety of Brolucizumab 6 mg in Prefilled Syringe in Patients With Neovascular Age Related Macular Degeneration. *ClinicalTrials.gov*
<https://clinicaltrials.gov/ct2/show/NCT03930641?term=Brolucizumab&cond=AMD&draw=2&rank=4> (2019) doi:NCT03930641.
275. Study to Collect Safety and ECG Data on Brolucizumab 6 mg Intravitreal Treatment in Patients With Wet AMD. *ClinicalTrials.gov*
<https://clinicaltrials.gov/ct2/show/results/NCT03954626?term=Brolucizumab&cond=AMD&draw=2&rank=6> (2020) doi:NCT03954626.
276. Study of Safety and Efficacy of Brolucizumab 6 mg Drug Product Intended for Commercialization in Patients With nAMD. *ClinicalTrials.gov*
<https://clinicaltrials.gov/ct2/show/results/NCT03386474?term=Brolucizumab&cond=AMD&draw=2&rank=7> (2020) doi:NCT03386474.
277. Efficacy and Safety of RTH258 Versus Aflibercept - Study 1. *ClinicalTrials.gov*
<https://clinicaltrials.gov/ct2/show/NCT02307682?term=HAWK&cond=AMD&draw=2&rank=1> (2019) doi:NCT02307682.
278. Efficacy and Safety of RTH258 Versus Aflibercept - Study 2. *ClinicalTrials.gov*
<https://clinicaltrials.gov/ct2/show/NCT02434328?term=HARRIER&cond=AMD&draw=2&rank=1> (2019) doi:NCT02434328.
279. Agostini, H. *et al.* Comparison of the Efficacy of Brolucizumab with Natural Disease Progression in Wet AMD Using Clinical Data from the Phase III HAWK and HARRIER Trials and Modelled Placebo Data. *Curr. Eye Res.* 1–4 (2020) doi:10.1080/02713683.2020.1731832.
280. Novartis. Novartis receives FDA approval for Beovu®, offering wet AMD patients vision gains and greater fluid reductions vs aflibercept. <https://novartis.gcs-web.com/Novartis-receives-FDA-approval-for-Beovu-offering-wet-AMD-patients-vision-gains-and-greater-fluid-reductions-vs-aflibercept> (2019).
281. Yorston, D. Intravitreal injection technique. *Community Eye Heal. J.* **27**, 47 (2014).
282. Martin, D. F. *et al.* Ranibizumab and bevacizumab for neovascular age-related macular degeneration. *N. Engl. J. Med.* **364**, 1897–1908 (2011).
283. Zhang, M. *et al.* A phase 1 study of KH902, a vascular endothelial growth factor receptor decoy, for exudative age-related macular degeneration. *Ophthalmology* **118**, 672–678 (2011).
284. Sun, X. & Lu, X. Profile of conbercept in the treatment of neovascular age-related macular degeneration. *Drug Des. Devel. Ther.* (2015) doi:10.2147/DDDT.S67536.
285. Nguyen, T. T. & Guymer, R. Conbercept (KH-902) for the treatment of neovascular age-related macular degeneration. *Expert Rev. Clin. Pharmacol.* **8**, 541–548 (2015).
286. A Study Assessing the Safety and Efficacy of Multiple Intravitreal KH902 in Patients With CNV Due to AMD. *ClinicalTrials.gov*
<https://clinicaltrials.gov/ct2/show/NCT01242254?term=KH902&recrs=eh&cond=AMD&draw=2&rank=2> (2014) doi:NCT01242254.
287. A Randomized, Double-masked, Multicenter, Controlled Study of Intravitreal KH902 in Patients With Neovascular AMD. *ClinicalTrials.gov*
<https://clinicaltrials.gov/ct2/show/NCT01157715?term=NCT+01157715&recrs=eh&cond=AMD&draw=2&rank=1> (2014) doi:NCT01157715.
288. Li, X. *et al.* Safety and efficacy of conbercept in neovascular age-related macular degeneration:

- Results from a 12-month randomized phase 2 Study: AURORA study. *Ophthalmology* **121**, 1740–1747 (2014).
289. A Randomized, Double-masked, Multicenter, Sham-controlled, Safety and Efficacy Study of KH902 in Patients With Wet AMD. *ClinicalTrials.gov*
<https://clinicaltrials.gov/ct2/show/NCT01436864?term=Conbercept&recrs=eh&cond=AMD&draw=2&rank=2> (2014) doi:NCT01436864.
 290. Head to Head Study of Anti-VEGF Treatment. *ClinicalTrials.gov*
<https://clinicaltrials.gov/ct2/show/NCT02577107?term=Conbercept&recrs=eh&cond=AMD&draw=2&rank=1> (2017) doi:NCT02577107.
 291. Zhang, J. *et al.* Conbercept for patients with age-related macular degeneration: A systematic review. *BMC Ophthalmol.* **18**, 1–12 (2018).
 292. Zuo, W. *et al.* The interpretation of China national essential medicines list 2018. *Expert Rev. Clin. Pharmacol.* **13**, 191–200 (2020).
 293. Kunitomo, D. *et al.* Evaluation of abicipar pegol (an anti-VEGF DARPIN therapeutic) in patients with neovascular age-related macular degeneration: Studies in Japan and the United States. *Ophthalmic Surg. Lasers Imaging Retin.* **50**, E10–E22 (2019).
 294. Rodrigues, G. A. *et al.* Functional characterization of abicipar-pegol, an anti-VEGF DARPIn therapeutic that potently inhibits angiogenesis and vascular permeability. *Investig. Ophthalmol. Vis. Sci.* **59**, 5836–5846 (2018).
 295. Safety and Pharmacokinetics of Abicipar Pegol Intravitreal Injections in Patients With Neovascular AMD. *ClinicalTrials.gov*
<https://clinicaltrials.gov/ct2/show/NCT02859766?term=Abicipar+pegol&cond=AMD&draw=2&rank=1> (2018) doi:NCT02859766.
 296. Safety and Pharmacokinetics of Abicipar Pegol Intravitreal Injections in Japanese Patients With Neovascular AMD. *ClinicalTrials.gov*
<https://clinicaltrials.gov/ct2/show/NCT03335852?term=Abicipar+pegol&cond=AMD&draw=2&rank=2> (2018) doi:NCT03335852.
 297. A Study of Abicipar Pegol in Patients With Neovascular Age-related Macular Degeneration. *ClinicalTrials.gov*
<https://clinicaltrials.gov/ct2/show/NCT02181517?term=CYPRESS&cond=AMD&draw=2&rank=1> (2016) doi:NCT02181517.
 298. A Study of Abicipar Pegol in Japanese Patients With Neovascular Age-related Macular Degeneration. *ClinicalTrials.gov*
<https://clinicaltrials.gov/ct2/show/NCT02181504?term=BAMBOO&cond=AMD&draw=2&rank=1> (2017) doi:NCT02181504.
 299. Evaluation of AGN-150998 in Exudative Age-related Macular Degeneration (AMD). *ClinicalTrials.gov*
<https://clinicaltrials.gov/ct2/show/NCT01397409?term=NCT01397409&cond=AMD&draw=2&rank=1> (2019) doi:NCT01397409.
 300. Callanan, D. *et al.* Double-masked, randomized, phase 2 evaluation of abicipar pegol (an Anti-VEGF DARPIn Therapeutic) in neovascular age-related macular degeneration. *J. Ocul. Pharmacol. Ther.* **34**, 700–709 (2018).
 301. Allergen. A Safety and Efficacy Study of Abicipar Pegol in Patients With Neovascular Age-related Macular Degeneration - CDER. *ClinicalTrials.gov*

- <https://clinicaltrials.gov/ct2/show/NCT02462928?term=NCT02462928&draw=2&rank=1>
(2019) doi:NCT02462928.
302. Allergen. Safety and Efficacy of Abicipar Pegol in Patients With Neovascular Age-related Macular Degeneration - SEQUOIA. *ClinicalTrials.gov*
<https://clinicaltrials.gov/ct2/show/NCT02462486?term=NCT02462486&draw=2&rank=1>
(2019) doi:NCT02462486.
 303. Evaluating Abicipar for Safety and Treatment Effect in Patients With Neovascular Age-related Macular Degeneration (AMD). *ClinicalTrials.gov*
<https://clinicaltrials.gov/ct2/show/NCT03539549?term=Abicipar+pegol&cond=AMD&draw=2&rank=5> (2020) doi:NCT03539549.
 304. Study Evaluating the Safety, Pharmacokinetics and Pharmacodynamics of OPT-302 With or Without Lucentis™ in Patients With Wet AMD. *ClinicalTrials.gov*
<https://clinicaltrials.gov/ct2/show/NCT02543229?term=OPT-302&cond=AMD&draw=2&rank=2> (2017) doi:NCT02543229.
 305. Dugel, P. U. *et al.* Phase 1 Study of OPT-302 Inhibition of Vascular Endothelial Growth Factors C and D for Neovascular Age-Related Macular Degeneration. *Ophthalmol. Retin.* **4**, 250–263 (2020).
 306. A Dose Ranging Study of OPT-302 With Ranibizumab in Neovascular (Wet) AMD. *ClinicalTrials.gov*
<https://clinicaltrials.gov/ct2/show/NCT03345082?term=OPT-302&cond=AMD&draw=2&rank=1> (2020) doi:NCT03345082.
 307. Stein, M. N. & Flaherty, K. T. Sorafenib and sunitinib in renal cell carcinoma. *Clin. Cancer Res.* **13**, 3765–3770 (2007).
 308. Fda. *NEXAVAR (sorafenib) tablets, for oral use.* www.fda.gov/medwatch. (2011).
 309. Haute autorité de santé. *Nexavar.* https://www.bertelsmannstiftung.de/fileadmin/files/BSt/Publikationen/GrauePublikationen/MT_Globalization_Report_2018.pdf
http://eprints.lse.ac.uk/43447/1/India_globalisation%2C_society_and_inequalities%28Isero%29.pdf
<https://www.quora.com/What-is-the> (2008)
doi:10.11113/jt.v56.60.
 310. Kernt, M. *et al.* Sorafenib prevents human retinal pigment epithelium cells from light-induced overexpression of VEGF, PDGF and PIGF. *Br. J. Ophthalmol.* **94**, 1533–1539 (2010).
 311. Diago, T. *et al.* Ranibizumab combined with low-dose sorafenib for exudative age-related macular degeneration. *Mayo Clin. Proc.* **83**, 231–234 (2008).
 312. Kernt, M., Staehler, M., Stief, C., Kampik, A. & Neubauer, A. S. Resolution of macular oedema in occult choroidal neovascularization under oral Sorafenib® treatment. *Acta Ophthalmol.* **86**, 456–458 (2008).
 313. Zhao, H. L., Yang, F., Huang, X. & Zhou, Q. H. Overview of fundamental study of pazopanib in cancer. *Thorac. Cancer* **5**, 487–493 (2014).
 314. U.S. Food and Drug Administration. *Votrient.* (2012).
 315. A Study To Evaluate The Safety, Tolerability And Pk Of Pazopanib Eye Drops In Healthy Adult And Elderly Subjects. *ClinicalTrials.gov*
<https://clinicaltrials.gov/ct2/show/NCT00463320?term=pazopanib&cond=AMD&draw=2&rank=6> (2012) doi:NCT00463320.
 316. Study Of The Repeat Dosing Of Ketoconazole On The Pharmacokinetics Of A Single Dose Of

- Pazopanib (GW786034) Eye Drops. *ClinicalTrials.gov*
<https://clinicaltrials.gov/ct2/show/NCT00659555?term=pazopanib&cond=AMD&draw=2&rank=7> (2017) doi:NCT00659555.
317. A Study to Evaluate Pazopanib Tablets in Patients Who Have Neovascular Age-related Macular Degeneration. *ClinicalTrials.gov*
<https://clinicaltrials.gov/ct2/show/NCT01154062?term=pazopanib&cond=AMD&draw=2&rank=4> (2017) doi:NCT01154062.
318. A Safety Study in Healthy Volunteers to Evaluate Safety, How Fast the Drug is Absorbed, and the Side Effects of the Drug in Humans. *ClinicalTrials.gov*
<https://clinicaltrials.gov/ct2/show/NCT01051700?term=pazopanib&cond=AMD&draw=2&rank=9> (2017) doi:NCT01051700.
319. A Safety Study to Evaluate Pazopanib Eye Drops in Healthy Volunteers. *ClinicalTrials.gov*
<https://clinicaltrials.gov/ct2/show/NCT01072214?term=pazopanib&cond=AMD&draw=2&rank=8> (2017) doi:NCT01072214.
320. To Evaluate the Pharmacodynamics, Safety, and Pharmacokinetics of Pazopanib Drops in Adult Subjects With Neovascular AMD. *ClinicalTrials.gov*
<https://clinicaltrials.gov/ct2/show/NCT00612456?term=NCT00612456&draw=2&rank=1> (2017) doi:NCT00612456.
321. An Extension to Study MD7108240. *ClinicalTrials.gov*
<https://clinicaltrials.gov/ct2/show/NCT00733304?term=pazopanib&cond=AMD&draw=2&rank=5> (2017) doi:NCT00733304.
322. Dose Ranging Study of Pazopanib to Treat Neovascular Age-Related Macular Degeneration. *ClinicalTrials.gov*
<https://clinicaltrials.gov/ct2/show/NCT01134055?term=pazopanib&cond=wet+AMD&draw=2&rank=1> (2018) doi:NCT01134055.
323. 12 Week Patient Study in Neovascular Age-related Macular Degeneration (AMD). *ClinicalTrials.gov*
<https://clinicaltrials.gov/ct2/show/NCT01362348?term=pazopanib&cond=AMD&draw=2&rank=2> (2017) doi:NCT01362348.
324. McLaughlin, M. M. *et al.* Initial exploration of oral pazopanib in healthy participants and patients with age-related macular degeneration. *JAMA Ophthalmol.* **131**, 1595–1601 (2013).
325. Singh, R. *et al.* Clinical evaluation of pazopanib eye drops in healthy subjects and in subjects with neovascular age-related macular degeneration. *Retina* **34**, 1787–1795 (2014).
326. Csaky, K. G. *et al.* Clinical evaluation of pazopanib eye drops versus ranibizumab intravitreal injections in subjects with neovascular age-related macular degeneration. *Ophthalmology* **122**, 579–588 (2015).
327. Gross-Goupil, M., François, L., Quivy, A. & Ravaud, A. Axitinib: A review of its safety and efficacy in the treatment of adults with advanced renal cell carcinoma. *Clin. Med. Insights Oncol.* **7**, 269–277 (2013).
328. U.S. Food and Drug Administration. *Inlyta*. (2020).
329. Kang, S. *et al.* Antiangiogenic Effects of Axitinib, an Inhibitor of Vascular Endothelial Growth Factor Receptor Tyrosine Kinase, on Laser-Induced Choroidal Neovascularization in Mice. *Curr. Eye Res.* **38**, 119–127 (2013).

330. Giddabasappa, A. *et al.* Axitinib inhibits retinal and choroidal neovascularization in in vitro and in vivo models. *Exp. Eye Res.* **145**, 373–379 (2016).
331. Carr, B. I. *et al.* Effects of low concentrations of Regorafenib and Sorafenib on human HCC cell AFP, migration, invasion, and growth in vitro. *J. Cell. Physiol.* **228**, 1344–1350 (2013).
332. U.S. Food and Drug Administration. *Stivarga*. (2017) doi:10.1007/978-3-662-46875-3_102186.
333. Regorafenib Eye Drops: Investigation of Efficacy and Safety in Neovascular Age Related Macular Degeneration. *ClinicalTrials.gov* <https://clinicaltrials.gov/ct2/show/NCT02222207?term=NCT02222207&draw=2&rank=1> (2016) doi:NCT02222207.
334. Jousseaume, A. M. *et al.* The Developing Regorafenib Eye drops for neovascular Age-related Macular degeneration (DREAM) study: an open-label phase II trial. *Br. J. Clin. Pharmacol.* **85**, 347–355 (2019).
335. Rudolf, M. and Roizman, K. Treatment of age-related macular degeneration and other eye diseases with apolipoprotein mimetics. (2018) doi:US 2018 / 0207233 A1.
336. Tolentino, M. J., Dennrick, A., John, E. & Tolentino, M. S. Drugs in phase II clinical trials for the treatment of age-related macular degeneration. *Expert Opin. Investig. Drugs* **24**, 183–199 (2015).
337. Phase 1 Study of Topical Ocular PAN-90806 for Neovascular AMD. *ClinicalTrials.gov* <https://clinicaltrials.gov/ct2/show/NCT02022540?term=NCT02022540&draw=2&rank=1> (2016) doi:NCT02022540.
338. Study of PAN-90806 Eye Drops, Suspension for Neovascular AMD. *ClinicalTrials.gov* <https://clinicaltrials.gov/ct2/show/NCT03479372?term=NCT03479372&draw=2&rank=1> (2019) doi:NCT03479372.
339. Jackson, T. L. *et al.* Oral tyrosine kinase inhibitor for neovascular age-related macular degeneration: A phase 1 dose-escalation study. *JAMA Ophthalmol.* **135**, 761–767 (2017).
340. EyePoint Pharmaceuticals, I. *Securities and Exchange Commission. Federal Regulatory Guide* vol. 1933 (2020).
341. Pilot Study of X-82 in Patients With Wet AMD. *ClinicalTrials.gov* <https://clinicaltrials.gov/ct2/show/NCT01674569?term=NCT01674569&draw=1&rank=1> (2018) doi:NCT01674569.
342. X-82 to Treat Age-related Macular Degeneration. *ClinicalTrials.gov* <https://clinicaltrials.gov/ct2/show/NCT02348359?term=NCT02348359&draw=2&rank=1> (2018) doi:NCT02348359.
343. U.S. Food and Drug Administration. *LENVIMA*. www.fda.gov/medwatch. (2018).
344. Costa, R. *et al.* Spotlight on lenvatinib in the treatment of thyroid cancer: Patient selection and perspectives. *Drug Des. Devel. Ther.* **10**, 873–884 (2016).
345. Wiegand, A. *et al.* E7080 (Lenvatinib), a Multi-Targeted Tyrosine Kinase Inhibitor, Demonstrates Antitumor Activities Against Colorectal Cancer Xenografts. *Neoplasia* **16**, 972–981 (2014).
346. Wei, X. *et al.* Efficacy of Lenvatinib, a multitargeted tyrosine kinase inhibitor, on laser-induced CNV mouse model of neovascular AMD. *Exp. Eye Res.* **168**, 2–11 (2018).
347. Allen, E., Walters, I. B. & Hanahan, D. Brivanib, a dual FGF/VEGF inhibitor, is active both 1st and

- 2nd line against mouse pancreatic neuroendocrine tumors (PNET) developing adaptive/evasive resistance to VEGF inhibition. *Clin Cancer Res.* **17**, 5299–5310 (2011).
348. Bhide, R. S. *et al.* The antiangiogenic activity in xenograft models of brivanib, a dual inhibitor of vascular endothelial growth factor receptor-2 and fibroblast growth factor receptor-1 kinases. *Mol. Cancer Ther.* **9**, 369–378 (2010).
 349. Li, L. *et al.* Brivanib, a multitargeted small-molecule tyrosine kinase inhibitor, suppresses laser-induced CNV in a mouse model of neovascular AMD. *J. Cell. Physiol.* **235**, 1259–1273 (2020).
 350. Brycki, B., Koenig, H. & Pospieszny, T. Quaternary alkylammonium conjugates of steroids: Synthesis, molecular structure, and biological studies. *Molecules* **20**, 20887–20900 (2015).
 351. Pietras, R. J. & Weinberg, O. K. Antiangiogenic Steroids in Human Cancer Therapy. *eCAM* **2**, 49–57 (2005).
 352. A Safety and Efficacy Study of MSI-1256F (Squalamine Lactate) To Treat ‘Wet’ Age-Related Macular Degeneration. *ClinicalTrials.gov*
<https://clinicaltrials.gov/ct2/show/NCT00089830?term=Squalamine&cond=AMD&draw=2&rank=7> (2007) doi:NCT00089830.
 353. A Study of MSI-1256F (Squalamine Lactate) To Treat ‘Wet’ Age-Related Macular Degeneration. *ClinicalTrials.gov*
<https://clinicaltrials.gov/ct2/show/NCT00333476?term=Squalamine&cond=AMD&draw=2&rank=6> (2007) doi:NCT00333476.
 354. MSI-1256F (Squalamine Lactate) in Combination With Verteporfin in Patients With ‘Wet’ Age-Related Macular Degeneration (AMD). *ClinicalTrials.gov*
<https://clinicaltrials.gov/ct2/show/NCT00094120?term=Squalamine&cond=AMD&draw=2&rank=3> (2008) doi:NCT00094120.
 355. A Safety and Efficacy Study of Squalamine Lactate for Injection (MSI-1256F) for ‘Wet’ Age-Related Macular Degeneration. *ClinicalTrials.gov*
<https://clinicaltrials.gov/ct2/show/NCT00139282?term=NCT00139282&draw=2&rank=1> (2007) doi:NCT00139282.
 356. Efficacy and Safety of Squalamine Lactate Eye Drops in Subjects With Neovascular (Wet) Age-related Macular Degeneration (AMD). *ClinicalTrials.gov*
<https://clinicaltrials.gov/ct2/show/NCT01678963?term=NCT01678963&draw=2&rank=1> (2015) doi:NCT01678963.
 357. Cunningham Jr., E. T. Impact of the OHR-102 IMPACT Data. <https://www.retina-specialist.com/article/impact-of-the-ohr102-impact-data>.
 358. Efficacy and Safety Study of Squalamine Ophthalmic Solution in Subjects With Neovascular AMD. *ClinicalTrials.gov*
<https://clinicaltrials.gov/ct2/show/NCT02727881?term=NCT02727881&cond=AMD&draw=2&rank=1> (2018) doi:NCT02727881.
 359. Tura, A., Ranjbar, M., Grisanti, S. & Grisanti, S. Squalamine and age-related macular degeneration. Did the Shark lose its teeth? *New Front. Ophthalmol.* **4**, (2018).
 360. Garba, A. O. & Mousa, S. A. Bevasiranib for the Treatment of Wet, Age-Related Macular Degeneration. *Ophthalmol. Eye Dis.* **2**, OED.S4878 (2010).
 361. Safety & Efficacy Study Evaluating the Combination of Bevasiranib & Lucentis Therapy in Wet AMD. *ClinicalTrials.gov*

- <https://clinicaltrials.gov/ct2/show/study/NCT00499590?term=Bevasiranib&cond=AMD&draw=2&rank=1> (2014) doi:NCT00499590.
362. Shen, J. *et al.* Suppression of ocular neovascularization with siRNA targeting VEGF receptor 1. *Gene Ther.* **13**, 225–234 (2006).
363. A Dose Escalation Trial of an Intravitreal Injection of Sirna-027 in Patients With Subfoveal Choroidal Neovascularization (CNV) Secondary to Age-Related Macular Degeneration (AMD). *ClinicalTrials.gov* <https://clinicaltrials.gov/ct2/show/NCT00363714?term=siRNA-027&cond=AMD&draw=2&rank=1> (2008) doi:NCT00363714.
364. A Study Using Intravitreal Injections of a Small Interfering RNA in Patients With Age-Related Macular Degeneration. *ClinicalTrials.gov* <https://clinicaltrials.gov/ct2/show/NCT00395057?term=siRNA-027&cond=AMD&draw=2&rank=2> (2015) doi:NCT00395057.
365. AGN-745 (Sirna-027) - Wet AMD Development was halted | www.amdbook.org. <https://amdbook.org/content/agn-745-sirna-027-wet-amd-development-was-halted>.
366. Campochiaro, P. A. *et al.* Lentiviral vector gene transfer of endostatin/angiostatin for macular degeneration (GEM) study. *Hum. Gene Ther.* **28**, 99–111 (2017).
367. Phase I Dose Escalation Safety Study of RetinoStat in Advanced Age-Related Macular Degeneration (AMD). *ClinicalTrials.gov* <https://clinicaltrials.gov/ct2/show/NCT01301443?term=RetinoStat&cond=AMD&draw=2&rank=1> (2017) doi:NCT01301443.
368. Kim, S., Kim, D., Cho, S. W., Kim, J. & Kim, J. Highly efficient RNA-guided genome editing in human cells via delivery of purified Cas9 ribonucleoproteins. *Genome Res.* **24**, 1012–1019 (2014).
369. Zuris, J. A. *et al.* Cationic lipid-mediated delivery of proteins enables efficient protein-based genome editing in vitro and in vivo. *Nat. Biotechnol.* **33**, 73–80 (2015).
370. Kim, K. *et al.* Genome surgery using Cas9 ribonucleoproteins for the treatment of age-related macular degeneration. *Genome Res.* **27**, 419–426 (2017).
371. Safety and Efficacy Study of rAAV.sFlt-1 in Patients With Exudative Age-Related Macular Degeneration. *ClinicalTrials.gov* <https://clinicaltrials.gov/ct2/show/NCT01494805?term=NCT01494805&draw=2&rank=1> (2017) doi:NCT01494805.
372. Constable, I. J. *et al.* Gene Therapy in Neovascular Age-related Macular Degeneration: Three-Year Follow-up of a Phase 1 Randomized Dose Escalation Trial. *Am. J. Ophthalmol.* **177**, 150–158 (2017).
373. Safety and Tolerability Study of AAV2-sFLT01 in Patients With Neovascular Age-Related Macular Degeneration (AMD). *ClinicalTrials.gov* <https://clinicaltrials.gov/ct2/show/NCT01024998?term=NCT01024998&draw=2&rank=1> (2018) doi:NCT01024998.
374. Heier, J. S. *et al.* Intravitreal injection of AAV2-sFLT01 in patients with advanced neovascular age-related macular degeneration: a phase 1, open-label trial. *Lancet* **390**, 50–61 (2017).
375. Jaffe, G. J. *et al.* Dual Antagonism of PDGF and VEGF in Neovascular Age-Related Macular Degeneration: A Phase IIb, Multicenter, Randomized Controlled Trial. *Ophthalmology* **124**, 224–234 (2017).

376. Tsioumpkou, M. *et al.* Specific targeting of PDGFR β in the stroma inhibits growth and angiogenesis in tumors with high PDGF-BB expression. *Theranostics* **10**, 1122–1135 (2020).
377. Sadiq, M. A. *et al.* Platelet derived growth factor inhibitors: A potential therapeutic approach for ocular neovascularization. *Saudi J. Ophthalmol.* **29**, 287–291 (2015).
378. A Phase 1, Safety, Tolerability and Pharmacokinetic Profile of Intravitreal Injections of E10030 (Anti-PDGF Pegylated Aptamer) in Subjects With Neovascular Age-Related Macular Degeneration. *ClinicalTrials.gov* <https://clinicaltrials.gov/ct2/show/NCT00569140> (2010) doi:NCT00569140.
379. A Safety and Efficacy Study of E10030 (Anti-PDGF Pegylated Aptamer) Plus Lucentis for Neovascular Age-Related Macular Degeneration. *ClinicalTrials.gov* <https://clinicaltrials.gov/ct2/show/NCT01089517> (2017) doi:NCT01089517.
380. A Phase 3 Safety and Efficacy Study of Fovista[®] (E10030) Intravitreal Administration in Combination With Lucentis[®] Compared to Lucentis[®] Monotherapy. *ClinicalTrials.gov* <https://clinicaltrials.gov/ct2/show/study/NCT01940900> (2018) doi:NCT01940900.
381. A Phase 3 Safety and Efficacy Study of Fovista[®] (E10030) Intravitreal Administration in Combination With Lucentis[®] Compared to Lucentis[®] Monotherapy. *ClinicalTrials.gov* <https://clinicaltrials.gov/ct2/show/NCT01944839?term=E10030&cond=AMD&draw=2&rank=3> (2018) doi:NCT01944839.
382. Park, E. J., Choi, J., Lee, K. C. & Na, D. H. Emerging PEGylated non-biologic drugs. *Expert Opin. Emerg. Drugs* **24**, 107–119 (2019).
383. A Phase 3 Safety and Efficacy Study of Fovista[®] (E10030) Intravitreal Administration in Combination With Either Avastin[®] or Eylea[®] Compared to Avastin[®] or Eylea[®] Monotherapy. *ClinicalTrials.gov* <https://clinicaltrials.gov/ct2/show/study/NCT01940887?term=E10030&cond=AMD&draw=2&rank=5> (2017) doi:NCT01940887.
384. Phase 1 Safety Study With Intravitreal (IVT) REGN2176-3 in Patients Aged 50 Years and Older With Wet AMD. *ClinicalTrials.gov* <https://clinicaltrials.gov/ct2/show/NCT02061865?term=REGN2176-3&cond=AMD&draw=2&rank=1> (2015) doi:NCT02061865.
385. Study of Intravitreal REGN2176-3 in Patients With Neovascular (‘Wet’) Age-Related Macular Degeneration (AMD). *ClinicalTrials.gov* <https://clinicaltrials.gov/ct2/show/NCT02418754?term=REGN2176-3&cond=AMD&draw=2&rank=2> (2017) doi:NCT02418754.
386. Scholz, A., Plate, K. H. & Reiss, Y. Angiopoietin-2: A multifaceted cytokine that functions in both angiogenesis and inflammation. *Ann. N. Y. Acad. Sci.* **1347**, 45–51 (2015).
387. Fukuhara, S. *et al.* Angiopoietin-1/Tie2 receptor signaling in vascular quiescence and angiogenesis. *Histol. Histopathol.* **25**, 387–396 (2010).
388. Parikh, S. M. The angiopoietin-Tie2 signaling axis in systemic inflammation. *J. Am. Soc. Nephrol.* **28**, 1973–1982 (2017).
389. Tabruyn, S. P. *et al.* Angiopoietin-2-driven vascular remodeling in airway inflammation. *Am. J. Pathol.* **177**, 3233–3244 (2010).
390. Wolf, A. & Langmann, T. Anti- VEGF -A/ ANG 2 combotherapy limits pathological angiogenesis in the eye: a replication study. *EMBO Mol. Med.* **11**, 10–11 (2019).

391. A Study of RO6867461 Administered in Single- and Multiple-Ascending Doses in Patients With Wet Age-Related Macular Degeneration. *ClinicalTrials.gov*
<https://clinicaltrials.gov/ct2/show/NCT01941082?term=NCT01941082&draw=2&rank=1>
 (2016) doi:NCT01941082.
392. A Proof-of-Concept Study of Faricimab (RO6867461) in Participants With Choroidal Neovascularization (CNV) Secondary to Age-Related Macular Degeneration (AMD). *ClinicalTrials.gov*
<https://clinicaltrials.gov/ct2/show/NCT02484690?term=NCT02484690&draw=2&rank=1>
 (2019) doi:NCT02484690.
393. A Study to Evaluate the Efficacy and Safety of Faricimab in Participants With Neovascular Age-Related Macular Degeneration (LUCERNE). *ClinicalTrials.gov*
<https://clinicaltrials.gov/ct2/show/NCT03823300?term=NCT03823300&draw=2&rank=1>
 (2021) doi:NCT03823300.
394. A Study to Evaluate the Efficacy and Safety of Faricimab in Participants With Neovascular Age-Related Macular Degeneration (TENAYA). *ClinicalTrials.gov*
<https://clinicaltrials.gov/ct2/show/NCT03823287?term=RG7716&cond=wet+AMD&draw=2&rank=1>
 (2021) doi:NCT03823287.
395. Study of Intravitreal (IVT) REGN910-3 and IVT REGN910 in Patients With Either Neovascular ('Wet') Age Related Macular Degeneration (AMD) or Diabetic Macular Edema (DME). *ClinicalTrials.gov*
<https://clinicaltrials.gov/ct2/show/NCT01997164?term=NCT01997164&draw=2&rank=1>
 (2016) doi:NCT01997164.
396. Anti-angiOpoetin 2 Plus Anti-vascular eNdothelial Growth Factor as a therapY for Neovascular Age Related Macular Degeneration: Evaluation of a fiXed Combination Intravitreal Injection. *ClinicalTrials.gov*
<https://clinicaltrials.gov/ct2/show/NCT02713204?term=NCT02713204&draw=2&rank=1>
 (2019) doi:NCT02713204.
397. Ishikawa, M., Jin, D., Sawada, Y., Abe, S. & Yoshitomi, T. Future Therapies of Wet Age-Related Macular Degeneration. *J. Ophthalmol.* **2015**, 1–10 (2015).
398. Anecortave Acetate in Patients With Exudative Age-related Macular Degeneration (AMD) - Full Text View. *ClinicalTrials.gov*
<https://clinicaltrials.gov/ct2/show/NCT00299507?term=Anecortave+acetate&cond=AMD&draw=2&rank=2>
 (2012) doi:NCT00299507.
399. Evaluate the Therapeutic Effects and Safety of ALK4290 in Patients With Refractory Wet Age-Related Macular Degeneration. *ClinicalTrials.gov*
<https://clinicaltrials.gov/ct2/show/NCT03558074?term=ALK4290&cond=AMD&draw=2&rank=2>
 (2020) doi:NCT03558074.
400. Evaluate the Effects and Safety of ALK4290 in Patients With Newly Diagnosed Wet Age-Related Macular Degeneration. *ClinicalTrials.gov*
<https://clinicaltrials.gov/ct2/show/NCT03558061?term=ALK4290&cond=AMD&draw=2&rank=1>
 (2012) doi:NCT03558061.
401. Safety and Efficacy of Intravitreal LFG316 in Wet Age Related Macular Degeneration (AMD). *ClinicalTrials.gov*
<https://clinicaltrials.gov/ct2/show/NCT01535950?term=NCT01535950&cond=AMD&draw=2&rank=1>
 (2016) doi:NCT01535950.

402. Safety and Tolerability of Intravenous LFG316 in Wet Age-related Macular Degeneration (AMD). *ClinicalTrials.gov*
<https://clinicaltrials.gov/ct2/show/NCT01624636?term=NCT01624636&cond=AMD&draw=2&rank=1> (2016) doi:NCT01624636.
403. Assessment of Safety, Tolerability and Pharmacokinetics of Intravitreal APL-2 for Patients With Wet AMD. *ClinicalTrials.gov* <https://clinicaltrials.gov/ct2/show/NCT02461771?term=APL-2&cond=AMD&draw=2&rank=1> (2020) doi:NCT02461771.
404. APL-2 in Neovascular AMD. *ClinicalTrials.gov*
<https://clinicaltrials.gov/ct2/show/NCT03465709?term=APL-2&cond=AMD&draw=2&rank=2> (2020) doi:NCT03465709.
405. AAVCAGsCD59 for the Treatment of Wet AMD. *ClinicalTrials.gov*
<https://clinicaltrials.gov/ct2/show/NCT03585556?term=AAVCAGsCD59&cond=AMD&draw=2&rank=1> (2020) doi:NCT03585556.
406. Triple Combination Therapy of Choroidal Neovascularization in AMD, a Cost Effect and Efficient Therapeutic Treatment. *ClinicalTrials.gov*
<https://clinicaltrials.gov/ct2/show/NCT02287298?term=Triple+combination+therapy&cond=AMD&draw=2&rank=1> (2016) doi:NCT02287298.
407. Khatol, P., Saraf, S. & Jain, A. Peroxisome proliferated activated receptors (PPARs): Opportunities and challenges for ocular therapy. *Crit. Rev. Ther. Drug Carrier Syst.* **35**, 65–97 (2018).
408. Choudhary, M. *et al.* PPAR β/δ selectively regulates phenotypic features of age-related macular degeneration. *Aging (Albany. NY)*. **8**, 1952–1978 (2016).
409. Vallée, A., Lecarpentier, Y., Guillevin, R. & Vallée, J. N. PPAR γ agonists: Potential treatments for exudative age-related macular degeneration. *Life Sci.* **188**, 123–130 (2017).
410. A Safety And Efficacy Study Of ALG-1001 In Human Subjects With Wet Age-Related Macular Degeneration. *ClinicalTrials.gov* <https://clinicaltrials.gov/ct2/show/NCT01749891?term=ALG-1001&cond=AMD&draw=2&rank=1> (2017) doi:NCT01749891.
411. A Phase 1 Safety Study of Single and Repeated Doses of JSM6427 (Intravitreal Injection) to Treat AMD. *ClinicalTrials.gov*
<https://clinicaltrials.gov/ct2/show/NCT00536016?term=JSM6427&cond=AMD&draw=2&rank=1> (2010) doi:NCT00536016.
412. A Phase 1 Ascending and Parallel Group Trial to Establish the Safety, Tolerability and Pharmacokinetics Profile of Volociximab (Alpha 5 Beta 1 Integrin Antagonist) in Subjects With Neovascular Age-Related Macular Degeneration. *ClinicalTrials.gov*
<https://clinicaltrials.gov/ct2/show/NCT00782093?term=Volociximab&cond=AMD&draw=2&rank=1> (2012) doi:NCT00782093.
413. Safety and Efficacy of ATG003 in Patients With AMD Receiving Anti-VEGF. *ClinicalTrials.gov*
<https://clinicaltrials.gov/ct2/show/NCT00607750?term=ATG003&cond=AMD&draw=2&rank=1> (2010) doi:NCT00607750.
414. Safety and Efficacy of ATG003 in Patients With Wet Age-Related Macular Degeneration (AMD). *ClinicalTrials.gov*
<https://clinicaltrials.gov/ct2/show/NCT00414206?term=ATG003&cond=AMD&draw=2&rank=2> (2010) doi:NCT00414206.
415. Lim, J. I. Neovascular age-related macular degeneration. (2020).

416. Kurup, S. K., Gee, C. & Greven, C. M. Intravitreal methotrexate in therapeutically resistant exudative age-related macular degeneration. *Acta Ophthalmol.* **88**, e145–e146 (2009).
417. Soheilian, M., Movaseghi, M., Ramezani, A. & Peyman, G. A. Pilot study of safety and effect of combined intravitreal bevacizumab and methotrexate for neovascular age-related macular degeneration. *Eur. J. Ophthalmol.* **21**, 77–82 (2011).
418. Infliximab, Sirolimus and Daclizumab to Treat Age-Related Macular Degeneration. *ClinicalTrials.gov*
<https://clinicaltrials.gov/ct2/show/NCT00304954?term=Sirolimus&cond=AMD&draw=2&rank=7> (2016) doi:NCT00304954.
419. Phase 1/2 Study of an Ocular Sirolimus (Rapamycin) Formulation in Patients With Age-Related Macular Degeneration. *ClinicalTrials.gov*
<https://clinicaltrials.gov/ct2/show/NCT00712491?term=Sirolimus&cond=AMD&draw=2&rank=4> (2013) doi:NCT00712491.
420. Sirolimus Versus Anti-Vascular Endothelial Growth Factor (antiVEGF) for Wet AMD. *ClinicalTrials.gov*
<https://clinicaltrials.gov/ct2/show/NCT02357342?term=Sirolimus&cond=AMD&draw=2&rank=2> (2017) doi:NCT02357342.
421. Sirolimus in Conjunction With Eylea vs Eylea Alone for Exudative AMD. *ClinicalTrials.gov*
<https://clinicaltrials.gov/ct2/show/NCT02732899?term=Sirolimus&cond=AMD&draw=2&rank=1> (2018) doi:NCT02732899.
422. Anecortave Acetate Versus Placebo in AMD Patients Following PDT. *ClinicalTrials.gov*
<https://clinicaltrials.gov/ct2/show/NCT00346866?term=Anecortave+acetate&cond=AMD&draw=2&rank=1> (2008) doi:NCT00346866.
423. TAC-PF, Avastin® in Combination With Photodynamic Therapy to Treat Age Related Macular Degeneration. *ClinicalTrials.gov*
<https://clinicaltrials.gov/ct2/show/NCT00464347?term=Triamcinolone+acetamide&cond=wet+AMD&draw=2&rank=1> (2010) doi:NCT00464347.
424. Study of the Combination of Anecortave Acetate and Triamcinolone Acetonide for the Treatment of Exudative Age-Related Macular Degeneration (AMD). *ClinicalTrials.gov*
<https://clinicaltrials.gov/ct2/show/NCT00211419?term=Triamcinolone+acetamide&cond=wet+AMD&draw=2&rank=4> (2012) doi:NCT00211419.
425. ARC1905 (ANTI-C5 APTAMER) Given Either In Combination Therapy With Lucentis® 0.5 mg/Eye In Subjects With Neovascular Age-Related Macular Degeneration. *ClinicalTrials.gov*
<https://clinicaltrials.gov/ct2/show/NCT00709527?term=NCT00709527&cond=AMD&draw=2&rank=1> (2012) doi:NCT00709527.
426. ZIMURA in Combination With LUCENTIS in Patients With Neovascular Age Related Macular Degeneration (NVAMD). *ClinicalTrials.gov*
<https://clinicaltrials.gov/ct2/show/NCT03362190?term=Zimura&cond=AMD&draw=2&rank=1> (2019) doi:NCT03362190.
427. Safety of Intravitreal POT-4 Therapy for Patients With Neovascular Age-Related Macular Degeneration (AMD). *ClinicalTrials.gov*
<https://clinicaltrials.gov/ct2/show/NCT00473928?term=POT-4&cond=AMD&draw=2&rank=1> (2010) doi:NCT00473928.
428. Evaluation of AL-78898A in Exudative Age-Related Macular Degeneration. *ClinicalTrials.gov*

- <https://clinicaltrials.gov/ct2/show/NCT01157065?term=AL-78898A&cond=AMD&draw=2&rank=1> (2013) doi:NCT01157065.
429. Kanemura, H. *et al.* Tumorigenicity studies of induced pluripotent stem cell (iPSC)-derived retinal pigment epithelium (RPE) for the treatment of age-related macular degeneration. *PLoS One* **9**, 1–11 (2014).
 430. Chakradhar, S. An eye to the future: Researchers debate best path for stem cell-derived therapies. *Nat. Med.* **22**, 116–119 (2016).
 431. A Study Of Implantation Of Retinal Pigment Epithelium In Subjects With Acute Wet Age Related Macular Degeneration. *ClinicalTrials.gov* <https://clinicaltrials.gov/ct2/show/NCT01691261?term=Stem+cells&cond=wet+AMD&draw=2&rank=1> doi:NCT01691261.
 432. Retinal Pigment Epithelium Safety Study For Patients In B4711001. *ClinicalTrials.gov* <https://clinicaltrials.gov/ct2/show/NCT03102138?term=Stem+cells&cond=wet+AMD&draw=2&rank=2> (2019) doi:NCT03102138.
 433. Ferris, F. L., Fine, S. L. & Hyman, L. Age-Related Macular Degeneration and Blindness Due to Neovascular Maculopathy. *Arch. Ophthalmol.* **102**, 1640–1642 (1984).
 434. Eng, V. A., Id, N. R., Id, H. V. N. & Id, T. L. Complete RPE and outer retinal atrophy in patients receiving anti-VEGF treatment for neovascular age-related macular degeneration. *PLoS One* **15**, 1–13 (2020).
 435. Dufies, M. *et al.* New CXCR1/CXCR2 inhibitors represent an effective treatment for kidney or head and neck cancers sensitive or refractory to reference treatments. *Theranostics* **9**, 5332–5346 (2019).
 436. Ha, H., Debnath, B. & Neamati, N. Role of the CXCL8-CXCR1/2 axis in cancer and inflammatory diseases. *Theranostics* **7**, 1543–1588 (2017).
 437. Giuliano, S., Guyot, M., Grépin, R. & Pagès, G. The ELR+CXCL chemokines and their receptors CXCR1/CXCR2: A signaling axis and new target for the treatment of renal cell carcinoma. *Oncoimmunology* **3**, 8–11 (2014).
 438. Vandercappellen, J., Damme, J. Van & Struyf, S. The role of CXC chemokines and their receptors in cancer. *Cancer Lett.* **267**, 226–244 (2008).
 439. Boshagh, M. A. *et al.* ELR positive CXCL chemokines are highly expressed in an animal model of ulcerative colitis. 167–174 (2019).
 440. Waugh, D. J. J. & Wilson, C. The interleukin-8 pathway in cancer. *Clin. Cancer Res.* **14**, 6735–6741 (2008).
 441. Mélik-Parsadaniantz, S. & Rostène, W. Chemokines and neuromodulation. *J. Neuroimmunol.* **198**, 62–68 (2008).
 442. Baggiolini, M. Chemokines and leukocyte traffic. *Nature* **392**, 565–568 (1998).
 443. Sallusto, F. & Baggiolini, M. Chemokines and leukocyte traffic. *Nat. Immunol.* **9**, 949–952 (2008).
 444. Che, J., Song, R., Chen, B. & Dong, X. Targeting CXCR1/2: The medicinal potential as cancer immunotherapy agents, antagonists research highlights and challenges ahead. *Eur. J. Med. Chem.* **185**, 111853 (2020).
 445. Qi, J., Mcclelland, B. W., Palovich, M. R. & Widdowson, K. L. Hydroxy diphenyl urea sulfonamides as IL-8 receptor antagonists. (2000) doi:WO0035442A1.

446. White, J. R. *et al.* Identification of a Potent, Selective Non-peptide CXCR2 Antagonist That Inhibits Interleukin-8-induced Neutrophil Migration*. *J. Biol. Chem.* **273**, 10095–10098 (1998).
447. Jin, Q. *et al.* Discovery of potent and orally bioavailable N , N -diarylurea antagonists for the CXCR2 chemokine receptor. *Bioorg. Med. Chem. Lett.* **14**, 4375–4378 (2004).
448. Lazaar, A. L. *et al.* CXCR2 antagonist for patients with chronic obstructive pulmonary disease with chronic mucus hypersecretion: A phase 2b trial. *Respir. Res.* **21**, (2020).
449. Palovich, M. R., Mcclelland, B., Bi, G., Werner, M. & Widdowson, K. L. IL-8 receptor antagonists. (2001) doi:WO0192202A1.
450. Schott, A. F. *et al.* Phase Ib pilot study to evaluate reparixin in combination with weekly paclitaxel in patients with HER-2–negative metastatic breast cancer. *Clin. Cancer Res.* **23**, 5358–5365 (2017).
451. Goldstein, L. J. *et al.* A window-of-opportunity trial of the CXCR1/2 inhibitor reparixin in operable HER-2-negative breast cancer. *Breast Cancer Res.* **22**, 1–9 (2020).
452. Grepin, R. *et al.* Acceleration of clear cell renal cell carcinoma growth in mice following bevacizumab/Avastin treatment: The role of CXCL cytokines. *Oncogene* **31**, 1683–1694 (2012).
453. Grepin, R. *et al.* The CXCL7/CXCR1/2 axis is a key driver in the growth of clear cell renal cell carcinoma. *Cancer Res.* **74**, 873–883 (2014).
454. White, J. R. *et al.* Identification of a Potent, Selective Non-peptide CXCR2 Antagonist That Inhibits Interleukin-8-induced Neutrophil Migration*. *J. Biol. Chem.* **273**, 10095–10098 (1998).
455. Benhida, R. *et al.* Urea derivatives for treating and/or preventing cancer. (2020) doi:WO2020079184A2.
456. May, J. A. ., Bingaman, D. P. . & Romano, C. Urea compounds for the treatment of posterior segment disorders and other ocular diseases. (2012) doi:WO2012003141A1.
457. Kim, J. *et al.* Urea derivatives as antiangiogenic agents. (2014) doi:WO2014201127A2.
458. Imidazole-Hazardous Substances Data Bank (HSDB): 8449 - PubChem. <https://pubchem.ncbi.nlm.nih.gov/source/hsdb/8449>.
459. Garratt, P. J. 1,2,4-Triazoles. in *Comprehensive Heterocyclic Chemistry II: A Review of the Literature 1982-1995* vol. 4 127–163 (Elsevier Ltd, 1996).
460. Mahboobi, S. *et al.* Inhibition of PDGFR tyrosine kinase activity by a series of novel N-(3-(4-(pyridin-3-yl)-1H-imidazol-2-ylamino)phenyl)amides - A SAR study on the bioisosterism of pyrimidine and imidazole. *Eur. J. Med. Chem.* **43**, 1444–1453 (2008).
461. Capua, M. *et al.* An expeditious and greener synthesis of 2-aminoimidazoles in deep eutectic solvents. *Molecules* **21**, 1–11 (2016).
462. Millet, A. *et al.* Discovery and Optimization of N-(4-(3-Aminophenyl)thiazol-2-yl)acetamide as a Novel Scaffold Active against Sensitive and Resistant Cancer Cells. *J. Med. Chem.* **59**, 8276–8292 (2016).
463. Dornow, A., Machens, H. & Bruncken, K. Uber einige Aminoalkohole der Pyridyl- und Dipyridyl-iithanreih. *Chem. Ber.* **84**, 147–246 (1951).
464. Ha, H. H., Kim, J. S. & Kim, B. M. Novel heterocycle-substituted pyrimidines as inhibitors of NF- κ B transcription regulation related to TNF- α cytokine release. *Bioorganic Med. Chem. Lett.* **18**, 653–656 (2008).

465. Diab, S. *et al.* Discovery of 5-(2-(phenylamino)pyrimidin-4-yl)thiazol-2(3H)-one derivatives as potent Mnk2 inhibitors: Synthesis, SAR analysis and biological evaluation. *ChemMedChem* **9**, 962–972 (2014).
466. Tsubokura, K. *et al.* Direct guanylation of amino groups by cyanamide in water: Catalytic generation and activation of unsubstituted carbodiimide by scandium(iii) triflate. *Synlett* **25**, 1302–1306 (2014).
467. Horwitz, J. P. & Rila, C. C. A Comparison of the Reactions of Some Amines with Nitrosoguanidine, Cyanamide and S-Methylisothiurea Hydrochlorides. *J. Am. Chem. Soc.* **80**, 431–437 (1958).
468. Ciufolini, M., Benjahad, A., Giethlen, B., Moussy, A. & Wermuth, C. Aminoaryl substituted five-membered ring heterocyclic compounds for the treatment of diseases. (2006) doi:WO2006064375A2.
469. Scott, F. L., O'Donovan, D. G. & Reilly, J. Studies in the Pyrazole Series. III. Substituted Guanidines. *J. Am. Chem. Soc.* **75**, 4053–4054 (1953).
470. Little, T. L. & Webber, S. E. A Simple and Practical Synthesis of 2-Aminoimidazoles. *J. Org. Chem.* **59**, 7299–7305 (1994).
471. Ando, N. & Terashima, S. A novel synthesis of the 2-amino-1H-imidazol-4-carbaldehyde derivatives and its application to the efficient synthesis of 2-aminoimidazole alkaloids, oroidin, hymenidin, dispacamide, monobromodispacamide, and ageladine A. *Tetrahedron* **66**, 6224–6237 (2010).
472. Iwata, T. *et al.* One-Pot Evolution of Ageladine A through a Bio-Inspired Cascade towards Selective Modulators of Neuronal Differentiation. *Chem. - A Eur. J.* **22**, 14707–14716 (2016).
473. Bracht, C., Hauser, D. R. J., Schattel, V., Albrecht, W. & Laufer, S. A. Synthesis and biological testing of N-aminoimidazole-based p38 α MAP kinase inhibitors. *ChemMedChem* **5**, 1134–1142 (2010).
474. Günther, M. *et al.* Trisubstituted Pyridinylimidazoles as Potent Inhibitors of the Clinically Resistant L858R/T790M/C797S EGFR Mutant: Targeting of Both Hydrophobic Regions and the Phosphate Binding Site. *J. Med. Chem.* **60**, 5613–5637 (2017).
475. Li, K. *et al.* Oxa, Thia, Heterocycle, and Carborane Analogues of SQ109: Bacterial and Protozoal Cell Growth Inhibitors. *ACS Infect. Dis.* **109**, 215–221 (2015).
476. Sudarsanam, V. *et al.* Nitroimidazoles: Part VIII -2-amino-1-methyl-5-nitroimidazoles & derivatives. *Indian J. Chem.* **21B**, 989–996 (1982).
477. Lan, P. *et al.* An efficient method to access 2-substituted benzimidazoles under solvent-free conditions. *Tetrahedron Lett.* **49**, 1910–1914 (2008).
478. Lukasik, P. M. *et al.* Synthesis and biological evaluation of imidazo [4 , 5- b] pyridine and 4-heteroaryl- pyrimidine derivatives as anti-cancer agents. *Eur. J. Med. Chem.* **57**, 311–322 (2012).
479. D'Sidocky, N. R. . *et al.* Amino-substituted heterocycles, compositions thereof, and methods of treatment therewith. (2008) doi:WO2008036308A2.
480. Ibáñez, E. *et al.* Synthesis and antiproliferative activity of novel symmetrical alkylthio- and alkylseleno-imidocarbamates. *Eur. J. Med. Chem.* **46**, 265–274 (2011).
481. Steenackers, H. P. L. *et al.* Structure-activity relationship of 2-hydroxy-2-aryl-2,3-dihydroimidazo[1, 2-a]pyrimidinium salts and 2N-substituted 4(5)-aryl-2-amino-1H-imidazoles as inhibitors of biofilm formation by Salmonella Typhimurium and Pseudomonas aeruginosa.

- Bioorganic Med. Chem.* **19**, 3462–3473 (2011).
482. Delvos, L. B., Begouin, J. M. & Gosmini, C. Zinc base assisted amination of 2-chloropyrimidines by aniline derivatives at room temperature. *Synlett* **16**, 2325–2328 (2011).
483. Hao, X. *et al.* Air-stable and highly efficient indenyl-derived phosphine ligand: Application to Buchwald-Hartwig amination reactions. *J. Organomet. Chem.* **706–707**, 99–105 (2012).
484. Shaw, J. W., Grayson, D. H. & Rozas, I. Synthesis of cyclic guanidines: 2-arylamino-1,4,5,6-tetrahydropyrimidines. *Archive Org. Chem.* **2014**, 161–174 (2014).
485. Huang, X. *et al.* A copper-mediated tandem reaction through isocyanide insertion into N-H bonds: Efficient access to unsymmetrical tetrasubstituted ureas. *Chem. Commun.* **50**, 1465–1468 (2014).
486. Castillo-Meléndez, J. A. & Golding, B. T. Optimisation of the synthesis of guanidines from amines via nitroguanidines using 3,5-dimethyl-N-nitro-1H-pyrazole-1-carboxamide. *Synthesis (Stuttg)*. 1655–1663 (2004) doi:10.1055/s-2004-829130.
487. Solodenko, W., Bröker, P., Messinger, J., Schön, U. & Kirschning, A. Amidination of amines under microwave conditions using recyclable polymer-bound 1H-pyrazole-1-carboxamide. *Synthesis (Stuttg)*. **2006**, 461–466 (2006).
488. Earle, H. N., Hurst, N. B. & Andrew, W. T. Novel imidazole derivatives useful for the treatment of arthritis. (2012) doi:WO 2012/161965.
489. Amberg, W. *et al.* 5-Ring Heteroaromatic compounds and their use as binding partners for 5-HT₅ receptors. (2007).
490. Nishimura, T. & Kitajima, K. Reaction of guanidines with α -diketones. Syntheses of 4,5-disubstituted-2-aminoimidazoles and 2,6-unsymmetrically substituted imidazo[4,5-d]imidazoles. *J. Org. Chem.* **44**, 818–824 (1979).
491. Congreve, M. S., Andrews, S. P., Mason, J. S., Richardson, C. M. & Brown, G. A. 1,2,4-triazine-4-amine derivatives. doi:WO2011095625A1.
492. Zidar, N. *et al.* Substituted 4-phenyl-2-aminoimidazoles and 4-phenyl-4,5-dihydro-2-aminoimidazoles as voltage-gated sodium channel modulators. *Eur. J. Med. Chem.* **74**, 23–30 (2014).
493. Zidar, N. *et al.* Antimicrobial activity of the marine alkaloids, clathrocin and oroidin, and their synthetic analogues. *Mar. Drugs* **12**, 940–963 (2014).
494. Charrier, C., Khan, N. & Meo, P. Antibacterial compounds. (2019) doi:WO2019086890A1.
495. Trinka, P. & Reiter, J. Triazoles. XXXVI. The arylation of 5-amino-3-(methylthio)-1H-1,2,4-triazole with activated aryl chlorides. *J. Heterocycl. Chem.* **32**, 1359–1371 (1995).
496. BAUER, U., BRAILSFORD, W., GUSTAFSSON, L. & SVENSSON, T. GABA-B Receptor modulators. (2007) doi:WO2007073300A1.
497. Romagnoli, R. *et al.* Synthesis, antimitotic and antivasular activity of 1-(3',4', 5'-trimethoxybenzoyl)-3-arylamino-5-amino-1,2,4-triazoles. *J. Med. Chem.* **57**, 6795–6808 (2014).
498. Dolzhenko, A. V., Dolzhenko, A. V. & Chui, W. K. Synthesis of 5,7-diamino-1,2,4-triazolo[1,2-a]1,3,5-triazines via annulation of 1,3,5-triazine ring onto 3(5)-amino-1,2,4-triazoles. *Heterocycles* **71**, 429–436 (2007).
499. Reiter, J. & Pongo, L. On Triazoles. V [1,2]. Synthesis of 1- and 2-R'-3-R₂,R₃-Amino-5-amino-1

- ,2,4-triazoles. *J. Heterocycl. Chem.* **23**, 401 (1986).
500. FREDRIK, B. & CHRISTENSEN, M. K. Novel Cyanoguanidines. (2009) doi:WO2009086835A1.
 501. Christensen, M. K. *et al.* Nicotinamide phosphoribosyltransferase inhibitors, design, preparation, and structure-activity relationship. *J. Med. Chem.* **56**, 9071–9088 (2013).
 502. BAIR, K. W. *et al.* Guanidine compounds and compositions for the inhibition of NAMPT. (2012) doi:WO2012031199A1.
 503. Zheng, X. *et al.* Discovery of potent and efficacious cyanoguanidine-containing nicotinamide phosphoribosyltransferase (Namp1) inhibitors. *Bioorganic Med. Chem. Lett.* **24**, 337–343 (2014).
 504. Lin, R. *et al.* 1-Acyl-1H-[1,2,4]triazole-3,5-diamine analogues as novel and potent anticancer cyclin-dependent kinase inhibitors: Synthesis and evaluation of biological activities. *J. Med. Chem.* **48**, 4208–4211 (2005).
 505. Malerich, J. P. *et al.* Diamino-1,2,4-triazole derivatives are selective inhibitors of TYK2 and JAK1 over JAK2 and JAK3. *Bioorganic Med. Chem. Lett.* **20**, 7454–7457 (2010).
 506. Chen, Z. *et al.* 5-(Heteroaryl-amino)-1H-1,2,4-triazol-3-amines as antiviral compounds and their preparation. (2014) doi:WO2014135483A1.
 507. Er-Rhaimini, A. & Mornet, R. Synthesis and photochemical degradation of N-arylmethyl derivatives of the herbicide 3-amino-1,2,4-triazole. *J. Heterocycl. Chem.* **29**, 1561–1566 (1992).
 508. Liu, K. *et al.* Structural basis of CXC chemokine receptor 2 activation and signalling. *Nature* **585**, (2020).
 509. Fabre, M. *et al.* Synthesis, 3D-structure and stability analyses of NRPa-308, a new promising anti-cancer agent. *Bioorganic Med. Chem. Lett.* **29**, 126710 (2019).
 510. Kathuria, D., Bankar, A. A. & Bharatam, P. V. “What’s in a structure?” The story of biguanides. *J. Mol. Struct.* **1152**, 61–78 (2018).
 511. Elmar, B., Stach, K., Schmidt, F. H., Heerdt, R. & Weber, H. Biguanide compounds and anti-diabetic compositions. (1977) doi:US4017539A.
 512. Mayer, S., Daigle, D. M., Brown, E. D., Khatri, J. & Organ, M. G. An expedient and facile one-step synthesis of a biguanide library by microwave irradiation coupled with simple product filtration. Inhibitors of dihydrofolate reductase. *J. Comb. Chem.* **6**, 776–782 (2004).
 513. Smolka, A. & Friedreich, A. Über eine neue Darstellungsweise der Biguanide und über einige Derivate des Phenylbiguanids. *Monatshefte für Chemie* **9**, 227–241 (1888).
 514. Tonelli, M., Espinoza, S., Gainetdinov, R. R. & Cichero, E. Novel biguanide-based derivatives scouted as TAAR1 agonists: Synthesis, biological evaluation, ADME prediction and molecular docking studies. *Eur. J. Med. Chem.* **127**, 781–792 (2017).
 515. van Kuijk, S. J. A. *et al.* New approach of delivering cytotoxic drugs towards CAIX expressing cells: A concept of dual-target drugs. *Eur. J. Med. Chem.* **127**, 691–702 (2017).
 516. Suyama, T., Soga, T. & Miyauchi, K. A method for the preparation of substituted biguanides. *Nippon Kagaku Kaishi* **5**, 884–887 (1989).
 517. Obianom, O. N. *et al.* Incorporation of a Biguanide Scaffold Enhances Drug Uptake by Organic Cation Transporters 1 and 2. *Mol. Pharm.* **14**, 2726–2739 (2017).

518. Kim, S. W.; Kim, H. W.; Yoo, S. H.; Lee, J. S.; Heo, H. J.; Lee, H. B.; Kook, J. A.; Lee, Y. W.; Kim, M. J.; Cho, W. Guanidine compounds and use thereof. (2015) doi:WO2015160220A1.
519. Fortun, S. & Schmitzer, A. R. Synthesis and Characterization of Biguanide and Biguanidium Surfactants for Efficient and Recyclable Application in the Suzuki–Miyaura Reaction. *ACS omega* **3**, 1889–1896 (2018).
520. Guo, Z., Cainmlde, A. N. & Mckilop, A. N- vs O-Alkylation in 2(1H)-quinolinone derivatives. *Tetrahedron Lett.* **40**, 6999–7002 (1999).
521. Chen, H. Y. *et al.* β -Biguanidinium-cyclodextrin: A supramolecular mimic of mitochondrial ADP/ATP carrier protein. *Tetrahedron* **70**, 2378–2382 (2014).
522. Yan, Q. & Zhao, Y. ATP-triggered biomimetic deformations of bioinspired receptor-containing polymer assemblies. *Chem. Sci.* **6**, 4343–4349 (2015).
523. Hao, X., Sang, W., Hu, J. & Yan, Q. Pulsating Polymer Micelles via ATP-Fueled Dissipative Self-Assembly. *ACS Macro Lett.* **6**, 1151–1155 (2017).
524. Shuhui, C., Zhifei, F., Jian, L., Miaorong, L. & Yang, Z. IDO1 inhibitor and preparation method and application thereof. (2018) doi:AU2017306487A1.
525. Vaillancourt, V. A. *et al.* Synthesis and biological activity of aminoguanidine and diaminoguanidine analogues of the antidiabetic/antiobesity agent 3-guanidinopropionic acid. *J. Med. Chem.* **44**, 1231–1248 (2001).
526. Igashira-Kamiyama, A., Kajiwarra, T., Nakano, M., Konno, T. & Ito, T. Syntheses, structures, and magnetic properties of tetramanganese(III) and hexamanganese(III) complexes containing derivative of biguanidate ligand: Ferromagnetic interaction via imino nitrogen. *Inorg. Chem.* **48**, 11388–11393 (2009).
527. Eilingsfeld, H. & Scheuermann, H. Synthese von 1.3.5-Triazinen. *Chem. Ber.* **100**, 1874–1891 (1967).
528. Bando, S., Ichikawa, E. & Odo, K. Synthesis of Guanylmelamines. *J. Synth. Org. Chem. Japan* **28**, 521–525 (1970).
529. KAWANO & Kentaro. Synthesis of Guanyl-O-Alkylisourea Salt by the Additive Reaction of Alcohol with Dicyandiamide. *Bull. Kyushu Inst. Technol.* 69–78 (1962).
530. Liu, W.-Q. *et al.* NRPa-308, a new neuropilin-1 antagonist, exerts in vitro anti-angiogenic and anti-proliferative effects and in vivo anti-cancer effects in a mouse xenograft model. *Cancer Lett.* **414**, 88–98 (2018).
531. Weitman, M. *et al.* Facile structural elucidation of imidazoles and oxazoles based on NMR spectroscopy and quantum mechanical calculations. *Tetrahedron* **66**, 1465–1471 (2010).
532. Armitage, I. *et al.* The Use of Chloroformamidine Hydrochloride as a Reagent for the Synthesis of Guanidines from Electron Deficient Aromatic Amines. *J. Heterocycl. Chem.* **54**, 728–734 (2017).
533. Tavares, F. X. *et al.* N-Phenyl-4-pyrazolo [1 , 5- b] pyridazin-3-ylpyrimidin-2-amines as Potent and Selective Inhibitors of Glycogen Synthase Kinase 3 with Good Cellular Efficacy. *J. Med. Chem.* 4716–4730 (2004) doi:10.1021/jm040063i.
534. Prajapati, V. G. & Sen, D. J. Synthesis and Biological Evaluation of Some Novel Coumarin and Guanidine Derivatives by Oral Glucose Tolerance Test. *Am. J. Adv. Drug Deliv.* **2**, 141–148 (2013).

535. Alix, K. *et al.* Super-agonist, full agonist, partial agonist and antagonist actions of arylguanidines at h5-HT3A receptors Super-agonist, full agonist, partial agonist and antagonist actions of arylguanidines at h5-HT 3 A receptors. *ACS Chem. Neurosci.* **7**, 1565–1574 (2016).
536. Khair, N. Z. *et al.* Discovery of CDK5 Inhibitors through Structure-Guided Approach. *ACS Med. Chem. Lett.* **10**, 786–791 (2019).
537. Kim, D.-Y. *et al.* New N-phenyl-2-pyrimidine-amine derivatives related to imatinib mesylate, useful as antitumor agents, and process for the preparation thereof. (2004) doi:WO2004099186A1.
538. Yasuhara, A., Sun, X.-M., Sakagami, K. & Hayashi, M. Preparation of amino-imidazole derivatives having stimulatory action on the activity of metabotropic glutamate receptor mGluR5. doi:WO2009099177A1.
539. Hendrix, M. *et al.* Preparation of acylaminoimidazoles as cardiovascular agents. (2007) doi:DE 102006001574 A1.
540. Chen, J., Pang, Q., Sun, Y. & Li, X. Synthesis of N-(2-pyridyl)indoles via Pd(II)-catalyzed oxidative coupling. *J. Org. Chem.* **76**, 3523–3526 (2011).
541. Porcheddu, A. *et al.* A “ Catch and Release ” Strategy for the Parallel Synthesis of 2,4,5-Trisubstituted Pyrimidines. *J. Comb. Chem.* **6**, 105–111 (2004).
542. Liu, Z., Chen, Z. C. & Zheng, Q. G. Hypervalent iodine in synthesis 92. A facile synthesis of 3-substituted-5,6-dihydroimidazo[2,1-b]thiazoles by cyclocondensation of alkynyl(phenyl)iodonium salts and imidazolidine-2-thione. *J. Chem. Res. - Part S* 715–717 (2003) doi:10.3184/030823403322863058.
543. Duca, M., Malnuit, V., Barbault, F. & Benhida, R. Design of novel RNA ligands that bind stem-bulge HIV-1 TAR RNA. *Chem. Commun.* **46**, 6162–6164 (2010).
544. Tilley, J. W. & Ramuz, H. The Synthesis of 3,5-Diamino-1,2,4-oxadiazol. *Helv. Chim. Acta* **63**, 832–840 (1980).
545. Davidson, J. S. & Peak, D. A. Dithiobiurets. Part III. 1,1-Disubstituted derivatives. *J. Chem. Soc.* 3327–3333 (1963) doi:10.1039/JR9630003327.
546. Curd, F. H. S., Cliven, E. C. & Richardson, D. N. Alkyl(halophenyl)dicyandiamides. (1945) doi:GB619497A.
547. Karnail, A. & Grover, G. J. Method of treating or prevention of fibrillation of the heart. (1994) doi:US5278169A.
548. Pierce, A. C. *et al.* Preparation of 3,5-diamino[1,2,4]triazoles as protein kinase inhibitors. (2004) doi:WO2004046120A2.
549. Pollack, S. J. *et al.* A comparative study of fragment screening methods on the p38 α kinase: New methods, new insights. *J. Comput. Aided. Mol. Des.* **25**, 677–687 (2011).
550. Kim, H. W. *et al.* Preparation of biguanide compounds for the treatment of cancer. *PCT Int. Appl.* 82 pp. (2016).
551. Shapiro, S. L., Parrino, V. A. & Freedman, L. Hypoglycemic Agents. III. N1-Alkyl-and Aralkylbiguanides. *J. Am. Chem. Soc.* **81**, 3728–3736 (1959).
552. Kim, S. W. *et al.* Preparation of guanidine compounds for inhibiting mitochondrial oxidative phosphorylation (OXPHOS). *PCT Int. Appl.* 148 pp. (2015).

553. Ma, X. *et al.* Synthesis and antimicrobial activity of N 1-benzyl or N 1-benzyloxy-1,6-dihydro-1,3,5-triazine-2,4-diamines. *Bioorganic Med. Chem. Lett.* **21**, 5428–5431 (2011).
554. Makowska, A., Saczewski, F., Bednarski, P. J., Saczewski, J. & Balewski, Ł. Hybrid molecules composed of 2,4-diamino-1,3,5-triazines and 2-imino-coumarins and coumarins. Synthesis and cytotoxic properties. *Molecules* **23**, 1–16 (2018).
555. Husain, M. I. . & Srivastava, V. P. Synthesis of 4-methyl-1-piperazino/piperidinobiguanides as oral hypoglycemic agents. *Indian J. Chem. Sect. B Org. Chem. Incl. Med. Chem.* **23B**, 789–792 (1984).
556. Corbellini, A., Lugaro, G., Giannattasio, G. & Torti, G. Research on the antitumoral activity of the biguanides. IV. *Arch. Ital. Patol. Clin. Tumori* **10**, 197–210 (1967).
557. Shapiro, S. L. & Freedman, L. Oral anti-diabetic compositions and methods. (1957) doi:US2961377A.
558. Kim, H. W. *et al.* Biguanide compound and use thereof. (2020) doi:US10626085B2.